PREDICTION OF THE TABLET STRENGTH: DEVELOPMENT OF THE UNIFIED COMPACTION CURVE MODEL FOR WET GRANULATION

DOCTOR OF PHILOSOPHY THESIS

Submitted by

Thanh Huynh Nguyen

BEng(Hons)/MEngSci

Supervisor: **Prof. Karen Hapgood**

Co-supervisor: **A/Prof. David Morton**

Monash Advanced Particle Engineering Laboratory
Monash Institute of Pharmaceutical Sciences

Department of Chemical Engineering
Faculty of Engineering, Monash University

February, 2014

ꕥ In dedication to those
who believed in me and
encouraged me to sprout
wings and fly,

"No bird soars too high, if he soars with his own wings"
-William Blake- ꕥ

DECLARATION

In accordance with Monash University Doctorate Regulation 17: Doctor of Philosophy and Research Master's regulations the following declarations are made:

I hereby declare that this thesis contains no material which has been accepted for the award of any other degree or diploma at any university or equivalent institution and that, to the best of my knowledge and belief, this thesis contains no material previously published or written by another person, except where due reference is made in the text of the thesis.

This thesis includes one original paper published in peer reviewed journals and two unpublished publications. The core theme of the thesis is the understanding the fundamental driving forces from the wet granulation process on the final tablet strength in tablet manufacture. The ideas, development and writing up of all the papers in the thesis were the principal responsibility of myself, the candidate, working within the chemical engineering department under the supervision of Prof. Karen Hapgood [main supervisor, 75%] and A/Prof. David Morton [co-supervisor, 25%].

In the case of chapter four my contribution to the work involved the following:

Thesis chapter	Publication title	Publication status*	Nature and extent of candidate's contribution
4	Application of the Unified Compaction Curve to Link Wet Granulation and Tablet Compaction Behaviour	In press	Experimental and journal paper write-up

I have not renumbered sections of submitted or published papers in order to generate a consistent presentation within the thesis.

Signed: Thanh Huynh Nguyen

Copyright Notices

Notice 1

Under the Copyright Act 1968, this thesis must be used only under the normal conditions of scholarly fair dealing. In particular no results or conclusions should be extracted from it, nor should it be copied or closely paraphrased in whole or in part without the written consent of the author. Proper written acknowledgment should be made for any assistance obtained from this thesis.

Notice 2

I certify that I have made all reasonable efforts to secure copyright permissions for third-party content included in this thesis and have not knowingly added copyright content to my work without the owner's permission.

ACKNOWLEDGEMENTS

"*The only way of finding the limits of the possible is by going beyond them into the impossible.*"

-Arthur C. Clarke, Author -

Looking back to when I began my postgraduate studies, to where I am now with this thesis in my hand, I have realised that the past few years have been a major journey of discovery - both professionally and personally. I am honoured to be given the opportunity to achieve my vision as a four year-old to be a "scientist" or an independent researcher. Although the journey seemed impossible, I hope this thesis can show that anyone can achieve their dreams – *anyone*, who has their heart set to their goals. However, breaking through traditional boundaries and venturing into the impossible cannot be done without the help and encouragement of everyone around me. Words cannot express my sincere gratitude to everyone for instilling the confidence in me to persevere and be bold in my research studies.

It feels like yesterday when I was pacing back and forth across Prof. Karen Hapgood's office door (for what feels like the umpteenth time), feeling nervous about whether or not to ask her about wet granulation for my final year undergraduate research project (I know…"*It's Karen!*" but I was shy…). I am glad I had courage that day; since meeting and working with Karen, that was it - research became my life! Karen has been a huge source of support in my research and personal life. I could not have asked for a better supervisor/mentor. I am so honoured to have worked with Karen and be able to foster a unique supervisor-student relationship with her over the years (one consisting of various discussions/stories and chocolate fairies). Seeing Karen from the first day she stepped into academia to the academic researcher she is now and the research group she has established has been an absolute joy to watch and support. Thank you for everything Karen, your words and enthusiasm will stay with me a life-time and will shine in my future endeavours.

That is not to say that I didn't receive additional enthusiasm, encouragement and knowledge from A/Prof. David Morton. Working with David is awesome; his enthusiasm, curiosity and extensive knowledge help bring the project together and add more depth. David has been an enormous source of support for me, helping to ignite my curiosity and can always steer me on the right path when I become astray. His patience and understanding in my research and personal life I cannot fathom. Thank you David for making the research journey an absolute delight to undertake. I am absolutely honoured and proud to have worked with you and your enthusiasm is inspiring.

One of my major driving forces in moving forward comes from Ms. Shyama Fuad. No amount of words can express my appreciation for Shyama going beyond her duty of care with her patience, time, effort, support and compassion to encourage me follow my dreams and live out the life that I deserve. Shyama, for simplicity I can only say thank you so much for everything. To have you in my life is a blessing. I carry your words with me with confidence and enthusiasm in my personal and research lives.

Another major driving force comes from Dr. Kirsty McIntyre. I would not be able to achieve my childhood dream and go through the journey of discovery without Kirsty's patience, understanding, sincerity and encouragement. Kirsty, I cannot express through words how much I appreciate your time and compassion for me. You have helped to open my eyes and see that sometimes life presents blessings in disguise or in unconventional ways. Sometimes unconventional ways of thinking can help bring out the talent within us and make a positive contribution to society. Thank you for standing by my side, believing in me and encouraging me to persist towards achieving my dreams.

Another driving factor has been my time at the university gym. I have been able to achieve this thesis, one punch and one core at a time with Shar Campell-Smith and Christelle Schang. Thank you so much Shar and Christelle, for helping and motivating me to stay strong physically and mentally. The motivation and enthusiasm you both show is inspiring! To combat warriors Teresa Tran, June Treerat and Bianca Taylor, may we continue to stay with the fight!

My journey beyond the impossible would not have been possible without the support from my friends. To my board-game and nerdy buddies: Nazra Hameed, Ryan Moo, Fiona Low, Ronald Halim, Shaun Rimos and Bithi Roy, thank you for being there for me. I cannot tell you how much having you all in my life has changed my life for the better. May our love of games and nerdiness continue! Sincere gratitude is also sent to David Barling, Yao Zeng, Waithira Kariuki, Hasnul Rahman, Dr. Yuan Fang, Dr. Jenny Ho and Dr. Mohid Khan.

A special mention is given to Dr. Winnie Au-Yeung, Melanie Gribble, Kath Lloyd, Rachael Carter, Leanne Donald, Becky Hinman, Ahona Guha and, Sandra and Ian Jacobson – I could not have made it this far without being inspired by your strength and belief in me.

Being in the chemical engineering department in what appears to be “forever”, sincere gratitude goes to the chemical engineering administration staff including Chloe Priebee, Garry Thunder, Wren Schoppe and Jill Crisfield. I could not have organised the administration details and conference/research trips without the staff. Everyone always brightens up my day. A special mention is given to Jane Moodie for helping me to navigate through the thesis writing process.

I would like to especially express my gratitude to Lilyanne Price – you have provided much support, understanding and motivation. I would also like to sincerely express my gratitude to Prof. Raman Singh, who has been a source of consistent encouragement since my first day in undergraduate studies to the present day. Despite the changes in the department throughout my undergraduate and postgraduate studies, I am grateful to have constant support in my studies. At this point I would also like to express my gratitude to James Cartwright, who has been a consistent source of support in my research studies and adds a dimension of (cool) quirkiness to research life.

At this point I do not want to forget to thank the chemical, safety, and workshop staff: Kim Phu, Ron Graham, Ross Ellingham and Martin Watkins. As much as I love research, talking to you all really makes my day and thank you so much for being here for me.

I would also like to sincerely express my appreciation to Monash University; not only for providing the Australian Post-graduate Award but also for all the support I have received over the years from various Monash staff members including Dr. Nhan Le, Liz Kemp, Bronwyn Drake, Cindy Tarczon, Kay Gardner and Carol Triantafyllidis. It really does take a university community to help a student make something positive out of their life.

What makes my journey to do a PhD more wonderful is the support from my family. I am so fortunate that my family supports me in taking the rough and unbeaten road of research. I send my loving gratitude to Tracy Nguyen, Chloe and Shaun Price, Uncle Grahame and Aunty Khanh Tindale, Phuong and Kim-Kim Phan. I really would not be able to get to where I am today, without your love and support. I consider myself to be very lucky to have you all in my life.

This is quite a lengthy acknowledgement (I applaud you for reading this far!) but as someone wise once told me, it takes many droplets of water to turn into a powerful ocean and I wanted to make sure I did not miss a droplet. Last but not least, thank you for taking the time to read my thesis.

Warm regards,

Thanh Nguyen

SUMMARY

The complexity of tablet is often overlooked. A simple compressed mass of active and inactive ingredients hides the complex relationship between achieving the desired drug potency, the tablet strength and the tablet dissolution. The resulting tablet properties, particularly the tablet strength, are driven by the wet granulation process, an up-stream particle size enlargement process. Studies on the influence of the wet granulation process on the tablet properties show that there is still confusion over the influence of the wet granulation on the final tablet strength due to the lack of investigation in the direct impact between wet granulation and tabletting, which paves the path for the objective of this thesis.

The influence of the wet granulation process on the final tablet strength was investigated by conducting wet granulation case studies looking at the effects of the liquid level, wet massing time, impeller speed and binder flow rate on a standard formulation of 1:1 lactose and microcrystalline cellulose granulated with polyvinyl pyrrolidine polymer in various solutions. A model called the “Unified Compaction Curve” was adopted from the dry roller compaction process and applied to the wet granulation case studies to see the feasibility of the model and understand how the model bridges the relationship between the wet granulation operating conditions and the final tablet strength. To understand this, granules from selected granulation batches were analysed to determine the granule properties including the circularity factor, surface roughness and granule porosity. The effect of the wet massing process, presence of moisture, liquid binder acidity and the presence of hydrogen-bonding in the granule liquid bridges on the microcrystalline cellulose properties was also investigated. The Unified Compaction Curve model was also extended to investigate the effect of the granulator scale on the final tablet strength to explore the possibility of a new up-scale guideline.

The results demonstrate that the wet granulation process can have a direct effect on the subsequent tablet strength. As the liquid level, wet massing time and impeller speed increases, the tablet strength decreases from a maximum tablet hardness of approximately 45kp (from direct compaction) to lowest tablet hardness of 23.5kp after 10 minutes of wet massing time. Therefore there is a “loss of compactability” when the formulation is exposed to processing conditions in wet granulation and even in dry roller compaction

(Kochhar *et al.*, 1995; Bultmann, 2002; Freitag and Kleinebudde, 2003; Shi *et al.*, 2011; Shi *et al.*, 2011). The loss of compactability in the formulation by the processing compaction forces sets up the fundamental conditions for the Unified Compaction Curve model to be applied.

The Unified Compaction Curve model was found to be a feasible model for the wet granulation process in which the model was able to translate the wet granulation compaction curves for various liquid levels, wet massing times, impeller speeds and binder flow rates and overlap them onto the master direction compaction curve, which allows the prediction of the resulting tablet strength. The Unified Compaction Curve is able to quantify the amount of compaction pressure exerted on the granules during wet granulation through the "effective wet granulation compaction pressure", P_{WGC}. When the P_{WGC} is coupled with the cumulative number of impeller revolutions, the liquid level, wet massing time, impeller speed and binder flow-rate wet granulation data all coincide onto a first-order exponential curve. This makes the Unified Compaction Curve a potentially powerful tool in visually seeing the magnitude of deterioration in the tablet strength by the wet granulation process, which allows the prediction of the final tablet strength.

The deterioration in the tablet strength with increasing wet granulation processing time is attributed to the decrease in the granule surface and rounding of the granule structure. This was evident by the increase in the circularity factor with increasing number of impeller revolutions and SEM images. The granulator impeller consolidates the granules, consequently destroying the granule surface roughness and decreases the granule porosity. If the granule porosity is seen as a function of the cumulative number of impeller revolutions, it can be seen that the relationship is the inverse relationship of the P_{WGC} and the cumulative number of impeller revolutions. This demonstrates that the granule porosity is one of the main driving factors for the deterioration of the tablet strength with increasing residence time in the granulator. The transition of the granule morphology and porosity during wet granulation can be attributed to the irreversible plastic deformation of microcrystalline cellulose particles, which wrap and encase the lactose particles during the consolidation and densification of the granules during the wet granulation process. This destroys the mechanical inter-locking ability of the granules during the tabletting process, hence leading to the "loss of compactability" and reduction in the final tablet strength.

However, the Unified Compaction Curve model will only be valid for granulation formulations comprising at least 30% liquid level and with at least 50% microcrystalline cellulose in the formulation used in this study, to effectively translate the kinetic forces from the impeller into compaction forces for significant deformation to occur. This was evident in granulation case studies where a liquid level less than 30% leads to the compaction data not conforming to the Unified Compaction Curve model. A recent study into the Unified Compaction Curve model found that a formulation comprising of 49% of microcrystalline cellulose (Avicel Ph-101) was not successful for the model to be valid (Dave and Dudhat, 2013).

Investigations into the presence or absence of intra-granular hydrogen bonding in the granule liquid bridges can influence the final tablet. When hydrogen bonding is present (by using water-based liquid binder) between the granules, the granule strength increases which in turn compromises the table strength. The inverse trend was found for the absence of hydrogen-bonding (by using an ethanol-based liquid binder). Therefore strength of the liquid bridges can play a part in controlling the final tablet strength.

The exploration of the effect of the liquid binder on the microcrystalline cellulose properties revealed that microcrystalline cellulose swells upon exposure to liquid binder. The swelling of the cellulose would increase the bonding area and confer strength to the tablet. The acidity of the liquid binder appears to influence the crystallite size of microcrystalline cellulose granules. The crystallite size was found to be larger for granulation experiments using a liquid binder with a neutral pH level (such as calcium oxide liquid binders), compared to the crystallite size in granules produced with more acidic liquid binders (such as PVP or hydrochloric acid). The wet massing time did not have any significant effect on the crystalline or amorphous regions of microcrystalline cellulose.

The effects of the wet granulator scale was also investigated which revealed that Unified Compaction Curve demonstrates different mixing intensities between the 1litre and 5 litre granulator bowls in the relationship between the wet granulation compaction pressure (denoted as χ) and the cumulative number of impeller revolutions. The compaction pressure per revolution was found to be greater for the 1L granulator in comparison to the

5L granulator scale. This formed the basis for the proposal of a new wet granulation scale-up rule which looks at maintaining 'constant compaction pressure' during the wet granulation scale-up process. This scale-up rule is a function of the compaction pressure per revolution and the cumulative number of impeller revolutions. The compaction pressure per revolution, χ, is able to compensate for the differences in the granulator bowl geometry and impeller design between the two granulator scales. The proposed rule is anticipated to be a useful tool to help maintain constant granule properties during wet granulation scale-up but also to target the desired tablet.

The studies in this thesis will allow a deeper insight into the mechanisms in the relationship between the wet granulation process and the final tablet strength, which would enable the wet granulation to be tailored for optimisation and target tablet specifications, make trouble-shooting easier to carry out and reduce resources for wet granulation case studies. This is of great importance and benefit to the pharmaceutical industry.

PUBLICATIONS AND AWARDS

Publications from research project:

Journal publication(s):

1. **T.H. Nguyen**, D. Morton and K.P. Hapgood (2013), "*Application of the Unified Compaction Curve to Link Wet Granulation and Tablet Compaction Behaviour",* Powder Technology Journal, vol. 240, special issue: 3rd International Conference on Particulate Processes in the Pharmaceutical Industry.

Conference publication(s):

2. **T.H. Nguyen**, D. Morton and K. Hapgood (2013), "*Linking the wet Granulation conditions to the tablet properties through the Unified Compaction Curve*", 6th International granulation workshop, 26th -28th June, Sheffield, UK,
3. **T.H. Nguyen**, D. Morton and K. Hapgood (2012), "*Understanding the Unified Compaction Curve model for wet granulation and subsequent tablet strength*", CHEMECA, 23-26 September, Wellington, New Zealand, IChemE/IEAust.,
4. **T.H. Nguyen**, D. Morton and K. Hapgood (2011), "*Unified Compaction Curve: A potential link between the wet granulation and tabletting processes*", 5th International granulation workshop, 20th -22th June, Lausanne, Switzerland,
5. K. Hapgood, **T.H. Nguyen** and D. Morton (2011), "*Using the Unified Compaction Curve to bridge the wet granulation and tabletting processes*", Particulate processes in the pharmaceutical industry III, 24th -29th July, Gold Coast, Australia (Keynote presentation by A/Prof. Hapgood),
6. **T.H. Nguyen**, D. Morton and K. Hapgood (2011), "*Linking the wet granulation conditions to the tablet properties through the Unified Compaction Curve*", CHEMECA, 18-21 September, Sydney, Australia, IChemE/IEAust.

Publications from other fields of research:

Journal publication(s):

7. M.X.L. Tan, **T.H. Nguyen** and K. Hapgood (2013), "*Drug distribution in wet granulation: foam versus spray*", Drug Development and Industrial Pharmacy, 39(9), pp.1389-1400.

Conference publication(s):

8. K. Hapgood, T.H. Nguyen and N. Eshtiaghi (2011), "*Wet granulation of hydrophobic powders: Drop penetration, drug distribution and liquid marbles*", 5th International granulation workshop, 20th -22th June, Lausanne, Switzerland,
9. **T.H. Nguyen**, W. Shen and K. Hapgood (2010), "*Predicting distribution of a hydrophobic drug using drop penetration time*", American Association of Pharmaceutical Scientists (AAPS) Annual meeting, 14-18 November, New Orleans, US,
10. **T.H. Nguyen**, W. Shen and K. Hapgood, "*Transitional drop penetration time: a guideline for an even drug distribution in heterogeneous-wetting formulations in wet granulation*", CHEMECA conference, September, 2010, Adelaide, Australia.

11. **T.H. Nguyen**, W. Shen and K. Hapgood, "*Transitional drop penetration time: a guideline for an even drug distribution in heterogeneous-wetting formulations in wet granulation*", 6th World Congress on Particle Technology, 26th-29th April, 2010, Nuremberg, Germany.
12. **T.H. Nguyen**, W. Shen and K. Hapgood, "*Influence of spray viscosity on the rewetting effect and dimensionless spray flux in wet granulation*", 6th World Congress on Particle Technology, 26th-29th April, 2010, Nuremberg, Germany.

Award(s):

2nd place speaker in 3rd annual Monash University chemical engineering conference 2013

TABLE OF CONTENTS

Page number

DECLARATION **II**

ACKNOWLEDGEMENTS **III**

SUMMARY **V**

PUBLICATIONS AND AWARDS **IX**

TABLE OF CONTENTS **XI**

LIST OF FIGURES **XV**

LIST OF TABLES **XXIII**

1 INTRODUCTION **2**

1.1 INTRODUCTION TO SOLID DOSAGE FORM: TABLETS **2**
1.2 LIMITATION OF KNOWLEDGE: INFLUENCE OF WET GRANULATION PROCESS ON TABLET STRENGTH **4**
1.3 RESEARCH AIMS **5**
1.4 REPORT OUTLINE **5**

2 LITERATURE REVIEW **10**

2.1 OVERVIEW OF TABLET MANUFACTURE **10**
2.2 TABLETTING PROCESS **14**
2.2.1 COMPRESSION OF TABLETS 14
2.2.2 PARTICLE RE-ARRANGEMENT AND DEFORMATION 16
2.2.3 PARTICLE-PARTICLE BONDING 20
2.3 TABLET CHARACTERISTICS **20**
2.3.1 TABLET BONDING MECHANISMS 20
2.3.2 TABLET POROSITY 21
2.3.3 TABLET HARDNESS 22
2.4 EXAMINATION OF WET GRANULATION PROCESS **25**
2.4.1 WETTING AND NUCLEATION 25
2.4.2 COALESCENCE AND CONSOLIDATION 26
2.4.3 ATTRITION AND BREAKAGE 30

2.5 GRANULE CHARACTERISTICS 30
2.5.1 GRANULE LIQUID SATURATION 30
2.5.2 GRANULE SIZE DISTRIBUTION 31
2.5.3 GRANULE MORPHOLOGY 33
2.5.4 GRANULE SURFACE AREA 35
2.5.5 GRANULE POROSITY 35
2.5.6 GRANULE STRENGTH 37
2.6 EFFECT OF WET GRANULATION CONDITIONS ON GRANULE PROPERTIES AND TABLET PROPERTIES 39
2.6.1 EFFECT OF THE FORMULATION 40
2.6.2 EFFECT OF THE LIQUID LEVEL 43
2.6.3 EFFECT OF THE WET MASSING TIME 44
2.6.4 EFFECT OF THE IMPELLER SPEED AND TORQUE 46
2.6.5 GRANULATOR SCALE-UP 47
2.6.6 COMPACTION PRESSURE PRIOR TO TABLETTING 50
2.7 UNIFIED COMPACTION CURVE MODEL 52
2.8 LITERATURE SUMMARY AND GAP ANALYSIS 55

3 MATERIAL AND EXPERIMENTAL PROCEDURES 60

3.1 LIQUID BINDER 61
3.2 POWDER FORMULATION 62
3.2.1 MICROCRYSTALLINE CELLULOSE 62
3.2.2 LACTOSE MONOHYDRATE 64
3.3 WET GRANULATION EXPERIMENTS 66
3.4 TABLETTING EXPERIMENTS 71
3.4.1 DIRECT COMPACTION TABLETTING 72
3.4.2 WET-GRANULATED TABLET COMPACTION 73
3.5 GRANULE AND TABLET CHARACTERISATION 73
3.5.1 PARTICLE SIZE DISTRIBUTION MEASUREMENT 74
3.5.2 SKELETAL DENSITY MEASUREMENT 74
3.5.3 BULK SPECIFIC SURFACE AREA 75
3.5.4 GRANULE POROSITY 77
3.5.5 GRANULE STRUCTURE IMAGING AND ANALYSIS 78
3.5.6 TABLET DIMENSIONS AND WEIGHT MEASUREMENTS 80
3.5.7 TABLET HARDNESS AND TENSILE STRENGTH MEASUREMENTS 80

4 USING THE UNIFIED COMPACTION CURVE TO PREDICT THE TABLET STRENGTH FROM THE WET GRANULATION PROCESS 83

4.1 INTRODUCTION 83
4.2 MATERIALS AND EXPERIMENTAL PROCEDURE 85
4.3 ADAPTING THE UNIFIED COMPACTION CURVE FOR WET GRANULATION 88

4.3.1 THEORY 88
4.3.2 MODELLING THE UNIFIED COMPACTION CURVE MODEL IN WET GRANULATION 91
4.4 RESULTS 95
4.4.1 EFFECT OF LIQUID LEVEL AND WET MASSING TIME ON GRANULE SIZE DISTRIBUTION 96
4.4.2 EFFECT OF LIQUID LEVEL ON TABLET STRENGTH 99
4.4.3 EFFECT OF WET MASSING TIME 103
4.5 APPLICATION OF THE UNIFIED COMPACTION CURVE TO WET GRANULATION 106
4.5.1 FEASIBILITY OF THE UNIFIED COMPACTION CURVE MODEL TO WET GRANULATION 106
4.5.2 QUANTITATIVE ANALYSIS FROM THE UNIFIED COMPACTION CURVE 110
4.6 DISCUSSION 115
4.6.1 WET GRANULATION COMPACTION PRESSURE, P_{WGC} 115
4.6.2 QUANTIFYING THE IMPELLER COMPACTION PRESSURE PER REVOLUTION 119
4.7 LIMITATIONS OF UNIFIED COMPACTION CURVE MODEL 121
4.8 IMPLICATIONS OF THE UNIFIED COMPACTION CURVE 123
4.9 CONCLUSIONS 124

5 EFFECT OF THE GRANULATOR COMPACTION PRESSURE ON THE GRANULE PROPERTIES 128

5.1 INTRODUCTION 128
5.2 EXPERIMENTAL PROCEDURE 129
5.3 CHARACTERISATION RESULTS 132
5.3.1 GRANULE TOPOLOGY AND MORPHOLOGY 132
5.3.2 GRANULATION MEAN SIZE 134
5.3.3 GRANULE AND TABLET SKELETAL DENSITY 135
5.3.4 GRANULE SPECIFIC SURFACE AREA 137
5.3.5 GRANULE POROSITY 139
5.4 DISCUSSION 141
5.5 CONCLUSIONS 144

6 EFFECT OF THE GRANULATOR COMPACTION PRESSURE AND THE LIQUID BINDER ON THE MICROCRYSTALLINE CELLULOSE MATERIAL PROPERTIES AND SUBSEQUENT TABLET STRENGTH 148

6.1 INTRODUCTION 148
6.2 MATERIALS AND EXPERIMENTAL PROCEDURE 149
6.2.1 DRY POWDER MIXING EXPERIMENT 149
6.2.2 POWDER RE-HUMIDIFICATION 150
6.2.3 WETTED POWDER, NO SHEAR EXPERIMENT 151
6.2.4 ETHANOL-BASED WET GRANULATION EXPERIMENT 151
6.2.5 EFFECT OF LIQUID BINDER ACIDITY ON THE TABLET STRENGTH EXPERIMENT 152

6.2.6 EFFECT OF LIQUID BINDER ACIDITY ON THE MICROCRYSTALLINE CELLULOSE CRYSTALLINITY 152
6.2.7 TABLETTING EXPERIMENTS 154
6.3 RESULTS 155
6.3.1 EFFECT OF POWDER DRY MIXING ON THE TABLET STRENGTH 155
6.3.2 EFFECT OF RE-HUMIDIFICATION OF POWDER ON THE TABLET STRENGTH 156
6.3.3 EFFECT OF LIQUID BINDER POWDER SATURATION WITH VERY LOW SHEAR 159
6.3.4 EFFECT OF THE LIQUID BINDER SOLVENT ON THE TABLET STRENGTH 161
6.3.5 EFFECT OF THE LIQUID BINDER SOLVENT ACIDITY ON THE TABLET STRENGTH 165
6.3.6 EFFECT OF THE MICROCRYSTALLINE CELLULOSE AMORPHOUS AND CRYSTALLINITY PROPERTIES ON THE TABLET STRENGTH 169
6.4 DISCUSSION 174
6.5 CONCLUSIONS 177

7 EFFECT OF THE GRANULATOR SCALE ON THE TABLET STRENGTH 180

7.1 INTRODUCTION 180
7.2 MATERIALS AND EXPERIMENTAL PROCEDURE 181
7.3 RESULTS 184
7.3.1 EFFECT OF 1 LITRE GRANULATOR SCALE ON THE TABLET STRENGTH 184
7.3.2 EFFECT OF THE GRANULATOR SCALE ON THE UNIFIED COMPACTION CURVE 189
7.4 DISCUSSION 191
7.5 CONCLUSIONS 195

8 FINAL REMARKS, CONCLUSIONS AND RECOMMENDATIONS 198

8.1 CONCLUSIONS 198
8.2 RECOMMENDATIONS 204

NOMENCLATURE AND ACRONYMS 206

REFERENCES 209

LIST OF FIGURES

Page number

Figure 1.1: Summary of the tablet manufacturing process using wet granulation. 3
Figure 2.1: Schematic diagram of direct compaction tablet manufacturing process. Raw powder is fed directly to the tablet press to produce a tablet. 11
Figure 2.2: Schematic diagram of roller compaction tablet manufacturing process. Raw powder is fed to compactor rollers to produce a ribbon, before being milled into granules. The granules are then fed to the tablet press to produce the tablet. 11
Figure 2.3: Schematic diagram of wet granulation tablet manufacturing process. Raw powder is fed to the wet granulator along with liquid binder to produce granules. The granules are then fed to the tablet press to produce a tablet. 12
Figure 2.4: Schematic diagram of the rotary tabletting process, adapted from Augsburger and Hoag (2008). 15
Figure 2.5: The mechanisms involved in particle compression in a cylindrical die. The definition of particle in this diagram can be taken to be either a raw particle or a granule. Adopted from (Salman *et al.*, 2007). 17
Figure 2.6: Compression cycle, adopted from Cartensen (2001). 18
Figure 2.7: Stress-strain plot representing tablet behaviour under an applied force. The arrows represent the change in tablet property if the profile is modified. Adopted from Hartsuijker and Welleman (2007). 23
Figure 2.8: Schematic diagram of the wetting and nucleation in the spray zone during wet granulation, inset from Perry and Green (1997) and Iveson (2001). 25
Figure 2.9: Schematic diagram of the coalescence and consolidation stage during wet granulation. Inset from Perry and Green (1997) and Iveson *et al.* (2001). 26
Figure 2.10: Schematic graph of steady granule growth (left) and induction granulate growth (right). Taken from (Iveson and Litster, 1998; Salman *et al.*, 2007).....28
Figure 2.11: Granule growth regime map developed by Iveson *et al.* (2001). 29
Figure 2.12: Schematic diagram of the coalescence and consolidation stage during wet granulation Inset from Perry and Green (1997) and Iveson *et al.* (2001). 30
Figure 2.13: Stages of liquid content in a granule. Redrawn from Capes (1980).....31
Figure 2.14: Morphology of pure microcrystalline cellulose granules at different wet massing times: (A) 0mins; (B) 1min; (C) 5mins; (D) 10mins; (E) 20mins and (F) 40mins. Figure taken from Shi, *et al.* (2001). 34
Figure 2.15: Reconstructed 3D x-ray tomography images of granules produced at (a) 230rpm; (b) 300rpm and 350rpm. Figure taken from Rahmanian, *et al.* (2009). 34
Figure 2.16: The relationships between: (left) granule strength and the granule porosity and (right) granule strength as a function of the granule density. Taken from Macias and Carvajal (2012). 37
Figure 2.17: The tablet (compact) strength as a function of the average granule strength. Figure taken from Macias and Carvajal (2012). 38
Figure 2.18: Schematic molecular structure of microcrystalline cellulose (left); and SEM image of microcrystalline cellulose, taken from Rowe *et al.* (2009) (right).....41

Figure 2.19: The rounding of microcrystalline cellulose (MCC) granule morphology (left) and changes in granule properties with increasing water level (right). Taken from Shi *et al. (2011).* 43
Figure 2.20: The granule density as a function of the number of impeller revolutions and impeller speed. Figure taken from Macias and Carvajal (2012). 45
Figure 2.21: The compact or tablet strength as a function of the number of impeller revolutions. Data taken from Macias *et al.* (2012). 45
Figure 2.22: Effect of the wet massing time (MWG) on the tablet tensile strength as a function of the compaction pressure (liquid level of 65%). Broken line indicates the threshold between desirable granulation and over-granulation. Figure taken from Shi *et al.*, (2011). 46
Figure 2.23: The reduction of the compaction behaviour profile or the "processing compaction" from the effects of: (left) liquid level and (right) wet massing time. Images taken from Shi *et al.* (2011a and 2011b). 51
Figure 2.24: (left) Schematic diagram of the loss of tablet compactability after Roller Compaction (RC) at low (L) and high (H) roller compaction forces; and (right) the same data combined onto a Unified Compaction Curve (UCC). The translation in origin points for the UCC allows for the roller compaction pressure (P_{RC}) to be extrapolated from the data (adapted from Farber *et al.* 2008). 52
Figure 3.1: Chemical molecular structure of Polyvinyl Pyrrolidone. 61
Figure 3.2: Chemical molecular structure of microcrystalline cellulose. 63
Figure 3.3: Schematic diagram of the Avicel manufacturing process, taken from Reier (2007). 63
Figure 3.4: Images of microcrystalline cellulose (Avicel, PH-101) with (left) Scanning Electron Microscopy (scale bar: 160µm) and; (right) optical microscope. 64
Figure 3.5: Molecular structure of lactose monohydrate. 65
Figure 3.6: Images of lactose monohydrate (200 mesh) with (left) Scanning Electron Microscopy (scale bar: 240µm) and; (right) optical microscope. 65
Figure 3.7: Schematic diagram of the wet granulation process. 66
Figure 3.8: Schematic diagram of wet granulation experiment set-up. 67
Figure 3.9: Images of (a) aerial view; and (b) internal view of 1L granulator bowl and main impeller with the powder contact surface area for different regions of the bowl (Key International). 67
Figure 3.10: Images of (a) aerial view; and (b) internal view of 5L granulator bowl and main impeller with the powder contact surface area for different regions of the bowl (Key International). 68
Figure 3.11: Experimental set up of wet granulation experiments using the granulator, spray pot and spray nozzle. 68
Figure 3.12: Images of (a) Carver automatic tablet press; and (b) tablet produced from the tablet press (scale bar in centimetres). 71
Figure 3.13: Schematic diagram of tablet press mould and punch set-up. 72
Figure 3.14: Schematic diagram of direct compaction. 72
Figure 3.15: Schematic diagram of wet-granulated tablet compaction process. 73
Figure 3.16: Image of the mechanical vibration sieve shaker (Retsch AS200). 74

Figure 3.17: Image of nitrogen gas adsorption BET surface area (left) instrument (Belsorp Mini II, Belsorp Japan) and (right) sample tubes. 76
Figure 3.18: Fitting the tangent line (Bold line) to the BET curve using linear regression in the *Belsorp Mini II* software. 77
Figure 3.19: Schematic diagram of the interstitial and internal pore of powder samples in mercury intrusion porosimetry analysis. 78
Figure 3.20: Refinement of SEM images to obtain the particle perimeter outline in preparation for circularity value analysis using *ImageJ*. 79
Figure 3.21: Dr. Schleuniger Pharmatron tablet hardness tester. 80
Figure 4.1: Schematic diagram of the roller compaction process. 84
Figure 4.2: (left) Schematic diagram of the loss of tablet compactability after Roller Compaction (RC) at low (L) and high (H) roller compaction forces; and (right) the same data combined onto a Unified Compaction Curve (UCC). The translation in origin points for the UCC allows for the roller compaction pressure (P_{RC}) to be extrapolated from the data (adapted from Farber *et al.* 2008). 84
Figure 4.3: Schematic diagram of (a) tablet produced from direct compaction; and (b) tablet produced from wet granulation. 85
Figure 4.4: Compaction profile of tablets produced from direct compaction for 1:1 microcrystalline cellulose:lactose 200mesh formulation with an experimental maximum tablet tensile strength of 3.34MPa. 92
Figure 4.5: An example of the calculations to data fit Leuenberger's model of compactability and compressibility (1982) to the experimental dry compaction tensile strength (TS) data with consistent theoretical tablet density. 93
Figure 4.6: An example of the calculations required to generate the dry compaction curve for the Unified Compaction Curve. 93
Figure 4.7: Compaction profile of tablets produced from wet granulation at 20wt% liquid level (LL) for 1:1 MCC:L2M formulation. 94
Figure 4.8: An example of the calculations required to generate the Unified Compaction Curve. 95
Figure 4.9: Application of the Unified Compaction Curve for wet granulated tablets at 30wt% liquid level, 10 minutes wet massing time for 1:1 MCC:L2M formulation. The blue curve represents the tabletting portion of the Unified Compaction Curve, while the green data points represent the translated Unified Compaction Curve. The blue curve is translated to the new origin of P_{WGC}, T_{WGC}. 95
Figure 4.10: Granule size distribution plots for varying liquid level quantities: (a) 20wt.%; (b) 30wt.%; (c) 40wt.%; and (d) 50wt.%. The granulation experiments are based on an impeller speed of 285rpm and 10 seconds wet massing time. 96
Figure 4.11: Relationship between the d_{50} particle size and the tablet hardness as a function of liquid level, binder flow rate and impeller speed. Wet massing time is 10 seconds. 97
Figure 4.12: Granule size distribution plots for varying wet massing time at: (a) 20wt.%; (b) 30wt.%; (c) 40wt.%; and (d) 50wt.% liquid level. The granulation experiments are based on an impeller speed of 285rpm. 98

Figure 4.13: Relationship between the d_{50} particle size and the tablet hardness as a function of wet massing time, liquid level, binder flow rate and impeller speed. 99
Figure 4.14: Tablettability (tablet hardness as a function of compaction pressure) behaviour for granules produced from varying liquid levels (a) 20%; (b) 30%; (c) 40%; and (d) 50%. 100
Figure 4.15: Compressibility (tablet density as a function of compaction pressure) behaviour for granules produced from varying liquid levels (a) 20%; (b) 30%; (c) 40%; and (d) 50%. Formulation comprises of 1:1 microcrystalline cellulose:lactose 200 mesh and 5w/v% PVP. 102
Figure 4.16: Compactability (tablet hardness as a function of tablet density) behaviour for granules produced from varying liquid levels (a) 20wt%; (b) 30wt%; (c) 40wt%; and (d) 50wt%. Formulation comprises of 1:1 microcrystalline cellulose:lactose 200 mesh and 5w/v% PVP. 103
Figure 4.17: Tablettabilty (tablet hardness as a function of compaction pressure) behaviour for granules produced from varying wet massing times (a) 0mins; (b) 2mins; (c) 6mins; and (d) 10mins. 104
Figure 4.18: Compactability (tablet hardness as a function of tablet density) behaviour for granules produced from varying wet massing times (a) 0mins; (b) 2mins; (c) 6mins; and (d) 10mins. 105
Figure 4.19: Unified Compaction Curve for the liquid level effects at varying impeller speeds. 107
Figure 4.20: Unified Compaction Curve for wet massing time effects with varying impeller speeds and liquid levels (130g/min). 108
Figure 4.21: Unified Compaction Curve for wet massing time effects and liquid levels. Binder flow rate is 280 g/min and impeller speed is 285 rpm. 108
Figure 4.22: Schematic representation of how the wet granulation process is related to the tabletting process in the Unified Compaction Curve. 109
Figure 4.23: Schematic representation of the Unified Compaction Curve model showing how the equivalent wet granulation compaction pressure (P_{WGC}) and the tableting compaction pressure (P') is related to the equivalent average granule strength (T_{WGC}) and the reduction of the maximum possible compaction pressure (T_{max}) to produce the final tablet strength (T'). 110
Figure 4.24: The relationship between the liquid level and the wet granulation compaction pressure P_{WGC} with low (130g/min) and high (280g/min) binder flow rates. 111
Figure 4.25: relationship between the wet massing time and the wet granulation compaction pressure P_{WGC} as a function of liquid level (LL). 112
Figure 4.26: Matrix graphs showing various relationships between the wet granulation compaction pressure P_{WGC}, wet massing time, liquid level, binder flow rate (BF) and impeller speed. (a) BF = 130g/min, 285rpm; (b) BF = 280g/min, 285rpm; (c) BF = 130g/min; and (d) BF = 280g/min. 113
Figure 4.27: The wet granulation compaction pressure as a function of the number of impeller revolutions. Solid line is fitted to the direct compaction data (Equation 4.11). 117

Figure 4.28: Application of the Unified Compaction Curve model to a formulation of pure microcrystalline cellulose with varying liquid level and wet massing time. Data taken from Shi *et al.* (2011). 119
Figure 4.29: Schematic diagram of the transition of granule surface roughness as a function of the number of impeller revolutions and the wet granulation compaction pressure. 120
Figure 5.1: Selected granular samples produced from wet granulation experiments (in Chapter 4), used to characterise the granule structure and observe the implications on the wet granulation compaction pressure, P_{WGC}. 130
Figure 5.2: SEM images of granules produced from varying number of impeller revolutions. Images are at 500 times magnification. Scale-bar represents 230µm..... 133
Figure 5.3: The Circularity dimension of the projected profile of granules as a function of the cumulative number of high-shear granulator impeller revolutions. 133
Figure 5.4: The mean granule size d_{50} as a function of the number of impeller revolutions. Each data-point is labelled with the sample number as described in Table 5.1..... 135
Figure 5.5: Granule skeletal density as a function of the number of impeller revolutions. 136
Figure 5.6: Tablet skeletal density as a function of the number of impeller revolutions. 137
Figure 5.7: Granule specific surface area as a function of the number of impeller revolutions. Each data-point is labelled with the sample number as described in Table 5.1. 138
Figure 5.8: The tablet tensile strength as a function of the granule specific surface area as measured by nitrogen adsorption analysis (Belsorp). 138
Figure 5.9: The effective wet granulation compaction pressure, P_{WGC}, as a function of the cumulative number of impeller revolutions. 139
Figure 5.10: Granule porosity as a function of the number of impeller revolutions as measured by mercury intrusion porosimetry analysis. 140
Figure 5.11: The tablet tensile strength as a function of the granule porosity as measured by the mercury intrusion porosimetry analysis. 140
Figure 5.12: The effective wet granulation compaction pressure, P_{WGC}, as a function of the granule porosity..... 141
Figure 6.1: Moisture Isotherm of microcrystalline cellulose. Data taken from (Wolf *et al.*, 1984; Khan and Pilpel, 1987; Kachrimanis *et al.*, 2006). 150
Figure 6.2: Schematic diagram of the peak height method (Terinte *et al.*, 2011). 153
Figure 6.3: The Scherrer crystallite size analysis on a XRD spectra peak, showing the width of the peak at half the peak, *B*. 154
Figure 6.4: Tablettabilty (tablet hardness as a function of compaction pressure) behaviour for powder dry mixed at: (a) 0mins; (b) 2mins; (c) 6mins; and (d) 10mins. Formulation comprises of 1:1 microcrystalline cellulose:lactose 200 mesh and 5w/v% PVP..... 155
Figure 6.5: Compactability (tablet hardness as a function of tablet density) behaviour for powder dry mixed at: (a) 0mins; (b) 2mins; (c) 6mins; and (d) 10mins. Formulation comprises of 1:1 microcrystalline cellulose:lactose 200 mesh and 5w/v% PVP..... 156

Figure 6.6: Tablettabilty (tablet hardness as a function of compaction pressure) behaviour for tablets produced from humidified powder and direct compaction. Formulation comprises of 1:1 microcrystalline cellulose:lactose 200 mesh and 5w/v% PVP.....157
Figure 6.7: Compressibility (tablet hardness as a function of tablet density) behaviour for tablets produced from humidified powder and direct compaction. Formulation comprises of 1:1 microcrystalline cellulose:lactose 200 mesh and 5w/v% PVP.....158
Figure 6.8: Compactability (tablet hardness as a function of tablet density) behaviour for tablets produced from humidified powder and direct compaction. Formulation comprises of 1:1 microcrystalline cellulose:lactose 200 mesh and 5w/v% PVP.....159
Figure 6.9: Tablettabilty behaviour for tablets produced from powder saturated with 5w/v% PVP liquid binder, with low shear (~50rpm) and high shear (600rpm) applied; and direct compaction. Powder formulation comprises of 1:1 microcrystalline cellulose:lactose 200 mesh.....160
Figure 6.10: Compactability behaviour for tablets produced from powder saturated with 5w/v% PVP liquid binder, with low shear (~50rpm) and high shear (600rpm) applied; and direct compaction. Powder formulation comprises of 1:1 microcrystalline cellulose:lactose 200 mesh.....161
Figure 6.11: Comparison of Tablettabilty (tablet hardness versus compaction pressure) behaviour for tablets produced from ethanol-based (E) and water-based (W) liquid binders in liquid level (LL) granulation experiments. Formulation comprises of 1:1 microcrystalline cellulose:lactose 200 mesh and 5w/v% PVP. 162
Figure 6.12: Compressibility (tablet hardness vs. tablet density) behaviour for tablets produced from ethanol-based (E) and water-based (W) liquid binders in liquid level (LL) granulation experiments. Formulation comprises of 1:1 microcrystalline cellulose:lactose 200 mesh and 5w/v% PVP.....163
Figure 6.13: Compactability (tablet hardness vs. tablet density) behaviour for tablets produced from ethanol-based (E) and water-based (W) liquid binders in liquid level (LL) granulation experiments. Formulation comprises of 1:1 microcrystalline cellulose:lactose 200 mesh and 5w/v% PVP.....163
Figure 6.14: Tablettabilty (tablet hardness vs. compaction pressure) behaviour for tablets produced from ethanol-based (E) and water-based (W) liquid binders in wet-massing time (WMT) granulation experiments. Formulation comprises of 1:1 microcrystalline cellulose:lactose 200 mesh and 5w/v% PVP. 164
Figure 6.15: Compactability (tablet hardness vs. tablet density) behaviour for tablets produced from ethanol-based (E) and water-based (W) liquid binders in wet-massing time (WMT) granulation experiments. Formulation comprises of 1:1 microcrystalline cellulose:lactose 200 mesh and 5w/v% PVP. 165
Figure 6.16: Tablettability (tablet hardness as a function of compaction pressure) behaviour for granules produced from varying wet massing times 30% liquid level. Formulation comprises of 1:1 microcrystalline cellulose:lactose 200 mesh and 5w/v% PVP. 166
Figure 6.17: Compactability (tablet hardness as a function of tablet density) behaviour for granules produced from varying wet massing times 30% liquid level. Formulation comprises of 1:1 microcrystalline cellulose:lactose 200 mesh and 5w/v% PVP.....167

Figure 6.18: Granule size distribution plots for varying wet massing time at 30wt% liquid level. The granulation experiments are based on an impeller speed of 285rpm. Formulation is 1:1 microcrystalline cellulose and lactose 200 mesh, granulated with 5w/v% polyvinyl pyrrolidone and calcium oxide (pH = 7). 168
Figure 6.19: Granule size distribution plots for varying wet massing time at 30wt% liquid level. The granulation experiments are based on an impeller speed of 285rpm. Formulation is 1:1 microcrystalline cellulose and lactose 200 mesh, granulated with 5w/v% polyvinyl pyrrolidone and hydrochloric acid (pH = 1). 168
Figure 6.20: Representative SEM images of granules (30wt.% liquid level, 400rpm, 10 minutes wet massing time) produced from liquid binders containing calcium oxide (pH = 7) and hydrochloric acid (pH = 1)..... 169
Figure 6.21: XRD analysis of the raw material components: microcrystalline cellulose (MCC); lactose 200mesh (L2M) which comprises the 1:1 microcrystalline cellulose/lactose 200mesh (MCC-L2M) formulation. 170
Figure 6.22: XRD of 1:1 raw microcrystalline cellulose and lactose 200 mesh, granulated with 5w/v% PVP liquid binder (pH = 4), as a function of the wet massing time. The colour of the wet massing time description in the legend corresponds to the XRD spectra of the same colour. 171
Figure 6.23: XRD of 1:1 raw microcrystalline cellulose and lactose 200 mesh, granulated with 5w/v% PVP and HCl liquid binder (pH = 1), as a function of the wet massing time. The colour of the wet massing time description in the legend corresponds to the XRD spectra of the same colour..... 172
Figure 6.24: XRD of 1:1 raw microcrystalline cellulose and lactose 200 mesh, granulated with 5w/v% PVP and CaO liquid binder (pH = 7.5), as a function of the wet massing time. The colour of the wet massing time description in the legend corresponds to the XRD spectra of the same colour. 172
Figure 7.1: Images of the (a) bowl; (b) impeller and (c) dimensional drawings of the small laboratory granulator (KG1 granulator) bowl (1L). 182
Figure 7.2: Images of the (a) bowl; (b) impeller and (c) dimensional drawings of the large laboratory granulator (KG5 granulator) bowl (5L). 183
Figure 7.3: Comparison of Tablettabilty behaviour for tablets produced from low (250rpm) and high (400rpm) impeller speeds in small scale (1L) granulation experiments for various liquid levels (LL). 185
Figure 7.4: Compressibility (tablet hardness versus tablet density) behaviour for tablets produced from low (250rpm) and high (400rpm) impeller speeds in small scale (1L) granulation experiments for various liquid levels (LL). 186
Figure 7.5: Compactability (tablet hardness versus tablet density) behaviour for tablets produced from low (250rpm) and high (400rpm) impeller speeds in small scale (1L) granulation experiments for various liquid levels (LL). 187
Figure 7.6: Comparison of Tablettabilty (tablet hardness versus compaction pressure) behaviour for tablets produced from low (250rpm) and high (400rpm) impeller speeds in small scale (1L) granulation experiments for various wet massing times (WMT)..... 188

Figure 7.7: Compactability (tablet hardness versus tablet density) behaviour for tablets produced from low (250rpm) and high (400rpm) impeller speeds in small scale (1L) granulation experiments for various wet massing times (WMT). 189
Figure 7.8: The wet granulation compaction pressure P_{WGC} as a function of the number of impeller revolutions, with varying wet massing times (WMT) and liquid levels (LL), from the application of the Unified Compaction Curve for small (1L) granulator bowls.....190
Figure 7.9: The wet granulation compaction pressure P_{WGC} as a function of the number of impeller revolutions, with varying wet massing times (WMT) and liquid levels (LL), from the application of the Unified Compaction Curve for small (1L, denoted by hollow symbols) and large (5L, denoted by filled symbols) granulator bowls.....191
Figure 7.10: The relationship between the wet granulation compaction pressure and the cumulative number of impeller revolutions for small (1L) and large (5L) granulator bowls. 195
Figure 8.1: Granule porosity as a function of the number of impeller revolutions. 199
Figure 8.2: The Unified Compaction Curve model for the wet massing time effects with varying impeller speed and liquid levels (binder flow rate = 130g/min).....201
Figure 8.3: The effective wet granulation compaction pressure, P_{WGC}, as a function of the cumulative number of impeller revolutions. 202

LIST OF TABLES

Page number

Table 2.1: Bonding mechanisms between primary particles. 27
Table 3.1: Summary of the powder properties of microcrystalline cellulose and lactose 200 mesh. 65
Table 3.2: Summary of wet granulation experiments conducted at impeller speed of 150rpm. Low binder flow rate (L) is 130g/min; high binder flow rate (H) is 280g/min. ..70
Table 3.3: Characterisation of granules and tablets. 73
Table 4.1: The granulation spray times for varying granulation liquid levels. 86
Table 4.2: Wet granulation experiments involving Liquid Level (LL), Wet Massing Time (WMT), and binder flow rate at an impeller speed of 150rpm. 87
Table 4.3: Wet granulation experiments involving Liquid Level (LL), Wet Massing Time (WMT), and binder flow rate at an impeller speed of 285rpm. 87
Table 4.4: Wet granulation experiments involving Liquid Level (LL), Wet Massing Time (WMT), and binder flow rate at an impeller speed of 600rpm. 87
Table 4.5: Summary of the wet granulation and tabletting conditions. 114
Table 4.6: The effective wet granulation compaction pressure as a function of liquid level and wet massing time for pure microcrystalline cellulose. Data taken from Shi *et al.* (2011). 119
Table 5.1: Summary of the wet granulation processing conditions for the twelve samples chosen for granule characterisation analysis. 130
Table 6.1: Summary of liquid binder formulation and acidity. 152
Table 6.2: Scherrer crystallite size and crystallinity analysis of wet granulated samples of varying wet massing times for microcrystalline cellulose granules prepared with calcium oxide liquid binder. 173
Table 6.3: Scherrer crystallite size and crystallinity analysis of wet granulated samples of varying wet massing times for microcrystalline cellulose granules prepared with PVP only liquid binder. 173
Table 6.4: Scherrer crystallite size and crystallinity analysis of wet granulated samples of varying wet massing times for microcrystalline cellulose granules prepared with hydrochloric acid liquid binder. 173

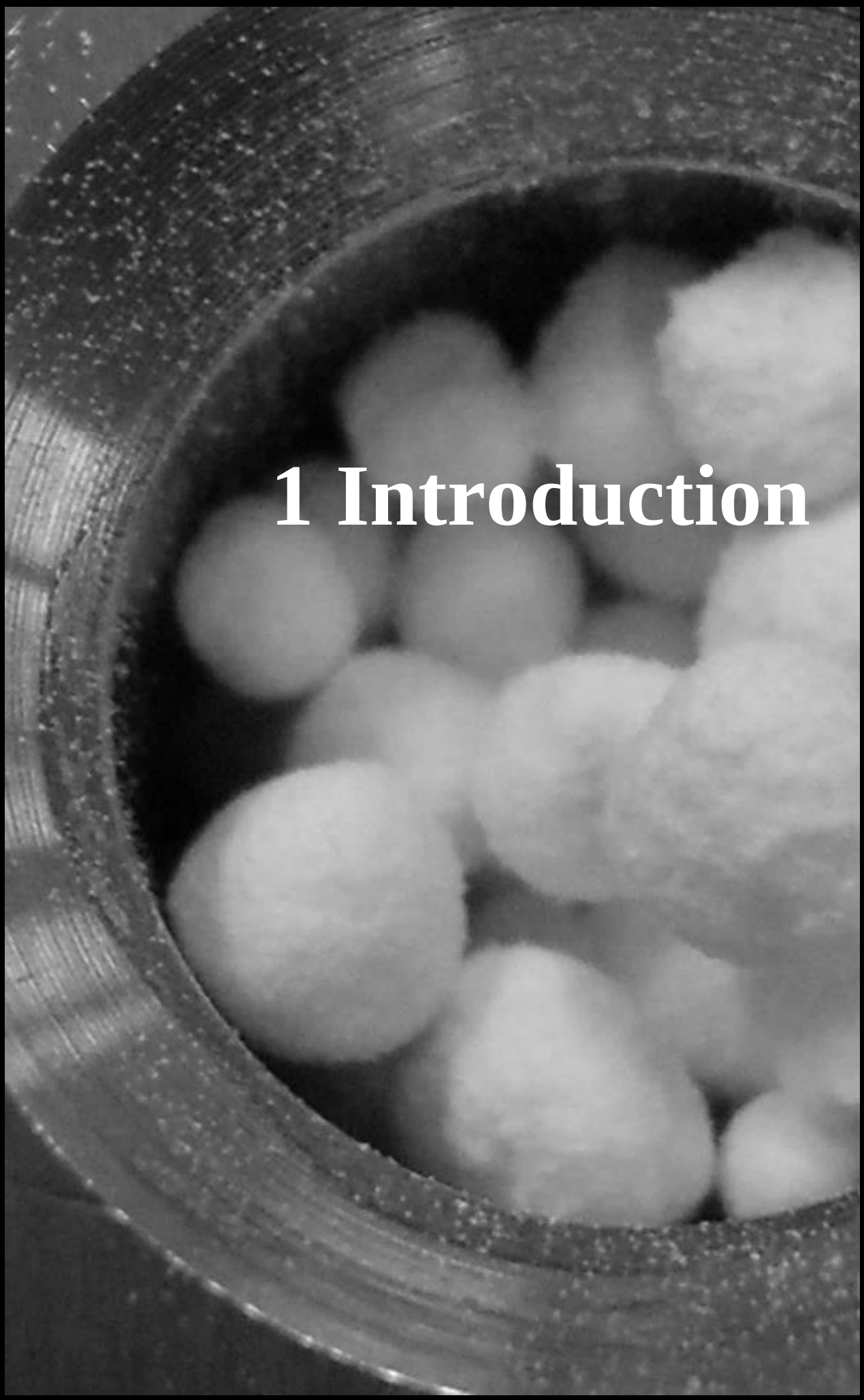

1 Introduction

1 INTRODUCTION

"*What we call the beginning is often the end. And to make an end is to make a beginning. The end is where we start from.*"

-T.S. Eliot, American Playwright-

1.1 INTRODUCTION TO SOLID DOSAGE FORM: TABLETS

Tablets are often taken for granted by the consumption of millions of tablets around the world annually. For aspirin alone, 100 billion tablets are consumed annually (Bullen, 2009). Fortunately the consumption of tablet medicines does not usually pose a significant safety risk due to the advancement of pharmaceutical manufacturing technology and uniformity criterion set in place to ensure that medicinal tablets are consistent in drug content for each batch. Tablets are still popular vehicles for drug administration today due to their benefits for the consumer and the producer, despite the prediction in 1985 that tablets will be phased out for new drug delivery vehicles (Salman *et al.*, 2007).

For the consumer, tablets are easy to handle and identify, and quick to administer. For the pharmaceutical manufacturer, tablets provide a more stable dosage form, particularly for poorly stable active components (Ansel, 1981; Augsburger and Hoag, 2008). On the macro-scale, tablets appear to be simplistic structures; the drug is contained in a compressed powder mass ready for consumption. However the simple nature of the tablet hides the complex chemical and engineering design which is needed to achieve consistent drug content for all tablets in the batch.

The manufacture of tablets can be carried out using three main procedures: direct compaction, dry granulation (such as roller compaction) and wet granulation, as illustrated in Figure 1.1.

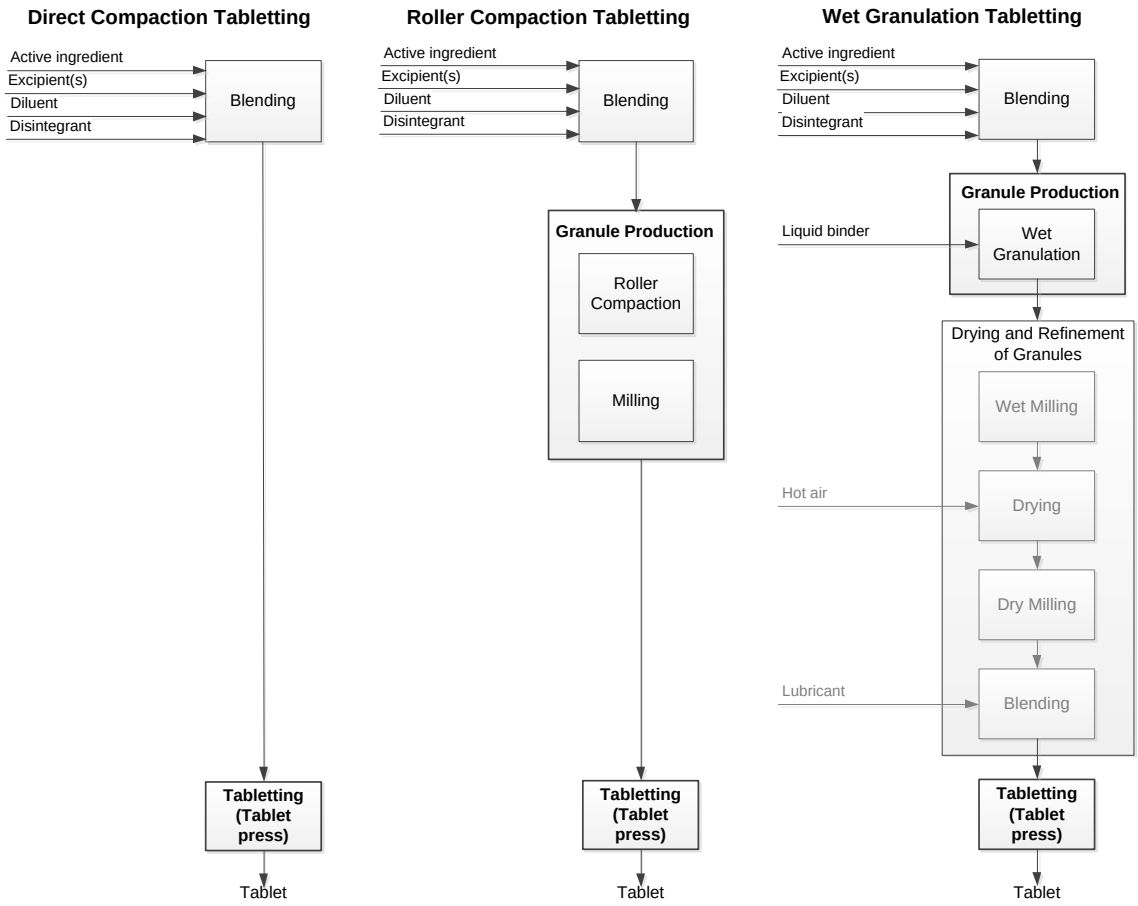

Figure 1.1: Summary of the tablet manufacturing process using wet granulation.

With the exception of the direct compaction tabletting process, during the manufacture of tablets, the raw ingredients go through a series of sub-processes to produce a tablet. The overall manufacturing process can be broken up into blending, granule formation and tabletting sub-processes. This means that prior to tabletting, the powder experiences compaction and potential irreversible material deformation to form granules. The "processing compaction" prior to tabletting has been noted in several studies (Kochhar *et al.*, 1995; Bultmann, 2002; Freitag and Kleinebudde, 2003; Shi *et al.*, 2011; Shi *et al.*, 2011), which has led to the development of the Unified Compaction Curve model to predict the final tablet strength from the roller compactor pressure (Farber *et al.*, 2008). However, due to the lack of understanding of how the compaction incurred during the wet granulation process affects the final tablet strength, a mathematical model has not yet been developed to predict the strength of wet-granulated tablets.

Therefore there is a need to better understand the effects of the wet granulation process conditions on the final tablet strength which forms the objective of this thesis. In this thesis, extensive research on the milling and blending processes will not form part of the

scope, instead the wet granulation and tabletting processes will be the focal-point of this research project.

1.2 LIMITATION OF KNOWLEDGE: INFLUENCE OF WET GRANULATION PROCESS ON TABLET STRENGTH

The production of tablets is a common pharmaceutical industrial process. The wet granulation process forms one of the integral components in tablet manufacture, while the tabletting process produces the final product. During tablet manufacture design, a series of granulation batches are produced at a range of processing conditions to establish a range of final tablet strengths possible at each compaction force, before a desired set of operating conditions is selected. These experimental case-studies are carried out based partly on operator experience and partly on a trial-and-error basis, which are time consuming. This also leads to a large amount of material waste, which is economically undesirable but necessary. By enhancing the knowledge of the connection between the wet granulation and tabletting processes, the amount of experimental batches can be minimised, thus allowing time and money to be saved.

A lot of research has been carried out to understand wet granulation and the tabletting processes. This has led to a better understanding of the powder-liquid binder interaction dynamics (Denesuk *et al.*, 1993; Doerr, 1998; Hapgood *et al.*, 2002; Hapgood *et al.*, 2003; Ax *et al.*, 2008; Emady *et al.*, 2011), granule growth through agglomeration and consolidation (Waldie, 1991; Iveson *et al.*, 1996; Iveson and Litster, 1998; Iveson, 2001; Iveson *et al.*, 2001; Iveson *et al.*, 2001) and the resultant granule properties (H., 1962; Bouwman *et al.*, 2005; Badawy *et al.*, 2006; Rahmanian *et al.*, 2011; Shi *et al.*, 2011; Shi *et al.*, 2011; Macias and Carvajal, 2012). In other studies, the tablet properties have been investigated for a given wet granulation formulation (Bergman *et al.*, 1998; Keleb *et al.*, 2001; Williams *et al.*, 2004; Vermeire *et al.*, 2005). However, a common trend that arises from these studies is the lack of insight into how the wet granulation process conditions influence the final granule properties and the final tablet strength, especially since different wet granulation and tabletting studies use different formulations. *There is little understanding in how the wet granulation conditions create a blue-print for the granule properties and ultimately the tablet strength*.

Therefore understanding which granule properties are enhanced or deteriorated by the wet granulation process and how this influences the tablet strength would provide many benefits for the pharmaceutical industry. Such knowledge would enable mathematical models to be developed, thus enabling "a more robust" prediction of the final tablet strength from the wet granulation process.

1.3 RESEARCH AIMS

The overall objective of this research is to better establish the relationship between the wet granulation process and the tablet strength. The broad objective will be achieved through a series of specific objectives which examine different aspects of the wet granulation process. The effect of the wet granulation operating conditions, the granule properties, the raw material used in granulation and the granulator scale on the final tablet strength, will be examined in this project. The specific aims of the research are:

1. To investigate the effect of the liquid level, wet massing time, binder flow-rate and impeller speed on the final tablet strength,
2. To examine the effect of the wet granulation process conditions on the granule properties, in particular, the granule size, surface area, skeletal density and porosity. This will allow the granule properties which control the final tablet strength to be determined,
3. To explore the effect of the crystalline and porous structure of microcrystalline cellulose on the interaction with the liquid binder and the material compaction behaviour, which in turn influence the tablet strength,
4. To determine the effect of the granulator scale and the resultant mechanical shear forces on the granule properties and the tablet strength,
5. To examine the feasibility of the Unified Compaction Curve model to predict the tablet strength for wet-granulated tablets from various granulation process conditions.

1.4 REPORT OUTLINE

To achieve an understanding of the effects of the wet granulation conditions on the final tablet strength, a series of studies will be conducted to establish which wet granulation process variables have a strong influence on the granule structure and the tablet strength. The thesis will present and discuss the key findings in the following chapters:

Chapter Two: Literature review

The fundamental mechanisms of the wet granulation and tabletting process are discussed, along with a review on previous research on wet granulation and the resulting granule properties or tablet strength.

Chapter Three: Material and Experimental Procedures

An in-depth description of granulation formulation is presented which enables the powder and liquid binder interaction to be understood during wet granulation. The wet granulation, tabletting and characterisation experiments are also discussed.

Chapter Four: Using the Unified Compaction Curve to predict the tablet strength from the Wet Granulation Process

The feasibility of the Unified Compaction Curve is investigated in this chapter, looking at the effects of the granulator liquid level and the wet massing time on the final tablet strength.

Chapter Five: Effect of the Granulator Compaction Pressure on the Granule Properties

The interaction between the granulator impeller and the powder and granules are examined in this chapter. The influence of the wet granulation compaction pressure on the granule properties and the final tablet strength are examined through the characterisation of the granule properties.

Chapter Six: Effect of the Granulator Compaction Pressure and Liquid Binder on the Microcrystalline Cellulose Material Properties

The effect of the physical and chemical conditions within the granulator on the extent of granulation and alteration of the microcrystalline cellulose properties are investigated in this chapter. The influence of the granulator shear, acidity/basic nature and moisture are the variables of focus for the final tablet strength.

Chapter Seven: Effect of the Granulator Scale on the Tablet Strength

The impact of the granulator scale on the final strength is explored to see whether the Unified Compaction Curve gives an insight into the magnitude of the shear at different granulator scales and their influence the tablet strength.

Chapter Eight: Summary of the wet granulation effects on tabletting

The investigations into the feasibility of the Unified Compaction Curve, the wet granulation conditions, granule properties and the granulator scale are summarised as a whole to provide an overall picture of the relationship between the wet granulation process and the final tablet strength.

Recommendations, Conclusions, Nomenclature and References

The establishment of the relationship between the wet granulation process and the final tablet strength from the experimental chapters are presented with recommendations for future work. The nomenclature and references follow the conclusions.

2 Literature Review

2 LITERATURE REVIEW

"It is not enough to take steps which may someday lead to a goal; each step must be itself a goal and a step likewise"

- Johann Wolfgang van Goethe, German writer and polymath -

From *Chapter One: Introduction*, it is clear that there is a need to improve the understanding of the relationship between the wet granulation process and the final tablet strength. Thus, this chapter presents a review of the existing research that has been conducted to investigate the wet granulation process and the tabletting process as well as the relationship between them. A brief review of the development of tablet manufacture is presented and then studies of the interaction between the liquid and powder during the wet granulation process and of the granule-to-granule interaction during the tabletting stage are reviewed.

2.1 OVERVIEW OF TABLET MANUFACTURE

Tablet manufacture finds itself in a wide range of applications including pharmaceutical, food, detergent and catalyst industries. For the pharmaceutical industry, tabletting has been carried out for thousands of years eventuating to a single-station tablet press using a hand crank by the 1800's. The mass production of tablets at the time was around 100 tablets per minute. The production of tablets increased to approximately 1,200 tablets per minute in the 1800's with the introduction of the first automated Stokes multi-station rotary press, developed by Frank J. Stokes, using a leather belt and a steam-driven power bar (Augsburger and Hoag, 2008; Natoli, 2008). By the 1900's the Stokes rotary tablet press was in full mass production across the world and in the 1950's shaped tablets were introduced into the market. The advancement of the tabletting technology has increased the production rate of tablets by twenty times, since the 1800's, to approximately 24,000 tablets per minute (Natoli, 2008). The production rate is expected to increase with advancement of the tabletting technology and better process control of the process.

The development of the tabletting technology is driven by the popularity of tablets as a solid drug dosage form which can be self-administered by the consumer. Tablets now make up a third of all types of dosage forms (Augsburger and Hoag, 2008) and are widely trusted by professions and consumers alike.

In the pharmaceutical industry there are three main types of processes for tablet manufacture: (1) direct compaction tabletting; (2) tabletting through roller compaction; and (3) tabletting through wet granulation. Hot-melt extrusion is also another tabletting process; however they are beyond the scope of this project and will not be considered in this thesis. These processes may include the use of a liquid binder to help compact the powder into a tablet. The selection of the type of agglomeration process is crucial during the drug research and development stage to ensure efficient tablet manufacture is achieved as it is difficult and costly to change the manufacturing process due to the strict enforcements in place by the Food and Drug Administration (FDA) for consistent tablet manufacture in each batch (Bennett and Cole, 2003).

The simplest procedure for manufacturing a tablet is through direct compaction (see Figure 2.1), in which the raw powder is fed directly into the tablet press and compacted into a tablet. Raw powders that are used for direct compaction are usually designed with good powder flow and compaction properties to make the tablet manufacturing process more efficient and robust.

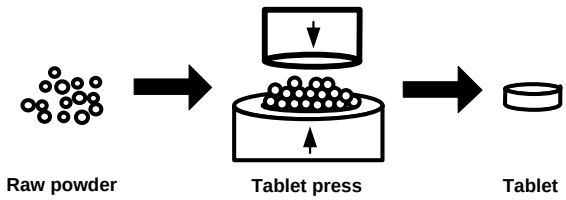

Figure 2.1: Schematic diagram of direct compaction tablet manufacturing process. Raw powder is fed directly to the tablet press to produce a tablet.

The second type of tablet manufacturing process is dry granulation or "roller compaction", which can be broken up into powder blending, initial compaction, milling, an optional addition of excipients and lubrication and tabletting stages (see Figure 2.2). Raw powder is fed through two rollers which compact the powder into a ribbon, before milling the ribbon into granules. The granules are then compacted into a tablet.

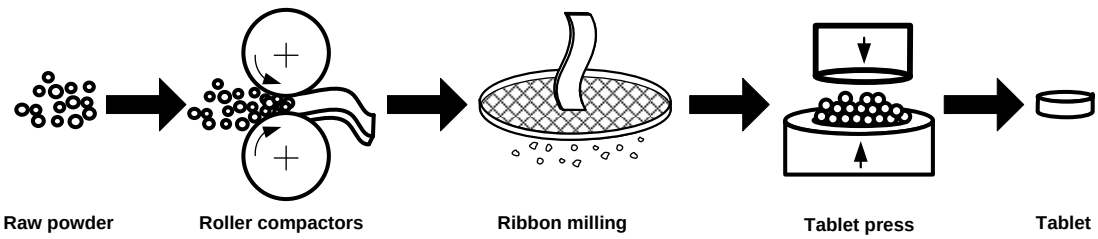

Figure 2.2: Schematic diagram of roller compaction tablet manufacturing process. Raw powder is fed to compactor rollers to produce a ribbon, before being milled into granules. The granules are then fed to the tablet press to produce the tablet.

The third type of tabletting manufacturing process is wet granulation in which a liquid binder is incorporated into the manufacturing process. A typical wet granulation process can be broken up into powder blending, particle size enlargement with the addition of liquid binder, drying and milling. Wet granulation can be carried in a variety of granulators, including the high-shear mixer granulator as shown in Figure 2.3. Raw powder is fed to the mixer granulator and agitated, while liquid binder is added from above. From the wet granulation process, the raw powder is grown into 'granules' which are then dried, milled to remove any large granules, and fed to the tablet press to be compacted into tablets.

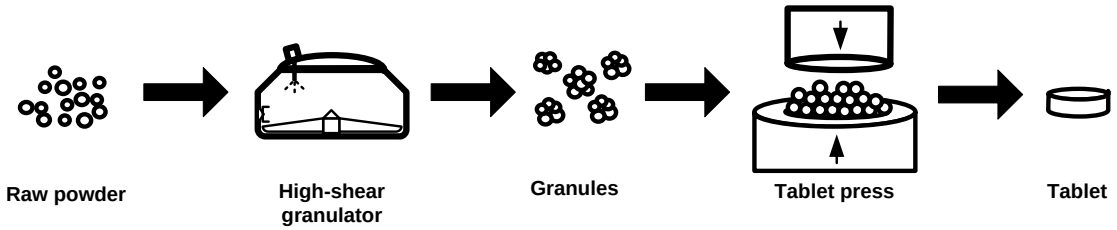

Figure 2.3: Schematic diagram of wet granulation tablet manufacturing process. Raw powder is fed to the wet granulator along with liquid binder to produce granules. The granules are then fed to the tablet press to produce a tablet.

Because the wet granulation tablet manufacturing process will be the primary focus of this project, the tablet manufacturing process will be described in detail as follows:

The tabletting process, via wet granulation, begins with the weighing and blending of the raw ingredients. The raw ingredients for the tablet are the active or drug compound, excipients, diluent and disintegrating agents. The purpose of the diluent is to improve the bulk packing, powder flowability and tablet compression. Disintegration agents are able to swell upon exposure to moisture which facilities the rupturing of the tablet within bodily environment or other the disintegrating medium for efficient absorption of the active compound. The blending of the powders take place in a mixer-granulator, which comprises of a main impeller and chopper to mix the powder for 3-15 minutes at approximately 15m/s for the main impeller tip speed and 3000-4000 rpm for the chopper speed (Bennett and Cole, 2003).

Wet granulation then occurs, in which liquid is added to the agitated powder to help the agglomerate the powder and promote granule growth. The primary objectives of the wet granulation process in the pharmaceutical industry are to improve the powder properties such as reducing dust explosion, improving the granular powder flowability into the tablet

press, and increasing the bulk density to ensure that the bulk tablet batch has a narrow tablet weight distribution with uniform tablet composition (Bennett and Cole, 2003). The typical impeller speed during wet granulation is lower compared to the blending stage which is approximately 5-10m/s for the main impeller. Once the liquid is added to the powder, the wetted powder may be mixed further for another 2-10 minutes to promote granule growth and break down any coarse over-wetted granules (Bennett and Cole, 2003). The wet granulation process will be described more in detail in *Section 2.4: Wet granulation Mechanisms*

The wet granules from the particle size enlargement process may be then screened through specialised wet milling equipment by extrusion (Ansel, 1981). Granules are then dried by levitating them with hot air in a fluidised-bed dryer.

Following the drying stage, the granules pass through another sieving mill with an aperture size of approximately 800-1600µm. The resulting granule size will determine the tablet strength, tablet porosity and the tablet punch size, which relies on even packing of the granules to produce a desirable tablet (Ansel, 1981).

Prior to the tabletting stage, the granules are lubricated, typically with magnesium stearate, in a powder blender (Rowe *et al.*, 2009). The lubricant usually makes up to between 0.1-5% of the tablet weight (Ansel, 1981), and typically approximately 1% of lubricant is used in the formulation. The lubrication of the granules improves the flowability of the granules into the tablet die press, minimise adhesion of the compressed powder mass to the tablet die wall and allow efficient ejection of the tablet from the tablet press.

The lubricated granules are then transported to the tablet press die for compression into a tablet. The tabletting conditions depend on the mechanics of the tablet press, the tablet porosity, tablet strength and the tablet size. The tablet products are then ready for coating, packaging and distribution.

The tablet production through dry granulation and wet granulation share similar characteristics in which the powder is compacted by the roller or the granulator impeller prior to the tabletting process. However the amount of compaction from the high-shear

mixer granulator impeller would be expected to be greater than the amount of compaction experienced in the roller compaction process.

Despite the popularity of tablets and the tablet manufacturing process is well established, there is still some confusion about the relationship between the wet granulation and the tabletting process, in particular how the wet granulation processing conditions affect the final tablet strength.

2.2 TABLETTING PROCESS

The final stage of the tablet manufacturing process relies on the formation of bonds between the powder particles or granules to produce tablets with the following desirable properties (Bennett and Cole, 2003):

- Able to resist mechanical and handling forces exerted (through packaging, shipping and dispensing) on the tablet,
- Able to be film-coated if required,
- Free from defects,
- Chemically and physically stable,
- Able to produce a drug release (dissolution) profile that is reproducible and predictable.

Therefore understanding the tabletting process in detail will help provide an insight into the contributing factors that control the final tablet strength.

2.2.1 COMPRESSION OF TABLETS

The compression of tablets is typically carried out in a multi-station rotary tablet press which operates between 1-200rpm. The rotary press is a turret with typically between 16-75 sets of punches and dies which rotates and the granules passes through four different stages to produce a tablet, which are illustrated in Figure 2.4 (Augsburger and Hoag, 2008):

1. Die filling
2. Powder fill weight adjustment
3. Powder compaction
4. Tablet ejection from die

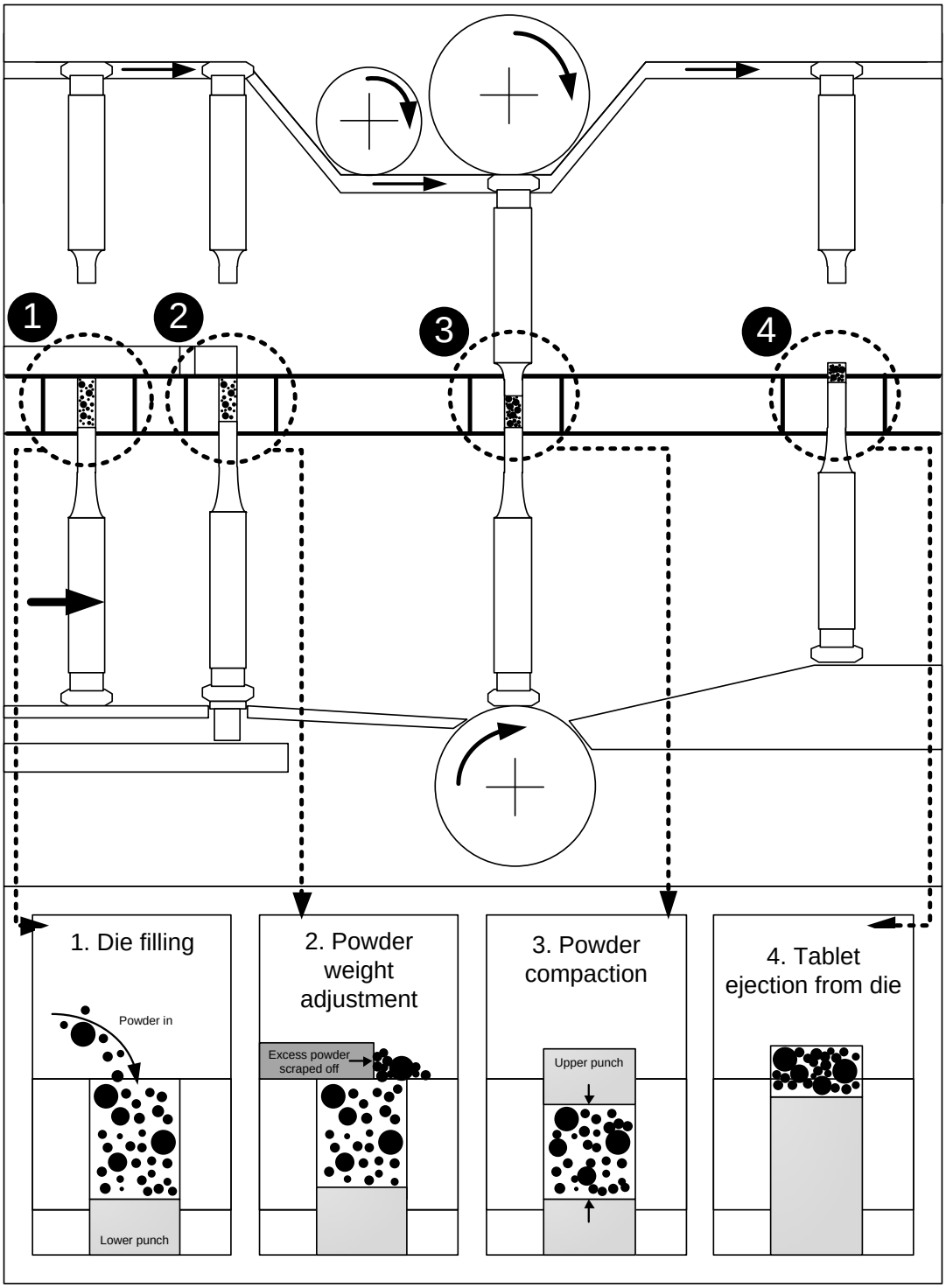

Figure 2.4: Schematic diagram of the rotary tabletting process, adapted from Augsburger and Hoag (2008).

During the die filling stage (stage 1 of Figure 2.4), the granules fill the tablet die which is held up by the bottom punch. The uniformity of granule packing within the tablet die is essential for producing a tablet where the pressure applied by the tablet press is evenly distributed across the cross-section of the tablet (Augsburger and Hoag, 2008).

Once the granules fill the tablet die, the weight of the granules is measured by adjusting how far down the bottom die punch is positioned in the tablet die and scraping off the powder excess, to manually achieve a tablet volume which corresponds to the desired tablet weight (stage 2 of Figure 2.4). Therefore maintaining the desired tablet weight relies on a constant bulk density of the granules filling the tablet die. During the tabletting process, the bottom die punch is checked frequently (approximately every 10-15 minutes) to re-adjust the position, to achieve consistent tablet weight, if required (Salman *et al.*, 2007; Augsburger and Hoag, 2008).

When the correct tablet weight is achieved, the bottom and top punches begin to move in towards each other and compact the powder mass (see stage 3 of Figure 2.4). The compaction of the granules involves pressure forces exerted by both the top and bottom tablet punches. The tablet strength, porosity and density are dependent on the magnitude of the compaction forces from the punches. In industry, the punches usually have an embossing to leave an imprint on the tablet for easy identification (Augsburger and Hoag, 2008).

The resulting tablet is ejected from the tablet die after the compaction stage. The bottom punch pushes the tablet out of the die whilst the top punch is removed from the tablet die (see stage 4 of Figure 2.4). The entire process takes a fraction of a second per tablet. The tablet can then be transported toward the coating or packaging stages (Augsburger and Hoag, 2008).

2.2.2 PARTICLE RE-ARRANGEMENT AND DEFORMATION

The compression of the granular mass enables molecular contact between the granules to form chemical bonds through plastic deformation or brittle fracture (Carstensen, 2001). Although compressibility and compactability are often used inter-changeably, there is a difference between compactibility and compressibility. The *compressibility* of a powder is the ability to *reduce its original loose bulk volume* as a result of an exerted force on the powdered mass, while *compactibility* is the ability for a powder to *produce a cohesive mass* (Leuenberger, 1982; Chulia, 1994).

The compression of a powder mass to form a solid compact or tablet undergoes four main stages (Salman *et al.*, 2007):

1. Once the particles are filled in the tablet die, the particles are arranged in a random, loosely packed condition
2. As soon as compression pressure is applied to the granular mass, the particles slide across each other to fill voids that are of the same size as the primary particles and rearrange into a denser random packing arrangement (Cooper and Eaton, 1962; Salman *et al.*, 2007).
3. More compression pressure is applied to the powder mass and the particles begin to fill the smaller voids by undergoing elastic deformation. The deformation process is reversible because there is no interaction or permanent connection at the contact points between the particles, hence allowing the deformed particles to return to its original state as soon as compression pressure is lifted.
4. Further increasing the compression pressure induces the particles to undergo plastic deformation to force the particles to fill the smaller voids and produce a coherent powder mass (Cooper and Eaton, 1962; Salman *et al.*, 2007). During this stage particle-to-particle contact bonds and pores are created within the powder mass. The densification of the powder mass can occur in two ways: for ductile powder, densification occurs through plastic deformation while for more brittle materials, densification occurs though splitting or crushing.

A schematic diagram of the mechanisms involved in tablet compression can be seen in Figure 2.5.

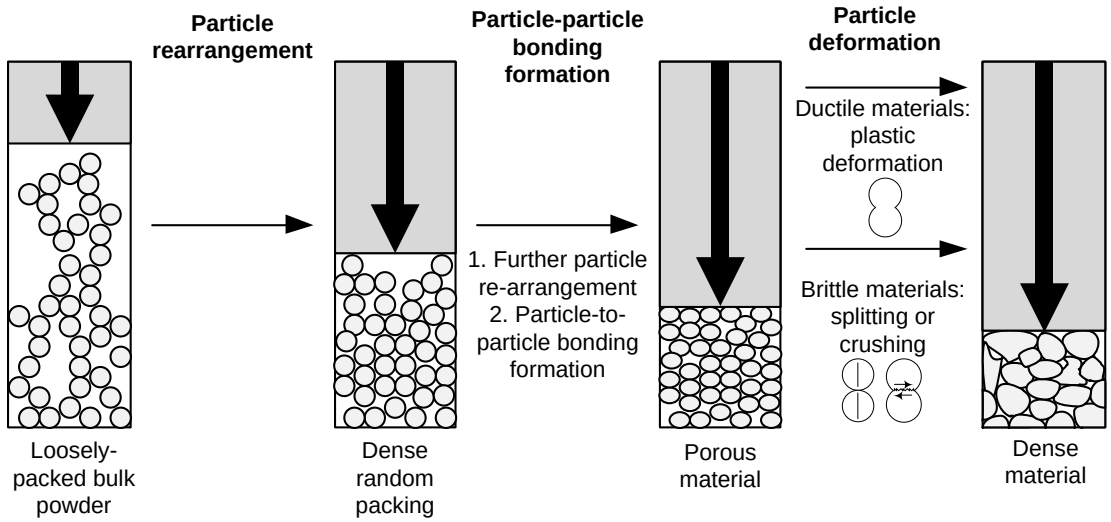

Figure 2.5: The mechanisms involved in particle compression in a cylindrical die. The definition of particle in this diagram can be taken to be either a raw particle or a granule. Adopted from (Salman *et al.*, 2007).

The compression of powder can be represented by a compression cycle (as schematically illustrated in Figure 2.6) showing the relationship between the pressure from the upper

punch, P_{upper}, and the pressure stress experienced by the die wall, $P_{die\ wall}$. The compression cycle comprises of three main steps (Carstensen, 2001):

1. Compression by elastic deformation
2. Compression by plastic deformation
3. Release of the upper punch from the tablet

The tablet also undergoes brittle fracture (Vromans *et al.*, 1985; Wikberg and Alderborn, 1990; Wikberg and Alderborn, 1992) and elastic relaxation (Augsburger and Hoag, 2008), however these are beyond the scope of this project and will not be considered in this thesis.

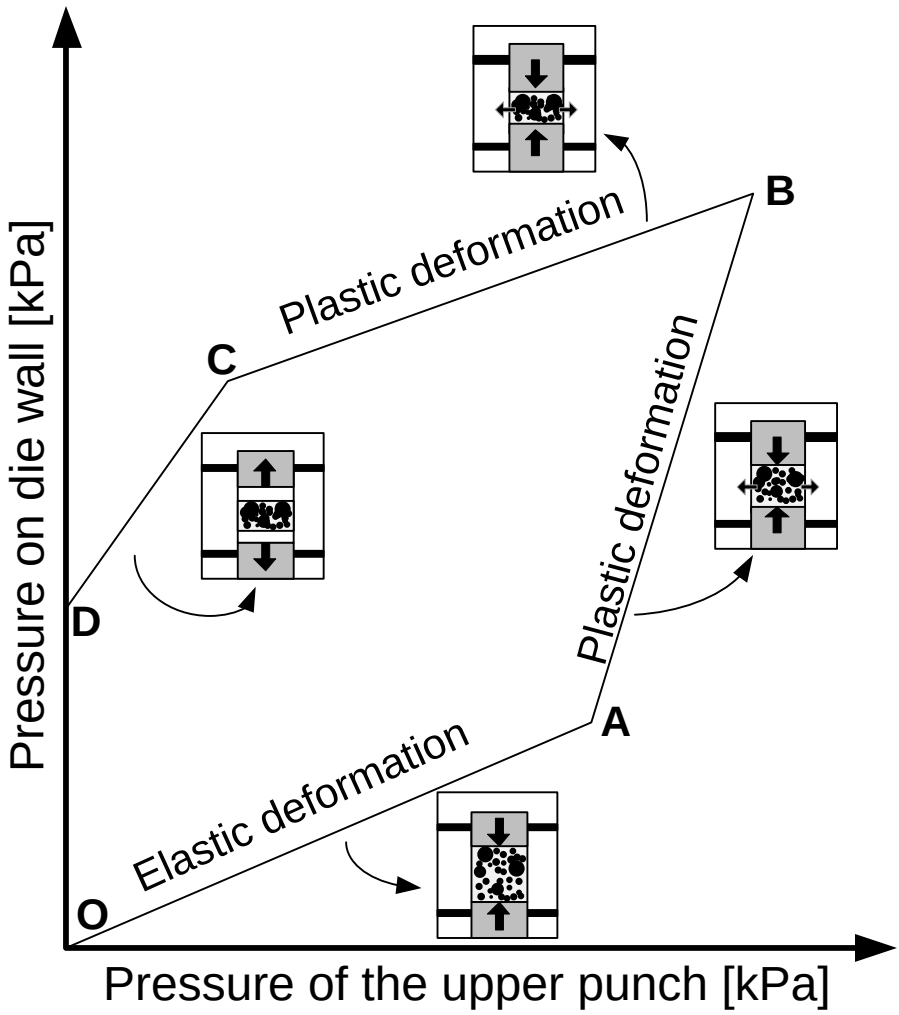

Figure 2.6: Compression cycle, adopted from Cartensen (2001).

The first stage of elastic deformation (represented by line OA in Figure 2.6) involves the re-arrangement of the particles to fill as many voids as possible in the powder volume before being compressed into a tablet. When the applied force is removed from the powder, the compressed particle returns to its original volume and shape, demonstrating reversible elastic deformation. The slope of line OA in Figure 2.6 is equivalent to the

slope of Poisson's ratio, v (Equation 2.1) or a more accurate function of Poisson's ratio (Equation 2.2).

$$P_{die\ wall} = vP_{upper} \tag{2.1}$$

$$P_{die\ wall} = \left(\frac{v}{1-v}\right)P_{upper} \tag{2.2}$$

Plastic deformation (represented by line AB in Figure 2.6) begins to dominate when the applied pressure surpasses a threshold pressure ϕ (represented by point A in Figure 2.6) and usually at a fractional powder density of approximately 0.85 (the fractional powder density f is defined as the ratio between the bulk powder density ρ_b and the particle density ρ_p , $f = \rho_b/\rho_p$) (German, 1989; Carstensen, 2001; Sevillano, 2001). The threshold pressure represents the elastic limit or yield of the powder (Carstensen, 2001). Unlike elastic deformation, plastic deformation is an irreversible process. If the exerted force on the powder mass is removed, the powder will not return to its original volume and shape. Plastic deformation occurs in two stages: firstly, the die wall experiences increasing stress as the pressure from the compressed powder is translated to the die wall (represented by line AB in Figure 2.6). The tablet die wall pressure is represented by the different in the pressure of the upper punch pressure and the threshold pressure (Equation 2.3).

$$P_{die\ wall} = P_{upper} - \phi \tag{2.3}$$

In the second stage, plastic deformation is occurring in conjunction with the decrease in die wall pressure when the upper punch begins to lift away from the tablet die (represented by line BC in Figure 2.6) (Carstensen, 2001), which is described in Equation 2.4.

$$P_{die\ wall} = \left(\frac{v}{1-v}\right)P_{upper} + \left[1-\left(\frac{v}{1-v}\right)\right]P_{upper,\max} - \phi \tag{2.4}$$

During the release of the upper punch (represented by line CD in Figure 2.6), the upper punch continues to lift away from the tablet die, further reducing the pressure experienced by the die wall. The die wall pressure then becomes the summation of the upper die punch pressure with the threshold pressure as can be seen in Equation 2.5.

$$P_{die\ wall} = P_{upper} + \phi \tag{2.5}$$

The compression mechanism with respect to the rearrangement of the particles can also be represented by various compaction models and curves (Walker, 1923; Heckel, 1961a; Cooper and Eaton, 1962; Kawakita and Tsutsumi, 1966). However the compression models are out of the scope of this project and hence will not be described in detail.

2.2.3 PARTICLE-PARTICLE BONDING

To produce a tablet with sufficient strength that can sustain processing and handling forces, sufficient bonding must occur between the particles. However achieving strong particle-particle bonds is dependent upon close molecular contact. The three main types of bonding during tabletting are:

1. Weak forces (for example van der Waals, electrostatic and hydrogen bonding)
2. Mechanical interlocking
3. Solid bridges

There are also capillary and condensation attraction forces, however this is mostly relevant to wet granulation (see Section 2.4.1). The type of bonding that will occur between the particles is dependent on the material used and the particle size. The combination of particle deformation and the creation of contact bonds between the particles are important in tablet production and the resultant tablet properties (Carstensen, 2001).

The particle-particle bonding can also be influenced by the particle surface area. An investigation of the sodium chloride particle surface area on the deformation and bonding behaviour by direct compression was conducted (Adolfsson *et al.*, 1998). The sodium chloride powder was separated into milled and unmilled powder of the same sieve fraction size (250-355µm). The findings showed that the milled particles are irregular in shape with a greater surface area compared to the unmilled sodium chloride powder. Consequently, the non-uniform packing and larger surface area of the milled particles increased the area of the intra-particle bond and increased the final tablet tensile strength (Adolfsson *et al.*, 1998).

2.3 TABLET CHARACTERISTICS

One of the objectives of the tablet manufacturing process is to produce a drug delivery vehicle that has a high mechanical strength to withstand processing and handling forces downstream (Murakami *et al.*, 2001) but still retains sufficiently fast rates of disintegration and dissolution. The key tablet properties are the tablet porosity and the tablet hardness, which are essential properties to control to achieve an optimum tablet.

2.3.1 TABLET BONDING MECHANISMS

The mechanisms in the bonding of granules to form a tablet is similar to the bonding of primary particles to form a granule, however the contact area topology for bonding

between primary particles and granules are different. The contact area for a primary particle is considered to be smooth and can be representative of a sphere, while the contact area for a granule is considered to be more irregular (Augsburger and Hoag, 2008).

2.3.2 TABLET POROSITY

The tablet porosity is defined as the proportion of free volume in the apparent volume of the tablet. The tablet porosity can be found from the ratio of the apparent to true density which is defined in Equation 2.6 (Murakami *et al.*, 2001):

$$\text{Porosity } (\varepsilon) = \left(1 - \frac{\text{Apparent density}}{\text{True density}}\right) \times 100 \tag{2.6}$$

The ratio of the apparent density to the true density can also define the solid fraction, *SF* of the tablet which is the proportion of solid in the apparent volume of the tablet as can be seen in Equation 2.7 (Tye *et al.*, 2005).

$$SF = \frac{m}{\rho_{true} \cdot v} \tag{2.7}$$

where m is the tablet weight, ρ_{true} is the true density of the tablet and v is the apparent volume of the tablet. From the solid fraction, the porosity can be calculated as (Tye *et al.*, 2005):

$$\text{Porosity}(\varepsilon) = (1 - SF) \times 100\% = \left(1 - \frac{m}{\rho_{true} \cdot v}\right) \times 100\% \tag{2.8}$$

As the tablet porosity decreases, the tablet strength increases. However the tablet porosity cannot ever reach zero due to pores, imperfect bonds and cracks within the tablet structure (Salman *et al.*, 2007). The compression force has a significant influence on the tablet porosity. As the compression force increases, the porosity of the tablet decreases, resulting in a stronger tablet (Johansson and Alderborn, 2001; Agrawal *et al.*, 2003).

The direct compression of fine and coarse particles can give an insight into the deformation mechanisms of the materials which affect the tablet porosity and the compression pressure the material can resist (Carstensen, 2001). There is a difference in the brittle fracture behaviour for different-sized particles. The deformation of fine particles leads to higher tablet porosity compared to a tablet produced at the same conditions but with a coarser size fraction. As the compression on the powder increases, the tablet porosity reduces and at a certain compression pressure threshold, the tablet

porosity becomes the same for tablets produced with either fine or coarse particles. This suggests that there is no difference in the fractural behaviour at high compression pressures. For materials which deform by plastic deformation, the tablets produced are generally of lower porosity compared to those tablets composed of brittle material. Unlike tablets made from brittle material, the particle size affects the tablet porosity across the entire compression pressure range. The deformation behaviour trend for fine and coarse particles mirror each other, with the fine particles producing higher tablet porosity compared to the coarse particle size fraction (Carstensen, 2001).

The trend in fine particles resulting in high tablet porosity can also be seen in another direct compaction study by Nicklasson and Podczeck (2007) with crystalline sucrose powder. For fine sucrose particles of 20-40µm, the highest tablet porosity was found to be 0.309, compared to coarse sucrose particle of 355-500µm having the highest tablet porosity of 0.207. However, although the fine sucrose particles led to high tablet porosity, the tablet tensile strength was found to be higher than the tablet strength found in tablets produced from coarse particles, in which the tablet strength was 0.55MPa and 0.38MPa for the 20-40µm and the 355-500µm size fractions respectively. Therefore the tablet porosity is not the sole parameter determining the final tablet strength.

2.3.3 TABLET HARDNESS

The deformation behaviour of any material under exerted forces and deformations are characterised by the stress and strain experienced by the material. As tablets are made under compression forces, the stress experienced by the tablet dominates the study of tablet hardness in literature. The normal stress, σ, is defined by the average force applied perpendicular to the material cross section (Equation 2.9), hence having the units of N/m^2 (Hartsuijker and Welleman, 2007).

$$\sigma = \frac{F}{A} \tag{2.9}$$

The strain of the material, ε, is defined by the dimensionless ratio of material elongation by the original length of the material (Equation 2.10) (Hartsuijker and Welleman, 2007).

$$\varepsilon = \frac{\Delta \ell}{\ell} \tag{2.10}$$

The compression of granulated powder can undergo a couple of steps, namely elastic deformation and plastic deformation leading to either deformation or fracture.

The stress and strain experience by a tablet can be represented through a stress-strain plot as shown in Figure 2.7. During elastic deformation of the tablet, the stress increases in a linear manner with increasing strain (Equation 2.11).

$$\sigma = E\varepsilon \tag{2.11}$$

The slope of the linear region or the proportionality factor, E, is typically termed the Young's modulus or modulus of elasticity (Hartsuijker and Welleman, 2007) but in the tabletting literature, the proportionality factor is sometimes incorrectly termed the Poisson's ratio v (Carstensen, 2001). When the elastic deformation region is surpassed, the tablet undergoes plastic deformation or exhibits viscoelastic behaviour until the tablet bonds and breaks under brittle fracture.

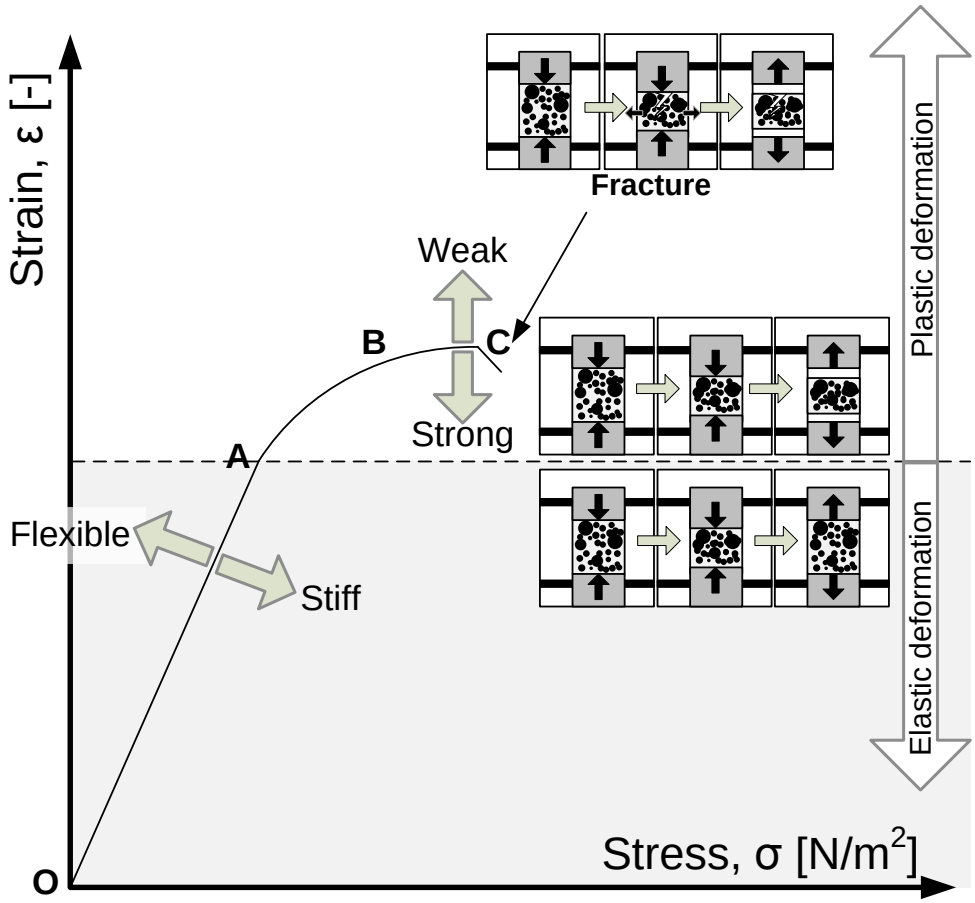

Figure 2.7: Stress-strain plot representing tablet behaviour under an applied force. The arrows represent the change in tablet property if the profile is modified. Adopted from Hartsuijker and Welleman (2007).

The stress-strain plot of Figure 2.7 can reveal a lot about the tablet properties and the potential to change the material properties to optimise the tablet strength. The stress-strain plot shows that a stronger and more rigid tablet is produced by adopting a formulation

that increases the stress of the tablet. Using a formulation that increases the strain of the tablet leads to a more flexible and softer tablet (Hartsuijker and Welleman, 2007). A strong tablet is favourable to withstand the downstream processing of packaging and transportation, and tablet handling.

The "hardness" of the tablet is measured by its tensile strength. This is typically determined by measuring the raw "crushing" hardness strength (the strength of the tablet than can resist fragmentation by an applied compaction force) of the tablet using a uni-axial tablet hardness tester. The "crushing" strength is then converted into a tensile strength using the crushing strength, tablet dimensions and the tabletting compaction force. A tablet, when first made, would possess a certain hardness which would usually change rapidly over a period of time due to "relaxation" and plateau to the equilibrium hardness (Carstensen, 2001). The tensile strength of a flat-faced tablet σ can be calculated by Equation 2.12 (Fell and Newton, 1970):

$$\sigma = \frac{2F}{\pi dh} \tag{2.12}$$

where F is the compaction force, d is the tablet diameter and the h is the tablet height. The tablet tensile strength developed by Fell and Newton was intended for round, flat-surfaced tablets that fail under tension forces. An equivalent relation for convex tablet has been developed by Pitt *et al.* (1989).

The tablet hardness in relation to the compaction force and tablet porosity was investigated by Tye *et al.* (2005) by direct compressing varying mixtures of microcrystalline cellulose, starch and lactose. From the study it was found that the tablet strength can be affected by compression speed of the tablet press depending on the extent of fragmentation during the tabletting process. For the compression of both plastically deforming (microcrystalline cellulose) and brittle fracturing materials (lactose), the tablet strength was largely independent of the compression speed (the tabletting dwell time) and hence was not strain-dependent (Tye *et al.*, 2005). However the material deformation and fragmentation behaviour results in different resultant tablet strengths. Microcrystalline cellulose tablets had a maximum tensile strength of approximately 14MPa, while for lactose tablets the tensile strength was approximately 4MPa, which may suggest that plastic deformation increases the tensile strength, although this was not speculated in the study (Tye *et al.*, 2005).

2.4 EXAMINATION OF WET GRANULATION PROCESS

Wet granulation forms part of the tablet manufacturing process in which the objective is to enhance the powder flow and physical properties by increasing the particle size into "granules". In wet granulation, atomised liquid binder is added to an agitated powder bed, to form liquid bridges between the raw particles and agglomerate them into granules. The production of granules improves the physical properties and handling of the powder which include:

- Minimising dust formation, particularly where potent powders are involved,
- Reduce the cohesiveness of the powder to promote powder flow,
- Minimising the risk of segregation of the active pharmaceutical ingredient,
- Increase bulk density of the powder,
- Improve uniform packing of the powder in the tablet die,
- Ensure the tablet weight, thickness and strength is uniform throughout the pharmaceutical batch.

In the wet granulation process, three simultaneous process occur in the granulator, as illustrated in Figure 2.8, Figure 2.9 and Figure 2.12 (Litster and Ennis, 2004):

1. Wetting, binder dispersion and nucleation
2. Consolidation and growth
3. Granule attrition and breakage

The understanding of each of the three stages is important to produce a granulation batch that is uniform in size, morphology and composition and therefore will be described more in detail in the following sections.

2.4.1 WETTING AND NUCLEATION

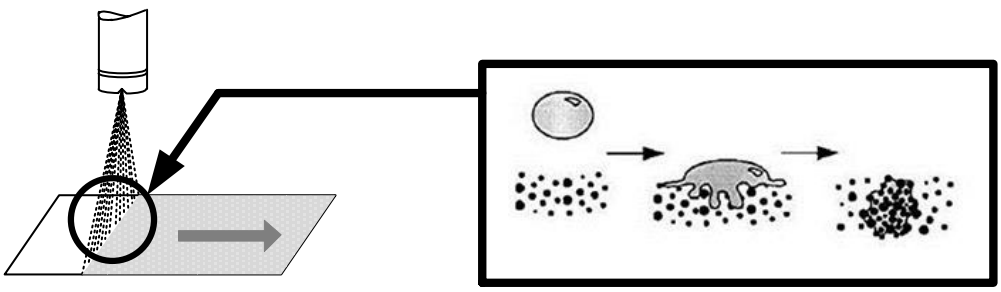

Figure 2.8: Schematic diagram of the wetting and nucleation in the spray zone during wet granulation, inset from Perry and Green (1997) and Iveson (2001).

The wetting, binder dispersion and nucleation stage occurs within the *spray zone* where the binder droplets make the initial contact with the powder bed (underneath the spray

nozzle or spray port as illustrated in Figure 2.8). Atomised binder droplets are formed by the spray nozzle which then impacts and interacts with the agitated powder. Upon contact with the powder bed, the droplet can penetrate into the powder bed to form the initial nucleus and/or coalesce with other particles and granules (Iveson *et al.*, 2001). If the powder is hydrophobic or non-wetting, then the raw particles remains on the droplet surface to form a liquid marble (Aussillous and Quéré, 2006). Therefore the wettability between the liquid and powder is essential to make strong liquid bridges and improve the resistance of the granule to attrition and breakage which can otherwise, lead to a large variation in tablet weight, tablet hardness and drug content. The degree of wettability between the liquid and the powder can be described by the surface tension and the contact angle of the liquid/powder system, or by measuring the drop penetration time. A fast drop penetration time is desirable to avoid producing over-wet clumps in the granulation batch (Hapgood *et al.*, 2002).

Once the liquid is able to wet the powder, the penetration of liquid through the powder pores becomes essential for the nucleation process. The percolation of liquid is driven by the surface tension and contact angle, creating a pressure gradient between the bulk liquid and the capillary walls to drive the advancing liquid through the pores. The liquid binder within the powder is then dispersed by mechanical forces from the granulator impeller.

2.4.2 COALESCENCE AND CONSOLIDATION

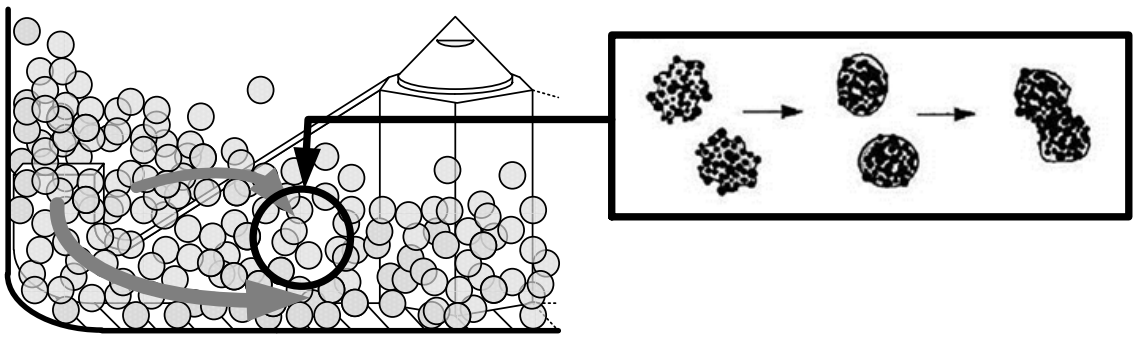

Figure 2.9: Schematic diagram of the coalescence and consolidation stage during wet granulation. Inset from Perry and Green (1997) and Iveson *et al.* (2001).

During mechanical dispersion of liquid throughout the powder bed, coalescence and consolidation takes place to encourage the raw particles and granules to grow in size. The mechanical forces from the impeller promote collision and adhesion between the particles, granules and/or the granulator, provided the adhesive forces between the particles are large enough to overcome the rebound kinetic energy and the separation

force (Litster and Ennis, 2004). When further forces are applied to the agglomerated particles, consolidation of the granules occurs which promotes granule densification. The rate of coalescence and consolidation are dependent upon the granule saturation and the granulation operating conditions such as the granulator liquid level (the amount of liquid added to the formulation) and impeller speed.

During coalescence and consolidation, there are five types of inter-particle bonding that are recognised to occur, as listed in Table 2.1:

Table 2.1: Bonding mechanisms between primary particles.

Bonding mechanism	Examples
Intermolecular, long-range weak forces:	Van der Waals, hydrogen bonding, electrostatic, surface charge
Mechanical interlocking:	Interlocking of particles and/or fibres
Liquid bridges:	Surface tension and capillary forces
Solid bridges	
Adhesion and cohesion:	Viscous fluids

The combination of the long-range forces, mechanical and liquid bridges enables a strong granule to be produced, which can sustain down-stream processing of the granulated powder.

The liquid content and deformation behaviour of the wet granules determines the type of granule growth occurring during wet granulation. There are two main granule growth phenomena defined: steady growth and induction growth, both of which are dependent on the rate of consolidation and the extent of deformation of the granules (Iveson and Litster, 1998). Steady granule growth exhibits a constant rate of granule growth during the entire granulation period. Therefore the granule size is proportional to the length of granulation time. This phenomenon is encountered when coarse particles are granulated with a non-viscous fluid and/or a high impeller force during wet granulation (Iveson and Litster, 1998; Salman *et al.*, 2007).

Induction growth involves minimum or no growth occurring in the initial stages of granulation. During this period, the granules are consolidating and the internal liquid binder within the pores are driven out to the granule surface. When the internal moisture reaches the granule surface, the granules undergo a rapid increase in growth. In contrast

to the steady growth phenomenon, induction growth typically occurs in granulation of fine particles and viscous fluids (Iveson and Litster, 1998; Salman *et al.*, 2007).

In terms of the effect of granule saturation, when additional liquid is added to a steady growth system, the slope (represents the granule growth rate increases), while additional liquid added to an induction growth system shortens the minimal growth period, as shown in Figure 2.10.

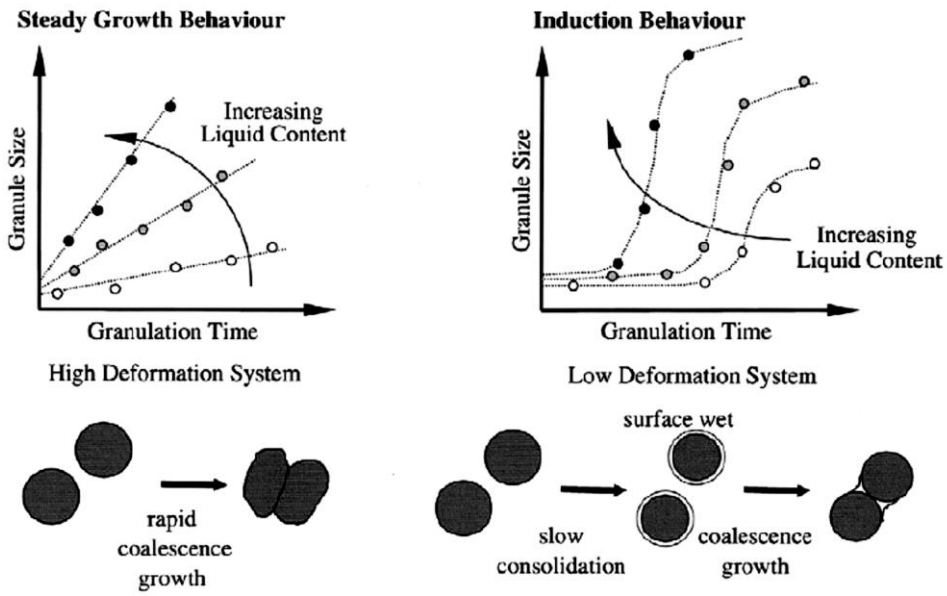

Figure 2.10: Schematic graph of steady granule growth (left) and induction granulate growth (right). Taken from (Iveson and Litster, 1998; Salman *et al.*, 2007).

The steady state and induction growth phenomena give an insight to the behaviour of granules under exerted forces. For steady growth rate of granules, the granule surface must be wet at all times in order for liquid bridges to be formed between particles. This indicates that the granules in this type of system deform easily under exerted forces. For induction growth, the deformation of granules is not extensive and hence time is required to push the liquid from the centre to the granule surface.

The magnitude of granule deformation under collision or exerted forces can be described by the powder agitation intensity, the impact kinetic energy, the granule mechanical properties and the plastic energy absorbed per strain, which constitutes the Stokes deformation number (Equation 2.15) which was developed by Iveson and Litster (1998):

$$St_{def} = \frac{\rho_g U_c^2}{2Y_d} \tag{2.15}$$

where ρ_g is the granule density, U_c is the collision velocity and Y_d is the granule yield stress.

The liquid content in the granule can influence the granule growth and the resulting granule properties. The amount of liquid present in the granule is known as the granule liquid saturation (a detailed description of the granule saturation is given in *Section 2.5.1.: Granule liquid saturation*). For low liquid content in the granulation system (low granule saturation), the powder behaves as a bulk dry powder. As the liquid content increases, granule nuclei are produced but they will not grow further unless additional liquid is added to the system. When there is a large amount of liquid in the system, the granular material will form a slurry. If the granules show intermediate strength, steady growth will take place, while stronger granules will exhibit induction growth, however induction growth will dominate for very high liquid content systems with little or no minimal growth period (Iveson *et al.*, 2001).

To describe and predict the different granule growth phenomena, granule growth regime maps were developed for high-shear and drum-granulation (Iveson *et al.*, 2001). A granule growth regime map was developed based on the effect of the formulation properties.

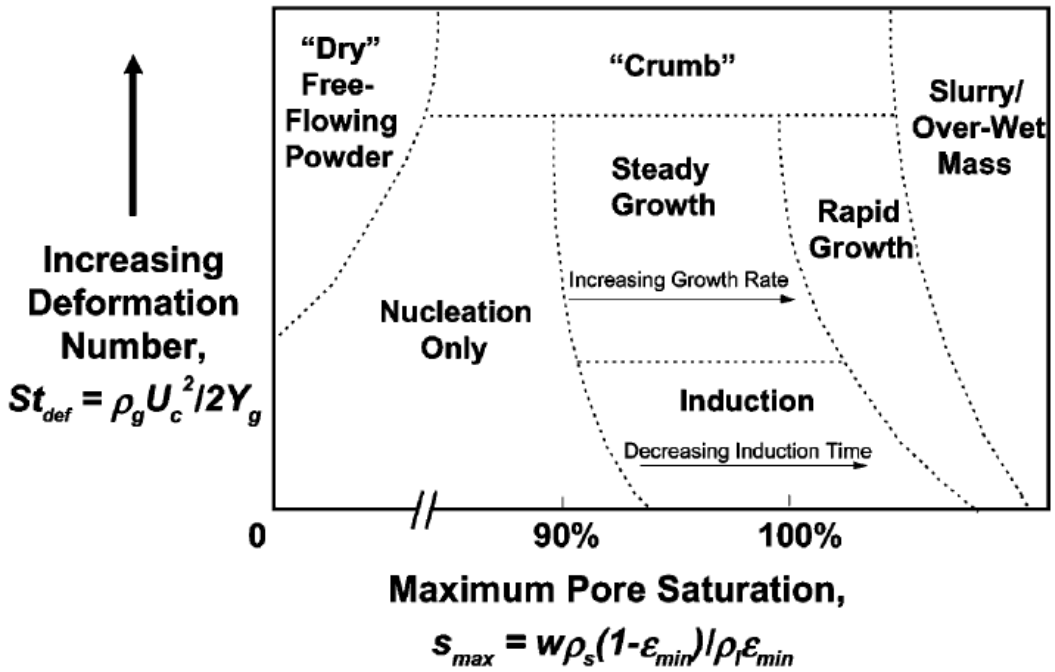

Figure 2.11: Granule growth regime map developed by Iveson *et al.* (2001).

2.4.3 ATTRITION AND BREAKAGE

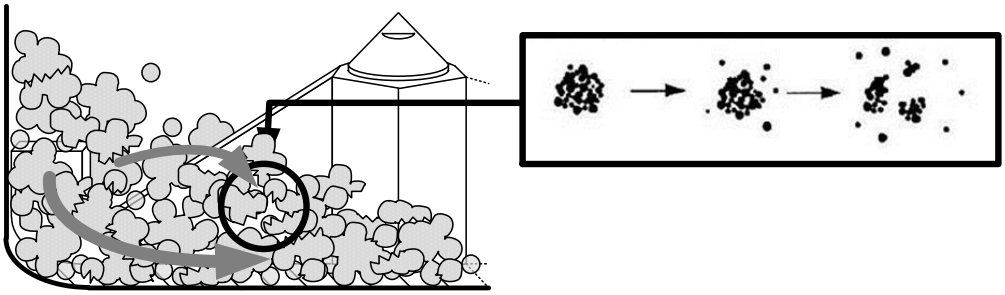

Figure 2.12: Schematic diagram of the coalescence and consolidation stage during wet granulation Inset from Perry and Green (1997) and Iveson *et al.* (2001).

The breakage and attrition stage describes the partial fracture of the granule and deterioration of the granule structure, which facilitates with liquid binder dispersion during wet granulation. The granule structure can break from the impact of the impeller and/or granulator or by the handling of the granule. Attrition occurs when part of the granule surface is removed due to the friction or collision with other granules (Litster and Ennis, 2004).

2.5 GRANULE CHARACTERISTICS

The quality of the granules produced from the wet granulation process is determined by the consistency of the granule physical properties throughout the whole granulation batch. Therefore the characteristics of the granules become important to ensure tablets with desirable tablet strength, consistent drug content and consistent weight are produced.

The granule characteristics that are of interest to studies on tabletting are:

- Liquid saturation,
- Size distribution,
- Surface area,
- Porosity,
- Strength.

These characteristics will be discussed in detail in this section.

2.5.1 GRANULE LIQUID SATURATION

During the initial stage of the binder droplets impacting and making contact with the powder bed, the binder spreads, penetrates and surrounds the particles, through immersion wetting. There are four states of the liquid binder content in a granule:

pendular, funicular, capillary and particles in a liquid (slurry) (Capes, 1980). These stages are illustrated in Figure 2.13.

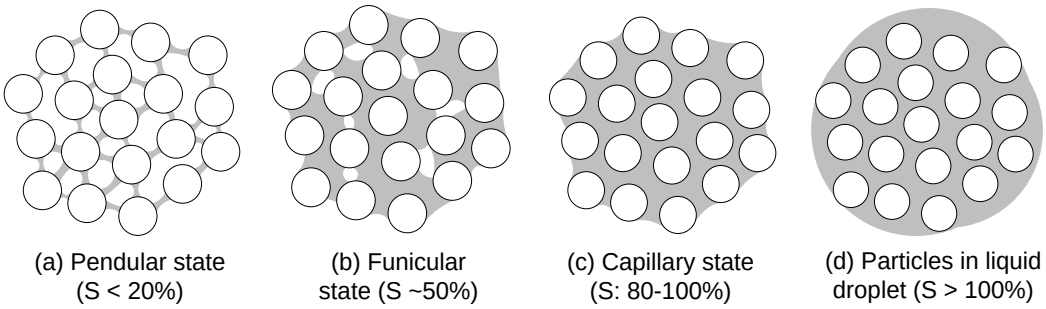

Figure 2.13: Stages of liquid content in a granule. Redrawn from Capes (1980).

From Figure 2.13, it can be seen that in the pendular stage (Figure 2.13a), the bonds are localised to the point of contact between two particles. As the liquid content within the granule increases, the liquid begins to permeate through the voids and the contact area between the liquid bridges and the raw particles enlarges, constituting the funicular stage (Figure 2.13b). When the voids are saturated with liquid, the granule is recognised to be in the capillary stage (Figure 2.13c). With additional liquid binder added to the granule, the mixture becomes a granulated slurry and the granules are seen to be in submerged in liquid (Figure 2.13d). The liquid saturation of the granule is a function of the solid and liquid mass, density and minimum porosity, as described in Equation 2.16 (Capes, 1980):

$$S_{\max} = \frac{w\rho_s\left(1-\varepsilon_{\min}\right)}{\rho_L\varepsilon_{\min}} \tag{2.16}$$

where w is the liquid mass to solid mass ratio, ρ_S and ρ_L are the solid and liquid densities respectively and ε_{min} is the minimum granule porosity for a given wet granulation process. The granule liquid saturation plays an important role for determining the quality of the granules produced from the granulation process. If there is insufficient liquid available within the pores at the granule surface (such as a granule in a pendular saturation state), then strong intra-granular liquid bridges cannot be formed, leading to the presence of un-granulated powder in the granulation batch.

2.5.2 GRANULE SIZE DISTRIBUTION

The efficiency and outcome of the tabletting process is to some extent dependent upon the initial granule properties. The average size and distribution of the final granules also relies on the fine balance between the breakage and growth of the agglomerates. This balance is determined by the particle-particle collisions and flow pattern of the particles.

The granule size distribution is often influenced by the impeller speed as suggested in a granulation study comprising of sericite, a form of cosmetic powder (Oulahna *et al.*, 2003). For a given solid to liquid ratio, the granule mass size distribution was broad with fine particles present for low impeller speeds (100rpm). The low amount of agitation applied to the powder and granules during wet granulation did not sufficiently distribute the liquid binder evenly in the powder mass and hence there was a low extent of granulation and granule growth.

At higher impeller speeds (500rpm and 1000rpm), the extent of granulation increased, which led to granule growth resulting in a narrower granule size distribution coarser granules. However at 1000rpm, it was observed that fine particles were present which were otherwise absent from the 500rpm granulation batch. The reoccurrence of fine particles signified the attrition and break-up of the granules due to the high impact and/or shear forces from the impeller. A similar trend was found from measuring the chord lengths of calcium carbonate granules for three different impeller speeds (230, 300 and 350rpm) in Rahmanian *et al.*'s work (2009). As the impeller speed increased, the average chord length of the granules increased from approximately 50µm to 75µm (Rahmanian *et al.*, 2009). However, the studies discussed above did not look into the effect of the impeller speed on the final tablet strength.

In a factorial study of wet granulation of a binary mixture of paracetamol and isomalt GS, it was found that increasing the granulator impeller speed from 1000rpm to 2000rpm in a 5L granulator decreased the average granule size from 300µm to 180 µm for formulations with both an active ingredient:excipient ratio (API:EXC) of 5:3 and 1:1, while the average granule size did not change for the formulation with API:EXC of 5:1. The increase in the impeller speed (from 1000rpm to 2000rpm) also decreased the tablet tensile strength, for API:EXC of 5:3, from 1.0024kg/cm^2 to 0.8866kg/cm^2 at a compaction force of 15kN, while there was not a significant change in the tablet tensile strength for formulations containing API:EXC of 5:1 and 1:1 (Sáska *et al.*, 2011). However the factorial gave no mechanistic reason for the findings, although the decrease in the average granule size with increasing impeller speed could suggest the consolidation of the granules (Sáska *et al.*, 2011) or breakage and attrition of the granules which were not investigated by the authors. This study is typical of many simplistic investigations

into the effect of the granulator shear on the granule size and ultimately the final tablet strength.

The relationship between the liquid saturation and the granule size was investigated by Ritala *et al.* (1988) in wet granulation studies involving calcium hydrogen phosphate (dicalcium phosphate) and various binder solutions of polyvinyl pyrrolidone (PVP) and hydroxypropylmethyl cellulose (HPMC). The average granule size was influenced strongly by the liquid saturation of the granule, rather than the liquid bonding strength through the surface tension. The granule size increased from approximately 30µm to 700µm for a PVP binder liquid level range of approximately 5 to 33.5v/v%, while HPMC binder increased the granule size from 30µm to 300µm for 5 to 34.5v/v% HPMC liquid level respectively (Ritala *et al.*, 1988).

The effect of the particle size on the compactibility efficiency was examined by Wu and co-workers (2001). The study looked at the granulation and compression of microcrystalline cellulose (Avicel PH 101 and PH 301) and found that coarse granules form weaker tablets. This was attributed to coarse granules having a lower surface area and consequently less bonding area to form strong inter-particular bonds. The study also found that the combination of a high compression force and fine granules increased the tablet strength due to the formation of strong inter-particular bonds during the compression process with a decrease in disintegration efficiency due to the high compression force producing a low porosity tablet. In summary, for a given formulation, the compression force and the particle size are the primary factors in predicting the tablet strength (Wu *et al.*, 2001).

2.5.3 GRANULE MORPHOLOGY

The deformation of the powder and granules during wet granulation results in changes in the granule topology and morphology. Studies by Shi *et al.* (2011) and Bouwman *et al.* (2005) using pure microcrystalline cellulose, showed a reduction in the granule surface roughness and sphericity with increasing wet massing time as shown in the SEM images in Figure 2.14 (Shi *et al.*, 2011). X-ray tomography images and image analysis of calcium carbonate granules also demonstrated that at high impeller speeds (350rpm), the granules produced had a higher degree of sphericity than those produced at lower impeller speeds (250rpm) as shown in Figure 2.15 (Rahmanian *et al.*, 2009).

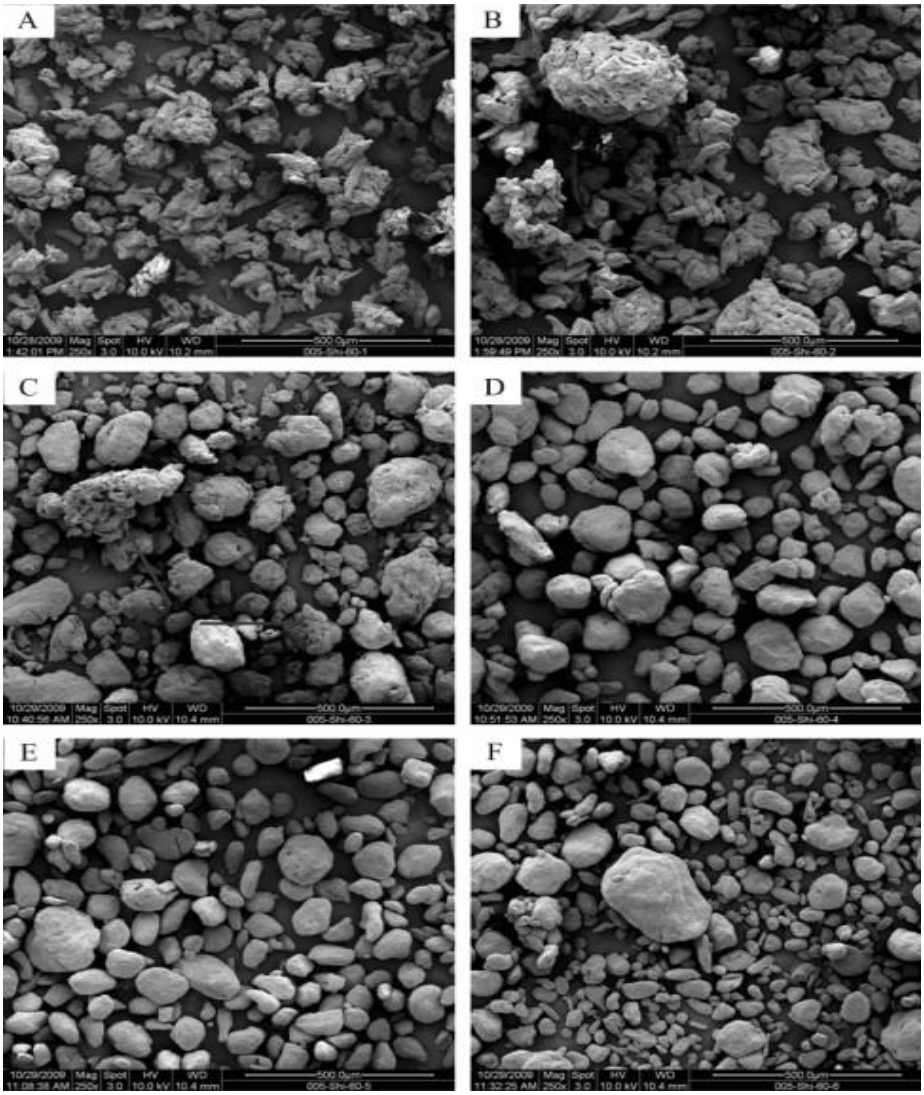

Figure 2.14: Morphology of pure microcrystalline cellulose granules at different wet massing times: (A) 0mins; (B) 1min; (C) 5mins; (D) 10mins; (E) 20mins and (F) 40mins. Figure taken from Shi, *et al.* (2001).

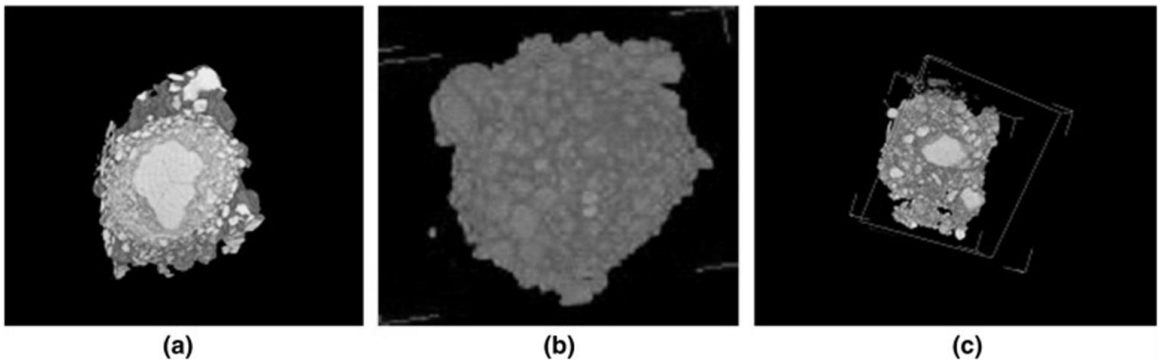

Figure 2.15: Reconstructed 3D x-ray tomography images of granules produced at (a) 230rpm; (b) 300rpm and 350rpm. Figure taken from Rahmanian, *et al.* (2009).

The granule shape plays a role in the tablet strength. Irregular shaped granules are more compressible than regular shaped granules and the irregular shape of the granules contributed to the increasing strength of tablet. This was speculated to be due to the

attrition of the granules during compression, facilitating in the formation of new intergranular bonds (Johansson and Alderborn, 2001).

2.5.4 GRANULE SURFACE AREA

The granule surface area is the area of the external roughness and the internal pore area. The granule surface area can also be affected by the shear and impact forces from the impeller. By using nitrogen gas adsorption BET analysis, Badawy and co-workers (2006) observed a 51 - 69% decrease in the surface area for microcrystalline cellulose granules compared to un-granulated microcrystalline cellulose. Shi *et al.* (2011) showed a decrease in the surface area from 0.9 to 0.5m^2/g as the granulation liquid level increased from 0 to 45% respectively. Their finding could also be seen as evidence that an increase in the granulation time (increasing the granulation liquid level) decreases the granular surface area. However from literature studies, there appears to be a lack of examination into the effect of granulation time on the surface area of granules.

2.5.5 GRANULE POROSITY

The mechanical energy from the granulator impeller has been shown to have a significant impact on the granule porosity. As the granules are subjected to the compaction forces from the impeller during wet granulation, the granules consolidate and the granule porosity is reduced.

Evidence of this trend has been found in a wide range of formulations including the granulation of cosmetic powder (Oulahna *et al.*, 2003), pure microcrystalline cellulose (Bouwman *et al.*, 2005; Badawy *et al.*, 2006; Shi *et al.*, 2011; Macias and Carvajal, 2012), a mixture of microcrystalline cellulose and hydroxypropyl cellulose (Badawy *et al.*, 2006) and calcium carbonate granules (Rahmanian *et al.*, 2009) and other powder formulations (Wikberg and Alderborn, 1991; Zuurman *et al.*, 1994). These studies show that the decrease in the granule porosity represents the consolidation stage of wet granulation and/or that the granules have a higher compressibility (Bacher *et al.*, 2008). Consolidation of the granules improves the granule strength, but compromises the compactability of the granule which consequently reduces the final tablet strength, particularly in roping regime powder flow in the granulator (Macias and Carvajal, 2012). Therefore it would be expected that the impeller speed and/or total granulation time

would play a major role in determining the final tablet strength since the consolidation mechanism compromises the granule's ability to compact and increase the tablet strength.

The compressibility of granules (prepared with microcrystalline cellulose and magnesium stearate) with varying porosity was investigated by Johansson and Alderborn (2001). By comparing the porosity (8.92-33% porosity) and shape of granules and spheronised granules (pellets), Johansson and Alderborn found that the dominant compression mechanism is deformation but the extent of deformation varies with granule porosity. Low porosity granules (less than 50%) underwent little deformation as evident by the similar de-agglomerated granule size to the original granule size. For high porosity granules, the compression process resulted in the granules being significantly deformed and fragmentated as the granules were de-agglomerated by delicately shaking a tablet in a petri dish manually until the tablet deteriorated into granules. The de-agglomerated granule size distribution was broad, suggesting that granule breakage occurred (Johansson and Alderborn, 2001). A similar trend was also found in other studies (Wikberg and Alderborn, 1991; Zuurman *et al.*, 1994; Bacher *et al.*, 2008).

The tablet porosity also appears to indirectly depend on the granule porosity through the granule bulk density. From granules produced from microcrystalline cellulose and magnesium stearate (less than 710µm in size), the granule bulk density has a more significant effect on the tablet porosity for a system of narrow granule size distribution and similar-shaped granules. The granule bulk density also had a significant effect on the tablet tensile strength in which low bulk density granules resulted in a higher tensile strength tablet compared to higher bulk density granules (Johansson and Alderborn, 2001). This suggests that a large extent of granular compressibility increases the tablet strength as the deformation of low bulk density granules increases the granule-granule contact area thus forming stronger inter-granular bonds (Johansson and Alderborn, 2001).

A study carried out by Marcias and Carvajal (2012) showed that the granule porosity is dependent on the number of impeller revolutions from the wet granulation process. Microcrystalline cellulose granules were produced using water as the liquid binder (liquid level was 90%). The change in the granule porosity was shown through the granule strength. The granule porosity decreased from 0.7 to 0.27 as the granule strength increased from 1MPa to 55MPa (left image of Figure 2.16). Therefore this led to an

increase in the granule density from 0.5 to 1.1g/cm^3 with increasing granule strength as can be seen in Figure 2.16 (Macias and Carvajal, 2012).

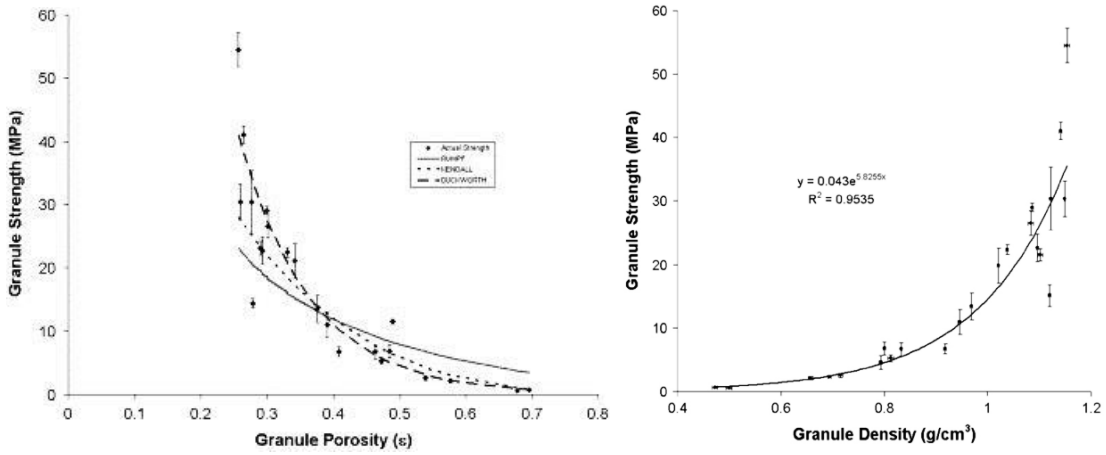

Figure 2.16: The relationships between: (left) granule strength and the granule porosity and (right) granule strength as a function of the granule density. Taken from Macias and Carvajal (2012).

2.5.6 GRANULE STRENGTH

The granule strength is an important parameter to ensure that a narrow granule size distribution is attained with consistent granule morphology, porosity and surface area (Litster and Ennis, 2004), which ultimately leads to the production of tablets with consistent strength and dissolution profile.

The granule strength σ_t is a function of the bed porosity, particle-particle adhesion forces, granule size and empirical coefficients. This can be calculated using Equation 2.17, which was developed by Rumf (1962).

$$\sigma_t = \frac{1-\varepsilon}{\pi} k \frac{A}{x^2} = \frac{1-\varepsilon}{\pi} k \frac{\sum_i A_i}{x^2} \tag{2.17}$$

where ε is the bed porosity, π is an empirical approximation, k is the average co-ordination number, A is the particle-particle adhesion forces and x is the particle size. If the empirical approximation is such that $\pi = \varepsilon k$, then the granule strength simplifies to Equation 2.18.

$$\sigma_t = \frac{1-\varepsilon}{\varepsilon} \frac{A}{x^2} \tag{2.18}$$

The adhesive forces can take into account different types of weak forces such as the van der Waals, electrostatic and capillary forces.

The granule strength has been correlated to the strength of the compact or tablet, produced from the granulation of microcrystalline cellulose powder and water (Macias and Carvajal, 2012). An increase of the granule porosity from 0.27 to 0.7, leads to a reduction in the granule strength from 57MPa to 1MPa as shown in the left image of Figure 2.16. The increase in the granule strength leads to a reduction in the tablet (compact) strength from approximately 7MPa to 0.2MPa, as demonstrated in Figure 2.17. The impeller speed and liquid level was found to not significantly affect the granule strength (Macias and Carvajal, 2012). Although the reason behind the decrease in the granule strength with increasing tablet strength was not directly explained in the study, we speculate that the high liquid level would promote densification of the granule and the reduction in the granule surface roughness, consequently decreasing the final tablet strength. The increase in the granule density from 0.45 to 1.1g/cm^3 (see right figure of Figure 2.16) would decrease the ability of the granule to deform further to confer strength to the granule (Macias and Carvajal, 2012). However the increase in the granule density would indicate a large area of intra-granular bonding which increases the tablet strength.

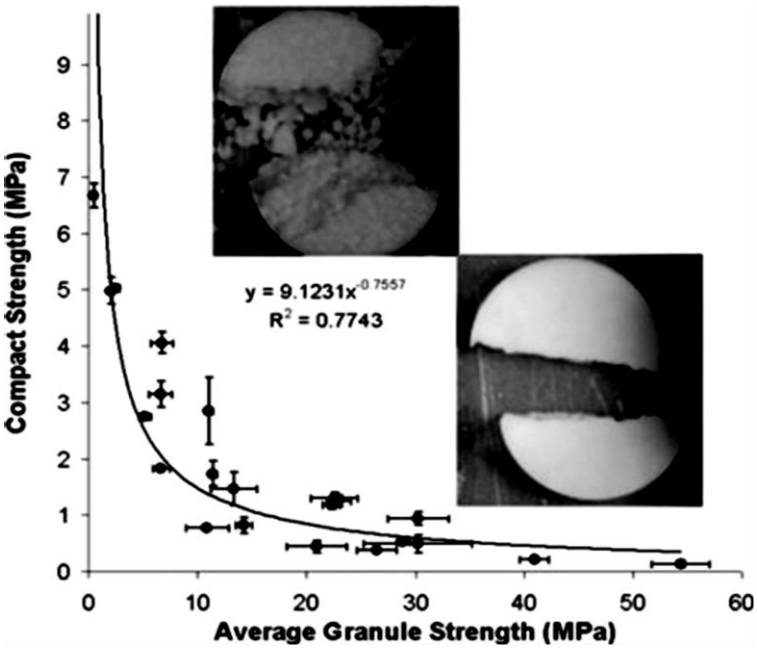

Figure 2.17: The tablet (compact) strength as a function of the average granule strength. Figure taken from Macias and Carvajal (2012).

In contrast, Jarosz and Parrot (1983) found that the liquid binder concentration and the tabletting compaction force have a greater influence on the final tablet strength than the granule strength (Jarosz and Parrott, 1983). The effect of the granule strength on the tablet strength was investigated by using dibasic calcium phosphate dihydrate, lactose monohydrate, starch and povidone. Wet granulation experiments varied the binder

concentration of povidone (1-8%) and starch (1-7%) liquid binders and tablets were compressed at 2268kg_f, 1134kg_f and 4536kg_f. The granule crushing strength was measured by determining the mass of mercury required to fragment a granule in a small chamber with a movable platen, while the tablet strength was measured using a tensiometer (Jarosz and Parrott, 1983).

From the study, it was found that the profile representing the granule crushing strength produced from dibasic calcium phosphate dehydrate and povidone or starch was similar to the tensile strength profile of tablets produced from the same formulation. For formulations comprising of dibasic calcium phosphate and povidone, the granule crushing strength increased from approximately 15g to 530g of mercury and the tablet tensile strength (compressed at 2268kg_f) increased from 3kg/cm^2 to 18kg/cm^2 with increasing povidone binder concentration. A similar trend was also observed when the compression force increased to 4536kg_f, in which the tablet strength increased from approximately 3kg/cm^3 to 45kg/cm^3. (Jarosz and Parrott, 1983). Similar findings were found for formulations containing dibasic calcium phosphate and starch. However for tablets prepared with lactose, the tablet tensile strength was fairly consistent at 200kg/cm^2 (for a compaction force of 1134kg_f) with increasing povidone concentration, in comparison to tablets produced with dibasic calcium phosphate dehydrate. The lactose granule crushing strength was found to be stronger with a maximum of 720g of mercury in comparison to dibasic calcium phosphate dehydrate granules. The findings were attributed to the formation of the intra-granular solid bridges from the deformation and consolidation of the granules within the tablet during the tabletting process (Jarosz and Parrott, 1983).

2.6 EFFECT OF WET GRANULATION CONDITIONS ON GRANULE PROPERTIES AND TABLET PROPERTIES

The quality of the tablets produced from the tabletting process is only as good as the initial quality of granules to obtain the desired tablet characteristics. The wet granulation process facilitates tablet manufacture by improving the powder flow by: (i) increasing the mean particle size, (ii) improving the drug distribution within the powder mixture, particularly with low-dosage drug batches, and (iii) improving the packing of the powder in the tablet die which reduces the variation in tablet weight and thickness. It is expected that the wet granulation process would directly or inherently affect the final tablet properties, as shown in a study comparing the granule and tablet properties from two

different types of mixer granulators (Hegedus and Pintye-Hodi, 2007). In literature, the main effects of the granule and/or granulation variables on the final tablet properties that are studied include:

- Granule size distribution,
- Granule saturation,
- Granule porosity,
- Granulator operating conditions such as the impeller speed, wet massing period and granulator scale-up.

The effect of the granule properties and the granulation operating conditions on the resultant tablet strength are discussed in more detail in the following sections.

The wet granulation process is expected to have a significant effect on the final tablet properties. However the study of how significant the wet granulation process is on the tablet properties is difficult to determine due to the complexity of the process. It is difficult to distinguish between which operating parameter has the most effect on the tablet properties and many sub-processes within the granulation process are occurring simultaneously. Hence many studies are carried out as a factorial experimental design, which simplifies the number of experiments by using statistical analysis to determine the significance of various operating parameters. However, this approach treats the relationship between wet granulation and the final tablet properties as a “black-box” with a series of inputs and outputs, and does not usually explain the underlying mechanism.

2.6.1 EFFECT OF THE FORMULATION

In tablet manufacture, many ingredients, besides the active ingredient, are incorporated into the formulation to help with increasing the tablet volume (excipients and diluents), assist with tablet disintegration and dissolution (disintegrants). These ingredients are known as “excipients” and will be the primary focus of this study since this ingredient makes up the majority of the tablet volume. There are many different types of excipients used in tablet manufacture including lactose monohydrate, croscarmellose sodium, corn starch, hydroxylpropyl cellulose and hydroxylpropylmethyl cellulose. One the most common types of excipient is microcrystalline cellulose and many studies have incorporated the material into the wet granulation formulation (Suzuki and Nakagami, 1999; Johansson and Alderborn, 2001; Suzuki *et al.*, 2001; Shi *et al.*, 2010; Shi *et al.*, 2011; Shi *et al.*, 2011; Shi *et al.*, 2011). Despite the prevalence use of microcrystalline

cellulose in tablet formulations, the behaviour of microcrystalline cellulose during wet granulation and tabletting is not fully understood.

Microcrystalline cellulose (MCC) is a partially depolymerised cellulose derivative that is commonly used as a binder/diluent in tablet manufacture as well as in the cosmetics and food industries (Rowe *et al.*, 2009).

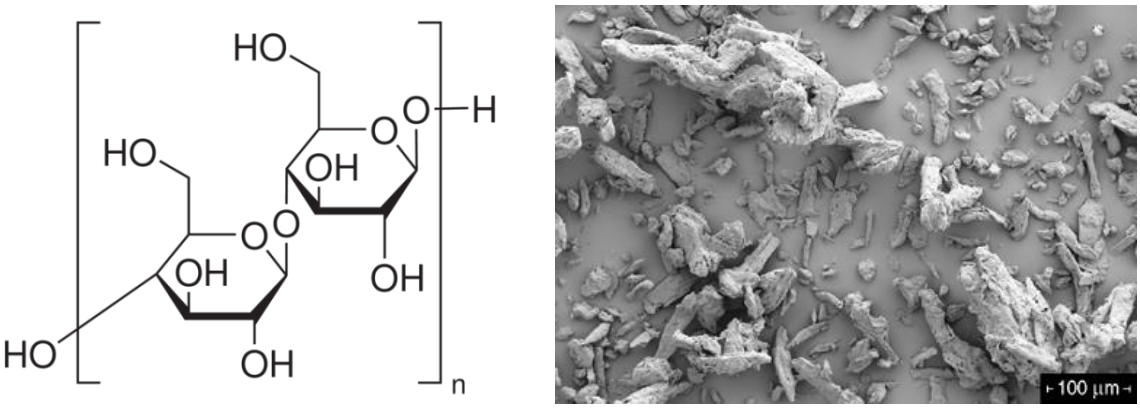

Figure 2.18: Schematic molecular structure of microcrystalline cellulose (left); and SEM image of microcrystalline cellulose, taken from Rowe *et al.* (2009) (right).

The wide range of applications leads to microcrystalline cellulose being available in different grades and moisture content. Microcrystalline cellulose is produced from the partial hydrolysis by dilute mineral acid solution of α-cellulose. The hydrolysed cellulose then undergoes a filtration process to purify the material before spray drying to dry the suspension of microcrystals or crystallites, leaving the microcrystalline cellulose powder behind (Kleinebudde, 1997; Rowe *et al.*, 2009). Microcrystalline cellulose does not have good powder flowability properties and hence wet granulation can be used to improve the flowability. Microcrystalline cellulose is porous in nature and the porous network allows liquid to be absorbed into the microcrystalline cellulose particles before it becomes saturated (Suzuki *et al.*, 2001).

Microcrystalline cellulose exhibits plastic deformation during compaction, undergoing deformation and densification to form a strong tablet whether the tablet is produced through wet granulation or direct compaction (Nicklasson *et al.*, 1999; Gohel *et al.*, 2003; Zhuikova *et al.*, 2010). This is particularly evident in comparison to other tablets produced from mixtures of microcrystalline cellulose and harder, less ductile material such as dicalcium phosphate dihydrate or lactose (Nicklasson *et al.*, 1999; Zhuikova *et al.*, 2010).

A few studies have studied the production of tablets through wet granulation using microcrystalline cellulose as part of the formulation (Roberts and Rowe, 1987; Kornchankul *et al.*, 2001; Suzuki *et al.*, 2001; Wu *et al.*, 2001; Gohel *et al.*, 2003). The wet granulation of microcrystalline cellulose has been speculated to conform to a crystalline-gel model proposed by Kleinebudde (1997) which describes the breaking down of the microcrystalline cellulose fibres into smaller crystalline units by shear forces, including the granulator impellers. These smaller units can then form an intricate gel-network which is dependent on the crystallites and amount of shear exerted on the microcrystalline cellulose (Kleinebudde, 1997). However no wet granulation experiments were carried out in the study, instead the study focussed on the stresses exerted by extrusion. The authors speculated that stresses induced on microcrystalline cellulose during wet granulation would be the same for extrusion.

The wet granulation process can reduce the compactibility of microcrystalline cellulose (Gohel *et al.*, 2003; Augsburger and Hoag, 2008). To study the internal transformation within the microcrystalline cellulose during wet granulation, Suzuki *et al.* (2001) analysed microcrystalline cellulose granules using mercury porosimetry (apparent particle density), helium-air pcynometer (true density), nitrogen gas adsorption (surface area) and X-Ray Diffraction (change of crystallite size). From their study, microcrystalline cellulose granulated with water can produce hard tablets even after long granulation times and increasing amount of water added to the process (Suzuki *et al.*, 2001). Nitrogen gas and water adsorption analysis showed that wet granulation decreases the surface area of the granules. This potentially may be due to the reduction in the number of pores in the microcrystalline cellulose and the creation of continuous microcrystalline cellulose phase in the granules (Suzuki *et al.*, 2001). By measuring the crystallite size of the microcrystalline cellulose by wide angle powder X-ray diffraction, it was found that the crystallite size decreased from 3.65nm to 3.30nm as the granulation time increased from 1 minute to 10 minutes (for 100mL of water added to the granulation process) and the crystallite size decreased from 3.87nm to 3.30nm as water addition increased from 80mL to 100mL, suggesting that the shear forces of the granulator impellers break up the fibrous microcrystalline cellulose (Suzuki *et al.*, 2001), which supports the finding by Kleinebudde (1997).

2.6.2 EFFECT OF THE LIQUID LEVEL

The granulation liquid level is the mass of liquid as a proportion of dry powder that is added to the granulator by mass. The granulation liquid level has also been shown to reduce the tablet strength (Oulahna *et al.*, 2003; Shi *et al.*, 2011; Macias and Carvajal, 2012). In Shi *et al.*'s study on microcrystalline cellulose granulation with water, the tablet tensile strength decreased from 11MPa to 4.5MPa, as the liquid level increased from 0% to 45%, as shown in the right image of Figure 2.19 (Shi *et al.*, 2011). The granule morphology and properties were also affected by the liquid level. As the liquid level increased towards 45%, the granules became rounder (see left image of Figure 2.19) while the granule porosity, specific surface area (SSA) decreased from 14-11% and 0.9-0.5m^2/g respectively. The powder flow factor (ff) also increased. A similar trend was found in Macias and Carvajal's (2012) granulation work with microcrystalline cellulose and distilled water in which it was found that the incorporation of more than 60% liquid significantly increased the granule strength for a given impeller speed with the greatest increase in the granule strength being from 2.15MPa to 30.34MPa for an impeller speed of 175rpm (Macias and Carvajal, 2012).

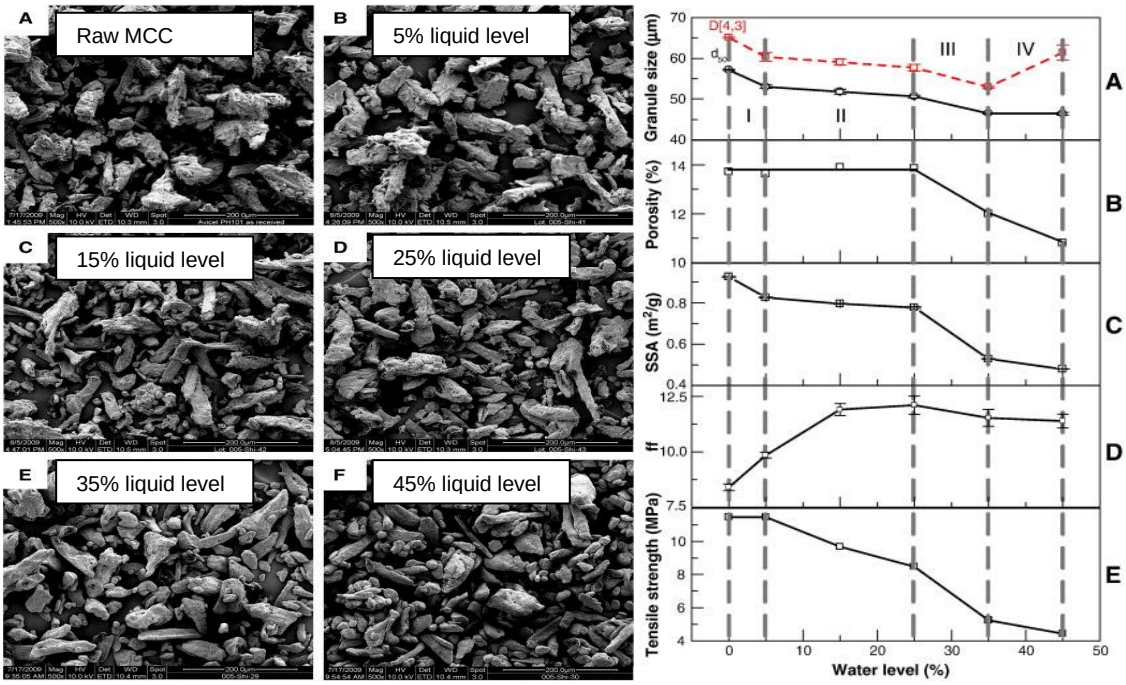

Figure 2.19: The rounding of microcrystalline cellulose (MCC) granule morphology (left) and changes in granule properties with increasing water level (right). Taken from Shi *et al. (2011)*.

The granule liquid content having a significant effect on the tablet tensile strength was also noted by Rangaiah *et al.* (1994). Norfloxacin powder was granulated with starch liquid binders with liquid levels varying from 6-20%. As the liquid level increased

towards 20%, the tablet strength began to decrease from 8.5kg/cm^2 (at around 10% liquid level) to 3.5kg/cm^2. At liquid levels of 17% and above, there was no change in the tablet strength. The finding was attributed to the decrease in the intra-granular bonding strength as water leaves a film around the granules with increasing liquid levels (Rangaiah *et al.*, 1994). The granule properties were not examined further in this study, only the final tablet properties which included the disintegration agents and disintegration time.

The densification of the granules with increasing water addition was also seen in the work conducted by (Sheskey and Williams, 1996). In their study, low shear and high shear granulations were carried out and granules between the size fractions of 180µm to 1mm were compressed into tablets. The amount of water added to the formulation did not significantly affect the tablet strength for both low and high shear granulation (Sheskey and Williams, 1996). This is also supported by ethenzamide and milled acetaminophen tablet hardness data from (Emori *et al.*, 1997). However what was noticed from Sheskey and William's study (1996) was that the addition of more water in the formulation produced more dense granules although no explanation for the reasoning behind the trend was given.

2.6.3 EFFECT OF THE WET MASSING TIME

Wet massing time is the amount of time, after the addition of the liquid binder, in which the wetted powder mass is mixed by the granulator to help with liquid distribution and coalescence and consolidation of the granules. During wet massing, the powder and granules are subjected to the compaction and deformation forces by the impeller. The loss of powder compactability may be attributed to the duration of the wet massing time during wet granulation. The effect of the wet massing time on the tablet strength has been investigated in several studies (Shi *et al.*, 2011; Shi *et al.*, 2011; Macias and Carvajal, 2012).

In Macias and Carvajal's study (2012), the number of impeller revolutions was found to have a profound effect on the granule strength and compact or tablet strength. This was shown through an inter-relationship between the granule porosity, granule strength and the tablet strength. The granulation results show that the granule strength increased (from approximately 1MPa to 55MPa) while the granule density increased (from 0.45 to 1.15) as shown previously in Figure 2.20.

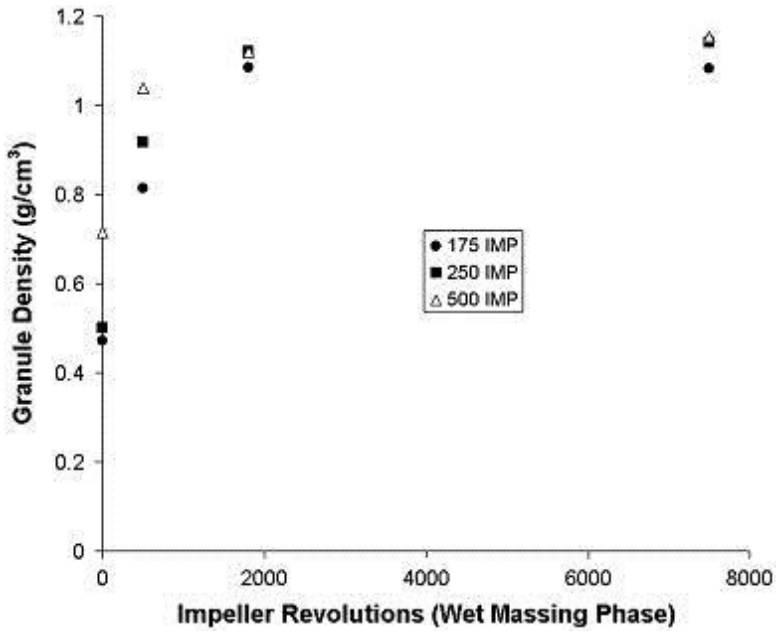

Figure 2.20: The granule density as a function of the number of impeller revolutions and impeller speed. Figure taken from Macias and Carvajal (2012).

There is also a decrease in tablet strength from approximately 7MPa to 0.2MPa with increasing average granule strength as shown in Figure 2.17. Macias and Carvajal (2012) fitted empirical models to the relationship between the granule strength and the granule density, as well as the tablet strength and the granule strength. From this, Figure 2.21 demonstrates that the tablet strength decreases with increasing number of impeller revolutions (hence a longer wet massing time), provided the mixing behaviour of the powder was in roping regime (Macias and Carvajal, 2012).

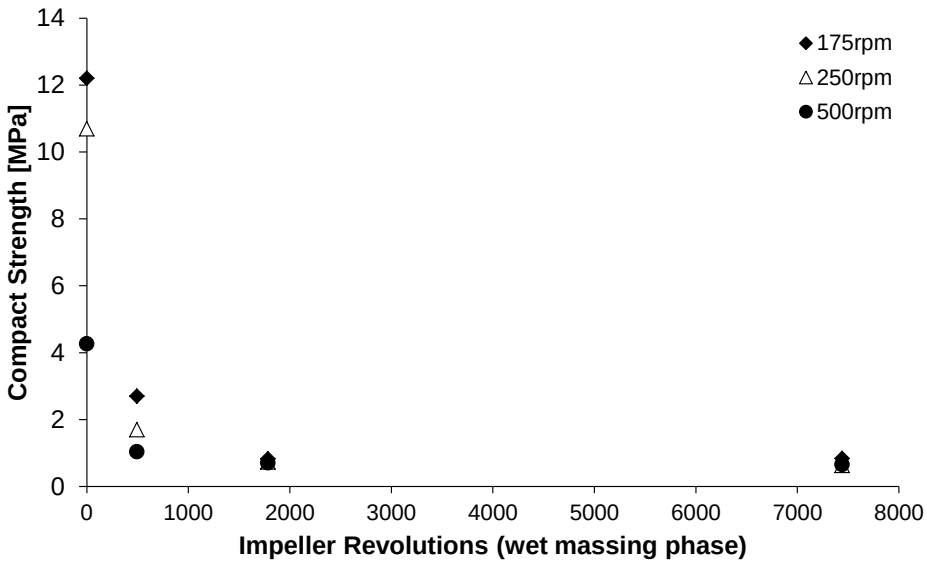

Figure 2.21: The compact or tablet strength as a function of the number of impeller revolutions. Data taken from Macias *et al.* (2012).

The trend was attributed to the combination of the granule strength and the granule porosity amount of inter-granular bonding within the tablet. A similar reduction in the tablet strength with an increase in the wet massing time was also noted in Shi *et al.*'s (2011) study. As the wet massing time increased from 0 minutes to 40 minutes, the tablet strength decreased from 7MPa to 0.8MPa, showing the cumulative impact of the impeller revolution and wet massing time on the tablet strength as shown in Figure 2.22.

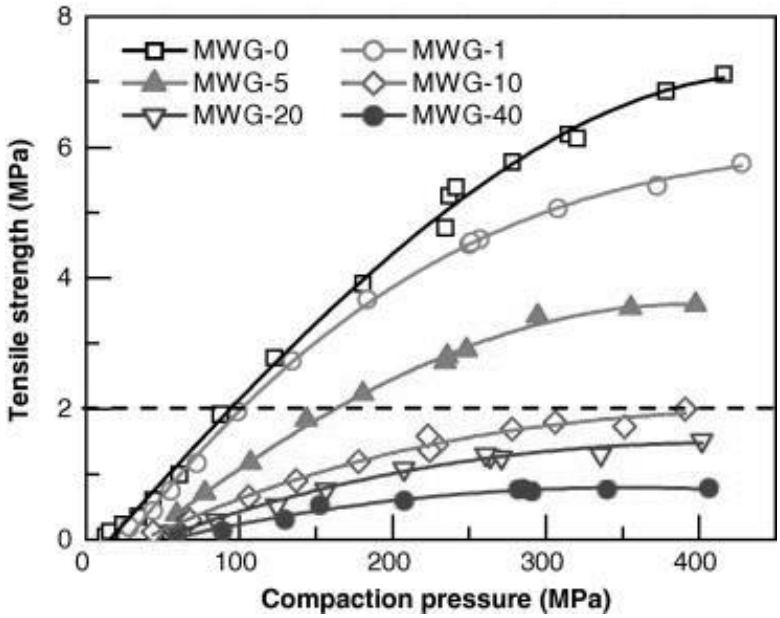

Figure 2.22: Effect of the wet massing time (MWG) on the tablet tensile strength as a function of the compaction pressure (liquid level of 65%). Broken line indicates the threshold between desirable granulation and over-granulation. Figure taken from Shi *et al.*, (2011).

2.6.4 EFFECT OF THE IMPELLER SPEED AND TORQUE

The granulator impeller speed and torque can also influence the final tablet properties. The impeller speed and torque would affect the magnitude of the impact force on the granules during the wet granulation process, thereby affecting the granule strength and ultimately the final tablet properties.

A study carried out by Kornchankul *et al.* (2001) looked at the effects of the granulation rate, granulation time and the torque applied by the impeller on the granule, on the tablet hardness, compaction pressure, friability and disintegration time. This study was based on granulating a formulation based on microcrystalline cellulose in a 2^k factorial experiment. The end torque, granulation rate and granulation extent (a ratio of the granulation energy input from the impeller to the wet powder mass) were statistically significant (Kornchankul *et al.*, 2001). With a high end torque and granulation extent, the granulation rate increased which reduced the tablet strength. No explicit explanation for this was

provided. The direct effect of the wet-massing time, granule saturation and binder concentration was difficult to see, although the authors varied these granulation and formulation properties in their work. Because the granulation extent, granulation rate and end torque had a significant effect on the tablet hardness, these granulation parameters also had a pronounced effect on the tablet friability (Kornchankul *et al.*, 2001). The compaction pressure was significantly influenced by the granulation rate and granulation extent, while the granulation time had no significance. In terms of the disintegration time, none of the granulation parameters investigated had a statistically significant effect (Kornchankul *et al.*, 2001).

In contrast, the impeller speed was not found to have a significant effect on the granule density and tablet strength in Macias and Carvajal's study (2012). The impeller speed was varied at 175, 250 and 500rpm and was investigated as a function of the number of impeller revolutions and granule density. Below 1500 impeller revolutions, the granule density varies approximately between 0.47 to 0.82g/cm^3 for an impeller speed of 175rpm, while the granule density varies from 0.50 to 0.92g/cm^3 and 0.71 to 1.04g/cm^3 for impeller speeds of 250rpm and 500rpm respectively. Beyond 1500 impeller revolutions, the granule density does not vary significantly and remains relatively consistent between 1.08 to 1.15g/cm^3 across all impeller speeds (see Figure 2.20). The impeller revolution did not have a significant influence on the final tablet tensile strength for a given liquid level. Therefore the influence of the liquid level and the impeller speed on the tablet strength was found to be more significant (Macias and Carvajal, 2012).

2.6.5 GRANULATOR SCALE-UP

Due to limitation of the quantity of active ingredient and economic resources, the need for designing and optimising the wet granulation process for tablet manufacture at a small scale (at a scale hundred times smaller than industrial scale) is imperative (Jones *et al.*, 2005).

Once the wet granulation process conditions are established, the process is then scaled-up to suit industrial production. The lack of understanding behind wet granulation made the scaling-up procedure difficult to control, in terms of maintaining the qualitative properties of the granules. With increasing knowledge about the three stages of wet granulation (wetting and nucleation, coalescence and consolidation, and attrition and breakage)

through experimental and computer simulation work, the scale-up of granulation processes is now recognised to have a greater scientific foundation recently rather than a work of art (Litster, 2003). Therefore the understanding of the granule properties from the wet granulation process allows the wet granulation scale-up procedure to be designed more efficiently.

During the scaling-up procedure, maintaining similar granulation dynamics between the small and large scale is imperative to conserve the quality of the granules. To achieve this in a mixer granulator, the three main options for scale-up are constant tip-speed (Landin *et al.*, 1996; Faure *et al.*, 1999; Faure *et al.*, 2001; Hassanpour *et al.*, 2009), or constant shear stress (Tardos *et al.*, 2004) or constant Froude number (Horsthuis *et al.*, 1993). The three scale-up rules can be evaluated using Equation 2.19 (Tardos *et al.*, 2004; Rahmanian *et al.*, 2008).

$$\frac{N_x}{N_y} = \left(\frac{D_y}{D_x}\right)^n \tag{2.19}$$

where N represents the impeller speed, D the impeller diameter, x and y the scales of the granulators and n a constant based on the scaling guideline. For the constant impeller tip speed, n = 1.0, constant Froude number, n = 0.5 and constant shear stress, n = 0.8 (Rahmanian *et al.*, 2008).

The constant impeller tip speed represents the shear rate during wet granulation and was first introduced to granulation scale-up by Horsthuis *et al.* (1993) using lactose granulated with PVP liquid binder. Although the constant tip speed rule is considered to the be easiest scale-up guideline (Tardos, 2005), there has been inconsistency in regards to the success of applying the constant tip speed rule to wet granulation. Horsthuis *et al.* (1993) found that the tip speed did not lead to comparable end-point times (the time at which there is no change in granule size distribution) across granulator scales of 10, 75 and 300L. Another study showed that the constant impeller tip speed may not be suitable for formulations incorporating hydrophobic components such as the HIV active ingredient Aplaviroc (He *et al.*, 2008). However, the constant tip speed rule has been found to be successful for granulator scale-up where the granule strength (comprising of calcium carbonate and aqueous polyethylene glycol solution) were similar for 5L and 50L Cyclomix granulators. This was attributed to the flow pattern of the granules during

Positron Emission Particle Tracking (PEPT) granulation experiments (Rahmanian *et al.*, 2008; Rahmanian *et al.*, 2008; Hassanpour *et al.*, 2009). The constant tip speed has also been successful in up-scaling high-shear granulators based on consistent granule size distribution (Rekhi *et al.*, 1996; Ameye *et al.*, 2002; Aikawa *et al.*, 2008).

The Froude number (*Fr*) represents the ratio of the centrifugal to gravitational forces, as described in Equation 2.20:

$$Fr = \frac{N^2 D}{g} \tag{2.20}$$

where N represents the impeller speed, D the impeller diameter and g the gravitational force. The Froude number was also first introduced to vertical high shear granulators by Horsthuis *et al.* (1993), using lactose powder and PVP liquid binder. The Froude number was found to suitable for producing comparable granule size distributions for 10, 75 and 300L granulators. The correlation between the Froude number and the impeller blade power and design has also been proposed as an important factor for consistent granulation dynamics during scale-up from 25, 65, 150 and 300L Fielder PMA granulators. The Froude number was successfully able to predict the dissolution time of tablets produced from the granulation of microcrystalline cellulose, povidone, sodium starch glycolate, Opadry and water (Campbell *et al.*, 2011). Another study proposed the use of process control to retain consistent Froude number and power consumption in the scaling up of fluidised bed granulation based on the granule moisture content (Faure *et al.*, 2001). However the Froude number was found to not be successful in scaling up granulation processes, using calcium carbonate and aqueous polyethylene glycol solution, based on maintaining a consistent granule strength from 1L to 250L Cyclomix granulators (Rahmanian *et al.*, 2008; Rahmanian *et al.*, 2008). Maintaining a constant Froude number along with the spray flux (Ψ_a) has also been proposed to be a useful tool for granulation scale-up (Litster *et al.*, 2002).

The constant-shear scale-up guideline is based on the scale-up of granulation processes with “equal shear stress” exerted on the granules (Tardos *et al.*, 2004). The constant-shear scale-up rule was initially developed from the investigation of the shear force from the fluidised bed Couette device (using glass ballotini powder and PVP solution) and varying scales of agitated fluidised beds granulating lactose, cornstarch and hydroxypropyl cellulose (Watano *et al.*, 1995; Tardos *et al.*, 1997), which was then expanded to high-

shear Fukae and Fielder granulators using mannitol, lactose, microcrystalline cellulose, starch and sucrose as test powders, granulated with water or hydroxypropyl cellulose or an aqueous ethanol solution (Tardos *et al.*, 2004). The high-shear granulation experiments revealed that the constant-shear rule was able to produce similar granule size distributions from 2L, 7.5L and 25L, provided the geometry of the granulator bowl is similar for all scales (Tardos *et al.*, 2004). Tardos *et al.*'s studies are supported by a scale-up high-shear granulation study using lactose, microcrystalline cellulose, hydroxypropyl cellulose, croscarmellose Na, active ingredient, citric acid and magnesium stearate (Michaels *et al.*, 2009). In contrast, the constant-shear stress rule was not found to be suitable for producing granules with consistent granule strength in both simulation studies and experimental (using calcium carbonate and aqueous polyethylene glycol solution) from 1L to 5L Cyclomix granulators (Hassanpour *et al.*, 2007; Rahmanian *et al.*, 2008; Hassanpour *et al.*, 2009), although similar granule strength was found for the up-scale from 5L to 50L Cyclomix granulators (Hassanpour *et al.*, 2009).

Another guideline is based on the power consumption during wet granulation through dimensionless power groups for torque profile. The reproducibility of the torque profile has been correlated to achieving a similar granule size distribution (Leuenberger, 2001; Chitu *et al.*, 2011), while maintaining the power consumption dimensionless group during scale-up to produce master curves (based on a combination of the Froude, pseudo Reynold's number and a powder filling ratio) was also proposed (Landin *et al.*, 1996; Faure *et al.*, 1999).

2.6.6 COMPACTION PRESSURE PRIOR TO TABLETTING

The granulator impeller can often exert significant shear and force on the powder and granules during wet granulation to allow homogeneous powder mixing and liquid distribution to take place. Therefore the compaction forces from the impeller could be one of the primary influences for the resulting granule properties and the tablet strength. Compaction and consolidation of the granules inherently leads to a reduction in the tablet strength, commonly known as a "*loss of compactibility*" and "*reduction in tablet crushing strength*". This has been noted in several studies in which some form of "processing compaction", including those from roller compaction and wet granulation, decreases the tablet strength (Kochhar *et al.*, 1995; Bultmann, 2002; Freitag and Kleinebudde, 2003; Shi *et al.*, 2011; Shi *et al.*, 2011). An example of this trend in wet granulation can be

found in Shi *et al.*'s work (Shi *et al.*, 2011; Shi *et al.*, 2011) with the reduction of the compactability profile from the effects of the liquid level and the wet massing time in Figure 2.23. The decline in the overall compaction behaviour is not well understood but has been speculated to be due to the reduction in the "*working potential*" of the powder, particularly for materials with high crushing strength (Kochhar *et al.*, 1995).

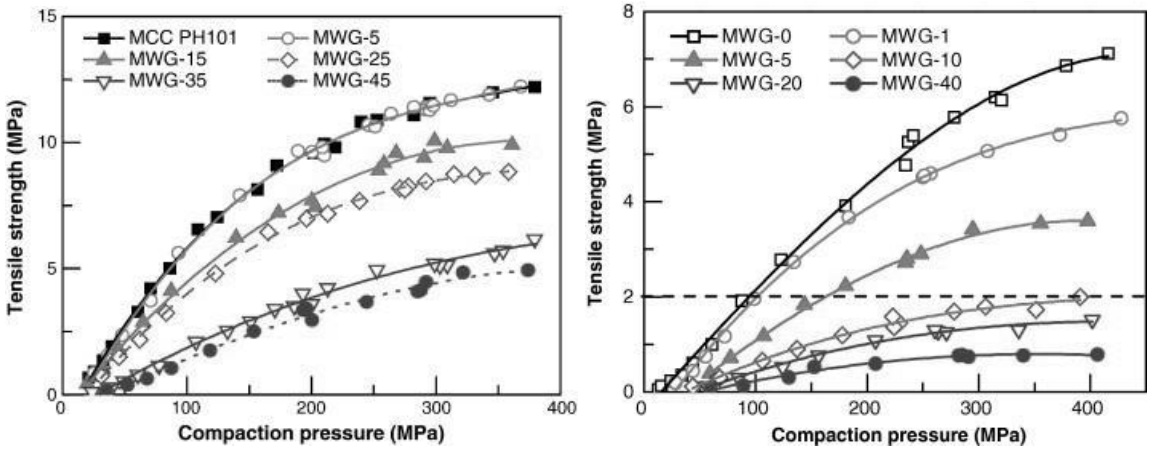

Figure 2.23: The reduction of the compaction behaviour profile or the "processing compaction" from the effects of: (left) liquid level and (right) wet massing time. Images taken from Shi *et al.* (2011a and 2011b)

Other studies have considered the consumption of the bonding potential and the release of energy from plastic, brittle fracture or elastic deformation during compaction of the material in both dry and wet granulation (Kochhar *et al.*, 1995; Bultmann, 2002). The reduction of the tensile strength after pre-compression has also been attributed to the "*work hardening*" of the material, consequently increasing the resistance of the material to irreversible deformation (Kochhar *et al.*, 1995).

The loss of powder compactability and reduction in the tablet tensile strength after pre-compression from the studies discussed (Kochhar *et al.*, 1995; Freitag and Kleinebudde, 2003; Shi *et al.*, 2011; Shi *et al.*, 2011) appear to be based on the fact that the number of contact bonds in the tablet determines the tablet strength. However other studies do not give an insight into the reasons for the reduction in tablet strength after pre-compression (Bultmann, 2002; Freitag and Kleinebudde, 2003; Bacher *et al.*, 2008). Hence more work is required in this area to understand the mechanisms controlling the tablet strength.

One useful approach in understanding the consumption of the material tensile strength from processing compaction, prior to the tabletting process, is the Unified Compaction Curve model, which will be described in the following section.

2.7 UNIFIED COMPACTION CURVE MODEL

Based on the concept of loss of powder compactability from processing compaction, Farber and co-workers (2008) proposed the Unified Compaction Curve model to link roller compaction pressure and the final tablet strength in roller compaction tablet manufacturing. Powder formulations containing at least 50wt.% microcrystalline cellulose were fed through roller compactors to produce a ribbon, prior to milling the ribbon into granules and tabletting. Plots of the tablet strength as a function of the compaction pressure showed that the compaction behaviour has the same overall "shape" as by-passing the rollers and allow the raw powder to be directly compacted (Direct compaction). However as the roller compaction force increased, the maximum tablet strength decreased (Figure 2.24). Farber *et al.* (2008) proposed that the final tablet strength was controlled by the cumulative compaction history of the powder and showed that final tablet strength for roller compacted granules could be predicted from a "Unified Compaction Curve".

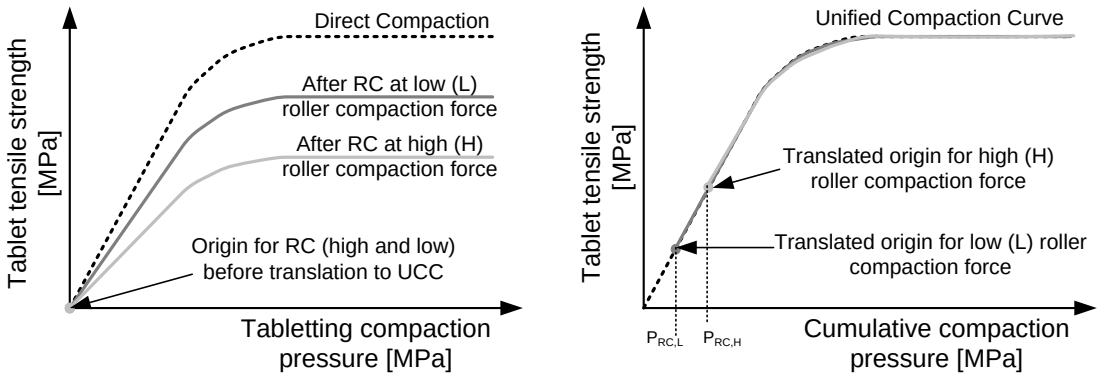

Figure 2.24: (left) Schematic diagram of the loss of tablet compactability after Roller Compaction (RC) at low (L) and high (H) roller compaction forces; and (right) the same data combined onto a Unified Compaction Curve (UCC). The translation in origin points for the UCC allows for the roller compaction pressure (P_{RC}) to be extrapolated from the data (adapted from Farber *et al.* 2008).

The roller compaction step was considered to be equivalent to direct compaction of the powder but the milling process destroyed the bonds in the ribbon. Due to the loss of powder compactability during the process, the maximum final tablet strength was reduced by an amount equal to the ribbon strength generated during the roller compaction step. The Unified Compaction Curve represents the cumulative compaction history from both roller compaction and tabletting compaction on a "master" direct compaction curve (see Figure 2.24). Mathematically, this was represented by translating the roller-compaction data along the formulation's direct compaction curve. The starting point is represented by the roller compaction pressure, P_{RC}, and the roller compaction ribbon tensile strength T_{RC} (Farber *et al.*, 2008).

The model gives a quantitative value for the amount of compaction pressure exerted on the raw powder by the rollers, which is equivalent to compressing the powder with a compaction pressure of P_{RC}. The ribbon produced from the rollers has a tensile strength of approximately T_{RC}. When the ribbon is milled into granules, the mechanical strength of the ribbon is destroyed but the roller compaction history remains, meaning that the maximum compactability of the granules is reduced. Therefore after the tabletting stage, the maximum tablet strength reduces to T_{max} - T_{RC} (the difference between the maximum tablet strength by direct compaction and the roller compaction ribbon tensile strength). Hence during the final stage of tabletting, the granules experience in total the compaction pressure from the tablet press in addition to the roller compaction pressure (Farber *et al.*, 2008).

The Unified Compaction Curve was created by measuring and fitting the tablet tensile strength of direct-compacted tablets to a simple empirical compaction model developed by Leuenberger (1982). The direct compaction curve serves as a master reference curve to align both the roller compaction and tabletting compaction profiles. Using the Unified Compaction Curve model (Equation 2.19), the origins of P_{RC} and T_{RC} for varying roller compaction pressures are used to translate the roller compaction curves along the reference curve. The final tablet strength T produced at any tabletting compaction pressure P' is:

$$T = T_{RC} + T_{\max}\left(e^{-bP_{RC}} - e^{-b(P'+P_{RC})}\right) \tag{2.19}$$

where T_{max} is the maximum tablet tensile strength that can be obtained by the formulation with direct compaction; T_{RC} is the ribbon tensile strength, P_{RC} is the pressure imparted on the powder during roller compaction; and b is the material-dependent exponent parameter that is a function of the relative density of the tablet and the compactability of the formulation (Leuenberger, 1982; Farber *et al.*, 2008). By unifying both the maximum tablet strength for the formulation through direct compaction and the tablet strength attained from roller compaction, the Unified Compaction Curve can enable the tablet strength to be predicted as well as give a quantitative measure of the amount of pressure applied to the powder during roller compaction.

The Unified Compaction Curve model has been studied in roller compaction (Mosig and Kleinebudde, 2013) and wet granulation studies (Dave and Dudhat, 2013). The Unified

Compaction Curve model was applied to the roller compaction of magnesium carbonate, a brittle fracturing material, and microcrystalline cellulose, a plastically deforming material. It was found that the model is not suitable for brittle fracturing materials. Tablets that were prepared with magnesium carbonate did not conform to the exponential Unified Compaction Curve model; instead the compaction curve had a linear profile (Mosig and Kleinebudde, 2013). The Unified Compaction Curve model was also not suited for roller compaction pressures below 200MPa. For microcrystalline cellulose granules, compacted at 2, 4, 8, 10 and 12kN/cm, tablet density was found to be consistent for granules for all compaction pressures. However the compaction curve deviated away from the Unified Compaction Curve at 12kN/cm. The reasoning behind the deviation was attributed to the granule being able to preserve its morphology, after tabletting, at high compaction pressures (e.g. 12kN/cm) (Mosig and Kleinebudde, 2013).

The Unified Compaction Curve has recently been applied to wet granulation using a formulation of 49% microcrystalline cellulose (MCC), 49% lactose and 2% plasdone (Dave and Dudhat, 2013). Two different grades of microcrystalline cellulose were investigated (MCC-101 with an average particle size of 50µm, and MCC-200 with an average particle size of 180 µm) to see the effect of the particle size on the tablet strength. The study revealed that MCC-200 was able to conform to the Unified Compaction Curve while MCC 101 did not (Dave and Dudhat, 2013). However the Unified Compaction Curve was able to show that MCC-101 exhibits higher compaction compared to MCC-200 which was due to the higher cohesiveness (compared to MCC-200) and smaller particle size of MCC-101 (Dave and Dudhat, 2013). The deviation of the MCC-101 away from the Unified Compaction Curve would not be expected given that the model was based on the same material. However further analysis of the granules were not revealed in this study to understand why the MCC-101 material could not conform to the model. In comparison to Farber *et al.*'s study (2008), one possible explanation for MCC-101 not conforming to the Unified Compaction Curve model is that the model may be more strongly reliant on the formulation having at least 50% MCC-101, which may not be as important for other grades of microcrystalline cellulose.

The Unified Compaction Curve has the potential to offer many benefits such as a basis for roller compaction scale-up and roller compaction design and troubleshooting. The roller compaction pressure can be used to predict what roller compaction pressure is

required to achieve a specified tensile strength. The P_{RC} and T_{RC} origins also demonstrate the reduction in tablet crushing strength as noted in previous studies (Kochhar *et al.*, 1995; Bultmann, 2002; Freitag and Kleinebudde, 2003). The benefits seen for roller compaction provide an incentive for this project to adopt the Unified Compaction Curve and apply it to the wet granulation process for the first time. The compaction pressure from the granulator impeller can be seen to be equivalent to the compaction pressure from the rollers.

2.8 LITERATURE SUMMARY AND GAP ANALYSIS

From this review of the research into the relationship between the wet granulation process and the resultant tablet strength, it is known that the wet granulation conditions have a strong influence on the granule properties such as the granule morphology, granule size distribution and the granule porosity. High liquid levels and long wet massing times promote granule growth and consolidation and densification of granules, which improves the spherity and reduces the granule surface roughness. It is also known that wet granulation affects the final tablet properties such as the friability, dissolution rate and the tensile strength.

However, the relationship between the wet granulation process and the final tablet strength remains unknown as the studies carried out do not take a systematic approach for a given formulation to understand the effect of each wet granulation condition (such as liquid level, wet massing time and the impeller speed) on the granule properties and consequently the tablet strength. Therefore there is a lack of a general and clear consensus on the effect of the wet granulation operating process on the tablet properties. The effect of the wet granulation process on the tablet properties becomes lost among the varying secondary effects of different granulation formulations, granulator geometries and granulation and tabletting conditions.

The current studies on the effect of the wet granulation process on the final tablet strength do not allow scope for a mathematical model to be developed to predict the tablet strength. However the consideration of the effect of the compaction history in powder processing (such as roller compaction) on the final tablet strength, such as the Unified Compaction Curve in Farber *et al.*'s study can be a potential model to be used in wet-granulated tablets. Therefore systematic studies looking at both the wet granulation

conditions and magnitude of compaction during the process are required to understand the direct effect of the wet granulation process on the tablet strength.

Based on this, there is yet to be a study which proposes a mathematical model to predict the tablet strength from the wet granulation conditions. Therefore there is a need for a systematic approach to understand the fundamental effects of the granulation conditions on the resultant granule and tablet strength to develop a model which can enable the tablet strength to be predicted for a given wet granulation condition.

To achieve this goal, the aims of this research are as follows:

1. Apply the Unified Compaction Curve Model to Wet Granulation:
   The tablet strength can be predicted by the compaction pressure applied by the rollers in dry roller compaction, in Farber *et al.*'s work (2008), through the Unified Compaction Curve model. The compaction history of the powder prior to tabletting is taken into account in the model and a similar concept can be adopted for wet granulation in which the powder would undergo irreversible deformation by compaction from the impeller before the tabletting stage. *The Unified Compaction Curve may be applicable to the wet granulation process, although the process is a wet system, rather than a dry process in roller compaction.* The Unified Compaction Curve model can be extended to be an alternative method for granulation scale-up which takes into consideration both the wet granulation conditions and the tablet strength, a view which other granulation scale-up models do not share. *Hence, the Unified Compaction Curve would be the first mathematical model proposed to link the wet granulation and tabletting processes together.*
2. Conduct a systematic study of wet granulation and tabletting:
   A systematic approach to understanding how the wet granulation conditions affect the granule properties needs to be established. By using the same formulation used by Farber *et al.*'s work (1:1 microcrystalline cellulose and lactose), the liquid level, wet massing time, impeller speed and the liquid binder delivery rate can be varied and the resultant granule properties can be examined for small and large scale granulators. By observing the granule morphology, topology, specific surface area, skeletal density and the porosity, the effect of the wet granulation conditions on the granule properties can be better understood. This will allow the granule properties to be

correlated back to the Unified Compaction Curve and determine which granule properties are the driving force for the final tablet strength.

3. Understand the role of microcrystalline cellulose in wet granulation and tabletting:
   The Unified Compaction Curve model is based on the incorporation of a plastically deforming material in the formulation such as microcrystalline cellulose. Microcrystalline cellulose is a common ingredient for tablet manufacturing, however the fundamental understanding of the plastic deformation behaviour of the cellulose material, interaction of microcrystalline cellulose with liquid binder and the effect of shear forces during wet granulation is not well understood. Therefore this research will investigate the effect of moisture, liquid binder acidity and basic pH level, shear as well as examining the crystallinity of microcrystalline cellulose will enable the material properties to be better understood and correlate back to the Unified Compaction Curve and the final tablet strength.

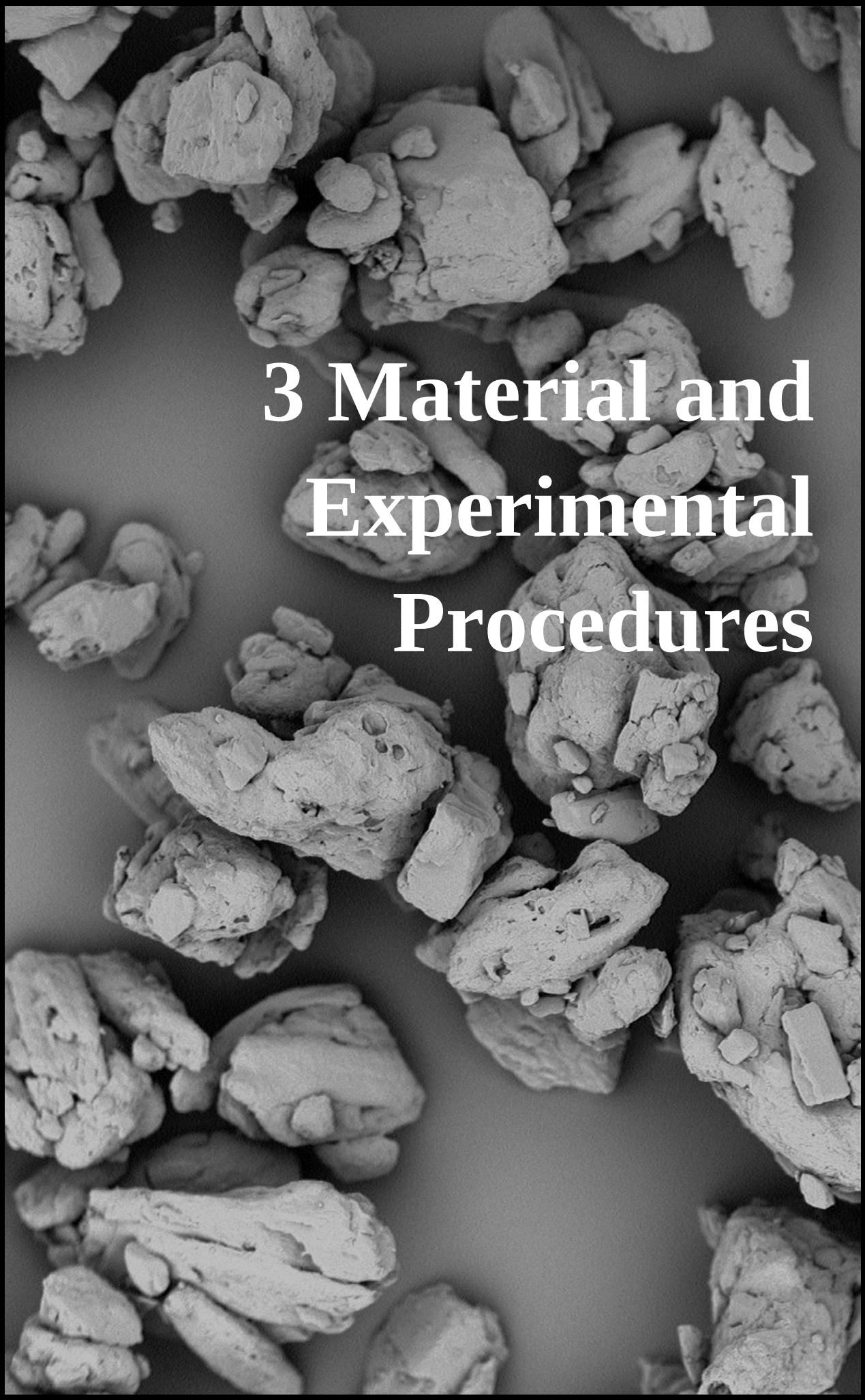

3 Material and Experimental Procedures

3 MATERIAL AND EXPERIMENTAL PROCEDURES

"*There is one thing even more vital to science than intelligent methods; and that is, the sincere desire to find out the truth, whatever it may be*"

- Charles Pierce, American actor -

To establish a clear picture of the relationship between the wet granulation process and the tablet strength, the selection of a model formulation (the powder and liquid ingredients required to produce the tablets) and establishing a set of systematic wet granulation experiments is imperative. The selection of the formulation and wet granulation experiments was based on studies on the application of compaction on raw powder in roller compaction (Farber *et al.*, 2008) and in wet granulation (Shi *et al.*, 2011; Shi *et al.*, 2011) where the wet granulation conditions (such as at the liquid level and wet massing time) have a significant effect on the granules. From the literature, there was a lack of experimental studies incorporating the variation of wet granulation conditions for a given formulation, which does not allow for the driving factors controlling the final tablet strength to be determined from the wet granulation and tabletting studies.

The Unified Compaction Curve model appears to depend on the presence of a sufficient amount of plastically deforming material in the formulation (at least 50% microcrystalline cellulose in Farber *et al.*'s (2008) study). Therefore to investigate the applicability of the Unified Compaction Curve to the wet granulation process, the granulation formulation must incorporate a plastically deforming material such as microcrystalline cellulose.

The chosen wet granulation formulation represents typical ingredients used in the pharmaceutical industry and is similar to the formulation used by Farber *et al.* (2008). The powder ingredients for the studies are microcrystalline cellulose and lactose, which show different deformation characteristics. Microcrystalline cellulose consists of fibre strands which deform plastically. Lactose particles (200 mesh grade), on the other hand, are crystalline and exhibit brittle fracture. The liquid binder chosen to bind the raw powder and produce granules is a polyvinyl pyrrolidone solution.

By examining these properties, the depths of the relationship between wet granulation and the tablet strength can be explored and better understood.

3.1 LIQUID BINDER

The standard liquid binder used in the studies was a 5w/v% solution of PolyVinyl Pyrrolidone (denoted as PVP, supplied by Sigma-Aldrich). Polyvinyl pyrrolidone is a common binder used in wet-granulated tablets in the pharmaceutical industry and is a common ingredient to incorporate in the wet granulation formulation (Jarosz and Parrott, 1983; Ritala *et al.*, 1988; Wikberg and Alderborn, 1991). The molecular chemical structure of PVP consists of a straight-chain polymer containing a 1-nitrogen cyclopentane ring, as illustrated in Figure 3.1. The polymer can contain various molecular chain length and weights, thus giving different grades of PVP. The PVP grade was used in this study was K90 which has a molecular weight of approximately 360,000.

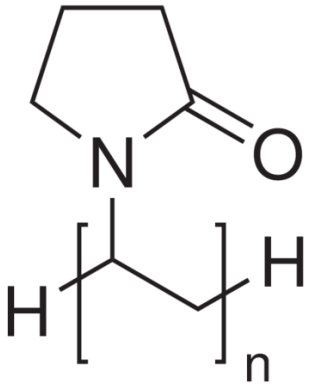

Figure 3.1: Chemical molecular structure of Polyvinyl Pyrrolidone.

Polyvinyl pyrrolidone is produced by the Reppe process, which involves acetylene and formaldehyde reacting with a copper catalyst to produce butynediol. Hydrogenation and cyclodehydrogenated chemical reactions occur in series to form butanediol and butyrolactone respectively. The PVP product is formed from the reaction of butyrolactone and ammonia (Rowe *et al.*, 2009). The PVP comes in a white powder form, roller-dried to give irregular-shaped particles with the majority of the particle size falling between approximately 75μm to 300μm (Rowe *et al.*, 2009).

The PVP liquid binder solution was prepared in two litre batches to ensure that a fresh supply of liquid binder was used in all wet granulation experiments. To make a 5w/v% PVP solution, 100 grams of the PVP powder was dissolved in distilled water (2 parts cold and 1 part hot water). The solution was left to stir over-night with aluminium foil covering the beaker to minimise evaporation of water from the solution. Once the PVP

powder was dissolved in the water solution, the water was topped up to make 2 litres to ensure the correct PVP concentration was made. A maximum of 6 droplets of food dye (Queens Fine Food Ltd. Pty.) was added to the solution to assist in observing the moisture content of the granules. It was assumed that the amount of food dye added to the formulation does not significantly alter the liquid characteristics (Litster *et al.*, 2001).

Generally, a water-based PVP solution was used which forms strong hydrogen bonds within the granules during wet granulation. For some selected experiments in *Chapter 6: Effect of the Granulator Compaction Pressure and Liquid Binder on the Microcrystalline Cellulose Material Properties*, an ethanol-based binder was used to see the effect of weak hydrogen bonds on the tablet strength.

3.2 POWDER FORMULATION

The standard formulation was 50% microcrystalline cellulose and 50% lactose monohydrate by weight. These are common ingredients in the pharmaceutical industry but were also chosen to compare the results of other studies (Farber *et al.*, 2008; Shi *et al.*, 2010; Shi *et al.*, 2011; Shi *et al.*, 2011; Shi *et al.*, 2011).

3.2.1 MICROCRYSTALLINE CELLULOSE

Microcrystalline cellulose is seen as a beneficial excipient to incorporate into pharmaceutical formulations due to its ease of compactability for low compaction pressures and has been used in several studies (Johansson *et al.*, 1995; Johansson and Alderborn, 2001; Bouwman *et al.*, 2005; Shi *et al.*, 2010; Shi *et al.*, 2011; Shi *et al.*, 2011; Shi *et al.*, 2011).

Microcrystalline cellulose is a white fibrous powder. Microcrystalline cellulose originates from a special grade of high-quality alpha cellulose, which can found in the walls of a special type of wood plant cells. The basic molecular structure of microcrystalline cellulose is $(C_6H_{10}O_5)_n$. The chemical structure of microcrystalline cellulose consists of a glucose back-bone with a 1-4 beta glycosidic bond (Tuason *et al.*, 2009). Microcrystalline cellulose is a polysaccharide, exhibiting two components: an amorphous region which comprises of flexible cellulose chains and a crystalline region which is made up of linear micro-fibril spiralled and bundled together. Microcrystalline cellulose has a chain length ranging between 50 to 5000 units. The length of polysaccharide chain makes microcrystalline cellulose insoluble in water (Tuason *et al.*, 2009).

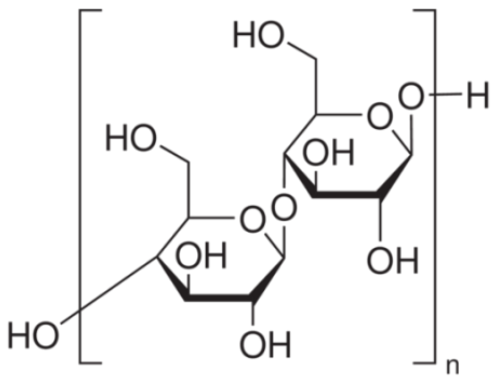

Figure 3.2: Chemical molecular structure of microcrystalline cellulose.

Microcrystalline cellulose is produced by separating the crystalline component of the weaker amorphous regions (otherwise known as dislocations) of the cellulose chemical structure. This is achieved through a series of steps, as schematically shown in Figure 3.3. The process begins with the shredding of alpha grade pulp sheets. The shredding pulp is then immersed in a mineral acid bath at a high temperature to dissolve the amorphous regions of the micro-fibrils, but leaving the microcrystalline regions intact. Hydrolysis of the micro-fibrils is then carried out to break down the polymer chains. The chemicals and impurities from the hydrolysis process is removed by washing the product with water before under-going spray drying to evaporate the water, and complete the microcrystalline cellulose manufacturing process (Reier, 2007; Tuason *et al.*, 2009).

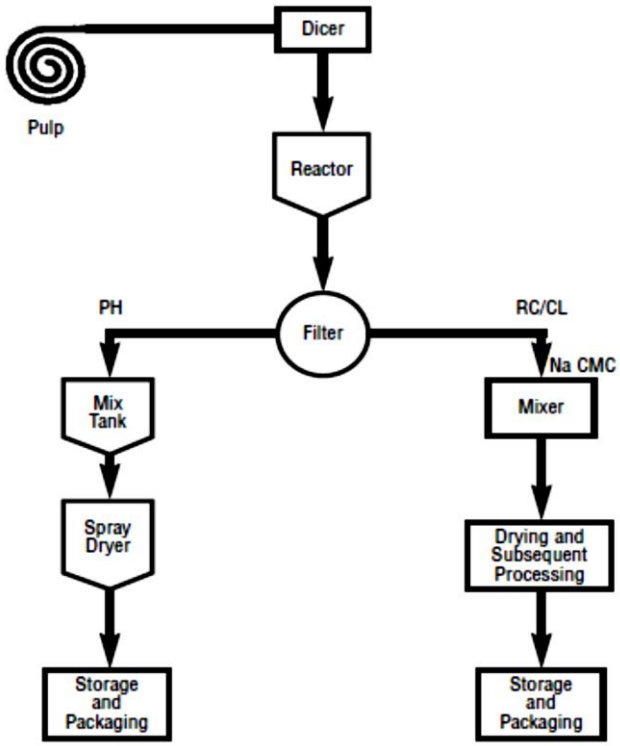

Figure 3.3: Schematic diagram of the Avicel manufacturing process, taken from Reier (2007).

The porous structure of microcrystalline cellulose exhibits plastic deformation and is desirable in direct compaction as well as wet granulation tablet manufacturing processes. Upon exposure to moisture, microcrystalline cellulose swells which can enhance the rate of disintegration and dissolution of the final tablet. In this research project, the wet granulation experiments used the most common grade of microcrystalline cellulose called Avicel (PH-101, FMC Biopolymer) which has an average particle size of 50 microns.

Figure 3.4: Images of microcrystalline cellulose (Avicel, PH-101) with (left) Scanning Electron Microscopy (scale bar: 160µm) and; (right) optical microscope.

3.2.2 LACTOSE MONOHYDRATE

Lactose monohydrate is a disaccharide carbohydrate comprising 2-8wt% in milk as sugar. Lactose is commonly used as a filler excipient in the pharmaceutical industry.

Lactose is made up of galactose and glucose compounds in which one group of these components can be linked together through a single molecule of water to form a 1:1 stoichiometric ratio of lactose to water (hence “monohydrate”) and form the molecular structure of $C_{12}H_{22}O_{11}{\cdot}H_2O$, as shown in Figure 3.5. Due to the presence of polar hydroxyl groups within the chemical structure, lactose exhibits hydrophilic wetting properties.

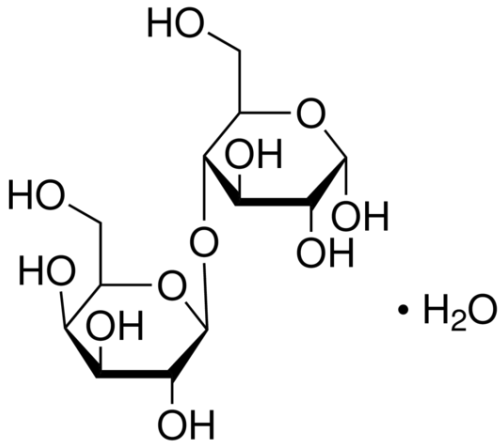

Figure 3.5: Molecular structure of lactose monohydrate.

Lactose is produced by the crystallisation of super-saturated solutions of whey below 95°C. The physical appearance of lactose consists is of a crystalline toma-hawk shaped particle. The bulk powder is white in colour and opaque as individual crystals. Lactose crystals are produced from whey (the residual from the production of cheese and casein) from the crystallisation of super-saturated whey solution.

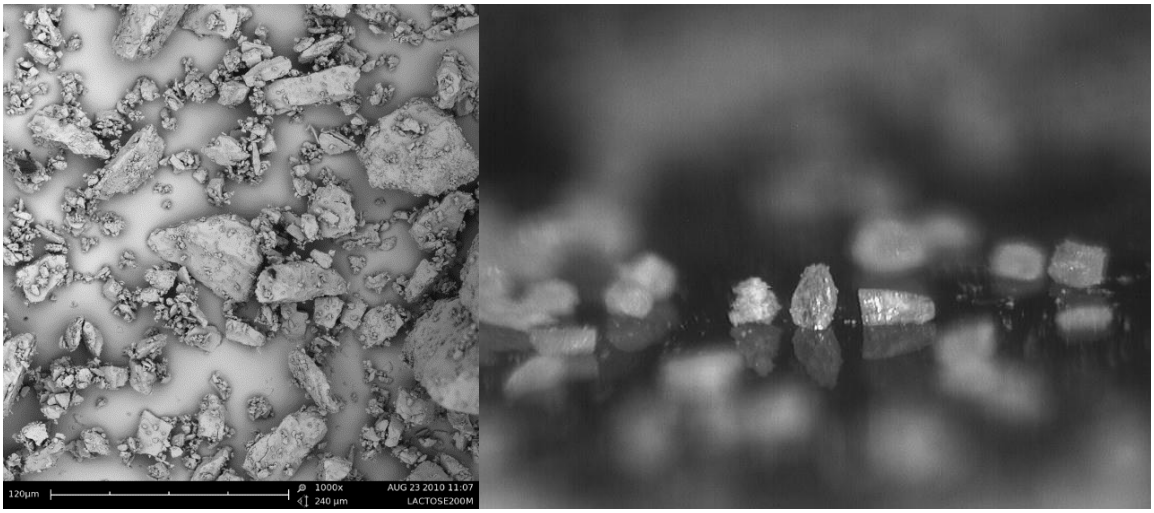

Figure 3.6: Images of lactose monohydrate (200 mesh) with (left) Scanning Electron Microscopy (scale bar: 240µm) and; (right) optical microscope.

The general properties of the powders used in this project are summarised in Table 3.1.

Table 3.1: Summary of the powder properties of microcrystalline cellulose and lactose 200 mesh.

Powder property \ Powder	Microcrystalline cellulose	Lactose 200 mesh
Appearance	Fibrous	White opaque, crystalline
Deformation mechanism	Plastic deformation	Brittle fracture
Mean particle size	50µm	75µm
True density	1577kg/m^3 (measured)[a] 1460kg/m^3 (corrected)[b]	1540kg/m^3
Solubility	insoluble	20g/100mL
Molecular weight	$(162.06)_n$	342.3

[a] Measured through helium pcynometry and is used to model the Unified Compaction Curve in this project.
[b] Sun, C., True density of microcrystalline cellulose. Journal of Pharmaceutical Sciences, 2005. 94(10): p. 2132-2134.

3.3 WET GRANULATION EXPERIMENTS

The wet granulation process is primarily the agglomeration of primary powder within the high-shear granulator with liquid binder sprayed from above using a spray nozzle (shown schematically in Figure 3.7).

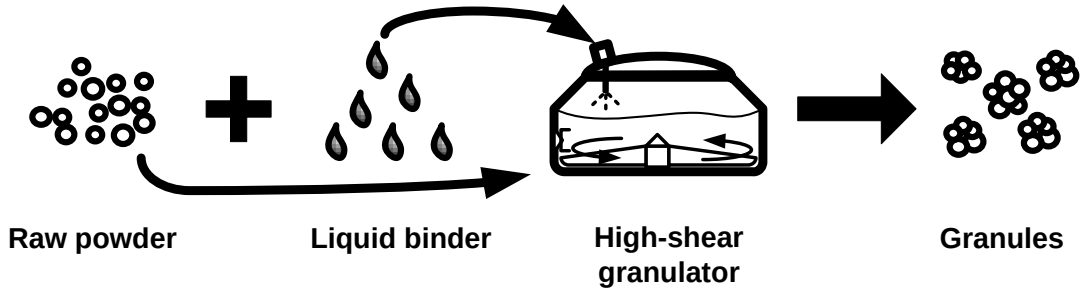

Figure 3.7: Schematic diagram of the wet granulation process.

To achieve a consistent granular product of narrow particle size distribution and drug content for tabletting, not only is the interaction of the liquid binder and powder important, but the wet granulation operating conditions are also important. The wet granulation operating conditions that were of interest in this project were:

- Liquid binder type (aqueous vs. non-aqueous)
- Liquid binder delivery rate
- Impeller speed
- Wet massing time
- Liquid level (mass proportion of liquid to mass of powder)

The wet granulation experiments were carried out using a laboratory-scale mixer granulator (KG5, Key International), spray pot (Spraying Systems) and nozzle (Spraying Systems), as shown in Figure 3.11.

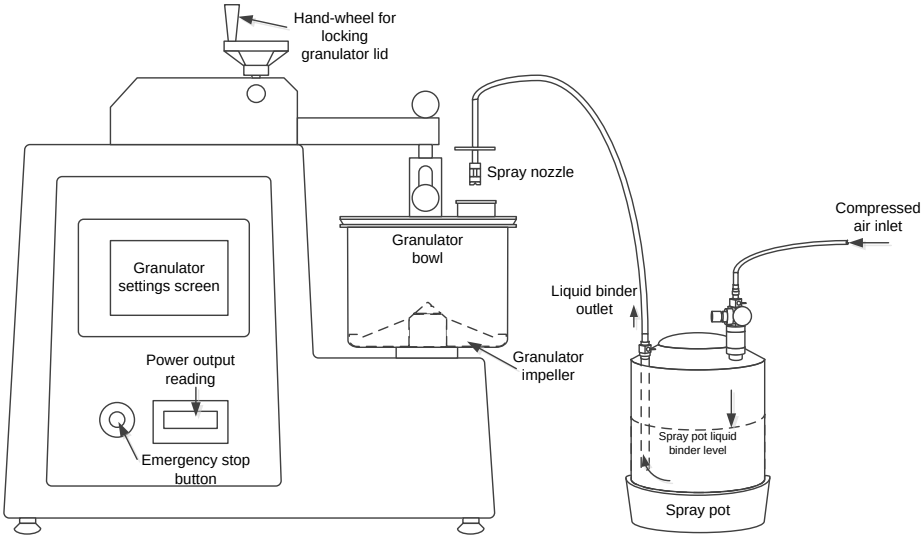

Figure 3.8: Schematic diagram of wet granulation experiment set-up.

The granulator has two granulator bowl sizes: a 1 litre (KG1, Key International) and a 5 litre bowl (KG5, Key International). The granulator bowls comprises of the main three-blade impeller only, however with different impeller geometries (as shown in Figure 3.9 and Figure 3.10). The impeller speed operated between 150-600rpm with the process impeller speed varying ±5rpm from the impeller speed set-point.

The one-litre main impeller blade geometry is a straight blade with no bowl scraper at the end, as shown in Figure 3.9. The bowl has a chute on the side for a chopper impeller blade to be installed, however this was not used during the wet granulation experiments and a Teflon cover was placed in the chute to prevent any powder from escaping the bowl volume.

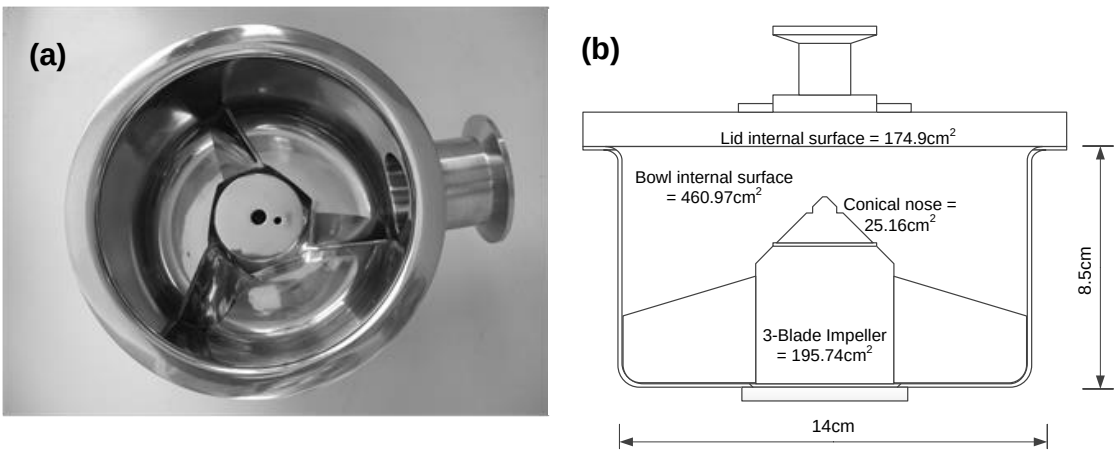

Figure 3.9: Images of (a) aerial view; and (b) internal view of 1L granulator bowl and main impeller with the powder contact surface area for different regions of the bowl (Key International).

For the five-litre bowl, the main impeller has a bowl scrapper at the impeller end, as presented in Figure 3.10. The large bowl has no side chute as the chopper impeller would be fitted to the granulator lid. The combination of the larger bowl size and the bowl scrapper at the end of the impeller leads to the five-litre bowl having a larger internal surface area that comes in contact with the powder, compared to the one-litre bowl.

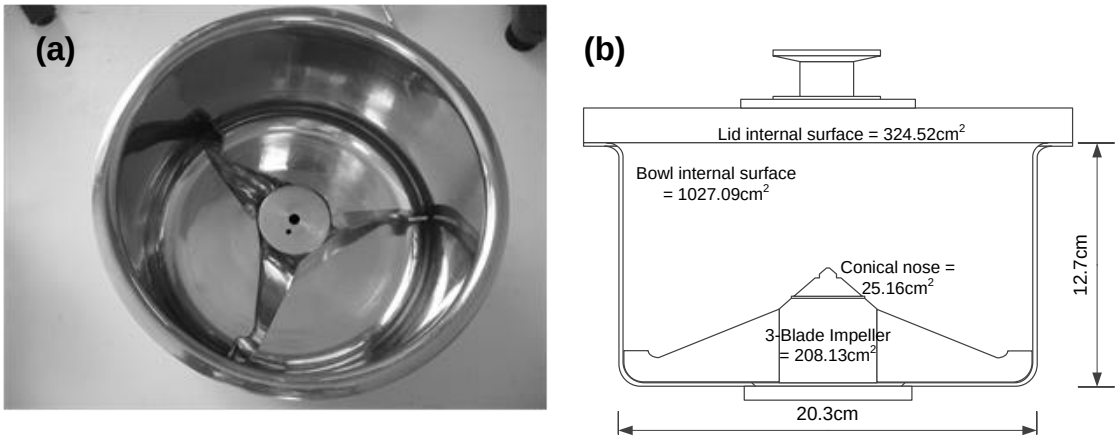

Figure 3.10: Images of (a) aerial view; and (b) internal view of 5L granulator bowl and main impeller with the powder contact surface area for different regions of the bowl (Key International).

The liquid binder was added to the granulation process through a spray nozzle above the agitated powder bed. The spray nozzle is connected to a liquid reservoir in a 5L spray pot (Spraying systems), as shown in Figure 3.11.

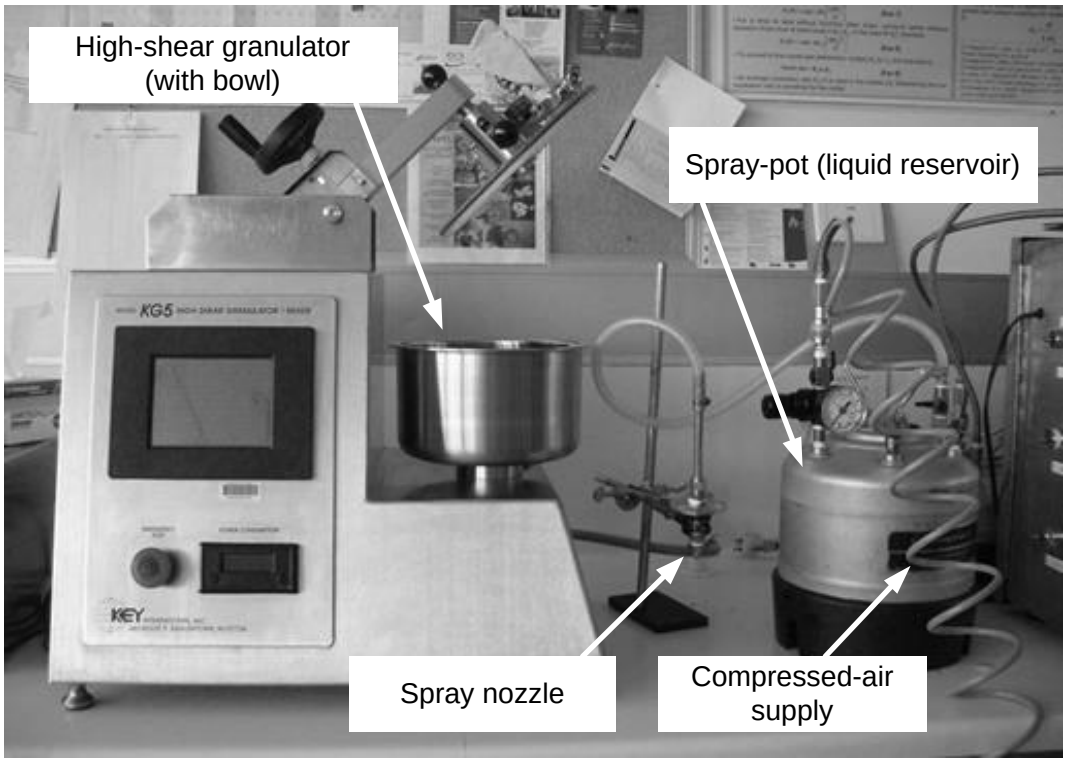

Figure 3.11: Experimental set up of wet granulation experiments using the granulator, spray pot and spray nozzle.

The process of droplet formation from a spray nozzle is called atomisation where a volume of liquid is driven through an orifice of a specific size by the pressure from the compressed-air in the spray pot. The pressure of the compressed air (providing potential energy to the liquid) and the geometry (orifice diameter and design) of the nozzle, allows the sheet of liquid to break up into strands of liquid called ligaments. The ligaments then break up further to produce droplets. The rate of binder delivery to the granulator is controlled by the spray pot pressure and spray nozzle design. For all experiments, the spray pot pressure was kept constant at 80psi (5.5bar) and the spray nozzle was varied to obtain a low and high binder flow rate. Two spray nozzles were chosen which gave a low (130g/min) flow rate using nozzle tip TP650017 and a high (280g/min) flow rate using nozzle tip TP65050.

The wet granulation experiments were conducted by adding 0.5kg of microcrystalline cellulose and 0.5kg of lactose powder into the granulator and pre-mixing it for at least 1 minute (at a minimum impeller speed of 285rpm) to ensure that the microcrystalline cellulose and lactose powders were mixed to be as close to a random mixture (a mixture in which the consistency of the powder blend is relatively uniform and the probability of finding a microcrystalline cellulose or lactose particle is the same for any sampling point within the granulator bowl (Rhodes, 2008)) as possible. In the wet granulation experiments, three impeller speeds were used which reflect the different mixing regimes: bumping (150rpm) and roping (285rpm and 600rpm) (Iveson and Litster, 1998).

The liquid binder was sprayed for at least 30 seconds, external to the granulator, to ensure that the spray flow rate was at steady state prior to the liquid being delivered to the granulator as atomised droplets. The spray nozzle was positioned in the granulator such that the spray was perpendicular to the direction of the agitating powder bed.

A systematic approach was applied to the wet granulation experiments. The effect of the granulator liquid level (20wt%, 30wt%, 40wt% and 50wt% on a dry basis), wet massing time (0, 2, 6 and 10 minutes), impeller speed (150, 285 and 600rpm) and the binder flow rate (130g/min and 280g/min) were investigated. For the liquid level experiments, a short wet massing time of 10 seconds was used, at the end of the spraying period, to ensure uniform liquid distribution throughout the powder bed. Each study of the liquid level or

wet massing time was conducted through a series of liquid addition, wet massing and sampling stages.

During the wet granulation experiments, multiple samples were taken from the one batch with increasing increments in the liquid level or wet massing time. The required amount of liquid to add to the granulator was determined through a wet and dry mass balance of the granulation process, based on the required dry sample weight and binder flow rate.

The granulation process was carried out by adding in the required liquid binder in the granulator to reach the desired liquid level. Once the liquid level was achieved, the impeller ran for an extra period of time (10 seconds for liquid level experiments and 0-10 minutes for wet massing time experiments) to evenly distribute the liquid and/or wet mass the powder. The granulator was stopped briefly to obtain a sample of the granulated product at three different locations around the granulator bowl from the powder surface to the bottom of the bowl using a scoop. Once the sample was obtained, the wet granulation process was restarted and additional liquid was added to reach the next liquid level and to compensate for the reduced batch size due to sampling. Further wet massing was then conducted. The combinations of the granulator liquid level, wet massing time, and binder flow rate at each of the three impeller speeds are summarised in Table 3.2.

Table 3.2: Summary of wet granulation experiments conducted at impeller speed of 150rpm. Low binder flow rate (L) is 130g/min; high binder flow rate (H) is 280g/min.

Wet massing time		0 mins		2 mins		6 mins		10 mins	
Impeller Speed	Liquid Level	L	H	L	H	L	H	L	H
150 (bumping mixing regime)	0%								
	20%								
	30%	✓		✓		✓		✓	
	40%								
	50%								
285 (roping mixing regime)	0%								
	20%	✓		✓		✓		✓	
	30%	✓		✓		✓		✓	
	40%	✓		✓		✓		✓	
	50%	✓		✓		✓		✓	
600 (roping mixing regime)	0%								
	20%								
	30%	✓		✓		✓		✓	
	40%								
	50%								

The granules produced from wet granulation were dried in a fan-forced oven at 60°C overnight (at least 12 hours for the granules to completely dry) on shallow trays lined with baking paper before conducting the tabletting experiments.

3.4 TABLETTING EXPERIMENTS

Tabletting is the process by which powder, in its original state or of granular form, is compacted into a tablet. In this project placebo tablets were produced using an automatic pneumatic single-station tablet press (Model 3887, Carver Inc, USA), as shown in Figure 3.12. The range of compaction forces the tablet press can produce is between 1,000lb_f to 50,000lb_f, although the tablet die mould has a limitation of withstanding up to 18,000lb_f. The compression and decompression rates on the tablet press were set to the fastest available setting and the dwell time was set to zero seconds to minimise the compression time. However it should be noted that the total compression/decompression period on the tablet press is approximately 1-2 minutes per tablet which is substantially longer than the milliseconds typically taken to produce a tablet by industrial tablet press stations. The dwell time was set to zero and the tablet ejection rate was set to the fastest rate to simulate an industrial tablet press as closely as possible. The tablets produced from the Carver press would have the maximum possible strength for the microcrystalline cellulose/lactose formulation and the tablets are assumed fracture in a similar way to tablets produced by an industrial press.

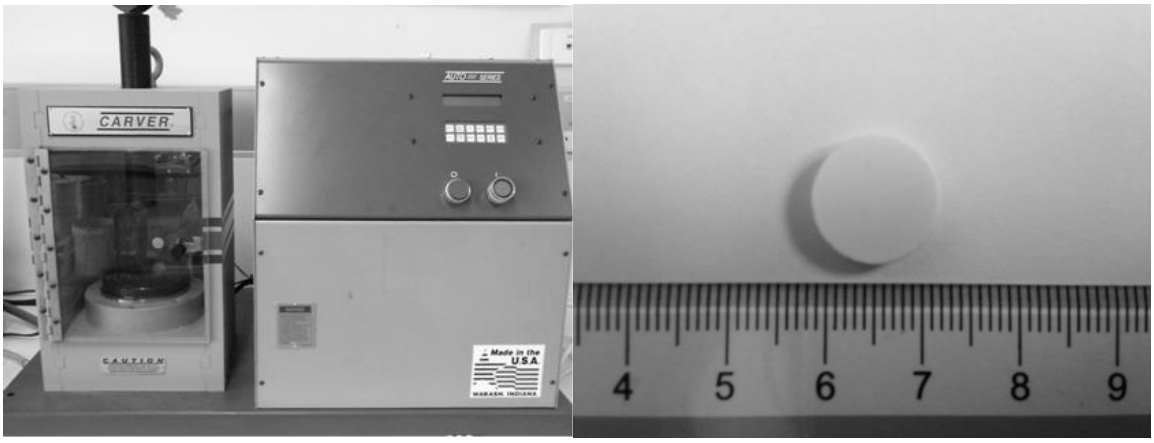

Figure 3.12: Images of (a) Carver automatic tablet press; and (b) tablet produced from the tablet press (scale bar in centimetres).

For each tablet, 500mg (±1mg) of powder was weighed out and transferred onto weighing paper before being added to the tablet die. The tablet press operates where the top tablet platen was held stationary, while the bottom platen raised up to compress the powder into a tablet. The tablet dimensions were 13mm in diameter and the tablet thickness varied

depending on the compaction force applied to the sample (see Figure 3.12b). Two types of tablets were produced in this project: direct compacted tablets and wet granulated-tablets.

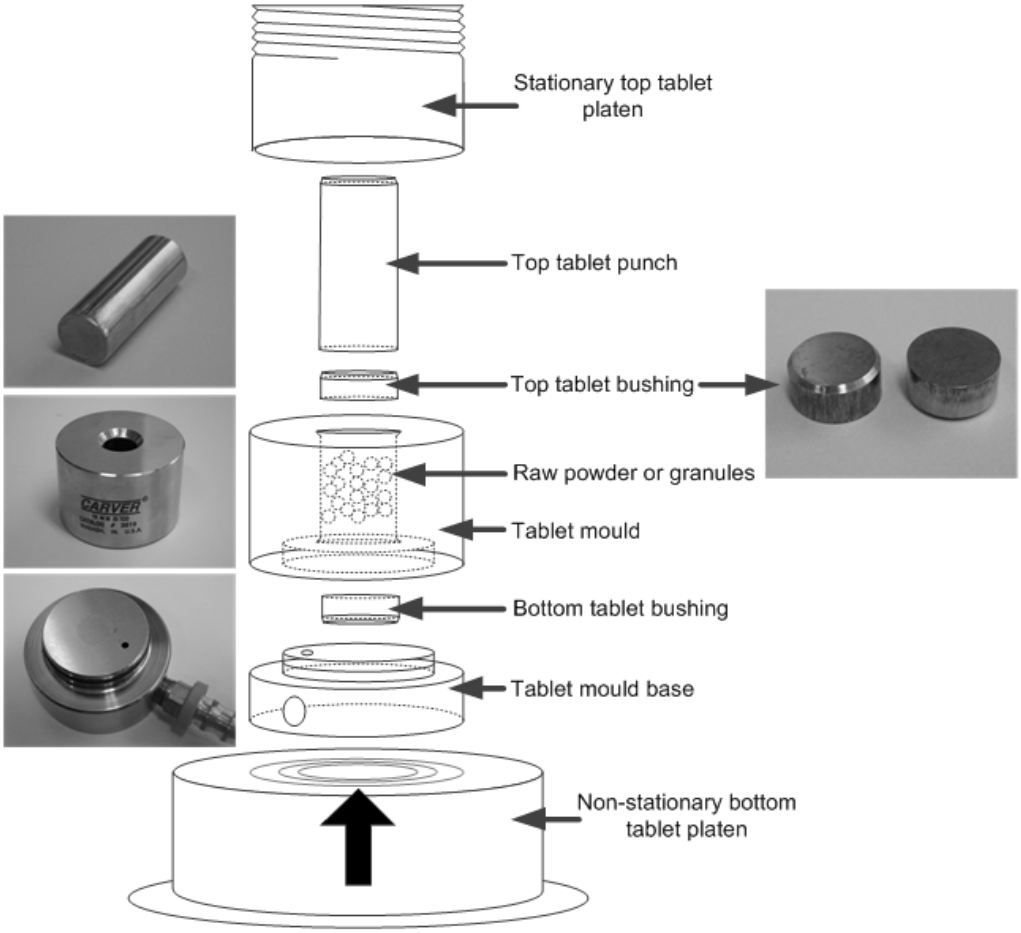

Figure 3.13: Schematic diagram of tablet press mould and punch set-up.

3.4.1 DIRECT COMPACTION TABLETTING

In direct compaction, the original powder is directly compacted into a tablet as shown in Figure 3.14.

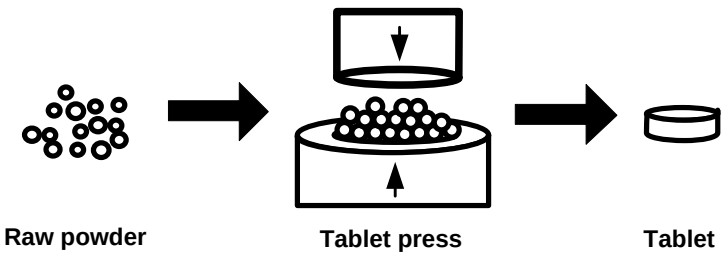

Figure 3.14: Schematic diagram of direct compaction.

For each tablet, 500mg of the 50:50 microcrystalline cellulose and lactose (no PVP present) powder blend was compacted directly in the tablet press with compaction forces

of 2000, 6000, 10,000, 12,000, 14,000 and 16,000lb_f. The tablet thicknesses produced from the process were between 2.54mm to 3.15mm for the highest compaction force (16,000lb_f) to the lowest compaction force (2,000lb_f) respectively. For each experimental batch, the tablets were produced in triplicate.

Direct compaction tabletting was also carried out on humidified powder to examine the effects of moisture up-take from the powder on the tablet strength. For this set of experiments, five tablets were produced per batch.

3.4.2 WET-GRANULATED TABLET COMPACTION

Tablets produced through wet granulation go through a series of processes of wet granulation, drying and tabletting, as illustrated in Figure 3.15.

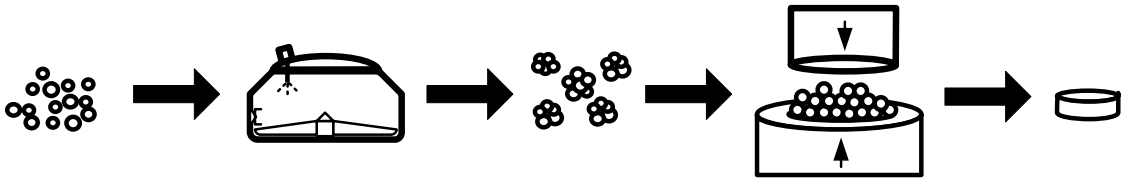

Figure 3.15: Schematic diagram of wet-granulated tablet compaction process.

The entire granule size distribution for each granulation batch was used during the tabletting process. The average equivalent granule diameter (d_{50}) for the batches ranged from 50µm to 425µm (see *Section 4.4.1.: Effect of Liquid level and wet massing time on granule size distribution*). The granules were compacted using compaction forces of 2000, 6,000, 10,000 and 16,000lb_f to produce five tablets (500mg) for each experimental batch and compaction force.

3.5 GRANULE AND TABLET CHARACTERISATION

The understanding of the powder properties is essential for understanding the formation of the granules and the subsequent properties of the tablets. This section will describe the process of characterising the powder and granules outlined in Figure 3.7 previously.

Table 3.3: Characterisation of granules and tablets.

Granule	Tablet
Size distribution	Volume
Porosity	Skeletal density
Surface area	Porosity
Skeletal density	Surface area
Fractal dimension	Physical structure of topology and cross-sectional area
Overall physical structure	

3.5.1 PARTICLE SIZE DISTRIBUTION MEASUREMENT

The particle size distribution was measured by dry mechanical sieve analysis. Although the resolution of the size distribution measurement in sieve analysis is lower compared to other particle size measuring techniques such as laser diffraction, the presence of large granules (greater than 2mm) in the granulation sample restricts the measuring technique to mechanical sieving. In this process, mechanical vibration encourages a sample of powder to pass through a nest of sieves of descending aperture size. A sieve shaker (Retsch AS200, shown in Figure 3.16) was used to mechanically segregate the powder sample into their size fractions. For each sieving experiment, approximately 20-50 grams of powder was deposited in a nest of nine sieves (pan, 63μm, 90μm, 125μm, 180μm, 355μm, 500μm, 710μm and 1mm). The sieving period for each sample was 10 minutes with the sieving amplitude of approximately 0.5 (sieving instrument setting of 50 amplitude). The powder loss from each sieving experiment was within 5% of the original sample weight. The particle size distribution was plotted on a basis of mass frequency.

Figure 3.16: Image of the mechanical vibration sieve shaker (Retsch AS200).

3.5.2 SKELETAL DENSITY MEASUREMENT

The skeletal density (or true density) is the mass of the sample over the volume that the sample occupies (excluding pore space). The skeletal density was measured using a helium pynometer (Micromeritics AccuPyc 1330). The helium pcynometer measures the skeletal density by measuring the volume of helium injected into a metal cylindrical container that has an exact volume (the volume of the metal container used was 6.314m^3).

Helium gas is used due to the small size of the helium gas molecules and hence the helium gas is able to penetrate deeply into all of the sample internal pores. By knowing the precise volume of the container and the helium injected, the volume of the sample can be measured. Hence using the weight of the sample, the skeletal density of the sample can be calculated.

The amount of sample measured was determined by the amount of powder it takes to fill one half or two-thirds of the sample container. The amount of sample measured is usually between 2.5 to 3 grams. The instrument was calibrated for every second measurement using calibration steel balls. For each measurement, the sample was purged with helium gas 50 times to clean the sample before the skeletal density measurement took place. For granular samples, a bulk sample comprising of the entire granule size distribution was measured as well as a sieved fraction of granules ranging from 90-250μm. The sieved granules were also compacted into tablets at 2722kg_f (6000lb_f) and the skeletal density for the tablet was measured.

For each sample, ten measurements of the skeletal density were taken to give an average value. The quality of the ten measurements (QOM) was determined using Equation 3.1:

$$QOM = \frac{\sigma}{V_{average}} \times 100\% \tag{3.1}$$

where σ is the standard deviation of the measurements (cm^3) and $V_{average}$ is the average volume (cm^3). If the QOM is less than two percent, then the measurement for the sample is considered to be of high quality. Therefore only helium pcynometer measurements with a QOM of less than two percent were taken as results.

3.5.3 BULK SPECIFIC SURFACE AREA

The Brunauer-Emmet-Teller (BET) specific surface area is the surface area of the granule per gram of sample. The BET model measures the specific surface area through the adsorption of gas molecules on the sample surface. The granular surface area was measured by nitrogen gas adsorption using the Belsorp Mini II instrument (Belsorp Mini II, Belsorp Japan), as shown in Figure 3.17.

Figure 3.17: Image of nitrogen gas adsorption BET surface area (left) instrument (Belsorp Mini II, Belsorp Japan) and (right) sample tubes.

Granules have a low specific surface area and therefore a minimum of 0.5 grams of the granular sample was deposited into the small sample tube (see Figure 3.17 right). Pharmaceutical powders easily absorb moisture and hence the sample was pre-treated under vacuum at room temperature (25°C) for 4 days before running the adsorption analysis, to ensure the sample was free from moisture and contaminants.

For the nitrogen adsorption analysis, the granular sample was further pre-treated for 4 hours on the Belsorp Mini II instrument to remove any contaminant and moisture from the sample before running the analysis. The analysis was conducted under cryogenic temperatures using liquid nitrogen (-196°C). The relative pressure (P/P_0) points taken for the gas adsorption ranged from 0.05 to 0.9. Duplicate measurements were carried out for each sample.

From the results of the analysis, the BET specific surface area was obtained using the software *Belsorp Mini*, in which a tangent line was fitted to the BET curve which gave a co-efficient of determination for linear regression R^2 value of at least 0.90. An example of this process is given in Figure 3.18.

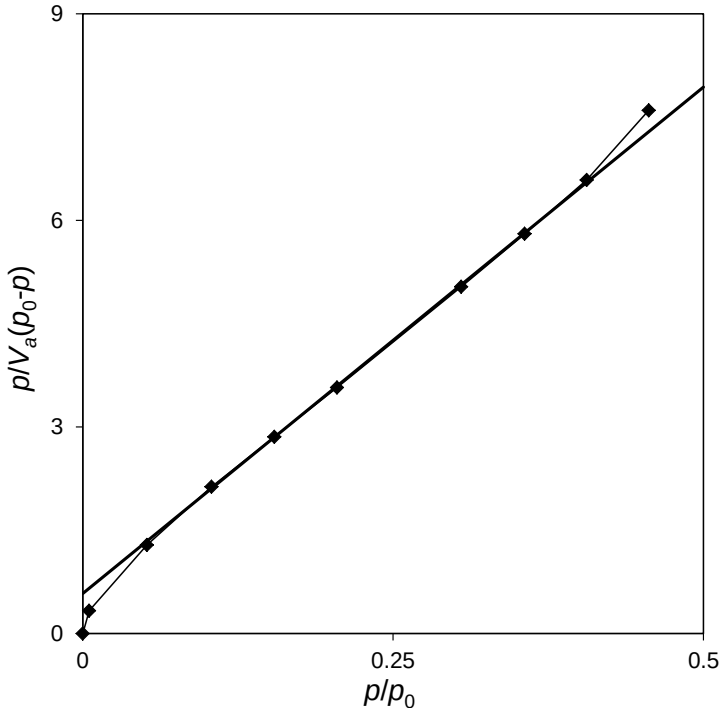

Figure 3.18: Fitting the tangent line (Bold line) to the BET curve using linear regression in the *Belsorp Mini II* software.

3.5.4 GRANULE POROSITY

The granule porosity was measured using mercury intrusion porosimetry. The instrument uses high pressure to drive the mercury into the sample pores and determine the sample density and porosity.

The sample placed under vacuum at room temperature (25°C) for at least four days to ensure the sample was thoroughly free of contaminant and moisture. The sample was measured in a 16 part glass penetrometer sample tube which has a calibrated volume of 3.9498mL. The sample was subject to pressures up to 65,000psia using both low and high pressure ports on the instrument in duplicate measurements.

Once the data was collected, the data was further analysed manually to calculate the granule porosity taking into account the granule internal pores only, using the pore size threshold between inter- and intra-granular pores to be 5µm (Shi *et al.*, 2011). The reason why the granule porosity needs to manually calculated from the porosimetry data is because during the low pressure test (0 to 33,000psia), the mercury penetrates into the interstitial pores (see Figure 3.19) between the granules to determine the bulk envelope volume. The absolute sample volume is then determined during the high pressure

(33,000psia to 65,000psia) test in which the mercury penetrates the internal pores of the sample (see Figure 3.19). Therefore from both the low and high pressure, the total volume of mercury filling the pores includes the interstitial and internal pores, which is then used to calculate the granule porosity. However, the volume of mercury filling the interstitial pores needs to be excluded so that the total volume of mercury filling the pores only takes into account the internal pores and hence the granule porosity can be more accurately measured. The calculations for the granule porosity from the mercury intrusion porosimetry data can be found in *Appendix: G: Mercury Intrusion Porosimetry Raw Data and Granule Porosity Calculations*.

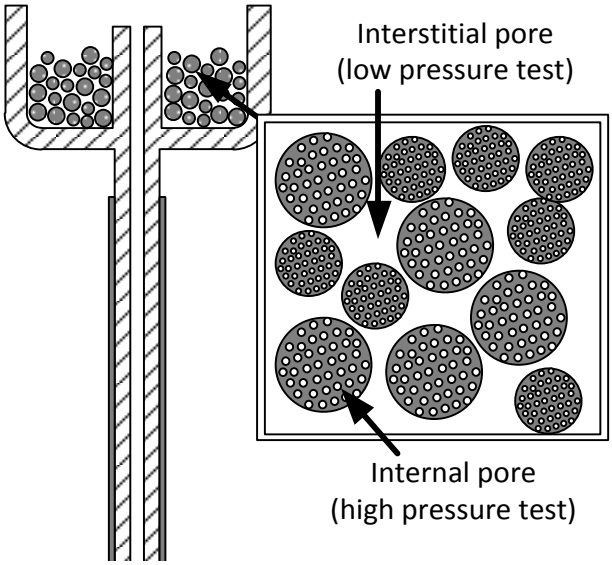

Figure 3.19: Schematic diagram of the interstitial and internal pore of powder samples in mercury intrusion porosimetry analysis.

3.5.5 GRANULE STRUCTURE IMAGING AND ANALYSIS

The granule structure was observed through a combination of optical microscopy (Motic Microscopes) and Scanning Electron Microscopy (SEM).

The external morphology of the granules was examined by taking Scanning Electron Microscopy (SEM, Phenom) imagining at 500× and 1000× magnification; and measuring the circularity of the granules through image analysis.

Based on the SEM images (Figure 3.20a), image analysis software *ImageJ* was used to adjust the threshold of each SEM image into a binary black and white image, and the colour inverted to capture as much of the projected area as possible (Figure 3.20b). The granule of interest was isolated from the surrounding image (Figure 3.20c) and the edge

of the granule was high-lighted (Figure 3.20d). Any white areas within the granule of interest were manually filled in to prevent any edges within the granule edge being high-lighted.

Once the image was modified, the imaging software was able to calculate the fractal number and circularity of the granules in the image. From the results, it was found that the circularity value reflected the granule projection area more accurately compared to the fractal number and therefore was used to measure the extent of rounding the granules (to see the fractal analysis of the granules, please refer to *Appendix E: Granule Sphericity and Porosity Characterisation Trial Experiments*). For each granule sample, ten granules were analysed for their circularity values to calculate the standard deviation of the mean. This is a statistically small sample given the size of the sample but additional SEM images were impractical.

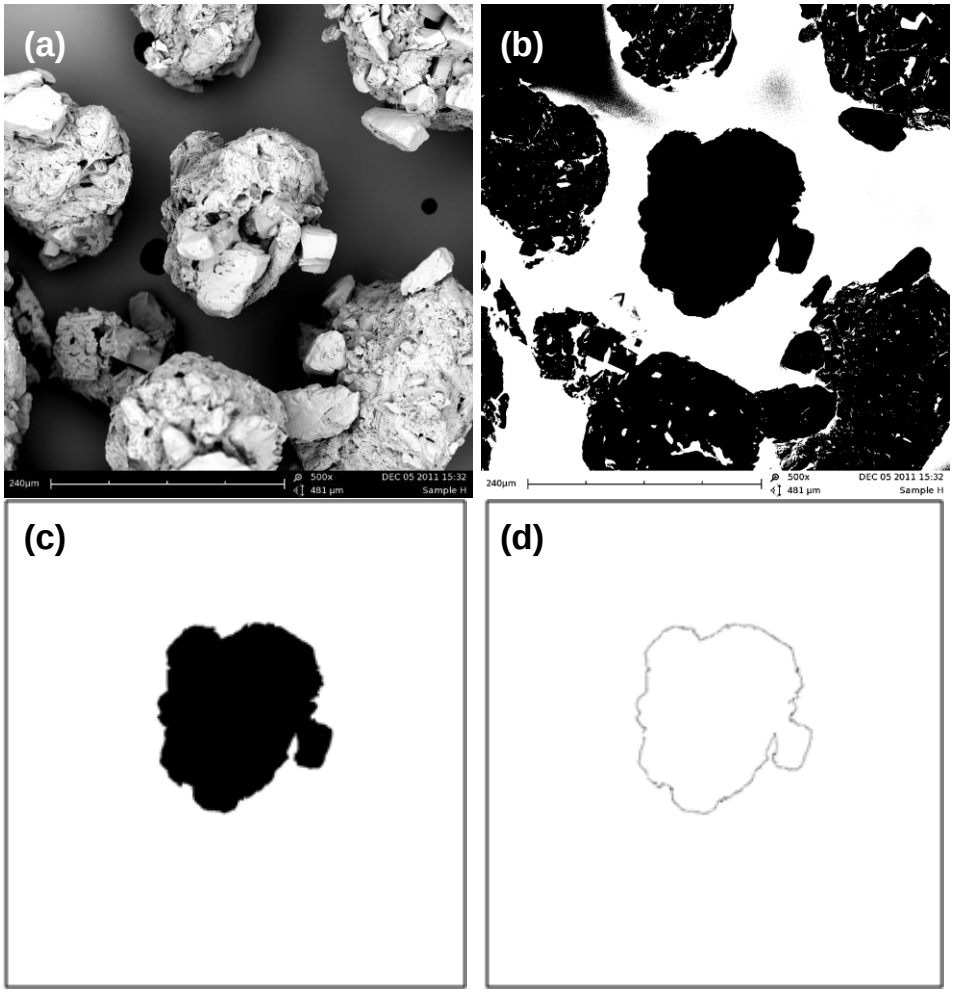

Figure 3.20: Refinement of SEM images to obtain the particle perimeter outline in preparation for circularity value analysis using *ImageJ*.

3.5.6 TABLET DIMENSIONS AND WEIGHT MEASUREMENTS

The tablet properties that were measured were the tablet height and the tablet weight. Tablets weighing 500mg were measured using an analytical balance with an error of ±1mg. The tablet height was measured using a digital calliper in which the tablet thickness varied depending on the compaction force applied to the sample. The tablet height varied between 0.55mm to 3.10mm depending on the sample and compaction force used. The tablet diameter was constrained by the width of the tablet die which was 13mm in diameter (see Figure 3.12 for an image of a typical tablet produced from the Carver tablet press).

3.5.7 TABLET HARDNESS AND TENSILE STRENGTH MEASUREMENTS

The tablet crushing force or "hardness" was measured using a tablet hardness tester (Dr. Schleuniger Pharmatron 6D model), as shown in Figure 3.21.

Figure 3.21: Dr. Schleuniger Pharmatron tablet hardness tester.

The tablet hardness tester measures the tablet strength by using a uni-axial force to compress the tablet until it fractures. Only the tablet strength from tablets that fractured into two separate pieces was recorded. Triplicate measurements were carried out for direct-compacted tablets while five measurements were carried out for wet granulated tablets. From the data collected, the tablet tensile strength was calculated (Equation 3.2) (Fell and Newton, 1970).

$$\sigma = \frac{2F}{\pi d t} \tag{3.2}$$

Where F is the crushing force ("hardness") of the tablet, d is the tablet diameter, and t is the tablet thickness. This equation is valid for the cylindrical, flat-faced tablets produced by the Carver tablet press.

4 Using the Unified Compaction Curve to Predict the Tablet Strength from the Wet Granulation Process

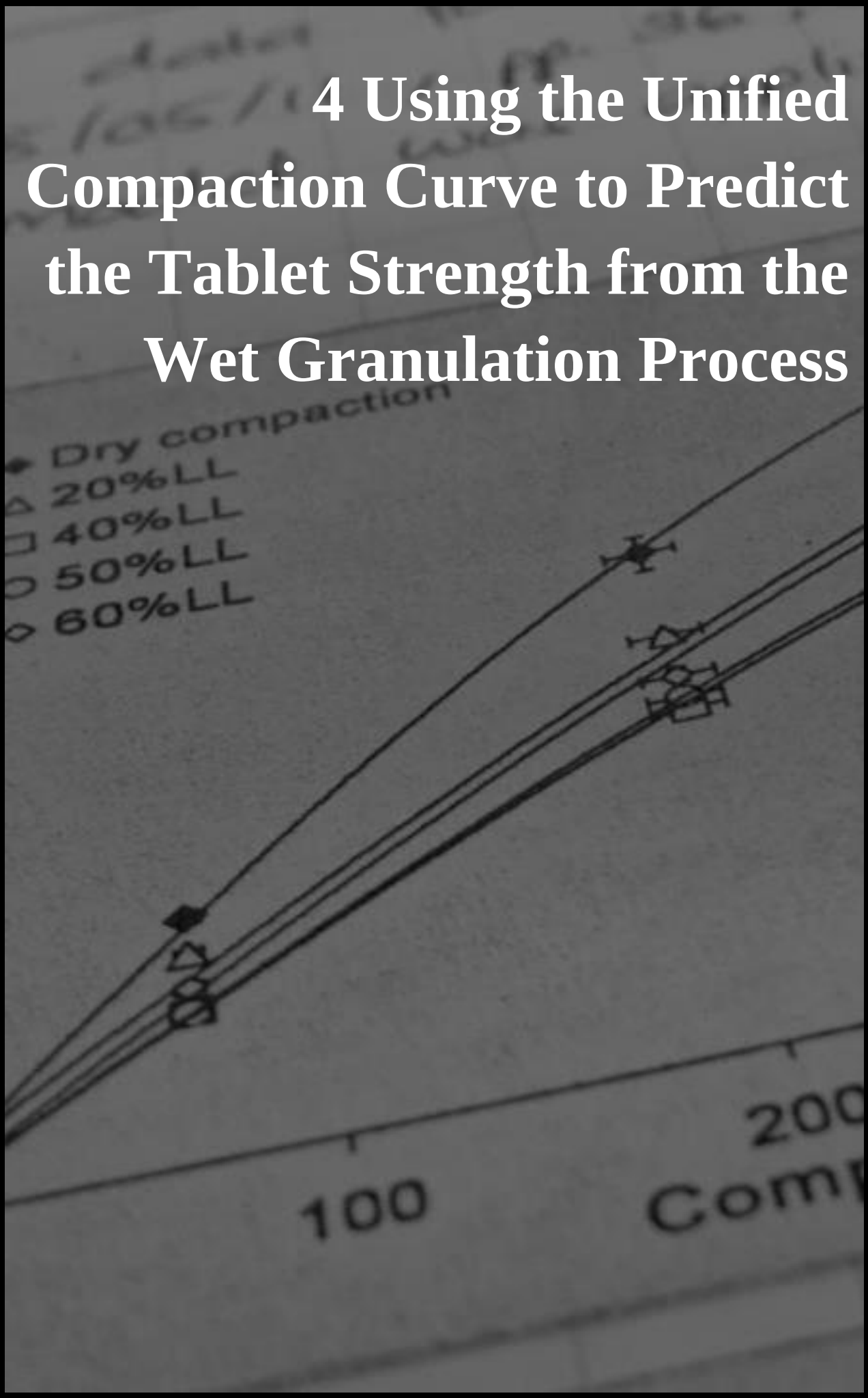

Monash University

Declaration for Thesis Chapter 4: Using the Unified Compaction Curve to Predict the Tablet Strength from the Wet Granulation Process

Declaration by candidate

In the case of Chapter 4, the nature and extent of my contribution to the work was the following:

Nature of contribution	**Extent of contribution (%)**
Experiment development, conducting experimental work, writing up of journal publication	100

The following co-authors contributed to the work. If co-authors are students at Monash University, the extent of their contribution in percentage terms must be stated:

Name	**Nature of contribution**	**Extent of contribution (%) for student co-authors only**
Not available, sole student author		

The undersigned hereby certify that the above declaration correctly reflects the nature and extent of the candidate's and co-authors' contributions to this work*.

Candidate's Signature		**Date**
Main Supervisor's Signature		**Date**

*Note: Where the responsible author is not the candidate's main supervisor, the main supervisor should consult with the responsible author to agree on the respective contributions of the authors.

4 USING THE UNIFIED COMPACTION CURVE TO PREDICT THE TABLET STRENGTH FROM THE WET GRANULATION PROCESS

"But words are things, and a small drop of ink, falling like dew, upon a thought, produces that, which makes thousands, perhaps millions, think..."
- Lord Byron, Poet -

4.1 INTRODUCTION

The studies on tablets show that wet granulation has a direct impact on the powder compaction behaviour and the tablet properties, such as the tablet strength (Bouwman *et al.*, 2005; Shi *et al.*, 2011; Shi *et al.*, 2011; Macias and Carvajal, 2012). The tablet strength must be able to withstand down-stream processing, such as coating, packaging and consumer handling during consumption of the tablet. In conjunction, the tablet must be able to break up within a reasonable amount of time during dissolution in the body after consumption of the tablet. It is remarkable that a simple structure of a tablet can hide the complex relationship between wet granulation and tabletting – looks can indeed be deceiving.

Despite tablet manufacturing being a common process in the pharmaceutical industry, the influence of the wet granulation conditions on the granule properties and the tablet strength is poorly understood, including:

- impeller speed
- granulator liquid level
- wet massing time
- binder flow rate.

Currently there are no mathematical models describing the relationship between wet granulation and the tablet strength which would enable the tablet strength to be predicted from the wet granulation operating conditions.

The Unified Compaction Curve has the potential to offer many benefits such as a basis for roller compaction scale-up and roller compaction design and troubleshooting. The roller compaction process is a *dry tabletting process*, in which powder is compacted into a ribbon and milled into granules before going through the tabletting stage, as schematically shown in Figure 4.1.

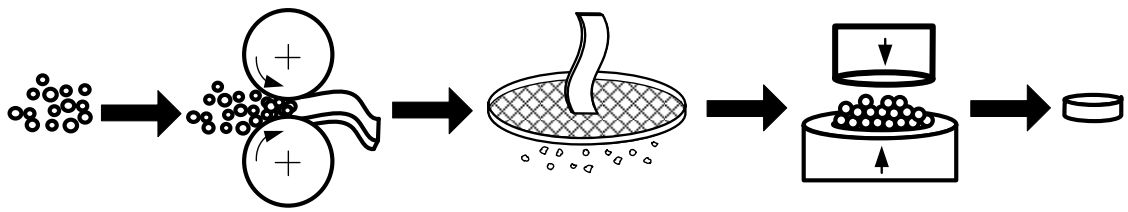

Figure 4.1: Schematic diagram of the roller compaction process.

The pressure from the roller compactor can be used to predict what roller compaction pressure is required to achieve a specified tensile strength. The P_{RC} and T_{RC} origins (see Figure 4.2) also demonstrate the reduction in tablet crushing strength as noted in previous studies (Bultmann, 2002, Freitag and Kleinebudde, 2003, Kochhar *et al.*, 1995). The benefits seen for roller compaction provide an incentive to adopt the Unified Compaction Curve and apply it to the wet granulation process for the first time. The "apparent compaction pressure" from the granulator impeller can be seen to be equivalent to the compaction pressure from the rollers. By investigating the role of the wet granulation condition(s), the compaction profiles for each granulation processing variable can be translated onto a direct compaction reference curve.

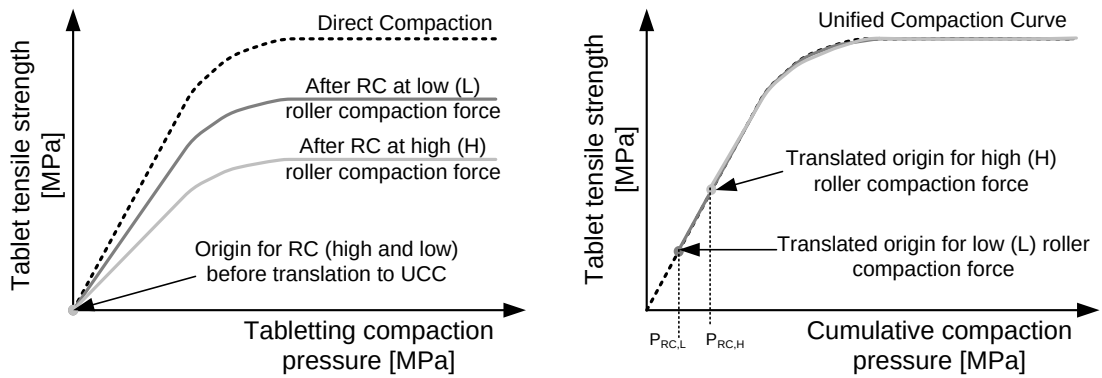

Figure 4.2: (left) Schematic diagram of the loss of tablet compactability after Roller Compaction (RC) at low (L) and high (H) roller compaction forces; and (right) the same data combined onto a Unified Compaction Curve (UCC). The translation in origin points for the UCC allows for the roller compaction pressure (P_{RC}) to be extrapolated from the data (adapted from Farber *et al.* 2008).

Therefore the Unified Compaction Curve provides an elegant model to quantitatively measure the amount of pressure applied to the powder and granules during wet granulation and visually see the relationship between the wet granulation conditions (liquid level, liquid binder flow rate, impeller speed and the wet massing time) and the final tablet strength. The information attained from the Unified Compaction Curve would be beneficial for tablet design, optimisation and troubleshooting in industry.

4.2 MATERIALS AND EXPERIMENTAL PROCEDURE

The formulation used in the wet granulation experiments was a 1:1 by weight binary powder mixture of microcrystalline cellulose (denoted as MCC, Avicel PH-101, FMC BioPolymer) and lactose monohydrate 200 mesh (denoted as L2M, Pharmatose 200M, DMV-Fonterra). The powders were used in their original form from the suppliers.

Two types of placebo tablets were produced: (1) direct-compacted tablets; and (2) wet-granulated tablets. As illustrated in Figure 4.3a below, in direct compaction, the original powder mixture was fed directly into the tablet press and compacted into a tablet. While for wet-granulated tablets (Figure 4.3b), the powder mixture goes through an intermediate stage of wet granulation in a 5L high-shear granulator (KG5, International Key) to produce granules prior to tabletting. For details of the high-shear granulator including geometry and operating specifications, please refer to *Section 3.3: Wet Granulation Experiments*.

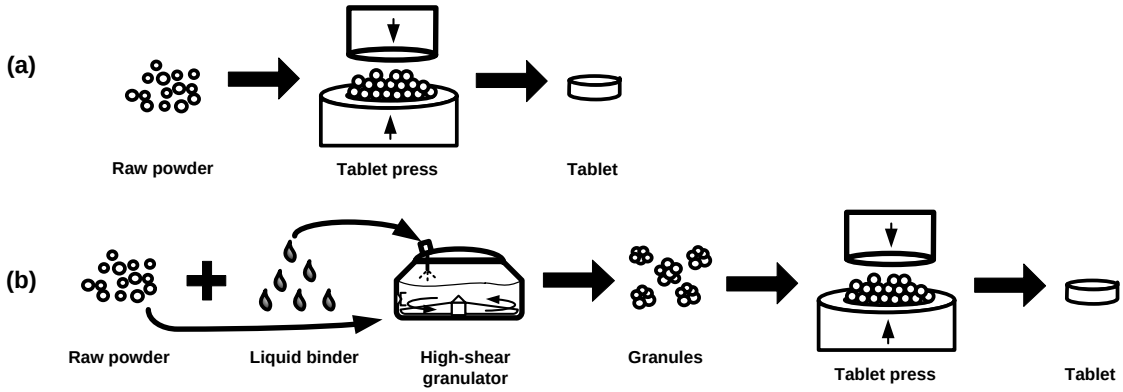

Figure 4.3: Schematic diagram of (a) tablet produced from direct compaction; and (b) tablet produced from wet granulation.

The liquid binder used to agglomerate the powder was a solution of 5w/v% polyvinyl pyrrolidone (denoted as PVP, K90, Sigma-Aldrich) which was delivered to the granulator as atomised droplets via a spray nozzle (Spraying systems: SS650017 to give 130g/min; and SS650050 to give 280g/min). The spray nozzle was connected to a liquid reservoir in 5L spray pot (Spraying systems). Prior to granulation, a 1 kg batch of primary powder mixture was pre-mixed in the granulator for at least 1 minute (at a minimum impeller speed of 250rpm to ensure the powder was well-mixed with a roping-regime mixing pattern (Iveson and Litster, 1998)). The liquid binder was sprayed for at least 30 seconds, external to the granulator, to ensure that the spray flow rate was at steady state before placing the spray nozzle into the granulator. The operating conditions were varied to see

the resulting effect on the final tablet strength; however the minimum wet massing time was 10 seconds to ensure that the liquid added to the granulator was well dispersed in the powder mass.

The wet granulation variables which were investigated included:

- Granulator liquid level (LL) 20wt.%, 30wt.%, 40wt.% and 50wt.%. A wet granulation experiment using 60wt.% liquid level was conducted, however the granules were found to be over-saturated with coarse granules produced. The results can be seen in *Appendix B: Tablet Dimension and Strength Raw Data*,
- Wet massing time (WMT) 0, 2, 6 and 10 minutes for all liquid levels. Where the granulator liquid level was the primary variable of interest, a wet massing time of 10 seconds was performed to ensure uniform dispersion of the liquid in the powder mass,
- Low (130g/min) and high (280g/min) liquid binder flow rate which corresponds to a spray time for a given granulation liquid level as described in Table 4.1,

Table 4.1: The granulation spray times for varying granulation liquid levels.

Granulation Liquid Level [%]	Liquid Binder Spray Time [mins; secs]	
	Low spray rate (130g/min)	High spray rate (280g/min)
20	1 min; 32 secs	45 secs
30	1 min; 10 secs	1 min; 3 secs
40	1 mins; 39 secs	1 min; 17 secs
50	2 mins; 3 secs	1 min; 29 secs

- Impeller speed (150rpm, 285rpm and 600rpm). The three impeller speeds used in these experiments reflect the different mixing regimes: bumping (150rpm); and roping (285rpm and 600rpm) (Iveson and Litster, 1998).

For the wet granulation experiments, different combinations of experimental conditions were investigated to see the effect of the processing “apparent compaction pressure” (this will be conveyed as the “compaction pressure” throughout this thesis). The processing compaction pressure is the equivalent compaction pressure exerted on the granules from the impeller from various impeller speeds, binder flow rate and granulator liquid levels and granulation time, on the tablet strength, as summarised in Table 4.2 to Table 4.4.

Table 4.2: Wet granulation experiments involving Liquid Level (LL), Wet Massing Time (WMT), and binder flow rate at an impeller speed of 150rpm.

LL / WMT	20wt.%		30wt.%		40wt.%		50wt.%	
	130g/min	280g/min	130g/min	280g/min	130g/min	280g/min	130g/min	280g/min
10 seconds	✓	✓	✓	✓	✓	✓	✓	✓
0 minutes			✓					
2 minutes			✓					
6 minutes			✓					
10 minutes			✓					

Table 4.3: Wet granulation experiments involving Liquid Level (LL), Wet Massing Time (WMT), and binder flow rate at an impeller speed of 285rpm.

LL / WMT	20wt.%		30wt.%		40wt.%		50wt.%	
	130g/min	280g/min	130g/min	280g/min	130g/min	280g/min	130g/min	280g/min
10 seconds	✓	✓	✓	✓	✓	✓	✓	✓
0 minutes	✓	✓	✓	✓	✓	✓	✓	✓
2 minutes	✓	✓	✓	✓	✓	✓	✓	✓
6 minutes	✓	✓	✓	✓	✓	✓	✓	✓
10 minutes	✓	✓	✓	✓	✓	✓	✓	✓

Table 4.4: Wet granulation experiments involving Liquid Level (LL), Wet Massing Time (WMT), and binder flow rate at an impeller speed of 600rpm.

LL / WMT	20wt.%		30wt.%		40wt.%		50wt.%	
	130g/min	280g/min	130g/min	280g/min	130g/min	280g/min	130g/min	280g/min
10 seconds	✓	✓	✓	✓	✓	✓	✓	✓
0 minutes			✓					
2 minutes			✓					
6 minutes			✓					
10 minutes			✓					

Approximately 30-50g of sample (on dry basis) was withdrawn at each time point. The amount of liquid to the granulator to reach the next liquid level was determined via a mass balance on the liquid and powder remaining in the granulator (details can be found in *Appendix A: Mass balance calculations for granulation experiments*).

The granules produced from the wet granulation experiments were dried on shallow oven trays in a fan-forced oven at 60°C overnight before conducting tabletting experiments. The minimum drying period for the granules is 10 hours to ensure that the granules are completely dried before tabletting.

For both direct-compacted and wet-granulated tablets, the tablets were compacted in a hydraulic single-station tablet press (Model 3887, Carver Inc. USA) to produce 500mg

tablets. The tablets were weighed with an error of ±1mg. The tablets produced are large compared to pharmaceutical tablets in which the tablet thickness ranged from 0.55mm to 3.10mm, while the tablet diameter was kept constant at 13mm.

The compaction force applied by the tablet press to produce the tablets range between 1000lb_f to 16,000lb_f (453.6kg_f to 7257.5kg_f). For each granulation batch, the entire granule size distribution, with the average equivalent granule diameter (d_{50}) ranging from 50μm to 425μm was compacted. The tablet press was set up to minimise the compaction time by setting the compression and decompression rates at the fastest available setting with the dwell time set to zero seconds. Despite these settings, the compression/decompression cycle took 1-2 minutes to complete per tablet which, comparing to the typical total time from an industrial tablet press of milliseconds, is very much longer than used in industry. This results in a tablet with high tablet hardness ranging between 25-45kPa. For details about the tablet press, please refer to *Section 3.4: Tabletting Experiments*.

The tablet properties measured were the tablet height, measured by a digital calliper, and the tablet crushing force or "hardness" using a tablet hardness tester (Dr. Schleuniger Pharmatron 6D model, please refer to *Section 3.5.7: Tablet Hardness and Tensile Strength* for more details). Triplicate measurements were carried out for direct-compacted tablets while five measurements were carried out for wet granulated tablets. The physical tablet dimensions were 13mm in diameter and the tablet thickness ranged from 2.54mm for the highest compaction force (16,000lb_f) to 3.15mm for the lowest compaction force (1,000lb_f). From the data collected, the tablet tensile strength was calculated (Equation 4.2) (Fell and Newton, 1970).

$$\sigma = \frac{2F}{\pi d t} \tag{4.2}$$

where F is the crushing force ("tablet hardness") of the tablet, d is the tablet diameter, and t is the tablet thickness.

4.3 ADAPTING THE UNIFIED COMPACTION CURVE FOR WET GRANULATION

4.3.1 THEORY

The Unified Compaction Curve from the roller compaction studies in Farber *et al.*'s work (2008) was adapted to wet granulation to see the compaction pressure from the granulator

impeller on the powder and granules during wet granulation. In Farber *et al.*'s work, the amount of pressure applied by the rollers to form a ribbon by the rollers was the driving force for the Unified Compaction Curve model. The roller compaction pressure was considered to irreversibly deform the powder prior to tabletting, and therefore the resulting granules from the milling process were not able to be compacted to the full extent that would have been possible for unprocessed powder.

The Unified Compaction Curve was adopted for wet granulation. During wet granulation, the impact of the granulator impeller on the powder and granules induces irreversible deformations which expend part of the final tablet strength. The impeller compaction pressure (which is usually unknown) that becomes the main driving force behind the Unified Compaction Curve model. The equivalent amount of compaction pressure from the granulation impeller impact on the powder and granules during wet granulation is defined as P_{WGC}, while the equivalent amount of tensile strength generated in the granules from wet granulation is defined as T_{WGC}.

In the Unified Compaction Curve model, the compaction profiles from different processing conditions are unified onto a single curve by translating the profiles along the 'unprocessed' master compaction profile. The master curve originates from the direct compaction of the unprocessed powder to determine the maximum tablet strength of the formulation for a range of compaction pressures. The direct compaction curve can be described by an empirical model developed by Leuenberger (1982):

$$T = T_{\max}\left(1 - e^{-bP}\right) \tag{4.3}$$

where T is the tablet tensile strength for a given compaction pressure, T_{max} is the maximum tablet strength for unprocessed powder, b represents the product of γ - a material-related constant representing the measure of compactability, and ρ - the ratio of the tablet density to the theoretical tablet density, and P is the maximum compaction pressure that can be exerted on a powder formulation which is usually the pressure applied in direct compaction tabletting (Leuenberger, 1982; Farber *et al.*, 2008). For simplicity the $\gamma\rho$ constant group was represented by constant b ($b = \gamma\rho$).

During wet granulation, some (unknown) compaction pressure is applied to the granules during agitation. We define this as "P_{WGC}" or the effective wet granulation pressure. At

P_{WGC}, the equivalent granule tensile strength, T_{WGC}, is related to the effective wet granulation compaction pressure P_{WGC} (Equation 4.4):

$$T_{WGC} = T_{\max}\left(1 - e^{-bP_{WGC}}\right) \tag{4.4}$$

Since the compaction pressure imparted on the granules and powder during wet granulation is irreversible, the resulting tablet strength will decrease from the strength attained from the compaction of unprocessed powder. This can be represented as:

$$T' = T - T_{WGC} \tag{4.5}$$

where T' is the tablet tensile strength produced after wet granulation. The tabletting pressure P' is the difference between the total cumulative compaction pressure (during granulation and compaction), and the effective wet granulation compaction pressure P_{WGC} (Equation 4.6):

$$P' = P - P_{WGC} \tag{4.6}$$

where P_{WGC} is the compaction pressure induced on the powder by the granulator impeller. By substituting Equations 4.3, 4.4 and 4.6 into Equation 4.5 and simplifying, the Unified Compaction Curve model can be derived to obtain the final tablet strength (Equation 4.7). A full derivation of the Unified Compaction Curve model for wet granulation can be found in *Appendix A: Derivation of the Unified Compaction Curve Model for Wet Granulation*.

$$T = T_{WGC} + T_{\max}\left(e^{-bP_{WGC}} - e^{-b(P'+P_{WGC})}\right) \tag{4.7}$$

where T is the final tablet strength, P' is the compaction pressure in the tablet press, T_{max} is the maximum tablet tensile strength that can be obtained by the formulation without any other compaction to the powder during the process (i.e. direct compaction) and b is the material-dependent exponent parameter that is a function of the tablet relative density and the compactability of the formulation. From Equation 4.7, it can be seen that the Unified Compaction Curve represents the sum of the granule tensile strength from the wet granulation process (T_{WGC}) and the tablet tensile strength ($T_{\max}\left(e^{-bP_{WGC}} - e^{-b(P'+P_{WGC})}\right)$).

The Unified Compaction Curve model would enable the prediction of the tablet strength for a given set of wet granulation conditions including the liquid level, wet massing time, impeller speed or the binder flow rate. The translation of the compaction curves along the reference curve would give a measure of the compaction pressure imparted on the powder and granules during wet granulation. This would serve to be a powerful prediction tool

for the pharmaceutical industry in designing and troubleshooting the tablet manufacturing process.

4.3.2 MODELLING THE UNIFIED COMPACTION CURVE MODEL IN WET GRANULATION

The procedure of constructing the Unified Compaction Curve for the wet granulation process involves creating a direct compaction backbone curve and allowing the compaction profiles for tablets produced from various wet granulation conditions to be collapsed onto the backbone curve. The Unified Compaction Curve is modelled in a similar manner to that modelled in roller compaction (Farber *et al.*, 2008) and will be demonstrated in the following section.

4.3.2.1 CONSTRUCTION OF THE DIRECT COMPACTION MASTER/REFERENCE CURVE

The reference curve for the Unified Compaction Curve was created by performing direct compaction tabletting at compaction forces varying from 1000lb_f (453.6kg_f) to 16,000lb_f (7257.5kg_f). By plotting the relationship between the tablet tensile strength and the compaction pressure, the compaction profile for the powder formulation was created. The data in the compaction profile is representative of 3 measurements with the *x*-axis error bars representing ±5% of the tabletting compaction pressure while the *y*-axis error bars represent the standard error of the mean. The direct compaction data representing the tablet strength as a function of the tabletting compaction pressure is shown in Figure 4.4.

To create the direct compaction reference curve, a model representing the compactibility of pharmaceutical powder (Equation 4.1), developed by Leuenberger (1982), was fitted to the compaction data using the Least Sum of the Errors Squared (LSES) in a conventional spread-sheet software using the "*goal-seek*" function. The LSES helps to minimise the error between the experimental and the theoretical (calculated) values.

$$LSES = \sum_{1}^{i} \left(Exp_i - Calc_i \right)^2 \tag{4.8}$$

The compactibility model was fitted to the direct compaction curve to determine T_{max} and *b* (Farber *et al.*, 2008), and is represented by the bold line in Figure 4.4.

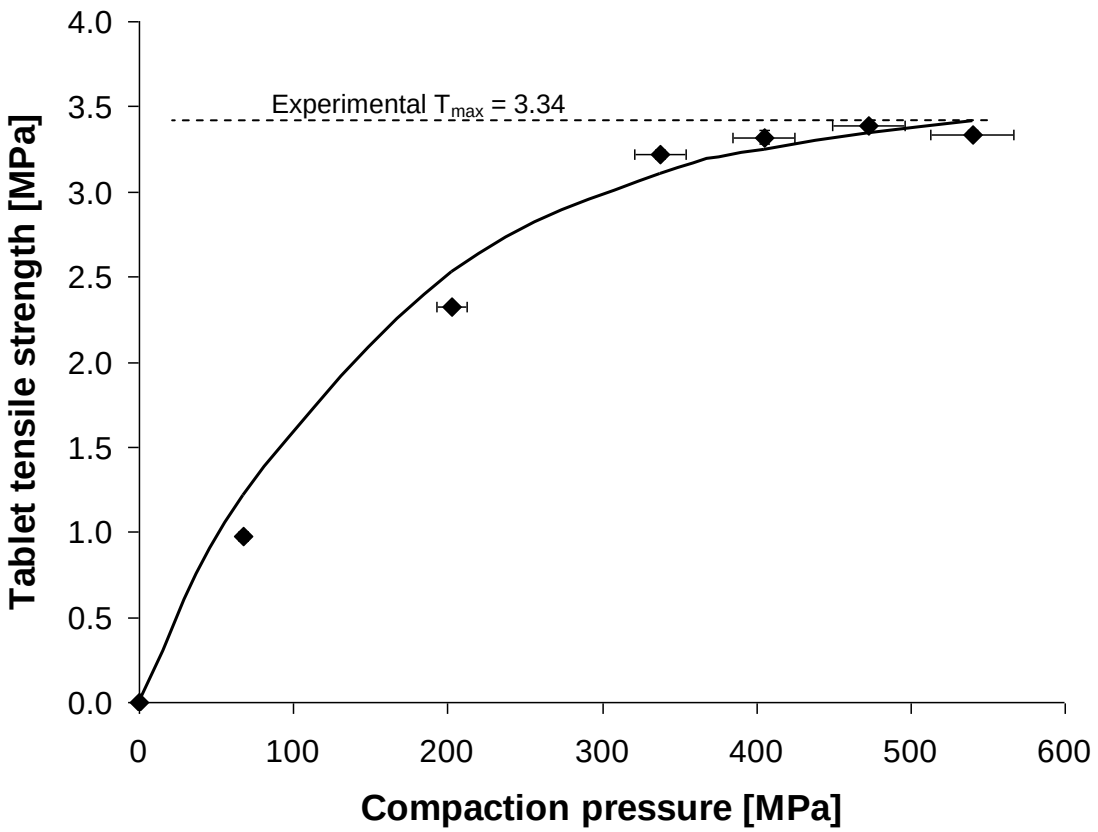

Figure 4.4: Compaction profile of tablets produced from direct compaction for 1:1 microcrystalline cellulose:lactose 200mesh formulation with an experimental maximum tablet tensile strength of 3.34MPa.

Data fitting was carried out by calculating the theoretical value of the tensile strength T_{max} from the compactibility model and using the LSES. The iterative calculations to fit the data involved estimating starting values of T_{max} and b. These values were chosen such that the calculated tensile strength was within ±5% of the experimental tensile strength. The iterative data-fitting calculations were carried out in a conventional spread-sheet, forming columns for the compaction pressure, the experimental tensile strength, the calculated tensile strength and the LSES (See Figure 4.5). The "*goal-seek*" function, in the spread-sheet software, was then used to set the LSES to be as close to zero as possible by varying first the b constant, then T_{max} (with b being the fitted value). An example of the data fitting calculations is shown in Figure 4.5.

	A	B	C	D
1	T_{max} [MPa] =	3.54	P_{WGC} [MPa] =	N/A
2	b [-] =	0.0062	T_{WGC} [MPa] =	N/A
3				
4	Direct compaction *Used Eqn(1) for Calculated TS*			
5	Compaction pressure [MPa]	Experimental TS [MPa]	Calculated TS [MPa]	$(Exp.-Calc.)^2$
6	67.50	0.98	1.21	0.05
7	202.51	2.32	2.53	0.04
8	337.51	3.22	3.10	0.01
9	405.01	3.32	3.25	0.00
10	472.52	3.39	3.35	0.00
11	540.02	3.34	3.41	0.01
12			Sum of error =	0.069

Figure 4.5: An example of the calculations to data fit Leuenberger's model of compactability and compressibility (1982) to the experimental dry compaction tensile strength (TS) data with consistent theoretical tablet density.

When the values of T_{max} and b were determined, the compactibility and compressibility model (Leuenberger, 1982) was calculated to extend the curve to higher compaction pressures and accommodate the translated compaction pressures for the fitted wet granulation Unified Compaction Curves, as shown in Figure 4.6.

	A	B	C	D
1	T_{max} [MPa] =	3.54	P_{WGC} [MPa] =	N/A
2	b [MPa] =	0.0062	T_{WGC} [MPa] =	N/A
3				
4	Direct compaction *Used Eqn(1) for Calculated TS*			
5	Compaction pressure [MPa]	Experimental TS [MPa]	Calculated TS [MPa]	$(Exp.-Calc.)^2$
6	0	0.00	0.00	0.00
7	67.50	0.98	1.21	0.05
8	202.51	2.32	2.53	0.04
9	337.51	3.22	3.10	0.01
10	405.01	3.32	3.25	0.00
11	472.52	3.39	3.35	0.00
12	540.02	3.34	3.41	0.01
13	550.00	N/A	3.42	N/A
14	600.00	N/A	3.45	N/A
15	700.00	N/A	3.49	N/A
16	800.00	N/A	3.51	N/A
17	900.00	N/A	3.52	N/A
18			Sum of error =	0.123

Figure 4.6: An example of the calculations required to generate the dry compaction curve for the Unified Compaction Curve.

The values of T_{max} and b were kept constant for a given formulation and hence T_{max} = 3.54 and b = 0.0062 were kept constant throughout the rest of the project and thesis. For a new type of formulation, the values of T_{max} and b would need to be recalculated.

The direct compaction curve forms the "reference master curve" for the Unified Compaction Curve and represents the theoretical tablet strength as a function of the cumulative compaction pressure (Farber *et al.*, 2008).

4.3.2.2 MODELLING THE WET GRANULATION COMPACTION DATA

To translate the wet granulation compaction curves onto the direct compaction reference curve, the data-points for the wet granulation samples were fitted to the compactibility model in Equation 4.3. An example of fitting 30% liquid level, 10 minutes wet massing time data to the Unified Compaction Curve is presented below. To achieve this, the tablet tensile strength was measured for tablets produced at varying compaction pressures, *P'*, (Figure 4.7) after the production and drying of the granules.

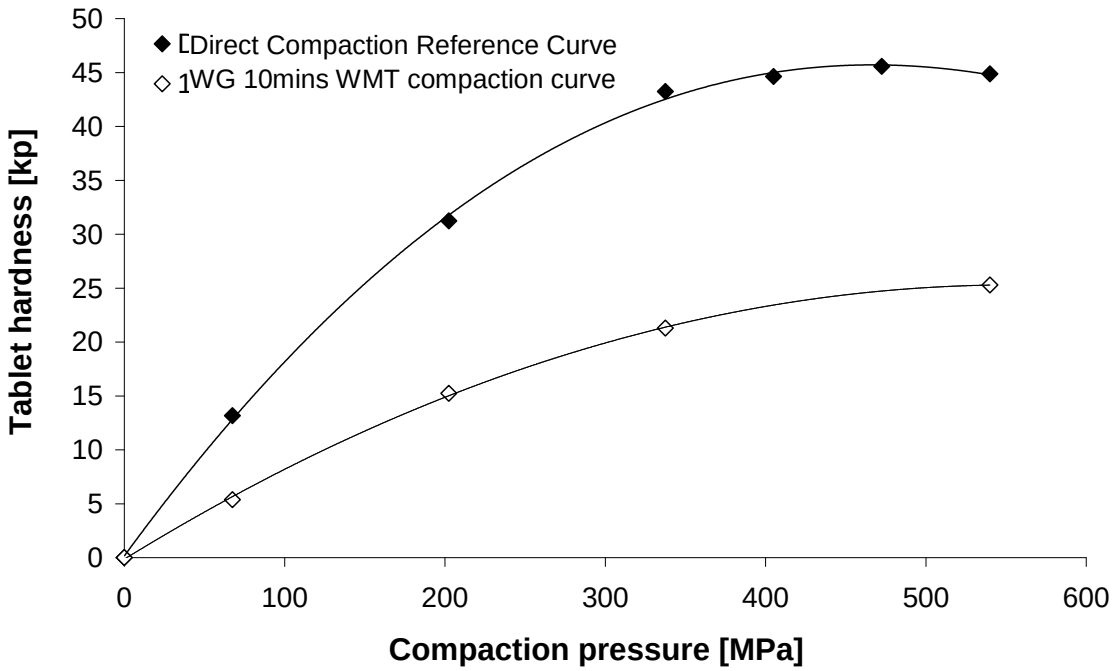

Figure 4.7: Compaction profile of tablets produced from wet granulation at 20wt% liquid level (LL) for 1:1 MCC:L2M formulation.

The values of T_{max} and b were already determined from the data fitting of the dry compaction data, carried out earlier. The wet granulation tablet data is fitted to the reference curve by adjusting the P_{WGC} value only. The T_{WGC} value is then calculated from the P_{WGC} from Equation 4.4.

The tabletting Unified Compaction Curve is generated for the wet granulation liquid level conditions using the P_{WGC}, T_{max} and b parameters determined earlier (column C, rows 6-12 of Figure 4.8). To translate the compaction curves for the Unified Compaction Curve, the P_{WGC} parameter is added to the experimental compaction pressure (P_{WGC} + data in column A, rows 6-10 of Figure 4.8) while T_{WGC} is added to the experimental tensile strength data (T_{WGC} + data in column B, rows 6-10 of Figure 4.8) (Farber *et al.*, 2008). This translates the wet granulation tablet data onto the direct compaction master curve,

using only a single fitting parameter, P_{WGC}. The same series of calculations and data fitting were carried out for all granulator liquid levels and wet massing times investigated in the study.

	A	B	C	D	E	F
1	T_{max} [MPa] =	3.54	P_{WGC} [MPa] =	108.68		
2	b [-] =	0.0062	T_{WGC} [MPa] =	1.74		
3						
4	10 mins WMT					
5	Compaction pressure [MPa]	Experimental TS [MPa]	Calculated TS [MPa]	$(Exp.-Calc.)^2$	P' [MPa]	TS [MPa]
6	0	0.00	0.00	0.00	108.68	1.74
7	67.50	0.40	0.62	0.05	176.18	2.14
8	202.51	1.13	1.29	0.02	311.18	2.87
9	337.51	1.55	1.58	0.00	446.19	3.29
10	540.02	1.97	1.74	0.06	648.69	3.71
11			Sum of error =	0.13		

Figure 4.8: An example of the calculations required to generate the Unified Compaction Curve.

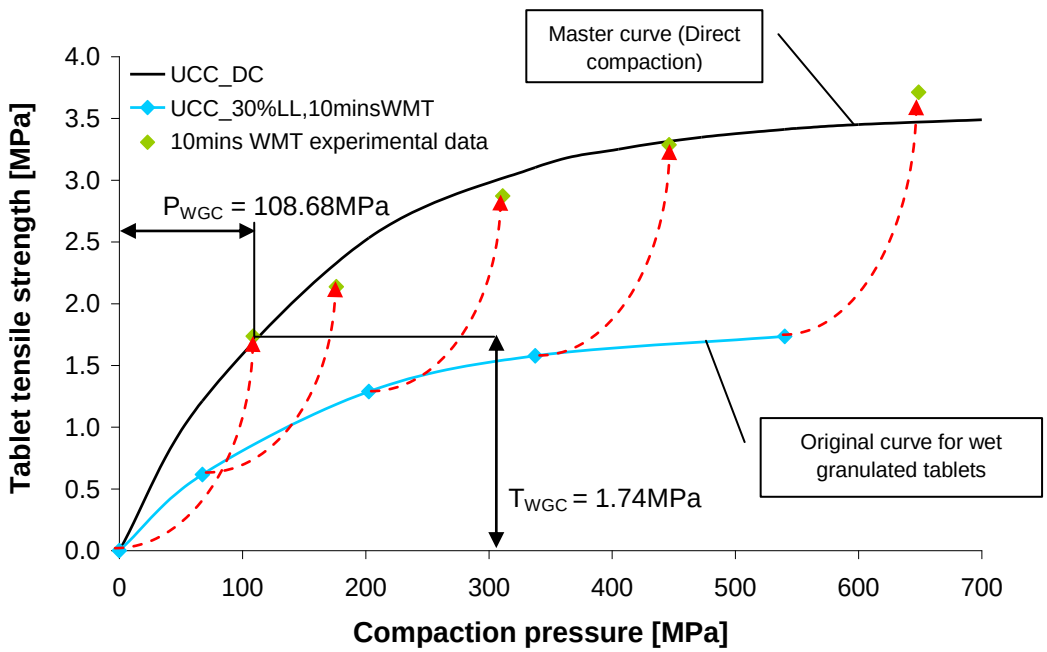

Figure 4.9: Application of the Unified Compaction Curve for wet granulated tablets at 30wt% liquid level, 10 minutes wet massing time for 1:1 MCC:L2M formulation. The blue curve represents the tabletting portion of the Unified Compaction Curve, while the green data points represent the translated Unified Compaction Curve. The blue curve is translated to the new origin of P_{WGC}, T_{WGC}.

4.4 RESULTS

The wet granulation conditions have been shown to significantly impact the compactability behaviour of the granules during tabletting as seen from Shi *et al.*'s study (Shi *et al.*, 2011; Shi *et al.*, 2011). The extent of granule compactability decreases as either the liquid level and/or wet massing time increases. This is supported by results present in this section in which the longer the powder and granules are subjected to the compaction forces from the granulator impeller from an increase in the liquid level, wet

massing time or impeller speed, the greater the decrease in the granule compactability ability and the tablet strength. The standard analysis of the granule size distribution and tablet compaction profile are presented first before the results are reanalysed using the Unified Compaction Curve to translate the data onto a single master curve.

4.4.1 EFFECT OF LIQUID LEVEL AND WET MASSING TIME ON GRANULE SIZE DISTRIBUTION

The liquid level and the wet massing time would be expected to influence the saturation of the granules required for granule growth and hence have profound effects on the granule size distribution as seen in Figure 4.10 to Figure 4.13.

The liquid level has a significant effect on the granule growth as presented in Figure 4.10. As the liquid level increases from 20wt.% to 50wt.%, the granule size distribution gradually becomes larger and shifts towards the coarse end of the granule size axis. As expected, at higher liquid levels, the granule is more saturated with liquid binder which allows a greater extent of agglomeration and granule growth to occur.

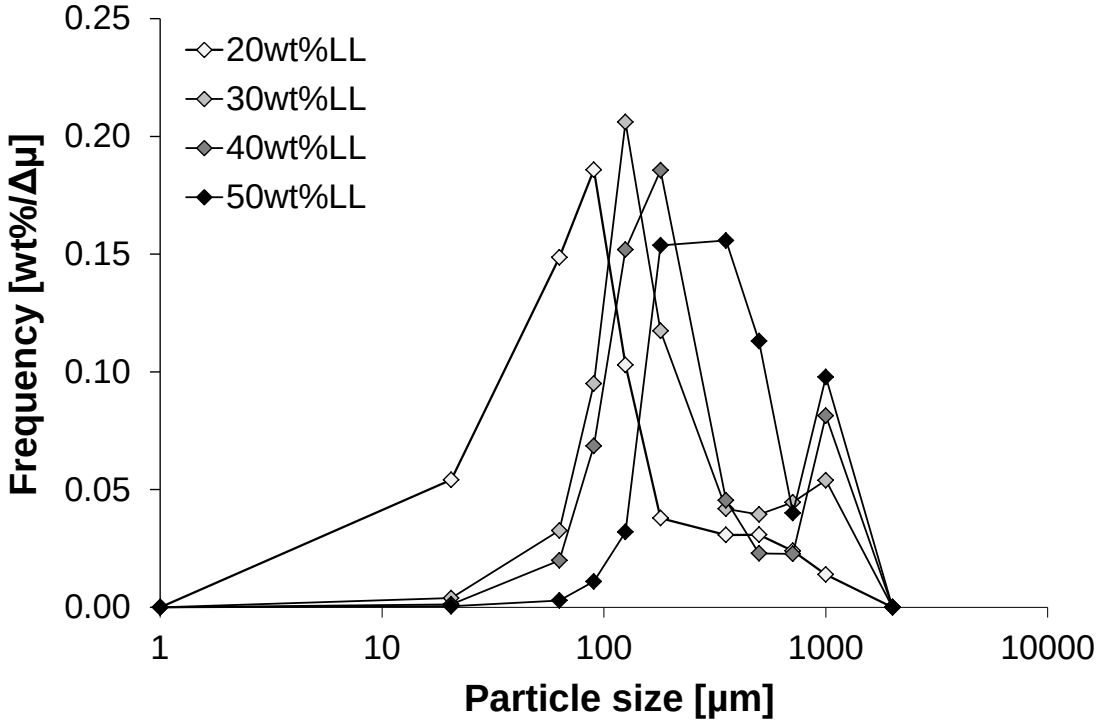

Figure 4.10: Granule size distribution plots for varying liquid level quantities: (a) 20wt.%; (b) 30wt.%; (c) 40wt.%; and (d) 50wt.%. The granulation experiments are based on an impeller speed of 285rpm and 10 seconds wet massing time.

The relationship between the granule size and the resulting tablet strength is presented in Figure 4.11. For given set of conditions, as the granules become larger in size, the tablet

hardness decreases. However, when different granulation batches are compared across different flow-rates and impeller speeds, the granule size appears to be independent to the tablet strength. For example, granulation batches resulting in an average d_{50} size of 150μm can have a tablet hardness ranging between 17-27kP, depending on the combination of the liquid level, liquid flow rate and impeller speed. This data illustrates the current lack of clarity about the relationship between the wet granulation process conditions and tablet strength.

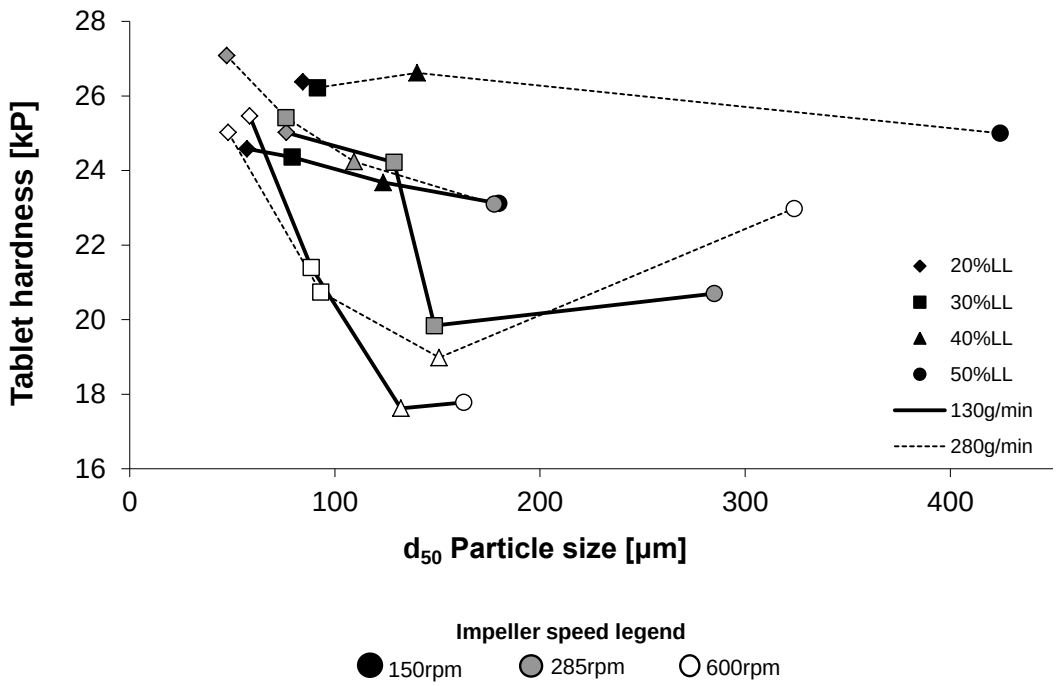

Figure 4.11: Relationship between the d_{50} particle size and the tablet hardness as a function of liquid level, binder flow rate and impeller speed. Wet massing time is 10 seconds.

The wet massing time also affects the granule size distribution as portrayed in Figure 4.12. For liquid levels 30wt.% and above, as the wet massing time increases towards 10 minutes, the granule size distribution shifts towards the right denoting the production of coarse granules. For the 20wt.% liquid level granulation batch, the granule size distribution does not vary much regardless of the wet massing time. The results presented demonstrate the importance of both the granule liquid saturation and the consolidation stage in wet granulation for determining the granule growth and find the granule size distribution.

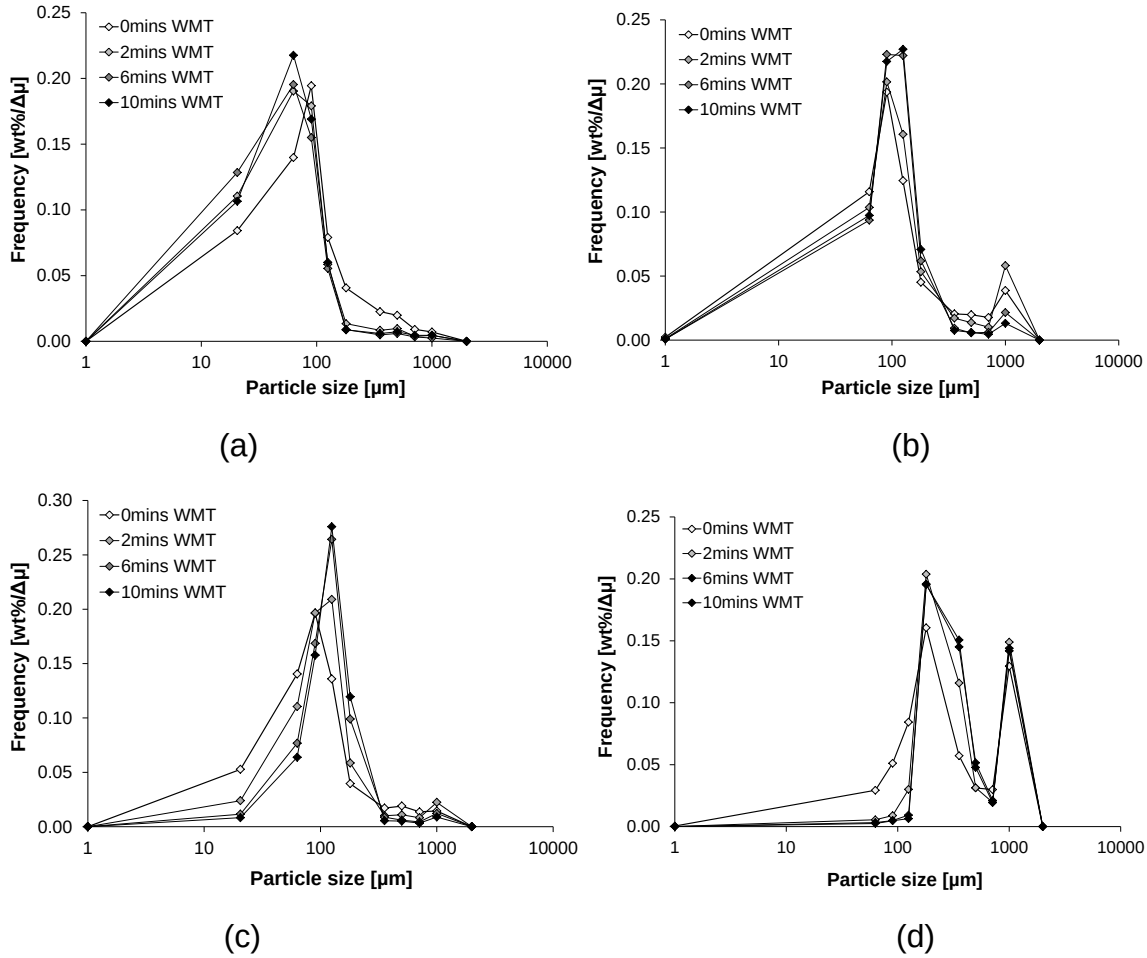

Figure 4.12: Granule size distribution plots for varying wet massing time at: (a) 20wt.%; (b) 30wt.%; (c) 40wt.%; and (d) 50wt.% liquid level. The granulation experiments are based on an impeller speed of 285rpm.

The average granule size, d_{50}, has no significant effect on the tablet hardness overall as shown in Figure 4.13. However the wet massing time appears to significantly affect the tablet hardness instead. The deterioration in the tablet hardness is more pronounced at higher impeller speeds, which can be seen by the tablet hardness beginning at approximately 20kPa (0 minutes wet massing time, 600rpm) and decreasing to 11kPa (at 10 minutes wet massing time, 600rpm), compared to the tablet hardness starting in between 26-27kPa for 150rpm and 285rpm impeller speeds. However the liquid level also plays a significant role in the decrease of the tablet hardness with increasing wet massing time, in which at a low liquid level of 20%, there is a 4kPa decrease in the tablet hardness, compared to 40% liquid level, which has a tablet hardness decrease of 15kPa.

For a given narrow d_{50} granule size range of 77-100μm, the tablet hardness varies from 11-27kP with the tablet hardness decreasing rapidly with longer periods of wet massing.

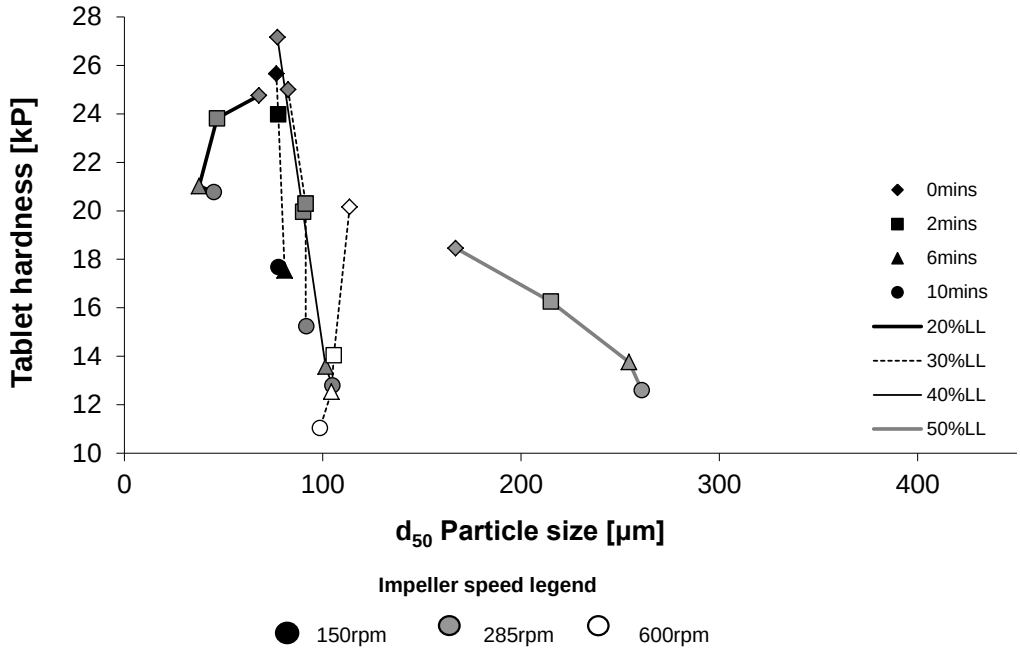

Figure 4.13: Relationship between the d_{50} particle size and the tablet hardness as a function of wet massing time, liquid level, binder flow rate and impeller speed.

4.4.2 EFFECT OF LIQUID LEVEL ON TABLET STRENGTH

The effect of the liquid level on the tablet strength in the 'tablettability' profile is shown in Figure 4.14. The tablet hardness as a function of the compaction pressure is plotted with varying liquid levels (20wt.% - 50wt.%), liquid binder flow rate (high: 280g/min; and low: 130g/min) and impeller speeds (150, 285 and 600rpm). Each data point contains results from five tablets with the *x*-error bars representing the ±5% of the compaction pressure and the *y*-error bars representing the error of the mean for five samples.

Figure 4.14, shows the direct compaction curve master curves, compared to the compaction data for wet granulation samples. Wet granulation appears to "consume" some of the compactability of the granulated powder. The maximum tablet hardness is always for the direct compaction samples, regardless of the granulation conditions. This has been noted to be the "loss of compactability" in several studies (Kochhar *et al.*, 1995; Bultmann, 2002; Freitag and Kleinebudde, 2003; Shi *et al.*, 2010; Shi *et al.*, 2011; Shi *et al.*, 2011). From the results in Figure 4.14, the magnitude of the compactability loss increases from approximately 45 kP at 20wt.% liquid level, 600rpm impeller speed and 130g/min binder flow rate (Figure 4.14a), to 30 kP at 50wt.% liquid level at the same impeller speed and binder flow rate (Figure 4.14d). Looking at the general trend across all liquid levels, the profiles reveal that the impact of higher granulator impeller speed on the powder and granules reduces the compactability behaviour of the granules.

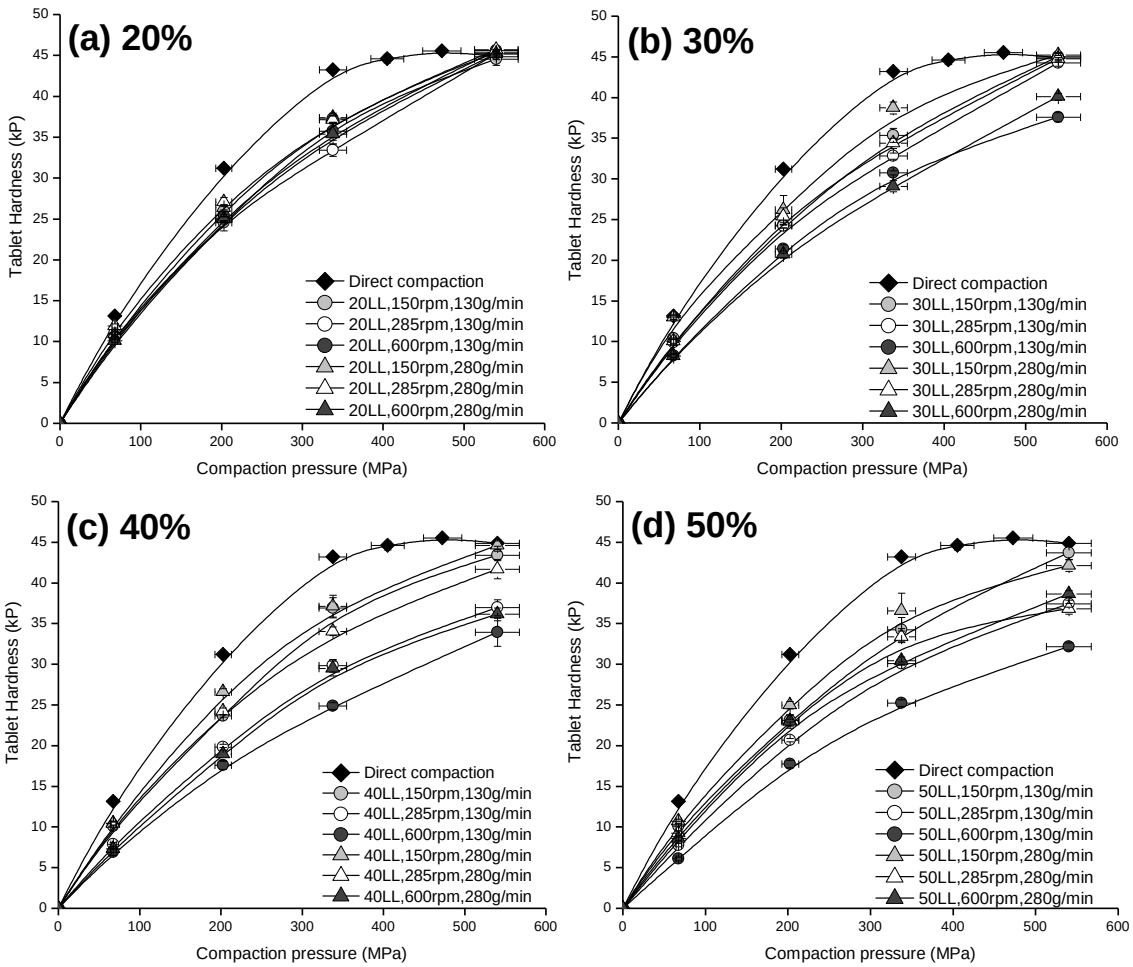

Figure 4.14: Tablettability (tablet hardness as a function of compaction pressure) behaviour for granules produced from varying liquid levels (a) 20%; (b) 30%; (c) 40%; and (d) 50%.

There are two potential causes of these results. First, it could be the higher liquid level which affects the material properties, thereby reducing compaction. Alternatively, the results could be attributed to granules being exposed to longer period of compaction forces with high liquid levels (longer solution delivery time) than for low liquid levels (shorter mixing time).

The low decrease in compactability for the 20wt.% liquid level granulation batch may suggest that a low degree of aggregation is occurring within the granulator as supported by the granule size distribution results in Figure 4.11 and Figure 4.13. The granulator liquid level and tabletting compaction pressure have the strongest influence on the tablet strength as seen in the in Figure 4.9, whilst the binder flow rate and the impeller speed have a minor effect.

During granulation, if there is sufficient liquid binder in the granulator, the liquid agglomerates the particles together and transform the kinetic energy from the granulator impeller into compaction forces to consolidate the particles. This is not shown in the 20wt.% liquid level granulation batch (Figure 4.9a), in which the data shows different behaviour. The powder compactability is not affected by binder flow rate or impeller speed. This implies that a minimum liquid level is required to effectively transfer the compaction forces to the granules for consolidation.

The compressibility behaviour of the powder (the relationship of the tablet density as a function of compaction pressure), provides evidence that the liquid level and the binder flow-rate do not have a significant influence on the tablet density, as seen in Figure 4.15. The tablet volume and density are primarily driven by the compaction pressure regardless of the liquid level, impeller speed or binder flow rate. Therefore the wet granulation operating conditions do not govern the tablet density. Comparing the granule size data in Figure 4.10 and Figure 4.12 with the compressibility data in Figure 4.15 shows that granule size had no effect on the tablet density.

The compactability behaviour (relationship between the tablet hardness and the tablet density) in Figure 4.16 demonstrates the strong influence of the tablet density on the tablet strength. For low liquid levels, such as 20wt.% liquid level, the tablet hardness is strongly dependent on the tablet density. As the liquid level increases towards 50wt.%, the tablet density range broadens for a given tablet strength. Examining the wet granulation conditions for 50wt.% liquid level batches (Figure 4.16d) reveals that higher impeller speeds (285rpm and 600rpm) and/or the binder flow rate (280g/min) tend to have a higher tablet density and broaden the tablet density range. Comparing this trend to that found for 20wt.% liquid level (Figure 4.16a) in which the tablet density range is small for a given tablet strength, shows that consolidation and densification of the granules during wet granulation can compromise the tablet strength.

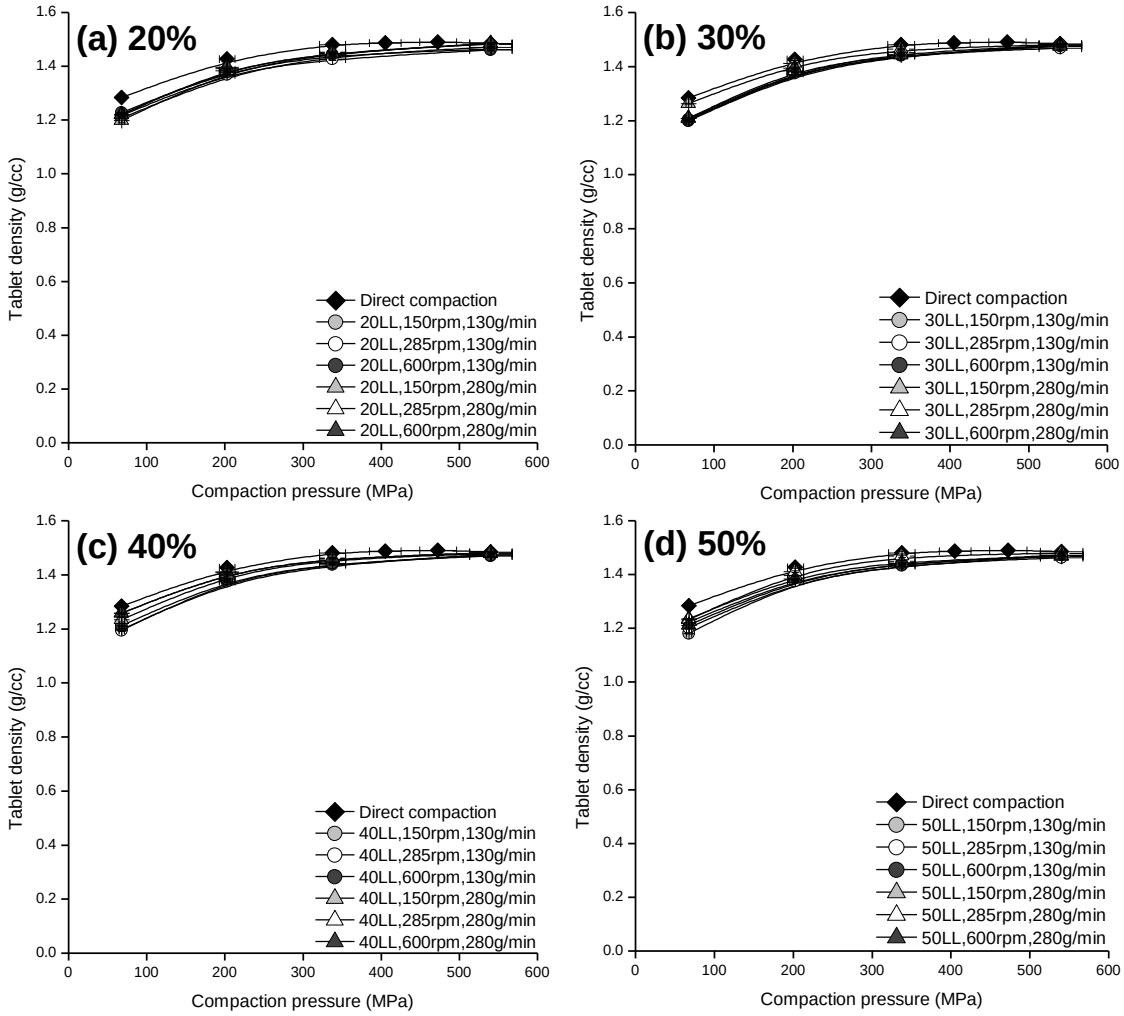

Figure 4.15: Compressibility (tablet density as a function of compaction pressure) behaviour for granules produced from varying liquid levels (a) 20%; (b) 30%; (c) 40%; and (d) 50%. Formulation comprises of 1:1 microcrystalline cellulose:lactose 200 mesh and 5w/v% PVP.

If an assumption of constant tablet density meaning a constant number of bonds for any given wet granulation and tabletting condition was made, then Figure 4.16(b) to (d) imply that the strength per bond is changing regardless of the liquid level, impeller speed or binder flow-rate. Therefore the decrease in the tablet strength can be considered to be driven primarily by the impeller impact and the consolidation of the granules, which can be seen indirectly by the reduction of the tablet density. The assumption for constant tablet density being contributed to a constant number of bonds is based on the principle that the granule size and shape are consistent. However, since the granule size and shape are not uniform, this is not an exact relationship and hence a control experiment is required to investigate this assumption further.

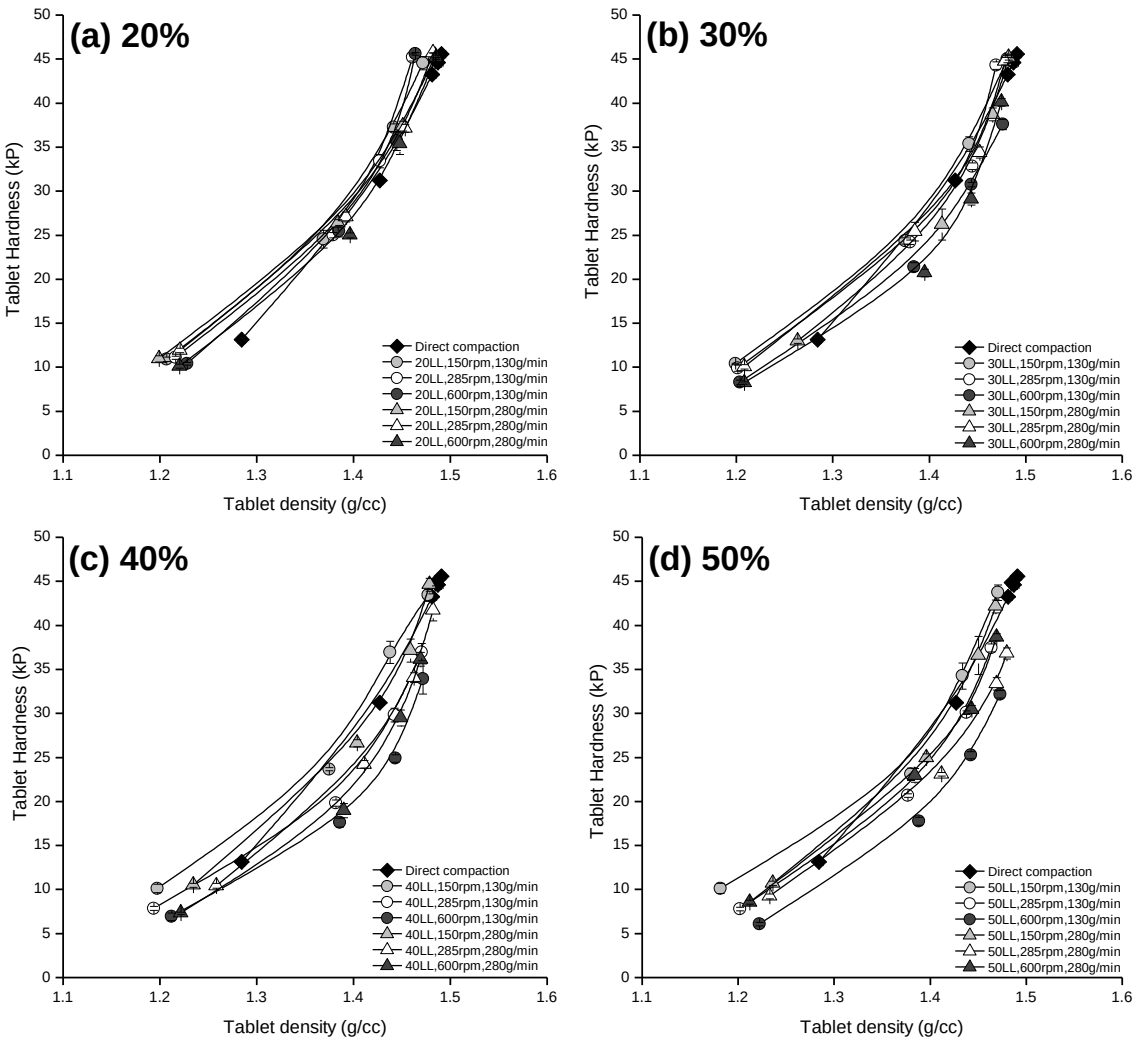

Figure 4.16: Compactability (tablet hardness as a function of tablet density) behaviour for granules produced from varying liquid levels (a) 20wt%; (b) 30wt%; (c) 40wt%; and (d) 50wt%. Formulation comprises of 1:1 microcrystalline cellulose:lactose 200 mesh and 5w/v% PVP.

4.4.3 EFFECT OF WET MASSING TIME

A significant reduction of the overall tablettability behaviour from the compaction of the granulator impeller on the powder and granules can be seen in Figure 4.17. As the wet massing time increases towards 10 minutes, the magnitude of the "loss of compactability' in tablet strength increases from approximately 7kp for 0 minutes wet massing time (direct compaction) to 25kp after 10 minutes wet massing time. When the granules are subjected to long periods of wet massing, the granules undergo compaction and densification from the impact of impeller blades (Iveson *et al.*, 1996; Shi *et al.*, 2011; Shi *et al.*, 2011). Therefore the impellor compaction during wet granulation reduces the amount of granule deformation and consolidation which is transferred to the tabletting stage. When the granules undergo tabletting, the extent of deformation and fragmentation of the granules to form contact bonds decreases. It is speculated that the decrease in the

number of bonds and/or the granule-granule bonding strength contributes to the reduction in the tablet strength.

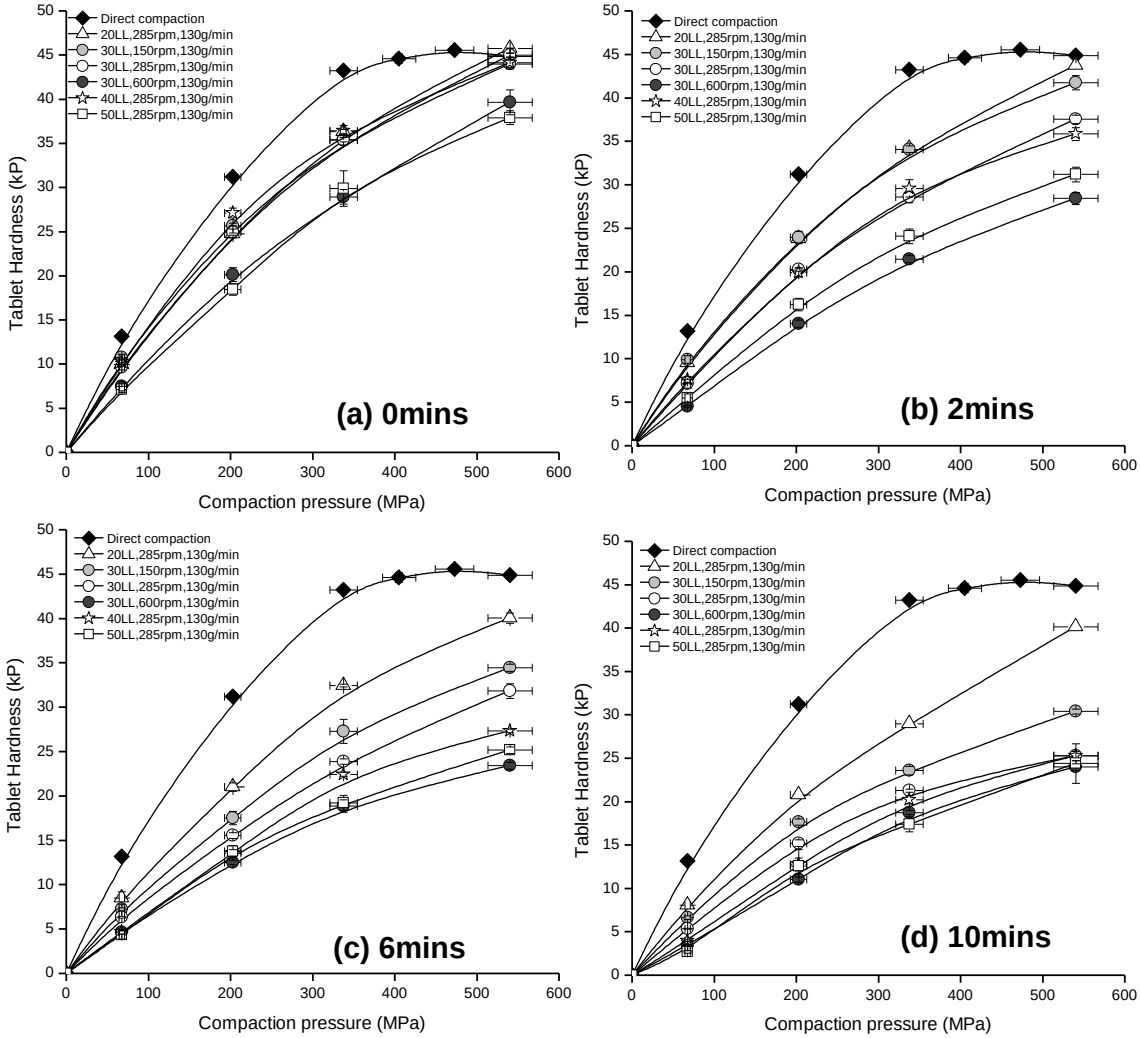

Figure 4.17: Tablettabilty (tablet hardness as a function of compaction pressure) behaviour for granules produced from varying wet massing times (a) 0mins; (b) 2mins; (c) 6mins; and (d) 10mins.

The tablet density was not affected by the wet massing time (please refer to Figure E.1 in *Appendix D: Tablet Compressibility Behaviour Profiles*), which is in agreement with the liquid level compressibility result in Figure 4.15. The tablet density is controlled by the tabletting compaction pressure regardless of the wet massing time, liquid level or binder flow-rate.

Evidence of granule consolidation and densification having a significant influence on the tablet strength can also be seen through the compactability behaviour in Figure 4.18. Across all liquid levels, the tablet hardness increases in an exponential-like function with increasing tablet density, similar to the trend found for the liquid level compactability

behaviour. Upon close examination of the compactability curves, for a given tablet density, a wide range of tablet hardness values can be seen across all wet massing times, indicating a significant reduction in granule compactability has occurred. Wet massing time and impeller speed both affect the total number of impeller impacts granules. However the granule properties, such as the morphology, porosity and surface area, resulting from the wet granulation process may also be a factor for the final tablet strength. This will be explored in *Chapter Five: Effect of the Granulator Compaction Pressure on the Granule Properties*.

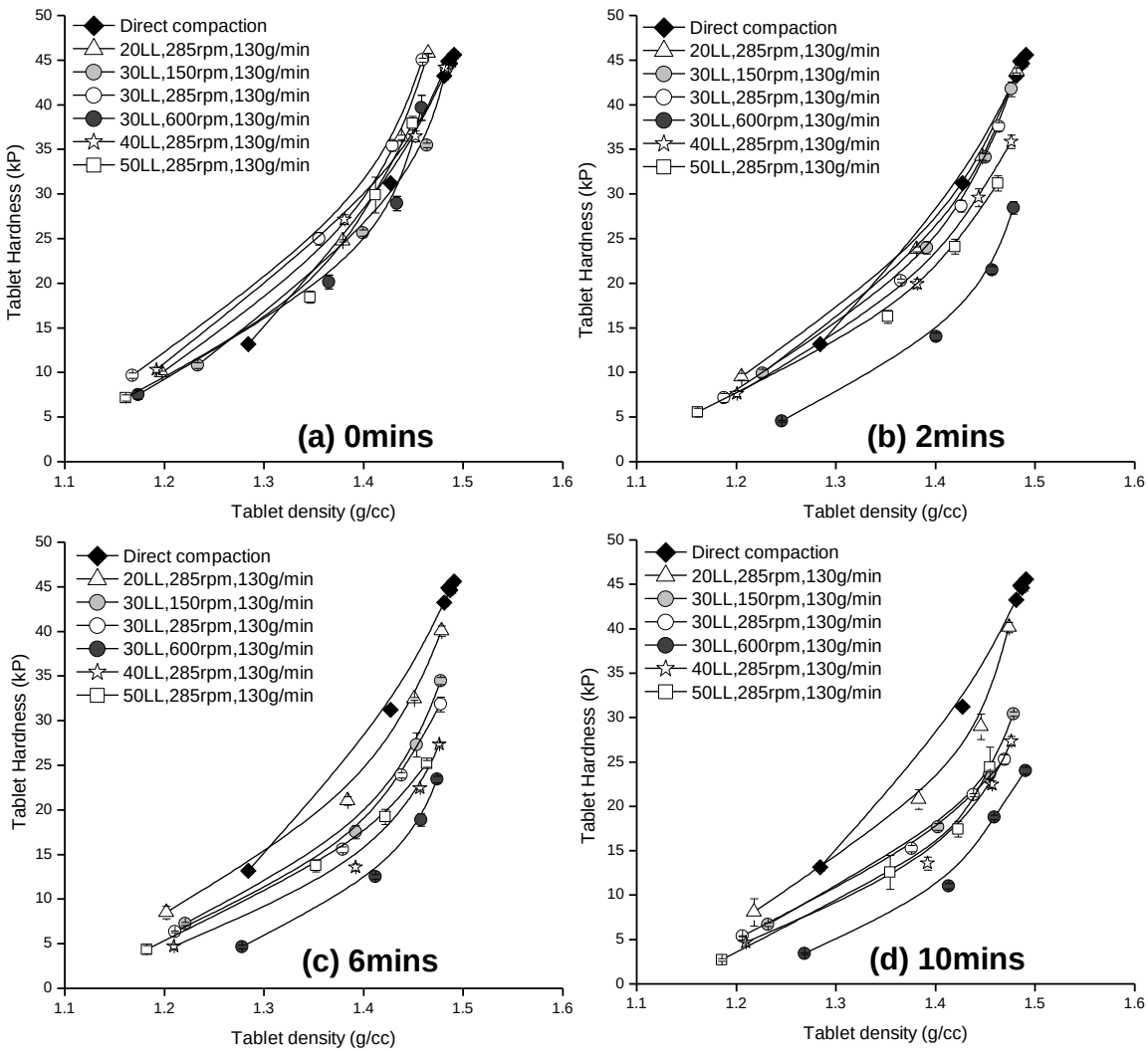

Figure 4.18: Compactability (tablet hardness as a function of tablet density) behaviour for granules produced from varying wet massing times (a) 0mins; (b) 2mins; (c) 6mins; and (d) 10mins.

4.5 APPLICATION OF THE UNIFIED COMPACTION CURVE TO WET GRANULATION

4.5.1 FEASIBILITY OF THE UNIFIED COMPACTION CURVE MODEL TO WET GRANULATION

To enable the prediction of the tablet strength from the wet granulation conditions, the Unified Compaction Curve model was applied to visualise the effect of the liquid level and the wet massing time on the tablet strength. The Unified Compaction Curve model is adopted here for the first time for wet granulation processes.

The tablet hardness results in Figure 4.14 and Figure 4.17, for the liquid level and the wet massing time respectively, were converted into tablet tensile strength data as described in Equation 4.2 to create tensile strength tablettability profiles, ready for the Unified Compaction Curve model to be applied.

The tablet strength data for all the wet granulation conditions were able to be collapsed onto a single curve using the Unified Compaction Curve model, using only P_{WGC} as the fitting parameter (See Figure 4.19, Figure 4.20, Figure 4.21). The wet granulation data can be collapsed onto a single curve regardless of the liquid levels, wet massing times, impeller speeds and binder flow-rates.

In Figure 4.19, for all liquid levels (20%LL to 50%LL), impeller speeds (150rpm, 285rpm and 600rpm) and liquid binder flow-rate (Low (L) - 130g/min; and High (H) – 280g/min), the liquid level wet granulation data collapses onto the direct compaction reference curve. The wet granulation data for varying liquid levels are clustered in four main groups, shifting across the curve from left to right, representing 20% to 50% liquid level respectively. As the liquid level increases, the tablet strength increases toward the maximum tablet strength of 3.54MPa.

The wet granulation data also collapses onto the reference curve for the wet massing data and varying binder flow-rates of 130g/min in Figure 4.20, and 280g/min in Figure 4.21. In Figure 4.20, as the wet massing time increases from 0 minutes to 10 minutes, the wet granulation data are positioned on the direct compaction curve with the data points shifting across the curve from left to right. Compared to the liquid level data, the wet

massing data are more spread out across the reference curve. Similar data fitting results can be seen for the higher binder flow rate wet massing data in Figure 4.21. The relationship between the wet massing time and the tablet strength is similar to the one between the liquid level and the tablet strength in Figure 4.19, in which the tablet strength increases toward the maximum tablet strength as the wet massing time increases towards 10 minutes.

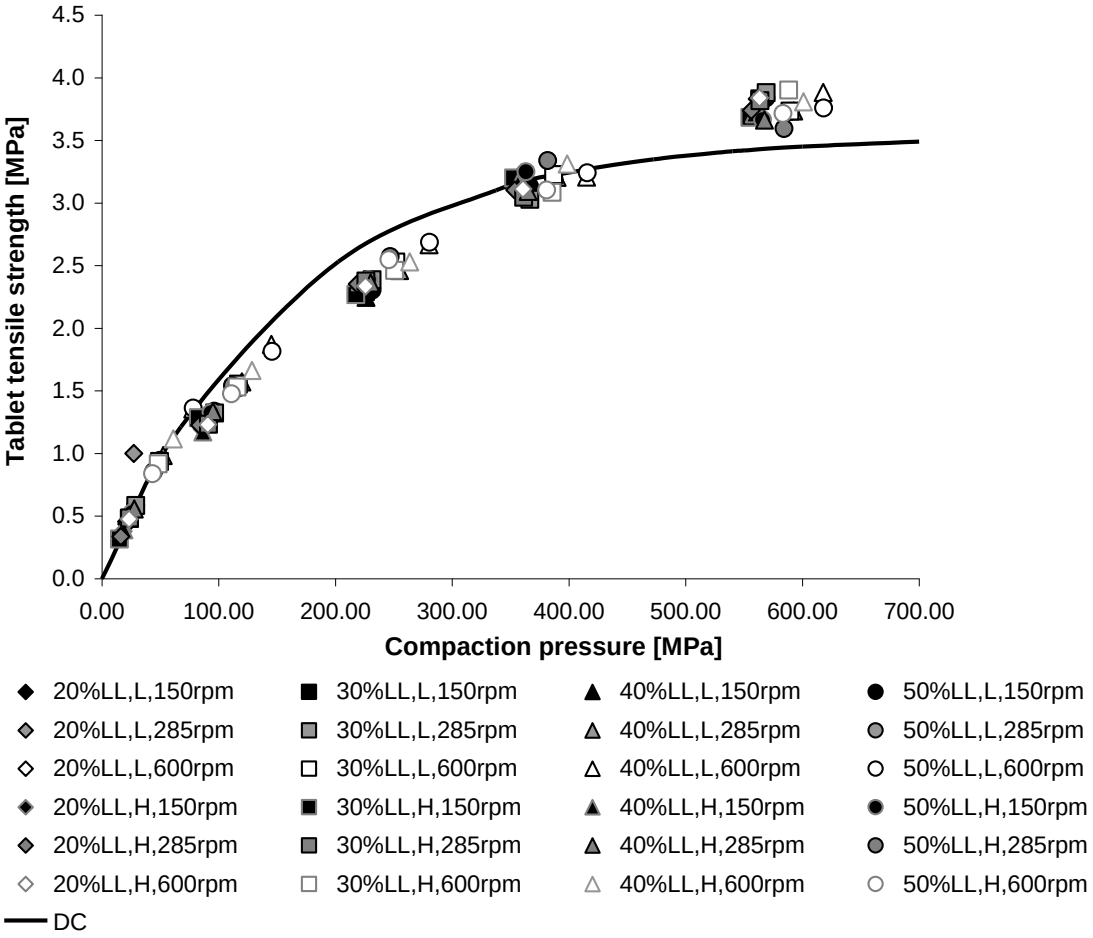

Figure 4.19: Unified Compaction Curve for the liquid level effects at varying impeller speeds.

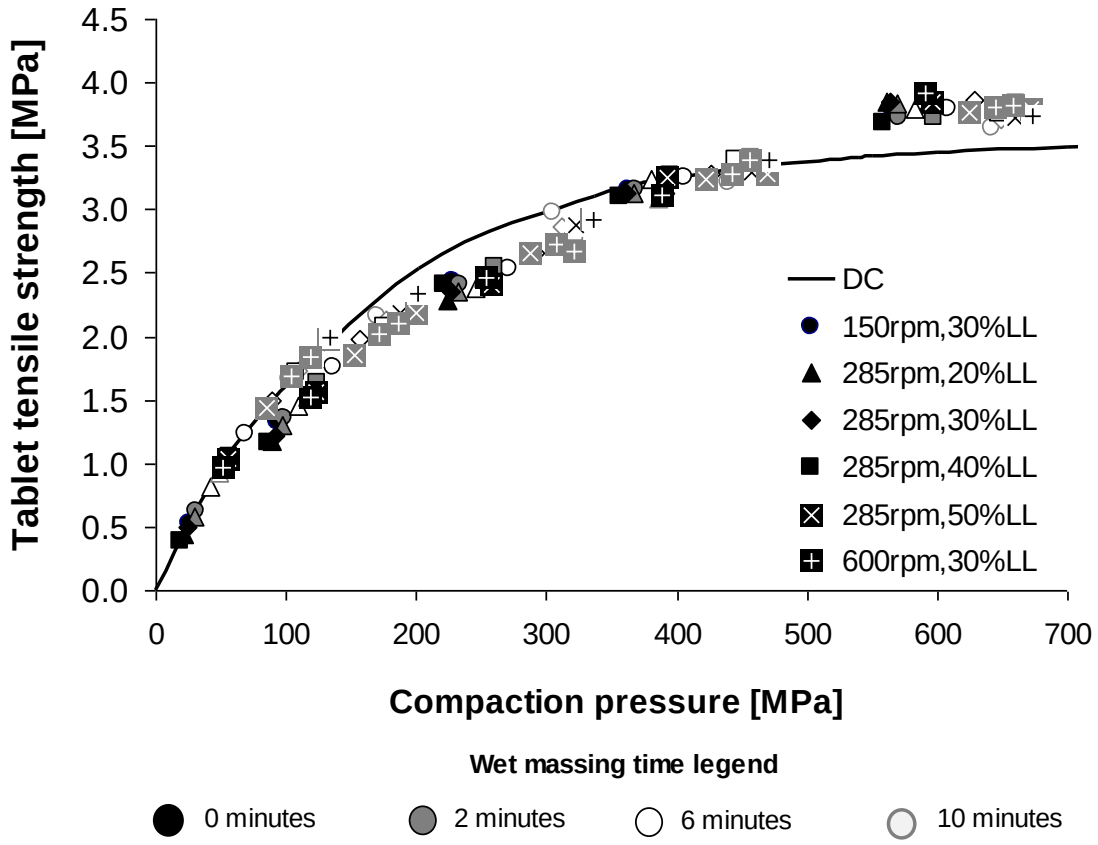

Figure 4.20: Unified Compaction Curve for wet massing time effects with varying impeller speeds and liquid levels (130g/min).

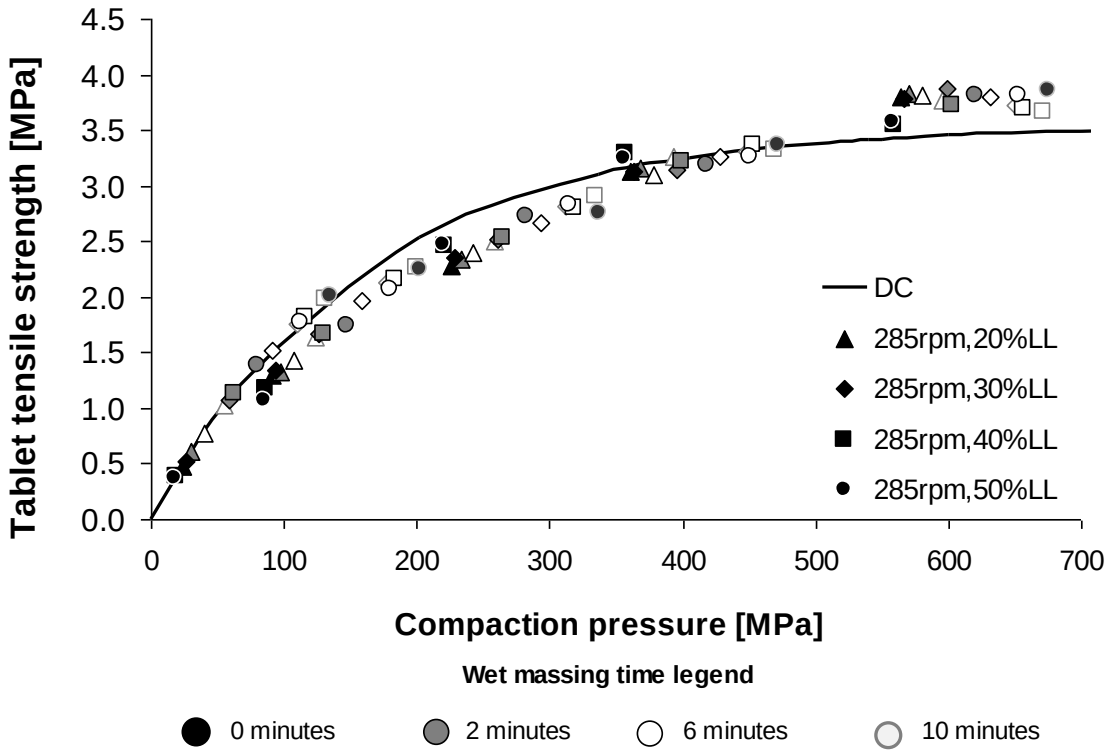

Figure 4.21: Unified Compaction Curve for wet massing time effects and liquid levels. Binder flow rate is 280 g/min and impeller speed is 285 rpm.

From the application of the Unified Compaction Curve, the tablet strength can be predicted from the direct compaction reference curve regardless of the liquid level, wet massing time, impeller speed and the binder flow-rate. All the granulation data for different granulation conditions can potentially be translated onto the reference curve to predict the tablet strength. This indicates that the *tablet strength is dependent on the compaction pressure of both the wet granulation and tabletting processes – in other words, the cumulative compaction history experienced by the powder,* as illustrated in Figure 4.22.

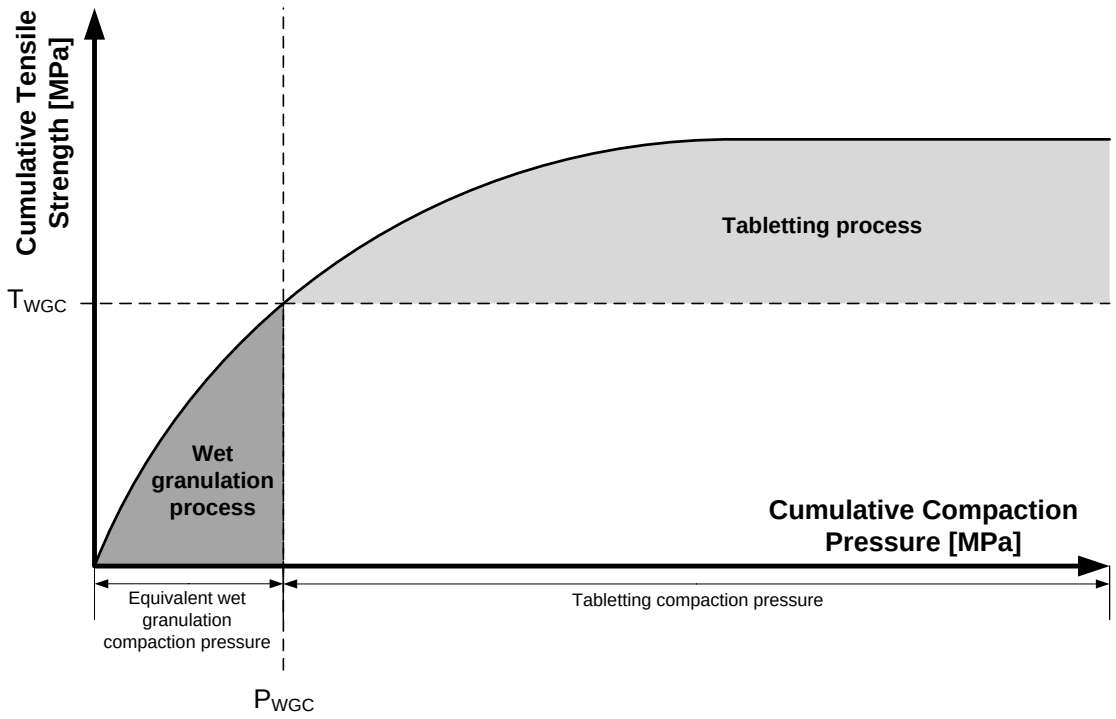

Figure 4.22: Schematic representation of how the wet granulation process is related to the tabletting process in the Unified Compaction Curve.

Therefore the Unified Compaction Curve model enables the tablet strength to be predicted for a given compaction pressure with varying liquid level and wet massing conditions as seen in Figure 4.19 to Figure 4.21. This indicates that the "loss of compactability" seen in the wet granulation is analogous to the forces applied during roller compaction by the rollers (Farber *et al.*, 2008) and that the total cumulative compaction history controls the final tablet strength.

The translation of the tabletability curves along the direct compaction reference curve signifies the amount of granule compaction and consolidation from the granulator

impeller. As the liquid level or the wet massing time increases (i.e. longer time of granules being subjected to the granulator impeller), the compaction curve is shifted upwards and to the right on the reference curve beginning forming a new origin point (P_{WGC}, T_{WGC}). The origin co-ordinates, P_{WGC} and T_{WGC}, quantitatively represents the equivalent amount of compaction applied to the granules during wet granulation ("wet granulation compaction pressure") and the amount of tensile strength in the granules generated ("wet granulation tensile strength") respectively. During wet granulation, the compaction and consolidation creates strength in the granules. However the increase in granule strength compromises the final tablet strength due to the reduction in the maximum possible compaction pressure (T_{max}). Therefore the "loss" of tensile strength in the tablet (T_{max} – T, see Figure 4.23) is driven by granule consolidation which will be investigated more in *Chapter 5: Effect of the Granulator Compaction Pressure on the Granule Properties*.

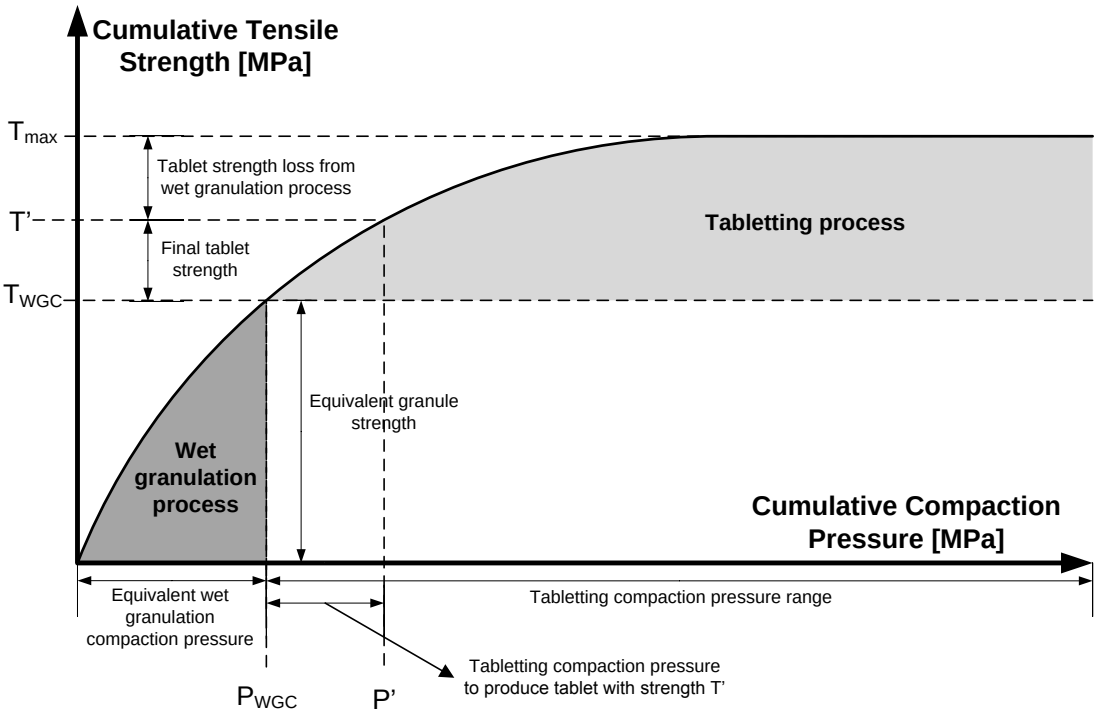

Figure 4.23: Schematic representation of the Unified Compaction Curve model showing how the equivalent wet granulation compaction pressure (P_{WGC}) and the tableting compaction pressure (P') is related to the equivalent average granule strength (T_{WGC}) and the reduction of the maximum possible compaction pressure (T_{max}) to produce the final tablet strength (T').

4.5.2 QUANTITATIVE ANALYSIS FROM THE UNIFIED COMPACTION CURVE

From the Unified Compaction Curve, an interesting insight that can be seen with this model is the *ability to quantitatively measure the compaction pressure of the impeller during the wet granulation process through the* P_{WGC}. Previous literature studies have

shown interest in determining the amount of impact, shear and compaction on the granules during wet granulation to predict the success of granule collision and coalescence and the resulting granule porosity, size and morphology (Iveson, 2001; Oulahna *et al.*, 2003). The Unified Compaction Curve model enables the amount of compaction applied to the granules by the impeller to be predicted for a variety of granulation conditions and without the use of sophisticated equipment to measure the compaction force or pressure.

The Unified Compaction Curve can reduce the amount of case-study experiments carried out to predict the amount of compaction the granules experience through the wet granulation compaction pressure P_{WGC}. By extracting the equivalent wet granulation compaction pressure from the Unified Compaction Curve, the relationship between the compaction pressure with the wet granulation operating conditions can be seen, as shown in Figure 4.24 and Figure 4.25 for the liquid level and wet massing time the respectively.

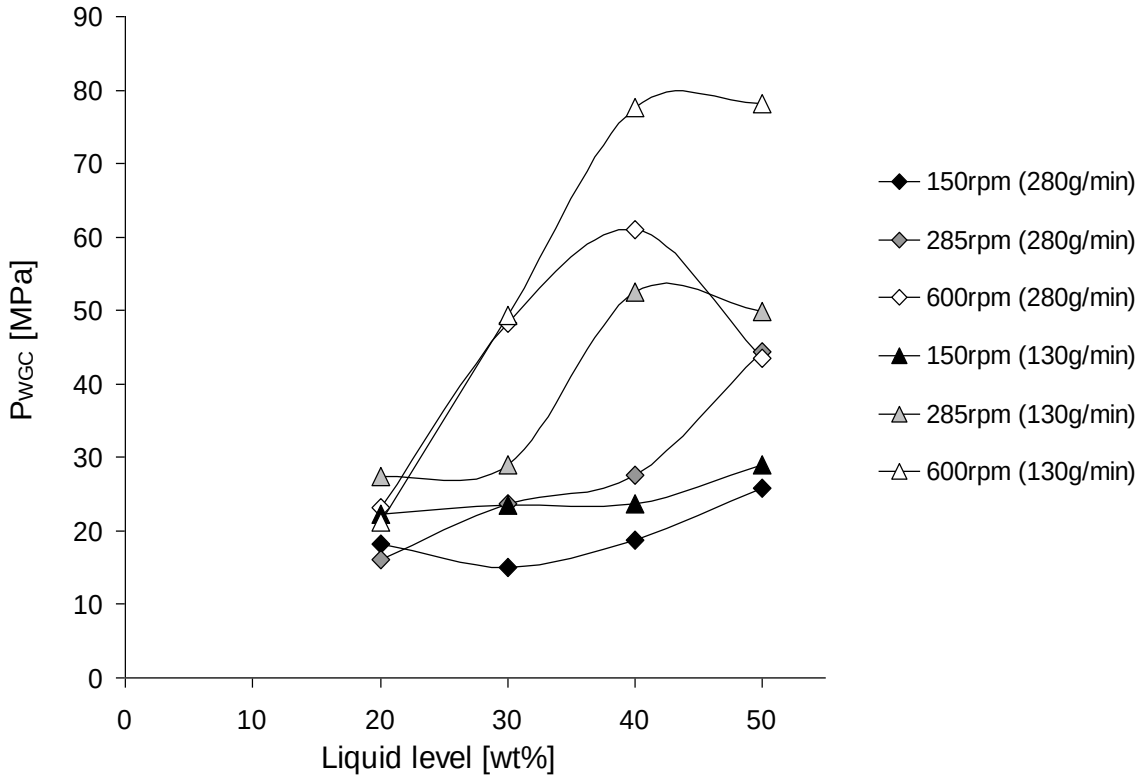

Figure 4.24: The relationship between the liquid level and the wet granulation compaction pressure P_{WGC} with low (130g/min) and high (280g/min) binder flow rates.

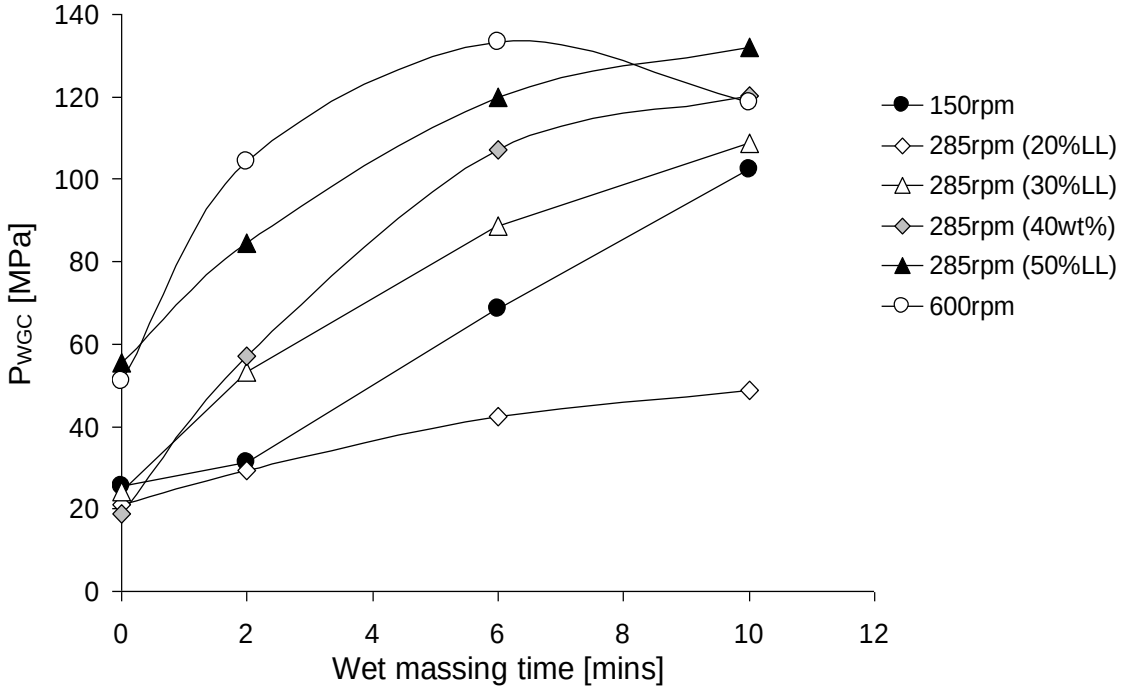

Figure 4.25: relationship between the wet massing time and the wet granulation compaction pressure P_{WGC} as a function of liquid level (LL).

The wet granulation compaction pressure P_{WGC} increases non-linearly with increasing liquid level or wet massing time, which implies that the granules would undergo a greater extent of deformation and consolidation with longer wet massing periods or granulation time with high liquid levels. Wet massing has the greatest effect on P_{WGC} as the wet granulation compaction pressure increases the compaction pressure from the impeller (maximum P_{WGC} is ~135MPa) compared to liquid level effects (maximum P_{WGC} is ~80MPa). An increase in P_{WGC} signifies that compaction from the impeller is higher and this is detrimental to the final tablet strength.

However this was not seen for 50 wt.% liquid level in which the P_{WGC} decreased at 600rpm with binder flow rate of 280g/min (seen in Figure 4.24). A possible reason for this deviation from the trend is due to the complete saturation of the microcrystalline cellulose porous structure at high liquid levels, which may alter the compaction properties of the granules. A similar trend is found in for granules produced at 600rpm with 10 minutes wet massing time in Figure 4.25. The combination of a high impeller speed and long wet massing time would facilitate in the consolidation of the granules which would increase the saturation of the microcrystalline cellulose structure. Subsequently, the granule compactability ability for the tableting stage decreases and the strength of the resultant tablet decreases. This speculation requires more investigation in future studies.

Therefore an insight into the extent of granule deformation and consolidation from different wet granulation conditions can be obtained, which can be correlated back to the extent of compactability during tabletting and ultimately the final tablet strength.

This form of insight can be beneficial in designing or troubleshooting the wet granulation process through matrix graphs to achieve the desired tablet strength, as presented in Figure 4.26.

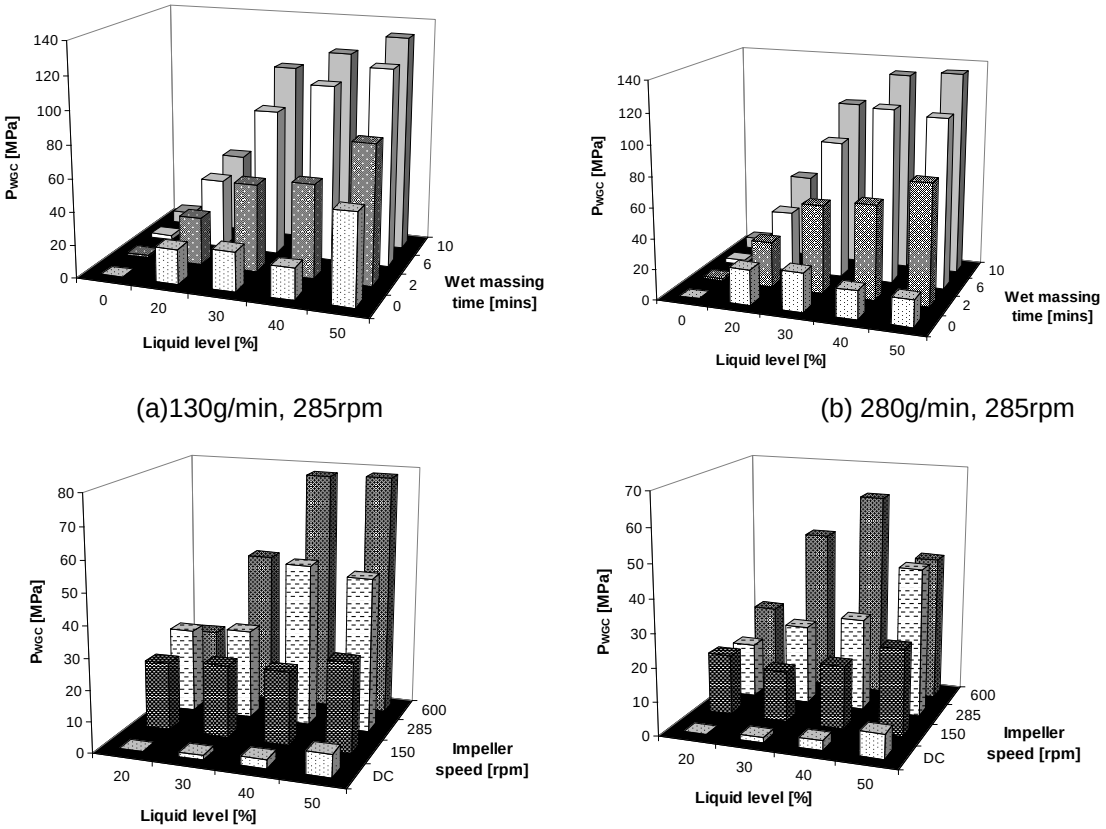

Figure 4.26: Matrix graphs showing various relationships between the wet granulation compaction pressure P_{WGC}, wet massing time, liquid level, binder flow rate (BF) and impeller speed. (a) BF = 130g/min, 285rpm; (b) BF = 280g/min, 285rpm; (c) BF = 130g/min; and (d) BF = 280g/min.

The matrix of P_{WGC} values in Figure 4.26 can be used as a "Quality-by-Design" (QbD) frame-work to design the wet granulation process to target the desired tablet strength. To understand the quality-by-design framework, an example will be presented. For a formulation comprising of 50% microcrystalline cellulose and 50% lactose, granulated with 5w/v% of PVP, a series of direct compaction profiles were produced to determine the Unified Compaction Curve co-efficient, *b* and the theoretical maximum tablet tensile strength, T_{max}, of 3.54MPa, using the procedure outlined in *Section 4.3.2.1: Construction*

of the Direct Compaction Master Curve. The tablet strength produced from the following wet granulation conditions (outlined in Table 4.5) needs to be determined:

Table 4.5: Summary of the wet granulation and tabletting conditions.

Wet granulation condition	Target value
Liquid level	40%
Wet massing time	6 minutes
Impeller speed	285rpm
Binder flow-rate	130g/min
Tabletting compression force	6000lb$_f$
UCC co-efficient, b	0.0062
Theoretical maximum tablet strength, T_{max}	3.54MPa

To determine the tablet strength, the matrix graph in Figure 4.26(a) is used to determine that the wet granulation compaction pressure, P_{WGC}, is 120MPa for the given wet granulation conditions. The P_{WGC} parameter is then substituted into Equation 4.4 to calculate the wet granulation tensile strength (granule tensile strength), T_{WGC}, and in Equation 4.7 along with the tabletting compression force, P', to determine the resultant tablet strength, T.

The data in Figure 4.26 can also be used to determine the wet granulation operating conditions to achieve a given tablet strength compressed at a given tabletting compaction pressure. For example, if a tablet strength of 3MPa is required that is compressed at a compression force of 6000lb$_f$, then the P_{WGC} value can be determined from the substitution of the UCC co-efficient, b, the maximum tablet strength, T_{max} and P' in Equation 4.4 and 4.7 (since P_{WGC} will be the only unknown variables in the equations). The obtained P_{WGC} can then be used in the matrix graphs to determine the wet granulation conditions that fall close to achieving the desired P_{WGC}. Another example of this is given in *Appendix H: Targeting the Tablet Strength using the Granulator Impeller Revolutions*.

Therefore the quality-by-design framework can be beneficial for optimising the wet granulation process and tabletting process conditions, in a visual and simple mathematical way that has not previously been possible. By setting up the Unified Compaction Curve from a small batch of experiments and standard compaction curves, the Unified Compaction Curve model will improve the efficiency for tablet manufacturing through minimisation of resources and finances to conduct case-studies and/or production of undesirable granulation batches.

4.6 DISCUSSION

4.6.1 WET GRANULATION COMPACTION PRESSURE, P_{WGC}

The investigation into the feasibility of the Unified Compaction Curve model to the wet granulation process reveals that the model can be used successfully to predict the final tablet strength for difference wet granulation processing conditions. The success of the Unified Compaction Curve model appears to be dependent upon the presence of a plastically deformable component in the formulation. In this study the incorporation of microcrystalline cellulose, a plastically deformation material, into the granulation formulation allows for the compaction pressure applied to the granules during wet granulation to be measured quantitatively for the first time.

The Unified Compaction Curve model is able to predict the tablet strength for varying liquid level and wet massing times, as evident from the unification of the liquid level and wet massing time tablettability profiles onto the Unified Compaction Curve in Figure 4.19 to Figure 4.24. The model gives a good prediction of the tablet strength for a given compaction pressure. However for compaction pressures beyond 500MPa, the model under-estimates the tablet strength. This may not be significant as the industrial tabletting compaction pressure ranges between 200MPa to 300MPa (Farber *et al.*, 2008). The wet granulation conditions which impart a significant amount of shear on the powder and granules have the most influence on the final tablet strength. This primarily comes from the wet massing time, in which the longer the residence time of the granules in the high-shear granulator, the greater the reduction of the tablet strength results until the wet massing reaches 6 minutes. Beyond this time, the additional wet massing time has little significant impact on the tablet strength.

The reduction of the tablet strength due to the impact of the granulator impeller on the powders and granules during wet massing is generally assumed to be due to the destruction of the potential contact bonds generated during the tabletting process. As the wet massing time increases, the impeller consolidates and densifies the granules conferring strength to the granules (Suzuki *et al.*, 2001). This would produce granules which are rounder and hence reduce the contact area between the granules during tabletting. The extent of mechanical inter-locking between the granules would also decrease which leads to the reduction in the tablet strength (Shesky and Williams, 1990;

Shi *et al.* 2010, 2011). However, Murakami *et al.* (2001) found contradictory results to the other studies. In this study, the results show that the number of contact bonds do not play a significant role in the final tablet strength. This is evident in the tablet density, which is consistent for all wet granulation conditions (liquid levels, wet massing times, binder flow rate and impeller speeds). The tablet density would be an indicator of the extent of contact bonds or bonding areas within the tablet which suggests that the consistent tablet density found in the results indicate a consistent number of contact bonds across all granulation conditions. Therefore this suggests that the number of contact bonds within the tablet is not the determining factor for the tablet strength. Instead the intra-granular bonding strength may be the driving force for the tablet strength. For this to occur, the granule structure is altered in some way during the wet granulation process which compromises at least one granule property and reducing the strength of the intra-granular contact bonds. The reduction in the intra-granular contact bond would consequently lead to a decrease in the tablet strength, assuming that the fracture line occurs through the granules rather than around the granule perimeter.

An interesting aspect of the Unified Compaction Curve model is the ability of the model to provide a deeper insight into the wet granulation dynamics through the wet granulation compaction pressure P_{WGC} (the equivalent force exerted by the impeller on the granules). The results presented so far demonstrate the importance of granule compaction and consolidation phenomena during wet granulation. The compaction and consolidation is driven by the granulator impeller and hence the number of impacts the impeller makes with the granules could be considered to be significant for understanding the relationship between the wet granulation conditions, potentially the modification in the granule properties during wet granulation and the final tablet strength.

To investigate this concept, the wet granulation compaction pressure was plotted against the total number of impeller revolutions for all liquid level and wet massing granulation experiments as can be seen in Figure 4.27. The relationship between the P_{WGC} and the wet granulation conditions reveal that the liquid level and wet massing time data all collapse onto a single curve, with the exception of the 20wt.% liquid level granulation batches. After 10 minutes wet massing time (equivalent to approximately 12.3 minutes of granulation time), the number of impeller revolutions reaches approximately 8000 revolutions, leading to a maximum wet granulation compaction pressure of P_{WGC} =

140MPa. Because P_{WGC} is related to both the wet granulation tensile strength and the tablet strength (through the Unified Compaction Curve), the wet granulation compaction pressure indirectly suggests that the final tablet strength is governed by the number of impeller revolutions as evident by the amalgamation of the all the wet granulation data onto a single curve.

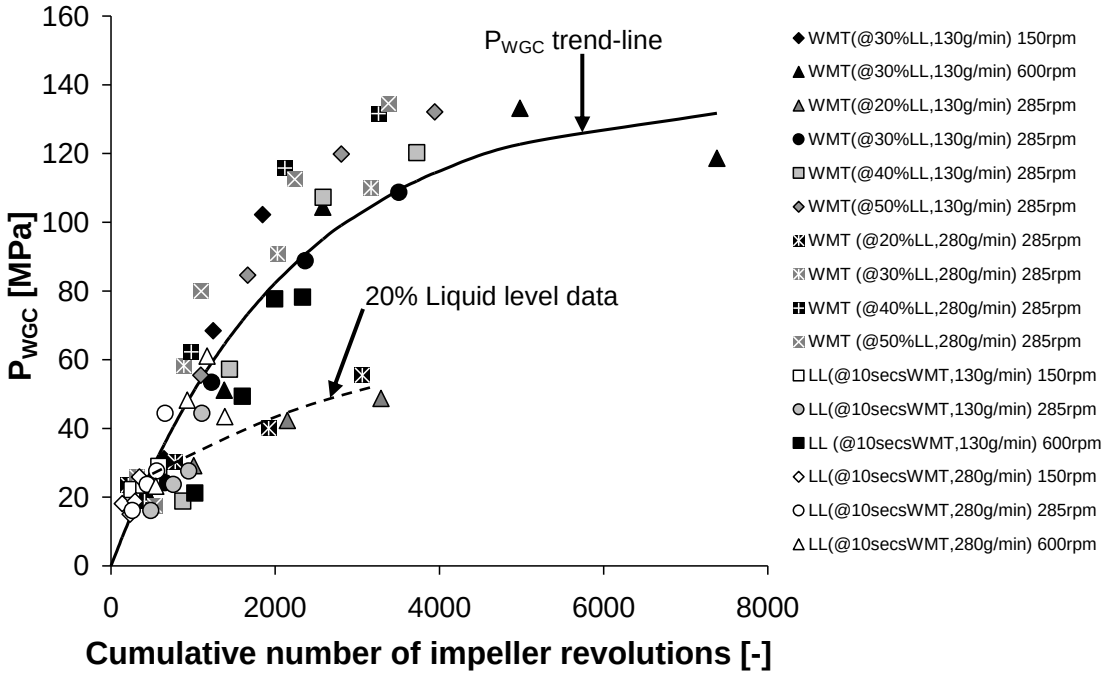

Figure 4.27: The wet granulation compaction pressure as a function of the number of impeller revolutions. Solid line is fitted to the direct compaction data (Equation 4.11).

The divergence of the 20wt.% granulation data from the main trend suggests that a minimum amount of liquid binder is required for the Unified Compaction Curve model to be valid. For this formulation, the liquid level needs to be above 30wt.% to ensure that the impeller force is transmitted to the powder for agglomeration, to cause a physio-chemical change in the microcrystalline cellulose or other alterations to the granule structure. Evidence of the 20wt.% liquid level granulation batches not conforming to the general trend can also be seen in the tablettability and compactability profiles in Figure 4.14, Figure 4.16, Figure 4.17 and Figure 4.18.

Figure 4.27 demonstrates that the Unified Compaction Curve tablet strength can optimise and control the tablet strength by the number of impeller revolutions during wet granulation. This offers great benefits in the simplification and by-passing of case-studies in tablet manufacturing design. The relationship between the cumulative number of impeller revolutions and the wet granulation compaction pressure can be can be fitted,

using the Least Sum of the Errors Squared (LSES), to a first-order exponential equation (represented by the solid line in Figure 4.27) using:

$$P_{WGC} = P_{WGC,\max}\left(1 - e^{-bN}\right) \tag{4.11}$$

Where b is a material-dependent exponent (-), P_{WGC} is the wet granulation compaction pressure (MPa), $P_{WGC,max}$ is the maximum wet granulation compaction pressure (MPa) and N is the total number of impeller revolutions (-) the granules are subjected to. For the formulation and high-shear granulator used in this project (1:1 of microcrystalline cellulose and lactose), b parameter was found to be 0.0062 and $P_{WGC,max}$ was approximately 135MPa. Figure 4.27 show that the kinetic energy from the impeller alters the granule structure which compromises at least one of the granule properties consequently reducing the tablet strength. By using both Equations 4.4 and 4.7, the final tablet strength, T, can be calculated.

The application of the Unified Compaction Curve can also be applied to different formulations. Pure microcrystalline cellulose was granulated by Shi *et al.* (2011) for varying liquid levels (15-95% liquid level) and wet massing times (0-20 minutes). Upon the application of the Unified Compaction Curve model to Shi *et al.*'s results, the tablettability profiles for each processing condition were successfully translated onto the microcrystalline cellulose direct compaction curve as shown in Figure 4.28. The results in Figure 4.28, demonstrate that the powder and granules are subjected to greater compaction pressures for long wet massing time and significant granulator liquid level (greater than 65% liquid level) as can be seen in Table 4.6.

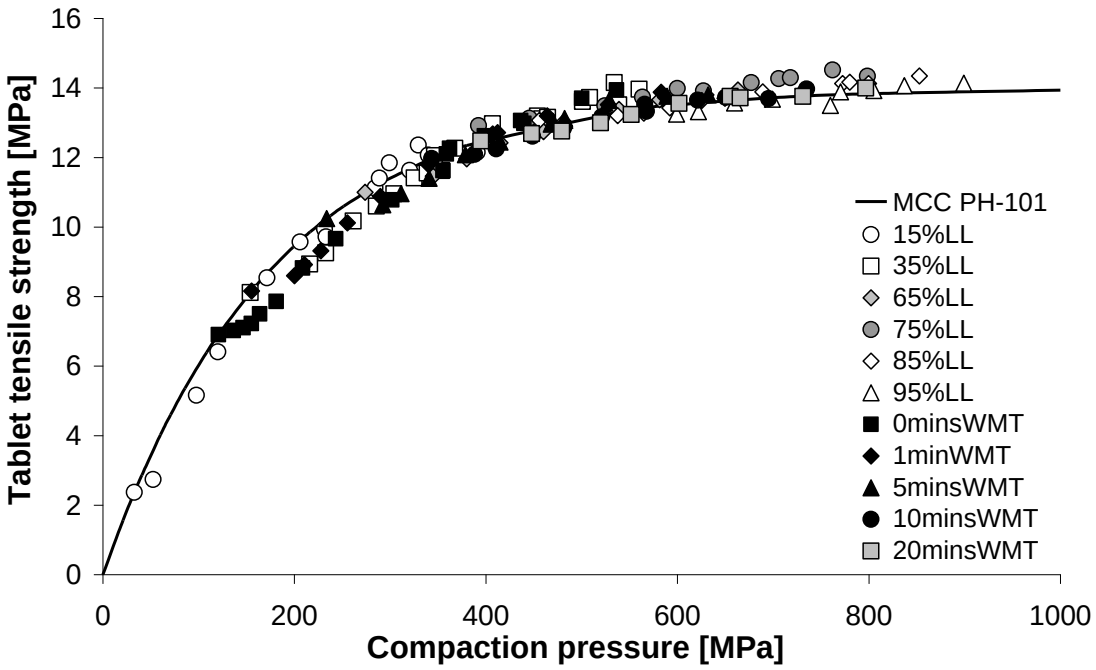

Figure 4.28: Application of the Unified Compaction Curve model to a formulation of pure microcrystalline cellulose with varying liquid level and wet massing time. Data taken from Shi *et al.* (2011).

Table 4.6: The effective wet granulation compaction pressure as a function of liquid level and wet massing time for pure microcrystalline cellulose. Data taken from Shi *et al.* (2011).

Liquid level [wt.%]	P_{WGC} [MPa]
15	32.90
35	153.90
65	273.88
75	392.37
85	455.80
95	482.50

Wet massing time [mins]	P_{WGC} [MPa]
0	120.66
1	155.25
5	233.74
10	343.49
20	394.75

4.6.2 QUANTIFYING THE IMPELLER COMPACTION PRESSURE PER REVOLUTION

Examining the wet granulation compaction curve (Figure 4.27) reveals that the curve has two regions, which can be represented by two intersecting linear lines which are shown in Figure 4.29. At low numbers of impeller revolutions, the wet granulation compaction pressure is proportional to the number of impeller revolutions. The slope of the line gives a quantitative measure of the equivalent wet granulation pressure per revolution of impeller (with units of MPa/rev) as defined in Equation 4.12:

$$\chi = \frac{P_{WGC}}{N} \qquad \text{for } N < 3500 \qquad (4.12)$$

Equation 4.12 represents the first quantitative, experimental, in-situ estimate of impeller force (or pressure) applied during wet granulation. For the formulation, used in this study, the effective wet granulation pressure applied by the 5L granulator (Key International) impeller to the powder and granules per revolution is approximately 44kPa/revolution for low numbers of impeller revolution (N < 3500 rev, linear line best fit, $R^2 = 0.77$). As the number of impeller revolutions increases beyond 3500 revolutions, the curve begins to plateau at approximately 130MPa. At this stage of the granulation process, the granules have reached upper limit of the powder compressibility and the maximum forces applied by the three-bladed impeller in the 5L high-shear granulator. The insight into the dynamics of the wet granulation process paves a potential path towards quantitative scaling-up guidelines, impeller design and formulation design to predict and achieve the desired tablet strength.

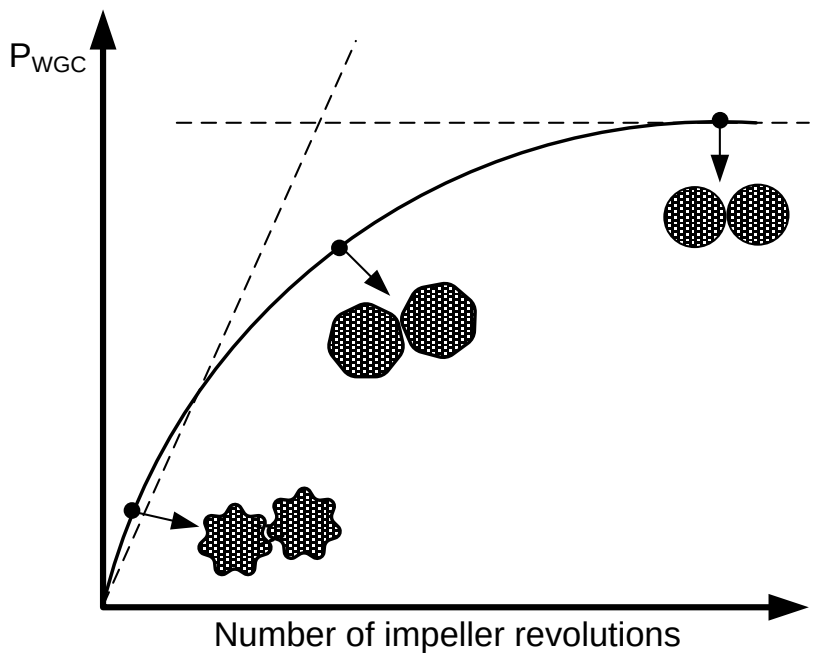

Figure 4.29: Schematic diagram of the transition of granule surface roughness as a function of the number of impeller revolutions and the wet granulation compaction pressure.

The reduction in the tablet strength with increasing granulation time is also supported by similar experiments conducted independently by Shi *et al.* (2010, 2011). The study concentrated on the granulation of microcrystalline cellulose with varying wet granulation conditions and it was found that the microcrystalline granules undergo significant surface smoothing during wet granulation which reduced the tablet strength. In other studies, it has been noted that irregular and rough granular surfaces enable the granule to undergo mechanical locking and confer strength to the tablet during compaction (Cooper and

Eaton, 1962; Salman *et al.*, 2007; Shi *et al.*, 2010; Shi *et al.*, 2011). Therefore it can be considered that the interaction between the granules and the impeller reduces the granule surface roughness, as represented by the first section of the curve in Figure 4.29. From the results from this study, below 3500 revolutions, the wet granulation compaction pressure provides kinetic energy to reduce the granule surface roughness. Eventually, the granules become dense, spherical and smooth and no further change in compressibility is possible, causing a plateau in tablet hardness. These speculations are illustrated in Figure 4.29 and change in the granule morphology and physical properties will be investigated further in *Chapter 5: Effect of the Granulation Compaction Pressure on the Granule Properties*. Therefore it would be expected that granules produced under different granulation conditions but having similar P_{WGC} values will have similar mechanical and structural properties.

4.7 LIMITATIONS OF UNIFIED COMPACTION CURVE MODEL

As with all empirical models, the Unified Compaction Curve has limitations which may not allow the Unified Compaction Curve to be applied to certain granulation conditions. The known limitations of the Unified Compaction Curve include:

- For the model to be valid, the formulation must include a sufficient amount of plastically deforming material such as microcrystalline cellulose. In this study, at least 50% of microcrystalline cellulose (Avicel Ph-101) is required for the Unified Compaction Curve to be valid (which is in line with Farber's *et al.* (2008) study). In another study, the grade of microcrystalline cellulose was shown to be important to the validity of the Unified Compaction Curve model (Dave and Dudhat, 2013). For Avicel Ph-101, the proportion of this grade of microcrystalline cellulose was less than 50% (In the study 49% of Avicel Ph-101 was used), which may not be sufficient enough to allow the Unified Compaction Curve to model the deformation of the granules during the wet granulation process. However the Unified Compaction Curve was valid for 49% of Avicel Ph-200 in the formulation.

- Sufficient liquid binder must also be included as part of the formulation for the model to be applicable. In this study, a minimum liquid level of 30wt.% was found to be valid for the Unified Compaction Curve model.

- Data-fitting can have inherent errors in which different starting values may be used for T_{WGC}, P_{WGC} and b. For all data fitting calculations carried out in this study, the

criterion for the chosen parameters obtained from iteration data-fitting process was based on the calculated tensile strength value being within ±5% of the experimental tensile strength to minimise any human error/variation.

- Good data-fitting of the compactability and Unified Compaction Curve models to the experimental data are very important, particularly with the direct compaction curve as it forms the reference or backbone curve of the Unified Compaction Curve. The data obtained from the experiments should correspond to a full a compaction profile (a profile that plateau out to a consistent tensile strength at high compaction pressures). In this study a wide range of tabletting compaction forces (ranging between 1000lb_f to 16,000lb_f (453.6kg_f to 7257.5kg_f)) were used to obtain the standard compaction profile.

- The data-fitting of Leuenberger's compactability model (1982) and the Unified Compaction Curve relies on the tablet density being consistent at typical industrial compaction pressures (above 200MPa), across all powder formulations used to model the Unified Compaction Curve (Farber *et al.*, 2008). Although a single powder formulation of 1:1 ratio of microcrystalline cellulose: lactose was used in the experiments, this is an important factor to keep in mind to avoid any misleading results from the Unified Compaction Curve model.

- In this study the granules produced from the wet granulation process were directly compacted in the tablet press. However this does not reflect the manufacture of tablets in industry where the powder undergoes a series of blending, agglomeration, milling and drying the powder before reaching the tabletting stage. Therefore in this study the effect of the subsequent processing of granules (milling and blending) are not taken into account. This would mean in industry, there are additional stress and compaction induced on the granules during the milling and blending processes. These processes all occur once the granules have been dried and therefore are less able to affect the granule structure except from attrition and breakage.

  However it is assumed that the Unified Compaction Curve model will take the additional stresses into account during the data fitting process as the granules used to generate that Unified Compaction Curve would represent granules with the effects of

compaction from the wet granulation, milling and blending processes having an influence on the granule mechanical properties.

4.8 IMPLICATIONS OF THE UNIFIED COMPACTION CURVE

The Unified Compaction Curve can be seen to be an important model for tablet manufacture, design, optimization and troubleshooting. The Unified Compaction Curve can have significant implications including:

- Investigating the amount of compaction pressure exerted on the powder and granules during wet granulation, which can be translated in quantifying the amount of energy applied on the powder/granules.
- The insight into the effect of the number of impeller revolutions on the wet granulation compaction pressure can lead to expressing the impeller revolutions as a function of the Froude number (a dimensionless group used to represent the ratio between the inertia forces to gravitational forces of the granulator as a function of the impeller diameter, impeller speed and gravitational force. $Fr = n^2d/g$) which could then help with scaling up procedures. Also the Unified Compaction Curve could potentially facilitate with scaling up procedures in which different scales would have different mixing intensities and pressure exerted on the powder/granules during granulation. This would help determine an impeller speed for an industrial-scale granulation process from laboratory-scale investigations to match the tablet strength or other properties.
- The use of the Unified Compaction Curve can also predict the tablet hardness from the relationship between the compaction profile, liquid level and wet massing time. The wet granulation process can be tailored to a specific tablet strength based on the number of impeller revolutions. An example of how this could be achieved is given in *Appendix H: Targeting the Tablet Strength using the Granulator Impeller Revolutions*. This would help with the design and optimization of the tablet manufacturing process.
- By-passing the need for sophisticated equipment to measure the compaction forces applied to the granules during wet granulation, the wet granulation compaction curve can potentially simplify the tablet manufacturing process. This would potentially by-pass any sophisticated equipment required to measure the compaction pressures in the granulator (Iveson, 2001; Oulahna *et al.*, 2003).

- Provide a new insight into the compaction mechanisms and the role granule morphology.

Therefore the Unified Compaction Curve can be a very useful model that can be used by the tablet manufacturing industry. However the mechanisms behind the UCC in terms of seeing how the granulation conditions (such as the impeller speed, liquid level, wet massing time and binder flow rate) influences the granule properties, and linking the granule properties to the tablet strength are required to be understood to fully utilise the Unified Compaction Curve model.

4.9 CONCLUSIONS

The Unified Compaction Curve has been demonstrated to be successfully applied to the wet granulation process, in which the granulation data collapsed onto a master reference curve, enabling the tablet strength to be predicted for a given cumulative compaction pressure. The model provided a good prediction of the tablet strength for varying liquid levels, wet massing times, binder flow-rate and impeller speeds. The wet massing time was a stronger influence on the tablet strength compared to the liquid level, binder flow-rate or the impeller speed. The Unified Compaction Curve model was applied to a 50/50 wt.% microcrystalline cellulose and lactose formulation, and a pure microcrystalline cellulose formulation (Shi *et al.*, 2011). The influence of the wet massing time reflected the driving force of the number of impeller revolutions on the tablet strength.

The model also shows potential for showing the dynamics of wet granulation, through the wet granulation compaction pressure P_{WGC}. The wet granulation compaction pressure gives a quantitative measure of the cumulative compaction pressure the granules experience per revolution of the impeller during wet granulation and χ indicates the equivalent compaction pressure per revolution. Therefore P_{WGC} is a quantitative value of the amount of strength the impeller confers to the granules from deformation and consolidation. The final tablet strength can be calculated from P_{WGC} through the Unified Compaction Curve model. Therefore the effective compaction pressure from the wet granulation operating condition is linked to the stresses in the granulator for the first time. It is speculated that the strength of the bonds through mechanical inter-locking and/or physio-chemical changes in the material properties, particularly microcrystalline cellulose, may play a role in the tablet strength.

The Unified Compaction Curve model can be used for quantitative scaling-up guidelines, understanding the dynamics of the impeller and powder/granule interactions during wet granulation, and design of the impeller and formulation to target the desired tablet strength without the need for extensive case-study investigations. Therefore the Unified Compaction Curve serves as an elegant link between the wet granulation and tabletting processes.

Publication(s):

From the study into the wet granulation conditions and the influence on the final tablet strength, a journal and two conference papers have been published:

- **T.H. Nguyen**, D. Morton and K.P. Hapgood, "*Application of the Unified Compaction Curve to Link Wet Granulation and Tablet Compaction Behaviour*", Accepted 28th of July 2012 for Special issue of Powder Technology Journal (invited article).
- **T.H. Nguyen**, D. Morton and K. Hapgood (2011), "*Unified Compaction Curve: A Potential link between the wet granulation and tabletting processes*", 5th International granulation workshop, 20th -22th June, Lausanne, Switzerland,
- K. Hapgood, **T.H. Nguyen** and D. Morton (2011), "*Using the Unified Compaction Curve to bridge the wet granulation and tabletting processes*", Particulate processes in the pharmaceutical industry III, 24th -29th July, Gold Coast, Australia (Keynote presentation by A/Prof. Hapgood),
- **T.H. Nguyen**, D. Morton and K. Hapgood (2011), "*Linking the wet granulation conditions to the tablet properties through the Unified Compaction Curve*", CHEMECA, 18-21 September, Sydney, Australia, IChemE/IEAust.

5 Effect of the Granulator Compaction Pressure on the Granule Properties

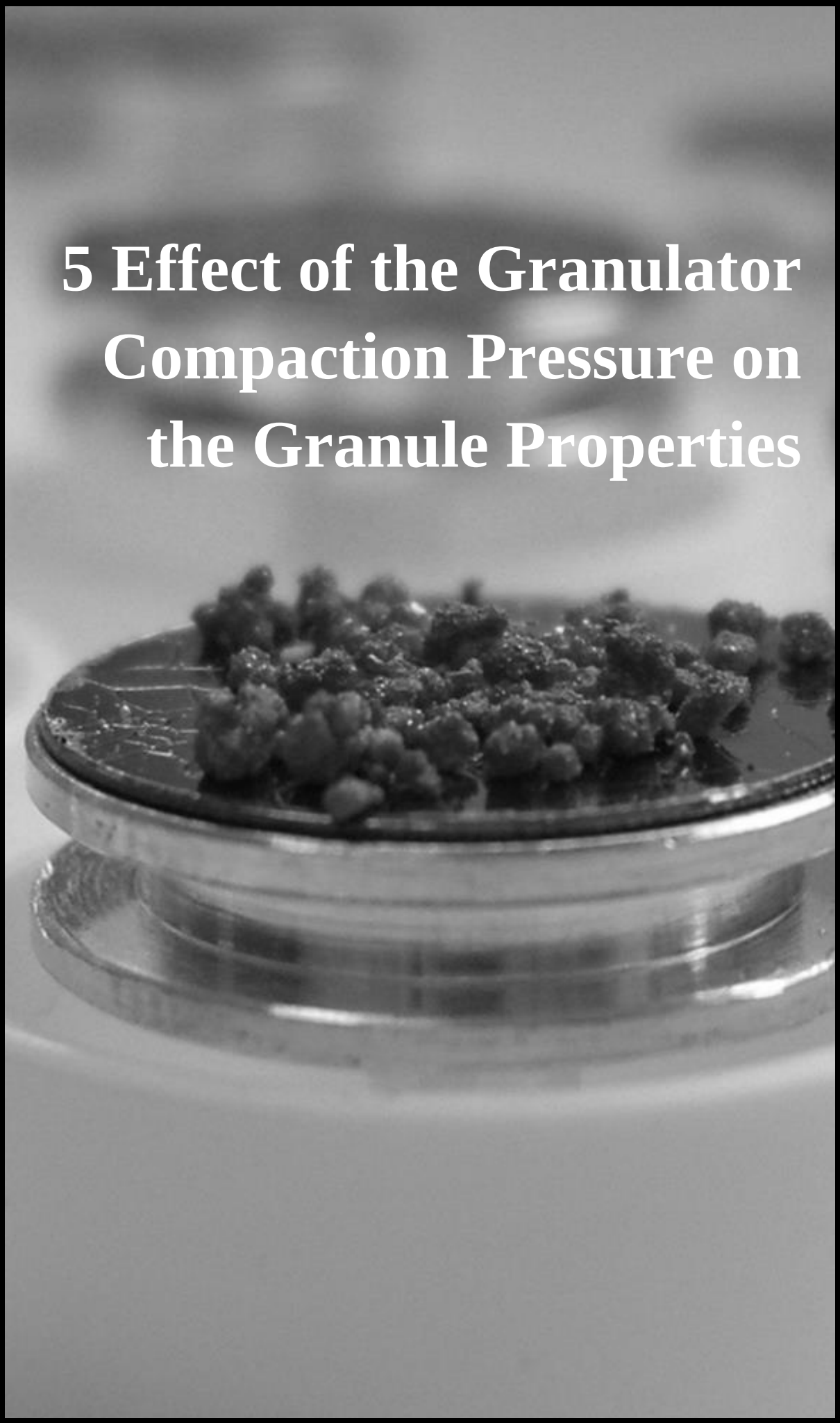

5 EFFECT OF THE GRANULATOR COMPACTION PRESSURE ON THE GRANULE PROPERTIES

"*When you are face to face with a difficulty, you are up against a discovery*"

- Lord Kelvin (William Thompson), Physicist and engineer -

5.1 INTRODUCTION

In the previous chapter, the Unified Compaction Curve was found to be a feasible model to predict the final tablet strength from the wet granulation process. The granulation data for varying liquid level and wet massing times collapsed onto a master reference curve, enabling the tablet strength to be predicted from the number of impeller revolutions. The model also quantitatively predicts the effective compaction pressure exerted on the granules by the impeller during granulation, which links granulation conditions and stresses in the granulator for the first time.

Although the Unified Compaction Curve model is able to be applied to the wet granulation process, what does the Unified Compaction Curve model really tell us in terms of why there is a relationship between the wet granulation conditions and the final compaction properties of the granules? What is it about the wet granulation conditions which influence how much the granules are able to compact to form a tablet? From the previous chapter, it can be seen that the number of impeller revolutions has a major influence on the tablet strength. Therefore it can be concluded that the impact of the impeller on the powder and granules compromises certain part(s) of the granule properties.

This chapter aims to explore and determine the granule properties which are compromised by the impact and shear forces during wet granulation and ultimately decreasing the tablet strength. To achieve this, the granule morphology along with the granule topology, granule specific surface area, density, porosity and tablet density were investigated for various numbers of impeller revolutions. By understanding the relationship between the granule properties and the tablet strength, the tablet strength can be predicted from the wet granulation conditions and optimised to achieve the desired

tablet strength. This would pave a way towards efficient pharmaceutical engineering and minimise economical and material waste and from un-successive granulation batches.

The introduction of mechanical energy from the granulator impeller and the impact on the powder and granules would be expected to refine the granule properties considerably, in particular the ability for the granules to compact, the granule porosity and the granule topology and morphology.

5.2 EXPERIMENTAL PROCEDURE

Twelve samples (as shown in Figure 5.1) were selected to represent granules with different impeller revolutions and wet granulation compaction pressure from the experiments in *Chapter 4: Using the Unified Compaction Curve to Predict the Tablet Strength from the Wet Granulation Process*, which is also described in *Section 4.2: Materials and Experimental Procedure*. The twelve samples represent a wide range of total impeller revolution from 500 to 7400 revolutions and a summary of the granulation conditions from which the granules were produced from are presented in Table 5.1.

Because the number of impeller revolutions was found to be the driving influence on the cumulative wet granulation compaction pressure, regardless of the wet granulation conditions, the selected granules also represent different liquid levels, binder flow rates, impeller speeds and wet massing times. Figure 5.1 shows the decrease in the tablet strength with increasing number of impeller revolutions as the curve translates towards the higher wet granulation compaction pressures (thereby a higher wet granulation tensile strength which lowers the tablet strength).

Table 5.1: Summary of the wet granulation processing conditions for the twelve samples chosen for granule characterisation analysis.

Sample	Number of Impeller revolutions [-]	Liquid Level [wt.%]	Wet Massing Time [mins]	Impeller speed [RPM]	Binder flow rate [g/min]	P_{WGC} [MPa]	Tablet Hardness [kp]
1	485	20	0.17	285	130	27.3	25.0
2	259	20	0.17	285	280	16.1	27.1
3	137	20	0.17	150	280	18.2	26.4
4	1226	30	2.00	285	130	53.4	20.3
5	1664	50	2.00	285	130	84.6	16.3
6	1387	50	0.17	600	280	43.4	23.0
7	2333	50	0.17	600	130	78.2	17.8
8	2366	30	6.00	285	130	88.8	15.6
9	2580	30	2.00	600	130	104.4	14.0
10	3506	30	10.0	285	130	108.7	15.2
11	4980	30	6.00	600	130	133.2	12.5
12	7380	30	10.0	600	130	118.6	11.0

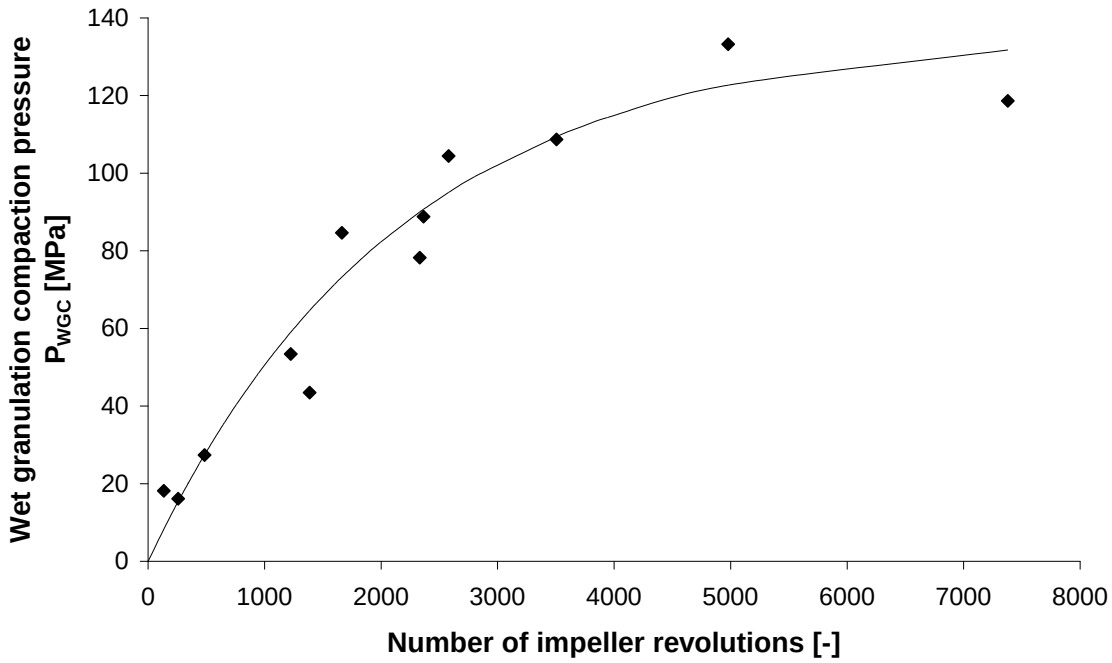

Figure 5.1: Selected granular samples produced from wet granulation experiments (in Chapter 4), used to characterise the granule structure and observe the implications on the wet granulation compaction pressure, P_{WGC}.

The granule characterisation included examining the external morphology, circularity and internal structure of the granules (skeletal density; apparent granule density and porosity; and specific surface area).

The surface roughness of the granules was examined to observe any changes to the granule external morphology with increasing impeller revolutions. The granule surface

was examined qualitatively by Scanning Electron Microscopy (SEM, Phenom) at 500× and 1000× magnification.

The circularity image analysis was based on the SEM images, captured using SEM at 500× magnification (Figure 3.20a). For each selected granulation batch, ten granules were analysed to determine the circularity value using the imaging software *ImageJ* and calculate the standard deviation of the mean for the data set. The process for the image modification and processing are outlined in *Section 3.5.5: Granule structure Imaging and Analysis*.

The skeletal density of the granules was measured using helium pycnometer (AccuPyc 1330, Micromertitics). To ensure accuracy of the results, the pycnometer was calibrated for every second measurement conducted using the calibration steel balls. The sample was purged with helium gas fifty times before the skeletal density measurement commenced. For each granular sample, the measurement was in two-fold: (1) bulk sample comprising of the complete granule size distribution; (2) sieved-fraction of granules between 90-250μm. For each sample, a total of ten measurements were performed with an average calculated for the total number of measurement runs. The skeletal density of a tablet produced by compaction of the 90-250μm sieved-fraction granular sample at 2722kg_f (6000lb_f) was also measured. Three tablets were used for each measurement with the average skeletal density calculated for the three tablets. The operating and analysing conditions for both granule and tablet samples were the same.

The apparent granule density and porosity was measured by two methods: (1) kerosene displacement; and (2) mercury intrusion porosimetry. For each granular sample, a sieved granule size range between 90-250μm was chosen to measure the apparent density and porosity. For the mercury intrusion porosimetry measurement, the sample was degassed with helium gas at room temperature (25°C) for at least four days to ensure the sample was thoroughly free of contaminant and moisture. The sample was subject to pressures up to 65,000 psia using both low and high pressure ports on the instrument, to allow the mercury to penetrate into the granules and measure the granule density accurately. Once the data was collected, the data was further analysed manually to calculate the granule porosity taking into the granule internal pores only (please refer to *Section 3.5.4: Granule*

Porosity and *Appendix G: Mercury Intrusion Porosimetry Raw Data and Granule Porosity Calculations*).

The granule surface area was measured by nitrogen gas adsorption (Belsorp Mini II, Belsorp) analysis. For each granulation batch, the sample was degassed with helium gas at room temperature (25°C) for at least four days prior to the analysis to ensure the sample was clean and dry. The adsorption analysis was conducted under cryogenic temperatures using liquid nitrogen (cryogenic temperature of (-196°C). The relative pressure points (ratio of P/P_0) in which the analysis took place were between 0.05 to 0.9.

Once the characterisation data was collected, the granule properties were compared to each other for varying number of impeller revolutions.

5.3 CHARACTERISATION RESULTS

5.3.1 GRANULE TOPOLOGY AND MORPHOLOGY

The SEM imaging reveals that there is a significant transition in the granule morphology and topology for increasing long residence times (high number of impeller revolutions) in the granulator as shown in Figure 5.2.

For short wet massing periods (low impeller revolutions) in the granulator, there is a low degree of wet granulation as there are un-granulated fibres of microcrystalline cellulose and lactose crystals evident in the granulation batch at 485 impeller revolutions. As the number of impeller revolutions increases, the powder begins to agglomerate to form loosely-packed granules at approximately 1,400 revolutions, before the microcrystalline cellulose eventually envelops the lactose crystals and densify the granules at 7,400 revolutions.

As the powder and granules are subjected to the impeller forces during wet granulation, the granular surface gradually smoothens as the microcrystalline cellulose plastically deforms during consolidation. The granule topology smoothens in conjunction with the rounding of the granules as seen in Figure 5.3.

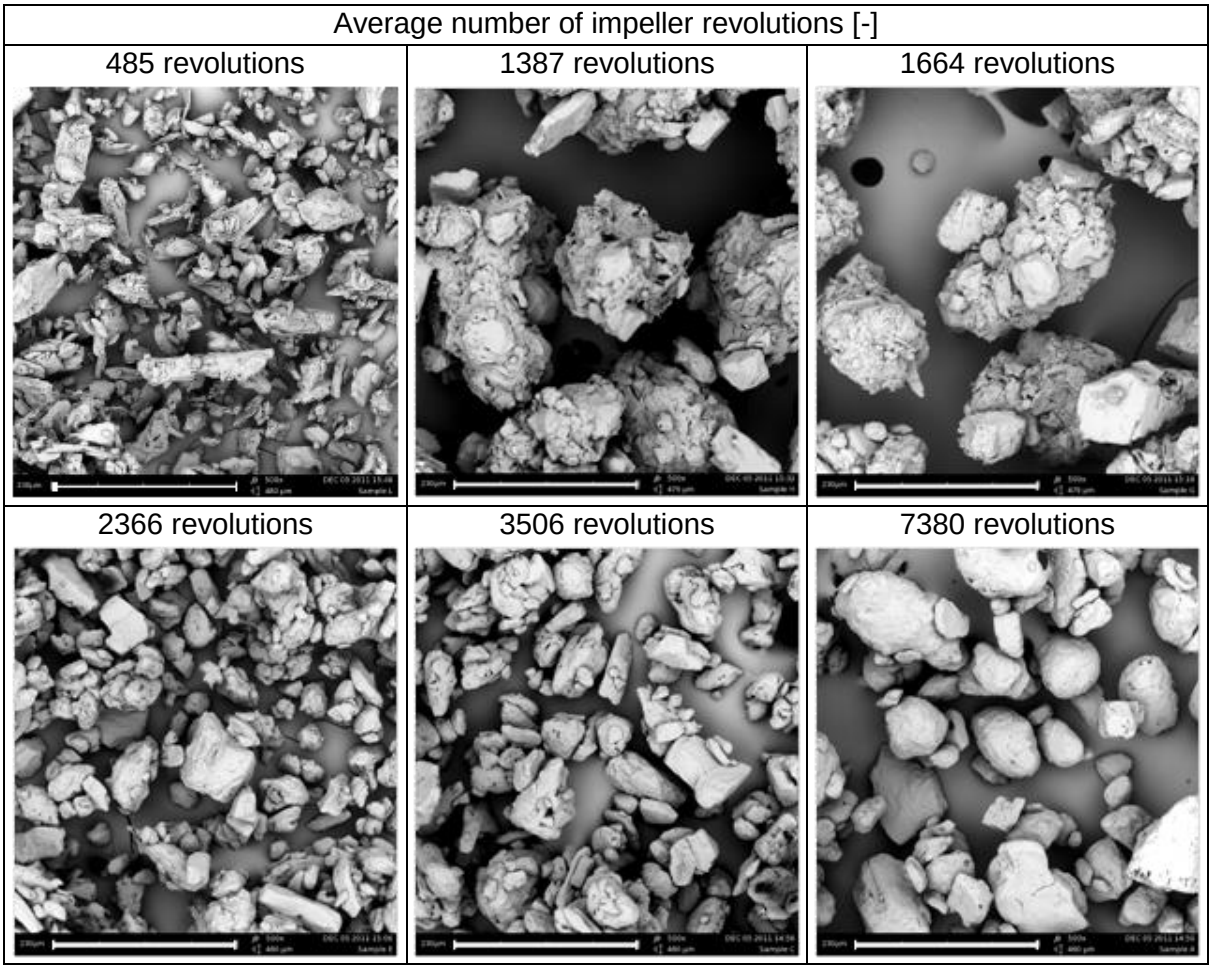

Figure 5.2: SEM images of granules produced from varying number of impeller revolutions. Images are at 500 times magnification. Scale-bar represents 230µm.

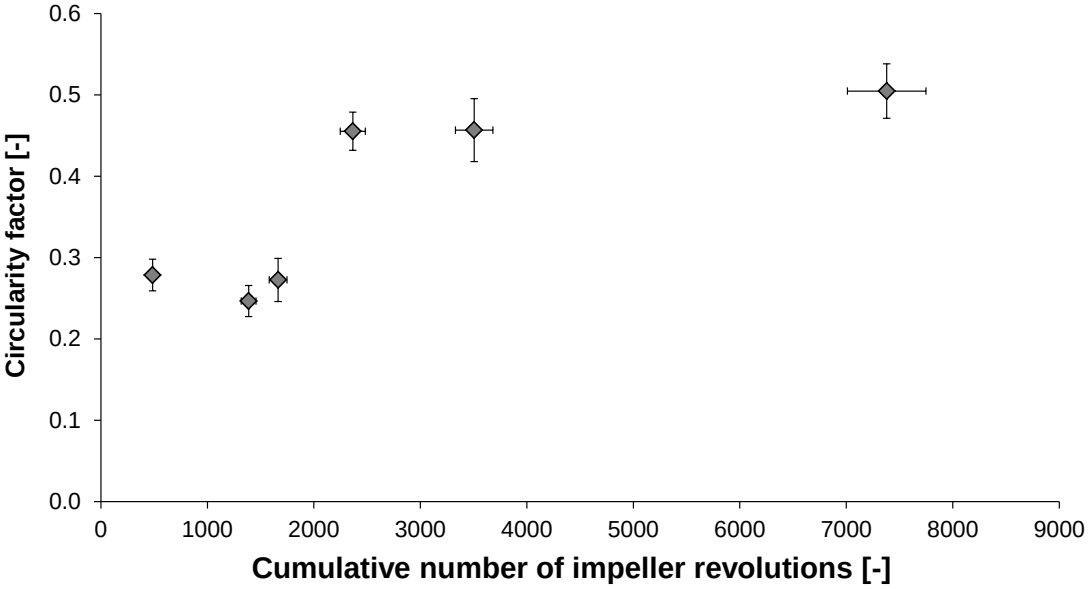

Figure 5.3: The Circularity dimension of the projected profile of granules as a function of the cumulative number of high-shear granulator impeller revolutions.

The smoothening and rounding of the granules can be seen in the circularity of the granule, as presented in Figure 5.3. Each data point in the figure represents ten granule shape analysis, with the error in the analysis represented by the standard deviation of circularity for the sample batch. The *x*-error bars represents ±5% of the impeller revolutions. The circularity results demonstrate that as the residence time of the granules in the granulator increases, the granules become more spherical as seen by the increase in the circularity value from the lowest value being 0.27 to the highest value of 0.50 (a spherical sample would have circularity value of 1.00). Observing the circularity profile, there appears to be a critical morphology transition condition in which there is an abrupt increase in the circularity value at approximately 2,500 impeller revolutions. The circularity value increases from 0.30 to 0.50. The critical morphology transition region may indicate a possible change in the consolidation mechanism where the particles in the granule may have reached its packing limiting and additional compaction forces from the impeller induces plastic deformation of the microcrystalline cellulose. However, this is yet to be proven.

5.3.2 GRANULATION MEAN SIZE

The granule size distribution of the bulk granular samples as a function of the number of impeller revolutions is presented in Figure 5.4. The data has an x-axis error of ±5% of the theoretical impeller revolutions. From the granule size distribution, the average size of the granules is consistent at approximately 100µm across most granulation batch samples; however the mean granule size can increase to 340µm. This was found for granule samples with 50wt.% liquid level, where the mean granule size was between 150µm to 340µm. Figure 5.4 shows that for this formulation, the granule size distribution does not found to influence the final tablet strength, contrary to previous literature studies on different formulations. This can also be seen in Figure 4.11, which showed similar data for the full set of granulation experiments.

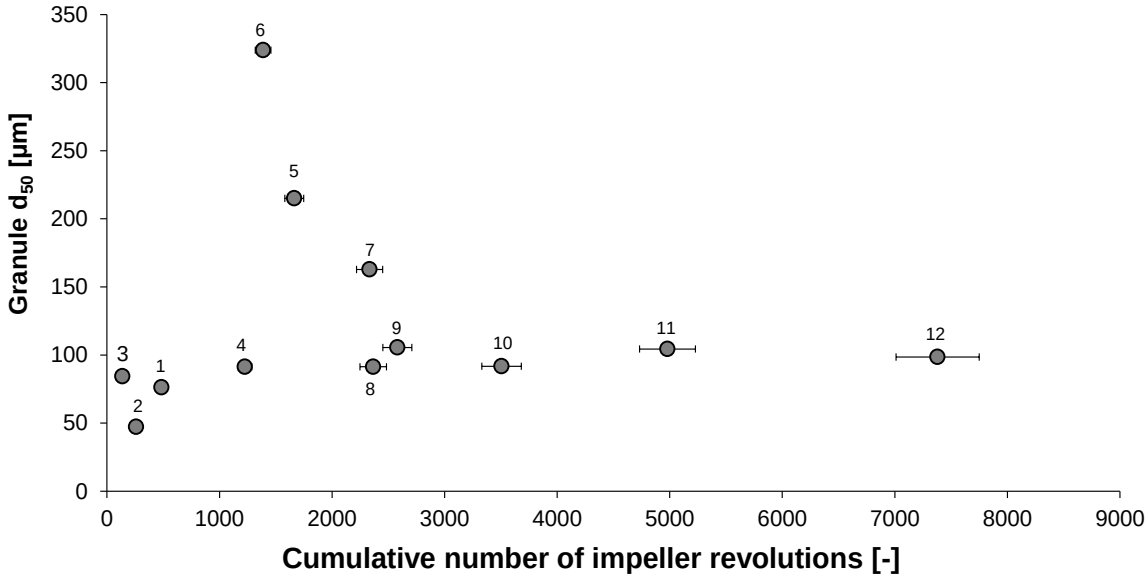

Figure 5.4: The mean granule size d_{50} as a function of the number of impeller revolutions. Each data-point is labelled with the sample number as described in Table 5.1.

5.3.3 GRANULE AND TABLET SKELETAL DENSITY

There is a transitional change in the average skeletal (true) density as a function of increasing number of impeller revolutions as seen in Figure 5.5. Each data point is representative of five replicates with the x-axis error bars representing ±5% of the impeller revolutions and the y-axis error bars denoting the standard error of the mean for the skeletal density. The granule skeletal density profile as a function of impeller revolutions demonstrate that the skeletal density decreases from 1.60g/cm^3 to 1.54g/cm^3 as the granules are subject to longer periods of compaction forces from the granulation process.

For both bulk and sieved granular samples, the overall profile is the similar; however the bulk sample exhibits a higher skeletal density, which may be due to the presence of coarse granules within the sample which are removed in the sieved sample (sieved between 90-250µm). The trend of decreasing granule density may be indicative of the consolidation of the granules during wet granulation (e.g. increasing number of impeller revolutions) in which the microcrystalline cellulose obstructs the granular pores as it envelopes the lactose particles and the granule densifies.

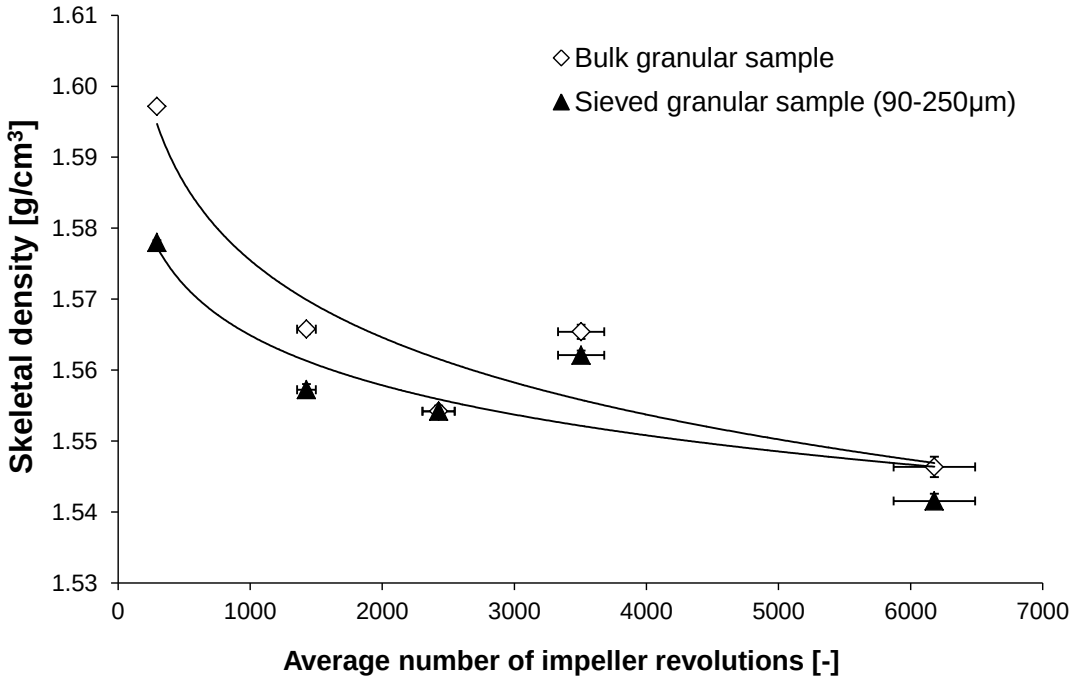

Figure 5.5: Granule skeletal density as a function of the number of impeller revolutions.

Bearing in mind that a high number of impeller revolutions leads to a reduction in the tablet strength (e.g. higher wet granulation compaction pressure P_{WGC} value), the decrease in the skeletal density also decreases the tablet strength. This finding appears to contradict logical expectations and literature studies. The trend in the skeletal density may be attributed to the physical changes in the granule structure or the material physical properties whilst wet, consequently leading to a reduction in the skeletal density. Further research into changes in the material properties upon exposure to moisture, in particular the swelling of microcrystalline cellulose, will be investigated in *Chapter 6: Effect of the Granulation Compaction Pressure and Liquid Binder on the Microcrystalline Cellulose Material Properties*.

However, when the bulk and sieved granule skeletal density profiles are examined (in Figure 5.5), the change in skeletal density value is minor and hence it can be demonstrated that the compaction pressure from the granulator impeller does not have a significant influence on the granule density and hence the final tablet strength.

Looking at the skeletal density profile for tablets as a function of the impeller revolutions (see Figure 5.6), the impeller revolutions do not have a major influence on the final tablet skeletal density. As seen in Figure 5.6, the tablet skeletal density ranges from 1.58g/cm^3 to approximately 1.61g/cm^3. Therefore for both granule and tablet skeletal density, the

compaction pressure from the wet granulation process is not a strong factor to establish the final tablet strength. Therefore the attention is now turned to the granule surface area and granule porosity characterisation in the following sections.

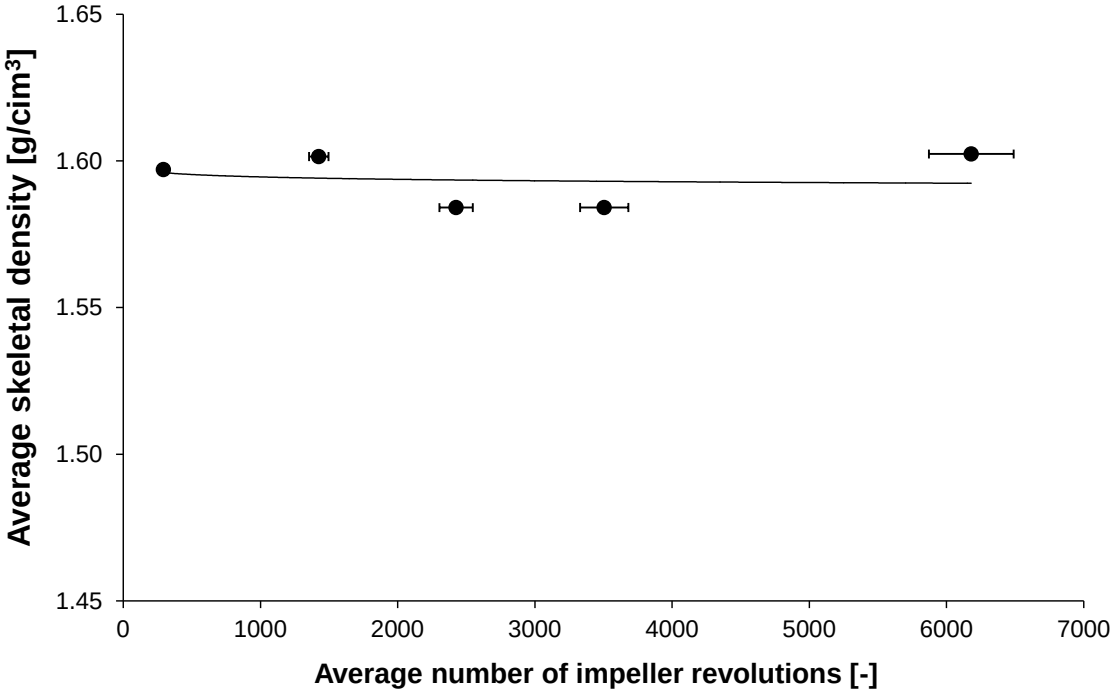

Figure 5.6: Tablet skeletal density as a function of the number of impeller revolutions.

5.3.4 GRANULE SPECIFIC SURFACE AREA

Examining the granular BET specific surface area revealed that the surface area is not a contributing factor to the final tablet strength as presented in Figure 5.7. Each data point in the figure represents duplicate samples with the measurement error shown by the standard error of the mean in the *y*-axis error bars. The *x*-axis error bars represent the variation in the granulator impeller speed, which is estimated to be within ±5% of theoretical number of impeller revolutions. Observing the profile in Figure 5.7 shows that the specific surface area can be large, up to 0.78m^2/g, for granules produced from very short granulation times (i.e. below 500 impeller revolutions). This finding supports the SEM images in Figure 5.2, in which the granules at 485 impeller revolutions have a rough granular surface. However the SEM image at 485 impeller revolutions also shows evidence of un-granulated powder, which may add to the large specific surface area for the granular sample. The presence of fine powder and granules would not significantly affect the final tablet hardness as shown in the granule size distribution in Figure 5.4. Beyond 500 impeller revolutions, the specific surface area remains in a narrow range from approximately 0.4-0.5 m^2/g.

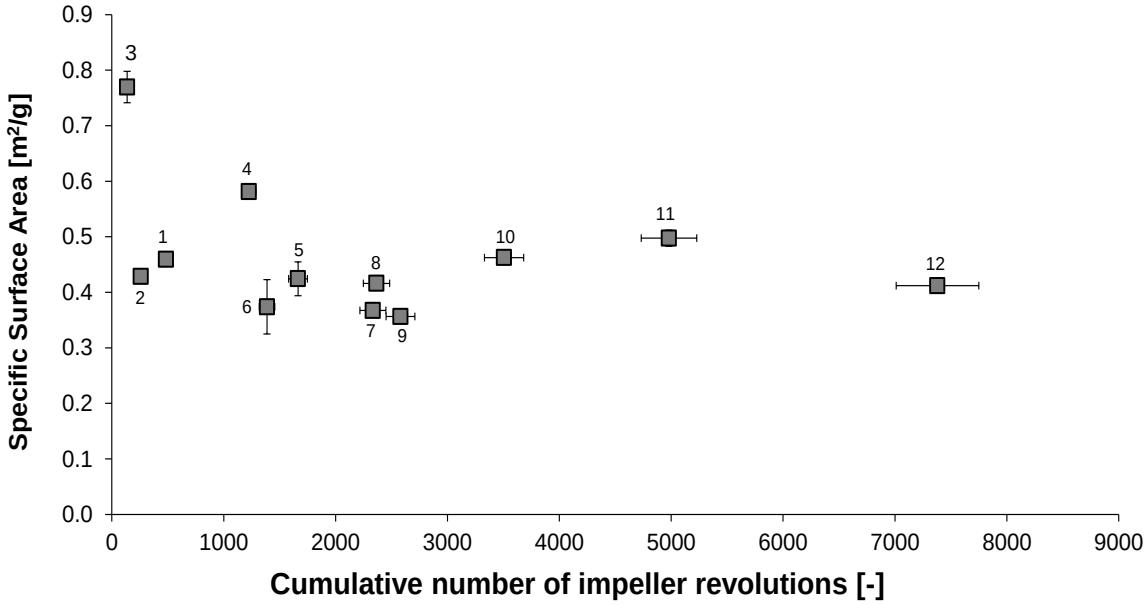

Figure 5.7: Granule specific surface area as a function of the number of impeller revolutions. Each data-point is labelled with the sample number as described in Table 5.1.

Because the specific surface area is not affected by the number of impeller revolutions, while the tablet strength is inversely proportional to the number of impeller revolutions, it can be established that the specific surface area of the granules is not the governing factor for the final tablet strength, as is demonstrated by the lack of trend in the relationship between the tablet tensile strength and the specific surface area in Figure 5.8.

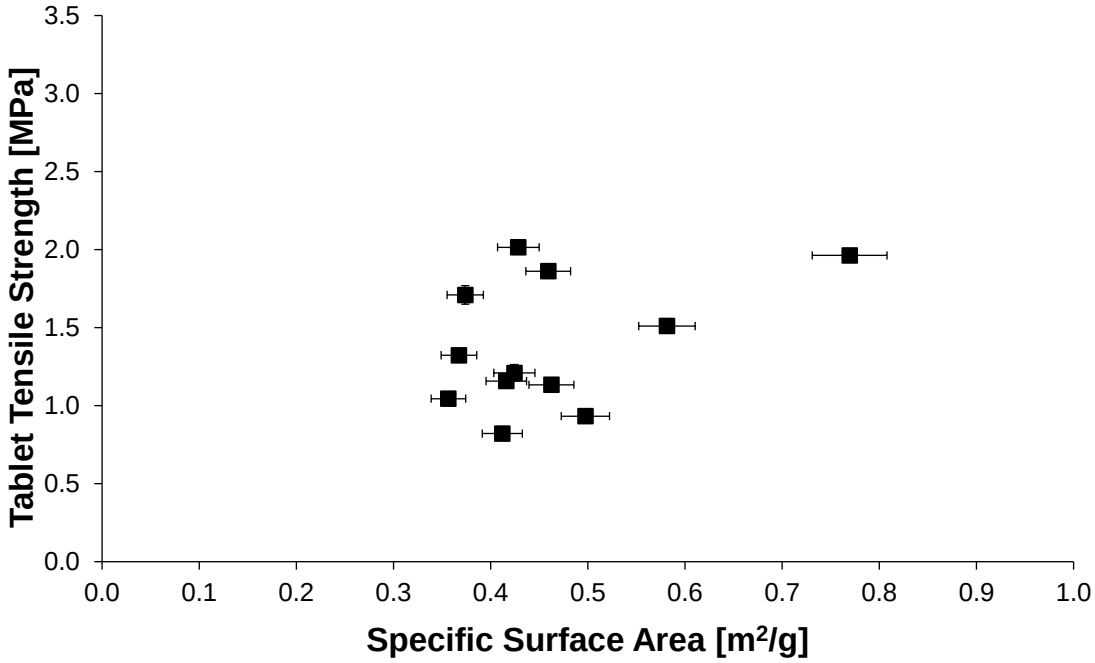

Figure 5.8: The tablet tensile strength as a function of the granule specific surface area as measured by nitrogen adsorption analysis (Belsorp).

5.3.5 GRANULE POROSITY

As was seen in the previous sections, the surface area and granule densities were not the driving factor for the change in tablet strength with increasing number of impeller revolutions. Therefore the granule porosity will now be examined with the results of the granule porosity measurements presented in Figure 5.10 (seen on the next page). The error bars represent ±5% of the chosen number of impeller revolutions and the standard error of the mean for duplicate measurements for the x-axis and y-axis respectively.

From Figure 5.10, it can be seen that the Analysis of the granule porosity as a function of the number of impeller revolutions shows that this is an important factor for the tablet strength. The granule porosity is inversely proportional to the number of impeller revolutions. As the residence time of the granules within the granulator increases (i.e. high number of impeller revolutions), the granule porosity decreases from 18% to approximately 8%. Figure 5.10 presents an interesting finding, in which the decrease in the granule porosity with increasing number of impeller revolutions mirrors the trend of the increase in the effective wet granulation compaction pressure (P_{WGC}) with increasing number of impeller revolutions (Figure 5.9). This finding demonstrates the importance of the residence time of the granules in the granulator (number of impeller revolutions) on the granule porosity and the effective wet granulation compaction pressure, which will ultimately effect the final tablet strength.

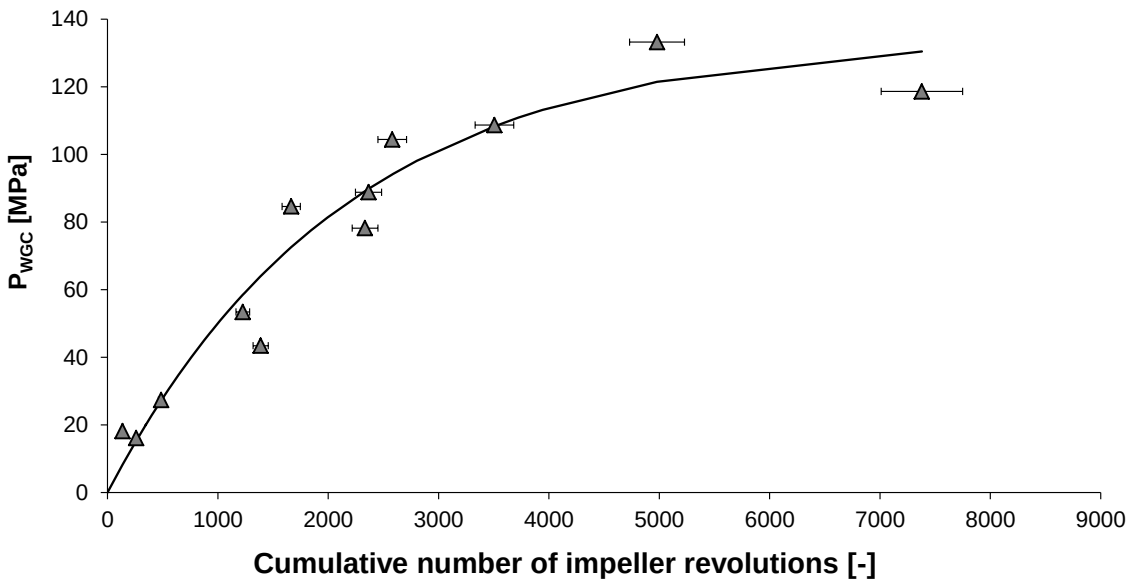

Figure 5.9: The effective wet granulation compaction pressure, P_{WGC}, as a function of the cumulative number of impeller revolutions.

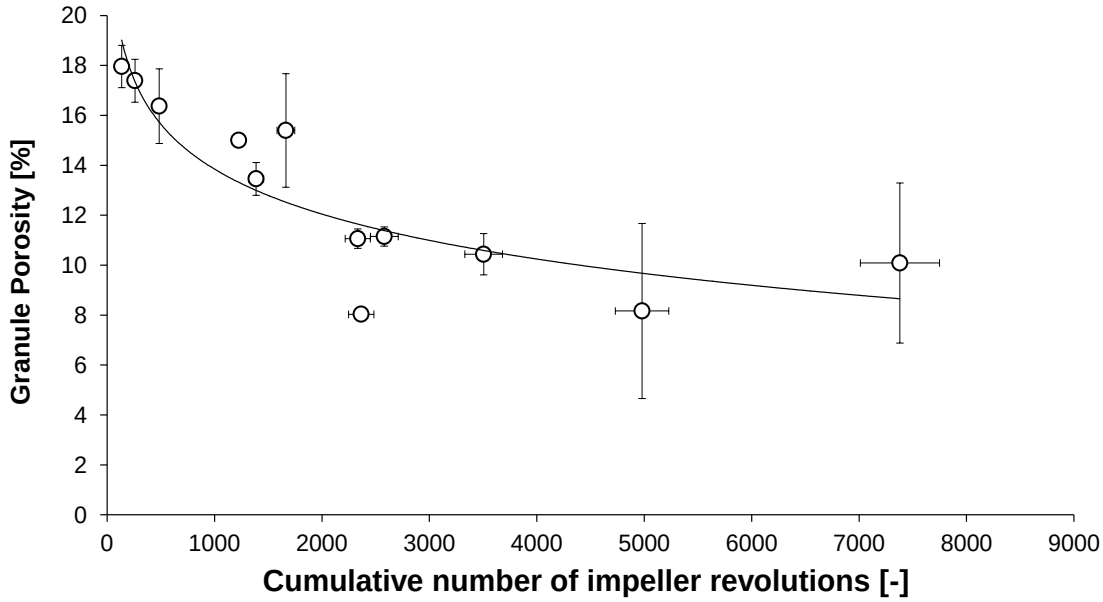

Figure 5.10: Granule porosity as a function of the number of impeller revolutions as measured by mercury intrusion porosimetry analysis.

The importance of the granule porosity on the tablet hardness is demonstrated in Figure 5.11. As the granule porosity increases from 8 to 17%, the tablet hardness increased from approximately 12.5 to 27MPa. This finding would support the SEM images and the circularity results, in which the consolidation and rounding of the granules during wet massing would decrease the granule porosity and reduce the tablet strength as seen in Figure 5.11.

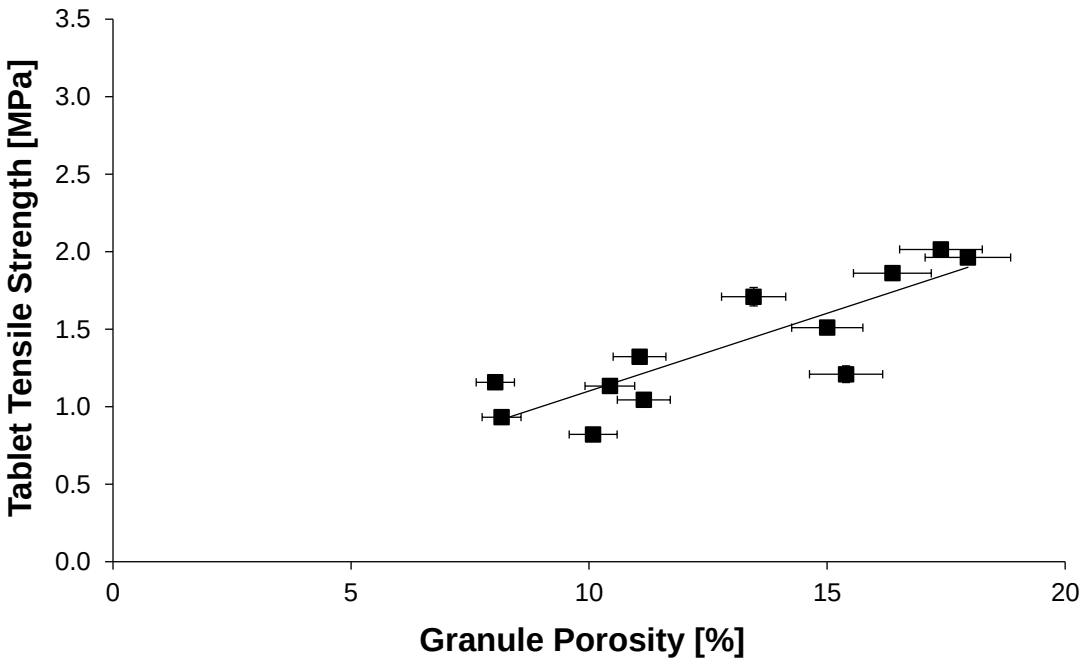

Figure 5.11: The tablet tensile strength as a function of the granule porosity as measured by the mercury intrusion porosimetry analysis.

The relationship between the tablet hardness and the granule porosity is supported by the relationship between the effective wet granulation compaction pressure and the granule porosity, presented in Figure 5.12. From the observation of Figure 5.11 and Figure 5.12, it can be seen that the two figures are also mirror images of each other, like the results in Figure 5.9 and Figure 5.10. Again this demonstrates that the granule porosity plays a vital role in controlling the final tablet strength.

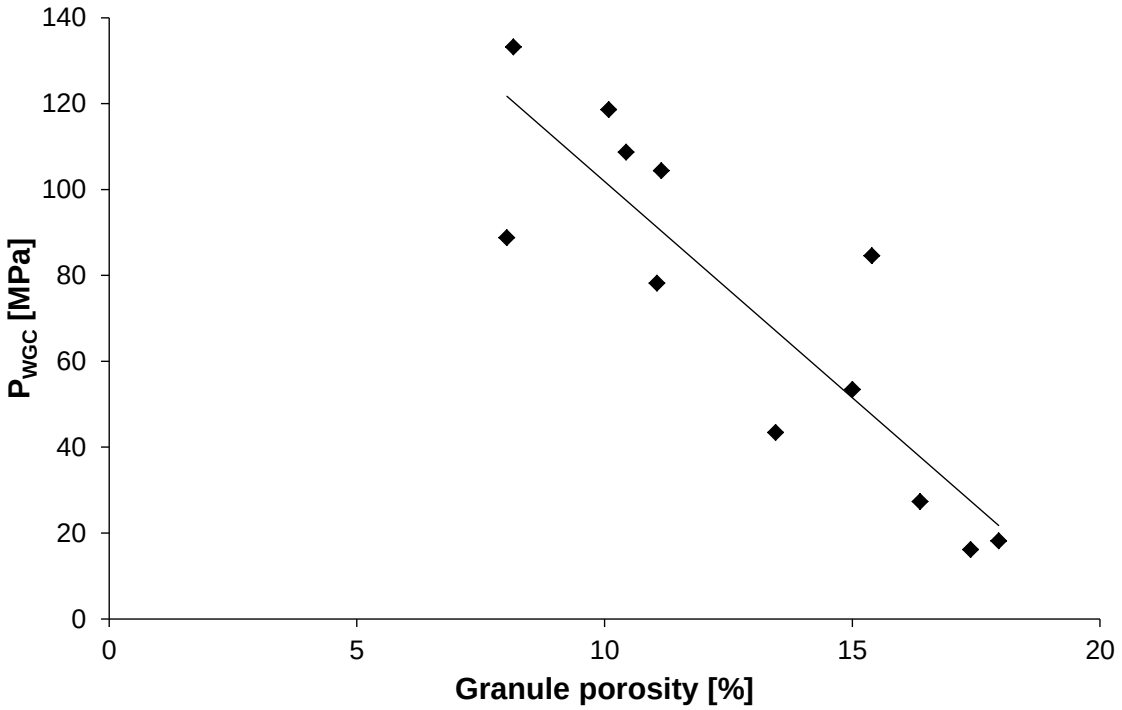

Figure 5.12: The effective wet granulation compaction pressure, P_{WGC}, as a function of the granule porosity.

5.4 DISCUSSION

The investigation into the effect of the compaction forces from the granulator impeller on the granule properties and ultimately the tablet strength reveal that the tablet strength appears to be dependent on the strength of the bonding between the granules. This is seen through the granule surface roughness, the granule circularity dimension and the granule porosity.

The findings from this study show that there is a transition in the granule surface roughness with increasing number of impeller revolutions. As the powder is subjected to longer periods of compaction from the granulator impeller, the powder begins to agglomerate with the aid of the liquid binder to form loosely-packed granules, such as those produced at approximately 1,500 impeller revolutions in Figure 5.2. These initial granules have a rough granular topology, with minimum irreversible deformation in the

powder particles. The combination of the rough surface and minimum particle deformation would help the granules undergo mechanical inter-locking during the final tabletting stage to form a tablet with high strength. If the loosely-packed granules are subjected to further wet massing during the granulation process, then the granules begin to consolidate and deform any protruding particles on the surface, which reduces the granular surface roughness and the granules appear more spherical in shape. This behaviour is consistent with Shi and co-workers wet granulation study (Johansson and Alderborn, 2001; Shi *et al.*, 2011; Shi *et al.*, 2011) which found similar topology and morphology changes for pure microcrystalline cellulose granules.

The formation of spherical granules with smooth surface is evidence that the powder formulation exhibits different deformation behaviours. From the SEM images, the lactose crystals remain relatively undeformed and fracture upon sufficient impact from the impeller. The porous microcrystalline cellulose fibres plastically deform and envelop the lactose crystals with increasing granulation time (i.e. large number of impeller revolutions). Therefore, it is primarily the microcrystalline cellulose powder that is responsible for the reduction in the granule surface roughness and the improvement of the sphericity. The effect of the number of impeller revolutions on the particle packing within the granule is evident in Figure 5.3. The abrupt increase in the circularity dimension may suggest that at low numbers of impeller revolutions (below ~1,800 impeller revolutions), the granule structure would be comprised of loosely-packed agglomerated particles which reach the critical transitional packing density at approximately 2,500 impeller revolutions before the microcrystalline cellulose particles begin to envelop the lactose particles at high impeller revolutions.

The granule porosity has been shown to be an important parameter to consider in controlling the tablet strength. The results in Figure 5.10 portray that the granule porosity is inversely proportional to the number of impeller revolutions. The reduction in the granule porosity with increasing granule residence time in the granulator is evident of consolidation occurring within the granules by the granulator impeller. The consolidation of the granules would affect the packing and deformation arrangement of the particles within the granules. Due to the plastic deformation ability of the microcrystalline cellulose particles, the granule porosity is speculated to be determined by the extent of “sacrificial deformation” of microcrystalline cellulose over the lactose crystals (lactose

particles are expected to rearrange and minimise the granule porosity). The decrease in the granule porosity is correlated with the increase in the wet granulation compaction pressure, suggesting that the consolidation and reduction in the granule porosity leads to a decline in the tablet strength.

The skeletal density, average granule size and the specific surface area were found not to be significant for the tablet strength. In Figure 5.4, Figure 5.5 and Figure 5.7, the results were not statistically significant to the final tablet strength for the average granule size, granule skeletal density and the granule specific surface area respectively. For the average granule size, the results from this study supports the finding found in McKenna and McCafferty's work (1982) in which they found that the particle size is independent from the chemical and physical particle-particle interactions for microcrystalline cellulose. The skeletal density was proportional to the number of impeller revolutions. Although this finding is unexpected, the densification of the granules from prolonged compaction could be attributed to a physiochemical change occurring in the microcrystalline cellulose fibres. The microcrystalline cellulose particles comprise of a porous cellulose network which may undergo changes due to water absorption and/or shear from the impeller. The lactose particles are not expected to undergo any physiochemical change due to its rigid crystalline structure. However, some of the lactose will dissolve in water and crystallise upon drying.

The increase in the skeletal density with increasing impeller revolutions may also be due to the presence of occluded pores which are blocked by the plastic deformation of microcrystalline cellulose and enveloping of the lactose particles. Work to understand the effect of exposure to liquid binder and/or impeller shear on the material properties will be explored in *Chapter 6: Effect of the Granulation Compaction Pressure and Liquid Binder on the Microcrystalline Cellulose Material Properties*.

The Unified Compaction Curve model enables the granule topology, circularity dimension and the granule porosity to be linked to the final tablet strength. The destruction of the protruding particles, which make up the rough granular surface, and the rounding of the granules demonstrate that the impeller speed is sufficiently high to have a large wet granulation compaction pressure, P_{WGC}, and irreversibly deform the granules. Consequently, the destruction of the mechanical-interlocking mechanism during

tabletting leads to a reduction in the inter-particulate bonds and hence the tablet strength. The Unified Compaction Curve is able to give an insight in that the strength of the bond is an important parameter to consider in controlling the tablet strength.

5.5 CONCLUSIONS

The investigation into the effect of the granule properties on the final tablet strength, revealed that the impact from the granulator impeller has an effect on the granule topology and morphology.

As the residence time of the granules within the granulator increased, the granule surface roughness decreases and the granules become more spherical with the circularity dimension increasing in value from 0.25 to 0.50. This is evident of the deformation and enveloping of the microcrystalline cellulose around the lactose particles as part of the consolidation process during wet granulation. As a result, the granules become more smooth externally and spherical, which decreases the tablet strength.

The granule porosity was also found to undergo significant changes as the number impeller revolutions increases. The granule porosity decreased from 18% to 8% as the impeller revolution increased, which coincides with the consolidation and deformation of the microcrystalline cellulose particles upon impact with the granulator impeller.

The Unified Compaction Curve demonstrated that the particle size, specific surface area and the skeletal density (or true density) are not significant factors for the final tablet strength. The skeletal density slightly decreases as the number of impeller revolutions increase for granules but remains relatively consistent for tablets. The data and the error bars for the particle size, specific area and the skeletal density as a function of increasing number of impeller revolutions show that the relationship between these granule properties are not statistically significant.

From the results of the investigation, it is speculated that the granule porosity and the strength of bonding between the particles are the controlling factors in the tablet strength, rather than the number of granule-granule bonding sites as suggested by literature. The bonding strength is speculated to be promoted by mechanical inter-locking between the granules during the tabletting process. Therefore the Unified Compaction Curve gives an

insight into the blue-print for the tablet strength which would allow efficient optimisation and trouble-shooting for granulation processes.

Publication(s):

From this study two conference papers has been written:

- **T.H. Nguyen**, D. Morton and K. Hapgood (2012), "*Understanding the Unified Compaction Curve model for wet granulation and subsequent tablet strength*", CHEMECA, 23-26 September, Wellington, New Zealand, IChemE/IEAust.
- **T.H. Nguyen**, D. Morton and K. Hapgood (2013), "*Using the Unified Compaction Curve Model to Predict the Strength of Wet-granulated Tablets*", 6th International Granulation Workshop, 26-28 June, Sheffield, UK.

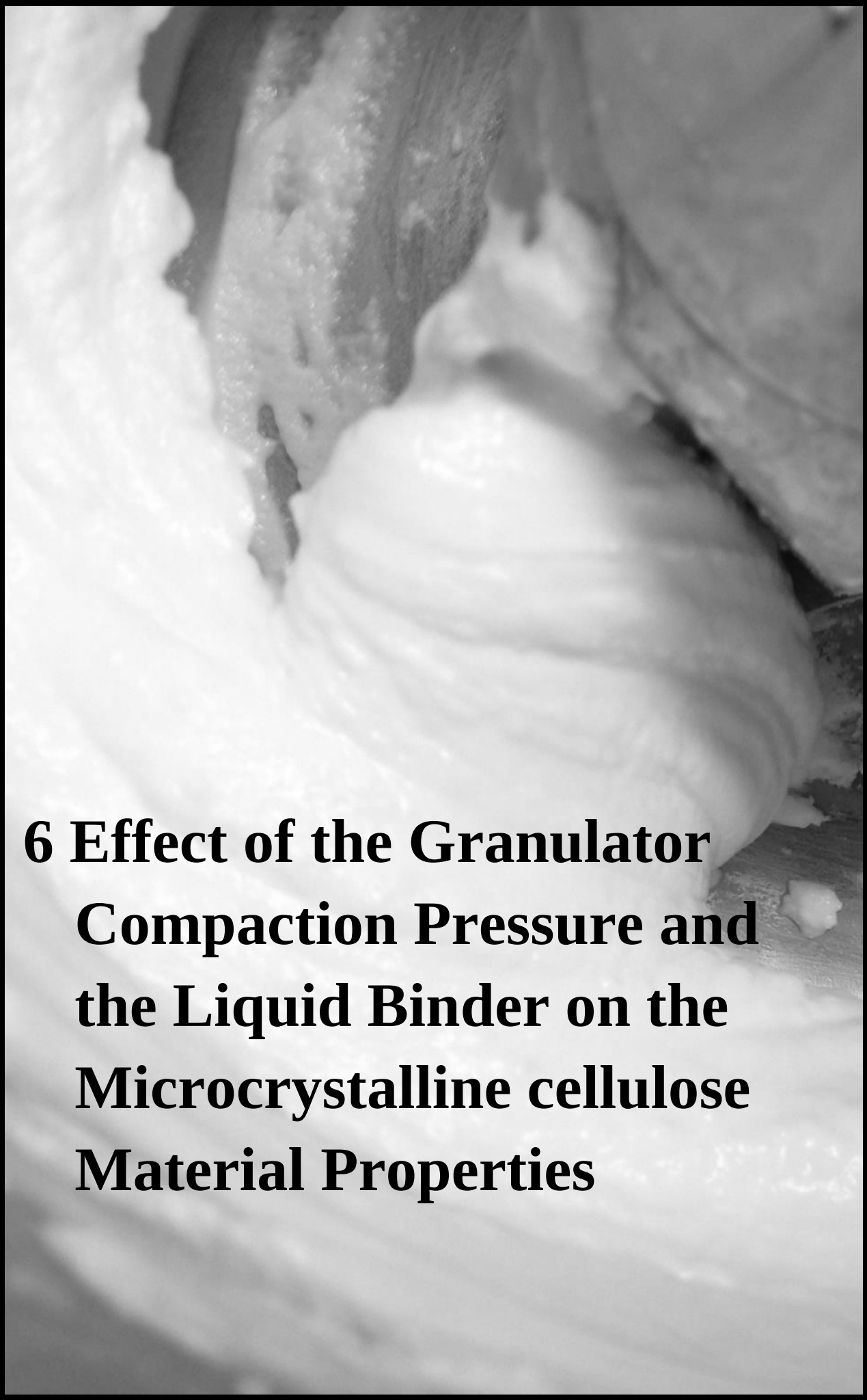

6 Effect of the Granulator Compaction Pressure and the Liquid Binder on the Microcrystalline cellulose Material Properties

6 EFFECT OF THE GRANULATOR COMPACTION PRESSURE AND THE LIQUID BINDER ON THE MICROCRYSTALLINE CELLULOSE MATERIAL PROPERTIES AND SUBSEQUENT TABLET STRENGTH

"*The whole of science is nothing more than a refinement of everyday thinking.*"

-Albert Einstein-

6.1 INTRODUCTION

So far in this thesis, the effects of the granulation conditions and granule properties on the ability of the Unified Compaction Curve model to predict the final tablet strength were investigated. The Unified Compaction Curve model has demonstrated the importance of the compaction pressure from the impeller in reducing the granule surface roughness and reducing the granule porosity. Consequently this leads to the deterioration of the mechanical interlocking between the granules during tabletting, which is vital for determining the final tablet strength. Therefore the Unified Compaction Curve relies on the ability of the microcrystalline cellulose material to plastically deform and allow for the granulation tabletability profiles to be translated along the direction of the compaction reference curve. Therefore a better understanding of the microcrystalline cellulose material properties would improve the design of wet granulation and the efficiency of the tablet manufacturing process.

During wet granulation, liquid binder is delivered to the process and therefore the presence of water, binding polymer or the liquid binder properties may alter the properties of microcrystalline cellulose. Evidence of this has been noted in literature studies (Zografi and Kontny, 1986; Fielden *et al.*, 1988; Zografi, 1988; Kumar and Kothari, 1999; Zhang *et al.*, 2003; Shrotri *et al.*, 2013). Although the wet granulation process, in particular, the wet massing time can have a strong effect on the granule morphology (Johansson and Alderborn, 2001; Shi *et al.*, 2011; Shi *et al.*, 2011; Macias and Carvajal, 2012), the wet massing period during wet granulation may alter the physiochemical properties of microcrystalline cellulose. Therefore the tablet strength will be investigated for various moisture addition levels (humidified powder or direct liquid addition of various liquid binder properties) to the microcrystalline cellulose and lactose powder mixture as a function of wet massing time. The amorphous and crystalline regions of the

microcrystalline cellulose powder will also be investigated from the wet granulation process.

6.2 MATERIALS AND EXPERIMENTAL PROCEDURE

The formulation used during this study was the standard 1:1 binary powder mixture of microcrystalline cellulose (Avicel PH-101, FMC BioPolymer) and lactose monohydrate 200 mesh (Pharmatose 200M, DMV-Fonterra) used in this project so far.

A series of experiments were conducted on the binary powder mixture to explore the different material properties of microcrystalline cellulose and its influence on the final tablet strength, as listed below:

- Dry powder mixing: to see if a reduction in compactability would occur after prolonged agitation in the granulator but without any liquid present,
- Powder re-humidification: to observe the compactablity of the powder at low moisture content,
- Liquid addition to the powder formulation no wet massing applied: to observe the compaction behaviour without any mixing shear applied to the wetted powder,
- Use of ethanol as a binder to see if changes in the microcrystalline cellulose-liquid binder (e.g. hydrogen bonding) affected the final tablet strength,
- Liquid binder solvent acidity: to see if a high or low pH affected the microcrystalline cellulose and changed the tablet strength,
- Microcrystalline cellulose amorphous and crystalline material properties: to observe if the microcrystalline structure was altered after wet granulation.

6.2.1 DRY POWDER MIXING EXPERIMENT

To examine the effect of shear on the microcrystalline cellulose and lactose powder mixture in the absence of moisture, the powder was dry blended (without any modification to the powder) in the 5L high-shear granulator (KG5, Key International). The powder was mixed for periods of 0 (direct compaction), 2, 8 and 10 minutes at two different impeller speeds (285rpm and 600rpm) to investigate the magnitude of shear during dry mixing. The impeller speeds were chosen such that the mixing behaviour of the powder was in roping regime (Iveson *et al.*, 2001). For each dry mixing batch, tablets were produced to measure the tablet crushing strength, as was described in *Chapter Three: Material and Experimental Procedures*.

6.2.2 POWDER RE-HUMIDIFICATION

The effect of the moisture up-take by the powder on the tablet strength was investigated by first mixing 50% microcrystalline cellulose and 50% lactose 200 mesh (by weight) in a 6L mixer (Hobart mixer, FP62) for at least 1 minute before humidifying the powder. The microcrystalline cellulose/lactose powder mixture was humidified using a saturated salt solution of sodium nitrate (Sigma-Aldrich). The powder was placed on shallow trays and onto a frame which fitted into a sealed container to ensure that the salt solution did not make contact with the powder. The powder was humidified for two weeks with relative humidity readings taken each day using a humidity reading device. The resulting relative humidity of the environment within the container was found to be approximately 63%. The relative humidity reading corresponds to a powder moisture up-take of approximately 7wt.% as noted by the moisture isotherms taken from previous literature studies (Wolf *et al.*, 1984; Khan and Pilpel, 1987; Kachrimanis *et al.*, 2006) and shown in Figure 6.1. The moisture isotherm was based on microcrystalline cellulose on the assumption that the crystalline structure of the lactose particles would not enable humidification of the lactose powder to take place.

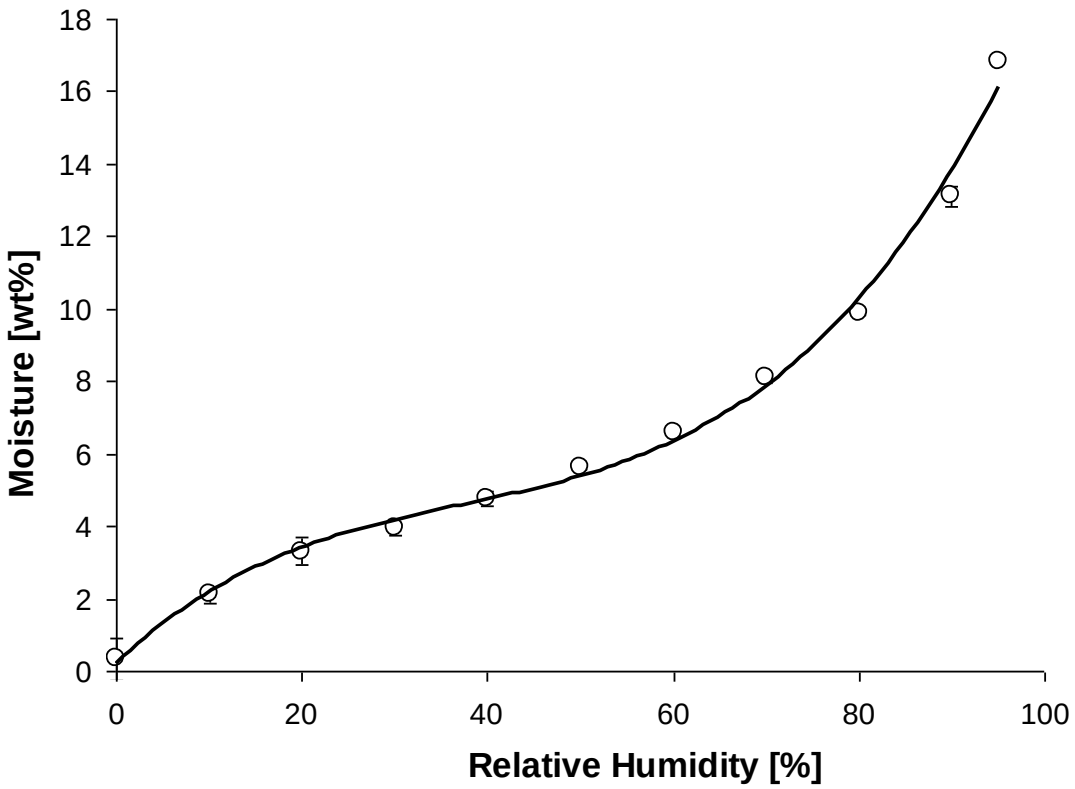

Figure 6.1: Moisture Isotherm of microcrystalline cellulose. Data taken from (Wolf *et al.*, 1984; Khan and Pilpel, 1987; Kachrimanis *et al.*, 2006).

Once the powder was humidified, the powder was removed from the humidifying environment and placed in the 5L high-shear granulator (KG5, Key International) as quickly as possible to ensure that the moisture content of the powder did not change significantly. The humidified powder was dry mixed at 600rpm for up to 12.3 minutes (the final dry mixing time being the longest total wet granulation time found in the wet granulation experiments) before undergoing tabletting.

6.2.3 WETTED POWDER, NO SHEAR EXPERIMENT

The effect of wetted powder but with no significant deforming shear on the final tablet strength was investigated. A powder mixture comprising of 50g of microcrystalline cellulose and 50g of lactose 200mesh was added into a beaker, which was placed under an over-head stirrer. The over-head stirrer was set to the lowest stirring setting (approximately 50rpm) to agitate the powder and 30g (to achieve a liquid level of 30%) of 5w/v% of PVP liquid binder was added to the powder drop-by-drop. After the liquid binder was delivered to the powder mixture, the wetted powder was mixed for 10 minutes before drying in the oven at 60°C overnight. The dried powder then underwent tabletting to see the effect of the wetted powder on the final tablet strength.

6.2.4 ETHANOL-BASED WET GRANULATION EXPERIMENT

The liquid binder solvent was also varied to investigate the effect of hydrogen-bonding within the liquid bridges and the resulting tablet strength. The liquid binder was prepared using ethanol as the solvent (previous experiments used distilled water as the liquid binder solvent). With the ethanol-based liquid binder, liquid level and wet massing granulation experiments were conducted at 600rpm. The wet massing experiment was conducted using 30wt.% liquid level, while the liquid level experiments had a wet massing time of 10 seconds. The large granulator bowl (5L, with the main impeller only, KG5 Key International) was used for the wet granulation experiments. The liquid binder was delivered to the granulator using a peristaltic pump in drop-by-drop fashion to minimise the formation of ethanol vapour. During the granulation experiments, the top of the bottle containing the liquid binder was covered with foil to minimise evaporation of the ethanol which may potentially alter the binder concentration. For each granulation batch, the granular product was placed in the fume-hood for at least an hour, prior to drying the granules in a fan-forced oven at 60°C. This was carried out to ensure that the ethanol was evaporated from the granules and minimise any hazards that may arise during

the drying process. Tablets were produced to examine the effect of the ethanol solvent on the tablet strength.

6.2.5 EFFECT OF LIQUID BINDER ACIDITY ON THE TABLET STRENGTH EXPERIMENT

The effect of the liquid binder acidity on the final tablet strength and the crystallinity of the microcrystalline cellulose were also investigated. Previous studies have shown that exposing microcrystalline cellulose to acidic liquids deteriorate the cellulosic chains thus reducing the crystallinity of microcrystalline cellulose for renewable biofuels (Zhang *et al.*, 2009; Shrotri *et al.*, 2013) and in wet granulation (Suzuki *et al.*, 2001). Therefore the exposure of acidic liquid binders to microcrystalline cellulose was carried out to investigate the extent of the cellulosic deterioration. Three liquid binders were used with varying pH levels were prepared according to the summary in Table 6.1.

Table 6.1: Summary of liquid binder formulation and acidity.

Liquid binder	Amount of PVP [g]	Amount of Acid/Basic component	Amount of Water	pH
PVP	5.26	0	100g	4
CaO	5.26	0.025g	100g	7
HCl	5.26	10mL (1M of HCl solution)	100mL	1

Wet massing time granulation experiments were carried out using each of the liquid binders. The granulation experiments were carried out in the small granulator bowl (1L, KG5 Key International) using 100g of microcrystalline cellulose and 100g of lactose 200mesh. The impeller speed was set to 400rpm and the wetted powder was wet massed for 0 (end of binder delivery time), 2, 6, 10 and 25 minutes with 65g samples taken out at each wet massing time. The liquid binder was delivered drop-wise to the granulation using a peristaltic pump. For the PVP liquid binder, the experimental results were taken from the small scale (1L) wet massing time experiments in *Chapter 7: Effect of the Granulator Scale on the Tablet Strength*. The granules were then dried in the oven at 60°C overnight, ready to be sieved (for the sieving details, please refer to *Section 3.5.1.: Granule size distribution*) and produced into tablets.

6.2.6 EFFECT OF LIQUID BINDER ACIDITY ON THE MICROCRYSTALLINE CELLULOSE CRYSTALLINITY

The effect of the liquid binder acidity on the crystallinity of microcrystalline cellulose was investigated using X-Ray Diffraction (XRD). Wet massing time granulation

experiments were carried out in the 1L bowl in the same manner as described above in *Section 6.2.5*, except that 200g of microcrystalline cellulose powder (no lactose 200mesh was present) was used as the powder formulation. Once the granules were dried in the oven, the granules were analysed using XRD. The granules were analysed using 2θ angles ranging from 10 to 50° under the following measurement conditions: Ni-filtered Cu-Kα (λ = 1.54) radiation; voltage, 40 kV; Current, 15 mA; scan speed, 0.02° per minute. For each liquid binder and wet massing time, the samples were analysed in duplicate.

From the XRD results, the crystallinity of the microcrystalline cellulose samples were calculated using a simple method based on the peak height method, as described in Equation 6.1 (Segal *et al.*, 1959; Terinte *et al.*, 2011).

$$C[\%] = \frac{I_{200} - I_{non-cr}}{I_{200}} \times 100\% \tag{6.1}$$

where C is the crystallinity percentage, I_{200} is the diffraction intensity of the maximum crystallinity peak which can be found between 2θ = 22-24°, I_{non-cr} is the diffraction intensity of the valley point for the non-crystalline region of microcrystalline cellulose, located at approximately 18°.

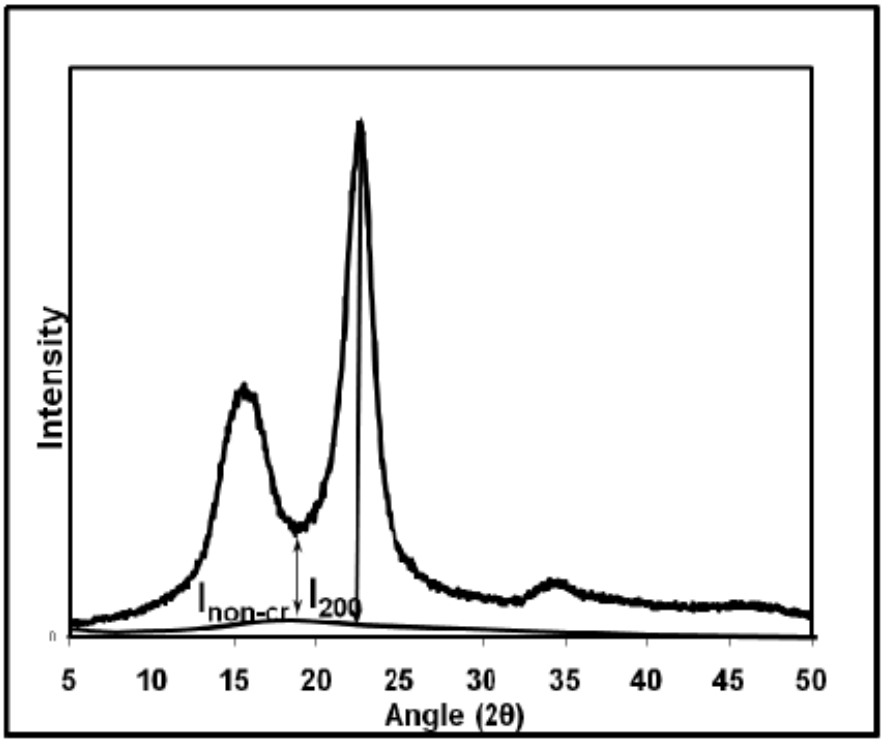

Figure 6.2: Schematic diagram of the peak height method (Terinte *et al.*, 2011).

The XRD spectra were also examined to determine the crystallite size using the Scherrer equation as described in Equation 6.2.

$$t = \frac{K\lambda}{B\cos(\theta)} \tag{6.2}$$

where t is the crystallite size, K is a constant relating to the particle shape (usually K varies from 0.9 to 1, and K = 0.9 is considered for this project), λ is the radiation wavelength (which is taken to be 0.154nm), B is the width of the peak at half the peak height of interest and θ is the diffraction angle of the peak of interest (in radians). An example of the Scherrer crystallite analysis on a XRD peak is given in Figure 6.3.

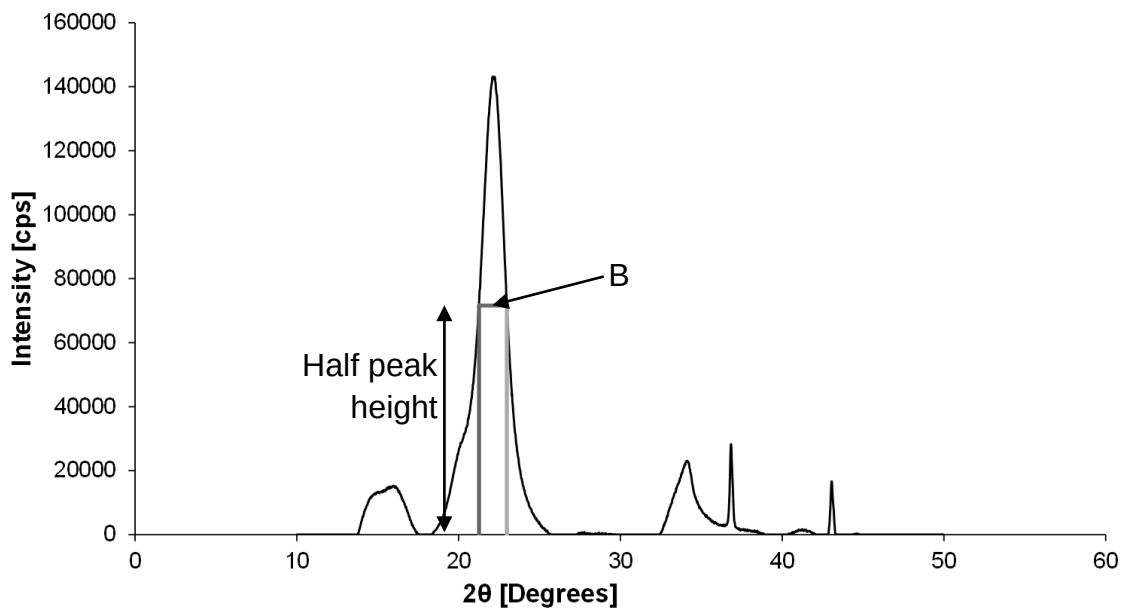

Figure 6.3: The Scherrer crystallite size analysis on a XRD spectra peak, showing the width of the peak at half the peak, *B*.

6.2.7 TABLETTING EXPERIMENTS

For each experimental batch, the resulting powder was compressed into flat-faced placebo tablets using a pneumatic single-station tablet press (Model 3887, Carver Inc. USA). The compaction forces applied by the tablet press were 2,000, 6,000, 10,000 and 16,000lb_f, to produce three to five tablets that weighed 500mg with an error of ±1mg. For each granulation batch, the entire granule size distribution was used to produce the tablets. The tablet "hardness" was measured using a tablet hardness tester (Dr. Schleuniger Pharmatron 6D model), while the tablet thickness was measured using a digital calliper. The tablet diameter from the tablet die was consistent at 13mm. The tablet properties were measured to calculate the tablet tensile strength as noted in Equation 3.2 (Fell and Newton, 1970).

6.3 RESULTS

Each data point represents five tablets with the *x*-error bars denoting ±5% of the compaction pressure or the standard error of the mean for the tablet density and the *y*-error bars representing the error of the mean for five samples.

6.3.1 EFFECT OF POWDER DRY MIXING ON THE TABLET STRENGTH

The effect of the shear force on dry powders with no addition of liquid binder was found to have no significant effect on the tablet strength as shown by the tablettability, compressibility and the compactability behaviour. The trends of the results were similar for both 285rpm and 600rpm granulation experiments and hence only the 600rpm granulation data is presented in Figure 6.4 to Figure 6.5.

For all tablettability, compressibility and the compactability behaviours, there was no change in the powder compactability behaviour (see Figure 6.4 and Figure 6.5 for the tabletability and compactability profiles respectively), even when the powder was dry mixed for 12.3 minutes at 600rpm. The tablet strength for vigorously dry-mixed powder and direct compressed powder were identical.

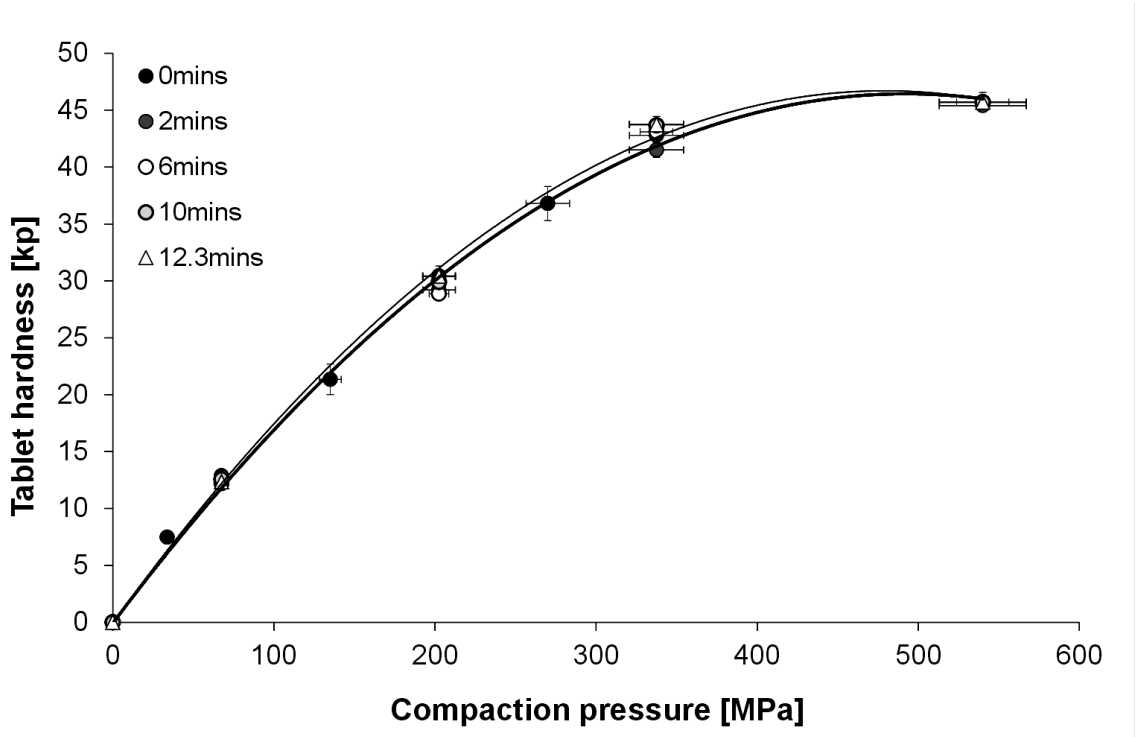

Figure 6.4: Tablettabilty (tablet hardness as a function of compaction pressure) behaviour for powder dry mixed at: (a) 0mins; (b) 2mins; (c) 6mins; and (d) 10mins. Formulation comprises of 1:1 microcrystalline cellulose:lactose 200 mesh and 5w/v% PVP.

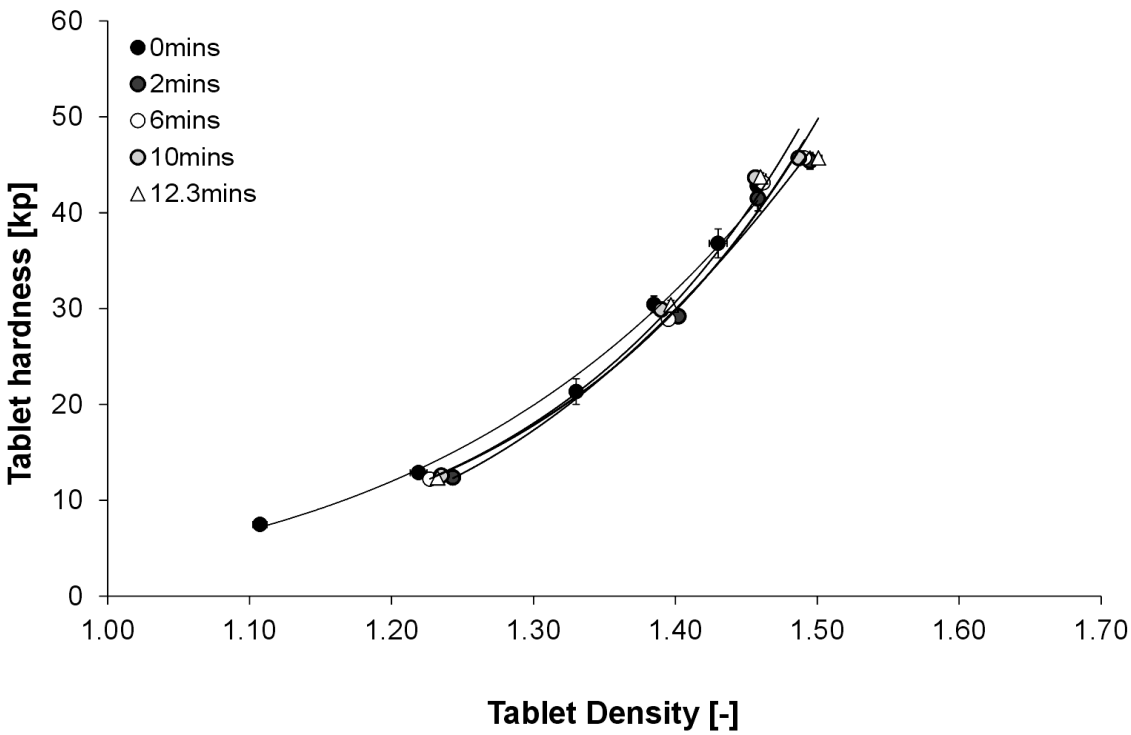

Figure 6.5: Compactability (tablet hardness as a function of tablet density) behaviour for powder dry mixed at: (a) 0mins; (b) 2mins; (c) 6mins; and (d) 10mins. Formulation comprises of 1:1 microcrystalline cellulose:lactose 200 mesh and 5w/v% PVP.

The compressibility behaviour was also seen to be identical for both direct compacted and dry-mixed tablets, as seen in other compressibility profiles in previous chapters. To see the compressibility behaviour of direct compacted tablets compared to dry-mixed tablets, please refer to *Appendix D: Tablet Compressibility Behaviour Profiles*.

6.3.2 EFFECT OF RE-HUMIDIFICATION OF POWDER ON THE TABLET STRENGTH

The re-humidification of the powder supports the results found for the liquid level granulation experiments in *Chapter 4: Using the Unified Compaction Curve to Predict the Tablet Strength from the Wet Granulation Process*. In Chapter 4 it was found that the strength of tablets produced from granulation batches containing 20wt.% did not change significantly from the strength of direct compacted tablets and the results did not conform to the Unified Compaction Curve model. This implied that there is a threshold granule liquid saturation above 20wt.%, where the Unified Compaction Curve model is valid.

Similar results were found in the tablettability behaviour in Figure 6.6 in which the effect of humidity does not alter the compaction behaviour; the tablet strength for both humidified (7% moisture) and non-humidified powder (direct compaction) were

consistent for a given compaction pressure. For microcrystalline cellulose/lactose/PVP formulation, the maximum tablet strength was found to be approximately 3.2MPa. The similarity in the tablettability profiles would imply that there is insufficient moisture within the granule structure to promote deformation or smoothing of the granule surface.

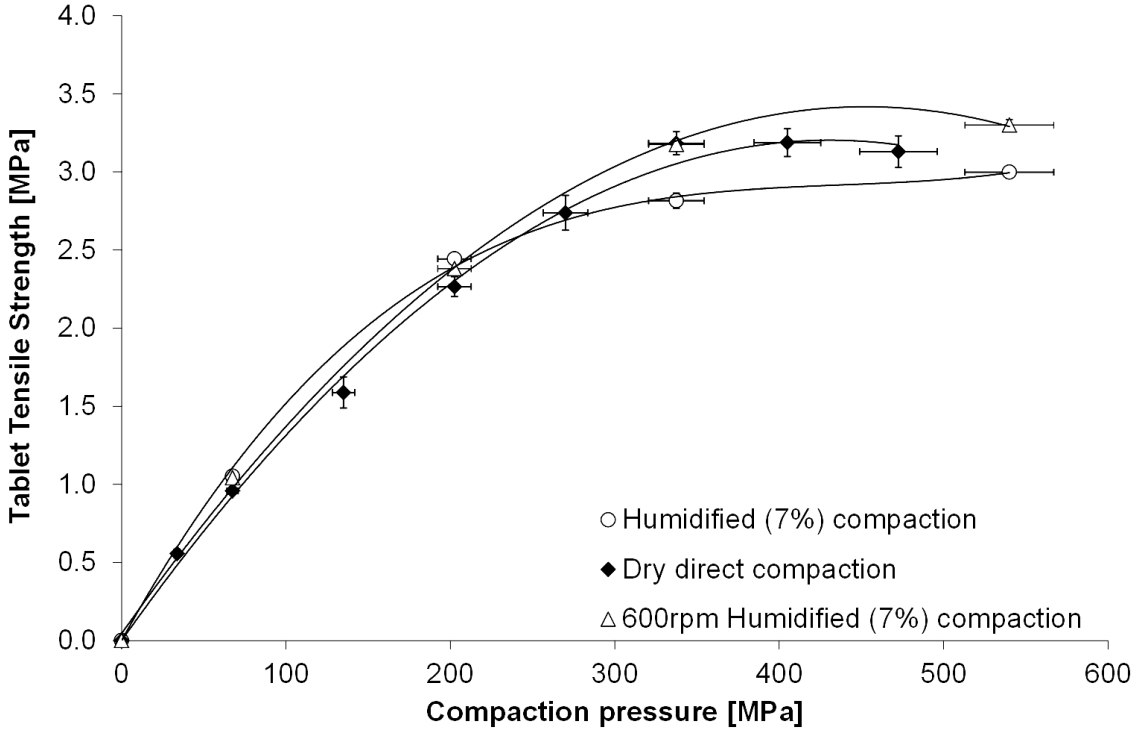

Figure 6.6: Tablettabilty (tablet hardness as a function of compaction pressure) behaviour for tablets produced from humidified powder and direct compaction. Formulation comprises of 1:1 microcrystalline cellulose:lactose 200 mesh and 5w/v% PVP.

The compressibility behaviour for humidified and non-humidified powder (Figure 6.7) portrays that there is a physical or chemical change occurring in the powder. For a given compaction pressure, the tablet density for the humidified powder is higher in comparison to the non-humidified tablet density. However as the compaction pressure increases towards 550MPa, the tablet density between the humidified and non-humidified powder becomes consistent at 1.5g/cm^3.

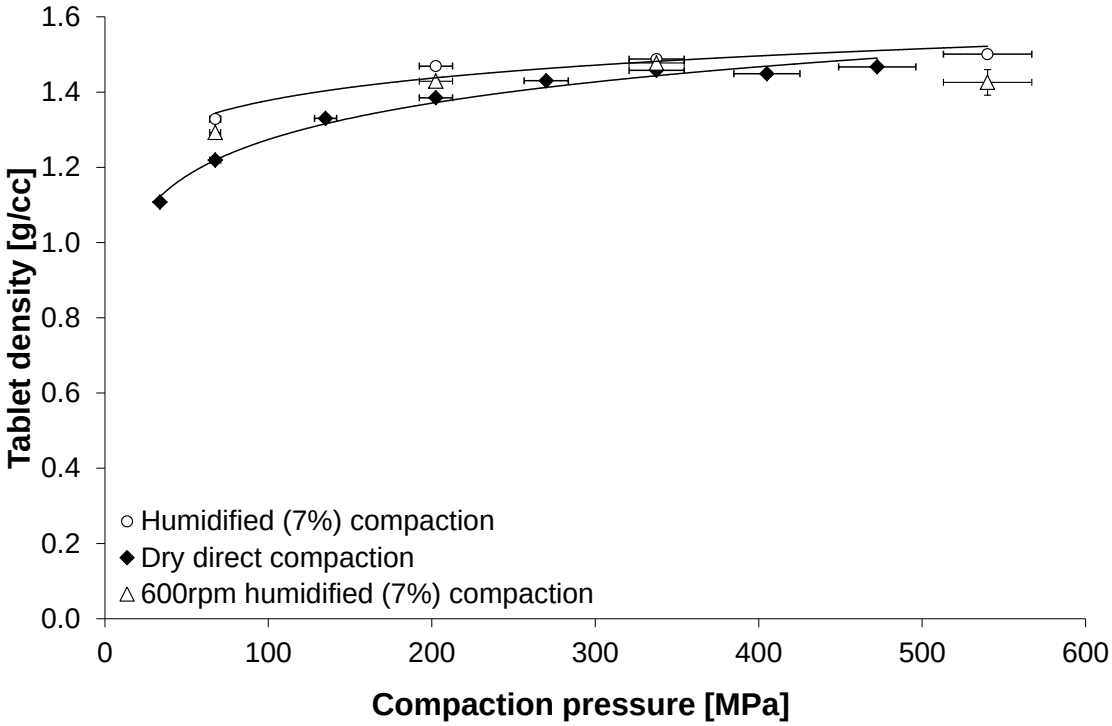

Figure 6.7: Compressibility (tablet hardness as a function of tablet density) behaviour for tablets produced from humidified powder and direct compaction. Formulation comprises of 1:1 microcrystalline cellulose:lactose 200 mesh and 5w/v% PVP.

The compactibility behaviour, shown in Figure 6.8, shows a similar trend for both non-humidified and humidified powder in which the tablet strength increases towards 3.2MPa as the tablet density increases towards 1.5g/cm^3. The humidity causes a slight increase in the tablet density for a given tablet strength. This implies that the microcrystalline cellulose material is swelling upon contact with water or there is a physical or chemical change in the powder structure. Although looking at the tablettability profile in Figure 6.6, this has no effect on the overall final tablet strength. Therefore humidification of the powder does not adversely impact the mechanical inter-locking of the particles during the tabletting process.

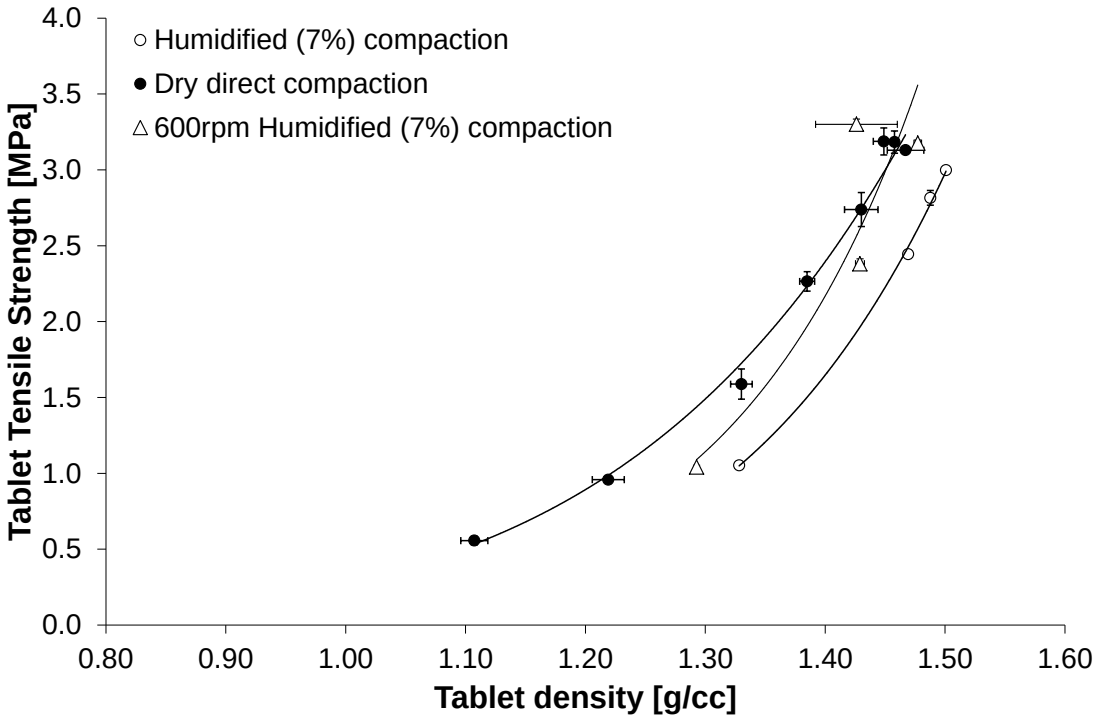

Figure 6.8: Compactability (tablet hardness as a function of tablet density) behaviour for tablets produced from humidified powder and direct compaction. Formulation comprises of 1:1 microcrystalline cellulose:lactose 200 mesh and 5w/v% PVP.

6.3.3 EFFECT OF LIQUID BINDER POWDER SATURATION WITH VERY LOW SHEAR

The addition of the liquid binder with very low shear exerted on microcrystalline cellulose powder has an effect on the physical properties of microcrystalline cellulose, supporting the results shown in *Section 6.3.2.: Effect of re-humidification of powder on the tablet strength*. The results of the powder conditioning with liquid binder addition and low shear are presented in Figure 6.9 and Figure 6.10. For each figure, the data represents the measurement of five tablets. Each data point in each plot represents the average result from five tablets with the *x*-error bars representing the ±5% of the compaction pressure or standard error of the mean for the tablet density and the *y*-error bars represent the error of the mean for the tablet hardness or tablet density.

In Figure 6.9, the tablet hardness for the tablets produced from powder with little shear applied is higher compared to tablets produced with shear applied and direct compacted tablets. The tablettability behaviour of tablets, produced from powder with no shear applied, may suggest that the microcrystalline cellulose structure is swelling with exposure to water or there is a physical and/or chemical alteration in the porous cellulose structure.

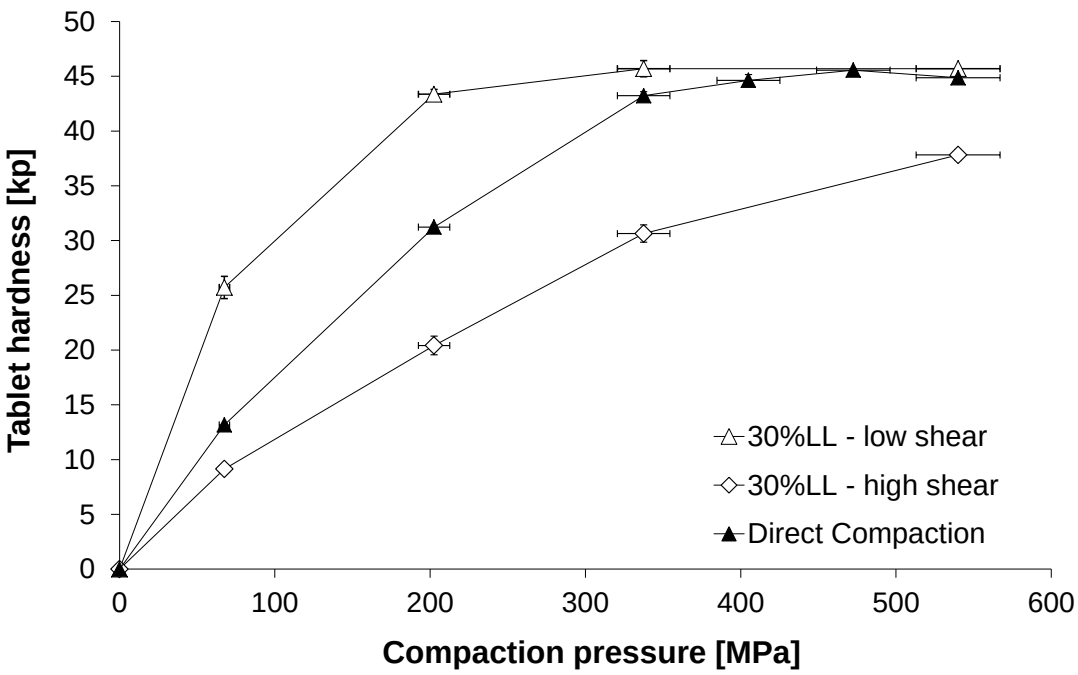

Figure 6.9: Tablettabilty behaviour for tablets produced from powder saturated with 5w/v% PVP liquid binder, with low shear (~50rpm) and high shear (600rpm) applied; and direct compaction. Powder formulation comprises of 1:1 microcrystalline cellulose:lactose 200 mesh.

Like the compressibility behaviour in tablets produced from re-humidified powder, the results show that the compaction pressure does not make a significant difference to the tablet density, whether a low or high degree of shear is applied to the powder prior to the tabletting process. The tablet density also does not appear to make a significant difference to the final tablet strength as seen in compactability behaviour in Figure 6.10. The tablet density varies between 1.25 to 1.5g/cm^3 for all tablet conditions, however the tablet hardness varies significantly. Similar to the tablettability behaviour, tablets produced from powder in which very low shear is applied has a higher tablet strength (tablet strength range of ~25kPa to 45kPa) compared to tablets produced with powder with shear applied (tablet strength range of ~10kPa to 38kPa) or by direct compaction (tablet strength range of ~12kPa to 45kPa). This would suggest that the liquid binder induces a change in the microcrystalline cellulose structure which ultimately increases the tablet strength.

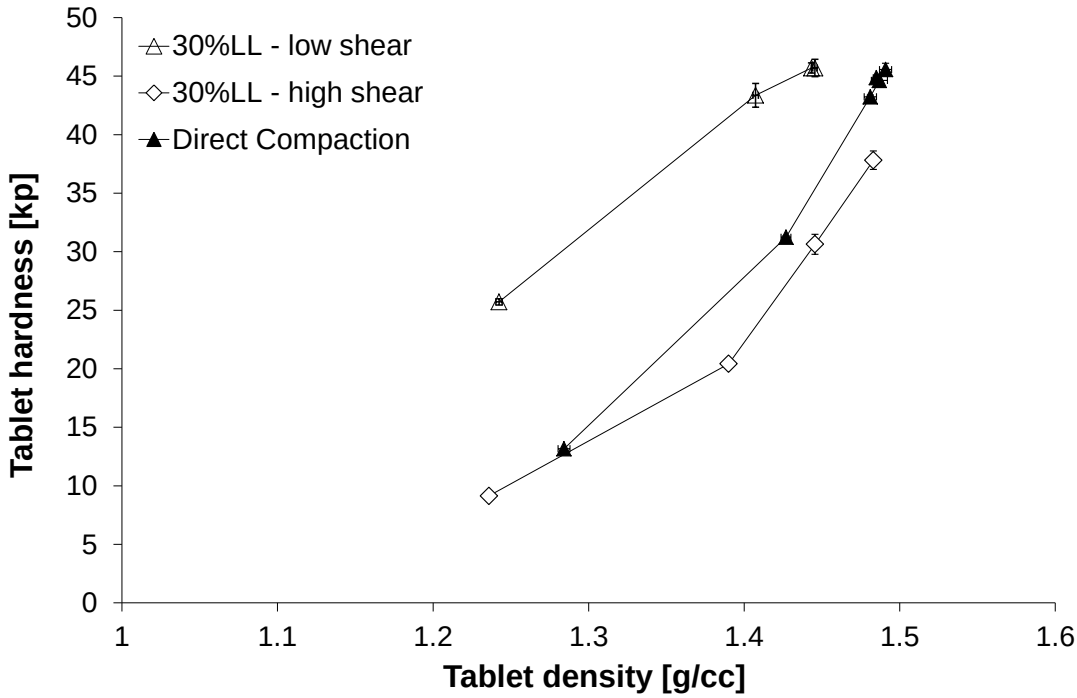

Figure 6.10: Compactability behaviour for tablets produced from powder saturated with 5w/v% PVP liquid binder, with low shear (~50rpm) and high shear (600rpm) applied; and direct compaction. Powder formulation comprises of 1:1 microcrystalline cellulose:lactose 200 mesh.

6.3.4 EFFECT OF THE LIQUID BINDER SOLVENT ON THE TABLET STRENGTH

The presence of hydrogen bonds within the liquid bridges that agglomerate the primary particles together makes a significance difference to the powder compactability in both liquid level and wet massing time granulation experiments as seen in Figure 6.11 to Figure 6.15. Each data point in each plot represents the average result from five tablets with the *x*-error bars representing the ±5% of the compaction pressure or standard error of the mean for the tablet density and the *y*-error bars represent the error of the mean for the tablet hardness or tablet density.

The comparison of the tablettability behaviour for water-based and ethanol-based liquid binder solvent reveals that the decrease in the hydrogen bonding in the ethanol-based liquid binder makes a significant change in the tablet hardness as seen in Figure 6.11. Ethanol-bound tablets retain almost all of their hardness with only a small drop in the tablet tensile strength. For the water-based liquid binder experiments, the tablet hardness decreases by a maximum magnitude of approximately 17kp from the direct compaction (maximum tablet strength that can be attained from a given compaction pressure) tablet hardness. This is significantly larger than the maximum magnitude of tablet hardness decrease of 5kp observed in the ethanol-based granulation experiments. Therefore

ethanol-based liquid binders produce granules with weaker intra-granular liquid bridges, which in turn leads to an increase in the tablet strength. The formation of hydrogen bonds in water-based liquid binders produces stronger granules which compromises the final tablet strength.

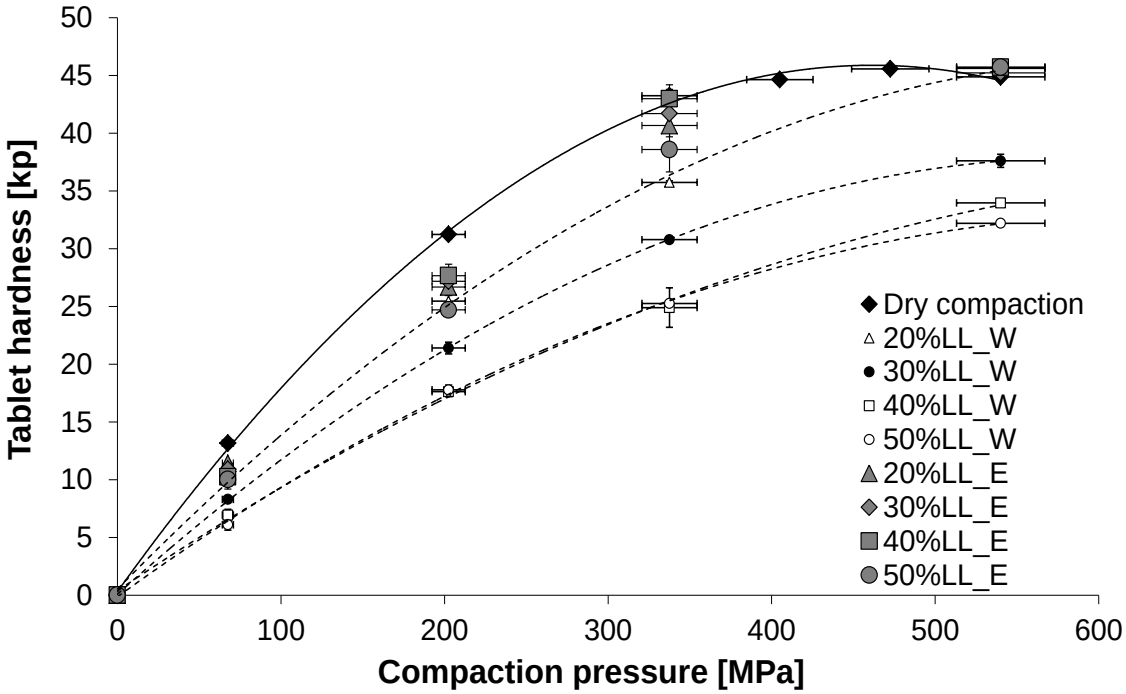

Figure 6.11: Comparison of Tablettabilty (tablet hardness versus compaction pressure) behaviour for tablets produced from ethanol-based (E) and water-based (W) liquid binders in liquid level (LL) granulation experiments. Formulation comprises of 1:1 microcrystalline cellulose:lactose 200 mesh and 5w/v% PVP.

The type of solvent used in the liquid binder does not appear to make any substantial difference in the compressibility behaviour as seen in Figure 6.12 or the compactability behaviour in Figure 6.13 for any given granulator liquid level. For the compactability behaviour, the tablet hardness for the ethanol-based liquid binder is marginally higher than the direct compaction curve and is similar in tablet hardness with the 60wt.% liquid level water-based granulation experiment as a function of the tablet density. The absence of hydrogen bonding in the ethanol-based liquid binder may not induce enough changes physio-chemically or chemically in the microcrystalline cellulose or lactose particles to make a significant change in the tablet hardness across all liquid levels. Therefore water-based liquid binders are more efficient in transferring the kinetic energy from the impeller to granules for deformation and/or consolidation.

This also implies that the Unified Compaction Curve does not apply to microcrystalline cellulose-ethanol formulations, and that there is something specific about the

microcrystalline cellulose-water interactions that causes the loss of compactability that is so often observed in industry and other microcrystalline cellulose granulation studies (Shi *et al.*, 2011; Macias and Carvajal, 2012).

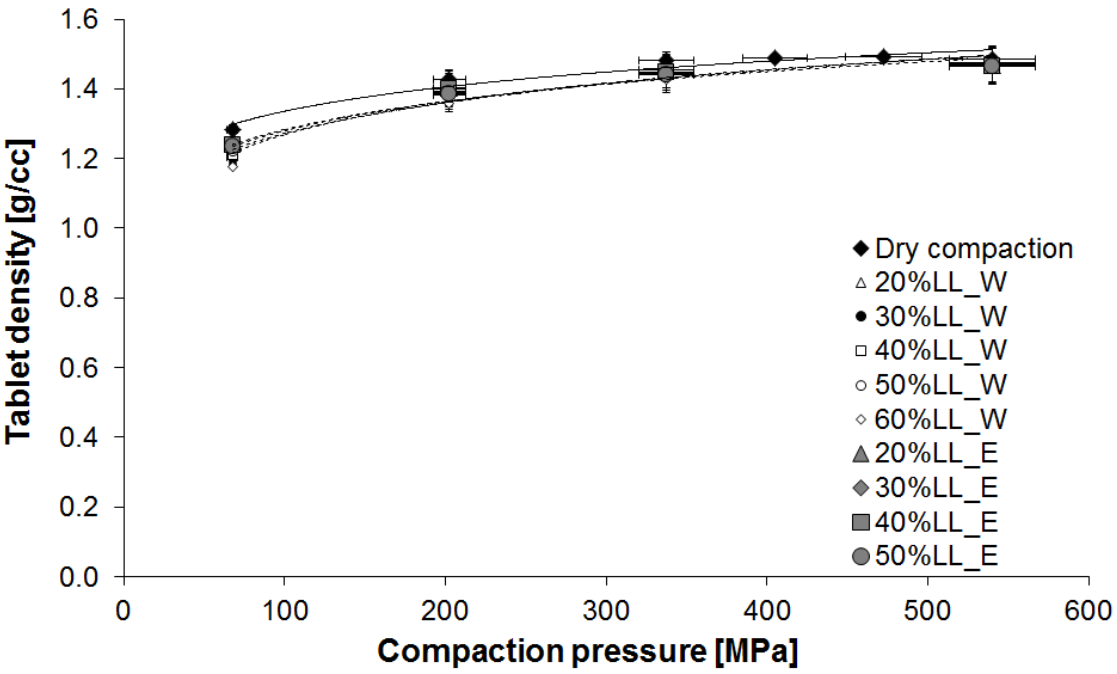

Figure 6.12: Compressibility (tablet hardness vs. tablet density) behaviour for tablets produced from ethanol-based (E) and water-based (W) liquid binders in liquid level (LL) granulation experiments. Formulation comprises of 1:1 microcrystalline cellulose:lactose 200 mesh and 5w/v% PVP.

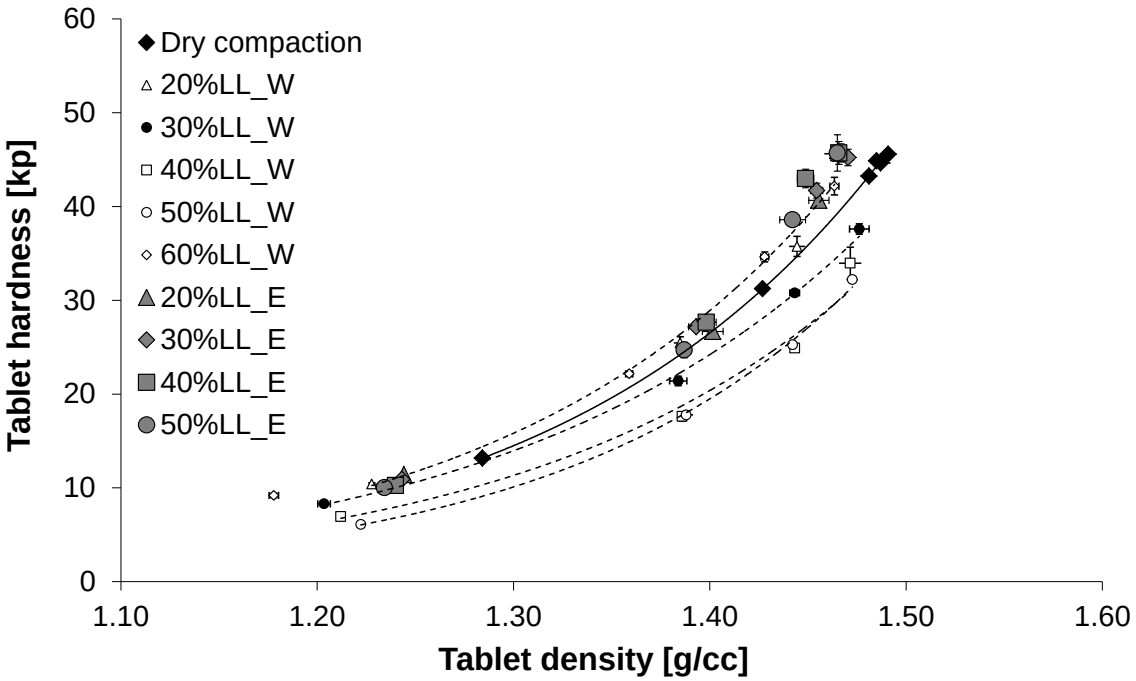

Figure 6.13: Compactability (tablet hardness vs. tablet density) behaviour for tablets produced from ethanol-based (E) and water-based (W) liquid binders in liquid level (LL) granulation experiments. Formulation comprises of 1:1 microcrystalline cellulose:lactose 200 mesh and 5w/v% PVP.

The wet massing granulation experiments also shows that the ethanol liquid binder does not affect the tablet hardness significantly, as seen in Figure 6.14. Similar to the liquid level experiments, the magnitude in the decrease of the tablet hardness, from the maximum possible tablet strength attainable (direct compacted tablets), is smaller for the ethanol-based liquid binder (5kp) compared to the water-based liquid binder (22.5kp).

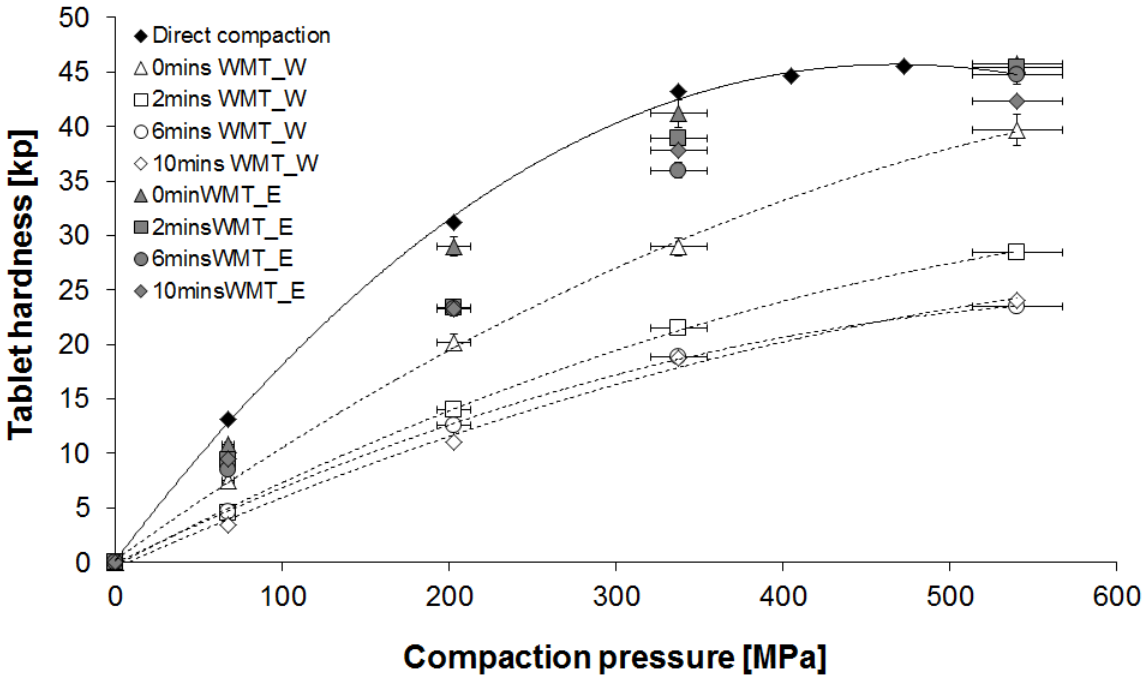

Figure 6.14: Tablettabilty (tablet hardness vs. compaction pressure) behaviour for tablets produced from ethanol-based (E) and water-based (W) liquid binders in wet-massing time (WMT) granulation experiments. Formulation comprises of 1:1 microcrystalline cellulose:lactose 200 mesh and 5w/v% PVP.

Similar trends to the liquid level results were found for the compressibility and the compactability behaviour for the wet massing time (portrayed in Figure 6.15). The tablet density for the ethanol-based wet massing experiments was found to be almost identical to the water-based wet massing experiments, showing that the strength of the liquid bridges does not play a governing role in the compressibility behaviour. For all wet massing times, the relationship between the tablet density and the tablet hardness is very similar for the ethanol-based experiments, which shows a different behaviour in comparison to the water-based wet massing experiments where the tablet hardness decreases with increasing wet massing time for a given tablet density. These results demonstrate that the hydrogen bonding in water-based liquid binders are more efficient in transferring deformation and consolidation forces to granules compared to ethanol-based liquid binders.

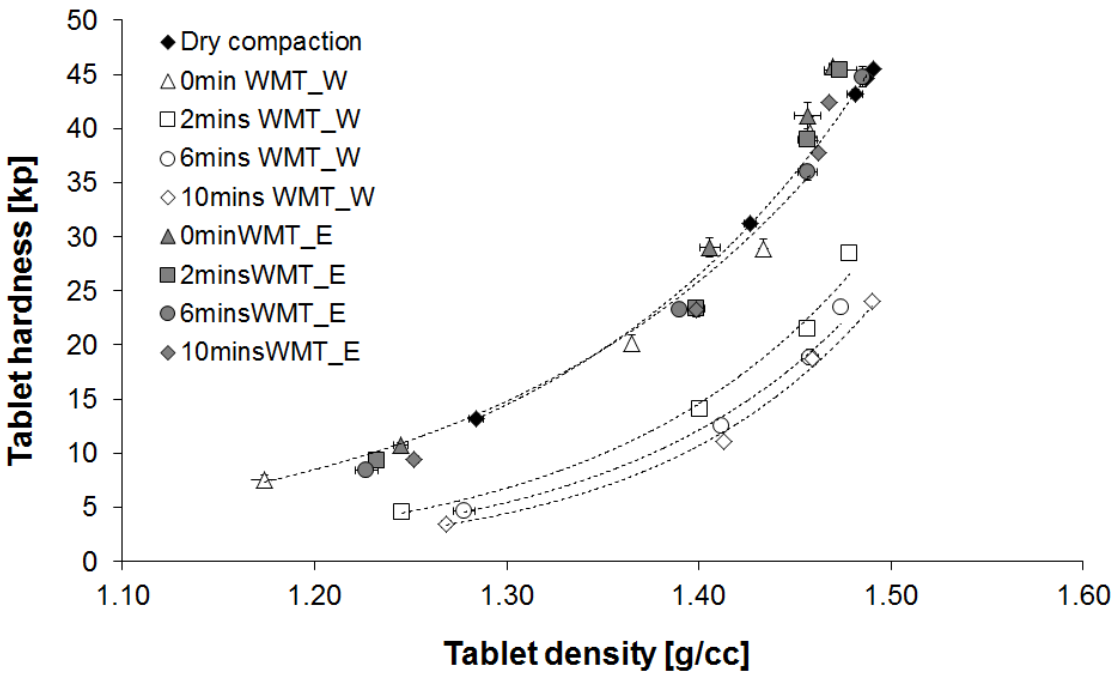

Figure 6.15: Compactability (tablet hardness vs. tablet density) behaviour for tablets produced from ethanol-based (E) and water-based (W) liquid binders in wet-massing time (WMT) granulation experiments. Formulation comprises of 1:1 microcrystalline cellulose:lactose 200 mesh and 5w/v% PVP.

6.3.5 EFFECT OF THE LIQUID BINDER SOLVENT ACIDITY ON THE TABLET STRENGTH

The effect of the acidity of the liquid binder solvent on the tablet strength was investigated with the results presented in Figure 6.16 to Figure 6.20. The data in Figure 6.16 and Figure 6.17 represents three tablet measurements with the *x*-error bars representing the ±5% of the compaction pressure or standard error of the mean for the tablet density and the *y*-error bars represent the error of the mean for the tablet hardness or tablet density.

From the tablettability results in Figure 6.16, it can be seen that the liquid binder acidity does not have a major influence on the compaction behaviour and the final tablet hardness, as the results appear to be segregated into different wet massing times (0, 2, 6 and 10 minutes). Regardless whether the liquid binder is acidic (liquid binder containing hydrochloric acid) or neutral (liquid binder containing calcium oxide), the tablet hardness does not have a large hardness range for a given wet massing time. For 0 minutes wet massing time, the tablet hardness is approximately 37kPa for all liquid binder acidity levels, while at 2 minutes wet massing time the tablet hardness varies between 26-30kPa. For 6 and 10 minutes wet massing time, the tablet hardness varies between 20-25kPa.

Similar to the results in *Chapter 4: Using the Unified Compaction Curve to predict the tablet strength from the wet granulation process*, the tablettability behaviour is similar for 6 and 10 minutes wet massing time. Therefore the liquid binder acidity would not be considered to influence the compaction behaviour of the powder and control the final tablet strength.

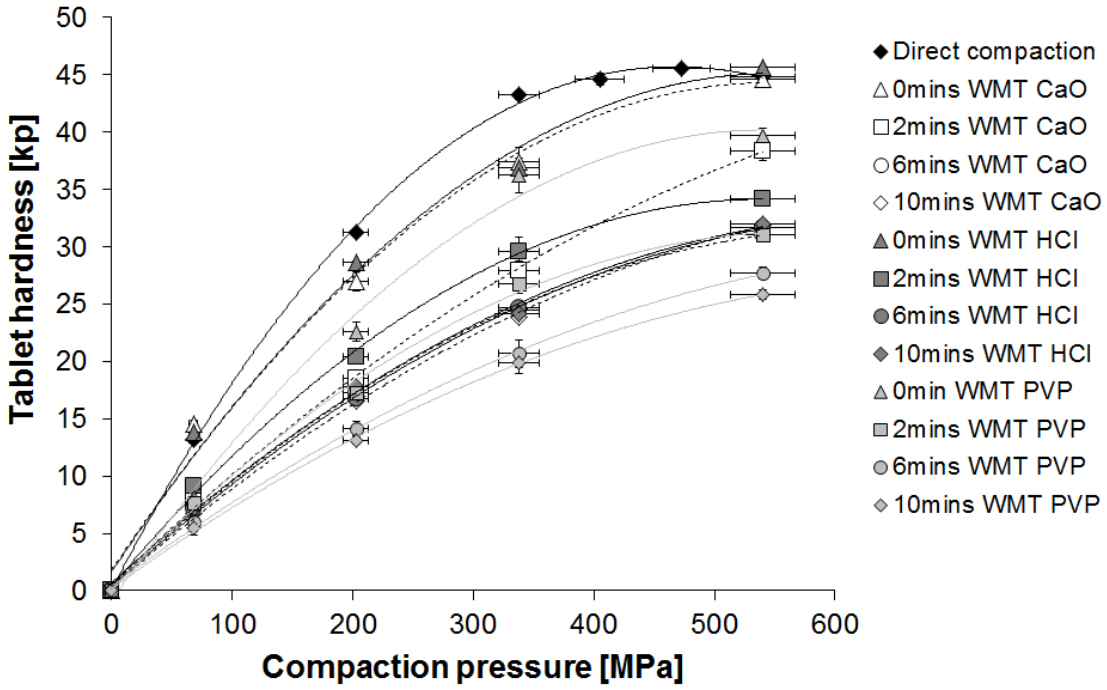

Figure 6.16: Tablettability (tablet hardness as a function of compaction pressure) behaviour for granules produced from varying wet massing times 30% liquid level. Formulation comprises of 1:1 microcrystalline cellulose:lactose 200 mesh and 5w/v% PVP.

The compactability behaviour, shown in Figure 6.17, demonstrates that the liquid binder acidity does not play a major influence on the microcrystalline cellulose structure. There are no clear trends seen in the relationship between the tablet density and the tablet hardness across all the liquid binder acidity levels and wet massing times. For all granulation batches, the tablet density falls within the range of 1.25 to 1.48g/cm^3, while the tablet hardness varies from 5-45kPa. However the variation in the tablet density for given tablet hardness indicates that there is a physical and/or chemical change occurring in the microcrystalline cellulose material, which is most likely attributed to the exposure of water, the swelling of the cellulose structure and the transference of the kinetic energy from the impeller to the granule for deformation and consolidation.

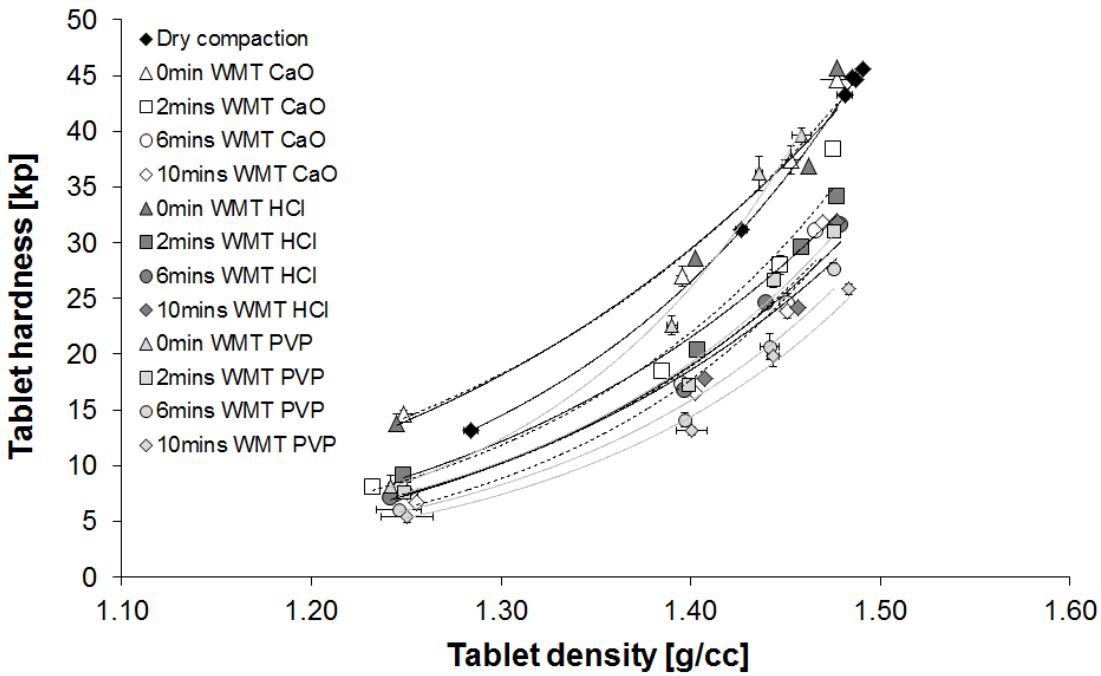

Figure 6.17: Compactability (tablet hardness as a function of tablet density) behaviour for granules produced from varying wet massing times 30% liquid level. Formulation comprises of 1:1 microcrystalline cellulose:lactose 200 mesh and 5w/v% PVP.

From the wet granulation experiments containing calcium oxide (corresponding to a liquid binder pH of 7) and hydrochloric acid (corresponding to a liquid binder pH of 1) liquid binders, the granules were sieved to measure the granule size distribution and the results from the size analysis are presented in Figure 6.18 and Figure 6.19 for calcium oxide and hydrochloric acid granules respectively. The granule size distributions of the calcium oxide and hydrochloric acid granules show little difference in the bi-modal distribution curves for all wet massing times. For each of the liquid binders, the granule size peaked at a mass-based frequency of approximately 0.23 in between 63-90µm. As the wet massing time increases to 10 minutes, the granule size distribution becomes narrower and the bi-modal distribution deteriorates to become a uni-modal distribution. The granule size distribution does not show any evidence of the physical/chemical change in the microcrystalline cellulose structure shown by the change in the tablet density for a given tablet hardness in Figure 6.17. Therefore the liquid binder acidity does not have any influence on the granule size distribution and is not the controlling factor for the final tablet strength.

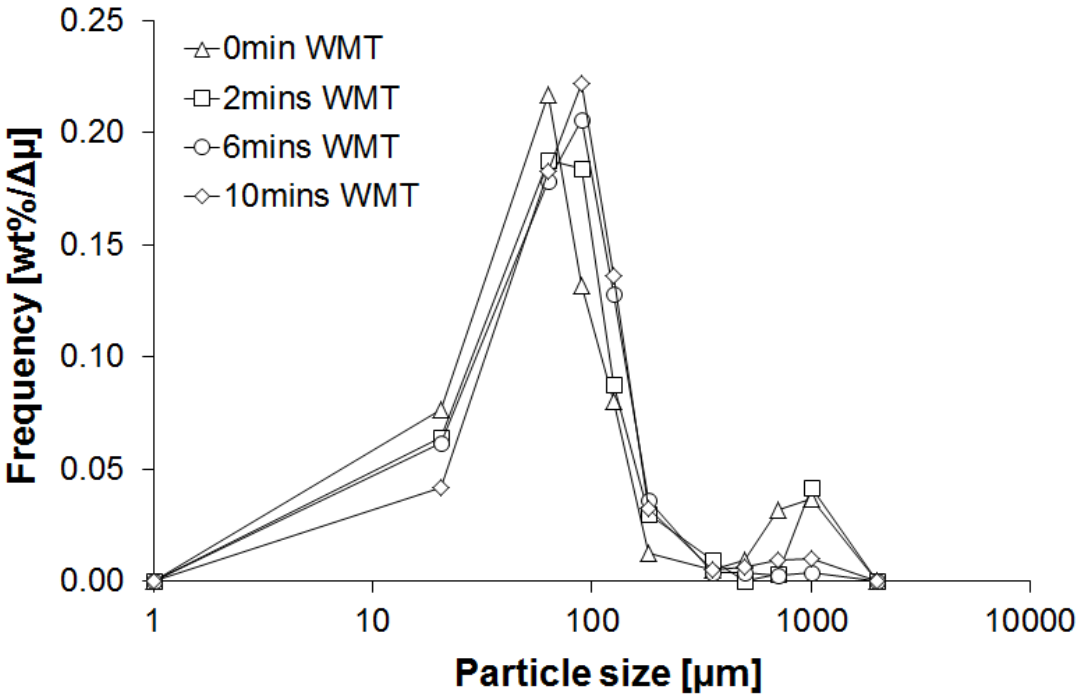

Figure 6.18: Granule size distribution plots for varying wet massing time at 30wt% liquid level. The granulation experiments are based on an impeller speed of 285rpm. Formulation is 1:1 microcrystalline cellulose and lactose 200 mesh, granulated with 5w/v% polyvinyl pyrrolidone and calcium oxide (pH = 7).

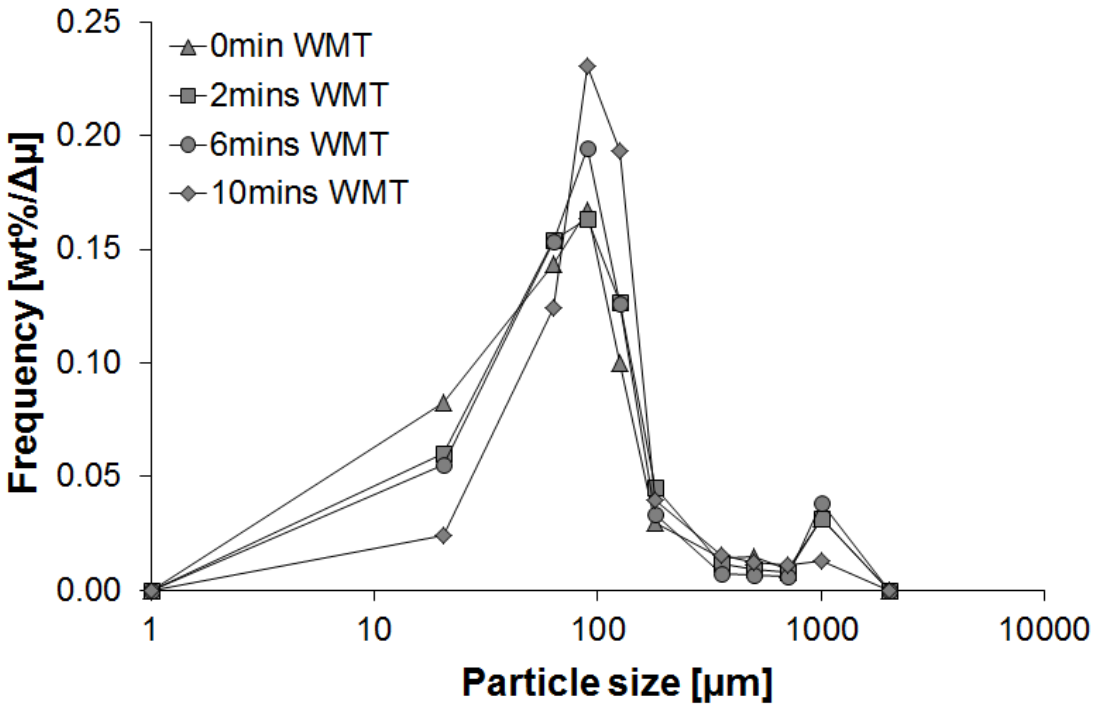

Figure 6.19: Granule size distribution plots for varying wet massing time at 30wt% liquid level. The granulation experiments are based on an impeller speed of 285rpm. Formulation is 1:1 microcrystalline cellulose and lactose 200 mesh, granulated with 5w/v% polyvinyl pyrrolidone and hydrochloric acid (pH = 1).

As well as the granule size distribution, the liquid binder acidity does not make any significant alterations in the overall granule morphology as seen in the SEM images in Figure 6.20. For each type of liquid binder (calcium oxide or hydrochloric acid), the SEM images are representative of granules from 90-180µm. From the images of the granules, it can be seen that the overall granule morphology is similar to the structure of granules produced from PVP liquid binder (pH = 4) in Figure 5.2. The granules are circular in shape with evidence of the microcrystalline cellulose components deformed and smoothing the granule surface. From Figure 6.20, it can be observed that there are more voids present on the topology of hydrochloric acid-based granules compared to granules produced from calcium oxide liquid binder; however this finding is not conclusive without doing further analysis such as measuring the granule porosity.

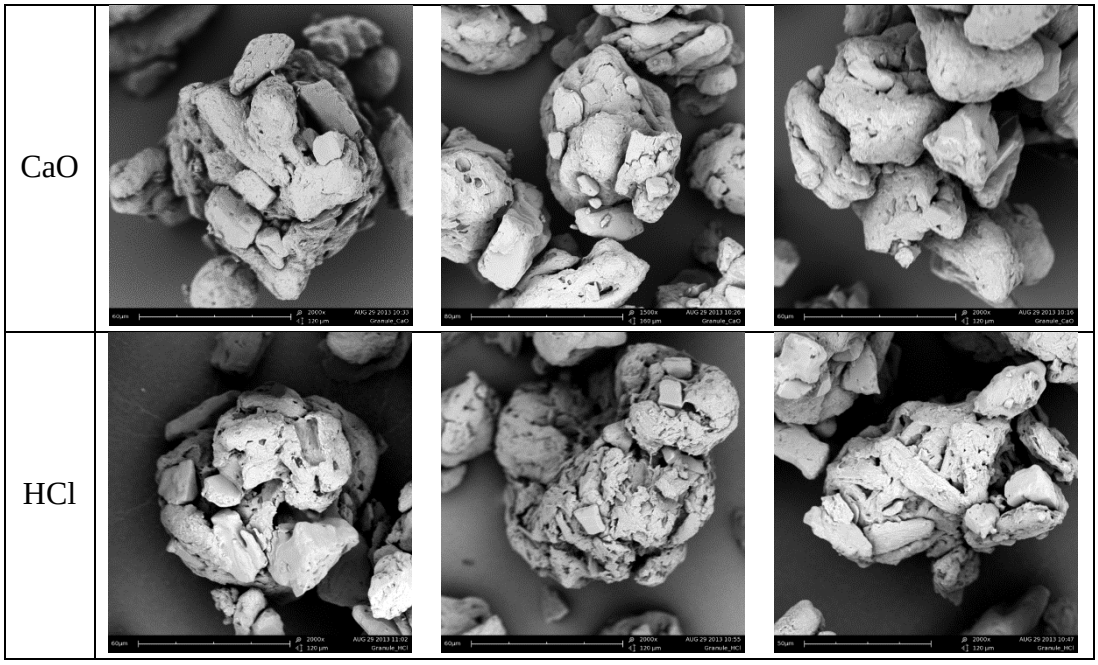

Figure 6.20: Representative SEM images of granules (30wt.% liquid level, 400rpm, 10 minutes wet massing time) produced from liquid binders containing calcium oxide (pH = 7) and hydrochloric acid (pH = 1).

6.3.6 EFFECT OF THE MICROCRYSTALLINE CELLULOSE AMORPHOUS AND CRYSTALLINITY PROPERTIES ON THE TABLET STRENGTH

The crystalline and amorphous regions were observed using X-Ray Diffraction (XRD) for microcrystalline cellulose and lactose 200mesh powders, with the results from the analysis presented in Figure 6.21 to Figure 6.24 and Table 6.2.

The XRD analysis of the microcrystalline cellulose and lactose 200mesh comprising the formulation are presented in Figure 6.21. The XRD spectra show that microcrystalline cellulose exhibits amorphous regions by the presence of broad peaks at approximately 14-

18°. Crystalline regions can also be seen by the narrow peaks at around 22, 34, 37 and 43°. Lactose 200 mesh is a crystalline material which is evident by the sharp narrow peaks present in the XRD spectrum. When the microcrystalline cellulose and lactose powder mixture is analysed, the amorphous and crystalline characteristics from the individual component analysis are combined into the overall spectrum.

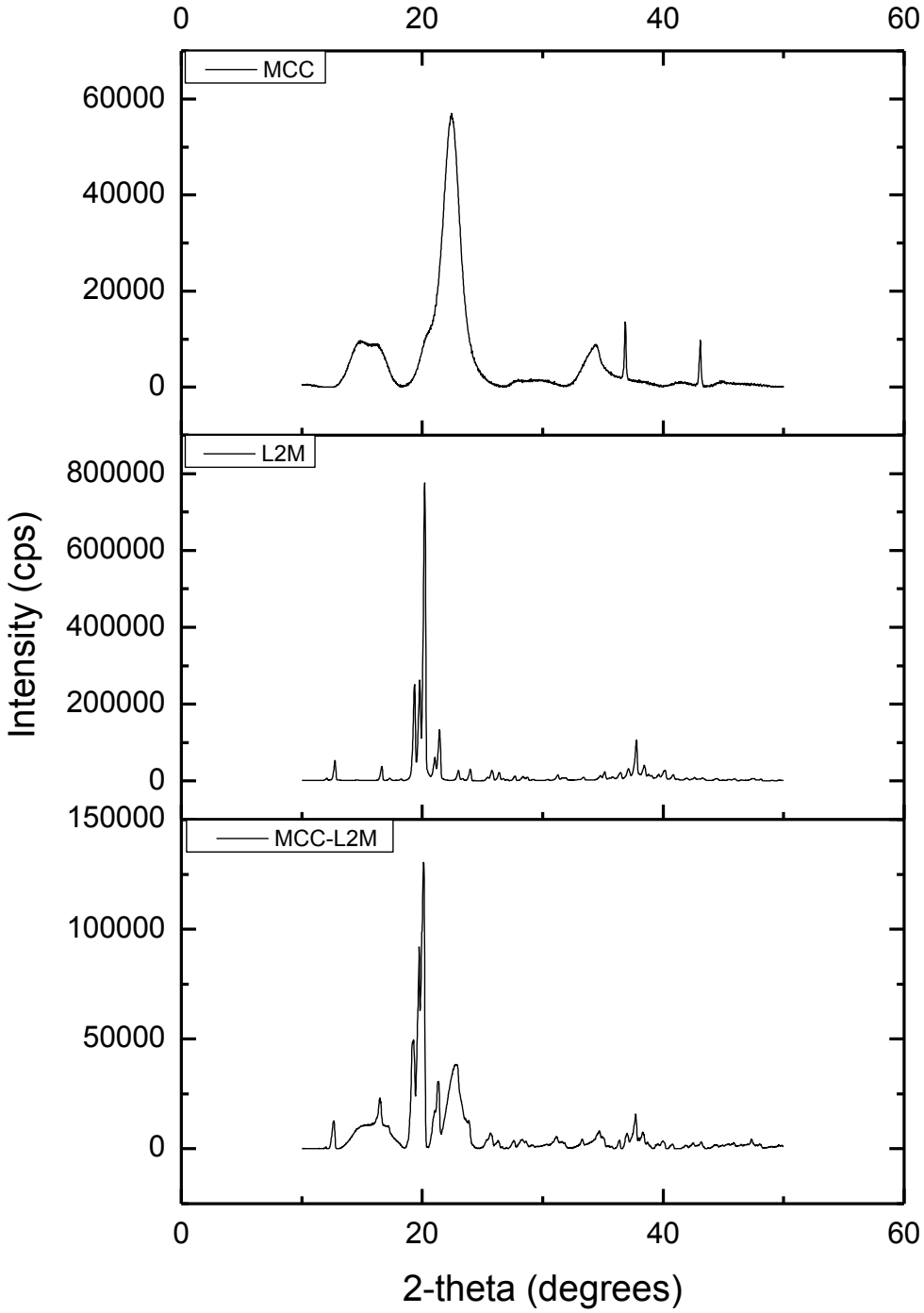

Figure 6.21: XRD analysis of the raw material components: microcrystalline cellulose (MCC); lactose 200mesh (L2M) which comprises the 1:1 microcrystalline cellulose/lactose 200mesh (MCC-L2M) formulation.

The XRD analysis was also carried out on wet-granulated samples which incorporated the various levels of liquid binder acidity, as presented in Figure 6.22, Figure 6.23 and Figure 6.24 for wet granulation experiments using PVP only, hydrochloric acid and calcium oxide liquid binders respectively. From the analysis of the wet granulation data, there does not appear to be any clear trend in amorphous or the crystalline peaks with increasing wet massing time. The spectrum shows varying levels of amorphous or crystallinity for different wet massing times, however this appears to scattering of the results and no conclusive finding can be determined from this. Therefore neither the liquid binder acidity nor the wet massing time has any effect on the micro-structure of the microcrystalline cellulose material.

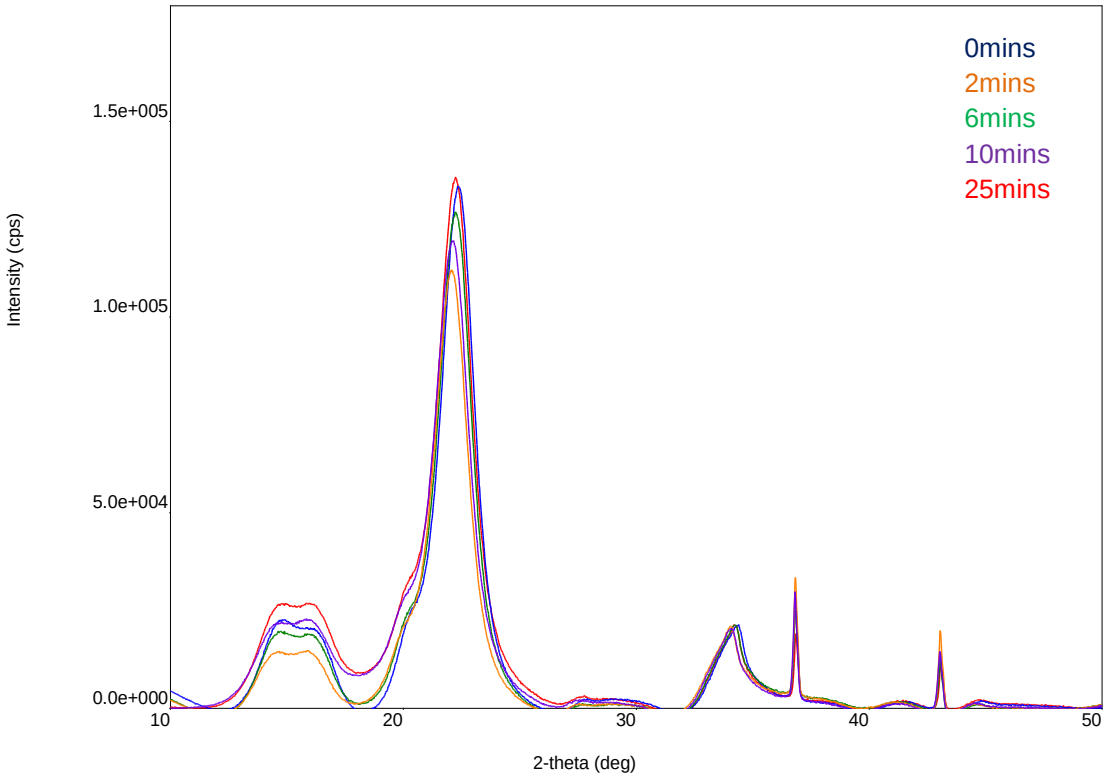

Figure 6.22: XRD of 1:1 raw microcrystalline cellulose and lactose 200 mesh, granulated with 5w/v% PVP liquid binder (pH = 4), as a function of the wet massing time. The colour of the wet massing time description in the legend corresponds to the XRD spectra of the same colour.

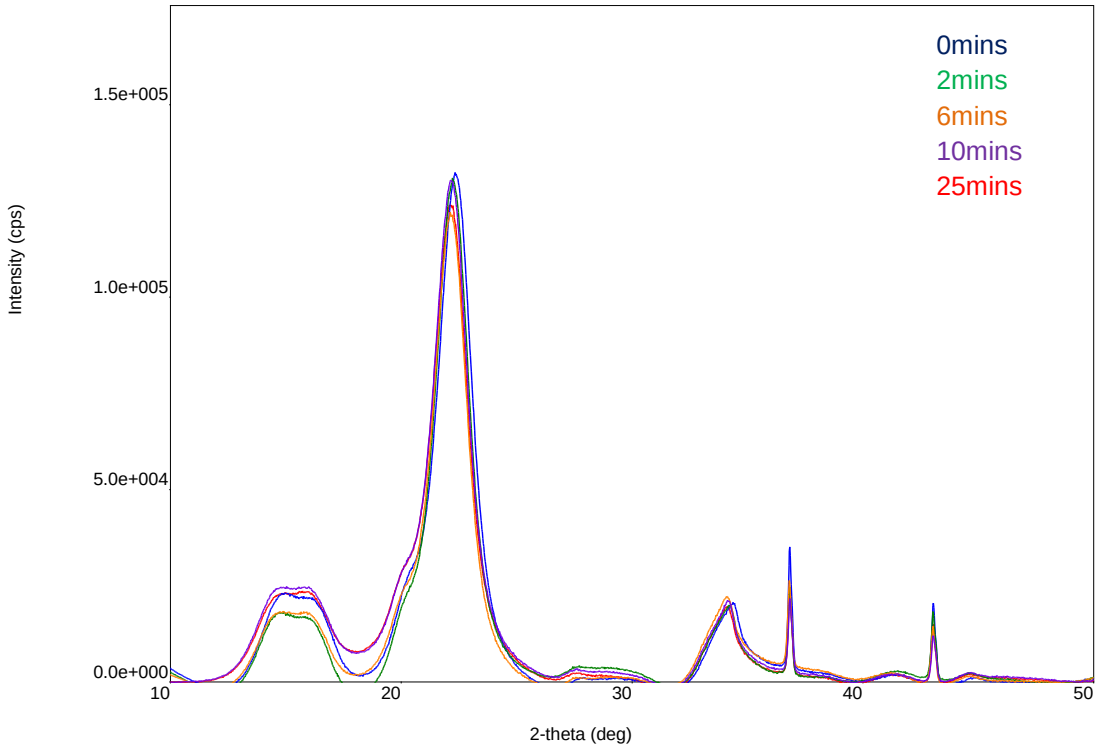

Figure 6.23: XRD of 1:1 raw microcrystalline cellulose and lactose 200 mesh, granulated with 5w/v% PVP and HCl liquid binder (pH = 1), as a function of the wet massing time. The colour of the wet massing time description in the legend corresponds to the XRD spectra of the same colour.

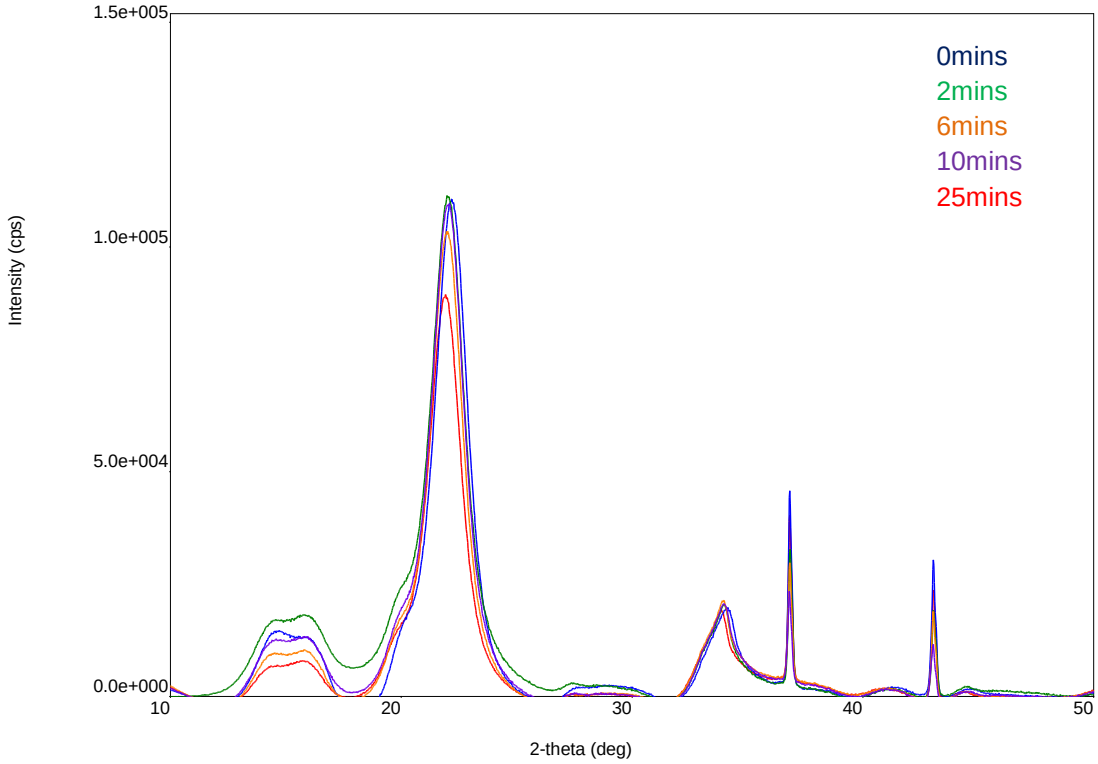

Figure 6.24: XRD of 1:1 raw microcrystalline cellulose and lactose 200 mesh, granulated with 5w/v% PVP and CaO liquid binder (pH = 7.5), as a function of the wet massing time. The colour of the wet massing time description in the legend corresponds to the XRD spectra of the same colour.

From the XRD crystalline spectrum peaks in Figure 6.22, Figure 6.23 and Figure 6.24, the crystallinity of the granule samples and the crystallite size was calculated using the Scherrer equation for all liquid binder types and wet massing times. The crystallinity and crystallite size as a function of the number of impeller revolutions are presented in Table 6.2 to Table 6.4.

Table 6.2: Scherrer crystallite size and crystallinity analysis of wet granulated samples of varying wet massing times for microcrystalline cellulose granules prepared with calcium oxide liquid binder.

Wet massing time [mins]	MCC/PVP/CaO (pH = 7)		
	Crystallite size [nm]	Number of impeller revolutions [-]	Crystallinity [%]
0	2.2	940	84
2	9.0	1740	85
6	15.2	3340	85
10	4.8	4940	85
25	48.5	10940	85

Table 6.3: Scherrer crystallite size and crystallinity analysis of wet granulated samples of varying wet massing times for microcrystalline cellulose granules prepared with PVP only liquid binder.

Wet massing time [mins]	MCC/PVP (pH = 4)		
	Crystallite size [nm]	Number of impeller revolutions [-]	Crystallinity [%]
0	1.2	932	83
2	1.9	1732	83
6	4.8	3332	84
10	2.5	4932	83
25	1.7	10932	83

Table 6.4: Scherrer crystallite size and crystallinity analysis of wet granulated samples of varying wet massing times for microcrystalline cellulose granules prepared with hydrochloric acid liquid binder.

Wet massing time [mins]	MCC/PVP/HCl (pH = 1)		
	Crystallite size [nm]	Number of impeller revolutions [-]	Crystallinity [%]
0	1.2	912	83
2	1.8	1712	84
6	3.3	3312	84
10	2.5	4912	84
25	2.5	10912	83

The crystallinity of the granule samples was found to be in the range of between 83-85%. The level of crystallinity for granules produced from calcium oxide was slightly higher, at ~85% crystallinity, compared to granules prepared from PVP (~83% crystallinity) and hydrochloric acid (~84% crystallinity). For all granule samples, the crystallinity did not change with increasing wet massing time. This suggests that the wet massing time and the

liquid binder acidity does not significantly alter the level of crystallinity within the microcrystalline cellulose material.

In a similar trend, the crystallite size was generally found to be larger for granules produced with calcium oxide liquid binder compared to the PVP only or with hydrochloric acid liquid binders. For granules produced with calcium oxide liquid binder, the crystallite size range was between 2.2 to 48.5nm, while for granules made with PVP liquid binder, the crystallite size varied between 1.2 to 4.8nm. For granules produced with hydrochloric acid, the crystallite size was similar to granules produced with PVP, where the crystallite size range was between 1.2 to 3.3nm. For granules composing of calcium oxide, the crystallite size increased with increasing number of impeller revolutions. A different trend was found for granules produced from PVP and hydrochloric acid. The crystallite size increased as the number of impeller revolutions increased towards approximately 3,500 revolutions, before the crystallite size started to decrease back down. The reasons behind these trends are unclear at this stage and more investigations are required to understand the changes that are occurring at a microscopic level in the microcrystalline cellulose structure.

6.4 DISCUSSION

This chapter investigated the effect of the wet granulation conditions, in particular the liquid binder properties and the wet massing time, on the crystallinity of the microcrystalline cellulose. The effects of dry mixing, powder re-humidification to approximately 7wt.% moisture content and the smoothness of the granule topology on the final tablet strength were also investigated. From the results presented in this chapter, it can be seen that the microcrystalline cellulose exhibits a complex structure which undergoes a physical and/or chemical transformation during the wet granulation process but is not easily understood by all the analysis presented in this chapter.

Although the liquid level does not play a significant role for the tablet strength, sufficient liquid is required during the wet granulation process to help transfer the kinetic energy from the granulator impeller to the granules for deformation and consolidation to occur. This supports the results in *Chapter 4: Using the Unified Compaction Curve to predict the tablet strength from the wet granulation process*, in which at 20% liquid level, the granulation data did not conform to the Unified Compaction Curve model. At 20% liquid

level and below (including re-humidification of the powder), there is not enough moisture to promote deformation of the microcrystalline cellulose components to form granules that are spherical and smooth in topology, thereby decreasing the granule density. The extent of deformation of the microcrystalline cellulose is strongly influenced by the number of impeller revolutions which then controls the final tablet strength, supporting the study by Marcias *et al.* (2012).

The need for sufficient liquid to be present in the wet granulation formulation indicates that the granule saturation is required to be in the pendular state to promote the compaction pressure or force from the granular impeller to deform the powder irreversibly. Therefore the presence of sufficient liquid binder within the granule facilitates the consolidation and densification of the granule which increases the granule strength, supporting the finding of the increase in the granule strength with increasing granule liquid saturation (Rumpf, 1962; Ennis, 2006). This implies that the granule liquid saturation is very important for the compaction behaviour of the powder and consequently, the tablet strength.

The effect of granule liquid saturation on the granule and tablet strength may be complicated by the ability of the microcrystalline cellulose to swell upon exposure to water. When liquid binder was added to the microcrystalline cellulose and lactose powder mixture (with no shear or wet massing applied), there was evidence of the microcrystalline cellulose structure swelling from the tablettability and compactabilty results in *Chapter 4: Using the Unified Compaction Curve to predict the tablet strength from the wet granulation process* and in this chapter. The swelling of the microcrystalline cellulose structure may increase the surface area within the granule to enable a greater bonding contact area to form and increase the tablet strength, compared to tablets produced from direct compaction.

Microcrystalline cellulose is known to have the ability to absorb moisture and liquid before becoming completely saturated (Zografi and Kontny, 1986; Fielden *et al.*, 1988; Zografi, 1988). Upon absorption, the moisture diffuses by Henry's law to the amorphous regions within the microcrystalline cellulose structure (Zografi, 1988) and can exist as free water (Fielden *et al.*, 1988), be bounded to the hydroxyl groups (one water molecule per anhydroglucose unit) within the cellulose structure or exist as an intermediate state of

bound water (Zografi and Kontny, 1986; Zografi, 1988). The water then fills up the "glassy" amorphous micro-pores until the pores are saturated with water, which then leads to the complete saturation of the microcrystalline cellulose powder (Zografi, 1988).

The strength of the liquid bridges was investigated through the presence and absence of hydrogen bonds from the liquid binder using water and ethanol solvents respectively. The presence of water in the liquid binder would form hydrogen bonds within the liquid bridges between the granules. The hydrogen bonds confer strength to the granules which subsequently compromises the tablet strength. When the solvent of the liquid binder was changed to ethanol, the strength of intra-granular bonds decreased which enabled the tablet strength to increase compared to granules produced with water-based liquid binders. From the Unified Compaction Curve model, it is understood that an increase in the granule strength leads to a decrease in the final tablet strength. If the granule strength can be increased by the presence of hydrogen bonding, this would mean that the final tablet strength is compromised, which is supported by the tablettability behaviour in Figure 6.11.

The micro-physiochemical change in the amorphous and/or crystallinity structure in microcrystalline cellulose was found to be complex to examine. There were no conclusive findings from the XRD analysis results in Figure 6.21 to Figure 6.24. The results imply that the liquid binder acidity or the wet massing time do not strongly affect the crystalline regions in the microcrystalline cellulose structure. However, the crystallite size of microcrystalline cellulose granules prepared using calcium oxide liquid binder was larger than granules produced from PVP or hydrochloric acid liquid binders. This finding supports the various studies using acidic solutions to saturate the cellulose material and de-crystallise or break up the long cellulosic chains into shorter chains to allow microcrystalline cellulose to hydrolyse or dissolve to produce renewable biofuels (Zhang *et al.*, 2009; Shrotri *et al.*, 2013) and a study demonstrating the deterioration of the long microcrystalline cellulose chains from wet granulation (Suzuki *et al.*, 2001). Also the presence of compaction forces from wet granulation may decrease the crystallinity of microcrystalline cellulose (Kumar and Kothari, 1999). However, the effective wet granulation compaction pressure was calculated to be approximately 39kPa/rev. in *Chapter 4*, which is below the 15MPa compaction pressure threshold, found in Kumar

and Kothari's (1999) study, to decrease the crystallinity of the microcrystalline cellulose material. This is supported by the crystallinity results in Figure 6.22 to Figure 6.24.

6.5 CONCLUSIONS

The investigation into the effect of the wet granulation formulation properties and conditions on the microcrystalline cellulose material properties was found to be mainly dependent on the presence of sufficient liquid binder and intra-granular hydrogen bonding.

The final tablet strength was not influenced by the re-humidification (7wt.% moisture content) of powder compared to the tablet strength of direct-compacted tablets. The tablet strength depends on the pendicular granule liquid saturation for deforming and consolidation to occur during the wet granulation process and the swelling of microcrystalline cellulose structure to increase the granule strength and compromise the consequent tablet strength. The final tablet strength also depends on the presence of hydrogen bonding within the intra-granular liquid bridges. The tablet strength was lower for granules produced using water-based liquid binders compared to tablets prepared using ethanol-based liquid binder.

The influence of the microcrystalline cellulose material properties on the granule and tablet strength was found to be dependent on the level of acidity of the liquid binder used in the wet granulation process. For granules prepared with calcium oxide liquid binder, corresponding to a pH of 7, the crystallite size was larger in comparison to granules prepared using PVP (corresponding to a pH of 4) or hydrochloric acid (corresponding to a pH of 1) liquid binders. However, the wet massing time did not have any significant effect on the crystalline or amorphous regions of microcrystalline cellulose. More studies are required to fully understand the impact of the wet granulation process on the microcrystalline cellulose material.

Therefore microcrystalline cellulose is a complex material which can be strongly influenced by the liquid binder properties. Although its properties are beneficial as an excipient for prolonging the wet granulation process or promoting the compaction behaviour during tabletting, there is more that can be understood about microcrystalline cellulose behaviour during wet granulation.

7 Effect of the Granulator Scale on the Tablet Strength

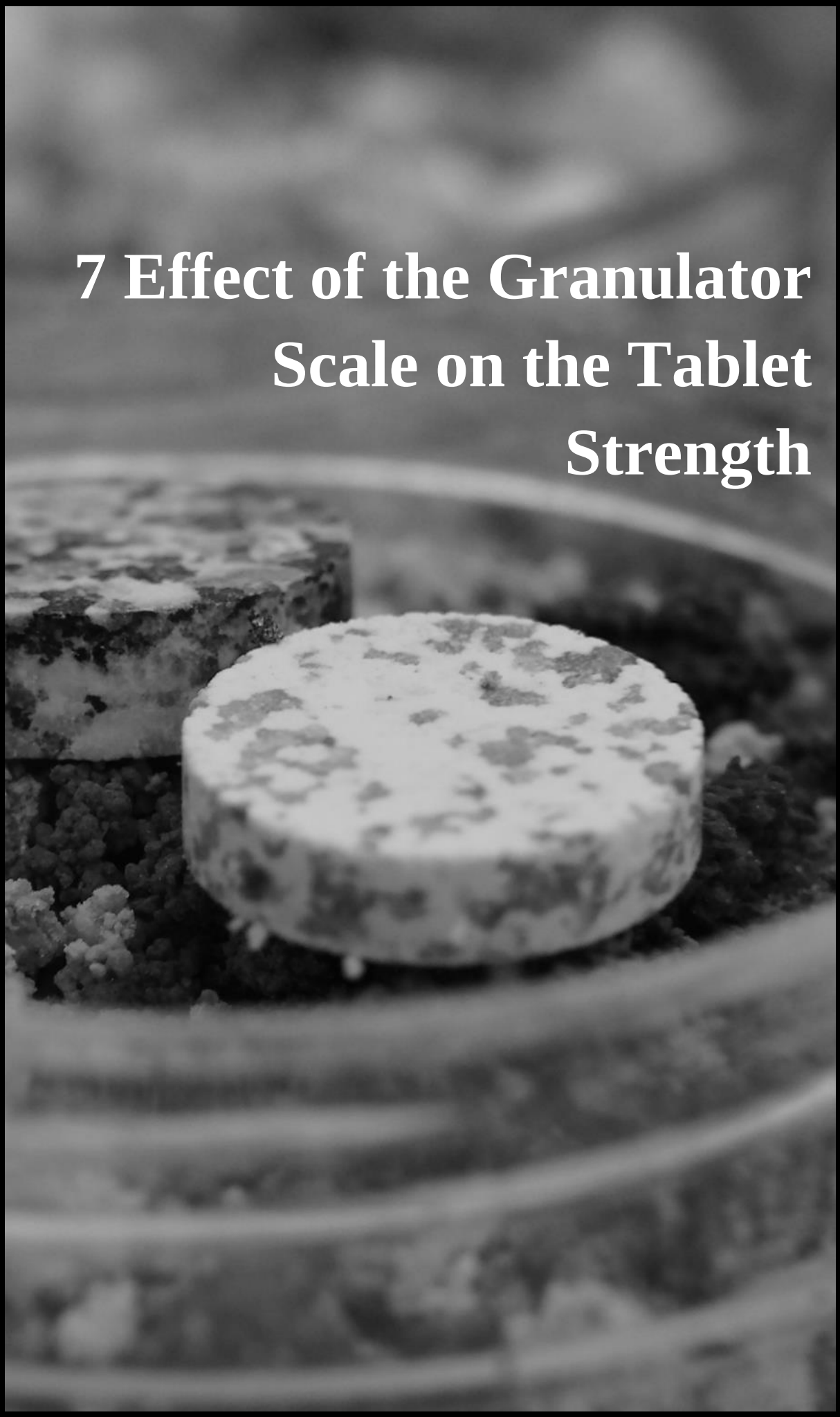

7 EFFECT OF THE GRANULATOR SCALE ON THE TABLET STRENGTH

"The most exciting phrase to hear in science, the one that heralds the most discoveries, is not "Eureka!"(I found it!) but 'That's funny...'"

- Isaac Asimov-

7.1 INTRODUCTION

From the previous chapters, the effect of the wet granulation operating conditions and the granule properties on the final tablet strength was investigated. The material properties of the raw materials, in particular microcrystalline cellulose was examined to understand how the plastic deformation properties of microcrystalline cellulose can deteriorate from exposure to agitation whilst saturated with liquid binder. These investigations were conducted at laboratory scale using the largest granulator bowl available (5L size).

Does the Unified Compaction Curve model give a quantitative prediction the final tablet strength for granules produced at varying scales? The applicability of the Unified Compaction Curve model may be extended to be an elegant scale-up tool and provide an alternative set of scaling-up guidelines based on the number of impeller revolutions and the wet granulation compaction pressure.

Due to frequent limitations in the quantity of active ingredient and economic resources, the need for designing and optimising the wet granulation process for tablet manufacture at a small scale (at a scale hundred times smaller than industrial scale) is imperative (Jones *et al.*, 2005). Once the wet granulation process conditions are established, the process is then up-scaled to suit industrial production. However wet granulation is a complex process and scaling up the wet granulation process can pose issues with inherently altering the granule properties such as size distribution, moisture content, porosity and compactability behaviour of granules which consequently influence the final tablet strength, disintegration time and dissolution profile of the active ingredient (Landin *et al.*, 1996; Leuenberger, 2001; He *et al.*, 2008).

The lack of understanding of the relationship between the wet granulation and the final tablet strength makes the scaling-up procedure difficult to control, in terms of maintaining

the qualitative properties of the granules. With increasing knowledge about the three stages of wet granulation (wetting and nucleation, coalescence and consolidation, and attrition and breakage) through experimental and computer simulation work, the scale-up of granulation processes is now recognised to have a greater scientific foundation recently rather than a work of art (Litster, 2003). Therefore the understanding of the granule properties from the wet granulation process allows the wet granulation scale-up procedure to be designed more efficiently.

The scale-up of the granulation process is based on keeping the granulation dynamics or the granulation operation process constant. This is reflected in the three main rules for scale-up; the constant tip-speed (Faure *et al.*, 1998; Bock and Kraas, 2001) is based on maintaining constant granulation mixing velocity, while the constant shear stress (Tardos *et al.*, 2004; Tardos, 2005) and the constant Froude number (Landin *et al.*, 1996; Faure *et al.*, 1999) rules maintain constant granulation dynamics. Other rules for scale-up include the spray flux (Litster *et al.*, 2002), constant power dimensionless group (Faure *et al.*, 1999; Faure *et al.*, 2001). The application and success of the scale-up rules appear to be dependent on the granulation formulation and/or the granulator geometry, as discussed in *Section 2.6.5*.

From the scale-up wet granulation investigations conducted so far, there are limitations in the knowledge of the relationship between the granulator scale and the tablet strength. The literature studies conducted so far have looked at the effect of scale up on the granule properties but have not extended the study to include the effect on the final tablet strength. Therefore the scaling-up guidelines assume that achieving granules with certain desired attributes (usually size) will lead to tablets with desirable properties. However, these guidelines may overlook the compaction effects from the granulator impeller, as seen in *Chapter Five*. Therefore the Unified Compaction Curve model may provide a visual qualitative guide for enhancing the understanding of the granulator scale-up on the final tablet strength.

7.2 MATERIALS AND EXPERIMENTAL PROCEDURE

The same microcrystalline cellulose and lactose formulation was used in the granulation experiments (see *Chapter 4: Using the Unified Compaction Curve to Predict the Tablet Strength from the Wet Granulation Process*).

The wet granulation experiments took place in two high-shear granulator bowls (KG5, International Key): 1 litre and 5 litre granulator. Only the main impeller was present (no chopper). The main difference between the small and the large bowls was the bowl and impeller geometry. It is conservatively assumed that the bowl and impeller geometries will not make a significant difference to the wet granulation dynamics. For the small granulator bowl, the side chute was covered by a Teflon chute cover to prevent the powder being thrown out the bowl.

The impeller design for the 1L granulator was also quite different (see Figure 7.1): the blade diameter to height ratio was 3:1 for the 1L bowl impeller compared to 4.5:1 for the 5L bowl impeller (see Figure 7.2).

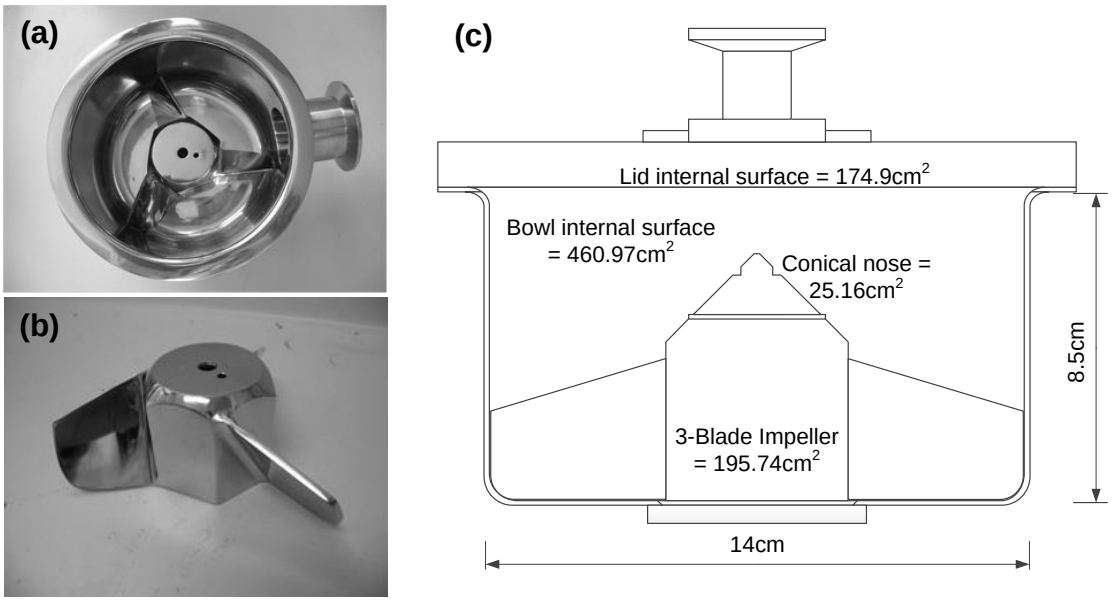

Figure 7.1: Images of the (a) bowl; (b) impeller and (c) dimensional drawings of the small laboratory granulator (KG1 granulator) bowl (1L).

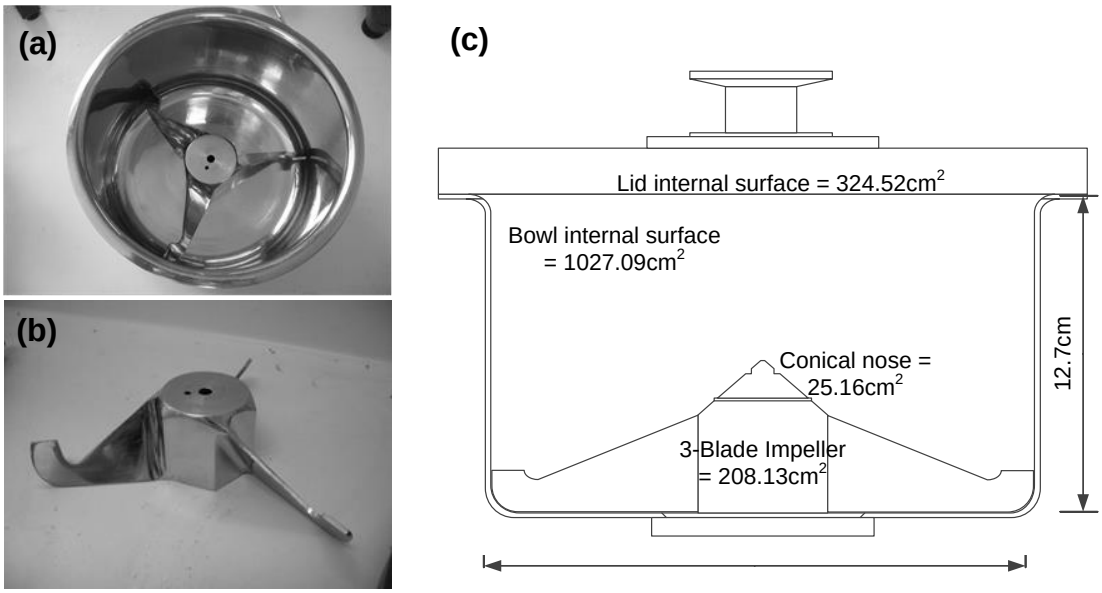

Figure 7.2: Images of the (a) bowl; (b) impeller and (c) dimensional drawings of the large laboratory granulator (KG5 granulator) bowl (5L).

The 5L scale experiments were based on the wet granulation experiments performed in *Chapter 4*. These experiments are described in detail in *Section 4.2*. The 1L wet granulation experiments, the wet granulation experiments were designed such that the total wet granulation time was approximately 12.3 minutes which is identical to the total wet granulation time for the 5L scale wet granulation experiments. The 1L experiments were conducted in the small granulator bowl, using 200g of powder with the liquid binder delivered in a drop-wise fashion using a peristaltic pump. The peristaltic pump speed was set to 23mL/min which gave a PVP liquid binder flow rate of approximately 26g/min and a total liquid binder delivery time of 2 minutes 30 seconds.

Prior to granulation, the primary powder mixture was pre-mixed in the granulator for at least 1 minute (at a minimum impeller speed of 200rpm to ensure the powder was well-mixed with a roping-regime mixing pattern (Iveson and Litster, 1998)). For the 1L bowl, 200g of the primary powder was used, while for the 5L bowl, 1kg of the binary powder mixture was deposited. The liquid binder was sprayed for at least 30 seconds, external to the granulator, to ensure that the spray flow rate was at steady state before placing the spray nozzle into the granulator. The operating conditions were varied to see the resulting effect on the final tablet strength; as follows:

- Granulator liquid level (30wt.%, 40wt.% and 50wt.%). A wet massing time of 10 seconds was performed to ensure uniform dispersion of the liquid in the powder mass,

- Wet massing time (0, 2, 6, 10 and 20 minutes) at 30wt.% liquid level,
- Impeller speed (250rpm and 400rpm for the 1L bowl, and 285rpm and 600rpm for the 5L bowl). The two impeller speeds correspond to low-intensity and high-intensity roping mixing regime respectively (Iveson and Litster, 1998).

The granules produced from the wet granulation experiments were dried in shallow trays in a fan-forced oven at 60°C overnight.

The granules were compacted into 500mg tablets in a pneumatic single-station tablet press (Model 3887, Carver Inc. USA). The tablets were weighed with an error of ±1mg. The compaction force applied by the tablet press to produce the tablets ranged between 1000lb_f to 16,000lb_f (453.6kg_f to 7257.5kg_f). The tablet press was set up with the same settings as those used in *Chapter 4*.

The tablet height was measured by a digital calliper, while the tablet "hardness" was measured using a tablet hardness tester (Dr. Schleuniger Pharmatron 6D model). The physical tablet dimensions were 13mm in diameter and the tablet thickness ranged from 2.54mm for the highest compaction force (16,000lb_f) to 3.15mm for the lowest compaction force (1,000lb_f). Three to five tablets were measured for each granulation batch, depending on the amount of powder granulated. From the tablet data, the tablet tensile strength was calculated according to Equation 4.2 (Fell and Newton, 1970).

7.3 RESULTS

The results for the effect of the granulator scale on the tablet strength are presented in this section. For each of the results presented, the data represents the average results for three to five tablets (depending on the amount of powder granulated), with the error in the x-axis symbolising 5% of the error in the compaction pressure or the standard error of the mean for the tablet density, while the y-axis error bars denote the standard error of the mean for the tablet hardness or the tablet density.

7.3.1 EFFECT OF 1 LITRE GRANULATOR SCALE ON THE TABLET STRENGTH

7.3.1.1 LIQUID LEVEL

The effect of the granulator liquid level and the impeller speed on the tablettability behaviour is presented in Figure 7.3. From the tablettablity behaviour, it can be observed that the impeller speed can be a strong influence on the final tablet strength. For tablets

produced from low (250rpm) impeller speeds, the tablet hardness decreases to approximately 30kp at 550MPa compaction pressure, while the tablet hardness decreases further to 25kp at the same compaction pressure for tablets produced from high impeller speeds (400rpm). Therefore similar to the results presented in previous chapters, a higher impeller speed can compromise the tablet strength.

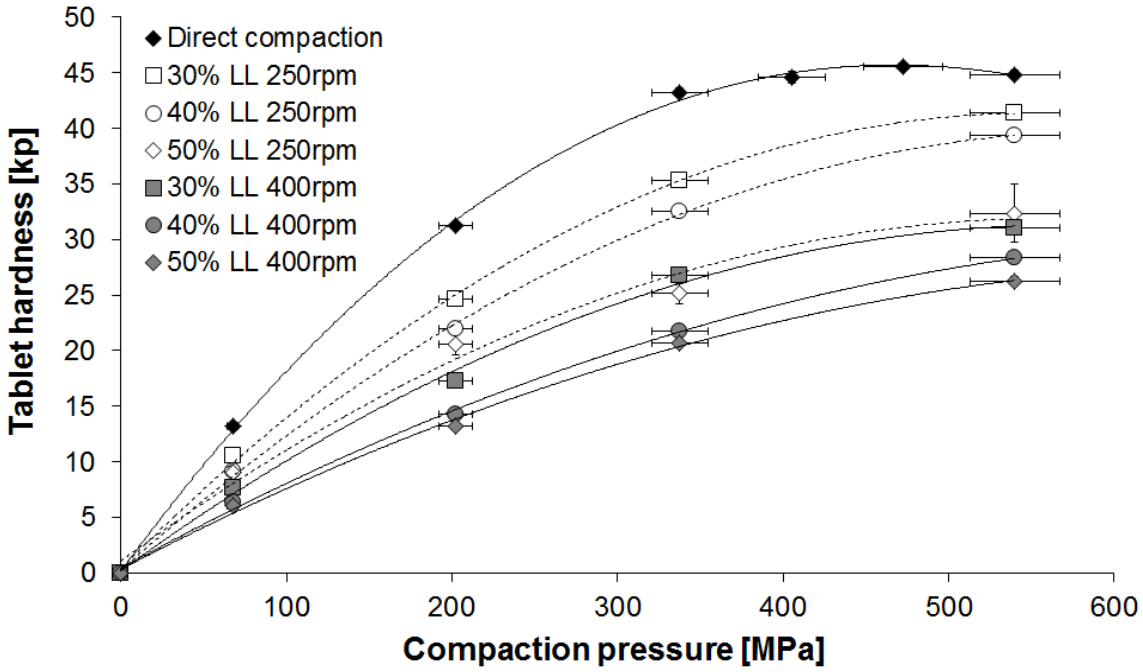

Figure 7.3: Comparison of Tablettabilty behaviour for tablets produced from low (250rpm) and high (400rpm) impeller speeds in small scale (1L) granulation experiments for various liquid levels (LL).

The compressibility behaviour for tablets produced in the small granulator bowl (1L) for varying liquid levels and impeller speeds can be seen in Figure 7.4. The compressibility behaviour as a function of the liquid level is similar to the results found in the 5L bowl (see Figure 4.15, Figure 6.7 and Figure 6.12). The results reconfirm that the liquid level or the impeller speed has very little effect on the tablet density as a function of the compaction pressure.

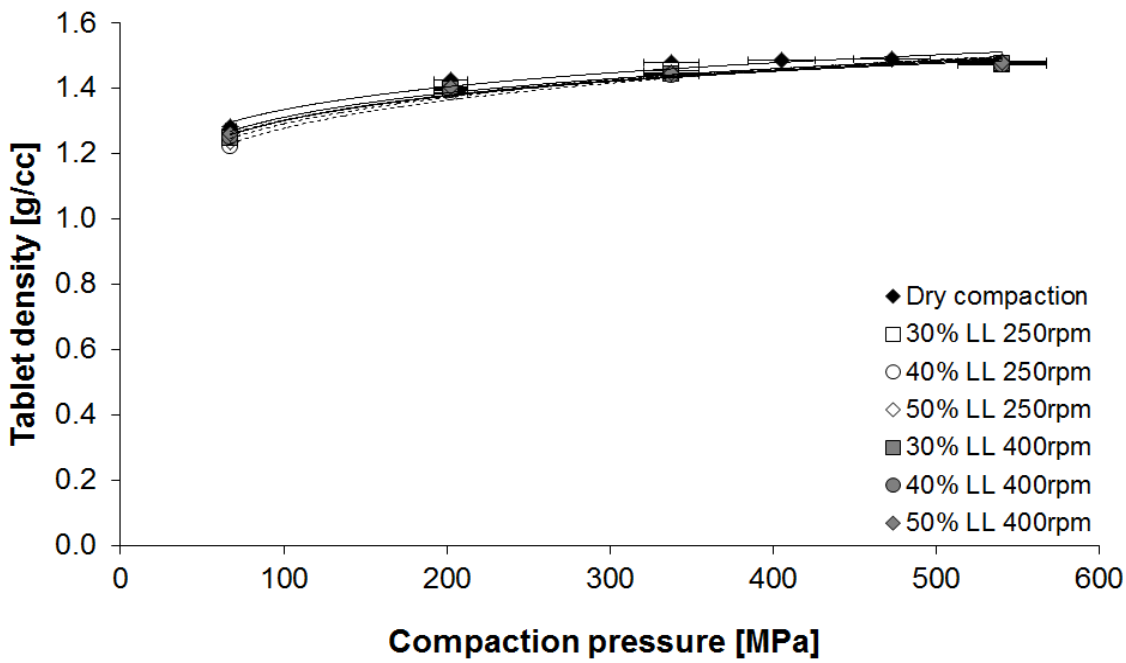

Figure 7.4: Compressibility (tablet hardness versus tablet density) behaviour for tablets produced from low (250rpm) and high (400rpm) impeller speeds in small scale (1L) granulation experiments for various liquid levels (LL).

The compactability behaviour demonstrates the significance of the impeller speed on the tablet hardness for a given tablet density in small-scale (1L) granulation experiments with varying liquid level and impeller speeds, as presented in Figure 7.5. The compactability plot shows that for low impeller speeds, the tablet strength for a given tablet density is similar for 30wt.% and 40wt.% liquid levels. However at 50wt.% liquid level, there appears to be sufficient liquid present in the powder and/or granules to decrease the tablet hardness to approximately 30kp at a tablet density of 1.48g/cm^3 (in comparison to approximately 38kp for a tablet density of 1.48g/cm^3 for 40wt.% liquid level). The tablet hardness decreases further to approximately 25kp for a similar tablet density when the impeller speed increases to 400rpm. Therefore the compactability behaviour demonstrates again that the increase in impeller speed promotes the deformation and consolidation of the granules, which profoundly increases the tablet density while compromising the tablet strength.

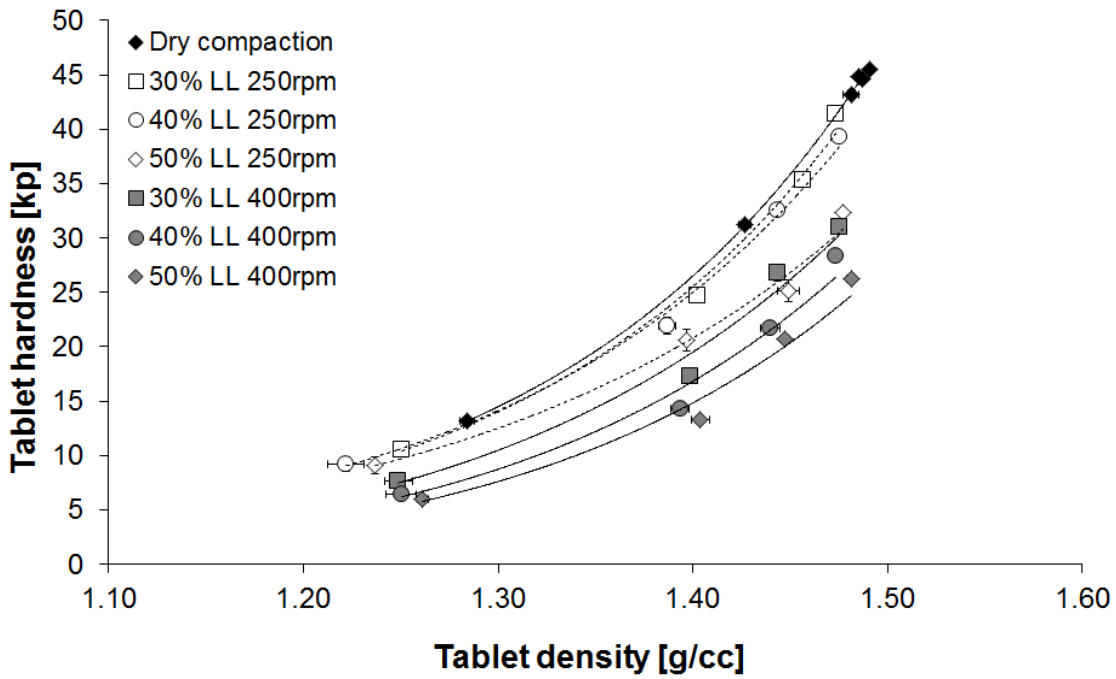

Figure 7.5: Compactability (tablet hardness versus tablet density) behaviour for tablets produced from low (250rpm) and high (400rpm) impeller speeds in small scale (1L) granulation experiments for various liquid levels (LL).

7.3.1.2 WET MASSING TIME

Evidence of the impact the impeller has on the deformation and consolidation of the granules can also be seen in the tablettability behaviour as a function of wet massing time seen in Figure 7.6. These results are at a constant liquid level of 30%. Although increasing the wet massing time decreases the tablet strength overall, when comparing the liquid level or the impeller speed, for wet massing times at 2 minutes and beyond, there is little difference in the tablet hardness between the different granulation conditions.

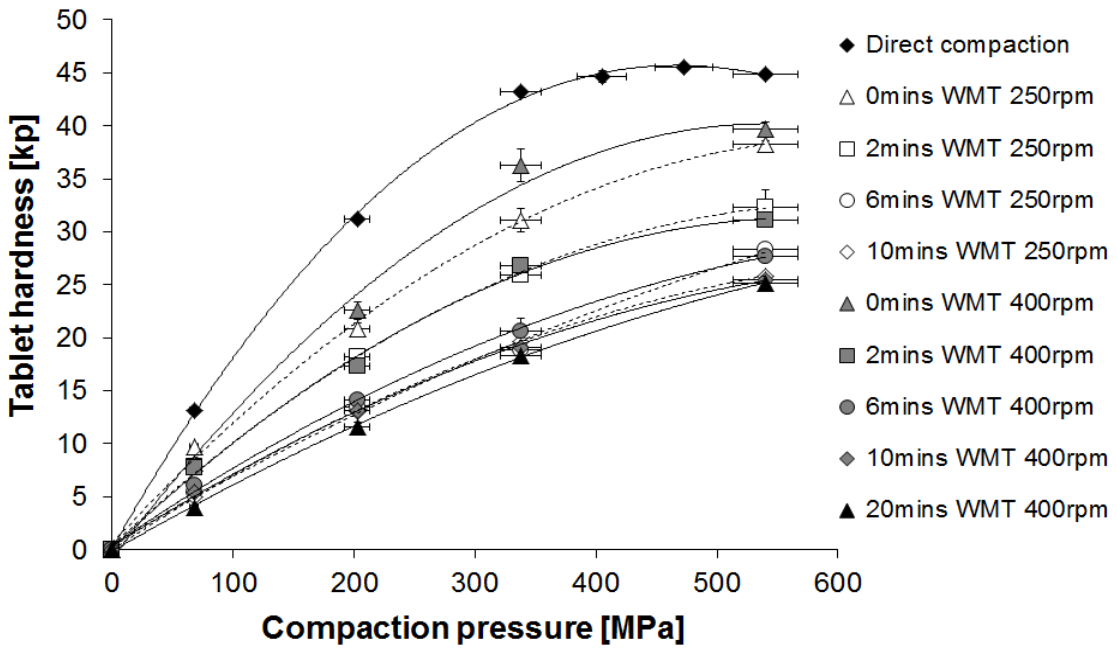

Figure 7.6: Comparison of Tablettabilty (tablet hardness versus compaction pressure) behaviour for tablets produced from low (250rpm) and high (400rpm) impeller speeds in small scale (1L) granulation experiments for various wet massing times (WMT).

The effect of wet massing time on the compressibility behaviour (not shown here, please see *Appendix D: Tablet Compressibility Behaviour Profiles*) was found to be similar to the liquid level effects in Figure 7.4. The effect of the liquid level and the impeller speed did not have any significant influence on the tablet density for a given compaction pressure.

The compactability behaviour showed that the liquid level and impeller speed gave similar trends and tablet hardness for a given tablet density as seen in Figure 7.7. Comparing the same wet massing time but with different impeller speeds revealed that for a given tablet density, the tablet hardness is similar, although it is clear that increasing the wet massing time and/or liquid level decreases the tablet hardness by approximately 15kp. However at wet massing times equal to and greater than 6 minutes, the compactability profile is identical regardless of the liquid level or impeller speed. This may signify that the granule has reached its maximum consolidation limit and hence any further wet massing would not alter the granule structure and subsequent final tablet strength.

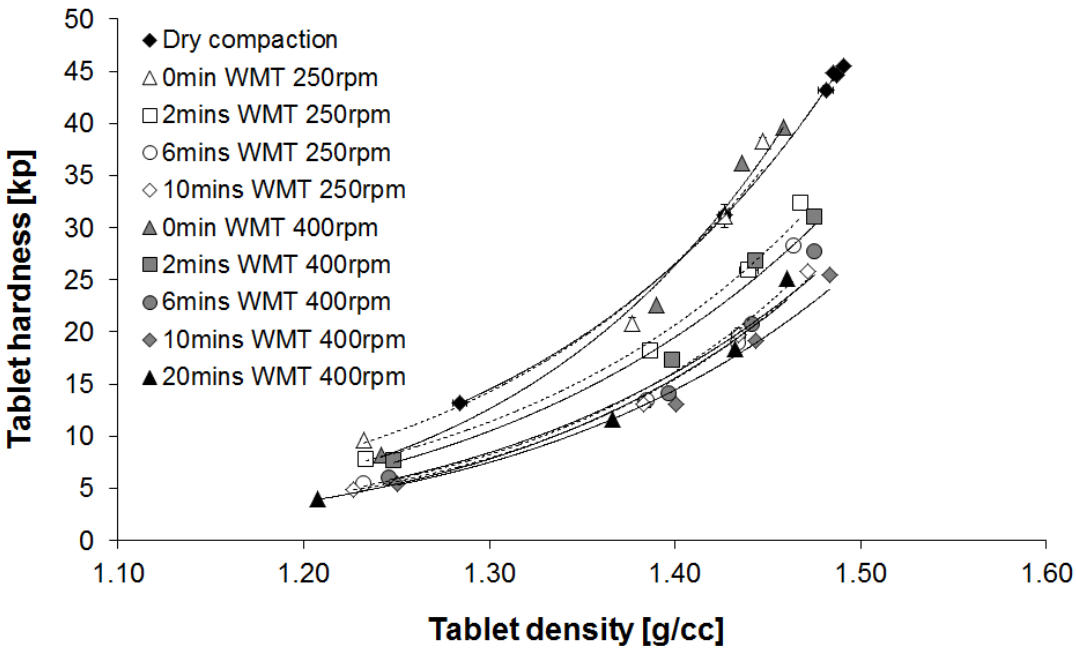

Figure 7.7: Compactability (tablet hardness versus tablet density) behaviour for tablets produced from low (250rpm) and high (400rpm) impeller speeds in small scale (1L) granulation experiments for various wet massing times (WMT).

7.3.2 EFFECT OF THE GRANULATOR SCALE ON THE UNIFIED COMPACTION CURVE

Taking into account the different granulator scales investigated in this study, the Unified Compaction Curve model was applied to the compaction curves for the small (1L) and large (5L) laboratory scale granulator bowls.

The application of the Unified Compaction Curve to wet granulation compaction curves for the one litre scale is presented in Figure 7.8 and the combination of the large (5L) and small scale can be seen in Figure 7.9. A first order exponential curve was also fitted to the relationship between the tensile strength and the number of impellor revolutions for the small 1L scale results ($P_{WGC,max}$ = 129.3MPa; b = 0.0006). For the large scale result in Figure 7.9, the curve fitting parameters was found to be $P_{WGC,max}$ = 134.8MPa; b = 0.0005. From the comparison of the fitting parameters between the small and large scale, it can be seen that there is a significant difference in the amount of compaction pressure exerted on the granules during granulation with the 5L scale exerting greater compaction forces compared to the smaller 1L scale.

From the data in Figure 7.8, the average effective wet granulation compaction pressure per revolution, χ, can be calculated and this was determined to be approximately 58kPa

per revolution. Compared to the large scale system, which has χ = 44kPa per revolution, the average compaction pressure experienced by the granules in the smaller bowl is greater. This could be attributed to the granulator bowl size and/or impeller geometry.

Overall, the size of the granulator bowl does not appear to have a significant effect on the final tablet strength as seen in Figure 7.9. The effect of the granulator impeller speed also does not have a significant effect on the tablet strength. However the granulation data fits better to the general curve at higher impeller speeds (400rpm in comparison to 250rpm). Because the wet granulation compaction pressure indirectly reflects the tablet strength obtained from the granulation process, the tablet strength is not significantly affected by the granulator scale. Rather it is the cumulative number of impeller revolutions that is the driving force for the tablet strength.

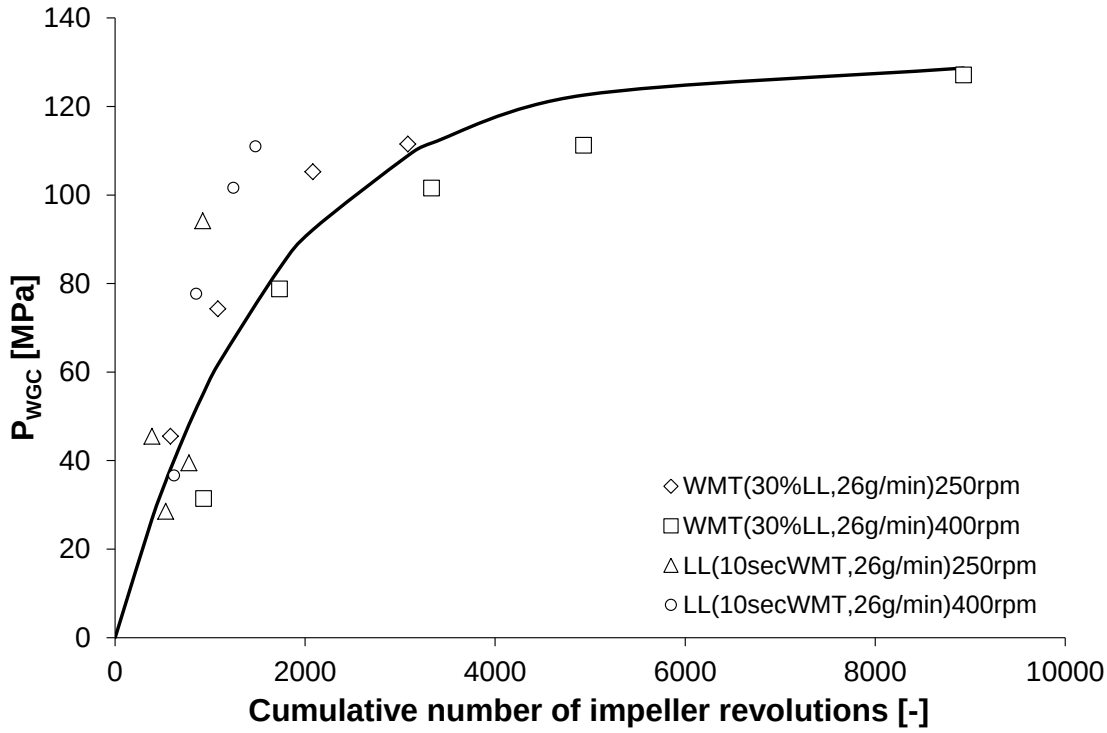

Figure 7.8: The wet granulation compaction pressure P_{WGC} as a function of the number of impeller revolutions, with varying wet massing times (WMT) and liquid levels (LL), from the application of the Unified Compaction Curve for small (1L) granulator bowls.

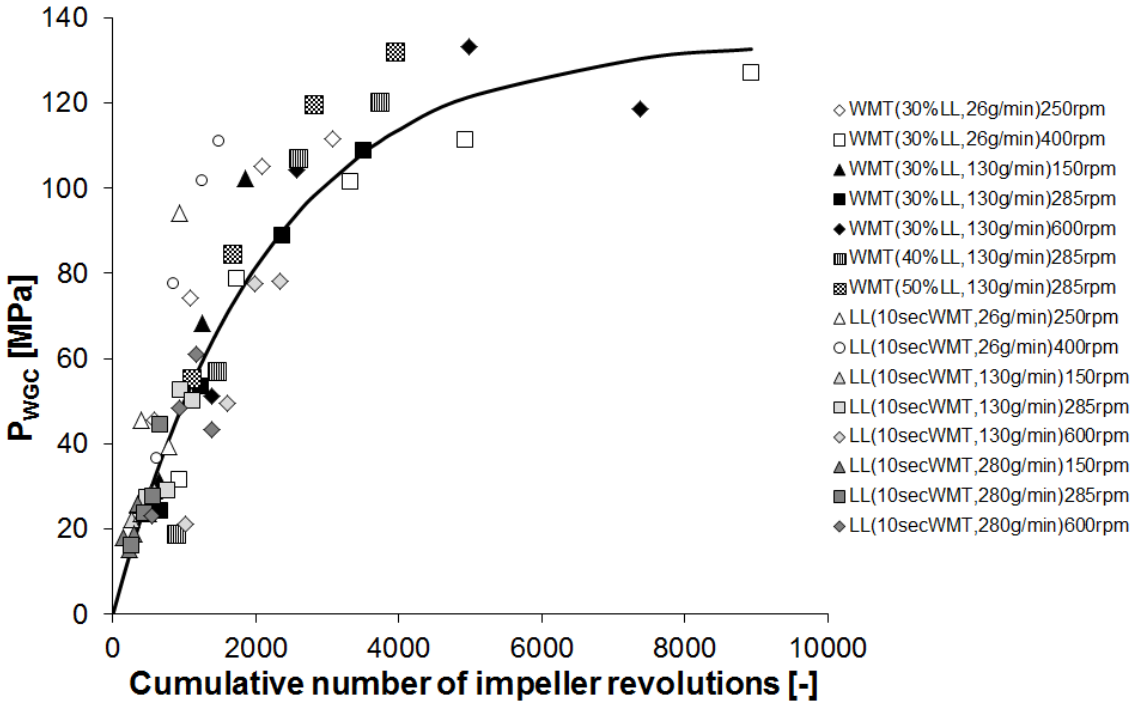

Figure 7.9: The wet granulation compaction pressure P_{WGC} as a function of the number of impeller revolutions, with varying wet massing times (WMT) and liquid levels (LL), from the application of the Unified Compaction Curve for small (1L, denoted by hollow symbols) and large (5L, denoted by filled symbols) granulator bowls.

7.4 DISCUSSION

The Unified Compaction Curve has proven to be able to represent the tablet strength attained from different granulator scales, impellor and bowl geometries. At low numbers of impeller revolutions (up to 2000 revolutions), the wet granulation compaction pressure for the different granulator scales and operating conditions coincide each other to form a linear relationship. At low impeller revolutions, the raw powder would be agglomerated into nuclei as part of the wetting and nucleation phase of wet granulation. Other studies have shown that nucleation occurs at low numbers of impeller revolutions, generally less than 500 revolutions (Hapgood *et al.*, 2003). Therefore from the results of Figure 7.9, during the first phase of granulation, the powder and initial nuclei experience the same compaction pressure no matter what the granulation operating condition is.

However beyond 2000 impeller revolutions, the wet granulation compaction pressure begins to vary for a given impeller revolution. This can be speculated to be due to the consolidation phase of wet granulation and the granulator operating conditions begin to have a significant role in the way the powder and/or granules are compacted and consolidated, hence leading to the scatter in the data at higher number of impeller revolutions.

From Figure 7.9, the average amount of impact and shear forces on the granules during wet granulation for the small and large scale can be seen by the linear slope of the first portion of the curve representing the relationship between the wet granulation compaction pressure and the number of impeller revolutions. It was found that the small-scale granulator induced a larger compaction pressure (χ = 50kPa per revolution) compared to the large-scale granulator (χ = 39kPa per revolution). The linear slope appears to give an insight into the mixing intensity of the powder and granules for a given granulation operating condition and granulator-scale. When the liquid level increases above 30wt.%, the microcrystalline cellulose particles and granules become saturated with liquid binder which alters the way the particles and granules deform and compact during wet granulation. Therefore the saturation of the microcrystalline cellulose particles deteriorates the ability of the microcrystalline cellulose to plastically deform but instead allow the granule to maintain rigid granule structure which is speculated to undergo brittle fracture and confers strength to the tablet during the tabletting stage.

Therefore the effect of granulator scale can give an insight into the compaction behaviour of microcrystalline cellulose during wet granulation and its sensitivity to the granulation operating conditions, particularly the impact with the impeller and the liquid saturation of the microcrystalline cellulose particles. The Unified Compaction Curve is able to unify the compaction data for varying granulation conditions at different scales, which enable manufacturers to design the wet granulation process with the primary basis being the number of impeller revolutions to achieve the desired tablet strength. Since the compaction pressure from the impeller is the variable of interest in the Unified Compaction Curve, the model is able to provide an alternative scale-up guideline to help design the wet granulation process.

The scale-up guideline is proposed to be based on maintaining “constant compaction” pressure between small and large scales. The granule properties (in particular the granule porosity) and the tablet strength was found to be dependent on the number of the impeller revolutions (N_{rev}) and the effective granulation compaction pressure per revolution, χ in *Chapter 4* and *5* (Equation 7.1).

$$\chi = \frac{P_{WGC}}{N_{rev}} \tag{7.1}$$

The size of the granulator would be expected to exhibit different compaction pressures based on the granulator bowl and impeller geometry. This would mean that to maintain the equivalent amount of compaction pressure, P_{WGC}, induced on the granules between the scales, the number of impeller revolutions would be dependent on χ, as described in Equation 7.3.

$$P_{WGC} = \chi \times N_{rev} \tag{7.2}$$

$$\chi_1 \times N_{rev,1} = \chi_2 \times N_{rev,2} \tag{7.3}$$

Therefore for a given χ_1 and χ_2 for the small and large scale respectively, for a given number of impeller revolutions for the small scale granulator, N_1, the number of impeller revolutions (N_2) required to achieve the same P_{WGC} for the small scale for the large scale is given by Equation 7.4.

$$N_{rev,2} = \frac{\chi_1}{\chi_2} \times N_{rev,1} \tag{7.4}$$

The number of impeller revolutions would be based on the impeller speed and the total granulation time. An example of using the constant compaction scale-up rule, based on the experiments conducted in this thesis, is given as follows:

<u>Known granulation conditions:</u>

Formulation: 1:1 microcrystalline cellulose and lactose 200mesh, granulated with 5w/v% aqueous PVP liquid binder (liquid level = 30%; wet massing time = 6mins)

χ for the small-scale 1L granulator, χ_1 = 50kPa/revolution

χ for the large-scale 5L granulator, χ_2 = 39kPa/revolution

Small-scale granulator impeller speed, $N_{speed,1}$ = 400rpm

Large-scale granulator impeller speed, $N_{speed,2}$ = 600rpm

Total granulation time for the small-scale 1L granulator, $t_{granulation,1}$ = 8.33 minutes

Tablet compaction pressure = 202.5MPa

Therefore the effective granulation compaction pressure for the small-scale granulator is:

$$P_{WGC,1} = \chi_1 \times N_{speed,1} \times t_{granulation,1} = 50\frac{kPa}{rev} \times 400rpm \times 8.33\min = 166{,}600kPa \text{ or } 166.6MPa$$

where $N_{speed,1}$ is the impeller speed of the small granulator and $t_{granulation,1}$ is the total granulation time conducted in the small granulator.

To achieve an effective granulation compaction pressure of 166.6MPa for the large granulator, the number of impeller revolutions, N_2, required is:

$$N_2 = \frac{\chi_1}{\chi_2} \times N_1 = \frac{50kPa/rev}{39kPa/rev} \times 400rpm \times 8.33\min = 4{,}272rev$$

Therefore to achieve 4,272 revolutions in the large-scale 5L granulator, the total granulation time required, for a given impeller speed of 600rpm, is:

$$t_{granulation,2} = \frac{N_{rev}}{N_{speed}} = \frac{4{,}272rev}{600rpm} = 7.1\min$$

Hence to maintain constant compaction pressure (P_{WGC} = 166.6MPa) while up-scaling from the 1L granulator to the 5L granulation to maintain a consistent tablet strength, the total wet granulation time required is 7.1 minutes.

By looking at granulation data for the 1L and 5L granulator bowls in Figure 7.10, the data supports the scale-up rule based on constant cumulative compaction pressure. At approximately 580 revolutions, the χ (compaction pressure/revolution) was found to be 58MPa/rev for the 1L granulator bowl, while at approximately 660 revolutions, the χ is 44MPa/rev for the 5L granulator bowl. Therefore the cumulative compaction pressure for both small and large granulator bowls was found to be similar in magnitude as shown below:

$$\chi_1 \times N_{rev,1} \approx \chi_2 \times N_{rev,2}$$

$$\chi_1 \times N_{rev,1} = 58MPa/rev \times 582.5rev = 33.8MPa$$

$$\chi_2 \times N_{rev,2} = 44MPa/rev \times 658.9rev = 29MPa$$

This would suggest that the scale-up rule is able to predict the tablet strength within ±5MPa based on the number of impeller revolutions and the wet granulation compaction pressure per impeller revolution. The scale-up of granulation processes based on the compaction pressure exerted on the granules is affected by the geometry of the granulator bowl and impeller design, which is captured in the parameter χ. The compaction pressure experienced by the granules may also be influenced by the batch-fill height and other granulation processing conditions which need to be taken into account in future investigations. This is particularly useful as laboratory or research scale granulators are not exact replicates of industrial granulators. Therefore the amount of compaction pressure exerted on the granules during granulation for small and large scale granulators

can be used as a scale-up rule for wet granulation processes to help predict the final tablet strength.

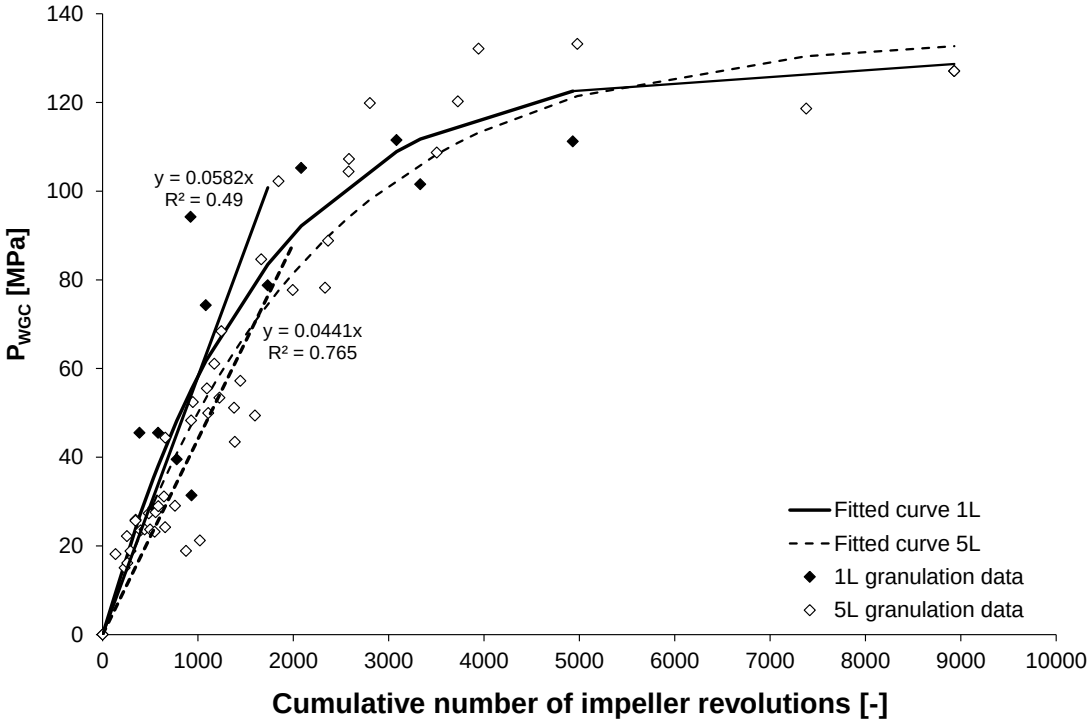

Figure 7.10: The relationship between the wet granulation compaction pressure and the cumulative number of impeller revolutions for small (1L) and large (5L) granulator bowls.

7.5 CONCLUSIONS

From the investigation of the effect of granulator scale on the final tablet strength and the Unified Compaction Curve model, it can be seen that the Unified Compaction Curve can differentiate the different scales between the 1L and 5L granulator bowls. A higher mixing intensity observed was observed for the 1L granulator bowl compared to the 5L bowl, which was seen in the compaction pressure per revolution parameter χ. The χ value for the 1L bowl was found to be 58MPa/rev, compared to 44MPa/rev for the 5L granulator bowl. Therefore for the 1L granulator scale, a steeper linear slope was observed in the relationship between the wet granulation compaction pressure and the number of impeller revolutions compared to the 5L granulator scale.

For each granulation scale, the wet massing time has a greater influence on the final tablet strength compared to the liquid level effects. As the wet massing time or the liquid level increases, a reduction in the tablet strength is observed. However at high liquid levels (50wt.%), the granules become saturated with liquid binder which alters the material properties and granule compaction behaviour which leads to a minor increase in the tablet

strength. This was seen for both the tablettability and the compactability relationships, however there was no influence of the granulator scale or the wet granulation conditions on the compressibility behaviour. The compressibility profile was almost identical for all granulation conditions.

Due to the differences in the compaction pressure per revolution (χ) for the 1L and 5L granulator bowls, a granulation scale-up rule based on maintaining 'constant compaction pressure' was proposed. This scale-up rule is a function of the compaction pressure per revolution and the cumulative number of impeller revolutions. The χ parameter compensates for the differences in the granulator bowl geometry and impeller design between the two granulator scales. Therefore the tablet strength would be dependent on the cumulative effective wet granulation compaction pressure, which is then related to the χ value and the number of impeller revolutions that accumulate during the wet granulation process. Although more investigations are required to validate the 'constant compaction pressure' scale-up rule, the proposed rule is anticipated to be a useful tool to help maintain constant granule properties during wet granulation scale-up but also to target the desired tablet.

Therefore the Unified Compaction Curve is able to be used as a scaling-up model to target the desired tablet strength by optimising the wet granulation conditions on a laboratory scale before up-scaling to industrial scale. This would save resources and be more economical for tablet manufacturers.

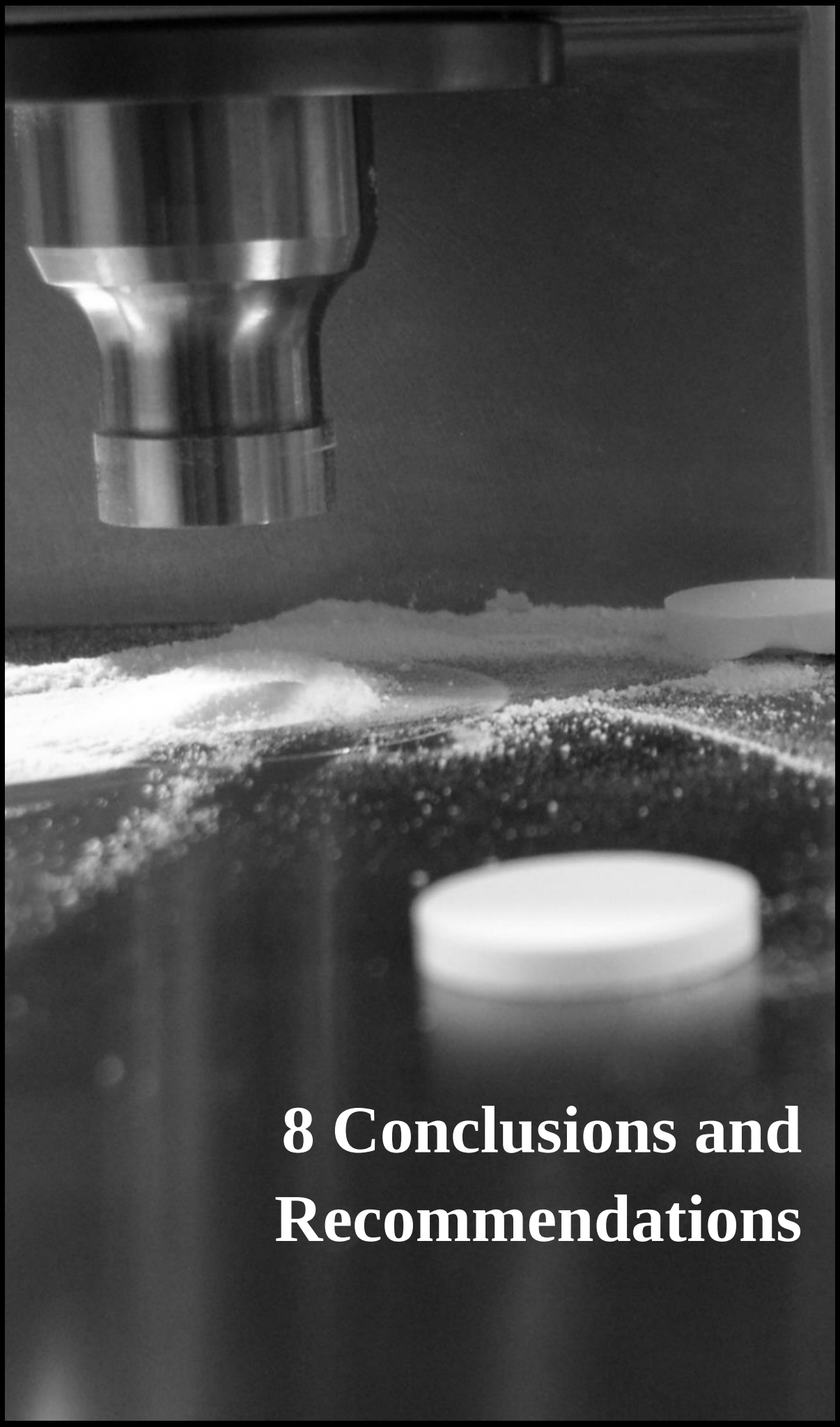

8 Conclusions and Recommendations

8 FINAL REMARKS, CONCLUSIONS AND RECOMMENDATIONS

"The most exciting phrase to hear in science, the one that heralds the most discoveries, is not "Eureka!"(I found it!) but 'That's funny...'"

- Isaac Asimov-

8.1 CONCLUSIONS

The driving force for this thesis is to fundamentally understand how the wet granulation operating conditions affect the final tablet strength. Although in literature there are studies which show that the wet granulation conditions influence the tablet strength (Bergman *et al.*, 1998; Keleb *et al.*, 2001; Murakami *et al.*, 2001; Williams *et al.*, 2004; Vermeire *et al.*, 2005), the mechanisms behind the change in the tablet strength are still not clear which has not enabled an efficient way to predict the tablet strength from the wet granulation process to be developed. Therefore this thesis aims to further understand the relationship between the wet granulation process and the final tablet strength by investigating the liquid level, wet massing time, impeller speed and binder flow-rate in a systematic manner to understand how the wet granulation process affects the granule morphology and the final tablet strength. These case studies can then be tied together through the Unified Compaction Curve model to predict the degree to which the wet granulation process affects and compromises the final tablet strength.

From this study using a base formulation of 1:1 lactose and microcrystalline cellulose, the tablet strength produced from various wet granulation conditions demonstrate that the liquid level (20-50wt%), wet massing time (0-10 minutes) and impeller speed (150rpm, 285rpm and 600rpm) can have a direct effect on the subsequent tablet strength. As the liquid level, wet massing time and impeller speed increases, the tablet strength decreases from a maximum tablet hardness of approximately 45kp (from direct compaction) to lowest tablet hardness of 23.5kp after 10 minutes of wet massing time. Therefore there is a "loss of compactability" when the formulation is exposed to processing conditions in wet granulation and even in dry roller compaction (Kochhar *et al.*, 1995; Bultmann, 2002; Freitag and Kleinebudde, 2003; Shi *et al.*, 2011; Shi *et al.*, 2011). The loss of

compactability in the formulation by the processing compaction forces sets up the fundamental conditions for the Unified Compaction Curve model to be applied.

The decrease in the tablet strength with increasing wet granulation processing time is partly due to the transition of the granule morphology in which the granule surface roughness decreases with increasing residence time of the granules in the granulator. The smoothing of the granule surface inherently produces rounder granules. This was shown through the circularity factor which suddenly increased in value from 0.27 to 0.5 at approximately 2600 revolutions (see Figure 5.3). The compaction forces from the granulator impeller consolidate the granules, which inherently destroys the granule surface roughness. Therefore the ability of the granule to undergo mechanical inter-locking during the tabletting process deteriorates, leading to a reduction in its potential contribution to the tablet strength.

The granule porosity also decreases significantly with increasing granulator residence time. The granules are densified during the coalescence and consolidation stages of the wet granulation process, which consequently decreases the granule porosity from 18% to approximately 8% (see Figure 8.1).

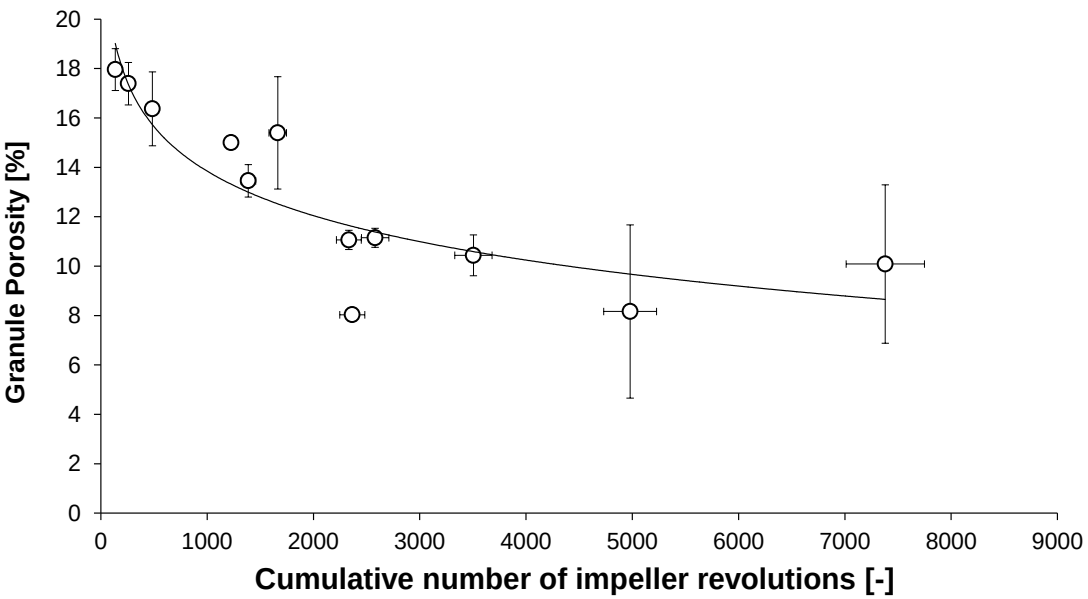

Figure 8.1: Granule porosity as a function of the number of impeller revolutions.

This also contributes to the deterioration of the mechanical inter-locking ability of the granules. The transition of the granule morphology and porosity during wet granulation can be attributed to the irreversible plastic deformation of microcrystalline cellulose

particles, which wrap and encase the lactose particles during the consolidation and densification of the granules during the wet granulation process.

The wet granulation processing conditions (liquid level, wet massing time, impeller speed) induce compaction forces from the impeller to the granules. Therefore the longer the wet granulation time, the more the granules are exposed to the compaction forces. This is an important factor in this study because there is the inclusion of microcrystalline cellulose in the formulation. Because microcrystalline cellulose is a plastically deforming material, the irreversible deformation behaviour affects the final tablet strength and becomes the driving force for the Unified Compaction Curve model.

From the wet granulation process, the subsequent decrease in the tablet strength or "loss of compactibility" with increasing granulator residence time allows the wet granulation compaction curves of varying processing conditions to be realigned onto a reference direct compaction curve to predict the final tablet strength from different operating conditions. In this study, the compaction curves produced from varying liquid levels, wet massing times, impeller speeds and binder flow-rates could be translated onto the reference compaction curve (direct compaction curve). An example of the Unified Compaction Curve model fitted to wet massing time granulation data is given in Figure 8.2.

As the wet granulation processing conditions increased, the wet granulation compaction curve translated further to the right of the reference curve, indicating that the difference between the maximum tablet strength (produced from direct compaction) and the "processed" tablet strength decreases ($T_{max} - T_{WGC}$), which is a reduction in the tablet tensile strength. The Unified Compaction Curve model was also feasible for granulation data in a different study in which pure microcrystalline cellulose was granulated with water (Shi *et al.*, 2011; Shi *et al.*, 2011).

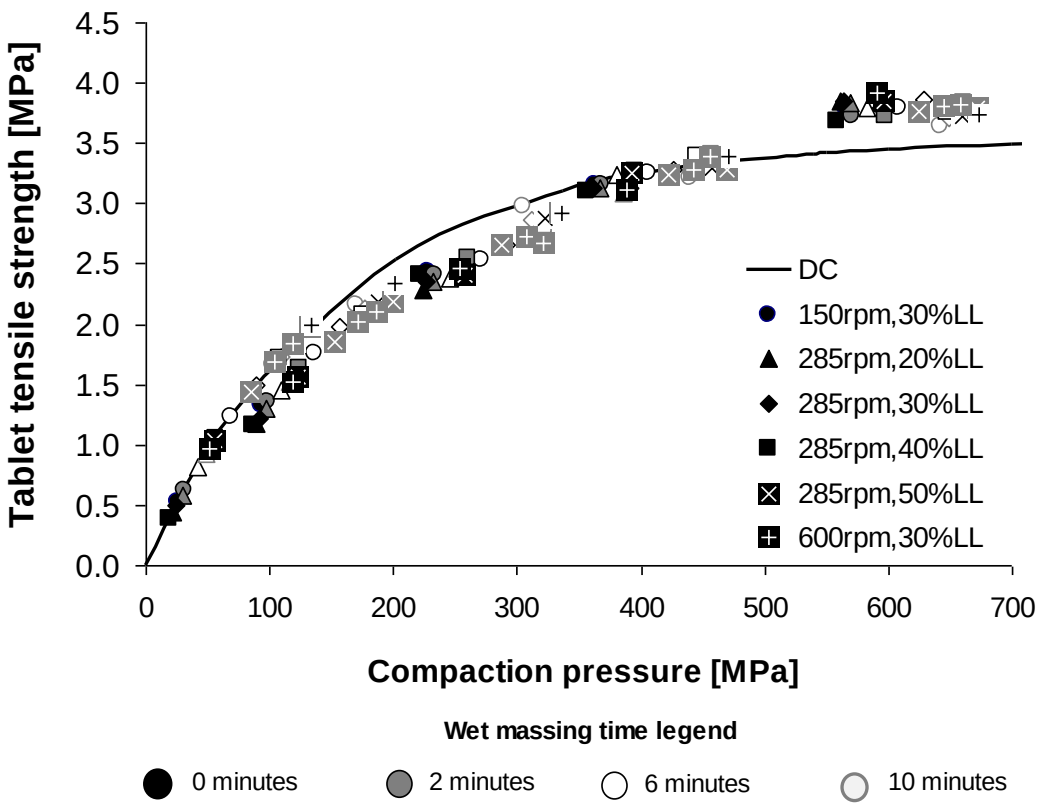

Figure 8.2: The Unified Compaction Curve model for the wet massing time effects with varying impeller speed and liquid levels (binder flow rate = 130g/min).

The Unified Compaction Curve model also shows the amount of compaction pressure the granules experience during wet granulation through the equivalent wet granulation compaction pressure parameter P_{WGC}. Therefore for the first time, the compaction pressure applied to the granules during wet granulation can be quantified without using sophisticated equipment. The most interesting aspect of the Unified Compaction Curve is the correlation between amount of compaction forces during the wet granulation and the tablet strength. When the relationship between the tablet strength and the number of impeller revolutions is taken into account, it can be seen that the liquid level, wet massing time, impeller speed and binder flow-rate wet granulation data all coincide onto a first-order exponential curve (see Figure 8.3).

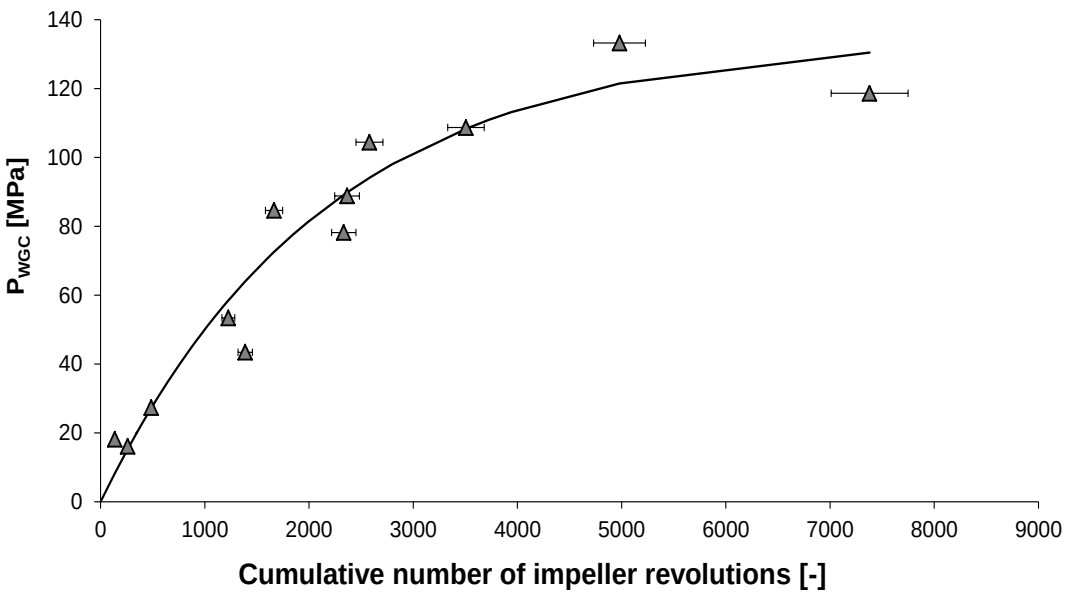

Figure 8.3: The effective wet granulation compaction pressure, P_{WGC}, as a function of the cumulative number of impeller revolutions.

This means that the tablet strength can be controlled using the number of impeller revolutions for a given wet granulation processing condition, which will help optimise the wet granulation process in an efficient way. Another interesting note to be made at this stage is that the relationship between the P_{WGC} and the cumulative number of impeller revolutions is the inverse trend of the relationship between the granule porosity and the number of impeller revolutions (Figure 8.2), indicating that the compaction forces from the impeller affects the granule porosity significantly. Consequently, the granule porosity becomes the driving force behind the rounding of the granules, the Unified Compaction Curve model and ultimately the final tablet strength.

However the Unified Compaction Curve has limitations in which the model will only be valid for granulation formulations comprising at least 30% liquid level and with at least 50% microcrystalline cellulose in the formulation used in this study. Other plastically deforming materials, such as starch, may also conform to the Unified Compaction Curve, however future studies are required to assess the use of other plastically deforming materials in the model. This is supported by studies where a liquid level less than 30% or re-humidified powder (with a moisture content of approximately 7wt%) leads to the compaction data not conforming to the relationship between the wet granulation compaction pressure (P_{WGC}) and the number of impeller revolutions. A formulation comprising of 25% microcrystalline cellulose/75% lactose was investigated and it was found this formulation did not show a trend that was consistent with the 50%

microcrystalline cellulose formulation. Instead of shifting right across the reference curve for longer granulation periods, the wet granulation compaction curve shifted left across the reference curve. This may indicate that the tablet becomes stronger, however this will be investigated in future studies.

The investigations into the effect of the wet granulation compaction pressure and the binder properties on the final tablet strength found that the presence or absence of intra-granular hydrogen bonding influences the final tablet. When hydrogen bonding is present in the liquid bridges (by using water-based liquid binder) between the granules, the granule strength increases which in turn compromises the table strength. Therefore the Unified Compaction Curve demonstrates that the strength of the intra-granule bonds inversely controls the tablet strength. The liquid binder can also contribute to the final tablet strength through the swelling of microcrystalline cellulose swells upon exposure to liquid binder. The swelling of the cellulose facilitates in increasing the bonding area and confer strength to the tablet.

The acidity of the liquid binder can influence the crystallite size of microcrystalline cellulose granules. For liquid binders with a neutral pH level (such as calcium oxide liquid binders), the crystallite size was larger in comparison to granules prepared using more acidic liquid binders (such as PVP or hydrochloric acid). The wet massing time did not have any significant effect on the crystalline or amorphous regions of microcrystalline cellulose.

The effects of the wet granulator scale was also investigated and it was found that for 1 litre and 5 litre granulator scales, the wet granulation compaction data exhibited different wet granulation compaction pressure per revolution which enabled a new wet granulation scale-up rule to be proposed based on the concept of maintaining “constant compaction pressure” to predict the final tablet strength. Therefore scaling-up the granulation process can be more efficient by basing the scale-up guidelines on the number of impeller revolutions.

Because the Unified Compaction Curve model was originally developed for tablets produced from roller compaction, further investigations into how the Unified Compaction Curve is applicable to the wet granulation process would help in understanding the

granulation dynamics and improve granulation process design, trouble-shooting and optimization of the process.

8.2 RECOMMENDATIONS

One such experiment that would help in enhancing the understanding of the Unified Compaction Curve model is granulating with different ratios of lactose and microcrystalline cellulose components in the formulation. In this study, only 25:75, 50:50 ratios of microcrystalline cellulose and lactose were studied. The studies showed that formulations with less than 50% microcrystalline cellulose produced tablets that did not follow the trend of shifting the compaction curves towards the right of the reference curve. This was supported by a recent study using 49% microcrystalline cellulose in the formulation (Dave and Dudhat, 2013). The use of different formulations in future studies will help to understand the limits of the Unified Compaction Curve model and understand the wet granulation dynamics through the equivalent wet granulation pressure per revolution of impeller χ. Other plastically deforming or visco-elastic materials such as starch or other grades of microcrystalline cellulose can also be incorporated into the wet granulation formulation to investigate the extent of deformation that is required by the material for the Unified Compaction Curve to be valid.

The effects of using a smaller tablet die or a different tablet press which uses a smaller dwell time that would replicate the strength of a pharmaceutical tablet would be beneficial in future studies. This will allow a wide range of microcrystalline cellulose proportions (such as 75% or 80% microcrystalline cellulose in the formulation) to be tested and understand the mechanisms behind the opposing trend of dominant brittle-fracturing formulations.

Dissolution studies can also be incorporated into future studies to investigate whether the Unified Compaction Curve gives an insight or predict the dissolution rate. It is possible that tablets produced with similar granule morphology can give similar dissolution profiles. Therefore the Unified Compaction Curve can be a useful tool to target dissolution times by using “designer” granules by Quality by Design (QbD).

The effect of using magnesium stearate to lubricate the tablets and die before tabletting can be included in future studies to reflect the pharmaceutical practice of lubricating the

tablet die or granules before tabletting. The tablet die in this study was not lubricated with magnesium stearate. The addition of magnesium stearate may alter the pressure applied to the granules to produce a tablet and hence influence the final tablet strength.

The effect of using ethanol-based liquid binders on the microcrystalline cellulose structure can be explored further by investigating the properties of the granules produced. Since the use of ethanol in the liquid binder increases the final tablet strength, this would indicate that the granule morphology is different to granules produced with aqueous-based liquid binders. Therefore the analysis of the granule porosity, BET surface and topology may reveal the reasoning behind the increase in the tablet strength for granules produced from ethanol-based liquid binders compared to water-based liquid binders. Similar investigations can be carried for granules produced with acidic liquid binders to compare the granule morphology with aqueous-based granules.

To investigate further into the scale of the wet granulation process and its effect on the final tablet strength, an industrial size granulator can be used in future studies to see if the wet granulation data can be translated onto the direct compaction reference curve like the 1 litre and 5 litre granulator scales. The up-scale from 1 litre to 5 litres granulator bowl may not be enough to see if different mixing dynamics, impeller blade design and bowl geometry results in different effective wet granulation pressures. By using an industrial granulator, the proposed scale-up guideline based on the “constant compaction pressure” can be tested further and assess the feasibility that constant wet granulation compaction pressure can be achieved especially with different impeller and bowl geometries. Other granulator processing conditions such as the batch fill height, impeller design and formulation type would be beneficial to investigate further to assess the ‘constant compaction pressure’ scale-up rule.

The studies on the effects of the wet granulation conditions on the final tablet strength, looking into the change in granule morphology, quantifying the wet granulation compaction pressure, understanding the material properties of microcrystalline cellulose and understanding the effects of down-scaling the wet granulation process is anticipated to help the pharmaceutical industry with improving the wet granulation process design and trouble-shooting as well as achieving the target tablet strength in an efficient manner.

NOMENCLATURE AND ACRONYMS

Symbol	Definition	Dimensions
A	Unit area generated by Gibbs' free energy (under isothermal and isobaric conditions) for surface free energy	[m^2]
A	Area in which a force is applied to the material	[m^2]
A	Particle-particle adhesion forces	[N/m^2]
b	Exponent constant for Unified Compaction Curve. Product of the formulation dependent pressure susceptibility constant and the ratio of the tablet density to the theoretical density ($b = \gamma\rho$)	[-]
d	Tablet diameter	[cm]
D	Impeller diameter	[m]
E	Young's modulus of elasticity	[N/m^2]
F	Force applied to an area of material	[N]
F	Tablet compaction force	[N]
Fr	Froude's number	[-]
g	Gravitational force	[m/s^2]
G	Gibbs' free energy	[J]
h	Tablet height	[m]
k	Average co-ordination number	[-]
ℓ , $\Delta\ell$	Length of material, change in length of material	[m]
L	Liquid phase	[-]
m	Tablet mass	[g]
N or N_{speed}	Impeller speed	[rpm]
N or N_{rev}	Number of impeller revolutions	[-]
P	Compaction pressure	[MPa]
P'	Compaction pressure of dry compaction	[MPa]
$P_{die\ wall}$	Pressure applied to die wall	[MPa]
P_{upper}	Pressure exerted by the upper tablet die punch	[MPa]
P_{RC}	Compaction pressure stress imparted on material during roller compaction	[MPa]
P_{WGC}	Compaction pressure stress imparted on material during wet granulation	[MPa]
$P_{WGC,max}$	Maximum compaction pressure stress imparted on material during wet granulation	[MPa]
S	Solid phase	[-]
S_{max}	Maximum granule liquid saturation	[-]
St_{def}	Stokes' deformation number	[-]
t	Tablet thickness	[cm]
$t_{granulation}$	Granulation time	[min]
T	Tablet tensile strength	[MPa]
T_{max}	Maximum tablet tensile strength that can be attained by the material	[MPa]

T_{RC}	Tensile strength of material generated during roller compaction	[MPa]
T_{WGC}	Tensile strength of material generated during wet granulation	[MPa]
U_C	Granule collision velocity	[m/s]
v	Poisson's ratio	[-]
v	Apparent volume of the tablet	[m^3]
V	Vapour phase	[-]
w	Liquid mass to solid mass ratio	[-]
x	Particle size	[m^2]
x	Small granulator scale notation	[-]
y	Large granulator scale notation	[-]
Y_d	Granule yield stress	[N/m^2]

Greek Symbols

γ	Surface free energy	[J/m^2]
γ_{SV}	Solid-vapour surface free energy	[J/m^2]
γ_{SL}	Solid-liquid surface free energy	[J/m^2]
γ_{LV}	Liquid-vapour surface free energy	[J/m^2]
γ	Pressure susceptibility constant	[-]
ε	Strain of the material	[-]
ε	Tablet or granule or bulk bed porosity	[-]
ε_{min}	Minimum porosity	[-]
θ	Equilibrium contact angle between the solid-liquid-vapour phases	[degrees,°]
σ	Normal material stress	[N/m^2]
σ_t	Granule strength	[-]
ρ	Ratio of tablet density to theoretical density	[-]
ρ_g	Granule density	[g/m^3]
ρ_S	Solid density	[g/m^3]
ρ_L	Solid density	[g/m^3]
$\rho_{theoretical,\ tablet}$	Theoretical tablet density representing ratio of apparent tablet density to true density of blend	[g/m^3]
$\rho_{apparent,\ tablet}$	Apparent tablet density incorporating the mass and dimensions of the tablet	[g/m^3]
ρ_{true}	True density of the material	[g/m^3]
$\rho_{true,\ blend}$	True material density of the blend	[g/m^3]
χ	Equivalent wet granulation compaction pressure per impeller revolution	[MPa/rev]
ϕ	Threshold pressure where plastic deformation begins to dominate	[MPa]

Acronyms	
BET	Brunauer-Emmet-Teller specific surface area
BF	Binder Flow-rate
CaO	Calcium Oxide
DC	Direct Compaction
FDA	Food and Drug Administration
HCl	Hydrochloric Acid
LL	(Granulator) Liquid Level
LSES	Least Sum of the Errors Squared
L2M	Lactose monohydrate 200 mesh
MCC	MicroCrystalline Cellulose
PVP	Polyvinyl Pyrrolidone
QbD	Quality by Design
QOM	Quality of Measurement for Helium Pcynometry
SEM	Scanning Electron Microscopy
SF	Solid Fraction
UCC	Unified Compaction Curve
WMT	(Granulator) Wet Massing Time
XRD	X-Ray Diffraction

REFERENCES

Adolfsson, Å., C. Caramella and C. Nyström (1998). "The effect of milling and addition of dry binder on the interparticulate bonding mechanisms in sodium chloride tablets." *International Journal of Pharmaceutics* **160**(2): 187-195, http://dx.doi.org/10.1016/S0378-5173(97)00307-4.

Agrawal, A. M., S. H. Neau and P. L. Bonate (2003). "Wet granulation fine particle ethylcellulose tablets: Effect of production variables and mathematical modelling of drug release." *AAPS Pharmaceutical Science* **5**(2): 1-13,

Aikawa, S., N. Fujita, H. Myojo, T. Hayashi and T. Tanino (2008). "Scale-up studies on high shear wet granulation process from mini-scale to commercial scale." *Chemical and Pharmaceutical Bulletin* **56**(10): 1431-1435,

Ameye, D., E. Keleb, C. Vervaet, J. P. Remon, E. Adams and D. L. Massart (2002). "Scaling-up of a lactose wet granulation process in mi-pro high shear mixers." *European Journal of Pharmaceutical Sciences* **17**(4–5): 247-251, http://dx.doi.org/10.1016/S0928-0987(02)00218-X.

Ansel, H. C. (1981). *Introduction to pharmaceutical dosage forms*. London, England, Lea & Febiger.

Augsburger, L. L. and S. W. Hoag (2008). *Pharmaceutical dosage forms: Tablets*. New York, USA, Informa Healthcare USA, Inc.

Augsburger, L. L. and S. W. Hoag (2008). *Pharmaceutical dosage forms: Tablets*. New York, USA, Informa Healthcare USA, Inc.

Aussillous, P. and D. Quéré (2006). "Properties of liquid marbles." *Proceedings of the Royal Society A: Mathematical, Physical and Engineering Science* **462**(2067): 973-999, 10.1098/rspa.2005.1581.

Ax, K., H. Feise, R. Sochon, M. Hounslow and A. Salman (2008). "Influence of liquid binder dispersion on agglomeration in an intensive mixer." *Powder Technology* **179**(3): 190-194,

Bacher, C., P. M. Olsen, P. Bertelsen and J. M. Sonnergaard (2008). "Compressibility and compactibility of granules produced by wet and dry granulation." *International Journal of Pharmaceutics* **358**: 69-74,

Badawy, S., D. Gray and M. Hussain (2006). "A study on the effect of wet granulation on microcrystalline cellulose particle structure and performance." *Pharmaceutical Research* **23**(3): 634-640, 10.1007/s11095-005-9555-z.

Bennett, B. and G. Cole (2003). *Pharmaceutical production : An engineers guide*. Rugby, UK, Institution of Chemical Engineers.

Bergman, R., M. E. Johansson, T. Lundstedt, E. Seifert and J. Aerg (1998). "Optimization of a granulation and tabletting process by sequential design and multivariate analysis." *Chemometrics and Intelligent Laboratory Systems* **44**(1-2): 271-286,

Bock, T. K. and U. Kraas (2001). "Experience with the diosna mini-granulator and assessment of process scalability." *European Journal of Pharmaceutics and Biopharmaceutics* **52**(3): 297-303, http://dx.doi.org/10.1016/S0939-6411(01)00197-7.

Bouwman, A. M., M. J. Henstra, D. Westerman, J. T. Chung, Z. Zhang, A. Ingram, J. P. K. Seville and H. W. Frijlink (2005). "The effect of the amount of binder liquid on the granulation mechanisms and structure of microcrystalline cellulose granules prepared by high shear granulation." *International Journal of Pharmaceutics* **290**(1–2): 129-136, http://dx.doi.org/10.1016/j.ijpharm.2004.11.024.

Bullen, A. (2009). *17 molecules that changed the world*. COSMOS Magazine (Online). Sydney, Australia, Luna Media Pty. Ltd.

Bultmann, J. M. (2002). "Multiple compaction of microcrystalline cellulose in a roller compactor." *European Journal of Pharmaceutics and Biopharmaceutics* **54**(1): 59-64,

Campbell, G. A., D. J. Clancy, J. X. Zhang, M. K. Gupta and C. K. Oh (2011). "Closing the gap in series scale up of high shear wet granulation process using impeller power and blade design." *Powder Technology* **205**(1–3): 184-192, http://dx.doi.org/10.1016/j.powtec.2010.09.009.

Capes, C. E. (1980). *Particle size enlargement*. Amsterdam, The Netherlands, Elsevier Scientific Publishing Company.

Carstensen, J. T. (2001). *Advanced pharmaceutical solids*. New York, Marcel Dekker, Inc.

Chitu, T. M., D. Oulahna and M. Hemati (2011). "Wet granulation in laboratory-scale high shear mixers: Effect of chopper presence, design and impeller speed." *Powder Technology* **206**(1–2): 34-43, http://dx.doi.org/10.1016/j.powtec.2010.07.016.

Chulia, D. (1994). *Powder technology and pharmaceutical processes*. Netherlands, Elsevier.

Cooper, A. R. and L. E. Eaton (1962). "Compaction behaviour of several ceramic powders." *Journal of the American Ceramic Society* **45**(3): 97-101,

Dave, R. H. and S. M. Dudhat (2013). *To evaluate wet granulated tablet properties through the unified compaction curve using microcrystalline cellulose (mcc, avicel 101 and 200).* American Association of Pharmaceutical Scientists Annual Meeting and Exposition, San Antonio, US, AAPS.

Denesuk, M., G. L. Smith, B. J. J. Zelinski, N. J. Kreidl and D. R. Uhlmann (1993). "Capillary penetration of liquid droplets into porous materials." *Journal of Colloid and Interface Science* **158**(1): 114-120,

Doerr, S. H. (1998). "On standardizing the 'water drop penetration time' and the 'molarity of an ethanol droplet' techniques to classify soil hydrophobicity: A case study using medium textured soils." *Earth Surface Processes and Landforms* **23**(7): 663-668,

Emady, H. N., D. Kayrak-Talay, W. C. Schwerin and J. D. Litster (2011). "Granule formation mechanisms and morphology from single drop impact on powder beds." *Powder Technology* **212**(1): 69-79,

Emori, H., Y. Sakuraba, K. Takahashi, T. Nishihata and T. Mayumi (1997). "Prospective validation of high-shear wet granulation process by wet granule sieving method. Ii. Utility of wet granule sieving method." *Drug Development and Industrial Pharmacy* **23**(2): 203-215,

Ennis, B. J. (2006). *Theory of granulation: An engineering perspective*. Handbook of pharmaceutical granulation technology. N. H. Parikh, Taylor & Francis.

Farber, L., K. P. Hapgood, J. N. Michaels, X.-Y. Fu, R. Meyer, M.-A. Johnson and F. Li (2008). "Unified compaction curve model for tensile strength of tablets made by roller compaction and direct compression." *International Journal of Pharmaceutics* **346**(1-2): 17-24,

Faure, A., I. M. Grimsey, R. C. Rowe, P. York and M. J. Cliff (1998). "A methodology for the optimization of wet granulation in a model planetary mixer." *Pharmaceutical Development and Technology* **3**(3): 413-422, doi:10.3109/10837459809009869.

Faure, A., I. M. Grimsey, R. C. Rowe, P. York and M. J. Cliff (1999). "Applicability of a scale-up methodology for wet granulation processes in collette gral high shear mixer-granulators." *European Journal of Pharmaceutical Sciences* **8**(2): 85-93, http://dx.doi.org/10.1016/S0928-0987(98)00063-3.

Faure, A., P. York and R. C. Rowe (2001). "Process control and scale-up of pharmaceutical wet granulation processes: A review." *European Journal of Pharmaceutics and Biopharmaceutics* **52**(3): 269-277, http://dx.doi.org/10.1016/S0939-6411(01)00184-9.

Fell, J. T. and J. M. Newton (1970). "Determination of tablet strength by the diametral-compression test." *Journal of Pharmaceutical Sciences* **59**(5): 688-691,

Fielden, K. E., J. M. Newton, P. O'Brien and R. C. Rowe (1988). "Thermal studies on the interaction of water and microcrystalline cellulose." *Journal of Pharmacy and Pharmacology* **40**(10): 674-678, 10.1111/j.2042-7158.1988.tb06993.x.

Freitag, F. and P. Kleinebudde (2003). "How do roll compaction/dry granulation affect the tableting behaviour of inorganic materials? Comparison of four magnesium carbonates." *European Journal of Pharmaceutical Sciences* **19**(4): 281-289, http://dx.doi.org/10.1016/S0928-0987(03)00133-7.

German, R. M. (1989). *Particle packing characteristics*, Metal Powder Industries Federation.

H., R. (1962). *The strength of granules and agglomerates*. New York, Wiley-Interscience.

Hapgood, K. P., J. D. Litster, S. R. Biggs and T. Howes (2002). "Drop penetration into porous powder beds." *Journal of Colloid and Interface Science* **253**(2): 353-366,

Hapgood, K. P., J. D. Litster and R. Smith (2003). "Nucleation regime map for liquid bound granules." *AIChE Journal* **49**(2): 350-361,

Hartsuijker, C. and J. W. Welleman (2007). *Engineering mechanics: Stresses, strains and displacements*. Dordrecht, Netherlands, Springer.

Hassanpour, A., S. J. Antony and M. Ghadiri (2007). "Modeling of agglomerate behavior under shear deformation: Effect of velocity field of a high shear mixer granulator on the structure of agglomerates." *Advanced Powder Technology* **18**(6): 803-812,

Hassanpour, A., C. C. Kwan, B. H. Ng, N. Rahmanian, Y. L. Ding, S. J. Antony, X. D. Jia and M. Ghadiri (2009). "Effect of granulation scale-up on the strength of granules." *Powder Technology* **189**(2): 304-312, 10.1016/j.powtec.2008.04.023.

He, X., K. A. Lunday, L.-c. Li and M. J. Sacchetti (2008). "Formulation development and process scale up of a high shear wet granulation formulation containing a poorly wettable drug." *Journal of Pharmaceutical Sciences* **97**(12): 5274-5289, 10.1002/jps.21410.

Heckel, R. W. (1961a). "Density-pressure relationships in powder compaction." *Transactions of the Metallurgical Society of AIME* **221**: 671–675,

Hegedus, A. and K. Pintye-Hodi (2007). "Influence of the type of the high-shear granulator on the physico-chemical properties of granules." *Chemical Engineering and Processing* **46**: 1012-1019,

Horsthuis, G. J. B., J. A. H. van Laarhoven, R. C. B. M. van Rooij and H. Vromans (1993). "Studies on upscaling parameters of the gral high shear granulation process." *International Journal of Pharmaceutics* **92**(1–3): 143-150, http://dx.doi.org/10.1016/0378-5173(93)90273-I.

Iveson, S. M. (2001). "Granule coalescence modelling: Including the effects of bond strengthening and distributed impact separation forces." *Chemical Engineering Science* **56**(6): 2215-2220,

Iveson, S. M. and J. D. Litster (1998). "Growth regime map for liquid-bound granules." *AIChE Journal* **44**(7): 1510-1518,

Iveson, S. M., J. D. Litster and B. J. Ennis (1996). "Fundamental studies of granule consolidation part 1: Effects of binder content and binder viscosity." *Powder Technology* **88**(1): 15-20,

Iveson, S. M., J. D. Litster, K. P. Hapgood and B. J. Ennis (2001). "Nucleation, growth and breakage phenomena in agitated wet granulation processes: A review." *Powder Technology* **117**(1-2): 3-39,

Iveson, S. M., P. A. L. Wauters, S. Forrest, J. D. Litster, G. M. H. Meesters and B. Scarlett (2001). "Growth regime map for liquid-bound granules: Further development and experimental validation." *Powder Technology* **117**(1-2): 83-97,

Jarosz, P. J. and E. L. Parrott (1983). "Comparison of granule strength and tablet tensile strength." *Journal of Pharmaceutical Sciences* **72**(5): 530-535, 10.1002/jps.2600720513.

Johansson, B. and G. Alderborn (2001). "The effect of shape and porosity on the compression behaviour and tablet forming ability of granular materials formed from microcrystalline cellulose." *European Journal of Pharmaceutics and Biopharmaceutics* **52**(3): 347-357, http://dx.doi.org/10.1016/S0939-6411(01)00186-2.

Johansson, B. and G. Alderborn (2001). "The effect of shape and porosity on the compression behaviour and tablet forming ability of granular materials formed from microcrystalline cellulose." *European Journal of Pharmaceutics and Biopharmaceutics* **52**: 347-357,

Johansson, B., M. Wikberg, R. Ek and G. Alderborn (1995). "Compression behaviour and compactability of microcrystalline cellulose pellets in relationship to their pore structure and mechanical properties." *International Journal of Pharmaceutics* **117**(1): 57-73, http://dx.doi.org/10.1016/0378-5173(94)00295-G.

Jones, D. M., M. A. S. Donsmark, G. Betz and H. Leuenberger (2005). *Scale-up in the field of granulation and drying*. Pharmaceutical process scale-up**:** 241-287.

Kachrimanis, K., M. F. Noisternig, U. J. Griesser and S. Malamataris (2006). "Dynamic moisture sorption and desorption of standard and silicified microcrystalline cellulose." *European Journal of Pharmaceutics and Biopharmaceutics* **64**(3): 307-315, http://dx.doi.org/10.1016/j.ejpb.2006.05.019.

Kawakita, K. and Y. Tsutsumi (1966). "A comparison of equations for powder compression." *Bulletin of the Chemical Society of Japan* **39**(7): 1364-1368,

Keleb, E. I., A. Vermeire, C. Vervaet and J. P. Remon (2001). "Cold extrusion as a continuous single-step granulation and tabletting process." *European Journal of Pharmaceutics and Biopharmaceutics* **52**(3): 359-368,

Khan, F. and N. Pilpel (1987). "An investigation of moisture sorption in microcrystalline cellulose using sorption isotherms and dielectric response." *Powder Technology* **50**(3): 237-241, http://dx.doi.org/10.1016/0032-5910(87)80069-4.

Kleinebudde, P. (1997). "The crystallite-gel-model for microcrystalline cellulose in wet-granulation, extrusion, and spheronization." *Pharmaceutical Research* **14**(6): 804-809, 10.1023/a:1012166809583.

Kochhar, S. K., M. H. Rubinstein and D. Barnes (1995). "The effects of slugging and recompression on pharmaceutical excipients." *International Journal of Pharmaceutics* **115**(1): 35-43, http://dx.doi.org/10.1016/0378-5173(94)00250-9.

Kornchankul, W., N. H. Parikh and A. Sakr (2001). "Correlation between wet granulation kinetic parameters and tablet characteristics." *Drugs Made in Germany* **44**(3): 78-87,

Kumar, V. and S. H. Kothari (1999). "Effect of compressional force on the crystallinity of directly compressible cellulose excipients." *International Journal of Pharmaceutics* **177**(2): 173-182, http://dx.doi.org/10.1016/S0378-5173(98)00340-8.

Landin, M., P. York, M. J. Cliff, R. C. Rowe and A. J. Wigmore (1996). "Scale-up of a pharmaceutical granulation in fixed bowl mixer-granulators." *International Journal of Pharmaceutics* **133**(1–2): 127-131, http://dx.doi.org/10.1016/0378-5173(95)04427-2.

Leuenberger, H. (1982). "The compressibility and compactibility of powder systems." *International Journal of Pharmaceutics* **12**: 41-55,

Leuenberger, H. (2001). "New trends in the production of pharmaceutical granules: The classical batch concept and the problem of scale-up." *European Journal of Pharmaceutics and Biopharmaceutics* **52**(3): 279-288, http://dx.doi.org/10.1016/S0939-6411(01)00200-4.

Litster, J. D. (2003). "Scaleup of wet granulation processes: Science not art." *Powder Technology* **130**(1): 35-40, 10.1016/s0032-5910(02)00222-x.

Litster, J. D. and B. J. Ennis (2004). *The science and engineering of granulation processes*. Particle technology series. P. B. Scarlett. Dordrecht, The Netherlands, Kluwer Academic Publishers.

Litster, J. D., K. P. Hapgood, J. N. Michaels, A. Sims, M. Roberts and S. K. Kameneni (2002). "Scale-up of mixer granulators for effective liquid distribution." *Powder Technology* **124**(3): 272-280, http://dx.doi.org/10.1016/S0032-5910(02)00023-2.

Litster, J. D., K. P. Hapgood, J. N. Michaels, A. Sims, M. Roberts, S. K. Kameneni and T. Hsu (2001). "Liquid distribution in wet granulation: Dimensionless spray flux." *Powder Technology* **114**(1-3): 32-39,

Macias, K. A. and M. T. Carvajal (2012). "The influence of granule density on granule strength and resulting compact strength." *Chemical Engineering Science* **72**(0): 205-213, http://dx.doi.org/10.1016/j.ces.2012.01.026.

McKenna, A. and D. F. McCafferty (1982). "Effect on particle size on the compaction mechanism and tensile strength of tablets." *J Pharm Pharmacol* **34**(6): 347-51,

Michaels, J. N., L. Farber, G. S. Wong, K. Hapgood, S. J. Heidel, J. Farabaugh, J.-H. Chou and G. I. Tardos (2009). "Steady states in granulation of pharmaceutical powders with application to scale-up." *Powder Technology* **189**(2): 295-303, http://dx.doi.org/10.1016/j.powtec.2008.04.028.

Mosig, J. and P. Kleinebudde (2013). *Critical assessment of the unified compaction curve model*. 6th International Granulation Workshop, Sheffield, UK.

Murakami, H., T. Yoneyama, K. Nakajima and M. Kobayashi (2001). "Correlation between loose density and compactibility of granules prepared by various granulation methods." *International Journal of Pharmaceutics* **216**: 159-164,

Natoli, D. (2008). "Time for a world tooling standard." from http://ezproxy-authcate.lib.monash.edu.au/cgi-bin/authcate.pl?url=http://proquest.umi.com/pqdweb?did=1458629791&Fmt=7&clientId=16397&RQT=309&VName=PQD.

Nicklasson, H. and F. Podczeck (2007). "Evaluation of the role of pores during strength testing in compacts made from different particle size fractions of sucrose." *Chemical Pharmaceutical Bulletin* **55**(1): 29-33,

Oulahna, D., F. Cordier, L. Galet and J. A. Dodds (2003). "Wet granulation: The effect of shear on granule properties." *Powder Technology* **130**(1-3): 238-246,

Oulahna, D., F. Cordier, L. Galet and J. A. Dodds (2003). "Wet granulation: The effect of shear on granule properties." *Powder Technology* **130**(1–3): 238-246, http://dx.doi.org/10.1016/S0032-5910(02)00272-3.

Perry, R. H. and D. W. Green (1997). *Size reduction and size enlargement*. Perry's chemical engineers' handbook. New York, USA, McGraw-Hill**:** 20-56-20-89.

Pitt, K. G., J. M. Newton, R. Richardson and P. Stanley (1989). "The material tensile strength of convex-faced aspirin tablets." *Journal of Pharmacy and Pharmacology* **41**(5): 289-292, 10.1111/j.2042-7158.1989.tb06458.x.

Rahmanian, N., M. Ghadiri and Y. Ding (2008). "Effect of scale of operation on granule strength in high shear granulators." *Chemical Engineering Science* **63**(4): 915-923,

Rahmanian, N., M. Ghadiri, X. Jia and F. Stepanek (2009). "Characterisation of granule structure and strength made in a high shear granulator." *Powder Technology* **192**(2): 184-194, http://dx.doi.org/10.1016/j.powtec.2008.12.016.

Rahmanian, N., A. Naji and M. Ghadiri (2011). "Effects of process parameters on granules properties produced in a high shear granulator." *Chemical Engineering Research and Design* **89**(5): 512-518, http://dx.doi.org/10.1016/j.cherd.2010.10.021.

Rahmanian, N., B. Ng, A. Hassanpour and X. Jia (2008). "Scale-up of high shear mixer granulators."

Rangaiah, K. V., S. C. Chattaraj and S. K. Das (1994). "Effects of process variables and excipients on tabletting parameters of norfloxacin tablets." *Drug Development and Industrial Pharmacy* **20**(13): 2175-2182,

Reier, G. (2007). *Avicel ph microcrystalline cellulose, nf, ph eur., jp, bp*, FMC Biopolymer**:** 1-27.

Rekhi, G. S., R. B. Caricofe, D. M. Parikh and L. L. Augsburger (1996). "A new approach to scale-up of a high-shear granulation process." *Pharm Technol* **20**: 58-67,

Rhodes, M. (2008). *Introduction to particle technology*. West Sussex, England, John Wiley & Sons Ltd.

Ritala, M., P. Holm, T. Schaefer and H. G. Kristensen (1988). "Influence of liquid bonding strength on power consumption during granulation in a high shear mixer." *Drug Development and Industrial Pharmacy* **14**(8): 1041-1060,

Rowe, R. C., P. J. Sheskey and P. J. Weller (2009). *Handbook of pharmaceutical excipients.* London, UK, Pharmaceutical Press.

Rumpf, H. (1962). *The strength of granules and agglomerates*. Agglomeration. New York, Interscience**:** 379.

Salman, A. D., M. J. Hounslow and J. P. K. Seville (2007). *Chapter 16: Tabletting*. Amsterdam, The Netherlands, Elsevier.

Salman, A. D., M. J. Hounslow and J. P. K. Seville (2007). *Chapter 20: Granulation rate processes*. Amsterdam, The Netherlands, Elsevier.

Sáska, Z., J. Dredán, O. Luhn, E. Balogh, G. Shafir and I. Antal (2011). "Evaluation of the impact of mixing speed on the compressibility and compactibility of paracetamol-isomalt containing granules with factorial design." *Powder Technology* **213**(1–3): 132-140, http://dx.doi.org/10.1016/j.powtec.2011.07.019.

Segal, L., J. J. Creely, A. E. Martin and C. M. Conrad (1959). "An empirical method for estimating the degree of crystallinity of native cellulose using the x-ray diffractometer." *Textile Research Journal* **29**(10): 786-794, 10.1177/004051755902901003.

Sevillano, J. G. (2001). "Size effects in powder compaction." *Journal of Materials Research* **16**(05): 1238-1240, doi:10.1557/JMR.2001.0172.

Sheskey, P. J. and D. M. Williams (1996). *Comparison of low-shear and high-shear wet granulation techniques and the influence of percent water addition in the preparation of a controlled-release matrix tablet containing hpmc and a high-dose, highly water-soluble drug*. Pharmaceutical Technology. March issue.

Shi, L., Y. Feng and C. C. Sun (2010). "Roles of granule size in over-granulation during high shear wet granulation." *Journal of Pharmaceutical Sciences* **99**(8): 3322-3325, 10.1002/jps.22118.

Shi, L., Y. Feng and C. C. Sun (2011). "Initial moisture content in raw material can profoundly influence high shear wet granulation process." *International Journal of Pharmaceutics* **416**(1): 43-48, 10.1016/j.ijpharm.2011.05.080.

Shi, L., Y. Feng and C. C. Sun (2011). "Massing in high shear wet granulation can simultaneously improve powder flow and deteriorate powder compaction: A double-edged sword." *European Journal of Pharmaceutical Sciences* **43**(1-2): 50-56, 10.1016/j.ejps.2011.03.009.

Shi, L., Y. Feng and C. C. Sun (2011). "Origin of profound changes in powder properties during wetting and nucleation stages of high-shear wet granulation of microcrystalline cellulose." *Powder Technology* **208**(3): 663-668, 10.1016/j.powtec.2011.01.006.

Shrotri, A., L. K. Lambert, A. Tanksale and J. Beltramini (2013). "Mechanical depolymerisation of acidulated cellulose: Understanding the solubility of high molecular weight oligomers." *Green Chemistry* **15**(10): 2761-2768, 10.1039/C3GC40945G.

Suzuki, T., H. Kikuchi, S. Yamamura, K. Terada and K. Yamamoto (2001). "The change in characteristics of microcrystalline cellulose during wet granulation using a high-shear mixer." *Journal of Pharmacy and Pharmacology* **53**(5): 609-616, 10.1211/0022357011775938.

Suzuki, T. and H. Nakagami (1999). "Effect of crystallinity of microcrystalline cellulose on the compactability and dissolution of tablets." *European Journal of Pharmaceutics and Biopharmaceutics* **47**(3): 225-230, http://dx.doi.org/10.1016/S0939-6411(98)00102-7.

Tardos, G. I. (2005). "Wet-granulation research with application to scale-up." *China Particuology* **3**(3): 191-195, http://dx.doi.org/10.1016/S1672-2515(07)60085-2.

Tardos, G. I., K. P. Hapgood, O. O. Ipadeola and J. N. Michaels (2004). "Stress measurements in high-shear granulators using calibrated “test” particles: Application to scale-up." *Powder Technology* **140**(3): 217-227, http://dx.doi.org/10.1016/j.powtec.2004.01.015.

Tardos, G. I., M. I. Khan and P. R. Mort (1997). "Critical parameters and limiting conditions in binder granulation of fine powders." *Powder Technology* **94**(3): 245-258, http://dx.doi.org/10.1016/S0032-5910(97)03321-4.

Terinte, N., R. Ibbett and K. C. Schuster (2011). "Overview on native cellulose and microcrystalline cellulose i structures studied by x-ray diffraction (waxd): Comparison between measurement techniques." *Lenzinger Berichte* **89**: 118-131,

Tuason, D. C., G. R. Krawczyk and G. Buliga (2009). *Microcrystalline cellulose*. Food stabilisers, thickeners and gelling agents, Wiley-Blackwell**:** 218-236.

Tye, C. K., C. Sun and G. E. Amidon (2005). "Evaluation of the effects of tableting speed on the relationships between compaction pressure, tablet tensile strength, and tablet solid fraction." *Journal of Pharmaceutical Sciences* **94**(3): 465-472,

Vermeire, A., E. I. Keleb, F. Kiekens, I. Van Driessche, S. Hoste, J. P. Remon and C. Vervaet (2005). "Tablets prepared by single-step granulation/tabletting: Interparticulate binding mechanism and stability." *Pharmaceutical Development & Technology* **10**(3): 397-403,

Vromans, H., A. De Boer, G. Bolhuis, C. Lerk, K. Kussendrager and H. Bosch (1985). "Studies on tableting properties of lactose." *Pharmacy World & Science* **7**(5): 186-193, 10.1007/bf02307575.

Waldie, B. (1991). "Growth mechanism and the dependence of granule size on drop size in fluidized-bed granulation." *Chemical Engineering Science* **46**(11): 2781-2785,

Walker, E. E. (1923). "The properties of powders. Part vi. The compressibility of powders." *Transactions of Faraday Society* **19**: 73-82,

Watano, S., Y. Sato, K. Miyanami, T. Murakami, Y. Ito, T. Kamata and N. Oda (1995). "Scale-up of agitation fluidized bed granulation. I. Preliminary experimental approach for optimization of process variables." *Chemical and Pharmaceutical Bulletin* **43**(7): 1212-1216,

Wikberg, M. and G. Alderborn (1990). "Compression characteristics of granulated materials. Iii. The relationship between air permeability and mechanical strength of tablets of some lactose granulations." *International Journal of Pharmaceutics* **63**(1): 23-27, http://dx.doi.org/10.1016/0378-5173(90)90096-M.

Wikberg, M. and G. Alderborn (1991). "Compression characteristics of granulated materials. Iv. The effect of granule porosity on the fragmentation propensity and the compactibility of some granulations." *International Journal of Pharmaceutics* **69**: 239-253,

Wikberg, M. and G. Alderborn (1991). "Compression characteristics of granulated materials. Iv. The effect of granule porosity on the fragmentation propensity and the compatibility of some granulations." *International Journal of Pharmaceutics* **69**(3): 239-253, http://dx.doi.org/10.1016/0378-5173(91)90366-V.

Wikberg, M. and G. Alderborn (1992). "Compression characteristics of granulated materials: Vi. Pore size distributions, assessed by mercury penetration, of compacts of two lactose granulations with different fragmentation propensities." *International Journal of Pharmaceutics* **84**(2): 191-195, http://dx.doi.org/10.1016/0378-5173(92)90059-B.

Williams, A. C., V. B. Cooper, L. Thomas, L. J. Griffith, C. R. Petts and S. W. Booth (2004). "Evaluation of drug physical form during granulation, tabletting and storage." *International Journal of Pharmaceutics* **275**(1-2): 29-39,

Wolf, W., W. E. L. Spiess, G. Jung, H. Weisser, H. Bizot and R. B. Duckworth (1984). "The water-vapour sorption isotherms of microcrystalline cellulose (mcc) and of purified potato starch. Results of a collaborative study." *Journal of Food Engineering* **3**(1): 51-73, http://dx.doi.org/10.1016/0260-8774(84)90007-4.

Zhang, J., J. Zhang, L. Lin, T. Chen, J. Zhang, S. Liu, Z. Li and P. Ouyang (2009). "Dissolution of microcrystalline cellulose in phosphoric acid—molecular changes and kinetics." *Molecules* **14**(12): 5027-5041,

Zhang, Y., Y. Law and S. Chakrabarti (2003). "Physical properties and compact analysis of commonly used direct compression binders." *AAPS PharmSciTech.* **4**(4): 62,

Zografi, G. (1988). "States of water associated with solids." *Drug Development and Industrial Pharmacy* **14**(14): 1905-1926, doi:10.3109/03639048809151997.

Zografi, G. and M. Kontny (1986). "The interactions of water with cellulose- and starch-derived pharmaceutical excipients." *Pharmaceutical Research* **3**(4): 187-194, 10.1023/A:1016330528260.

Zuurman, K., K. A. Riepma, G. K. Bolhuis, H. Vromans and C. F. Lerk (1994). "The relationship between bulk density and compactibility of lactose granulations." *International Journal of Pharmaceutics* **102**(1–3): 1-9, http://dx.doi.org/10.1016/0378-5173(94)90033-7.

APPENDICES

Page number

A. DERIVATION OF THE UNIFIED COMPACTION CURVE MODEL FOR WET GRANULATION 219

B. MASS BALANCE CALCULATIONS FOR GRANULATION EXPERIMENTS 221

C. TABLET DIMENSION AND STRENGTH RAW DATA 229

D. UNIFIED COMPACTION CURVE MODELLING DATA 264

E. TABLET COMPRESSIBILITY BEHAVIOUR PROFILES 281

F. GRANULE SPHERICITY AND POROSITY CHARACTERISATION TRIAL EXPERIMENTS 285

G. GRANULE BET SPECIFIC SURFACE AREA PLOTS 287

H. MERCURY INTRUSION POROSIMETRY RAW DATA AND GRANULE POROSITY CALCULATIONS 289

I. TARGETING THE TABLET STRENGTH USING THE GRANULATOR IMPELLER REVOLUTIONS 292

A. DERIVATION OF THE UNIFIED COMPACTION CURVE MODEL FOR WET GRANULATION

In the Unified Compaction Curve model, developed by Farber *et al.* (2008), the compaction profiles from different roller compaction pressures in roller compaction are unified onto a single curve by translating the profiles along the 'unprocessed' master compaction profile. This principle can potentially be applied to wet granulation. Therefore the derivation of the Unified Compaction Curve model for wet granulation is derived in the same manner as the model developed for roller compaction. The only differences between the Unified Compaction Curve model for wet granulation and roller compaction is that the roller compaction pressure P_{RC} is replaced with the effective wet granulation compaction pressure P_{WGC} and the tensile strength of the ribbon produced in roller compaction T_{RC} is replaced with the equivalent granule tensile strength in wet granulation T_{WGC}.

The derivation of the Unified Compaction Curve model begins with the direct compaction curve, developed by Leuenberger (1982):

$$T = T_{\max}\left(1 - e^{-bP}\right) \tag{A.1}$$

where T is the tablet tensile strength at a given compaction pressure, T_{max} is the maximum tablet strength for unprocessed powder, b represents the product of γ - a material-related constant representing the measure of compactability, and ρ - the ratio of the tablet density to the theoretical tablet density, and P is the maximum compaction pressure that can be applied to a powder formulation (Leuenberger, 1982; Farber *et al.*, 2008). For simplicity the $\gamma\rho$ constant group was represented by constant b ($b = \gamma\rho$).

During wet granulation, some (unknown) compaction pressure is applied to the granules by the granulator impeller. This apparent compaction pressure is defined as "P_{WGC}" or the effective wet granulation pressure. At P_{WGC}, the equivalent granule tensile strength, T_{WGC}, is related to the effective wet granulation compaction pressure P_{WGC} (Equation A.2):

$$T_{WGC} = T_{\max}\left(1 - e^{-bP_{WGC}}\right) \tag{A.2}$$

Since the compaction pressure imparted on the granules and powder during wet granulation is irreversible, the resulting tablet strength will decrease from the strength attained from the compaction of unprocessed powder (Equation A.3):

$$T' = T - T_{WGC} \tag{A.3}$$

where T' is the tablet tensile strength produced after wet granulation. Equations A.1 and A.2 are then substituted in Equation A.3 to give A.5.

$$T' = T_{\max}\left(1 - e^{-bP}\right) - T_{\max}\left(1 - e^{-bP_{WGC}}\right) \tag{A.4}$$

$$T' = T_{\max}\left(e^{-bP_{WGC}} - e^{-bP}\right) \tag{A.5}$$

The tabletting pressure *P'* is the difference between the total cumulative compaction pressure (during granulation and compaction) or the maximum possible compaction pressure that can be applied to the powder, and the effective wet granulation compaction pressure P_{WGC} (Equation A.6):

$$P' = P - P_{WGC} \tag{A.6}$$

$$P = P' + P_{WGC} \tag{A.7}$$

where P_{WGC} is the compaction pressure induced on the powder by the granulator impeller. By substituting Equation A.7 into Equation A.5, the Unified Compaction Curve model can be derived to obtain the final tablet strength, *T* (Equation A.8).

$$T = T_{WGC} + T_{\max}\left(e^{-bP_{WGC}} - e^{-b(P'+P_{WGC})}\right) \tag{A.8}$$

where *T* is the final tablet strength, *P'* is the compaction pressure applied to the granules by the tablet press.

B. MASS BALANCE CALCULATIONS FOR GRANULATION EXPERIMENTS

The wet granulation experiments were designed such that for each granulation condition (e.g. liquid level or wet massing time) 100g of dry granular powder is taken from the wetted powder batch in the granulator. Mass balances were performed around the granulator and oven for the powder and granulation fluid components.

Sample calculations:

For 20% liquid level and starting with 1kg of powder mass in granulator:

Amount of liquid to be added to granulator = $0.2 \times 1000\text{g dry powder} = 200\text{g liquid}$

Total granulation mass = $200\text{g liquid} + 1000\text{g powder} = 1200g$

Mass granular mass to be sampled from granulator =

$$100\text{g sample} + 20\%\text{liquid} = 100 \times \left(1 + \frac{20}{100}\right) = 120\text{g sample}$$

Dry granulation powder mass remaining after sampling =

$$1000\text{g initial powder} - 100\text{g dry sample powder} = 900\text{g}$$

Liquid mass remaining in granulator after sampling =

$$200\text{g liquid added} - (120\text{g sample} - 100\text{g dry powder sample}) = 180g$$

Liquid level remaining in granulator after sampling =

$$\frac{180\text{g liquid remaining}}{900\text{g powder remaining}} \times 100\% = 20\%$$

Wet granulation moisture content sampling experiment

Data input cells

Liquid flow rate [g/min]
129.53

BF = 130g/min
RPM = 150, 285, 600rpm
WMT = 10secs
Powder:
50%MCC/50%L2M
Liquid binder: 5w/v%PVP

Liquid binder addition

Exp#	Liquid level target (relative to powder mass)	Amount liquid to be added [g]	Liquid binder addition period [mins]
0	20%	200	1.54
1	30%	90	0.69
2	40%	80	0.62
3	50%	70	0.54
4	60%	60	0.46
5	70%	50	0.39
6	80%	40	0.31
7	90%	30	0.23
8	100%	20	0.15
Total liquid added:		590	

Exp#	Liquid binder addition period [min, secs]	
0	1	32
1	0	42
2	0	37
3	0	32
4	0	28
5	0	23
6	0	19
7	0	14
8	0	9

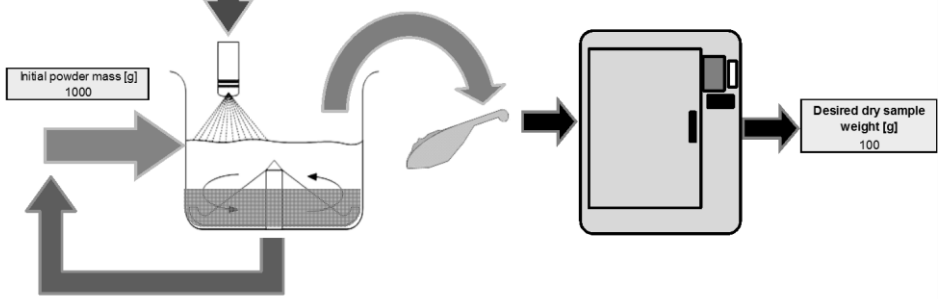

Granulation powder

Exp#	Powder mass [g]	Total granulation mass [g]
0	1000	1200
1	900	990
2	800	880
3	700	770
4	600	660
5	500	550
6	400	440
7	300	330
8	200	220

Remaining granulation powder bed

Exp#	Dry granulation powder mass [g]	Liquid mass remaining	Liquid level remaining
0	900	180	0.20
1	800	240	0.30
2	700	280	0.40
3	600	300	0.50
4	500	300	0.60
5	400	280	0.70
6	300	240	0.80
7	200	180	0.90
8	100	100	1.00

Sampling

Exp#	Wet sample weight to be taken out [g]
0	120
1	130
2	140
3	150
4	160
5	170
6	180
7	190
8	200

Figure B.1: Calculations for liquid level granulation experiments (BF = 130g/min; RPM=150, 285, 600rpm; WMT=10secs) for 5L granulator.

Wet granulation moisture content sampling experiment

Data input cells

Liquid flow rate [g/min]
269.17

BF = 280g/min
RPM = 150, 285, 600rpm
WMT = 10secs
Powder:
50%MCC/50%L2M
Liquid binder: 5w/v%PVP

Liquid binder addition

Exp#	Liquid level target (relative to powder mass)	Amount liquid to be added [g]	Liquid binder addition period [mins]
0	20%	200	0.74
1	25%	44	0.16
2	30%	38	0.14
3	40%	64	0.24
4	50%	52	0.19
5	60%	40	0.15
6	70%	28	0.10
7	80%	16	0.06
8	90%	4	0.01
Total liquid added:		466	

Exp#	Liquid binder addition period [min, secs]	
0	0	45
1	0	10
2	0	8
3	0	14
4	0	12
5	0	9
6	0	6
7	0	4
8	0	1

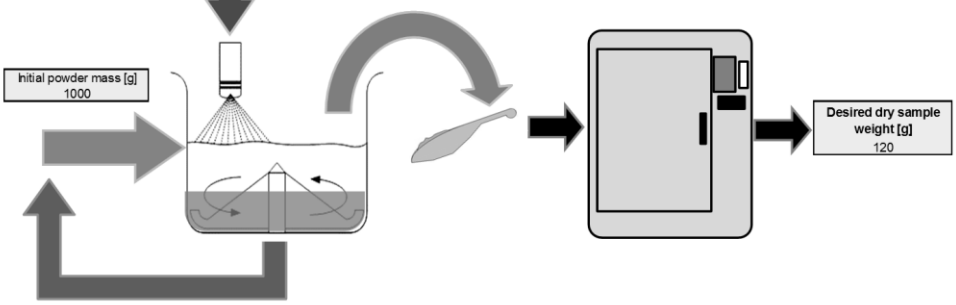

Granulation powder

Exp#	Powder mass [g]	Total granulation mass [g]
0	1000	1200
1	880	924
2	760	798
3	640	704
4	520	572
5	400	440
6	280	308
7	160	176
8	40	44

Remaining granulation powder bed

Exp#	Dry granulation powder mass [g]	Liquid mass remaining	Liquid level remaining
0	880	176	0.20
1	760	190	0.25
2	640	192	0.30
3	520	208	0.40
4	400	200	0.50
5	280	168	0.60
6	160	112	0.70
7	40	32	0.80
8	-80	-72	0.90

Sampling

Exp#	Wet sample weight to be taken out [g]
0	144
1	150
2	156
3	168
4	180
5	192
6	204
7	216
8	228

Figure B.2: Calculations for liquid level granulation experiments (BF = 280g/min; RPM=150, 285, 600rpm; WMT=10secs) for 5L granulator.

Wet granulation moisture content sampling experiment

Data input cells

Liquid flow rate [g/min]
130.25

BF = 130g/min
RPM = 285rpm
LL = 20%
Powder:
50%MCC/50%L2M
Liquid binder: 5w/v%PVP

Liquid binder addition			
Exp#	Liquid level target (relative to powder mass)	Amount liquid to be added [g]	Liquid binder addition period [mins]
0	20%	200	1.54
1	20%	0	0.00
2	20%	0	0.00
3	20%	0	0.00
4	20%	0	0.00
5	20%	0	0.00
6	20%	0	0.00
7	20%	0	0.00
8	20%	0	0.00
9	20%	0	0.00
10	20%	0	0.00
Total liquid added:		200	

Wet massing time [min]	Liquid binder addition period [min, secs]	
0	1	32
1	0	0
2	0	0
3	0	0
4	0	0
5	0	0
6	0	0
7	0	0
8	0	0
9	0	0
10	0	0

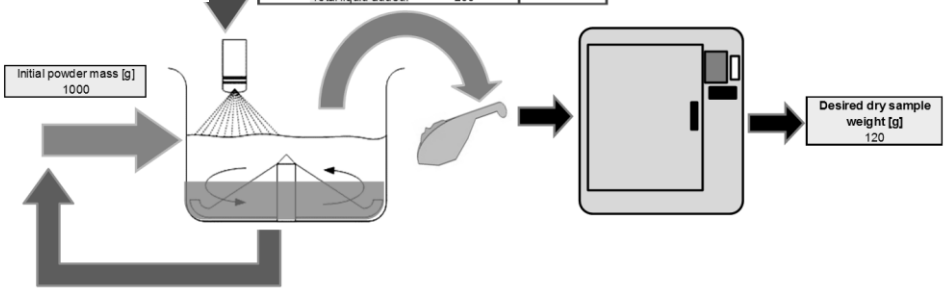

Granulation powder		
Exp#	Powder mass [g]	Total granulation mass [g]
0	1000	1200
1	880	880
2	760	760
3	640	640
4	520	520
5	400	400
6	280	280
7	160	160
8	40	40
9	-80	-80
10	-200	-200

Remaining granulation powder bed			
Exp#	Dry granulation powder mass [g]	Liquid mass remaining	Liquid level remaining
0	880	176	0.20
1	760	152	0.20
2	640	128	0.20
3	520	104	0.20
4	400	80	0.20
5	280	56	0.20
6	160	32	0.20
7	40	8	0.20
8	-80	-16	0.20
9	-200	-40	0.20
10	-320	-64	0.20

Sampling	
Exp#	Wet sample weight to be taken out [g]
0	144
1	144
2	144
3	144
4	144
5	144
6	144
7	144
8	144
9	144
10	144

Figure B.3: Calculations for wet massing time granulation experiments (LL = 20%; BF = 130g/min; RPM= 285rpm) for 5L granulator.

Wet granulation moisture content sampling experiment

Data input cells

Liquid flow rate [g/min]
269.41

BF = 280g/min
RPM = 285rpm
LL = 20%
Powder:
50%MCC/50%L2M
Liquid binder: 5w/v%PVP

Liquid binder addition			
Exp#	Liquid level target (relative to powder mass)	Amount liquid to be added [g]	Liquid binder addition period [mins]
0	20%	200	0.74
1	20%	0	0.00
2	20%	0	0.00
3	20%	0	0.00
4	20%	0	0.00
5	20%	0	0.00
6	20%	0	0.00
7	20%	0	0.00
8	20%	0	0.00
9	20%	0	0.00
10	20%	0	0.00
Total liquid added:		200	

Wet massing time [min]	Liquid binder addition period [min, secs]	
0	0	44
1	0	0
2	0	0
3	0	0
4	0	0
5	0	0
6	0	0
7	0	0
8	0	0
9	0	0
10	0	0

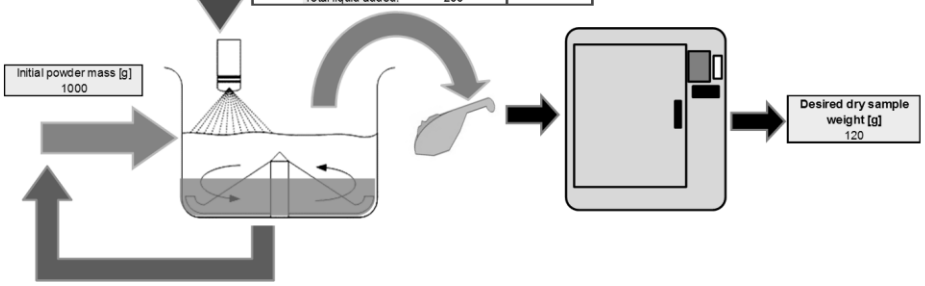

Granulation powder		
Exp#	Powder mass [g]	Total granulation mass [g]
0	1000	1200
1	880	880
2	760	760
3	640	640
4	520	520
5	400	400
6	280	280
7	160	160
8	40	40
9	-80	-80
10	-200	-200

Remaining granulation powder bed			
Exp#	Dry granulation powder mass [g]	Liquid mass remaining	Liquid level remaining
0	880	176	0.20
1	760	152	0.20
2	640	128	0.20
3	520	104	0.20
4	400	80	0.20
5	280	56	0.20
6	160	32	0.20
7	40	8	0.20
8	-80	-16	0.20
9	-200	-40	0.20
10	-320	-64	0.20

Sampling	
Exp#	Wet sample weight to be taken out [g]
0	144
1	144
2	144
3	144
4	144
5	144
6	144
7	144
8	144
9	144
10	144

Figure B.4: Calculations for wet massing time granulation experiments (LL = 20%; BF = 280g/min; RPM= 285rpm) for 5L granulator.

Wet granulation moisture content sampling experiment

Data input cells

Liquid flow rate [g/min]
130.25

BF = 130g/min
RPM = 150,285,600rpm
LL = 30%
Powder:
50%MCC/50%L2M
Liquid binder: 5w/v%PVP

Liquid binder addition

Exp#	Liquid level target (relative to powder mass)	Amount liquid to be added [g]	Liquid binder addition period [mins]
0	30%	300	2.30
1	30%	0	0.00
2	30%	0	0.00
3	30%	0	0.00
4	30%	0	0.00
5	30%	0	0.00
6	30%	0	0.00
7	30%	0	0.00
8	30%	0	0.00
8	30%	0	0.00
8	30%	0	0.00
Total liquid added:		300	

Wet massing time [min]	Liquid binder addition period [min, secs]	
0	2	18
1	0	0
2	0	0
3	0	0
4	0	0
5	0	0
6	0	0
7	0	0
8	0	0
9	0	0
10	0	0

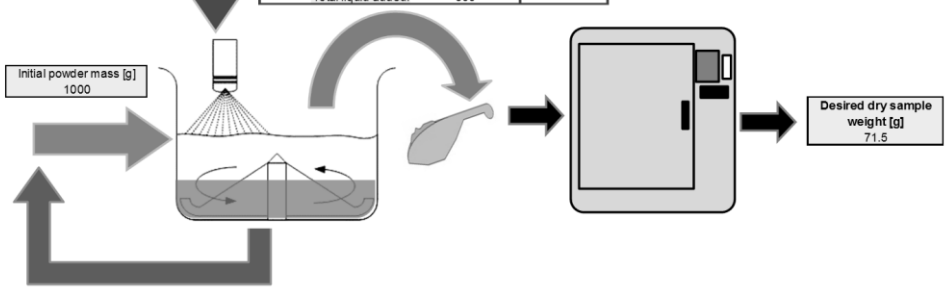

Granulation powder

Exp#	Powder mass [g]	Total granulation mass [g]
0	1000	1300
1	929	929
2	857	857
3	786	786
4	714	714
5	643	643
6	571	571
7	500	500
8	428	428
9	357	357
10	285	285

Remaining granulation powder bed

Exp#	Dry granulation powder mass [g]	Liquid mass remaining	Liquid level remaining
0	929	279	0.30
1	857	257	0.30
2	786	236	0.30
3	714	214	0.30
4	643	193	0.30
5	571	171	0.30
6	500	150	0.30
7	428	128	0.30
8	357	107	0.30
9	285	86	0.30
10	214	64	0.30

Sampling

Exp#	Wet sample weight to be taken out [g]
0	93
1	93
2	93
3	93
4	93
5	93
6	93
7	93
8	93
9	93
10	93

Figure B.5: Calculations for wet massing time granulation experiments (LL = 30%; BF = 130g/min; RPM= 150, 285, 600rpm) for 5L granulator.

Wet granulation moisture content sampling experiment

Data input cells

Liquid flow rate [g/min]
269.41

BF = 280g/min
RPM = 285rpm
LL = 30%
Powder:
50%MCC/50%L2M
Liquid binder: 5w/v%PVP

Liquid binder addition

Exp#	Liquid level target (relative to powder mass)	Amount liquid to be added [g]	Liquid binder addition period [mins]
0	30%	300	1.11
1	30%	0	0.00
2	30%	0	0.00
3	30%	0	0.00
4	30%	0	0.00
5	30%	0	0.00
6	30%	0	0.00
7	30%	0	0.00
8	30%	0	0.00
9	30%	0	0.00
10	30%	0	0.00
Total liquid added:		300	

Wet massing time [min]	Liquid binder addition period [min, secs]	
0	1	7
1	0	0
2	0	0
3	0	0
4	0	0
5	0	0
6	0	0
7	0	0
8	0	0
9	0	0
10	0	0

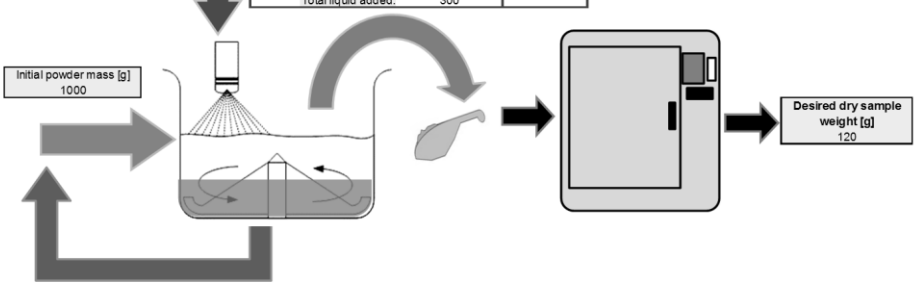

Granulation powder

Exp#	Powder mass [g]	Total granulation mass [g]
0	1000	1300
1	880	880
2	760	760
3	640	640
4	520	520
5	400	400
6	280	280
7	160	160
8	40	40
9	-80	-80
10	-200	-200

Remaining granulation powder bed

Exp#	Dry granulation powder mass [g]	Liquid mass remaining	Liquid level remaining
0	880	264	0.30
1	760	228	0.30
2	640	192	0.30
3	520	156	0.30
4	400	120	0.30
5	280	84	0.30
6	160	48	0.30
7	40	12	0.30
8	-80	-24	0.30
9	-200	-60	0.30
10	-320	-96	0.30

Sampling

Exp#	Wet sample weight to be taken out [g]
0	156
1	156
2	156
3	156
4	156
5	156
6	156
7	156
8	156
9	156
10	156

Figure B.6: Calculations for wet massing time granulation experiments (LL = 30%; BF = 280g/min; RPM= 285rpm) for 5L granulator.

Wet granulation moisture content sampling experiment

Data input cells

Liquid flow rate [g/min]
130.25

BF = 130g/min
RPM = 285rpm
LL = 40%
Powder:
50%MCC/50%L2M
Liquid binder: 5w/v%PVP

Liquid binder addition			
Exp#	Liquid level target (relative to powder mass)	Amount liquid to be added [g]	Liquid binder addition period [mins]
0	40%	400	3.07
1	40%	0	0.00
2	40%	0	0.00
3	40%	0	0.00
4	40%	0	0.00
5	40%	0	0.00
6	40%	0	0.00
7	40%	0	0.00
8	40%	0	0.00
8	40%	0	0.00
8	40%	0	0.00
Total liquid added:		400	

Wet massing time [min]	Liquid binder addition period [min, secs]	
0	3	5
1	0	0
2	0	0
3	0	0
4	0	0
5	0	0
6	0	0
7	0	0
8	0	0
9	0	0
10	0	0

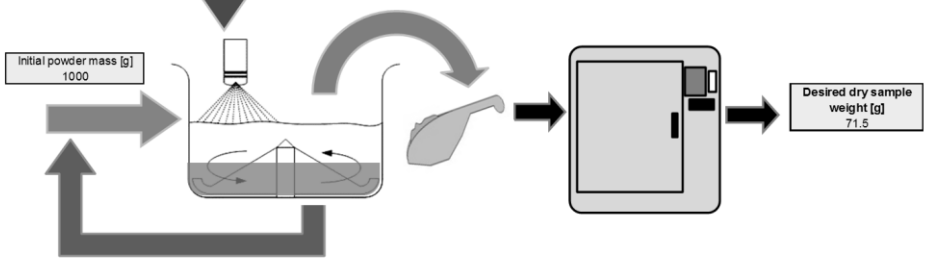

Granulation powder		
Exp#	Powder mass [g]	Total granulation mass [g]
0	1000	1400
1	929	929
2	857	857
3	786	786
4	714	714
5	643	643
6	571	571
7	500	500
8	428	428
9	357	357
10	285	285

Remaining granulation powder bed			
Exp#	Dry granulation powder mass [g]	Liquid mass remaining	Liquid level remaining
0	929	371	0.40
1	857	343	0.40
2	786	314	0.40
3	714	286	0.40
4	643	257	0.40
5	571	228	0.40
6	500	200	0.40
7	428	171	0.40
8	357	143	0.40
9	285	114	0.40
10	214	85	0.40

Sampling	
Exp#	Wet sample weight to be taken out [g]
0	100
1	100
2	100
3	100
4	100
5	100
6	100
7	100
8	100
9	100
10	100

Figure B.7: Calculations for wet massing time granulation experiments (LL = 40%; BF = 130g/min; RPM= 285rpm) for 5L granulator.

Wet granulation moisture content sampling experiment

Data input cells

Liquid flow rate [g/min]
279.62

BF = 280g/min
RPM = 285rpm
LL = 40%
Powder:
50%MCC/50%L2M
Liquid binder: 5w/v%PVP

Liquid binder addition			
Exp#	Liquid level target (relative to powder mass)	Amount liquid to be added [g]	Liquid binder addition period [mins]
0	40%	400	1.43
1	40%	0	0.00
2	40%	0	0.00
3	40%	0	0.00
4	40%	0	0.00
5	40%	0	0.00
6	40%	0	0.00
7	40%	0	0.00
8	40%	0	0.00
8	40%	0	0.00
8	40%	0	0.00
Total liquid added:		400	

Wet massing time [min]	Liquid binder addition period [min, secs]	
0	1	26
1	0	0
2	0	0
3	0	0
4	0	0
5	0	0
6	0	0
7	0	0
8	0	0
9	0	0
10	0	0

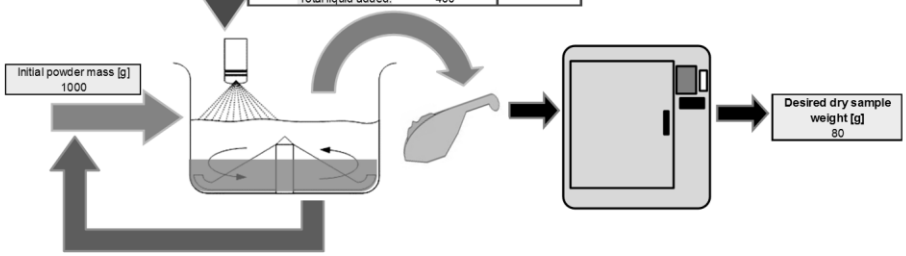

Granulation powder		
Exp#	Powder mass [g]	Total granulation mass [g]
0	1000	1400
1	920	920
2	840	840
3	760	760
4	680	680
5	600	600
6	520	520
7	440	440
8	360	360
9	280	280
10	200	200

Remaining granulation powder bed			
Exp#	Dry granulation powder mass [g]	Liquid mass remaining	Liquid level remaining
0	920	368	0.40
1	840	336	0.40
2	760	304	0.40
3	680	272	0.40
4	600	240	0.40
5	520	208	0.40
6	440	176	0.40
7	360	144	0.40
8	280	112	0.40
9	200	80	0.40
10	120	48	0.40

Sampling	
Exp#	Wet sample weight to be taken out [g]
0	112
1	112
2	112
3	112
4	112
5	112
6	112
7	112
8	112
9	112
10	112

Figure B.8: Calculations for wet massing time granulation experiments (LL = 40%; BF = 280g/min; RPM= 285rpm) for 5L granulator.

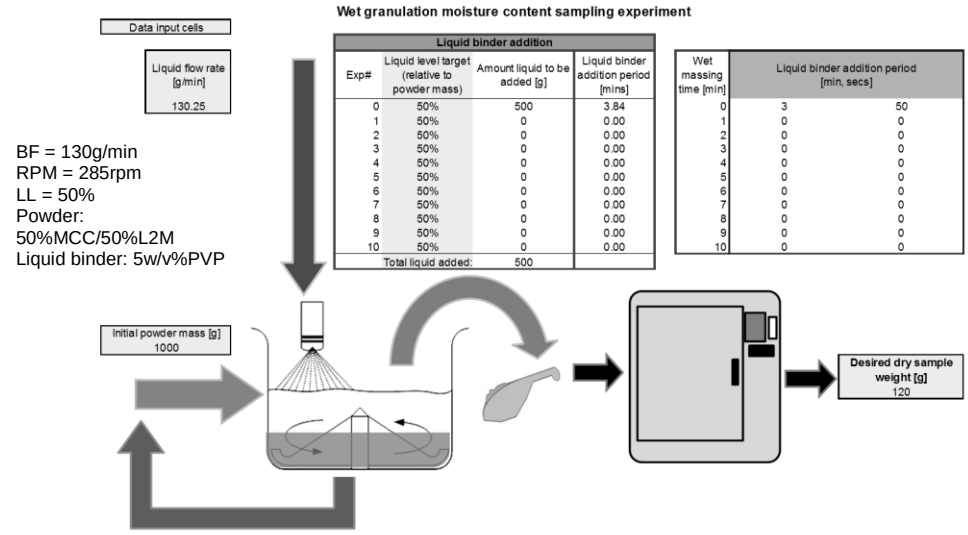

Wet granulation moisture content sampling experiment

Liquid binder addition			
Exp#	Liquid level target (relative to powder mass)	Amount liquid to be added [g]	Liquid binder addition period [mins]
0	50%	500	3.84
1	50%	0	0.00
2	50%	0	0.00
3	50%	0	0.00
4	50%	0	0.00
5	50%	0	0.00
6	50%	0	0.00
7	50%	0	0.00
8	50%	0	0.00
9	50%	0	0.00
10	50%	0	0.00
Total liquid added:		500	

Wet massing time [min]	Liquid binder addition period [min, secs]	
0	3	50
1	0	0
2	0	0
3	0	0
4	0	0
5	0	0
6	0	0
7	0	0
8	0	0
9	0	0
10	0	0

Granulation powder		
Exp#	Powder mass [g]	Total granulation mass [g]
0	1000	1500
1	880	880
2	760	760
3	640	640
4	520	520
5	400	400
6	280	280
7	160	160
8	40	40
9	-80	-80
10	-200	-200

Remaining granulation powder bed			
Exp#	Dry granulation powder mass [g]	Liquid mass remaining	Liquid level remaining
0	880	440	0.50
1	760	380	0.50
2	640	320	0.50
3	520	260	0.50
4	400	200	0.50
5	280	140	0.50
6	160	80	0.50
7	40	20	0.50
8	-80	-40	0.50
9	-200	-100	0.50
10	-320	-160	0.50

Sampling	
Exp#	Wet sample weight to be taken out [g]
0	180
1	180
2	180
3	180
4	180
5	180
6	180
7	180
8	180
9	180
10	180

Figure B.9: Calculations for wet massing time granulation experiments (LL = 50%; BF = 130g/min; RPM= 285rpm) for 5L granulator.

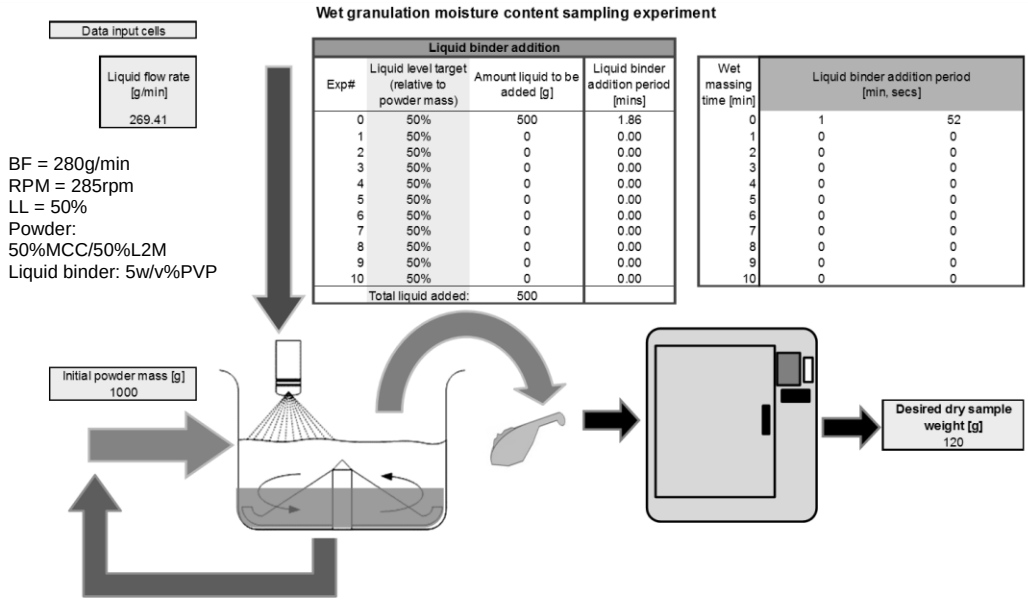

Wet granulation moisture content sampling experiment

Liquid binder addition			
Exp#	Liquid level target (relative to powder mass)	Amount liquid to be added [g]	Liquid binder addition period [mins]
0	50%	500	1.86
1	50%	0	0.00
2	50%	0	0.00
3	50%	0	0.00
4	50%	0	0.00
5	50%	0	0.00
6	50%	0	0.00
7	50%	0	0.00
8	50%	0	0.00
9	50%	0	0.00
10	50%	0	0.00
Total liquid added:		500	

Wet massing time [min]	Liquid binder addition period [min, secs]	
0	1	52
1	0	0
2	0	0
3	0	0
4	0	0
5	0	0
6	0	0
7	0	0
8	0	0
9	0	0
10	0	0

Granulation powder		
Exp#	Powder mass [g]	Total granulation mass [g]
0	1000	1500
1	880	880
2	760	760
3	640	640
4	520	520
5	400	400
6	280	280
7	160	160
8	40	40
9	-80	-80
10	-200	-200

Remaining granulation powder bed			
Exp#	Dry granulation powder mass [g]	Liquid mass remaining	Liquid level remaining
0	880	440	0.50
1	760	380	0.50
2	640	320	0.50
3	520	260	0.50
4	400	200	0.50
5	280	140	0.50
6	160	80	0.50
7	40	20	0.50
8	-80	-40	0.50
9	-200	-100	0.50
10	-320	-160	0.50

Sampling	
Exp#	Wet sample weight to be taken out [g]
0	180
1	180
2	180
3	180
4	180
5	180
6	180
7	180
8	180
9	180
10	180

Figure B.10: Calculations for wet massing time granulation experiments (LL = 50%; BF = 280g/min; RPM= 285rpm) for 5L granulator.

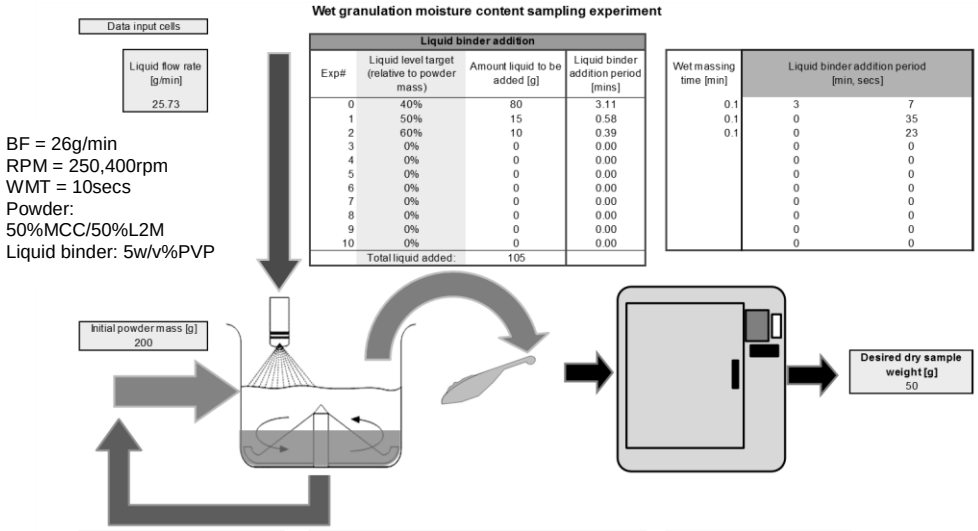

Liquid binder addition

Exp#	Liquid level target (relative to powder mass)	Amount liquid to be added [g]	Liquid binder addition period [mins]
0	40%	80	3.11
1	50%	15	0.58
2	60%	10	0.39
3	0%	0	0.00
4	0%	0	0.00
5	0%	0	0.00
6	0%	0	0.00
7	0%	0	0.00
8	0%	0	0.00
9	0%	0	0.00
10	0%	0	0.00
	Total liquid added:	105	

Wet massing time [min]	Liquid binder addition period [min, secs]	
0.1	3	7
0.1	0	35
0.1	0	23
	0	0
	0	0
	0	0
	0	0
	0	0
	0	0
	0	0

Granulation powder

Exp#	Powder mass [g]	Total granulation mass [g]
0	200	280
1	150	165
2	100	110
3	50	0
4	0	0
5	-50	0
6	-100	0
7	-150	0
8	-200	0
9	-250	0
10	-300	0

Remaining granulation powder bed

Exp#	Dry granulation powder mass [g]	Liquid mass remaining	Liquid level remaining
0	150	60	0.40
1	100	50	0.50
2	50	30	0.60
3	0	30	#DIV/0!
4	-50	30	-0.60
5	-100	30	-0.30
6	-150	30	-0.20
7	-200	30	-0.15
8	-250	30	-0.12
9	-300	30	-0.10
10	-350	30	-0.09

Sampling

Exp#	Wet sample weight to be taken out [g]
0	70
1	75
2	80
3	50
4	50
5	50
6	50
7	50
8	50
9	50
10	50

Figure B.11: Calculations for liquid level granulation experiments (WMT=10secs; BF = 26g/min; RPM= 250,400rpm) for 1L granulator.

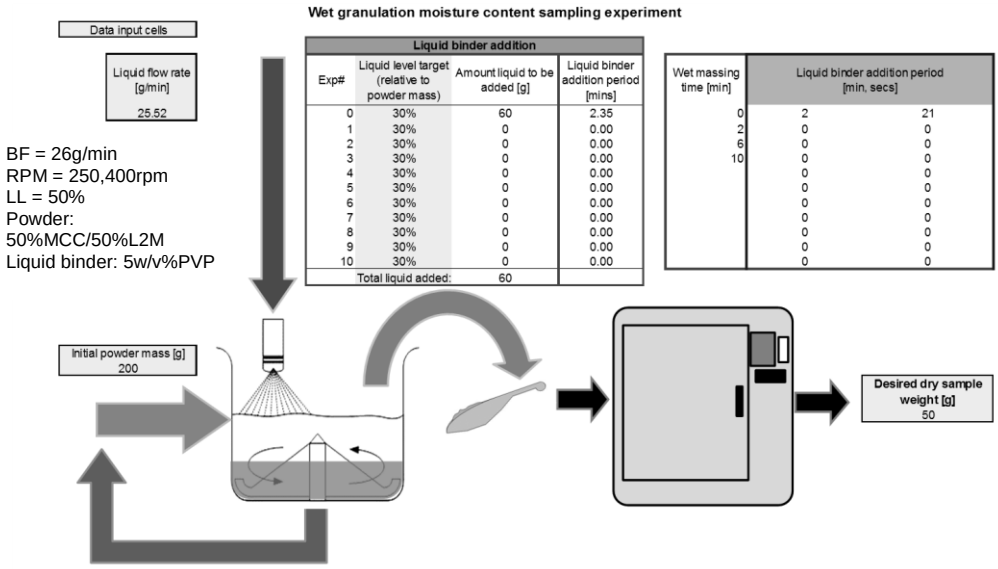

Liquid binder addition

Exp#	Liquid level target (relative to powder mass)	Amount liquid to be added [g]	Liquid binder addition period [mins]
0	30%	60	2.35
1	30%	0	0.00
2	30%	0	0.00
3	30%	0	0.00
4	30%	0	0.00
5	30%	0	0.00
6	30%	0	0.00
7	30%	0	0.00
8	30%	0	0.00
9	30%	0	0.00
10	30%	0	0.00
	Total liquid added:	60	

Wet massing time [min]	Liquid binder addition period [min, secs]	
0	2	21
2	0	0
6	0	0
10	0	0
	0	0
	0	0
	0	0
	0	0
	0	0
	0	0
	0	0

Granulation powder

Exp#	Powder mass [g]	Total granulation mass [g]
0	200	260
1	150	150
2	100	100
3	50	50
4	0	0
5	-50	-50
6	-100	-100
7	-150	-150
8	-200	-200
9	-250	-250
10	-300	-300

Remaining granulation powder bed

Exp#	Dry granulation powder mass [g]	Liquid mass remaining	Liquid level remaining
0	150	45	0.30
1	100	30	0.30
2	50	15	0.30
3	0	0	#DIV/0!
4	-50	-15	0.30
5	-100	-30	0.30
6	-150	-45	0.30
7	-200	-60	0.30
8	-250	-75	0.30
9	-300	-90	0.30
10	-350	-105	0.30

Sampling

Exp#	Wet sample weight to be taken out [g]
0	65
1	65
2	65
3	65
4	65
5	65
6	65
7	65
8	65
9	65
10	65

Figure B.12: Calculations for wet massing time granulation experiments (LL = 30%; BF = 26g/min; RPM= 250,400rpm) for 1L granulator.

Wet granulation moisture content sampling experiment

Data input cells

Liquid flow rate [g/min]
25.52

BF = 26g/min
RPM = 250,400rpm
LL = 50%
Powder:
50%MCC/50%L2M
Liquid binder:
5w/v%PVP/CaO

Liquid binder addition

Exp#	Liquid level target (relative to powder mass)	Amount liquid to be added [g]	Liquid binder addition period [mins]
0	30%	60	2.35
1	30%	0	0.00
2	30%	0	0.00
3	30%	0	0.00
4	30%	0	0.00
5	30%	0	0.00
6	30%	0	0.00
7	30%	0	0.00
8	30%	0	0.00
9	30%	0	0.00
10	30%	0	0.00
Total liquid added:		60	

Wet massing time [min]	Liquid binder addition period [min, secs]	
0	2	21
2	0	0
6	0	0
10	0	0
	0	0
	0	0
	0	0
	0	0
	0	0
	0	0
	0	0

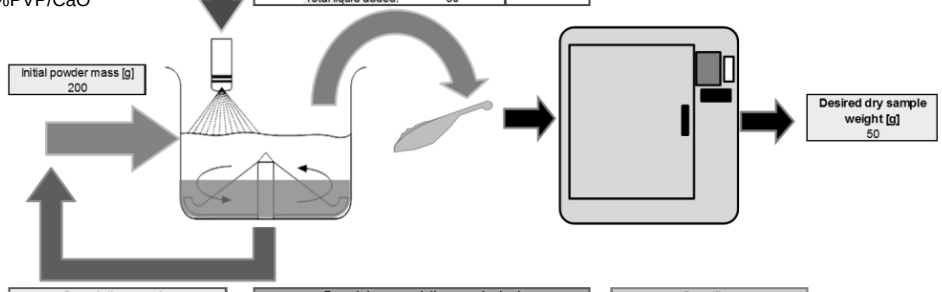

Granulation powder

Exp#	Powder mass [g]	Total granulation mass [g]
0	200	260
1	150	150
2	100	100
3	50	50
4	0	0
5	-50	-50
6	-100	-100
7	-150	-150
8	-200	-200
9	-250	-250
10	-300	-300

Remaining granulation powder bed

Exp#	Dry granulation powder mass [g]	Liquid mass remaining	Liquid level remaining
0	150	45	0.30
1	100	30	0.30
2	50	15	0.30
3	0	0	#DIV/0!
4	-50	-15	0.30
5	-100	-30	0.30
6	-150	-45	0.30
7	-200	-60	0.30
8	-250	-75	0.30
9	-300	-90	0.30
10	-350	-105	0.30

Sampling

Exp#	Wet sample weight to be taken out [g]
0	65
1	65
2	65
3	65
4	65
5	65
6	65
7	65
8	65
9	65
10	65

Figure B.13: Calculations for wet massing time granulation experiments (LL = 30%; BF = 26g/min; RPM= 250,400rpm, PVP/CaO liquid binder) for 1L granulator.

Wet granulation moisture content sampling experiment

Data input cells

Liquid flow rate [g/min]
26.26

BF = 26g/min
RPM = 400rpm
LL = 50%
Powder:
50%MCC/50%L2M
Liquid binder:
5w/v%PVP/HCl

Liquid binder addition

Exp#	Liquid level target (relative to powder mass)	Amount liquid to be added [g]	Liquid binder addition period [mins]
0	30%	60	2.28
1	30%	0	0.00
2	30%	0	0.00
3	30%	0	0.00
4	30%	0	0.00
5	30%	0	0.00
6	30%	0	0.00
7	30%	0	0.00
8	30%	0	0.00
9	30%	0	0.00
10	30%	0	0.00
Total liquid added:		60	

Wet massing time [min]	Liquid binder addition period [min, secs]	
0	2	17
2	0	0
6	0	0
10	0	0
	0	0
	0	0
	0	0
	0	0
	0	0
	0	0
	0	0

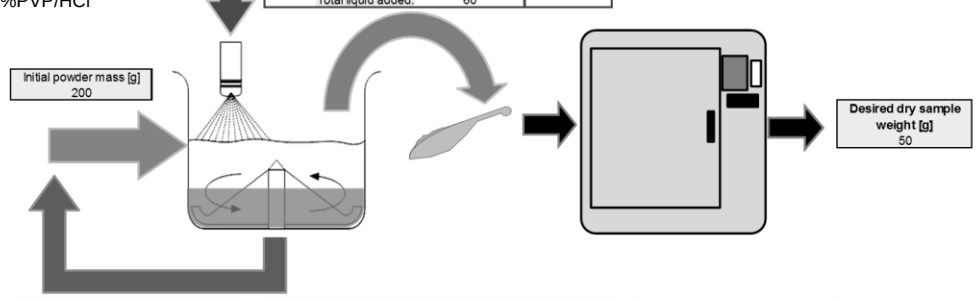

Granulation powder

Exp#	Powder mass [g]	Total granulation mass [g]
0	200	260
1	150	150
2	100	100
3	50	50
4	0	0
5	-50	-50
6	-100	-100
7	-150	-150
8	-200	-200
9	-250	-250
10	-300	-300

Remaining granulation powder bed

Exp#	Dry granulation powder mass [g]	Liquid mass remaining	Liquid level remaining
0	150	45	0.30
1	100	30	0.30
2	50	15	0.30
3	0	0	#DIV/0!
4	-50	-15	0.30
5	-100	-30	0.30
6	-150	-45	0.30
7	-200	-60	0.30
8	-250	-75	0.30
9	-300	-90	0.30
10	-350	-105	0.30

Sampling

Exp#	Wet sample weight to be taken out [g]
0	65
1	65
2	65
3	65
4	65
5	65
6	65
7	65
8	65
9	65
10	65

Figure B.14: Calculations for wet massing time granulation experiments (LL = 30%; BF = 26g/min; RPM= 400rpm, PVP/HCl liquid binder) for 1L granulator.

C. TABLET DIMENSION AND STRENGTH RAW DATA

Direct Compaction of Microcrystalline Cellulose and Lactose 200 mesh powder mixture:

Compaction Pressure [MPa]	Compression load [lb_f]	Thickness [cm]	Hardness [kp]	σ_μ	Tensile strength [MPa]	σ_μ	Porosity [-]	σ_μ	Tablet volume [cc]	Tablet Density [g/cc]	σ_μ
0.0	0	N/A	0.0	0.0	0.00	0.00	N/A	0.000	N/A	N/A	0.000
67.5	2000	0.29	13.2	0.1	0.98	0.01	0.19	0.002	0.39	1.28	0.004
202.5	6000	0.26	31.2	0.2	2.32	0.01	0.10	0.002	0.35	1.43	0.003
337.5	10000	0.25	43.2	0.4	3.22	0.03	0.06	0.002	0.34	1.48	0.004
405.0	12000	0.25	44.6	0.5	3.32	0.04	0.06	0.003	0.34	1.49	0.005
472.5	14000	0.25	45.6	0.1	3.39	0.01	0.06	0.002	0.34	1.49	0.004
540.0	16000	0.25	44.9	0.3	3.34	0.03	0.06	0.001	0.34	1.49	0.002

Liquid level Experiments using Microcrystalline Cellulose and Lactose 200 mesh, granulated with 5w/v% aqueous PVP:

Liquid level: 20% Wet massing time: 10 seconds
Impeller speed: 150rpm Binder flow rate: 130g/min

Compaction Pressure [MPa]	Compression load [lb_f]	Thickness [cm]	Hardness [kp]	σ_μ	Tensile strength [MPa]	σ_μ	Porosity [-]	σ_μ	Tablet volume [cc]	Tablet Density [g/cc]	σ_μ
0.0	0	N/A	0.0	0.0	0.00	0.00	N/A	0.000	N/A	N/A	0.000
67.5	2000	0.31	10.9	0.3	0.81	0.02	0.24	0.004	0.41	1.21	0.006
202.5	6000	0.28	24.6	1.0	1.83	0.08	0.13	0.004	0.37	1.37	0.007
337.5	10000	0.26	37.2	0.4	2.77	0.03	0.09	0.002	0.35	1.44	0.004
540.0	16000	0.26	44.6	0.7	3.32	0.05	0.07	0.002	0.34	1.47	0.003

Liquid level Experiments using Microcrystalline Cellulose and Lactose 200 mesh, granulated with 5w/v% aqueous PVP:

Liquid level: 30% Wet massing time: 10 seconds
Impeller speed: 150rpm Binder flow rate: 130g/min

Compaction Pressure [MPa]	Compression load [lb_f]	Thickness [cm]	Hardness [kp]	σ_μ	Tensile strength [MPa]	σ_μ	Porosity [-]	σ_μ	Tablet volume [cc]	Tablet Density [g/cc]	σ_μ
0.0	0	N/A	0.0	0.0	0.00	0.00	N/A	0.000	N/A	N/A	0.000
67.5	2000	0.31	10.4	0.1	0.77	0.00	0.24	0.002	0.42	1.20	0.003
202.5	6000	0.27	24.4	0.4	1.81	0.03	0.13	0.001	0.36	1.37	0.002
337.5	10000	0.26	35.4	0.8	2.63	0.06	0.09	0.003	0.35	1.44	0.004
540.0	16000	0.25	45.0	0.4	3.35	0.03	0.06	0.001	0.34	1.48	0.001

Liquid level: 40% Wet massing time: 10 seconds
Impeller speed: 150rpm Binder flow rate: 130g/min

Compaction Pressure [MPa]	Compression load [lb_f]	Thickness [cm]	Hardness [kp]	σ_μ	Tensile strength [MPa]	σ_μ	Porosity [-]	σ_μ	Tablet volume [cc]	Tablet Density [g/cc]	σ_μ
0.0	0	N/A	0.0	0.0	0.00	0.00	N/A	0.000	N/A	N/A	0.000
67.5	2000	0.31	10.1	0.5	0.75	0.03	0.24	0.003	0.42	1.20	0.004
202.5	6000	0.27	23.7	0.2	1.76	0.01	0.13	0.002	0.36	1.37	0.003
337.5	10000	0.26	37.0	1.3	2.75	0.09	0.09	0.001	0.35	1.44	0.002
540.0	16000	0.26	43.4	0.7	3.23	0.05	0.07	0.001	0.34	1.48	0.002

Liquid level: 50% Wet massing time: 10 seconds
Impeller speed: 150rpm Binder flow rate: 130g/min

Compaction Pressure [MPa]	Compression load [lb_f]	Thickness [cm]	Hardness [kp]	σ_μ	Tensile strength [MPa]	σ_μ	Porosity [-]	σ_μ	Tablet volume [cc]	Tablet Density [g/cc]	σ_μ
0.0	0	N/A	0	0.0	0.00	0.00	N/A	0.000	N/A	N/A	0.000
67.5	2000	0.32	10.1	0.6	0.75	0.04	0.25	0.002	0.42	1.18	0.003
202.5	6000	0.27	23.1	0.7	1.72	0.05	0.13	0.001	0.36	1.38	0.002
337.5	10000	0.26	34.3	1.5	2.55	0.11	0.09	0.003	0.35	1.43	0.004
540.0	16000	0.26	43.7	0.9	3.25	0.06	0.07	0.002	0.34	1.47	0.003

Liquid level Experiments using Microcrystalline Cellulose and Lactose 200 mesh, granulated with 5w/v% aqueous PVP:

Liquid level: 20% Wet massing time: 10 seconds
Impeller speed: 285rpm Binder flow rate: 130g/min

Compaction Pressure [MPa]	Compression load [lb_f]	Thickness [cm]	Hardness [kp]	σ_μ	Tensile strength [MPa]	σ_μ	Porosity [-]	σ_μ	Tablet volume [cc]	Tablet Density [g/cc]	σ_μ
0.0	0	N/A	0.0	0.00	0.00	0.00	N/A	0.000	N/A	N/A	0.000
67.5	2000	0.31	11.1	0.17	0.83	0.01	0.23	0.003	0.41	1.22	0.004
202.5	6000	0.27	25.0	0.32	1.86	0.02	0.13	0.002	0.36	1.38	0.004
337.5	10000	0.26	33.4	0.77	2.49	0.06	0.10	0.002	0.35	1.43	0.003
540.0	16000	0.26	45.2	0.38	3.36	0.03	0.08	0.002	0.34	1.46	0.003

Liquid level: 30% Wet massing time: 10 seconds
Impeller speed: 285rpm Binder flow rate: 130g/min

Compaction Pressure [MPa]	Compression load [lb_f]	Thickness [cm]	Hardness [kp]	σ_μ	Tensile strength [MPa]	σ_μ	Porosity [-]	σ_μ	Tablet volume [cc]	Tablet Density [g/cc]	σ_μ
0.0	0	N/A	0.0	0.00	0.00	0.00	N/A	0.000	N/A	N/A	0.000
67.5	2000	0.31	9.9	0.35	0.74	0.03	0.24	0.001	0.42	1.20	0.002
202.5	6000	0.27	24.2	0.24	1.80	0.02	0.13	0.001	0.36	1.38	0.002
337.5	10000	0.26	32.8	0.38	2.44	0.03	0.09	0.001	0.35	1.44	0.002
540.0	16000	0.26	44.3	0.42	3.30	0.03	0.07	0.002	0.34	1.47	0.004

Liquid level: 40% Wet massing time: 10 seconds
Impeller speed: 285rpm Binder flow rate: 130g/min

Compaction Pressure [MPa]	Compression load [lb_f]	Thickness [cm]	Hardness [kp]	σ_μ	Tensile strength [MPa]	σ_μ	Porosity [-]	σ_μ	Tablet volume [cc]	Tablet Density [g/cc]	σ_μ
0.0	0	N/A	0.0	0.00	0.00	0.00	N/A	0.000	N/A	N/A	0.000
67.5	2000	0.32	7.9	0.21	0.59	0.02	0.24	0.002	0.42	1.19	0.003
202.5	6000	0.27	19.8	0.35	1.48	0.03	0.13	0.002	0.36	1.38	0.003
337.5	10000	0.26	29.8	0.80	2.22	0.06	0.09	0.003	0.35	1.44	0.005
540.0	16000	0.26	37.0	0.99	2.75	0.07	0.07	0.002	0.34	1.47	0.003

Liquid level Experiments using Microcrystalline Cellulose and Lactose 200 mesh, granulated with 5w/v% aqueous PVP:

Liquid level: 50% Wet massing time: 10 seconds
Impeller speed: 285rpm Binder flow rate: 130g/min

Compaction Pressure [MPa]	Compression load [lb_f]	Thickness [cm]	Hardness [kp]	σ_μ	Tensile strength [MPa]	σ_μ	Porosity [-]	σ_μ	Tablet volume [cc]	Tablet Density [g/cc]	σ_μ
0.0	0	N/A	0.0	0.00	0.00	0.00	N/A	0.000	N/A	N/A	0.000
67.5	2000	0.31	7.8	0.19	0.58	0.01	0.24	0.002	0.42	1.20	0.004
202.5	6000	0.27	20.7	0.19	1.54	0.01	0.13	0.002	0.36	1.38	0.003
337.5	10000	0.26	30.1	0.20	2.24	0.01	0.09	0.002	0.35	1.44	0.003
540.0	16000	0.26	37.5	0.43	2.79	0.03	0.07	0.002	0.34	1.46	0.004

Liquid level: 20% Wet massing time: 10 seconds
Impeller speed: 600rpm Binder flow rate: 130g/min

Compaction Pressure [MPa]	Compression load [lb_f]	Thickness [cm]	Hardness [kp]	σ_μ	Tensile strength [MPa]	σ_μ	Porosity [-]	σ_μ	Tablet volume [cc]	Tablet Density [g/cc]	σ_μ
0.0	0	N/A	0.0	0.00	0.00	0.00	N/A	0.00	N/A	N/A	0.000
67.5	2000	0.31	10.4	0.14	0.78	0.01	0.22	0.001	0.41	1.23	0.001
202.5	6000	0.27	25.5	0.65	1.89	0.05	0.12	0.002	0.36	1.38	0.003
337.5	10000	0.26	35.7	1.08	2.66	0.08	0.09	0.003	0.35	1.44	0.004
540.0	16000	0.26	45.6	0.14	3.39	0.01	0.07	0.003	0.34	1.46	0.005

Liquid level: 30% Wet massing time: 10 seconds
Impeller speed: 600rpm Binder flow rate: 130g/min

Compaction Pressure [MPa]	Compression load [lb_f]	Thickness [cm]	Hardness [kp]	σ_μ	Tensile strength [MPa]	σ_μ	Porosity [-]	σ_μ	Tablet volume [cc]	Tablet Density [g/cc]	σ_μ
0.0	0	N/A	0.0	0.00	0.00	0.00	N/A	0.00	N/A	N/A	0.000
67.5	2000	0.31	8.3	0.26	0.62	0.02	0.24	0.002	0.42	1.20	0.003
202.5	6000	0.27	21.4	0.51	1.59	0.04	0.12	0.003	0.36	1.38	0.004
337.5	10000	0.26	30.8	0.25	2.29	0.02	0.09	0.002	0.35	1.44	0.002
540.0	16000	0.26	37.6	0.57	2.80	0.04	0.07	0.003	0.34	1.48	0.005

Liquid level Experiments using Microcrystalline Cellulose and Lactose 200 mesh, granulated with 5w/v% aqueous PVP:

Liquid level: 40% Wet massing time: 10 seconds
Impeller speed: 600rpm Binder flow rate: 130g/min

Compaction Pressure [MPa]	Compression load [lb_f]	Thickness [cm]	Hardness [kp]	σ_μ	Tensile strength [MPa]	σ_μ	Porosity [-]	σ_μ	Tablet volume [cc]	Tablet Density [g/cc]	σ_μ
0.0	0	N/A	0.0	0.00	0.00	0.00	N/A	0.000	N/A	N/A	0.000
67.5	2000	0.31	6.9	0.43	0.52	0.03	0.23	0.001	0.41	1.21	0.002
202.5	6000	0.27	17.6	0.50	1.31	0.04	0.12	0.001	0.36	1.39	0.002
337.5	10000	0.26	24.9	0.43	1.85	0.03	0.09	0.001	0.35	1.44	0.002
540.0	16000	0.26	34.0	1.71	2.53	0.13	0.07	0.004	0.34	1.47	0.006

Liquid level: 50% Wet massing time: 10 seconds
Impeller speed: 600rpm Binder flow rate: 130g/min

Compaction Pressure [MPa]	Compression load [lb_f]	Thickness [cm]	Hardness [kp]	σ_μ	Tensile strength [MPa]	σ_μ	Porosity [-]	σ_μ	Tablet volume [cc]	Tablet Density [g/cc]	σ_μ
0.0	0	N/A	0.0	0.00	0.00	0.00	N/A	0.000	N/A	N/A	0.000
67.5	2000	0.31	6.1	0.21	0.45	0.02	0.23	0.001	0.41	1.22	0.001
202.5	6000	0.27	17.8	0.46	1.32	0.03	0.12	0.002	0.36	1.39	0.003
337.5	10000	0.26	25.3	0.41	1.88	0.03	0.09	0.001	0.35	1.44	0.002
540.0	16000	0.26	32.2	0.44	2.40	0.03	0.07	0.002	0.34	1.47	0.003

Liquid level: 20% Wet massing time: 10 seconds
Impeller speed: 150rpm Binder flow rate: 280g/min

Compaction Pressure [MPa]	Compression load [lb_f]	Thickness [cm]	Hardness [kp]	σ_μ	Tensile strength [MPa]	σ_μ	Porosity [-]	σ_μ	Tablet volume [cc]	Tablet Density [g/cc]	σ_μ
0.0	0	N/A	0.0	0.00	0.00	0.00	N/A	0.000	N/A	N/A	0.000
67.5	2000	0.31	11.0	0.36	0.82	0.03	0.24	0.006	0.42	1.20	0.009
202.5	6000	0.27	26.4	0.38	1.96	0.03	0.12	0.003	0.36	1.38	0.004
337.5	10000	0.26	37.4	0.56	2.78	0.04	0.08	0.001	0.34	1.45	0.001
540.0	16000	0.25	45.4	0.24	3.38	0.02	0.06	0.002	0.34	1.48	0.004

Liquid level Experiments using Microcrystalline Cellulose and Lactose 200 mesh, granulated with 5w/v% aqueous PVP:

Liquid level: 30% Wet massing time: 10 seconds
Impeller speed: 150rpm Binder flow rate: 280g/min

Compaction Pressure [MPa]	Compression load [lb_f]	Thickness [cm]	Hardness [kp]	σ_μ	Tensile strength [MPa]	σ_μ	Porosity [-]	σ_μ	Tablet volume [cc]	Tablet Density [g/cc]	σ_μ
0.0	0	N/A	0.0	0.00	0.00	0.00	N/A	0.000	N/A	N/A	0.000
67.5	2000	0.30	13.0	0.27	0.97	0.02	0.20	0.001	0.40	1.26	0.002
202.5	6000	0.27	26.2	1.77	1.95	0.13	0.11	0.002	0.35	1.41	0.003
337.5	10000	0.26	38.7	0.72	2.88	0.05	0.07	0.001	0.34	1.47	0.002
540.0	16000	0.25	45.2	0.31	3.37	0.02	0.06	0.002	0.34	1.48	0.004

Liquid level: 40% Wet massing time: 10 seconds
Impeller speed: 150rpm Binder flow rate: 280g/min

Compaction Pressure [MPa]	Compression load [lb_f]	Thickness [cm]	Hardness [kp]	σ_μ	Tensile strength [MPa]	σ_μ	Porosity [-]	σ_μ	Tablet volume [cc]	Tablet Density [g/cc]	σ_μ
0.0	0	N/A	0.0	0.00	0.00	0.00	N/A	0.000	N/A	N/A	0.000
67.5	2000	0.31	10.5	0.24	0.78	0.02	0.22	0.005	0.41	1.23	0.008
202.5	6000	0.27	26.6	0.40	1.98	0.03	0.11	0.001	0.36	1.40	0.001
337.5	10000	0.26	37.2	1.33	2.76	0.10	0.08	0.002	0.34	1.46	0.003
540.0	16000	0.25	44.6	0.72	3.32	0.05	0.06	0.001	0.34	1.48	0.001

Liquid level: 50% Wet massing time: 10 seconds
Impeller speed: 150rpm Binder flow rate: 280g/min

Compaction Pressure [MPa]	Compression load [lb_f]	Thickness [cm]	Hardness [kp]	σ_μ	Tensile strength [MPa]	σ_μ	Porosity [-]	σ_μ	Tablet volume [cc]	Tablet Density [g/cc]	σ_μ
0.0	0	N/A	0.0	0.00	0.00	0.00	N/A	0.000	N/A	N/A	0.000
67.5	2000	0.30	10.7	0.24	0.80	0.02	0.22	0.001	0.40	1.24	0.002
202.5	6000	0.27	25.0	0.44	1.86	0.03	0.12	0.001	0.36	1.40	0.002
337.5	10000	0.26	36.6	2.18	2.72	0.16	0.08	0.002	0.34	1.45	0.003
540.0	16000	0.26	42.2	0.73	3.14	0.05	0.07	0.001	0.34	1.47	0.002

Liquid level Experiments using Microcrystalline Cellulose and Lactose 200 mesh, granulated with 5w/v% aqueous PVP:

Liquid level: 20% Wet massing time: 10 seconds
Impeller speed: 285rpm Binder flow rate: 280g/min

Compaction Pressure [MPa]	Compression load [lb_f]	Thickness [cm]	Hardness [kp]	σ_μ	Tensile strength [MPa]	σ_μ	Porosity [-]	σ_μ	Tablet volume [cc]	Tablet Density [g/cc]	σ_μ
0.0	0	N/A	0.0	0.00	0.00	0.00	N/A	0.000	N/A	N/A	0.000
67.5	2000	0.31	11.9	0.26	0.89	0.02	0.23	0.001	0.41	1.22	0.002
202.5	6000	0.27	27.1	0.55	2.01	0.04	0.12	0.001	0.36	1.39	0.001
337.5	10000	0.26	37.2	0.45	2.76	0.03	0.08	0.002	0.34	1.45	0.003
540.0	16000	0.25	45.7	0.02	3.40	0.00	0.06	0.001	0.34	1.48	0.001

Liquid level: 30% Wet massing time: 10 seconds
Impeller speed: 285rpm Binder flow rate: 280g/min

Compaction Pressure [MPa]	Compression load [lb_f]	Thickness [cm]	Hardness [kp]	σ_μ	Tensile strength [MPa]	σ_μ	Porosity [-]	σ_μ	Tablet volume [cc]	Tablet Density [g/cc]	σ_μ
0.0	0	N/A	0.0	0.00	0.00	0.00	N/A	0.000	N/A	N/A	0.000
67.5	2000	0.31	10.1	0.25	0.75	0.02	0.24	0.003	0.41	1.21	0.004
202.5	6000	0.27	25.4	1.05	1.89	0.08	0.12	0.002	0.36	1.38	0.003
337.5	10000	0.26	34.4	0.63	2.56	0.05	0.08	0.001	0.34	1.45	0.001
540.0	16000	0.25	44.8	0.41	3.33	0.03	0.06	0.001	0.34	1.48	0.002

Liquid level: 40% Wet massing time: 10 seconds
Impeller speed: 285rpm Binder flow rate: 280g/min

Compaction Pressure [MPa]	Compression load [lb_f]	Thickness [cm]	Hardness [kp]	σ_μ	Tensile strength [MPa]	σ_μ	Porosity [-]	σ_μ	Tablet volume [cc]	Tablet Density [g/cc]	σ_μ
0.0	0	N/A	0.0	0.00	0.00	0.00	N/A	0.000	N/A	N/A	0.000
67.5	2000	0.30	10.4	0.27	0.78	0.02	0.20	0.001	0.40	1.26	0.002
202.5	6000	0.27	24.2	0.42	1.80	0.03	0.11	0.001	0.35	1.41	0.002
337.5	10000	0.26	34.1	0.54	2.54	0.04	0.07	0.001	0.34	1.46	0.001
540.0	16000	0.25	41.7	1.18	3.10	0.09	0.06	0.002	0.34	1.48	0.003

Liquid level Experiments using Microcrystalline Cellulose and Lactose 200 mesh, granulated with 5w/v% aqueous PVP:

Liquid level: 50% Wet massing time: 10 seconds
Impeller speed: 285rpm Binder flow rate: 280g/min

Compaction Pressure [MPa]	Compression load [lb_f]	Thickness [cm]	Hardness [kp]	σ_μ	Tensile strength [MPa]	σ_μ	Porosity [-]	σ_μ	Tablet volume [cc]	Tablet Density [g/cc]	σ_μ
0.0	0	N/A	0.0	0.00	0.00	0.00	N/A	0.000	N/A	N/A	0.000
67.5	2000	0.31	9.2	0.26	0.69	0.02	0.22	0.002	0.41	1.23	0.004
202.5	6000	0.27	23.1	0.19	1.72	0.01	0.11	0.002	0.35	1.41	0.003
337.5	10000	0.26	33.4	0.71	2.49	0.05	0.07	0.002	0.34	1.47	0.004
540.0	16000	0.25	36.8	0.64	2.74	0.05	0.06	0.001	0.34	1.48	0.001

Liquid level: 20% Wet massing time: 10 seconds
Impeller speed: 600rpm Binder flow rate: 280g/min

Compaction Pressure [MPa]	Compression load [lb_f]	Thickness [cm]	Hardness [kp]	σ_μ	Tensile strength [MPa]	σ_μ	Porosity [-]	σ_μ	Tablet volume [cc]	Tablet Density [g/cc]	σ_μ
0.0	0	N/A	0.0	0.00	0.00	0.00	N/A	0.000	N/A	N/A	0.000
67.5	2000	0.31	10.1	0.23	0.75	0.02	0.23	0.006	0.41	1.22	0.009
202.5	6000	0.27	25.0	0.27	1.86	0.02	0.12	0.001	0.36	1.40	0.002
337.5	10000	0.26	35.4	1.22	2.64	0.09	0.08	0.002	0.35	1.45	0.003
540.0	16000	0.25	45.2	0.25	3.36	0.02	0.06	0.001	0.34	1.49	0.002

Liquid level: 30% Wet massing time: 10 seconds
Impeller speed: 600rpm Binder flow rate: 280g/min

Compaction Pressure [MPa]	Compression load [lb_f]	Thickness [cm]	Hardness [kp]	σ_μ	Tensile strength [MPa]	σ_μ	Porosity [-]	σ_μ	Tablet volume [cc]	Tablet Density [g/cc]	σ_μ
0	0	N/A	0.0	0	0.00	0.00	N/A	0.000	N/A	N/A	0.000
67.5	2000	0.31	8.2	0.14	0.61	0.01	0.24	0.002	0.41	1.21	0.003
202.5	6000	0.27	20.7	0.42	1.54	0.03	0.12	0.001	0.36	1.40	0.002
337.5	10000	0.26	29.1	0.69	2.17	0.05	0.09	0.002	0.35	1.44	0.003
540.0	16000	0.26	40.1	0.43	2.99	0.03	0.07	0.002	0.34	1.47	0.003

Liquid level Experiments using Microcrystalline Cellulose and Lactose 200 mesh, granulated with 5w/v% aqueous PVP:

Liquid level: 40% Wet massing time: 10 seconds
Impeller speed: 600rpm Binder flow rate: 280g/min

Compaction Pressure [MPa]	Compression load [lb_f]	Thickness [cm]	Hardness [kp]	σ_μ	Tensile strength [MPa]	σ_μ	Porosity [-]	σ_μ	Tablet volume [cc]	Tablet Density [g/cc]	σ_μ
0.0	0	N/A	0.0	0.00	0.00	0.00	N/A	0.000	N/A	N/A	0.000
67.5	2000	0.31	7.3	0.12	0.55	0.01	0.23	0.001	0.41	1.22	0.001
202.5	6000	0.27	19.0	0.81	1.41	0.06	0.12	0.002	0.36	1.39	0.003
337.5	10000	0.26	29.5	0.92	2.20	0.07	0.08	0.000	0.35	1.45	0.000
540.0	16000	0.26	36.2	0.79	2.69	0.06	0.07	0.001	0.34	1.47	0.002

Liquid level: 50% Wet massing time: 10 seconds
Impeller speed: 600rpm Binder flow rate: 280g/min

Compaction Pressure [MPa]	Compression load [lb_f]	Thickness [cm]	Hardness [kp]	σ_μ	Tensile strength [MPa]	σ_μ	Porosity [-]	σ_μ	Tablet volume [cc]	Tablet Density [g/cc]	σ_μ
0.0	0	N/A	0.0	0.00	0.00	0.00	N/A	0.000	N/A	N/A	0.000
67.5	2000	0.31	8.6	0.22	0.64	0.02	0.23	0.000	0.41	1.21	0.001
202.5	6000	0.27	23.0	0.80	1.71	0.06	0.12	0.001	0.36	1.38	0.001
337.5	10000	0.26	30.5	0.44	2.27	0.03	0.09	0.001	0.35	1.44	0.002
540.0	16000	0.26	38.7	0.39	2.88	0.03	0.07	0.002	0.34	1.47	0.003

Wet Massing Time Experiments using Microcrystalline Cellulose and Lactose 200 mesh, granulated with 5w/v% aqueous PVP:

Liquid level: 20% Wet massing time: 0 minutes
Impeller speed: 285rpm Binder flow rate: 130g/min

Compaction Pressure [MPa]	Compression load [lb_f]	Thickness [cm]	Hardness [kp]	σ_μ	Tensile strength [MPa]	σ_μ	Porosity [-]	σ_μ	Tablet volume [cc]	Tablet Density [g/cc]	σ_μ
0	0	N/A	0.0	0.00	0.00	0.00	N/A	0.000	N/A	N/A	0.000
67.5	2000	0.31	10.0	0.21	0.74	0.02	0.24	0.002	0.42	1.20	0.003
202.5	6000	0.27	24.8	0.12	1.84	0.01	0.13	0.003	0.36	1.38	0.004
337.5	10000	0.26	36.4	0.26	2.71	0.02	0.09	0.002	0.35	1.44	0.003
540.0	16000	0.26	45.8	0.02	3.41	0.00	0.07	0.001	0.34	1.46	0.002

Liquid level: 20% Wet massing time: 2 minutes
Impeller speed: 285rpm Binder flow rate: 130g/min

Compaction Pressure [MPa]	Compression load [lb_f]	Thickness [cm]	Hardness [kp]	σ_μ	Tensile strength [MPa]	σ_μ	Porosity [-]	σ_μ	Tablet volume [cc]	Tablet Density [g/cc]	σ_μ
0	0	N/A	0.0	0.00	0.00	0.00	N/A	0.000	N/A	N/A	0.000
67.5	2000	0.31	9.5	0.36	0.71	0.03	0.24	0.002	0.41	1.21	0.003
202.5	6000	0.27	23.8	0.27	1.77	0.02	0.13	0.002	0.36	1.38	0.003
337.5	10000	0.26	34.2	0.39	2.55	0.03	0.08	0.003	0.35	1.45	0.005
540.0	16000	0.25	43.7	0.39	3.25	0.03	0.06	0.001	0.34	1.48	0.002

Liquid level: 20% Wet massing time: 6 minutes
Impeller speed: 285rpm Binder flow rate: 130g/min

Compaction Pressure [MPa]	Compression load [lb_f]	Thickness [cm]	Hardness [kp]	σ_μ	Tensile strength [MPa]	σ_μ	Porosity [-]	σ_μ	Tablet volume [cc]	Tablet Density [g/cc]	σ_μ
0.0	0	N/A	0.0	0.00	0.00	0.00	N/A	0.000	N/A	N/A	0.000
67.5	2000	0.31	8.5	0.69	0.63	0.05	0.24	0.005	0.42	1.20	0.008
202.5	6000	0.27	21.0	0.49	1.56	0.04	0.12	0.001	0.36	1.38	0.001
337.5	10000	0.26	32.5	0.16	2.42	0.01	0.08	0.001	0.34	1.45	0.002
540.0	16000	0.25	40.0	0.57	2.98	0.04	0.06	0.001	0.34	1.48	0.002

Wet Massing Time Experiments using Microcrystalline Cellulose and Lactose 200 mesh, granulated with 5w/v% aqueous PVP:

Liquid level: 20% Wet massing time: 10 minutes
Impeller speed: 285rpm Binder flow rate: 130g/min

Compaction Pressure [MPa]	Compression load [lb_f]	Thickness [cm]	Hardness [kp]	σ_μ	Tensile strength [MPa]	σ_μ	Porosity [-]	σ_μ	Tablet volume [cc]	Tablet Density [g/cc]	σ_μ
0.0	0	N/A	0.0	0.00	0.00	0.00	N/A	0.000	N/A	N/A	0.000
67.5	2000	0.31	8.1	1.53	0.60	0.02	0.23	0.002	0.41	1.22	0.003
202.5	6000	0.27	20.8	1.11	1.55	0.03	0.12	0.002	0.36	1.38	0.003
337.5	10000	0.26	29.0	1.44	2.16	0.11	0.09	0.002	0.35	1.45	0.004
540.0	16000	0.26	40.2	0.56	2.99	0.04	0.07	0.001	0.34	1.47	0.002

Liquid level: 20% Wet massing time: 0 minutes
Impeller speed: 285rpm Binder flow rate: 280g/min

Compaction Pressure [MPa]	Compression load [lb_f]	Thickness [cm]	Hardness [kp]	σ_μ	Tensile strength [MPa]	σ_μ	Porosity [-]	σ_μ	Tablet volume [cc]	Tablet Density [g/cc]	σ_μ
0.0	0	N/A	0.0	0.00	0.00	0.00	N/A	0.000	N/A	N/A	0.000
67.5	2000	0.31	11.00	0.11	0.82	0.01	0.23	0.002	0.41	1.21	0.003
202.5	6000	0.28	24.10	1.61	1.79	0.12	0.13	0.005	0.37	1.37	0.007
337.5	10000	0.26	35.66	0.86	2.65	0.06	0.09	0.001	0.35	1.44	0.001
540.0	16000	0.26	44.60	0.88	3.32	0.07	0.07	0.002	0.34	1.47	0.003

Liquid level: 20% Wet massing time: 2 minutes
Impeller speed: 285rpm Binder flow rate: 280g/min

Compaction Pressure [MPa]	Compression load [lb_f]	Thickness [cm]	Hardness [kp]	σ_μ	Tensile strength [MPa]	σ_μ	Porosity [-]	σ_μ	Tablet volume [cc]	Tablet Density [g/cc]	σ_μ
0.0	0	N/A	0.0	0.00	0.00	0.00	N/A	0.000	N/A	N/A	0.000
67.5	2000	0.31	9.68	0.15	0.72	0.01	0.23	0.001	0.41	1.21	0.002
202.5	6000	0.27	23.30	0.45	1.73	0.03	0.13	0.001	0.36	1.38	0.002
337.5	10000	0.26	34.32	0.22	2.55	0.02	0.09	0.001	0.35	1.45	0.002
540.0	16000	0.25	43.22	0.50	3.22	0.04	0.07	0.001	0.34	1.48	0.001

Wet Massing Time Experiments using Microcrystalline Cellulose and Lactose 200 mesh, granulated with 5w/v% aqueous PVP:

Liquid level: 20% Wet massing time: 6 minutes
Impeller speed: 285rpm Binder flow rate: 280g/min

Compaction Pressure [MPa]	Compression load [lb_f]	Thickness [cm]	Hardness [kp]	σ_μ	Tensile strength [MPa]	σ_μ	Porosity [-]	σ_μ	Tablet volume [cc]	Tablet Density [g/cc]	σ_μ
0.0	0	N/A	0.0	0.00	0.00	0.00	N/A	0.000	N/A	N/A	0.000
67.5	2000	0.31	8.84	0.09	0.66	0.01	0.22	0.001	0.41	1.22	0.002
202.5	6000	0.27	21.86	0.30	1.63	0.02	0.12	0.001	0.36	1.39	0.002
337.5	10000	0.26	31.12	0.35	2.32	0.03	0.08	0.001	0.34	1.45	0.001
540.0	16000	0.26	40.82	1.12	3.04	0.08	0.07	0.002	0.34	1.48	0.003

Liquid level: 20% Wet massing time: 10 minutes
Impeller speed: 285rpm Binder flow rate: 280g/min

Compaction Pressure [MPa]	Compression load [lb_f]	Thickness [cm]	Hardness [kp]	σ_μ	Tensile strength [MPa]	σ_μ	Porosity [-]	σ_μ	Tablet volume [cc]	Tablet Density [g/cc]	σ_μ
0.0	0	N/A	0.0	0.00	0.00	0.00	N/A	0.000	N/A	N/A	0.000
67.5	2000	0.31	8.06	0.19	0.60	0.02	0.22	0.001	0.41	1.22	0.001
202.5	6000	0.27	19.80	0.68	1.47	0.03	0.12	0.001	0.36	1.39	0.002
337.5	10000	0.26	29.94	0.50	2.23	0.04	0.08	0.002	0.35	1.45	0.003
540.0	16000	0.25	36.86	0.27	2.74	0.02	0.06	0.001	0.34	1.48	0.002

Liquid level: 30% Wet massing time: 0 minutes
Impeller speed: 150rpm Binder flow rate: 130g/min

Compaction Pressure [MPa]	Compression load [lb_f]	Thickness [cm]	Hardness [kp]	σ_μ	Tensile strength [MPa]	σ_μ	Porosity [-]	σ_μ	Tablet volume [cc]	Tablet Density [g/cc]	σ_μ
0.0	0	N/A	0.0	0.00	0.00	0.00	N/A	0.000	N/A	N/A	0.000
67.5	2000	0.31	10.8	0.32	0.80	0.02	0.22	0.001	0.41	1.23	0.002
202.5	6000	0.27	25.7	0.34	1.91	0.03	0.11	0.002	0.36	1.40	0.003
337.5	10000	0.26	35.5	0.24	2.64	0.02	0.07	0.001	0.34	1.46	0.002
540.0	16000	0.25	44.0	0.55	3.28	0.04	0.06	0.002	0.34	1.48	0.003

Wet Massing Time Experiments using Microcrystalline Cellulose and Lactose 200 mesh, granulated with 5w/v% aqueous PVP:

Liquid level: 30% Wet massing time: 2 minutes
Impeller speed: 150rpm Binder flow rate: 130g/min

Compaction Pressure [MPa]	Compression load [lb_f]	Thickness [cm]	Hardness [kp]	σ_μ	Tensile strength [MPa]	σ_μ	Porosity [-]	σ_μ	Tablet volume [cc]	Tablet Density [g/cc]	σ_μ
0.0	0	N/A	0.0	0.00	0.00	0.00	N/A	0.000	N/A	N/A	0.000
67.5	2000	0.31	9.9	0.43	0.74	0.03	0.22	0.002	0.41	1.23	0.003
202.5	6000	0.27	24.0	0.69	1.78	0.05	0.12	0.003	0.36	1.39	0.004
337.5	10000	0.26	34.1	0.39	2.54	0.03	0.08	0.001	0.34	1.45	0.002
540.0	16000	0.26	41.8	0.81	3.11	0.06	0.07	0.002	0.34	1.48	0.003

Liquid level: 30% Wet massing time: 6 minutes
Impeller speed: 150rpm Binder flow rate: 130g/min

Compaction Pressure [MPa]	Compression load [lb_f]	Thickness [cm]	Hardness [kp]	σ_μ	Tensile strength [MPa]	σ_μ	Porosity [-]	σ_μ	Tablet volume [cc]	Tablet Density [g/cc]	σ_μ
0.0	0	N/A	0.0	0.00	0.00	0.00	N/A	0.000	N/A	N/A	0.000
67.5	2000	0.31	7.2	0.18	0.54	0.01	0.23	0.002	0.41	1.22	0.003
202.5	6000	0.27	17.5	0.77	1.31	0.06	0.12	0.002	0.36	1.39	0.003
337.5	10000	0.26	27.3	1.36	2.03	0.10	0.08	0.002	0.34	1.45	0.003
540.0	16000	0.26	34.5	0.40	2.56	0.03	0.07	0.002	0.34	1.48	0.003

Liquid level: 30% Wet massing time: 10 minutes
Impeller speed: 150rpm Binder flow rate: 130g/min

Compaction Pressure [MPa]	Compression load [lb_f]	Thickness [cm]	Hardness [kp]	σ_μ	Tensile strength [MPa]	σ_μ	Porosity [-]	σ_μ	Tablet volume [cc]	Tablet Density [g/cc]	σ_μ
0.0	0	N/A	0.0	0.00	0.00	0.00	N/A	0.000	N/A	N/A	0.000
67.5	2000	0.31	6.7	0.21	0.50	0.02	0.22	0.001	0.41	1.23	0.002
202.5	6000	0.27	17.7	0.38	1.32	0.03	0.11	0.001	0.36	1.40	0.002
337.5	10000	0.26	23.6	0.49	1.55	0.04	0.08	0.003	0.34	1.45	0.004
540.0	16000	0.25	30.4	0.26	1.97	0.02	0.06	0.003	0.34	1.48	0.005

Wet Massing Time Experiments using Microcrystalline Cellulose and Lactose 200 mesh, granulated with 5w/v% aqueous PVP:

Liquid level: 30% Wet massing time: 0 minutes
Impeller speed: 285rpm Binder flow rate: 130g/min

Compaction Pressure [MPa]	Compression load [lb_f]	Thickness [cm]	Hardness [kp]	σ_μ	Tensile strength [MPa]	σ_μ	Porosity [-]	σ_μ	Tablet volume [cc]	Tablet Density [g/cc]	σ_μ
0.0	0	N/A	0.0	0.00	0.00	0.00	N/A	0.000	N/A	N/A	0.000
67.5	2000	0.32	9.7	0.29	0.72	0.02	0.26	0.001	0.43	1.17	0.002
202.5	6000	0.28	25.0	0.69	1.86	0.05	0.14	0.001	0.37	1.36	0.002
337.5	10000	0.26	35.4	0.57	2.63	0.04	0.10	0.001	0.35	1.43	0.002
540.0	16000	0.26	45.0	0.23	3.35	0.02	0.08	0.002	0.34	1.46	0.004

Liquid level: 30% Wet massing time: 2 minutes
Impeller speed: 285rpm Binder flow rate: 130g/min

Compaction Pressure [MPa]	Compression load [lb_f]	Thickness [cm]	Hardness [kp]	σ_μ	Tensile strength [MPa]	σ_μ	Porosity [-]	σ_μ	Tablet volume [cc]	Tablet Density [g/cc]	σ_μ
0.0	0	N/A	0.0	0.00	0.00	0.00	N/A	0.000	N/A	N/A	0.000
67.5	2000	0.32	7.2	0.51	0.53	0.04	0.25	0.002	0.42	1.19	0.003
202.5	6000	0.28	20.3	0.19	1.51	0.01	0.14	0.003	0.37	1.36	0.004
337.5	10000	0.26	28.6	0.66	2.13	0.05	0.10	0.002	0.35	1.43	0.003
540.0	16000	0.26	37.6	0.49	2.79	0.04	0.07	0.001	0.34	1.46	0.001

Liquid level: 30% Wet massing time: 6 minutes
Impeller speed: 285rpm Binder flow rate: 130g/min

Compaction Pressure [MPa]	Compression load [lb_f]	Thickness [cm]	Hardness [kp]	σ_μ	Tensile strength [MPa]	σ_μ	Porosity [-]	σ_μ	Tablet volume [cc]	Tablet Density [g/cc]	σ_μ
0.0	0	N/A	0.0	0.00	0.00	0.00	N/A	0.000	N/A	N/A	0.000
67.5	2000	0.31	6.4	0.11	0.47	0.01	0.23	0.002	0.41	1.21	0.004
202.5	6000	0.27	15.6	0.33	1.16	0.02	0.13	0.002	0.36	1.38	0.004
337.5	10000	0.26	23.9	0.32	1.78	0.02	0.09	0.001	0.35	1.44	0.002
540.0	16000	0.26	31.8	0.81	2.37	0.06	0.07	0.001	0.34	1.48	0.002

Wet Massing Time Experiments using Microcrystalline Cellulose and Lactose 200 mesh, granulated with 5w/v% aqueous PVP:

Liquid level: 30% Wet massing time: 10 minutes
Impeller speed: 285rpm Binder flow rate: 130g/min

Compaction Pressure [MPa]	Compression load [lb_f]	Thickness [cm]	Hardness [kp]	σ_μ	Tensile strength [MPa]	σ_μ	Porosity [-]	σ_μ	Tablet volume [cc]	Tablet Density [g/cc]	σ_μ
0.0	0	N/A	0.0	0.00	0.00	0.00	N/A	0.000	N/A	N/A	0.000
67.5	2000	0.31	5.4	0.04	0.40	0.00	0.24	0.001	0.41	1.21	0.002
202.5	6000	0.27	15.2	0.36	1.13	0.03	0.13	0.002	0.36	1.38	0.003
337.5	10000	0.26	21.3	0.17	1.55	0.01	0.09	0.002	0.35	1.44	0.003
540.0	16000	0.26	25.3	0.52	1.97	0.04	0.07	0.002	0.34	1.47	0.003

Liquid level: 30% Wet massing time: 0 minutes
Impeller speed: 285rpm Binder flow rate: 280g/min

Compaction Pressure [MPa]	Compression load [lb_f]	Thickness [cm]	Hardness [kp]	σ_μ	Tensile strength [MPa]	σ_μ	Porosity [-]	σ_μ	Tablet volume [cc]	Tablet Density [g/cc]	σ_μ
0.0	0	N/A	0.0	0.00	0.00	0.00	N/A	0.000	N/A	N/A	0.000
67.5	2000	0.31	11.00	0.18	0.82	0.01	0.24	0.003	0.42	1.20	0.004
202.5	6000	0.27	24.58	0.70	1.83	0.05	0.12	0.002	0.36	1.39	0.003
337.5	10000	0.26	35.08	0.30	2.61	0.02	0.08	0.001	0.34	1.45	0.001
540.0	16000	0.26	43.78	0.67	3.26	0.05	0.07	0.002	0.34	1.48	0.003

Liquid level: 30% Wet massing time: 2 minutes
Impeller speed: 285rpm Binder flow rate: 280g/min

Compaction Pressure [MPa]	Compression load [lb_f]	Thickness [cm]	Hardness [kp]	σ_μ	Tensile strength [MPa]	σ_μ	Porosity [-]	σ_μ	Tablet volume [cc]	Tablet Density [g/cc]	σ_μ
0.0	0	N/A	0.0	0.00	0.00	0.00	N/A	0.000	N/A	N/A	0.000
67.5	2000	0.31	8.04	0.27	0.60	0.02	0.24	0.001	0.42	1.20	0.001
202.5	6000	0.27	19.42	0.24	1.44	0.02	0.12	0.001	0.36	1.38	0.002
337.5	10000	0.26	27.84	0.81	2.07	0.06	0.08	0.001	0.35	1.45	0.001
540.0	16000	0.26	37.58	0.65	2.80	0.05	0.07	0.003	0.34	1.47	0.005

Wet Massing Time Experiments using Microcrystalline Cellulose and Lactose 200 mesh, granulated with 5w/v% aqueous PVP:

Liquid level: 30% Wet massing time: 6 minutes
Impeller speed: 285rpm Binder flow rate: 280g/min

Compaction Pressure [MPa]	Compression load [lb_f]	Thickness [cm]	Hardness [kp]	σ_μ	Tensile strength [MPa]	σ_μ	Porosity [-]	σ_μ	Tablet volume [cc]	Tablet Density [g/cc]	σ_μ
0.0	0	N/A	0.0	0.00	0.00	0.00	N/A	0.000	N/A	N/A	0.000
67.5	2000	0.31	6.00	0.19	0.45	0.01	0.23	0.002	0.41	1.21	0.003
202.5	6000	0.27	15.42	0.45	1.15	0.03	0.13	0.002	0.36	1.38	0.003
337.5	10000	0.26	23.38	0.80	1.74	0.06	0.09	0.003	0.35	1.44	0.004
540.0	16000	0.25	30.56	1.06	2.27	0.08	0.06	0.001	0.34	1.48	0.002

Liquid level: 30% Wet massing time: 10 minutes
Impeller speed: 285rpm Binder flow rate: 280g/min

Compaction Pressure [MPa]	Compression load [lb_f]	Thickness [cm]	Hardness [kp]	σ_μ	Tensile strength [MPa]	σ_μ	Porosity [-]	σ_μ	Tablet volume [cc]	Tablet Density [g/cc]	σ_μ
0.0	0	N/A	0.0	0.00	0.00	0.00	N/A	0.000	N/A	N/A	0.000
67.5	2000	0.31	5.04	0.08	0.38	0.01	0.22	0.002	0.41	1.23	0.003
202.5	6000	0.27	14.36	0.24	1.07	0.02	0.12	0.002	0.36	1.38	0.003
337.5	10000	0.26	22.10	0.80	1.55	0.06	0.09	0.003	0.35	1.44	0.004
540.0	16000	0.25	28.55	1.06	1.97	0.08	0.06	0.001	0.34	1.48	0.002

Liquid level: 30% Wet massing time: 0 minutes
Impeller speed: 600rpm Binder flow rate: 130g/min

Compaction Pressure [MPa]	Compression load [lb_f]	Thickness [cm]	Hardness [kp]	σ_μ	Tensile strength [MPa]	σ_μ	Porosity [-]	σ_μ	Tablet volume [cc]	Tablet Density [g/cc]	σ_μ
0.0	0	N/A	0.0	0.00	0.00	0.00	N/A	0.000	N/A	N/A	0.000
67.5	2000	0.32	7.5	0.49	0.56	0.04	0.26	0.004	0.43	1.17	0.006
202.5	6000	0.28	20.2	0.77	1.50	0.06	0.14	0.001	0.37	1.36	0.002
337.5	10000	0.26	29.0	0.82	2.15	0.06	0.09	0.002	0.35	1.43	0.003
540.0	16000	0.26	39.7	1.41	2.95	0.10	0.08	0.001	0.34	1.46	0.002

Wet Massing Time Experiments using Microcrystalline Cellulose and Lactose 200 mesh, granulated with 5w/v% aqueous PVP:

Liquid level: 30% Wet massing time: 2 minutes
Impeller speed: 600rpm Binder flow rate: 130g/min

Compaction Pressure [MPa]	Compression load [lb_f]	Thickness [cm]	Hardness [kp]	σ_μ	Tensile strength [MPa]	σ_μ	Porosity [-]	σ_μ	Tablet volume [cc]	Tablet Density [g/cc]	σ_μ
0.0	0	N/A	0.0	0.00	0.00	0.00	N/A	0.000	N/A	N/A	0.000
67.5	2000	0.30	4.6	0.11	0.34	0.01	0.21	0.002	0.40	1.25	0.003
202.5	6000	0.27	14.0	0.41	1.04	0.03	0.11	0.001	0.36	1.40	0.002
337.5	10000	0.26	21.4	0.42	1.60	0.03	0.08	0.002	0.34	1.46	0.003
540.0	16000	0.25	28.5	0.69	2.12	0.05	0.06	0.003	0.34	1.48	0.004

Liquid level: 30% Wet massing time: 6 minutes
Impeller speed: 600rpm Binder flow rate: 130g/min

Compaction Pressure [MPa]	Compression load [lb_f]	Thickness [cm]	Hardness [kp]	σ_μ	Tensile strength [MPa]	σ_μ	Porosity [-]	σ_μ	Tablet volume [cc]	Tablet Density [g/cc]	σ_μ
0.0	0	N/A	0.0	0.00	0.00	0.00	N/A	0.000	N/A	N/A	0.000
67.5	2000	0.29	4.7	0.22	0.35	0.02	0.19	0.004	0.39	1.28	0.006
202.5	6000	0.27	12.5	0.26	0.93	0.02	0.11	0.002	0.35	1.41	0.003
337.5	10000	0.26	18.9	0.71	1.40	0.05	0.08	0.003	0.34	1.46	0.004
540.0	16000	0.26	23.4	0.38	1.74	0.03	0.07	0.004	0.34	1.47	0.007

Liquid level: 30% Wet massing time: 10 minutes
Impeller speed: 600rpm Binder flow rate: 130g/min

Compaction Pressure [MPa]	Compression load [lb_f]	Thickness [cm]	Hardness [kp]	σ_μ	Tensile strength [MPa]	σ_μ	Porosity [-]	σ_μ	Tablet volume [cc]	Tablet Density [g/cc]	σ_μ
0.0	0	N/A	0.0	0.00	0.00	0.00	N/A	0.000	N/A	N/A	0.000
67.5	2000	0.30	3.4	0.09	0.26	0.01	0.20	0.002	0.39	1.27	0.003
202.5	6000	0.27	11.0	0.30	0.82	0.02	0.11	0.001	0.35	1.41	0.001
337.5	10000	0.26	18.8	0.25	1.55	0.02	0.08	0.002	0.34	1.46	0.003
540.0	16000	0.25	24.0	0.38	1.97	0.03	0.06	0.003	0.34	1.49	0.005

Wet Massing Time Experiments using Microcrystalline Cellulose and Lactose 200 mesh, granulated with 5w/v% aqueous PVP:

Liquid level: 40% Wet massing time: 0 minutes
Impeller speed: 285rpm Binder flow rate: 130g/min

Compaction Pressure [MPa]	Compression load [lb_f]	Thickness [cm]	Hardness [kp]	σ_μ	Tensile strength [MPa]	σ_μ	Porosity [-]	σ_μ	Tablet volume [cc]	Tablet Density [g/cc]	σ_μ
0.0	0	N/A	0	0.00	0.00	0.00	N/A	0.000	N/A	N/A	0.000
67.5	2000	0.32	10.3	0.27	0.77	0.02	0.25	0.002	0.42	1.19	0.004
202.5	6000	0.27	27.2	0.55	2.02	0.04	0.13	0.002	0.36	1.38	0.002
337.5	10000	0.26	36.5	0.59	2.71	0.04	0.08	0.002	0.34	1.45	0.003
540.0	16000	0.25	44.2	0.56	3.29	0.04	0.06	0.001	0.34	1.48	0.001

Liquid level: 40% Wet massing time: 2 minutes
Impeller speed: 285rpm Binder flow rate: 130g/min

Compaction Pressure [MPa]	Compression load [lb_f]	Thickness [cm]	Hardness [kp]	σ_μ	Tensile strength [MPa]	σ_μ	Porosity [-]	σ_μ	Tablet volume [cc]	Tablet Density [g/cc]	σ_μ
0.0	0	N/A	0	0.00	0.00	0.00	N/A	0.000	N/A	N/A	0.000
67.5	2000	0.31	7.64	0.32	0.57	0.02	0.24	0.001	0.42	1.20	0.002
202.5	6000	0.27	19.96	0.51	1.49	0.04	0.13	0.003	0.36	1.38	0.004
337.5	10000	0.26	29.62	1.01	2.20	0.08	0.09	0.001	0.35	1.44	0.002
540.0	16000	0.26	35.88	0.74	2.67	0.05	0.07	0.001	0.34	1.48	0.001

Liquid level: 40% Wet massing time: 6 minutes
Impeller speed: 285rpm Binder flow rate: 130g/min

Compaction Pressure [MPa]	Compression load [lb_f]	Thickness [cm]	Hardness [kp]	σ_μ	Tensile strength [MPa]	σ_μ	Porosity [-]	σ_μ	Tablet volume [cc]	Tablet Density [g/cc]	σ_μ
0.0	0	N/A	0	0.00	0.00	0.00	N/A	0.000	N/A	N/A	0.000
67.5	2000	0.31	4.70	0.22	0.35	0.02	0.23	0.004	0.41	1.21	0.006
202.5	6000	0.27	13.58	0.41	1.01	0.03	0.12	0.002	0.36	1.39	0.003
337.5	10000	0.26	22.46	0.21	1.67	0.02	0.08	0.002	0.34	1.46	0.003
540.0	16000	0.26	27.36	0.19	2.04	0.01	0.07	0.002	0.34	1.48	0.003

Wet Massing Time Experiments using Microcrystalline Cellulose and Lactose 200 mesh, granulated with 5w/v% aqueous PVP:

Liquid level: 40% Wet massing time: 10 minutes
Impeller speed: 285rpm Binder flow rate: 130g/min

Compaction Pressure [MPa]	Compression load [lb_f]	Thickness [cm]	Hardness [kp]	σ_μ	Tensile strength [MPa]	σ_μ	Porosity [-]	σ_μ	Tablet volume [cc]	Tablet Density [g/cc]	σ_μ
0.0	0	N/A	0	0.00	0.00	0.00	N/A	0.000	N/A	N/A	0.000
67.5	2000	0.31	3.98	0.11	0.30	0.01	0.24	0.002	0.41	1.21	0.003
202.5	6000	0.27	12.80	0.74	0.95	0.06	0.13	0.003	0.36	1.38	0.004
337.5	10000	0.26	20.22	0.47	1.55	0.03	0.08	0.001	0.35	1.45	0.002
540.0	16000	0.26	25.29	0.52	1.97	0.04	0.07	0.002	0.34	1.47	0.003

Liquid level: 40% Wet massing time: 0 minutes
Impeller speed: 285rpm Binder flow rate: 280g/min

Compaction Pressure [MPa]	Compression load [lb_f]	Thickness [cm]	Hardness [kp]	σ_μ	Tensile strength [MPa]	σ_μ	Porosity [-]	σ_μ	Tablet volume [cc]	Tablet Density [g/cc]	σ_μ
0.0	0	N/A	0	0.00	0.00	0.00	N/A	0.000	N/A	N/A	0.000
67.5	2000	0.31	10.54	0.40	0.78	0.03	0.22	0.003	0.41	1.23	0.005
202.5	6000	0.27	27.74	0.35	2.06	0.03	0.11	0.002	0.36	1.41	0.003
337.5	10000	0.26	38.94	0.79	2.90	0.06	0.08	0.001	0.34	1.46	0.002
540.0	16000	0.25	42.34	1.11	3.15	0.08	0.06	0.002	0.34	1.48	0.003

Liquid level: 40% Wet massing time: 2 minutes
Impeller speed: 285rpm Binder flow rate: 280g/min

Compaction Pressure [MPa]	Compression load [lb_f]	Thickness [cm]	Hardness [kp]	σ_μ	Tensile strength [MPa]	σ_μ	Porosity [-]	σ_μ	Tablet volume [cc]	Tablet Density [g/cc]	σ_μ
0.0	0	N/A	0	0.00	0.00	0.00	N/A	0.000	N/A	N/A	0.000
67.5	2000	0.30	7.12	0.20	0.53	0.01	0.20	0.001	0.40	1.26	0.001
202.5	6000	0.27	18.86	0.34	1.40	0.03	0.11	0.002	0.35	1.41	0.004
337.5	10000	0.26	28.02	0.56	2.08	0.04	0.08	0.001	0.34	1.46	0.002
540.0	16000	0.26	34.80	2.15	2.59	0.16	0.07	0.004	0.34	1.47	0.006

Wet Massing Time Experiments using Microcrystalline Cellulose and Lactose 200 mesh, granulated with 5w/v% aqueous PVP:

Liquid level: 40% Wet massing time: 6 minutes
Impeller speed: 285rpm Binder flow rate: 280g/min

Compaction Pressure [MPa]	Compression load [lb_f]	Thickness [cm]	Hardness [kp]	σ_μ	Tensile strength [MPa]	σ_μ	Porosity [-]	σ_μ	Tablet volume [cc]	Tablet Density [g/cc]	σ_μ
0.0	0	N/A	0	0.00	0.00	0.00	N/A	0.000	N/A	N/A	0.000
67.5	2000	0.30	4.58	0.18	0.34	0.01	0.21	0.001	0.40	1.24	0.001
202.5	6000	0.27	13.24	0.17	0.99	0.01	0.11	0.001	0.36	1.40	0.001
337.5	10000	0.26	20.94	0.37	1.56	0.03	0.08	0.002	0.35	1.45	0.003
540.0	16000	0.26	25.30	0.59	1.88	0.04	0.07	0.001	0.34	1.47	0.002

Liquid level: 40% Wet massing time: 10 minutes
Impeller speed: 285rpm Binder flow rate: 280g/min

Compaction Pressure [MPa]	Compression load [lb_f]	Thickness [cm]	Hardness [kp]	σ_μ	Tensile strength [MPa]	σ_μ	Porosity [-]	σ_μ	Tablet volume [cc]	Tablet Density [g/cc]	σ_μ
0.0	0	N/A	0	0.00	0.00	0.00	N/A	0.000	N/A	N/A	0.000
67.5	2000	0.31	3.94	0.11	0.29	0.01	0.23	0.001	0.41	1.22	0.002
202.5	6000	0.27	12.46	0.20	0.93	0.01	0.12	0.002	0.36	1.39	0.003
337.5	10000	0.26	18.20	0.42	1.35	0.03	0.09	0.001	0.35	1.44	0.002
540.0	16000	0.25	22.64	0.54	1.68	0.04	0.06	0.002	0.34	1.48	0.003

Liquid level: 50% Wet massing time: 0 minutes
Impeller speed: 285rpm Binder flow rate: 130g/min

Compaction Pressure [MPa]	Compression load [lb_f]	Thickness [cm]	Hardness [kp]	σ_μ	Tensile strength [MPa]	σ_μ	Porosity [-]	σ_μ	Tablet volume [cc]	Tablet Density [g/cc]	σ_μ
0.0	0	N/A	0	0.00	0.00	0.00	N/A	0.000	N/A	N/A	0.000
67.5	2000	0.32	7.16	0.37	0.53	0.03	0.27	0.001	0.43	1.16	0.001
202.5	6000	0.28	18.46	0.66	1.37	0.05	0.15	0.001	0.37	1.35	0.001
337.5	10000	0.27	29.92	2.02	2.23	0.15	0.11	0.001	0.35	1.41	0.002
540.0	16000	0.26	37.94	0.78	2.82	0.06	0.08	0.002	0.35	1.45	0.004

Wet Massing Time Experiments using Microcrystalline Cellulose and Lactose 200 mesh, granulated with 5w/v% aqueous PVP:

Liquid level: 50% Wet massing time: 6 minutes
Impeller speed: 285rpm Binder flow rate: 130g/min

Compaction Pressure [MPa]	Compression load [lb_f]	Thickness [cm]	Hardness [kp]	σ_μ	Tensile strength [MPa]	σ_μ	Porosity [-]	σ_μ	Tablet volume [cc]	Tablet Density [g/cc]	σ_μ
0.0	0	N/A	0	0.00	0.00	0.00	N/A	0.000	N/A	N/A	0.000
67.5	2000	0.32	4.36	0.46	0.41	0.03	0.26	0.004	0.43	1.16	0.006
202.5	6000	0.28	13.76	0.73	1.21	0.05	0.14	0.002	0.37	1.35	0.004
337.5	10000	0.27	19.26	0.84	1.79	0.06	0.10	0.001	0.35	1.42	0.002
540.0	16000	0.26	25.18	0.85	2.32	0.06	0.07	0.001	0.34	1.46	0.002

Liquid level: 50% Wet massing time: 10 minutes
Impeller speed: 285rpm Binder flow rate: 130g/min

Compaction Pressure [MPa]	Compression load [lb_f]	Thickness [cm]	Hardness [kp]	σ_μ	Tensile strength [MPa]	σ_μ	Porosity [-]	σ_μ	Tablet volume [cc]	Tablet Density [g/cc]	σ_μ
0.0	0	N/A	0	0.00	0.00	0.00	N/A	0.000	N/A	N/A	0.000
67.5	2000	0.32	2.72	0.15	0.20	0.01	0.25	0.002	0.42	1.19	0.003
202.5	6000	0.28	12.60	1.90	0.94	0.14	0.14	0.003	0.37	1.35	0.005
337.5	10000	0.26	17.44	0.87	1.30	0.06	0.10	0.002	0.35	1.42	0.003
540.0	16000	0.26	24.42	2.29	1.82	0.17	0.08	0.004	0.34	1.45	0.006

Liquid level: 50% Wet massing time: 0 minutes
Impeller speed: 285rpm Binder flow rate: 280g/min

Compaction Pressure [MPa]	Compression load [lb_f]	Thickness [cm]	Hardness [kp]	σ_μ	Tensile strength [MPa]	σ_μ	Porosity [-]	σ_μ	Tablet volume [cc]	Tablet Density [g/cc]	σ_μ
0.0	0	N/A	0	0.00	0.00	0.00	N/A	0.000	N/A	N/A	0.000
67.5	2000	0.33	9.54	0.80	0.71	0.06	0.28	0.004	0.44	1.14	0.007
202.5	6000	0.28	28.34	0.68	2.11	0.05	0.16	0.002	0.37	1.33	0.003
337.5	10000	0.27	38.82	2.23	2.89	0.17	0.11	0.004	0.36	1.40	0.006
540.0	16000	0.26	43.20	0.89	3.21	0.07	0.08	0.001	0.34	1.45	0.002

Wet Massing Time Experiments using Microcrystalline Cellulose and Lactose 200 mesh, granulated with 5w/v% aqueous PVP:

Liquid level: 50% Wet massing time: 2 minutes
Impeller speed: 285rpm Binder flow rate: 280g/min

Compaction Pressure [MPa]	Compression load [lb_f]	Thickness [cm]	Hardness [kp]	σ_μ	Tensile strength [MPa]	σ_μ	Porosity [-]	σ_μ	Tablet volume [cc]	Tablet Density [g/cc]	σ_μ
0.0	0	N/A	0	0.00	0.00	0.00	N/A	0.000	N/A	N/A	0.000
67.5	2000	0.32	4.90	0.18	0.36	0.01	0.25	0.003	0.42	1.18	0.005
202.5	6000	0.28	18.10	1.26	1.35	0.09	0.14	0.002	0.37	1.35	0.004
337.5	10000	0.26	24.20	1.93	1.80	0.14	0.10	0.004	0.35	1.43	0.006
540.0	16000	0.26	32.64	2.95	2.43	0.22	0.08	0.006	0.34	1.46	0.010

Liquid level: 50% Wet massing time: 6 minutes
Impeller speed: 285rpm Binder flow rate: 280g/min

Compaction Pressure [MPa]	Compression load [lb_f]	Thickness [cm]	Hardness [kp]	σ_μ	Tensile strength [MPa]	σ_μ	Porosity [-]	σ_μ	Tablet volume [cc]	Tablet Density [g/cc]	σ_μ
0.0	0	N/A	0	0.00	0.00	0.00	N/A	0.000	N/A	N/A	0.000
67.5	2000	0.32	3.88	0.29	0.29	0.02	0.25	0.003	0.42	1.18	0.006
202.5	6000	0.28	14.08	1.08	1.05	0.08	0.14	0.003	0.37	1.36	0.006
337.5	10000	0.26	19.88	2.18	1.48	0.16	0.09	0.002	0.35	1.43	0.003
540.0	16000	0.26	27.36	2.37	2.04	0.18	0.07	0.002	0.34	1.46	0.004

Liquid level: 50% Wet massing time: 10 minutes
Impeller speed: 285rpm Binder flow rate: 280g/min

Compaction Pressure [MPa]	Compression load [lb_f]	Thickness [cm]	Hardness [kp]	σ_μ	Tensile strength [MPa]	σ_μ	Porosity [-]	σ_μ	Tablet volume [cc]	Tablet Density [g/cc]	σ_μ
0.0	0	N/A	0	0.00	0.00	0.00	N/A	0.000	N/A	N/A	0.000
67.5	2000	0.31	3.30	0.11	0.25	0.01	0.24	0.002	0.42	1.20	0.003
202.5	6000	0.28	10.06	0.22	0.75	0.02	0.14	0.001	0.37	1.36	0.002
337.5	10000	0.26	18.38	1.17	1.37	0.09	0.09	0.002	0.35	1.43	0.004
540.0	16000	0.26	24.84	2.77	1.85	0.21	0.07	0.002	0.34	1.47	0.003

Liquid Level Experiments using Microcrystalline Cellulose and Lactose 200 mesh, granulated with 5w/v% aqueous PVP (1L bowl):

Liquid level: 20% Wet massing time: 10 seconds
Impeller speed: 250rpm Binder flow rate: 130g/min

Compaction Pressure [MPa]	Compression load [lb_f]	Thickness [cm]	Hardness [kp]	σ_μ	Tensile strength [MPa]	σ_μ	Porosity [-]	σ_μ	Tablet volume [cc]	Tablet Density [g/cc]	σ_μ
0.0	0	N/A	0	0.00	0.00	0.00	N/A	0.000	N/A	N/A	0.000
67.5	2000	0.31	9.67	0.13	0.72	0.01	0.22	0.001	0.41	1.23	0.001
202.5	6000	0.27	20.87	0.54	1.55	0.04	0.13	0.001	0.36	1.38	0.002
337.5	10000	0.26	31.13	1.09	2.32	0.06	0.10	0.002	0.35	1.43	0.003
540.0	16000	0.26	38.27	0.33	2.85	0.02	0.08	0.001	0.35	1.45	0.002

Liquid level: 30% Wet massing time: 10 seconds
Impeller speed: 250rpm Binder flow rate: 130g/min

Compaction Pressure [MPa]	Compression load [lb_f]	Thickness [cm]	Hardness [kp]	σ_μ	Tensile strength [MPa]	σ_μ	Porosity [-]	σ_μ	Tablet volume [cc]	Tablet Density [g/cc]	σ_μ
0.0	0	N/A	0	0.00	0.00	0.00	N/A	0.000	N/A	N/A	0.000
67.5	2000	0.30	10.57	0.20	0.79	0.02	0.21	0.001	0.40	1.25	0.001
202.5	6000	0.27	24.67	0.43	1.84	0.03	0.11	0.002	0.36	1.40	0.003
337.5	10000	0.26	35.37	0.47	2.63	0.03	0.08	0.001	0.34	1.46	0.002
540.0	16000	0.26	41.37	0.03	3.08	0.00	0.07	0.001	0.34	1.47	0.002

Liquid level: 40% Wet massing time: 10 seconds
Impeller speed: 250rpm Binder flow rate: 130g/min

Compaction Pressure [MPa]	Compression load [lb_f]	Thickness [cm]	Hardness [kp]	σ_μ	Tensile strength [MPa]	σ_μ	Porosity [-]	σ_μ	Tablet volume [cc]	Tablet Density [g/cc]	σ_μ
0.0	0	N/A	0	0.00	0.00	0.00	N/A	0.000	N/A	N/A	0.000
67.5	2000	0.31	9.20	0.70	0.68	0.05	0.23	0.006	0.41	1.22	0.009
202.5	6000	0.27	21.93	0.82	1.63	0.06	0.12	0.003	0.36	1.39	0.005
337.5	10000	0.26	32.53	0.19	2.42	0.01	0.09	0.002	0.35	1.44	0.003
540.0	16000	0.26	39.33	0.79	2.93	0.06	0.07	0.002	0.34	1.48	0.004

Liquid Level Experiments using Microcrystalline Cellulose and Lactose 200 mesh, granulated with 5w/v% aqueous PVP (1L bowl):

Liquid level: 50% Wet massing time: 10 seconds
Impeller speed: 250rpm Binder flow rate: 130g/min

Compaction Pressure [MPa]	Compression load [lb_f]	Thickness [cm]	Hardness [kp]	σ_μ	Tensile strength [MPa]	σ_μ	Porosity [-]	σ_μ	Tablet volume [cc]	Tablet Density [g/cc]	σ_μ
0.0	0	N/A	0	0.00	0.00	0.00	N/A	0.000	N/A	N/A	0.000
67.5	2000	0.30	9.10	0.81	0.68	0.17	0.22	0.002	0.40	1.24	0.003
202.5	6000	0.27	20.60	1.01	1.53	0.08	0.12	0.001	0.36	1.40	0.002
337.5	10000	0.26	25.14	0.98	1.55	0.07	0.08	0.004	0.35	1.45	0.006
540.0	16000	0.26	32.37	2.65	1.97	0.20	0.07	0.002	0.34	1.48	0.003

Liquid level: 20% Wet massing time: 10 seconds
Impeller speed: 400rpm Binder flow rate: 130g/min

Compaction Pressure [MPa]	Compression load [lb_f]	Thickness [cm]	Hardness [kp]	σ_μ	Tensile strength [MPa]	σ_μ	Porosity [-]	σ_μ	Tablet volume [cc]	Tablet Density [g/cc]	σ_μ
0.0	0	N/A	0	0.00	0.00	0.00	N/A	0.000	N/A	N/A	0.000
67.5	2000	0.30	8.17	0.97	0.61	0.07	0.21	0.001	0.40	1.24	0.001
202.5	6000	0.27	22.57	0.84	1.68	0.06	0.12	0.002	0.36	1.39	0.003
337.5	10000	0.26	36.23	1.54	2.70	0.09	0.09	0.001	0.35	1.44	0.002
540.0	16000	0.26	39.70	0.64	2.95	0.05	0.08	0.003	0.34	1.46	0.005

Liquid level: 30% Wet massing time: 10 seconds
Impeller speed: 400rpm Binder flow rate: 130g/min

Compaction Pressure [MPa]	Compression load [lb_f]	Thickness [cm]	Hardness [kp]	σ_μ	Tensile strength [MPa]	σ_μ	Porosity [-]	σ_μ	Tablet volume [cc]	Tablet Density [g/cc]	σ_μ
0.0	0	N/A	0	0.00	0.00	0.00	N/A	0.000	N/A	N/A	0.000
67.5	2000	0.30	7.70	0.20	0.57	0.01	0.21	0.005	0.40	1.25	0.007
202.5	6000	0.27	17.27	0.47	1.28	0.03	0.11	0.002	0.36	1.40	0.003
337.5	10000	0.26	26.77	0.78	1.99	0.06	0.09	0.000	0.35	1.44	0.000
540.0	16000	0.26	31.07	0.52	2.31	0.04	0.07	0.001	0.34	1.48	0.002

Liquid Level Experiments using Microcrystalline Cellulose and Lactose 200 mesh, granulated with 5w/v% aqueous PVP (1L bowl):

Liquid level: 40% Wet massing time: 10 seconds
Impeller speed: 250rpm Binder flow rate: 130g/min

Compaction Pressure [MPa]	Compression load [lb_f]	Thickness [cm]	Hardness [kp]	σ_μ	Tensile strength [MPa]	σ_μ	Porosity [-]	σ_μ	Tablet volume [cc]	Tablet Density [g/cc]	σ_μ
0.0	0	N/A	0	0.00	0.00	0.00	N/A	0.000	N/A	N/A	0.000
67.5	2000	0.30	6.43	0.22	0.48	0.02	0.21	0.005	0.40	1.25	0.008
202.5	6000	0.27	14.33	0.42	1.07	0.03	0.12	0.003	0.36	1.39	0.005
337.5	10000	0.26	21.73	0.15	1.62	0.01	0.09	0.003	0.35	1.44	0.005
540.0	16000	0.26	28.33	0.52	2.11	0.04	0.07	0.001	0.34	1.47	0.002

Liquid level: 50% Wet massing time: 10 seconds
Impeller speed: 250rpm Binder flow rate: 130g/min

Compaction Pressure [MPa]	Compression load [lb_f]	Thickness [cm]	Hardness [kp]	σ_μ	Tensile strength [MPa]	σ_μ	Porosity [-]	σ_μ	Tablet volume [cc]	Tablet Density [g/cc]	σ_μ
0.0	0	N/A	0	0.00	0.00	0.00	N/A	0.000	N/A	N/A	0.000
67.5	2000	0.30	6.03	0.03	0.45	0.00	0.20	0.002	0.40	1.26	0.003
202.5	6000	0.27	13.27	0.32	0.99	0.02	0.11	0.003	0.36	1.40	0.005
337.5	10000	0.26	20.68	0.29	1.55	0.02	0.08	0.001	0.35	1.45	0.002
540.0	16000	0.25	26.29	0.33	1.97	0.02	0.06	0.001	0.34	1.48	0.002

Wet Massing Time Experiments using Microcrystalline Cellulose and Lactose 200 mesh, granulated with 5w/v% aqueous PVP (1L bowl):

Liquid level: 30% Wet massing time: 0 minutes
Impeller speed: 400rpm Binder flow rate: 130g/min

Compaction Pressure [MPa]	Compression load [lb_f]	Thickness [cm]	Hardness [kp]	σ_μ	Tensile strength [MPa]	σ_μ	Porosity [-]	σ_μ	Tablet volume [cc]	Tablet Density [g/cc]	σ_μ
0.0	0	N/A	0	0.00	0.00	0.00	N/A	0.000	N/A	N/A	0.000
67.5	2000	0.30	8.17	0.97	0.61	0.07	0.21	0.001	0.40	1.24	0.001
202.5	6000	0.27	22.57	0.84	1.68	0.06	0.12	0.002	0.36	1.39	0.003
337.5	10000	0.26	36.23	1.54	2.70	0.09	0.09	0.001	0.35	1.44	0.002
540.0	16000	0.26	39.70	0.64	2.95	0.05	0.08	0.003	0.34	1.46	0.005

Wet Massing Time Experiments using Microcrystalline Cellulose and Lactose 200 mesh, granulated with 5w/v% aqueous PVP (1L bowl):

Liquid level: 30% Wet massing time: 2 minutes
Impeller speed: 400rpm Binder flow rate: 130g/min

Compaction Pressure [MPa]	Compression load [lb_f]	Thickness [cm]	Hardness [kp]	σ_μ	Tensile strength [MPa]	σ_μ	Porosity [-]	σ_μ	Tablet volume [cc]	Tablet Density [g/cc]	σ_μ
0.0	0	N/A	0	0.00	0.00	0.00	N/A	0.000	N/A	N/A	0.000
67.5	2000	0.31	7.80	0.20	0.57	0.01	0.21	0.005	0.40	1.25	0.007
202.5	6000	0.27	18.20	0.47	1.28	0.03	0.11	0.002	0.36	1.40	0.003
337.5	10000	0.26	25.93	0.78	1.99	0.06	0.09	0.000	0.35	1.44	0.000
540.0	16000	0.26	32.33	0.52	2.31	0.04	0.07	0.001	0.34	1.48	0.002

Liquid level: 30% Wet massing time: 6 minutes
Impeller speed: 400rpm Binder flow rate: 130g/min

Compaction Pressure [MPa]	Compression load [lb_f]	Thickness [cm]	Hardness [kp]	σ_μ	Tensile strength [MPa]	σ_μ	Porosity [-]	σ_μ	Tablet volume [cc]	Tablet Density [g/cc]	σ_μ
0.0	0	N/A	0	0.00	0.00	0.00	N/A	0.000	N/A	N/A	0.000
67.5	2000	0.30	6.03	0.38	0.45	0.03	0.21	0.007	0.40	1.25	0.012
202.5	6000	0.27	14.10	0.65	1.05	0.05	0.12	0.001	0.36	1.40	0.002
337.5	10000	0.26	20.67	1.19	1.54	0.09	0.09	0.003	0.35	1.44	0.005
540.0	16000	0.26	27.70	0.50	2.06	0.04	0.07	0.001	0.34	1.48	0.002

Liquid level: 30% Wet massing time: 10 minutes
Impeller speed: 400rpm Binder flow rate: 130g/min

Compaction Pressure [MPa]	Compression load [lb_f]	Thickness [cm]	Hardness [kp]	σ_μ	Tensile strength [MPa]	σ_μ	Porosity [-]	σ_μ	Tablet volume [cc]	Tablet Density [g/cc]	σ_μ
0.0	0	N/A	0	0.00	0.00	0.00	N/A	0.000	N/A	N/A	0.000
67.5	2000	0.30	5.47	0.58	0.41	0.10	0.21	0.009	0.40	1.25	0.014
202.5	6000	0.27	13.13	0.39	0.98	0.03	0.11	0.005	0.36	1.40	0.008
337.5	10000	0.26	19.12	0.94	1.37	0.07	0.09	0.002	0.35	1.44	0.003
540.0	16000	0.25	25.48	0.47	1.87	0.03	0.06	0.000	0.34	1.48	0.000

Wet Massing Time Experiments using Microcrystalline Cellulose and Lactose 200 mesh, granulated with 5w/v% aqueous PVP (1L granulator bowl):

Liquid level: 30% Wet massing time: 10 minutes
Impeller speed: 250rpm Binder flow rate: 130g/min

Compaction Pressure [MPa]	Compression load [lb_f]	Thickness [cm]	Hardness [kp]	σ_μ	Tensile strength [MPa]	σ_μ	Porosity [-]	σ_μ	Tablet volume [cc]	Tablet Density [g/cc]	σ_μ
0.0	0	N/A	0	0.00	0.00	0.00	N/A	0.000	N/A	N/A	0.000
67.5	2000	0.31	4.93	0.35	0.37	0.09	0.22	0.004	0.41	1.23	0.006
202.5	6000	0.27	13.07	0.35	0.97	0.03	0.12	0.002	0.36	1.38	0.003
337.5	10000	0.26	19.68	0.68	1.55	0.05	0.09	0.002	0.35	1.43	0.004
540.0	16000	0.26	25.82	0.35	1.97	0.03	0.07	0.002	0.34	1.47	0.003

Liquid level: 30% Wet massing time: 0 minutes
Impeller speed: 400rpm Binder flow rate: 130g/min

Compaction Pressure [MPa]	Compression load [lb_f]	Thickness [cm]	Hardness [kp]	σ_μ	Tensile strength [MPa]	σ_μ	Porosity [-]	σ_μ	Tablet volume [cc]	Tablet Density [g/cc]	σ_μ
0.0	0	N/A	0	0.00	0.00	0.00	N/A	0.000	N/A	N/A	0.000
67.5	2000	0.30	8.17	0.97	0.61	0.07	0.21	0.001	0.40	1.24	0.001
202.5	6000	0.27	22.57	0.84	1.68	0.06	0.12	0.002	0.36	1.39	0.003
337.5	10000	0.26	36.23	1.54	2.70	0.09	0.09	0.001	0.35	1.44	0.002
540.0	16000	0.26	39.70	0.64	2.95	0.05	0.08	0.003	0.34	1.46	0.005

Liquid level: 30% Wet massing time: 2 minutes
Impeller speed: 400rpm Binder flow rate: 130g/min

Compaction Pressure [MPa]	Compression load [lb_f]	Thickness [cm]	Hardness [kp]	σ_μ	Tensile strength [MPa]	σ_μ	Porosity [-]	σ_μ	Tablet volume [cc]	Tablet Density [g/cc]	σ_μ
0.0	0	N/A	0	0.00	0.00	0.00	N/A	0.000	N/A	N/A	0.000
67.5	2000	0.31	7.80	0.20	0.57	0.01	0.21	0.005	0.40	1.25	0.007
202.5	6000	0.27	18.20	0.47	1.28	0.03	0.11	0.002	0.36	1.40	0.003
337.5	10000	0.26	25.93	0.78	1.99	0.06	0.09	0.000	0.35	1.44	0.000
540.0	16000	0.26	32.33	0.52	2.31	0.04	0.07	0.001	0.34	1.48	0.002

Wet Massing Time Experiments using Microcrystalline Cellulose and Lactose 200 mesh, granulated with 5w/v% aqueous PVP (1L granulator bowl):

Liquid level: 30% Wet massing time: 6 minutes
Impeller speed: 400rpm Binder flow rate: 130g/min

Compaction Pressure [MPa]	Compression load [lb_f]	Thickness [cm]	Hardness [kp]	σ_μ	Tensile strength [MPa]	σ_μ	Porosity [-]	σ_μ	Tablet volume [cc]	Tablet Density [g/cc]	σ_μ
0.0	0	N/A	0	0.00	0.00	0.00	N/A	0.000	N/A	N/A	0.000
67.5	2000	0.30	6.03	0.38	0.45	0.03	0.21	0.007	0.40	1.25	0.012
202.5	6000	0.27	14.10	0.65	1.05	0.05	0.12	0.001	0.36	1.40	0.002
337.5	10000	0.26	20.67	1.19	1.54	0.09	0.09	0.003	0.35	1.44	0.005
540.0	16000	0.26	27.70	0.50	2.06	0.04	0.07	0.001	0.34	1.48	0.002

Liquid level: 30% Wet massing time: 10 minutes
Impeller speed: 400rpm Binder flow rate: 130g/min

Compaction Pressure [MPa]	Compression load [lb_f]	Thickness [cm]	Hardness [kp]	σ_μ	Tensile strength [MPa]	σ_μ	Porosity [-]	σ_μ	Tablet volume [cc]	Tablet Density [g/cc]	σ_μ
0.0	0	N/A	0	0.00	0.00	0.00	N/A	0.000	N/A	N/A	0.000
67.5	2000	0.30	5.47	0.58	0.41	0.10	0.21	0.009	0.40	1.25	0.014
202.5	6000	0.27	13.13	0.39	0.98	0.03	0.11	0.005	0.36	1.40	0.008
337.5	10000	0.26	19.12	0.94	1.37	0.07	0.09	0.002	0.35	1.44	0.003
540.0	16000	0.25	25.48	0.47	1.87	0.03	0.06	0.000	0.34	1.48	0.000

Liquid Level Experiments using Microcrystalline Cellulose and Lactose 200 mesh, granulated with 5w/v% PVP in Ethanol:

Liquid level: 20% Wet massing time: 10 seconds
Impeller speed: 600rpm Binder flow rate: 130g/min

Compaction Pressure [MPa]	Compression load [lb_f]	Thickness [cm]	Hardness [kp]	σ_μ	Tensile strength [MPa]	σ_μ	Porosity [-]	σ_μ	Tablet volume [cc]	Tablet Density [g/cc]	σ_μ
0.0	0	N/A	0	0.00	0.00	0.00	N/A	0.000	N/A	N/A	0.000
67.5	2000	0.30	11.42	0.17	0.85	0.01	0.21	0.003	0.40	1.24	0.005
202.5	6000	0.27	26.68	0.73	1.99	0.05	0.11	0.003	0.36	1.40	0.005
337.5	10000	0.26	40.66	0.97	3.03	0.07	0.08	0.001	0.34	1.46	0.002
540.0	16000	0.26	45.70	0.00	3.40	0.00	0.07	0.002	0.34	1.47	0.003

Liquid level: 30% Wet massing time: 10 seconds
Impeller speed: 600rpm Binder flow rate: 130g/min

Compaction Pressure [MPa]	Compression load [lb_f]	Thickness [cm]	Hardness [kp]	σ_μ	Tensile strength [MPa]	σ_μ	Porosity [-]	σ_μ	Tablet volume [cc]	Tablet Density [g/cc]	σ_μ
0.0	0	N/A	0	0.00	0.00	0.00	N/A	0.000	N/A	N/A	0.000
67.5	2000	0.30	10.90	0.45	0.81	0.03	0.21	0.002	0.40	1.24	0.004
202.5	6000	0.27	27.18	0.79	2.02	0.06	0.12	0.002	0.36	1.39	0.003
337.5	10000	0.26	41.70	0.87	3.10	0.06	0.08	0.002	0.34	1.45	0.003
540.0	16000	0.26	45.22	0.48	3.36	0.04	0.07	0.004	0.34	1.47	0.006

Liquid level: 40% Wet massing time: 10 seconds
Impeller speed: 600rpm Binder flow rate: 130g/min

Compaction Pressure [MPa]	Compression load [lb_f]	Thickness [cm]	Hardness [kp]	σ_μ	Tensile strength [MPa]	σ_μ	Porosity [-]	σ_μ	Tablet volume [cc]	Tablet Density [g/cc]	σ_μ
0.0	0	N/A	0	0.00	0.00	0.00	N/A	0.000	N/A	N/A	0.000
67.5	2000	0.30	10.24	0.50	0.76	0.04	0.22	0.003	0.40	1.24	0.005
202.5	6000	0.27	27.66	0.99	2.06	0.07	0.11	0.003	0.36	1.40	0.004
337.5	10000	0.26	42.98	1.21	3.20	0.09	0.08	0.002	0.35	1.45	0.004
540.0	16000	0.26	45.70	0.00	3.40	0.00	0.07	0.002	0.34	1.47	0.003

Liquid Level Experiments using Microcrystalline Cellulose and Lactose 200 mesh, granulated with 5w/v% PVP in Ethanol:

Liquid level: 50% Wet massing time: 10 seconds
Impeller speed: 600rpm Binder flow rate: 130g/min

Compaction Pressure [MPa]	Compression load [lb_f]	Thickness [cm]	Hardness [kp]	σ_μ	Tensile strength [MPa]	σ_μ	Porosity [-]	σ_μ	Tablet volume [cc]	Tablet Density [g/cc]	σ_μ
0.0	0	N/A	0	0.00	0.00	0.00	N/A	0.000	N/A	N/A	0.000
67.5	2000	0.31	10.02	0.83	0.75	0.06	0.22	0.002	0.41	1.23	0.004
202.5	6000	0.27	24.70	0.43	1.84	0.03	0.12	0.004	0.36	1.39	0.007
337.5	10000	0.26	38.58	1.94	2.87	0.14	0.09	0.002	0.35	1.44	0.003
540.0	16000	0.26	45.70	0.00	3.40	0.00	0.07	0.007	0.34	1.46	0.012

Wet Massing Time Experiments using Microcrystalline Cellulose and Lactose 200 mesh, granulated with 5w/v% PVP in Ethanol:

Liquid level: 30% Wet massing time: 0 minutes
Impeller speed: 600rpm Binder flow rate: 130g/min

Compaction Pressure [MPa]	Compression load [lb_f]	Thickness [cm]	Hardness [kp]	σ_μ	Tensile strength [MPa]	σ_μ	Porosity [-]	σ_μ	Tablet volume [cc]	Tablet Density [g/cc]	σ_μ
0.0	0	N/A	0	0.00	0.00	0.00	N/A	0.000	N/A	N/A	0.000
67.5	2000	0.30	10.80	0.21	0.80	0.02	0.21	0.002	0.40	1.24	0.004
202.5	6000	0.27	29.03	0.89	2.16	0.07	0.11	0.003	0.36	1.41	0.005
337.5	10000	0.26	41.20	1.24	3.07	0.09	0.08	0.004	0.34	1.46	0.007
540.0	16000	0.26	45.70	0.00	3.40	0.00	0.07	0.001	0.34	1.47	0.002

Liquid level: 30% Wet massing time: 2 minutes
Impeller speed: 600rpm Binder flow rate: 130g/min

Compaction Pressure [MPa]	Compression load [lb_f]	Thickness [cm]	Hardness [kp]	σ_μ	Tensile strength [MPa]	σ_μ	Porosity [-]	σ_μ	Tablet volume [cc]	Tablet Density [g/cc]	σ_μ
0.0	0	N/A	0	0.00	0.00	0.00	N/A	0.000	N/A	N/A	0.000
67.5	2000	0.31	9.37	0.24	0.70	0.02	0.22	0.002	0.41	1.23	0.004
202.5	6000	0.27	23.40	0.80	1.74	0.06	0.11	0.003	0.36	1.40	0.005
337.5	10000	0.26	38.93	0.35	2.90	0.03	0.08	0.003	0.34	1.46	0.005
540.0	16000	0.26	45.40	0.30	3.38	0.02	0.07	0.005	0.34	1.47	0.008

Wet Massing Time Experiments using Microcrystalline Cellulose and Lactose 200 mesh, granulated with 5w/v% PVP in Ethanol:

Liquid level: 30% Wet massing time: 6 minutes
Impeller speed: 600rpm Binder flow rate: 130g/min

Compaction Pressure [MPa]	Compression load [lb_f]	Thickness [cm]	Hardness [kp]	σ_μ	Tensile strength [MPa]	σ_μ	Porosity [-]	σ_μ	Tablet volume [cc]	Tablet Density [g/cc]	σ_μ
0.0	0	N/A	0	0.00	0.00	0.00	N/A	0.000	N/A	N/A	0.000
67.5	2000	0.31	8.47	0.46	0.63	0.03	0.22	0.004	0.41	1.23	0.006
202.5	6000	0.27	23.23	0.22	1.73	0.02	0.12	0.000	0.36	1.39	0.000
337.5	10000	0.26	35.97	0.71	2.68	0.05	0.08	0.003	0.34	1.46	0.005
540.0	16000	0.25	44.77	0.93	3.33	0.07	0.06	0.001	0.34	1.49	0.002

Liquid level: 30% Wet massing time: 10 minutes
Impeller speed: 600rpm Binder flow rate: 130g/min

Compaction Pressure [MPa]	Compression load [lb_f]	Thickness [cm]	Hardness [kp]	σ_μ	Tensile strength [MPa]	σ_μ	Porosity [-]	σ_μ	Tablet volume [cc]	Tablet Density [g/cc]	σ_μ
0.0	0	N/A	0	0.00	0.00	0.00	N/A	0.000	N/A	N/A	0.000
67.5	2000	0.30	9.47	0.15	0.70	0.01	0.21	0.002	0.40	1.25	0.002
202.5	6000	0.27	23.30	0.06	1.73	0.00	0.11	0.001	0.36	1.40	0.002
337.5	10000	0.26	37.77	0.19	2.81	0.01	0.07	0.001	0.34	1.46	0.002
540.0	16000	0.26	42.37	0.15	3.15	0.01	0.07	0.001	0.34	1.47	0.002

Wet Massing Time Experiments using MCC and Lactose (L2M), granulated with 5w/v% aqueous PVP and Calcium Oxide (1L granulator bowl):

Liquid level: 30% Wet massing time: 0 minutes
Impeller speed: 250rpm Binder flow rate: 130g/min

Compaction Pressure [MPa]	Compression load [lb_f]	Thickness [cm]	Hardness [kp]	σ_μ	Tensile strength [MPa]	σ_μ	Porosity [-]	σ_μ	Tablet volume [cc]	Tablet Density [g/cc]	σ_μ
0.0	0	N/A	0	0.00	0.00	0.00	N/A	0.000	N/A	N/A	0.000
67.5	2000	0.31	9.67	0.13	0.72	0.01	0.22	0.001	0.41	1.23	0.001
202.5	6000	0.27	20.87	0.54	1.55	0.04	0.13	0.001	0.36	1.38	0.002
337.5	10000	0.26	31.13	1.09	2.32	0.06	0.10	0.002	0.35	1.43	0.003
540.0	16000	0.26	38.27	0.33	2.85	0.02	0.08	0.001	0.35	1.45	0.002

Wet Massing Time Experiments using MCC and Lactose (L2M), granulated with 5w/v% aqueous PVP and Calcium Oxide (1L granulator bowl):

Liquid level: 30% Wet massing time: 2 minutes
Impeller speed: 250rpm Binder flow rate: 130g/min

Compaction Pressure [MPa]	Compression load [lb_f]	Thickness [cm]	Hardness [kp]	σ_μ	Tensile strength [MPa]	σ_μ	Porosity [-]	σ_μ	Tablet volume [cc]	Tablet Density [g/cc]	σ_μ
0.0	0	N/A	0	0.00	0.00	0.00	N/A	0.000	N/A	N/A	0.000
67.5	2000	0.31	7.80	0.06	0.58	0.00	0.22	0.002	0.41	1.23	0.003
202.5	6000	0.27	18.20	0.00	1.35	0.00	0.12	0.001	0.36	1.39	0.002
337.5	10000	0.26	25.93	0.28	1.93	0.02	0.09	0.003	0.35	1.44	0.005
540.0	16000	0.26	32.33	1.58	2.41	0.12	0.07	0.003	0.34	1.47	0.005

Liquid level: 30% Wet massing time: 6 minutes
Impeller speed: 250rpm Binder flow rate: 130g/min

Compaction Pressure [MPa]	Compression load [lb_f]	Thickness [cm]	Hardness [kp]	σ_μ	Tensile strength [MPa]	σ_μ	Porosity [-]	σ_μ	Tablet volume [cc]	Tablet Density [g/cc]	σ_μ
0.0	0	N/A	0	0.00	0.00	0.00	N/A	0.000	N/A	N/A	0.000
67.5	2000	0.31	5.43	0.15	0.40	0.01	0.22	0.002	0.41	1.23	0.003
202.5	6000	0.27	13.43	0.64	1.00	0.05	0.12	0.002	0.36	1.38	0.003
337.5	10000	0.26	18.90	1.12	1.41	0.08	0.09	0.001	0.35	1.43	0.002
540.0	16000	0.26	28.30	0.40	2.11	0.03	0.07	0.005	0.34	1.46	0.008

Liquid level: 30% Wet massing time: 10 minutes
Impeller speed: 250rpm Binder flow rate: 130g/min

Compaction Pressure [MPa]	Compression load [lb_f]	Thickness [cm]	Hardness [kp]	σ_μ	Tensile strength [MPa]	σ_μ	Porosity [-]	σ_μ	Tablet volume [cc]	Tablet Density [g/cc]	σ_μ
0.0	0	N/A	0	0.00	0.00	0.00	N/A	0.000	N/A	N/A	0.000
67.5	2000	0.31	4.93	0.35	0.37	0.09	0.22	0.004	0.41	1.23	0.006
202.5	6000	0.27	13.07	0.35	0.97	0.03	0.12	0.002	0.36	1.38	0.003
337.5	10000	0.26	19.68	0.68	1.55	0.05	0.09	0.002	0.35	1.43	0.004
540.0	16000	0.26	25.82	0.35	1.97	0.03	0.07	0.002	0.34	1.47	0.003

Wet Massing Time Experiments using MCC and Lactose (L2M), granulated with 5w/v% aqueous PVP and Calcium Oxide (1L granulator bowl):

Liquid level: 30% Wet massing time: 0 minutes
Impeller speed: 400rpm Binder flow rate: 130g/min

Compaction Pressure [MPa]	Compression load [lb_f]	Thickness [cm]	Hardness [kp]	σ_μ	Tensile strength [MPa]	σ_μ	Porosity [-]	σ_μ	Tablet volume [cc]	Tablet Density [g/cc]	σ_μ
0.0	0	N/A	0	0.00	0.00	0.00	N/A	0.000	N/A	N/A	0.000
67.5	2000	0.30	14.60	0.32	1.09	0.02	0.21	0.004	0.40	1.25	0.006
202.5	6000	0.27	27.00	0.86	2.01	0.06	0.12	0.002	0.36	1.40	0.003
337.5	10000	0.26	37.43	1.25	2.79	0.07	0.08	0.003	0.34	1.45	0.005
540.0	16000	0.26	44.63	0.55	3.32	0.04	0.06	0.006	0.34	1.48	0.009

Liquid level: 30% Wet massing time: 2 minutes
Impeller speed: 400rpm Binder flow rate: 130g/min

Compaction Pressure [MPa]	Compression load [lb_f]	Thickness [cm]	Hardness [kp]	σ_μ	Tensile strength [MPa]	σ_μ	Porosity [-]	σ_μ	Tablet volume [cc]	Tablet Density [g/cc]	σ_μ
0.0	0	N/A	0	0.00	0.00	0.00	N/A	0.000	N/A	N/A	0.000
67.5	2000	0.31	8.07	0.20	0.57	0.03	0.22	0.002	0.41	1.23	0.003
202.5	6000	0.27	18.50	0.47	1.28	0.72	0.12	0.000	0.36	1.38	0.000
337.5	10000	0.26	27.97	0.78	1.99	0.84	0.08	0.001	0.35	1.45	0.002
540.0	16000	0.26	38.37	0.52	2.31	0.88	0.07	0.001	0.34	1.48	0.002

Liquid level: 30% Wet massing time: 6 minutes
Impeller speed: 400rpm Binder flow rate: 130g/min

Compaction Pressure [MPa]	Compression load [lb_f]	Thickness [cm]	Hardness [kp]	σ_μ	Tensile strength [MPa]	σ_μ	Porosity [-]	σ_μ	Tablet volume [cc]	Tablet Density [g/cc]	σ_μ
0.0	0	N/A	0	0.00	0.00	0.00	N/A	0.000	N/A	N/A	0.000
67.5	2000	0.30	7.40	0.32	0.55	0.02	0.21	0.001	0.40	1.24	0.001
202.5	6000	0.27	17.30	0.42	1.29	0.03	0.12	0.002	0.36	1.40	0.003
337.5	10000	0.26	24.50	1.00	1.82	0.07	0.08	0.001	0.34	1.45	0.002
540.0	16000	0.26	31.10	0.35	2.31	0.03	0.07	0.004	0.34	1.47	0.006

Wet Massing Time Experiments using MCC and Lactose (L2M), granulated with 5w/v% aqueous PVP and Calcium Oxide (1L bowl):

Liquid level: 30% Wet massing time: 10 minutes
Impeller speed: 400rpm Binder flow rate: 130g/min

Compaction Pressure [MPa]	Compression load [lb_f]	Thickness [cm]	Hardness [kp]	σ_μ	Tensile strength [MPa]	σ_μ	Porosity [-]	σ_μ	Tablet volume [cc]	Tablet Density [g/cc]	σ_μ
0.0	0	N/A	0	0.00	0.00	0.00	N/A	0.000	N/A	N/A	0.000
67.5	2000	0.30	6.70	0.31	0.50	0.16	0.21	0.002	0.40	1.26	0.002
202.5	6000	0.27	16.57	0.09	1.23	0.01	0.11	0.001	0.36	1.40	0.002
337.5	10000	0.26	23.90	0.64	1.78	0.05	0.08	0.001	0.34	1.45	0.002
540.0	16000	0.26	31.87	0.54	2.37	0.04	0.07	0.002	0.34	1.47	0.004

Wet Massing Time Experiments using MCC and Lactose (L2M) granulated with 5w/v% aqueous PVP and Hydrochloric Acid (1L bowl):

Liquid level: 30% Wet massing time: 0 minutes
Impeller speed: 400rpm Binder flow rate: 130g/min

Compaction Pressure [MPa]	Compression load [lb_f]	Thickness [cm]	Hardness [kp]	σ_μ	Tensile strength [MPa]	σ_μ	Porosity [-]	σ_μ	Tablet volume [cc]	Tablet Density [g/cc]	σ_μ
0.0	0	N/A	0	0.00	0.00	0.00	N/A	0.000	N/A	N/A	0.000
67.5	2000	0.30	13.83	0.73	1.03	0.05	0.21	0.001	0.40	1.24	0.001
202.5	6000	0.27	28.60	0.20	2.13	0.01	0.11	0.001	0.36	1.40	0.002
337.5	10000	0.26	36.87	0.39	2.74	0.02	0.07	0.001	0.34	1.46	0.002
540.0	16000	0.26	45.67	0.09	3.40	0.01	0.07	0.002	0.34	1.48	0.003

Liquid level: 30% Wet massing time: 2 minutes
Impeller speed: 400rpm Binder flow rate: 130g/min

Compaction Pressure [MPa]	Compression load [lb_f]	Thickness [cm]	Hardness [kp]	σ_μ	Tensile strength [MPa]	σ_μ	Porosity [-]	σ_μ	Tablet volume [cc]	Tablet Density [g/cc]	σ_μ
0.0	0	N/A	0	0.00	0.00	0.00	N/A	0.000	N/A	N/A	0.000
67.5	2000	0.31	0.30	9.13	0.68	0.02	0.21	0.001	0.40	1.25	0.001
202.5	6000	0.27	0.27	20.40	1.52	0.05	0.11	0.002	0.36	1.40	0.003
337.5	10000	0.26	0.26	29.63	2.20	0.09	0.08	0.001	0.34	1.46	0.002
540.0	16000	0.26	0.26	34.13	2.54	0.04	0.07	0.002	0.34	1.48	0.003

Wet Massing Time Experiments using MCC and Lactose (L2M) granulated with 5w/v% aqueous PVP and Hydrochloric Acid (1L bowl):

Liquid level: 30% Wet massing time: 6 minutes
Impeller speed: 400rpm Binder flow rate: 130g/min

Compaction Pressure [MPa]	Compression load [lb_f]	Thickness [cm]	Hardness [kp]	σ_μ	Tensile strength [MPa]	σ_μ	Porosity [-]	σ_μ	Tablet volume [cc]	Tablet Density [g/cc]	σ_μ
0.0	0	N/A	0	0.00	0.00	0.00	N/A	0.000	N/A	N/A	0.000
67.5	2000	0.30	7.17	0.44	0.53	0.03	0.21	0.002	0.40	1.24	0.004
202.5	6000	0.27	16.80	0.15	1.25	0.01	0.12	0.001	0.36	1.40	0.002
337.5	10000	0.26	24.63	0.12	1.83	0.01	0.09	0.005	0.35	1.44	0.008
540.0	16000	0.25	31.63	0.67	2.35	0.05	0.06	0.002	0.34	1.48	0.004

Liquid level: 30% Wet massing time: 10 minutes
Impeller speed: 400rpm Binder flow rate: 130g/min

Compaction Pressure [MPa]	Compression load [lb_f]	Thickness [cm]	Hardness [kp]	σ_μ	Tensile strength [MPa]	σ_μ	Porosity [-]	σ_μ	Tablet volume [cc]	Tablet Density [g/cc]	σ_μ
0.0	0	N/A	0	0.00	0.00	0.00	N/A	0.000	N/A	N/A	0.000
67.5	2000	0.30	7.70	0.15	0.57	0.14	0.21	0.001	0.40	1.25	0.001
202.5	6000	0.27	17.80	0.35	1.32	0.03	0.11	0.002	0.36	1.41	0.003
337.5	10000	0.26	24.20	0.68	1.80	0.05	0.08	0.001	0.34	1.46	0.002
540.0	16000	0.26	31.97	0.38	2.38	0.03	0.07	0.002	0.34	1.48	0.003

D. UNIFIED COMPACTION CURVE MODELLING DATA

This section presents the modelling work of the Unified Compaction Curve Model on the wet granulation experiments conducted during the project. The modelling of the data comprises of four formulas as described in Equations D.1 to D.4:

$$T = T_{\max}\left(1 - e^{-bP_{WGC}}\right) \tag{D.1}$$

$$T' = T_{\max}\left(e^{-bP_{WGC}} - e^{-b(P'+P_{WGC})}\right) \tag{D.2}$$

$$T_{WGC} = T_{\max}\left(1 - e^{-bP_{WGC}}\right) \tag{D.3}$$

$$T = T_{WGC} + T_{\max}\left(e^{-bP_{WGC}} - e^{-b(P'+P_{WGC})}\right) \tag{D.4}$$

The description for the fitting of the Unified Compaction Curve model to the direct compacted and wet granulated tablet data can be found in *4.3.2 Modelling the Unified Compaction Curve Model in Wet Granulation*. The Unified Compaction Curve model data for tablets produced through direct compaction and wet granulation experiments are presented below:

Direct Compaction modelling data (1:1 MCC/L2M):

T_{max} =	3.54	P_{WGC} =	N/A
b =	0.0062	T_{WGC} =	N/A

Dry compaction *Used Equation(C.1)*			
Compaction pressure [MPa]	Experimental TS [MPa]	Calculated TS [MPa]	$(\text{Exp.-Calc.})^2$
0	0.00	0.00	0.00
67.50	0.98	1.21	0.05
202.51	2.32	2.53	0.04
337.51	3.22	3.10	0.01
405.01	3.32	3.25	0.00
472.52	3.39	3.35	0.00
540.02	3.34	3.41	0.01
550.00	N/A	3.42	N/A
600.00	N/A	3.45	N/A
700	N/A	3.49	N/A
800	N/A	3.51	N/A
900	N/A	3.52	N/A
		Sum of error =	0.123

Liquid level granulation experiments (1:1 MCC/L2M, PVP; 150rpm; 130g/min):

Parameter P_{WGC} and T_{WGC} summary						
LL [%]	T_{max} [MPa]	b [-]	P_{WGC} [MPa]	T_{WGC} [MPa]	WGT [mins]	Rev [-]
DC	3.54	0.0062	N/A	N/A	N/A	N/A
20	3.54	0.0062	22.20	0.46	1.70	255.33
30	3.54	0.0062	23.50	0.48	2.67	399.77
40	3.54	0.0062	23.70	0.48	3.32	498.47
50	3.54	0.0062	28.95	0.58	3.89	583.36
60	3.54	0.0062	48.43	0.92	4.36	654.43

20% LL					
CP [MPa]	Experimental TS [MPa]	Calculated TS' [MPa]	$(Exp.-Calc.)^2$	P' [MPa]	TS [MPa]
0	0.00	0.00	0.00	22.20	0.46
67.50	0.81	1.06	0.06	89.70	1.27
202.51	1.83	2.21	0.14	224.71	2.28
337.51	2.77	2.70	0.00	359.71	3.23
540.02	3.32	2.97	0.12	562.22	3.77
		Sum of error =	0.3238		

30% LL					
CP [MPa]	Experimental TS [MPa]	Calculated TS' [MPa]	$(Exp.-Calc.)^2$	P' [MPa]	TS [MPa]
0	0.00	0.00	0.00	23.50	0.48
67.50	0.77	1.05	0.07	91.00	1.25
202.51	1.81	2.19	0.14	226.00	2.29
337.51	2.63	2.68	0.00	361.01	3.11
540.02	3.35	2.95	0.16	563.52	3.83
		Sum of error =	0.38		

40% LL					
CP [MPa]	Experimental TS [MPa]	Calculated TS' [MPa]	$(Exp.-Calc.)^2$	P' [MPa]	TS [MPa]
0	0.00	0.00	0.00	23.70	0.48
67.50	0.75	1.05	0.08	91.20	1.24
202.51	1.76	2.18	0.18	226.21	2.25
337.51	2.75	2.68	0.01	361.21	3.23
540.02	3.23	2.94	0.08	563.72	3.72
		Sum of error =	0.35		

50% LL					
CP [MPa]	Experimental TS [MPa]	Calculated TS' [MPa]	$(Exp.-Calc.)^2$	P' [MPa]	TS [MPa]
0	0.00	0.00	0.00	28.95	0.58
67.50	0.75	1.01	0.07	96.45	1.34
202.51	1.72	2.11	0.16	231.46	2.30
337.51	2.55	2.59	0.00	366.46	3.13
540.02	3.25	2.85	0.16	568.97	3.84
		Sum of error =	0.39		

Liquid level granulation experiments (1:1 MCC/L2M, PVP; 285rpm; 130g/min):

Parameter P_{WGC} and T_{WGC} summary						
LL [%]	T_{max} [MPa]	b [-]	P_{WGC} [MPa]	T_{WGC} [MPa]	WGT [mins]	Rev [-]
DC	3.54	0.0062	N/A	N/A	N/A	N/A
20	3.54	0.0062	27.34	0.55	1.70	485.13
30	3.54	0.0062	29.06	0.58	2.67	759.56
40	3.54	0.0062	52.44	0.98	3.32	947.10
50	3.54	0.0062	49.95	0.94	3.89	1108.39
60	3.54	0.0062	48.43	0.92	4.36	1243.41

20% LL					
CP [MPa]	Experimental TS [MPa]	Calculated TS' [MPa]	$(Exp.-Calc.)^2$	P' [MPa]	TS [MPa]
0	0.00	0.00	0.00	27.34	0.55
67.50	0.83	1.02	0.04	94.84	1.38
202.51	1.86	2.14	0.08	229.85	2.41
337.51	2.49	2.62	0.02	364.85	3.04
540.02	3.36	2.88	0.24	567.36	3.92
		Sum of error =	0.3663		

30% LL					
CP [MPa]	Experimental TS [MPa]	Calculated TS' [MPa]	$(Exp.-Calc.)^2$	P' [MPa]	TS [MPa]
0	0.00	0.00	0.00	29.06	0.58
67.50	0.74	1.01	0.07	96.56	1.32
202.51	1.80	2.11	0.10	231.56	2.39
337.51	2.44	2.59	0.02	366.57	3.03
540.02	3.30	2.85	0.20	569.07	3.88
		Sum of error =	0.39		

40% LL					
CP [MPa]	Experimental TS [MPa]	Calculated TS' [MPa]	$(Exp.-Calc.)^2$	P' [MPa]	TS [MPa]
0	0.00	0.00	0.00	52.44	0.98
67.50	0.59	0.87	0.08	119.94	1.57
202.51	1.48	1.83	0.12	254.95	2.46
337.51	2.22	2.24	0.00	389.95	3.20
540.02	2.75	2.46	0.08	592.46	3.74
		Sum of error =	0.29		

50% LL					
CP [MPa]	Experimental TS [MPa]	Calculated TS' [MPa]	$(Exp.-Calc.)^2$	P' [MPa]	TS [MPa]
0	0.00	0.00	0.00	49.95	0.94
67.50	0.58	0.89	0.09	117.45	1.52
202.51	1.54	1.86	0.10	252.45	2.48
337.51	2.24	2.27	0.00	387.46	3.18
540.02	2.79	2.50	0.08	589.97	3.73
		Sum of error =	0.28		

Liquid level granulation experiments (1:1 MCC/L2M, PVP; 600rpm; 130g/min):

Parameter P_{WGC} and T_{WGC} summary						
LL [%]	T_{max} [MPa]	b [-]	P_{WGC} [MPa]	T_{WGC} [MPa]	WGT [mins]	Rev [-]
DC	3.54	0.0062	N/A	N/A	N/A	N/A
20	3.54	0.0062	21.20	0.44	1.70	1021.33
30	3.54	0.0062	49.38	0.93	2.67	1599.07
40	3.54	0.0062	77.70	1.35	3.32	1993.90
50	3.54	0.0062	78.20	1.36	3.89	2333.44
60	3.54	0.0062	48.43	0.92	4.36	2617.71

20% LL					
CP [MPa]	Experimental TS [MPa]	Calculated TS' [MPa]	$(Exp.-Calc.)^2$	P' [MPa]	TS [MPa]
0	0.00	0.00	0.00	21.20	0.44
67.50	0.78	1.06	0.08	88.70	1.21
202.51	1.89	2.22	0.11	223.71	2.33
337.51	2.66	2.72	0.00	358.71	3.10
540.02	3.39	2.99	0.16	561.22	3.83
		Sum of error =	0.3546		

30% LL					
CP [MPa]	Experimental TS [MPa]	Calculated TS' [MPa]	$(Exp.-Calc.)^2$	P' [MPa]	TS [MPa]
0	0.00	0.00	0.00	49.38	0.93
67.50	0.62	0.89	0.08	116.89	1.55
202.51	1.59	1.86	0.07	251.89	2.53
337.51	2.29	2.28	0.00	386.89	3.23
540.02	2.80	2.51	0.08	589.40	3.73
		Sum of error =	0.23		

40% LL					
CP [MPa]	Experimental TS [MPa]	Calculated TS' [MPa]	$(Exp.-Calc.)^2$	P' [MPa]	TS [MPa]
0	0.00	0.00	0.00	77.70	1.35
67.50	0.52	0.75	0.05	145.20	1.87
202.51	1.31	1.56	0.06	280.21	2.67
337.51	1.85	1.91	0.00	415.21	3.21
540.02	2.53	2.10	0.18	617.72	3.88
		Sum of error =	0.30		

50% LL					
CP [MPa]	Experimental TS [MPa]	Calculated TS' [MPa]	$(Exp.-Calc.)^2$	P' [MPa]	TS [MPa]
0	0.00	0.00	0.00	78.20	1.36
67.50	0.45	0.75	0.08	145.70	1.82
202.51	1.32	1.56	0.05	280.71	2.68
337.51	1.88	1.91	0.00	415.71	3.24
540.02	2.40	2.10	0.09	618.22	3.76
		Sum of error =	0.23		

60% LL					
CP [MPa]	Experimental TS [MPa]	Calculated TS' [MPa]	$(Exp.-Calc.)^2$	P' [MPa]	TS [MPa]
0.00	0.00	0.00	0.00	48.43	0.92
67.50	0.68	0.90	0.05	115.93	1.60
202.51	1.65	1.87	0.05	250.93	2.57
337.51	2.58	2.30	0.08	385.94	3.50
540.02	3.14	2.52	0.38	588.44	4.06
		Sum of error =	0.549		

Liquid level granulation experiments (1:1 MCC/L2M, PVP; 150rpm; 280g/min):

Parameter P_{WGC} and T_{WGC} summary						
LL [%]	T_{max} [MPa]	b [-]	P_{WGC} [MPa]	T_{WGC} [MPa]	WGT [mins]	Rev [-]
DC	3.54	0.0062	N/A	N/A	N/A	N/A
20	3.54	0.0062	18.15	0.38	0.91	136.45
30	3.54	0.0062	15.08	0.32	1.55	232.15
40	3.54	0.0062	18.80	0.39	1.95	292.81
50	3.54	0.0062	25.88	0.53	2.31	346.79
60	3.54	0.0062	5.90	0.13	2.63	394.08

20% LL					
CP [MPa]	Experimental TS [MPa]	Calculated TS' [MPa]	$(Exp.-Calc.)^2$	P' [MPa]	TS [MPa]
0	0.00	0.00	0.00	18.15	0.38
67.50	0.82	1.08	0.07	85.65	1.19
202.51	1.96	2.26	0.09	220.66	2.34
337.51	2.78	2.77	0.00	355.66	3.16
540.02	3.38	3.05	0.11	558.17	3.76
		Sum of error =	0.2691		

30% LL					
CP [MPa]	Experimental TS [MPa]	Calculated TS' [MPa]	$(Exp.-Calc.)^2$	P' [MPa]	TS [MPa]
0	0.00	0.00	0.00	15.08	0.32
67.50	0.97	1.10	0.02	82.58	1.28
202.51	1.95	2.31	0.13	217.58	2.27
337.51	2.88	2.82	0.00	352.59	3.20
540.02	3.37	3.11	0.07	555.09	3.68
		Sum of error =	0.21		

40% LL					
CP [MPa]	Experimental TS [MPa]	Calculated TS' [MPa]	$(Exp.-Calc.)^2$	P' [MPa]	TS [MPa]
0	0.00	0.00	0.00	18.80	0.39
67.50	0.78	1.08	0.09	86.30	1.17
202.51	1.98	2.25	0.07	221.31	2.37
337.51	2.76	2.76	0.00	356.31	3.16
540.02	3.32	3.04	0.08	558.82	3.71
		Sum of error =	0.24		

50% LL					
CP [MPa]	Experimental TS [MPa]	Calculated TS' [MPa]	$(Exp.-Calc.)^2$	P' [MPa]	TS [MPa]
0	0.00	0.00	0.00	25.88	0.53
67.50	0.80	1.03	0.05	93.38	1.32
202.51	1.86	2.16	0.09	228.38	2.39
337.51	2.72	2.64	0.01	363.39	3.25
540.02	3.14	2.90	0.05	565.89	3.66
		Sum of error =	0.20		

60% LL					
CP [MPa]	Experimental TS [MPa]	Calculated TS' [MPa]	$(Exp.-Calc.)^2$	P' [MPa]	TS [MPa]
0.00	0.00	0.00	0.00	5.90	0.13
67.50	0.90	1.17	0.07	73.40	1.03
202.51	2.37	2.44	0.01	208.41	2.49
337.51	3.04	2.99	0.00	343.41	3.17
540.02	3.39	3.29	0.01	545.92	3.51
		Sum of error =	0.087		

Liquid level granulation experiments (1:1 MCC/L2M, PVP; 285rpm; 280g/min):

Parameter P_{WGC} and T_{WGC} summary						
LL [%]	T_{max} [MPa]	b [-]	P_{WGC} [MPa]	T_{WGC} [MPa]	WGT [mins]	Rev [-]
DC	3.54	0.0062	N/A	N/A	N/A	N/A
20	3.54	0.0062	16.12	0.34	0.91	259.26
30	3.54	0.0062	23.70	0.48	1.55	441.08
40	3.54	0.0062	27.60	0.56	1.95	556.35
50	3.54	0.0062	44.40	0.85	2.31	658.91
60	3.54	0.0062	25.95	0.53	2.63	748.76

20% LL					
CP [MPa]	Experimental TS [MPa]	Calculated TS' [MPa]	$(Exp.-Calc.)^2$	P' [MPa]	TS [MPa]
0	0.00	0.00	0.00	16.12	0.34
67.50	0.89	1.10	0.04	83.62	1.23
202.51	2.01	2.29	0.08	218.63	2.35
337.51	2.76	2.81	0.00	353.63	3.10
540.02	3.40	3.09	0.10	556.14	3.74
		Sum of error =	0.2203		

30% LL					
CP [MPa]	Experimental TS [MPa]	Calculated TS' [MPa]	$(Exp.-Calc.)^2$	P' [MPa]	TS [MPa]
0	0.00	0.00	0.00	23.70	0.48
67.50	0.75	1.05	0.09	91.20	1.23
202.51	1.89	2.18	0.09	226.21	2.38
337.51	2.56	2.68	0.01	361.21	3.04
540.02	3.33	2.94	0.15	563.72	3.82
		Sum of error =	0.34		

40% LL					
CP [MPa]	Experimental TS [MPa]	Calculated TS' [MPa]	$(Exp.-Calc.)^2$	P' [MPa]	TS [MPa]
0	0.00	0.00	0.00	27.60	0.56
67.50	0.78	1.02	0.06	95.10	1.33
202.51	1.80	2.13	0.11	230.11	2.36
337.51	2.54	2.61	0.01	365.11	3.09
540.02	3.10	2.87	0.05	567.62	3.66
		Sum of error =	0.23		

50% LL					
CP [MPa]	Experimental TS [MPa]	Calculated TS' [MPa]	$(Exp.-Calc.)^2$	P' [MPa]	TS [MPa]
0	0.00	0.00	0.00	44.40	0.85
67.50	0.69	0.92	0.05	111.90	1.54
202.51	1.72	1.92	0.04	246.91	2.57
337.51	2.49	2.35	0.02	381.91	3.34
540.02	2.74	2.59	0.02	584.42	3.59
		Sum of error =	0.14		

60% LL					
CP [MPa]	Experimental TS [MPa]	Calculated TS' [MPa]	$(Exp.-Calc.)^2$	P' [MPa]	TS [MPa]
0.00	0.00	0.00	0.00	25.95	0.53
67.50	0.86	1.03	0.03	93.45	1.38
202.51	1.95	2.15	0.04	228.46	2.48
337.51	2.68	2.64	0.00	363.46	3.21
540.02	3.06	2.90	0.02	565.97	3.59
		Sum of error =	0.098		

Liquid level granulation experiments (1:1 MCC/L2M, PVP; 600rpm; 280g/min):

Parameter P_{WGC} and T_{WGC} summary						
LL [%]	T_{max} [MPa]	b [-]	P_{WGC} [MPa]	T_{WGC} [MPa]	WGT [mins]	Rev [-]
DC	3.54	0.0062	N/A	N/A	N/A	N/A
20	3.54	0.0062	23.20	0.48	0.91	545.81
30	3.54	0.0062	48.26	0.92	1.55	928.60
40	3.54	0.0062	61.05	1.12	1.95	1171.26
50	3.54	0.0062	43.43	0.84	2.31	1387.17

20% LL					
CP [MPa]	Experimental TS [MPa]	Calculated TS' [MPa]	$(Exp.-Calc.)^2$	P' [MPa]	TS [MPa]
0	0.00	0.00	0.00	23.20	0.48
67.50	0.75	1.05	0.09	90.70	1.23
202.51	1.86	2.19	0.11	225.71	2.34
337.51	2.64	2.69	0.00	360.71	3.11
540.02	3.36	2.95	0.17	563.22	3.84
		Sum of error =	0.3673		

30% LL					
CP [MPa]	Experimental TS [MPa]	Calculated TS' [MPa]	$(Exp.-Calc.)^2$	P' [MPa]	TS [MPa]
0	0.00	0.00	0.00	48.26	0.92
67.50	0.61	0.90	0.08	115.76	1.53
202.51	1.54	1.88	0.11	250.77	2.46
337.51	2.17	2.30	0.02	385.77	3.08
540.02	2.99	2.53	0.21	588.28	3.90
		Sum of error =	0.42		

40% LL					
CP [MPa]	Experimental TS [MPa]	Calculated TS' [MPa]	$(Exp.-Calc.)^2$	P' [MPa]	TS [MPa]
0	0.00	0.00	0.00	61.05	1.12
67.50	0.55	0.83	0.08	128.55	1.66
202.51	1.41	1.73	0.10	263.56	2.53
337.51	2.20	2.12	0.01	398.56	3.31
540.02	2.69	2.33	0.13	601.07	3.81
		Sum of error =	0.31		

50% LL					
CP [MPa]	Experimental TS [MPa]	Calculated TS' [MPa]	$(Exp.-Calc.)^2$	P' [MPa]	TS [MPa]
0	0.00	0.00	0.00	43.43	0.84
67.50	0.64	0.93	0.08	110.93	1.48
202.51	1.71	1.93	0.05	245.94	2.55
337.51	2.27	2.37	0.01	380.94	3.10
540.02	2.88	2.60	0.07	583.45	3.71
		Sum of error =	0.22		

Wet massing time granulation experiments (1:1 MCC/L2M, PVP; 20%LL; 285rpm; 130g/min):

Parameter P_{WGC} and T_{WGC} summary						
WMT [mins]	T_{max} [MPa]	b [-]	P_{WGC} [MPa]	T_{WGC} [MPa]	WGT [mins]	Rev [-]
DC	3.54	0.0062	N/A	N/A	N/A	N/A
0	3.54	0.0062	21.20	0.44	1.54	437.63
2	3.54	0.0062	29.19	0.59	3.54	1007.63
6	3.54	0.0062	42.35	0.82	7.54	2147.63
10	3.54	0.0062	48.73	0.92	11.54	3287.63

0 mins WMT					
CP [MPa]	Experimental TS [MPa]	Calculated TS' [MPa]	$(Exp.-Calc.)^2$	P' [MPa]	TS [MPa]
0	0.00	0.00	0.00	21.20	0.44
67.50	0.74	1.06	0.10	88.70	1.18
202.51	1.84	2.22	0.14	223.71	2.28
337.51	2.71	2.72	0.00	358.71	3.14
540.02	3.41	2.99	0.17	561.22	3.84
		Sum of error =	0.4174		

2 mins WMT					
CP [MPa]	Experimental TS [MPa]	Calculated TS' [MPa]	$(Exp.-Calc.)^2$	P' [MPa]	TS [MPa]
0	0.00	0.00	0.00	29.19	0.59
67.50	0.71	1.01	0.09	96.69	1.30
202.51	1.77	2.11	0.12	231.69	2.36
337.51	2.55	2.59	0.00	366.70	3.13
540.02	3.25	2.85	0.17	569.20	3.84
		Sum of error =	0.37		

6 mins WMT					
CP [MPa]	Experimental TS [MPa]	Calculated TS' [MPa]	$(Exp.-Calc.)^2$	P' [MPa]	TS [MPa]
0	0.00	0.00	0.00	42.35	0.82
67.50	0.63	0.93	0.09	109.85	1.45
202.51	1.56	1.95	0.15	244.85	2.38
337.51	2.42	2.38	0.00	379.86	3.24
540.02	2.98	2.62	0.13	582.37	3.80
		Sum of error =	0.36		

10 mins WMT					
CP [MPa]	Experimental TS [MPa]	Calculated TS' [MPa]	$(Exp.-Calc.)^2$	P' [MPa]	TS [MPa]
0	0.00	0.00	0.00	48.73	0.92
67.50	0.60	0.90	0.09	116.23	1.53
202.51	1.55	1.87	0.10	251.24	2.47
337.51	2.16	2.29	0.02	386.24	3.08
540.02	2.99	2.52	0.22	588.75	3.91
		Sum of error =	0.43		

Wet massing time granulation experiments (1:1 MCC/L2M, PVP; 20%LL; 285rpm; 280g/min):

Parameter P_{WGC} and T_{WGC} summary						
WMT [mins]	T_{max} [MPa]	b [-]	P_{WGC} [MPa]	T_{WGC} [MPa]	WGT [mins]	Rev [-]
DC	3.54	0.0062	N/A	N/A	N/A	N/A
0	3.54	0.0062	23.50	0.48	0.74	211.57
2	3.54	0.0062	30.30	0.61	2.74	781.57
6	3.54	0.0062	40.05	0.78	6.74	1921.57
10	3.54	0.0062	55.50	1.03	10.74	3061.57

0 mins WMT					
CP [MPa]	Experimental TS [MPa]	Calculated TS' [MPa]	$(Exp.-Calc.)^2$	P' [MPa]	TS [MPa]
0	0.00	0.00	0.00	23.50	0.48
67.50	0.82	1.05	0.05	91.00	1.30
202.51	1.79	2.19	0.16	226.01	2.27
337.51	2.65	2.68	0.00	361.01	3.13
540.02	3.32	2.95	0.14	563.52	3.80
		Sum of error =	0.3459		

2 mins WMT					
CP [MPa]	Experimental TS [MPa]	Calculated TS' [MPa]	$(Exp.-Calc.)^2$	P' [MPa]	TS [MPa]
0	0.00	0.00	0.00	30.30	0.61
67.50	0.72	1.00	0.08	97.80	1.33
202.51	1.73	2.10	0.13	232.81	2.34
337.51	2.55	2.57	0.00	367.81	3.16
540.02	3.22	2.83	0.15	570.32	3.82
		Sum of error =	0.36		

6 mins WMT					
CP [MPa]	Experimental TS [MPa]	Calculated TS' [MPa]	$(Exp.-Calc.)^2$	P' [MPa]	TS [MPa]
0	0.00	0.00	0.00	40.05	0.78
67.50	0.66	0.94	0.08	107.55	1.44
202.51	1.63	1.97	0.12	242.56	2.41
337.51	2.32	2.42	0.01	377.56	3.10
540.02	3.04	2.66	0.14	580.07	3.82
		Sum of error =	0.36		

10 mins WMT					
CP [MPa]	Experimental TS [MPa]	Calculated TS' [MPa]	$(Exp.-Calc.)^2$	P' [MPa]	TS [MPa]
0	0.00	0.00	0.00	55.50	1.03
67.50	0.60	0.86	0.07	123.00	1.63
202.51	1.47	1.79	0.10	258.01	2.51
337.51	2.23	2.20	0.00	393.01	3.26
540.02	2.74	2.42	0.11	595.52	3.77
		Sum of error =	0.28		

Wet massing time granulation experiments (1:1 MCC/L2M, PVP; 30%LL; 150rpm; 130g/min):

Parameter P_{WGC} and T_{WGC} summary						
WMT [mins]	T_{max} [MPa]	b [-]	P_{WGC} [MPa]	T_{WGC} [MPa]	WGT [mins]	Rev [-]
DC	3.54	0.0062	N/A	N/A	N/A	N/A
0	3.54	0.0062	25.65	0.52	2.3	345
2	3.54	0.0062	31.15	0.62	4.3	645
6	3.54	0.0062	68.42	1.23	8.3	1245
10	3.54	0.0062	102.25	1.66	12.3	1845

0 mins WMT					
CP [MPa]	Experimental TS [MPa]	Calculated TS' [MPa]	$(Exp.-Calc.)^2$	P' [MPa]	TS [MPa]
0	0.00	0.00	0.00	25.65	0.52
67.50	0.80	1.03	0.05	93.15	1.32
202.51	1.91	2.16	0.06	228.16	2.43
337.51	2.64	2.64	0.00	363.16	3.16
540.02	3.28	2.91	0.13	565.67	3.80
		Sum of error =	0.25		

2 mins WMT					
CP [MPa]	Experimental TS [MPa]	Calculated TS' [MPa]	$(Exp.-Calc.)^2$	P' [MPa]	TS [MPa]
0	0.00	0.00	0.00	31.15	0.62
67.50	0.74	1.00	0.07	98.65	1.36
202.51	1.78	2.09	0.09	233.66	2.41
337.51	2.54	2.56	0.00	368.66	3.16
540.02	3.11	2.81	0.09	571.17	3.73
		Sum of error =	0.25		

6 mins WMT					
CP [MPa]	Experimental TS [MPa]	Calculated TS' [MPa]	$(Exp.-Calc.)^2$	P' [MPa]	TS [MPa]
0	0.00	0.00	0.00	68.42	1.23
67.50	0.54	0.79	0.06	135.93	1.76
202.51	1.31	1.65	0.12	270.93	2.53
337.51	2.03	2.03	0.00	405.94	3.26
540.02	2.56	2.23	0.11	608.44	3.79
		Sum of error =	0.30		

10 mins WMT					
CP [MPa]	Experimental TS [MPa]	Calculated TS' [MPa]	$(Exp.-Calc.)^2$	P' [MPa]	TS [MPa]
0	0.00	0.00	0.00	102.25	1.66
67.50	0.50	0.64	0.02	169.75	2.16
202.51	1.32	1.34	0.00	304.76	2.98
337.51	1.55	1.64	0.01	439.76	3.21
540.02	1.97	1.81	0.03	642.27	3.64
		Sum of error =	0.06		

Wet massing time granulation experiments (1:1 MCC/L2M, PVP; 30%LL; 285rpm; 130g/min):

Parameter P_{WGC} and T_{WGC} summary						
WMT [mins]	T_{max} [MPa]	b [-]	P_{WGC} [MPa]	T_{WGC} [MPa]	WGT [mins]	Rev [-]
DC	3.54	0.0062	N/A	N/A	N/A	N/A
0	3.54	0.0062	24.20	0.49	2.3	655.5
2	3.54	0.0062	53.40	1.00	4.3	1225.5
6	3.54	0.0062	88.80	1.50	8.3	2365.5
10	3.54	0.0062	108.68	1.74	12.3	3505.5

0 mins WMT					
CP [MPa]	Experimental TS [MPa]	Calculated TS' [MPa]	$(Exp.-Calc.)^2$	P' [MPa]	TS [MPa]
0	0.00	0.00	0.00	24.20	0.49
67.50	0.72	1.04	0.10	91.70	1.21
202.51	1.86	2.18	0.10	226.71	2.35
337.51	2.63	2.67	0.00	361.71	3.13
540.02	3.35	2.94	0.17	564.22	3.84
		Sum of error =	0.3781		

2 mins WMT					
CP [MPa]	Experimental TS [MPa]	Calculated TS' [MPa]	$(Exp.-Calc.)^2$	P' [MPa]	TS [MPa]
0	0.00	0.00	0.00	53.40	1.00
67.50	0.53	0.87	0.11	120.90	1.53
202.51	1.51	1.82	0.09	255.91	2.51
337.51	2.13	2.23	0.01	390.91	3.13
540.02	2.79	2.45	0.12	593.42	3.79
		Sum of error =	0.34		

6 mins WMT					
CP [MPa]	Experimental TS [MPa]	Calculated TS' [MPa]	$(Exp.-Calc.)^2$	P' [MPa]	TS [MPa]
0	0.00	0.00	0.00	88.80	1.50
67.50	0.47	0.70	0.05	156.30	1.97
202.51	1.16	1.46	0.09	291.31	2.66
337.51	1.78	1.79	0.00	426.31	3.28
540.02	2.37	1.96	0.16	628.82	3.87
		Sum of error =	0.30		

10 mins WMT					
CP [MPa]	Experimental TS [MPa]	Calculated TS' [MPa]	$(Exp.-Calc.)^2$	P' [MPa]	TS [MPa]
0	0.00	0.00	0.00	108.68	1.74
67.50	0.40	0.62	0.05	176.18	2.14
202.51	1.13	1.29	0.02	311.18	2.87
337.51	1.55	1.58	0.00	446.19	3.29
540.02	1.97	1.74	0.06	648.69	3.71
		Sum of error =	0.13		

Wet massing time granulation experiments (1:1 MCC/L2M, PVP; 30%LL; 285rpm; 280g/min):

Parameter P_{WGC} and T_{WGC} summary						
WMT [mins]	T_{max} [MPa]	b [-]	P_{WGC} [MPa]	T_{WGC} [MPa]	WGT [mins]	Rev [-]
DC	3.54	0.0062	N/A	N/A	N/A	N/A
0	3.54	0.0062	25.88	0.53	1.11	316.35
2	3.54	0.0062	58.30	1.08	3.11	886.35
6	3.54	0.0062	90.90	1.53	7.11	2026.35
10	3.54	0.0062	109.98	1.75	11.11	3166.35

0 mins WMT					
CP [MPa]	Experimental TS [MPa]	Calculated TS' [MPa]	$(Exp.-Calc.)^2$	P' [MPa]	TS [MPa]
0	0.00	0.00	0.00	25.88	0.53
67.50	0.82	1.03	0.05	93.38	1.34
202.51	1.83	2.16	0.11	228.38	2.35
337.51	2.61	2.64	0.00	363.39	3.14
540.02	3.26	2.90	0.12	565.89	3.78
		Sum of error =	0.2776		

2 mins WMT					
CP [MPa]	Experimental TS [MPa]	Calculated TS' [MPa]	$(Exp.-Calc.)^2$	P' [MPa]	TS [MPa]
0	0.00	0.00	0.00	58.30	1.08
67.50	0.60	0.84	0.06	125.80	1.67
202.51	1.44	1.76	0.10	260.81	2.52
337.51	2.07	2.16	0.01	395.81	3.15
540.02	2.80	2.37	0.18	598.32	3.87
		Sum of error =	0.35		

6 mins WMT					
CP [MPa]	Experimental TS [MPa]	Calculated TS' [MPa]	$(Exp.-Calc.)^2$	P' [MPa]	TS [MPa]
0	0.00	0.00	0.00	90.90	1.53
67.50	0.45	0.69	0.06	158.40	1.97
202.51	1.15	1.44	0.08	293.41	2.67
337.51	1.74	1.76	0.00	428.41	3.27
540.02	2.27	1.94	0.11	630.92	3.80
		Sum of error =	0.26		

10 mins WMT					
CP [MPa]	Experimental TS [MPa]	Calculated TS' [MPa]	$(Exp.-Calc.)^2$	P' [MPa]	TS [MPa]
0	0.00	0.00	0.00	109.98	1.75
67.50	0.38	0.61	0.06	177.49	2.13
202.51	1.07	1.28	0.04	312.49	2.82
337.51	1.55	1.56	0.00	447.49	3.30
540.02	1.97	1.72	0.06	650.00	3.73
		Sum of error =	0.16		

Wet massing time granulation experiments (1:1 MCC/L2M, PVP; 30%LL; 600rpm; 130g/min):

Parameter P_{WGC} and T_{WGC} summary						
WMT [mins]	T_{max} [MPa]	b [-]	P_{WGC} [MPa]	T_{WGC} [MPa]	WGT [mins]	Rev [-]
DC	3.54	0.0062	N/A	N/A	N/A	N/A
0	3.54	0.0062	51.13	0.96	2.3	1380
2	3.54	0.0062	104.40	1.69	4.3	2580
6	3.54	0.0062	133.20	1.99	8.3	4980
10	3.54	0.0062	118.61	1.84	12.3	7380

0 mins WMT					
CP [MPa]	Experimental TS [MPa]	Calculated TS' [MPa]	$(Exp.-Calc.)^2$	P' [MPa]	TS [MPa]
0	0.00	0.00	0.00	51.13	0.96
67.50	0.56	0.88	0.10	118.63	1.52
202.51	1.50	1.84	0.12	253.63	2.46
337.51	2.15	2.26	0.01	388.64	3.12
540.02	2.95	2.48	0.22	591.14	3.92
		Sum of error =	0.4532		

2 mins WMT					
CP [MPa]	Experimental TS [MPa]	Calculated TS' [MPa]	$(Exp.-Calc.)^2$	P' [MPa]	TS [MPa]
0	0.00	0.00	0.00	104.40	1.69
67.50	0.34	0.63	0.09	171.90	2.03
202.51	1.04	1.32	0.08	306.91	2.73
337.51	1.60	1.62	0.00	441.91	3.29
540.02	2.12	1.78	0.11	644.42	3.81
		Sum of error =	0.28		

6 mins WMT					
CP [MPa]	Experimental TS [MPa]	Calculated TS' [MPa]	$(Exp.-Calc.)^2$	P' [MPa]	TS [MPa]
0	0.00	0.00	0.00	133.20	1.99
67.50	0.35	0.53	0.03	200.70	2.34
202.51	0.93	1.11	0.03	335.71	2.92
337.51	1.40	1.35	0.00	470.71	3.40
540.02	1.74	1.49	0.06	673.22	3.74
		Sum of error =	0.13		

10 mins WMT					
CP [MPa]	Experimental TS [MPa]	Calculated TS' [MPa]	$(Exp.-Calc.)^2$	P' [MPa]	TS [MPa]
0	0.00	0.00	0.00	118.61	1.84
67.50	0.26	0.58	0.10	186.11	2.10
202.51	0.82	1.21	0.15	321.12	2.67
337.51	1.55	1.48	0.00	456.12	3.39
540.02	1.97	1.63	0.12	658.63	3.82
		Sum of error =	0.38		

Wet massing time granulation experiments (1:1 MCC/L2M, PVP; 40%LL; 285rpm; 130g/min):

Parameter P_{WGC} and T_{WGC} summary						
WMT [mins]	T_{max} [MPa]	b [-]	P_{WGC} [MPa]	T_{WGC} [MPa]	WGT [mins]	Rev [-]
DC	3.54	0.0062	N/A	N/A	N/A	N/A
0	3.54	0.0062	18.87	0.39	3.07	875.26
2	3.54	0.0062	57.22	1.06	5.07	1445.26
6	3.54	0.0062	107.23	1.72	9.07	2585.26
10	3.54	0.0062	120.24	1.86	13.07	3725.26

0 mins WMT					
CP [MPa]	Experimental TS [MPa]	Calculated TS' [MPa]	$(Exp.-Calc.)^2$	P' [MPa]	TS [MPa]
0	0.00	0.00	0.00	18.87	0.39
67.50	0.77	1.08	0.10	86.37	1.16
202.51	2.02	2.25	0.05	221.37	2.41
337.51	2.71	2.76	0.00	356.38	3.11
540.02	3.29	3.03	0.06	558.88	3.68
		Sum of error =	0.2163		

2 mins WMT					
CP [MPa]	Experimental TS [MPa]	Calculated TS' [MPa]	$(Exp.-Calc.)^2$	P' [MPa]	TS [MPa]
0	0.00	0.00	0.00	57.22	1.06
67.50	0.57	0.85	0.08	124.72	1.63
202.51	1.49	1.77	0.08	259.72	2.54
337.51	2.20	2.17	0.00	394.73	3.26
540.02	2.67	2.39	0.08	597.23	3.73
		Sum of error =	0.24		

6 mins WMT					
CP [MPa]	Experimental TS [MPa]	Calculated TS' [MPa]	$(Exp.-Calc.)^2$	P' [MPa]	TS [MPa]
0	0.00	0.00	0.00	107.23	1.72
67.50	0.35	0.62	0.07	174.73	2.07
202.51	1.01	1.30	0.08	309.73	2.73
337.51	1.67	1.59	0.01	444.74	3.39
540.02	2.04	1.75	0.08	647.25	3.76
		Sum of error =	0.25		

10 mins WMT					
CP [MPa]	Experimental TS [MPa]	Calculated TS' [MPa]	$(Exp.-Calc.)^2$	P' [MPa]	TS [MPa]
0	0.00	0.00	0.00	120.24	1.86
67.50	0.30	0.57	0.08	187.75	2.16
202.51	0.95	1.20	0.06	322.75	2.81
337.51	1.55	1.47	0.01	457.76	3.41
540.02	1.97	1.61	0.13	660.26	3.84
		Sum of error =	0.27		

Wet massing time granulation experiments (1:1 MCC/L2M, PVP; 40%LL; 285rpm; 280g/min):

Parameter P_{WGC} and T_{WGC} summary						
WMT [mins]	T_{max} [MPa]	b [-]	P_{WGC} [MPa]	T_{WGC} [MPa]	WGT [mins]	Rev [-]
DC	3.54	0.0062	N/A	N/A	N/A	N/A
0	3.54	0.0062	18.79	0.39	1.43	407.69
2	3.54	0.0062	62.30	1.14	3.43	977.69
6	3.54	0.0062	115.80	1.81	7.43	2117.69
10	3.54	0.0062	131.60	1.98	11.43	3257.69

0 mins WMT					
CP [MPa]	Experimental TS [MPa]	Calculated TS' [MPa]	$(Exp.-Calc.)^2$	P' [MPa]	TS [MPa]
0	0.00	0.00	0.00	18.79	0.39
67.50	0.78	1.08	0.09	86.29	1.17
202.51	2.06	2.25	0.04	221.30	2.45
337.51	2.90	2.76	0.02	356.30	3.29
540.02	3.15	3.04	0.01	558.81	3.54
		Sum of error =	0.1542		

2 mins WMT					
CP [MPa]	Experimental TS [MPa]	Calculated TS' [MPa]	$(Exp.-Calc.)^2$	P' [MPa]	TS [MPa]
0	0.00	0.00	0.00	62.30	1.14
67.50	0.53	0.82	0.09	129.80	1.67
202.51	1.40	1.72	0.10	264.81	2.54
337.51	2.08	2.11	0.00	399.81	3.22
540.02	2.59	2.32	0.07	602.32	3.73
		Sum of error =	0.26		

6 mins WMT					
CP [MPa]	Experimental TS [MPa]	Calculated TS' [MPa]	$(Exp.-Calc.)^2$	P' [MPa]	TS [MPa]
0	0.00	0.00	0.00	115.80	1.81
67.50	0.34	0.59	0.06	183.30	2.16
202.51	0.99	1.23	0.06	318.31	2.80
337.51	1.56	1.51	0.00	453.31	3.37
540.02	1.88	1.66	0.05	655.82	3.70
		Sum of error =	0.17		

10 mins WMT					
CP [MPa]	Experimental TS [MPa]	Calculated TS' [MPa]	$(Exp.-Calc.)^2$	P' [MPa]	TS [MPa]
0	0.00	0.00	0.00	131.60	1.98
67.50	0.29	0.53	0.06	199.10	2.27
202.51	0.93	1.12	0.04	334.11	2.90
337.51	1.35	1.37	0.00	469.11	3.33
540.02	1.68	1.50	0.03	671.62	3.66
		Sum of error =	0.13		

Wet massing time granulation experiments (1:1 MCC/L2M, PVP; 50%LL; 285rpm; 130g/min):

Parameter P_{WGC} and T_{WGC} summary						
WMT [mins]	T_{max} [MPa]	b [-]	P_{WGC} [MPa]	T_{WGC} [MPa]	WGT [mins]	Rev [-]
DC	3.54	0.0062	N/A	N/A	N/A	N/A
0	3.54	0.0062	55.50	1.03	3.84	1094.08
2	3.54	0.0062	84.60	1.45	5.84	1664.08
6	3.54	0.0062	119.85	1.86	9.84	2804.08
10	3.54	0.0062	132.11	1.98	13.84	3944.08

0 mins WMT					
CP [MPa]	Experimental TS [MPa]	Calculated TS' [MPa]	$(Exp.-Calc.)^2$	P' [MPa]	TS [MPa]
0	0.00	0.00	0.00	55.50	1.03
67.50	0.53	0.86	0.11	123.00	1.56
202.51	1.37	1.79	0.18	258.01	2.41
337.51	2.23	2.20	0.00	393.01	3.26
540.02	2.82	2.42	0.17	595.52	3.86
		Sum of error =	0.45		

2 mins WMT					
CP [MPa]	Experimental TS [MPa]	Calculated TS' [MPa]	$(Exp.-Calc.)^2$	P' [MPa]	TS [MPa]
0	0.00	0.00	0.00	84.60	1.45
67.50	0.41	0.72	0.09	152.10	1.86
202.51	1.21	1.50	0.08	287.11	2.66
337.51	1.79	1.83	0.00	422.11	3.24
540.02	2.32	2.02	0.09	624.62	3.77
		Sum of error =	0.27		

6 mins WMT					
CP [MPa]	Experimental TS [MPa]	Calculated TS' [MPa]	$(Exp.-Calc.)^2$	P' [MPa]	TS [MPa]
0	0.00	0.00	0.00	119.85	1.86
67.50	0.32	0.58	0.06	187.35	2.18
202.51	1.02	1.20	0.03	322.36	2.88
337.51	1.43	1.47	0.00	457.36	3.29
540.02	1.87	1.62	0.06	659.87	3.73
		Sum of error =	0.16		

10 mins WMT					
CP [MPa]	Experimental TS [MPa]	Calculated TS' [MPa]	$(Exp.-Calc.)^2$	P' [MPa]	TS [MPa]
0	0.00	0.00	0.00	132.11	1.98
67.50	0.20	0.53	0.11	199.61	2.18
202.51	0.94	1.11	0.03	334.62	2.92
337.51	1.30	1.36	0.00	469.62	3.28
540.02	1.82	1.50	0.10	672.13	3.80
		Sum of error =	0.24		

Wet massing time granulation experiments (1:1 MCC/L2M, PVP; 50%LL; 285rpm; 130g/min):

Parameter P_{WGC} and T_{WGC} summary						
WMT [mins]	T_{max} [MPa]	b [-]	P_{WGC} [MPa]	T_{WGC} [MPa]	WGT [mins]	Rev [-]
DC	3.54	0.0062	N/A	N/A	N/A	N/A
0	3.54	0.0062	17.55	0.37	1.86	528.93
2	3.54	0.0062	79.90	1.38	3.86	1098.93
6	3.54	0.0062	112.48	1.78	7.86	2238.93
10	3.54	0.0062	134.55	2.00	11.86	3378.93

0 mins WMT					
CP [MPa]	Experimental TS [MPa]	Calculated TS' [MPa]	$(Exp.-Calc.)^2$	P' [MPa]	TS [MPa]
0	0.00	0.00	0.00	17.55	0.37
67.50	0.71	1.09	0.14	85.05	1.08
202.51	2.11	2.27	0.03	220.06	2.47
337.51	2.89	2.78	0.01	355.06	3.25
540.02	3.21	3.06	0.02	557.57	3.58
		Sum of error =	0.20		

2 mins WMT					
CP [MPa]	Experimental TS [MPa]	Calculated TS' [MPa]	$(Exp.-Calc.)^2$	P' [MPa]	TS [MPa]
0	0.00	0.00	0.00	79.90	1.38
67.50	0.36	0.74	0.14	147.40	1.75
202.51	1.35	1.54	0.04	282.41	2.73
337.51	1.80	1.89	0.01	417.41	3.19
540.02	2.43	2.08	0.12	619.92	3.81
		Sum of error =	0.31		

6 mins WMT					
CP [MPa]	Experimental TS [MPa]	Calculated TS' [MPa]	$(Exp.-Calc.)^2$	P' [MPa]	TS [MPa]
0	0.00	0.00	0.00	112.48	1.78
67.50	0.29	0.60	0.10	179.98	2.07
202.51	1.05	1.26	0.04	314.98	2.83
337.51	1.48	1.54	0.00	449.99	3.26
540.02	2.04	1.69	0.12	652.49	3.81
		Sum of error =	0.26		

10 mins WMT					
CP [MPa]	Experimental TS [MPa]	Calculated TS' [MPa]	$(Exp.-Calc.)^2$	P' [MPa]	TS [MPa]
0	0.00	0.00	0.00	134.55	2.00
67.50	0.25	0.52	0.08	202.05	2.25
202.51	0.75	1.10	0.12	337.06	2.75
337.51	1.37	1.34	0.00	472.06	3.37
540.02	1.85	1.48	0.14	674.57	3.85
		Sum of error =	0.34		

E. TABLET COMPRESSIBILITY BEHAVIOUR PROFILES

This section presents the compressibility (tablet density as a function of compaction pressure) profiles of tablets produced from various wet granulation conditions. Despite the wide variation in the wet granulation operating conditions, the compressibility profiles are virtually identical with each other.

Compressibility profiles from Chapter 4: Using the Unified Compaction Curve for the Wet Granulation Process

Formulation for the following results: 1:1 microcrystalline cellulose and lactose 200mesh, granulated with 5w/v% PVP.

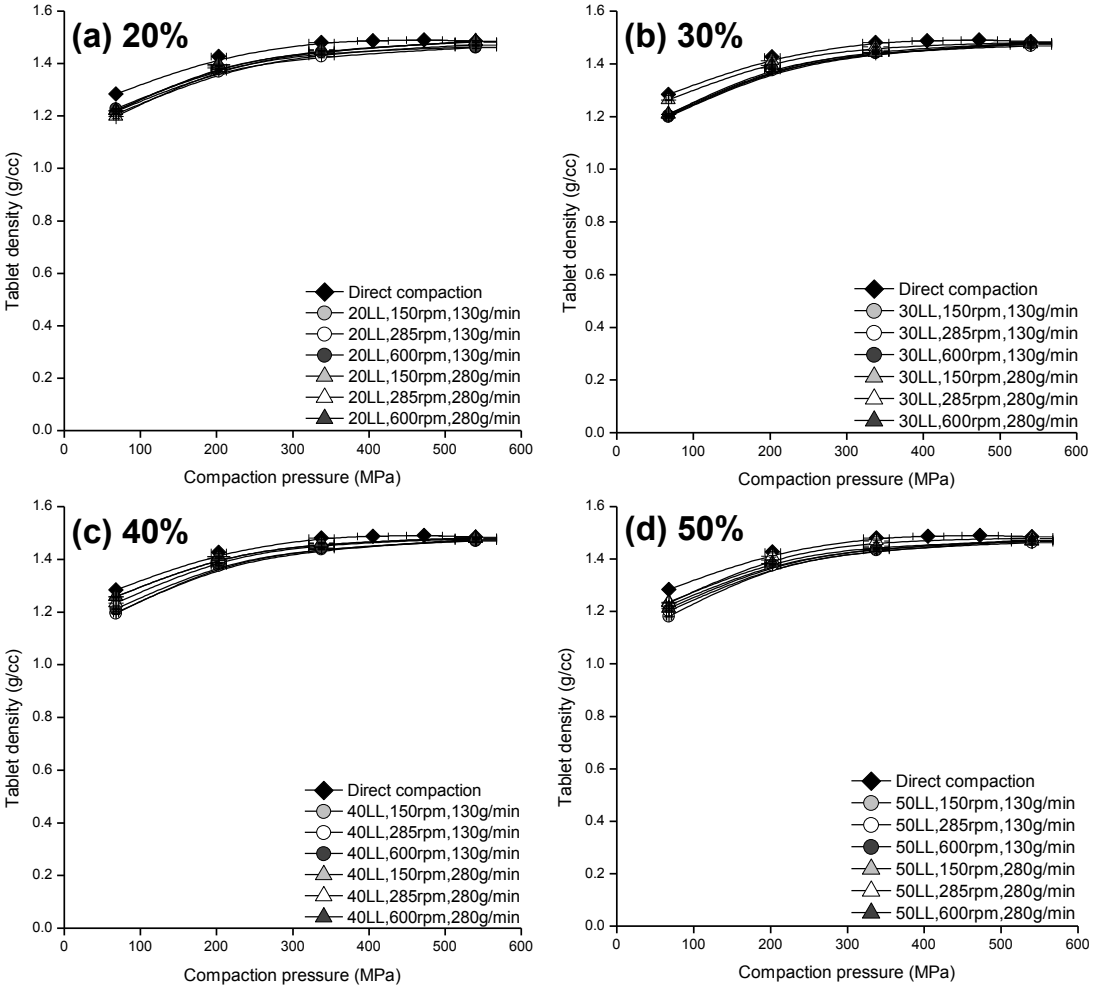

Figure E.1 Compressibility behaviour for granules produced from varying liquid level and binder flow rates (a) 20%; (b) 30%; (c) 40%; and (d) 50%.

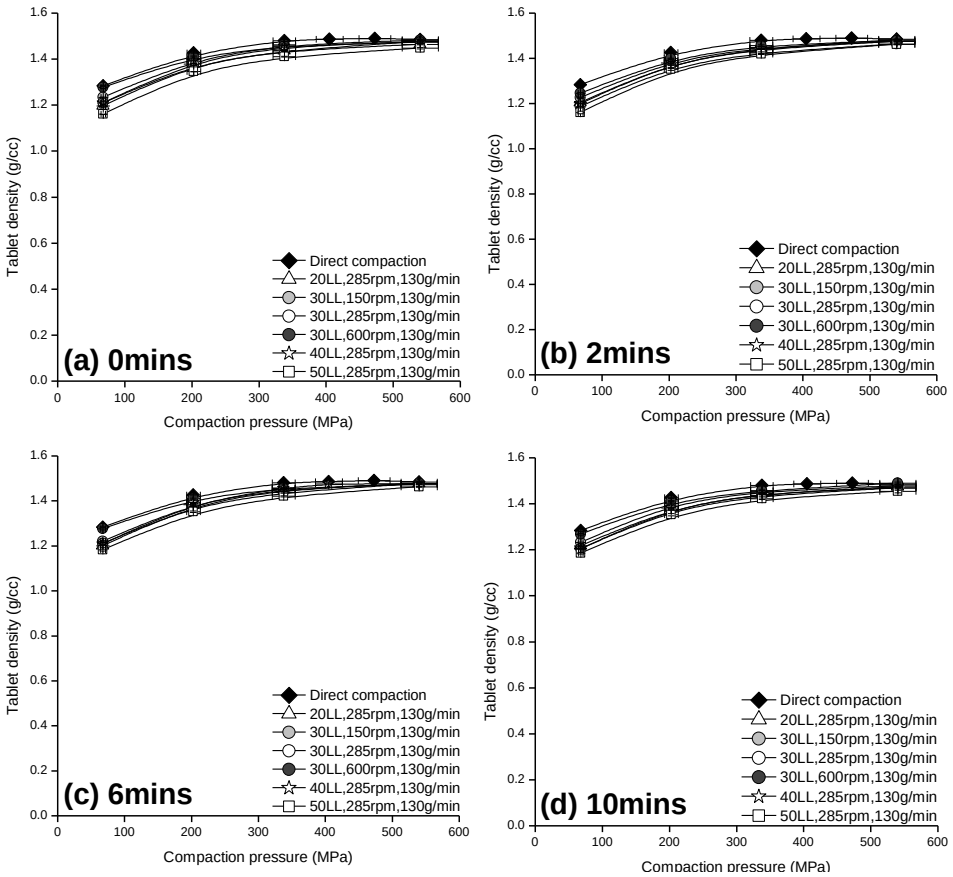

Figure E.2: Compressibility (binder flow rate = 130g/min) behaviour for granules produced from varying wet massing times (a) 0mins; (b) 2mins; (c) 6mins; and (d) 10mins.

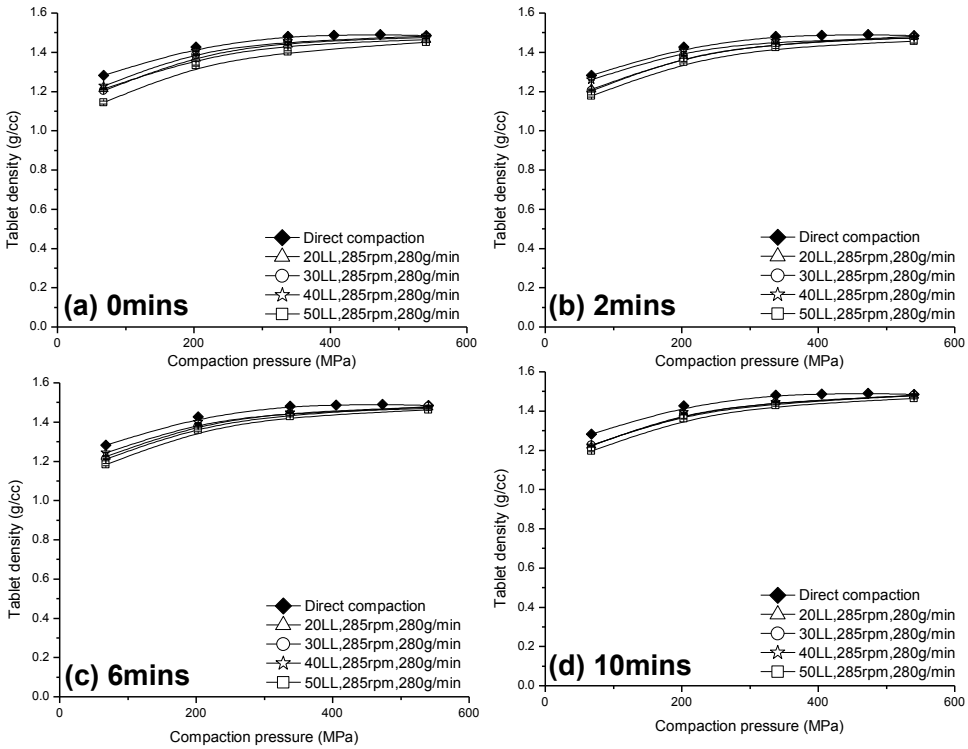

Figure E.3: Compressibility (binder flow rate = 280g/min) behaviour for granules produced from varying wet massing times (a) 0mins; (b) 2mins; (c) 6mins; and (d) 10mins.

Compressibility profiles from Chapter 6: Effect of the Granulator Compaction Pressure and the Liquid Binder on the Microcrystalline Cellulose Material Properties

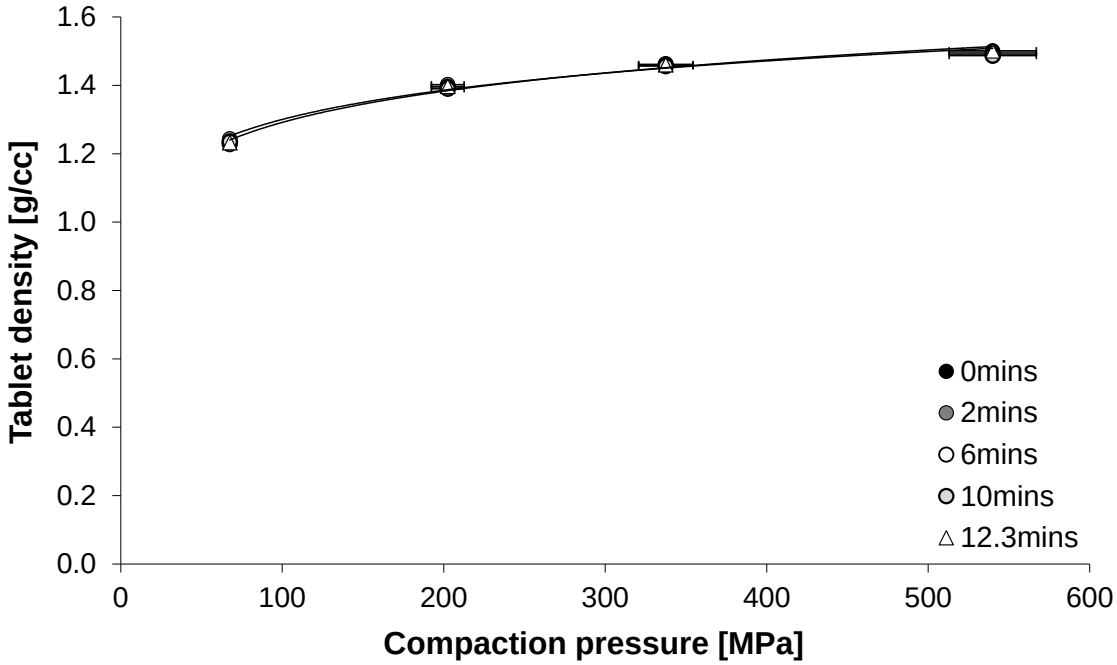

Figure E.4: Compressibility (tablet hardness as a function of tablet density) behaviour for powder dry mixed at: (a) 0mins; (b) 2mins; (c) 6mins; and (d) 10mins. Formulation comprises of 1:1 microcrystalline cellulose and lactose 200 mesh.

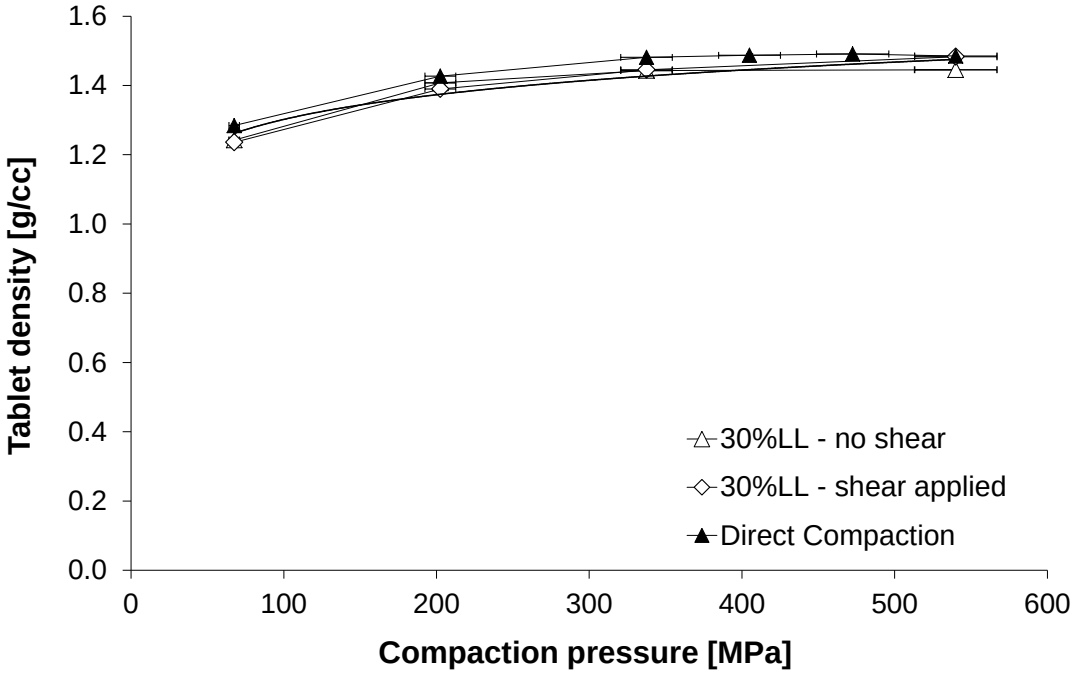

Figure E.5: Compressibility behaviour for tablets produced from powder saturated with 5w/v% PVP liquid binder (with shear and no shear applied) and direct compaction. Formulation comprises of 1:1 microcrystalline cellulose and lactose 200 mesh with 5w/v% PVP aqueous liquid binder added.

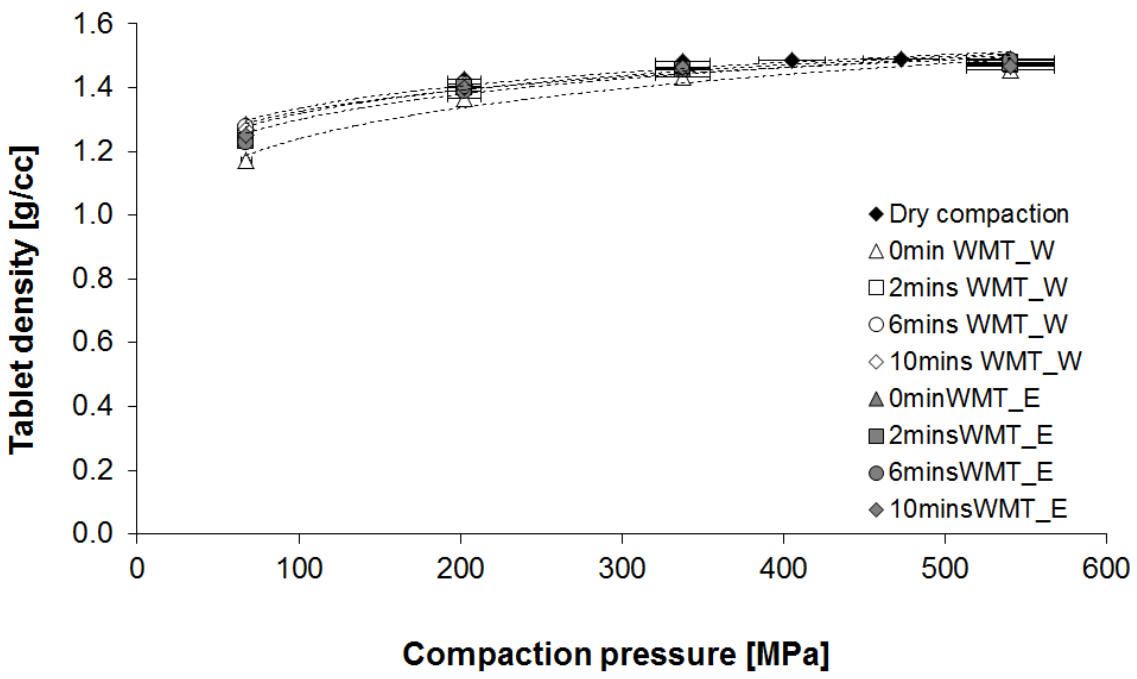

Figure E.6: Compressibility (tablet hardness versus tablet density) behaviour for tablets produced from ethanol-based (E) and water-based (W) liquid binders in wet-massing time (WMT) granulation experiments. Formulation comprises of 1:1 microcrystalline cellulose:lactose 200 mesh and 5w/v% PVP in ethanol.

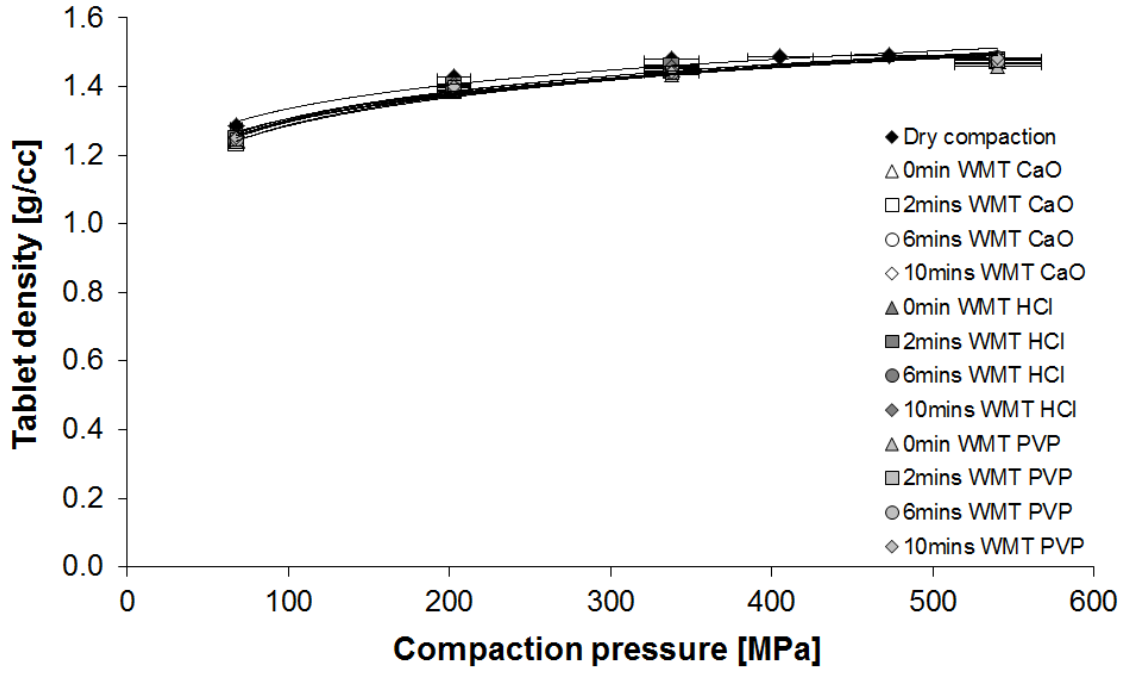

Figure E.7: Compressibility (tablet density as a function of compaction pressure) behaviour for granules produced from varying wet massing times 30% liquid level. Formulation comprises of 1:1 microcrystalline cellulose:lactose 200 mesh and 5w/v% PVP in Water, Calcium Oxide (CaO), Hydrochloric Acid (HCl).

F. GRANULE SPHERICITY AND POROSITY CHARACTERISATION TRIAL EXPERIMENTS

During analysis of the projected granular shape profile, the fractal number was investigated to be a potential parameter for observing the change in the surface roughness. However as seen in Figure F.1, the fractal dimension was not an effective parameter to represent the transition of the granule morphology with increasing number of impeller revolutions. The fractal dimension demonstrated an insignificant gradual increase in the fractal dimension from 1.23 to 1.26 as the number of impeller revolutions decreased, showing that at low impeller revolutions the granule surface roughness is greater. This may be attributed to the limitation of the 2D analysis of the SEM imaging and not being able to take into account the surface smoothing of the granules. Hence the circularity dimension was a better parameter to use to reflect the transition of the granule surface roughness as a function of the number of impeller revolutions.

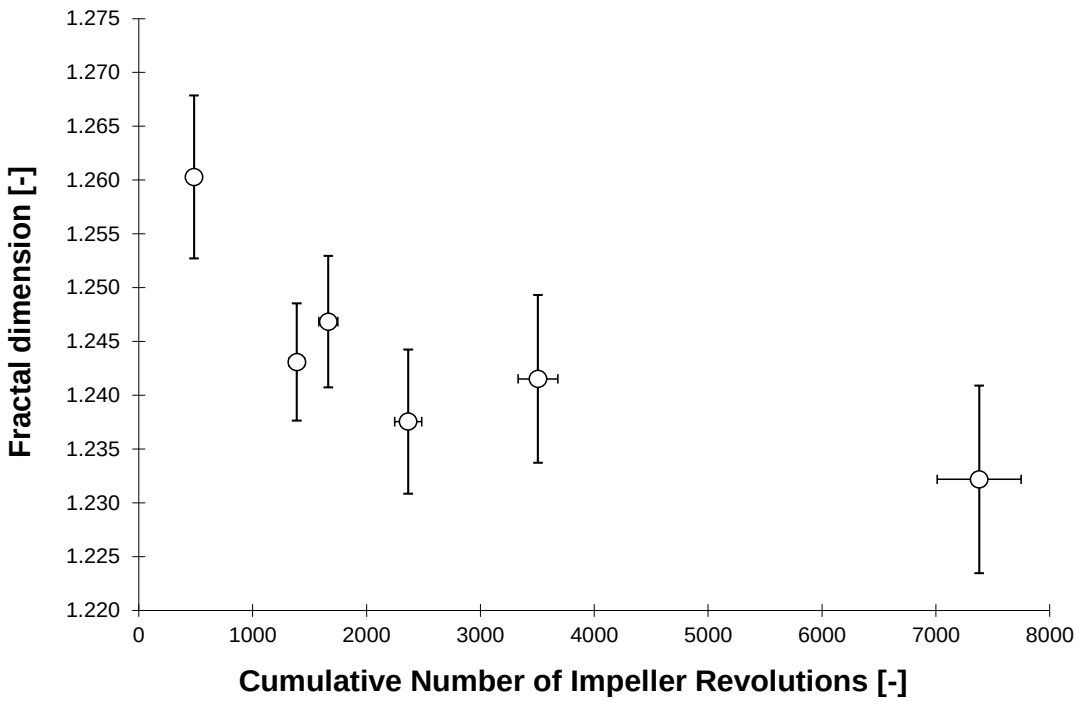

Figure F.1: The Fractal dimension of the projected profile of granules as a function of the cumulative number of high-shear granulator impeller revolutions.

The findings from the measurements demonstrate that the kerosene displacement experiment is not a favourable method for measuring the granule porosity. The magnitudes of the standard error of the mean for the duplicate measurements render the

findings to be statistically insignificant. This would be attributed to the errors in measuring the mass of the flask with both the granular sample and kerosene. Since kerosene does not penetrate into the granule pores, the mass of the kerosene after the samples have been deposited into the flask would not be accurate in determining the mass of the granule to calculate the porosity. Therefore the mercury intrusion porosimetry experiments were considered to accurately determine the granule porosity since pressure is applied to the mercury fluid to drive the mercury into the granular pores.

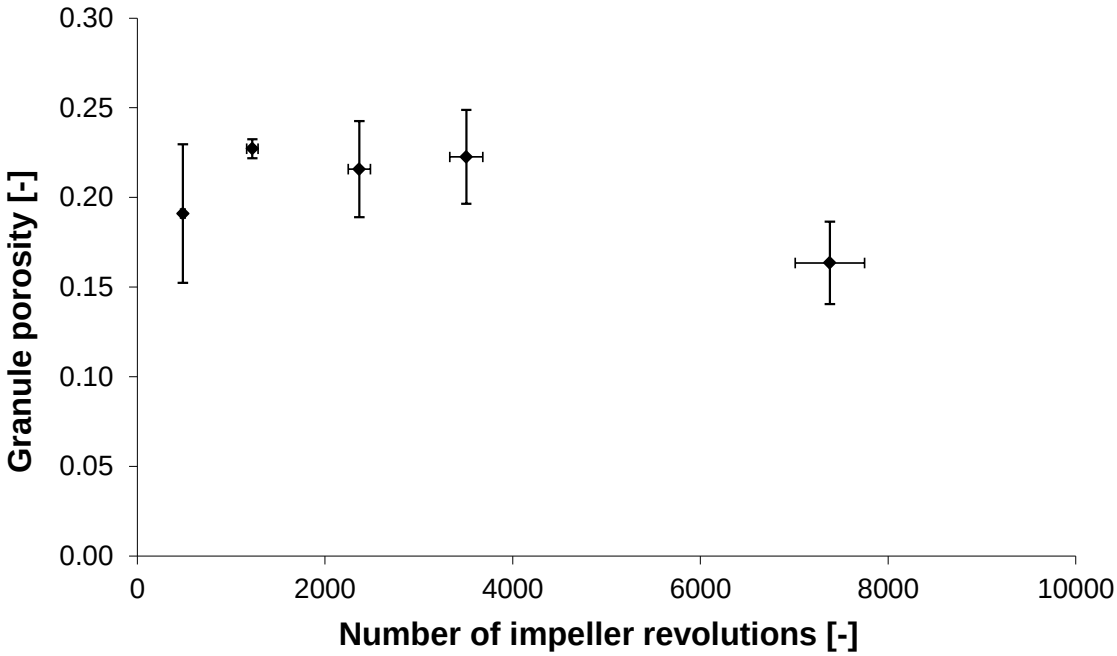

Figure F.2: Granule porosity as a function of the number of impeller revolutions using the kerosene displacement method.

G. GRANULE BET SPECIFIC SURFACE AREA PLOTS

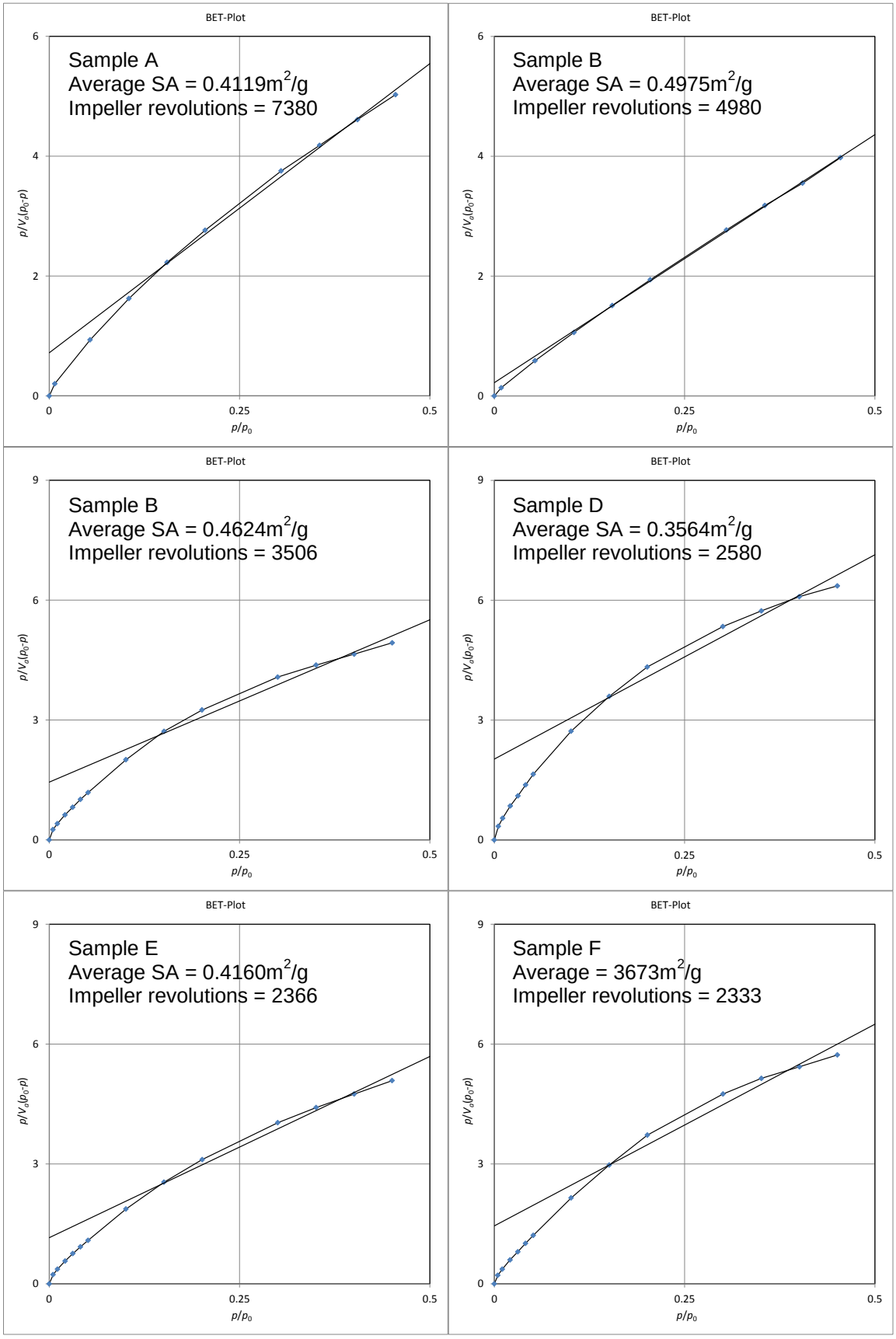

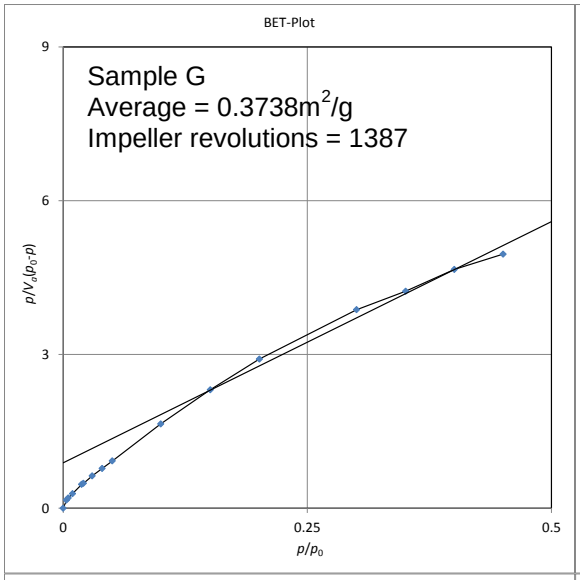
BET-Plot
Sample G
Average = 0.3738m²/g
Impeller revolutions = 1387
p/Va(p0-p)
p/p0
0
3
6
9
0.25
0.5

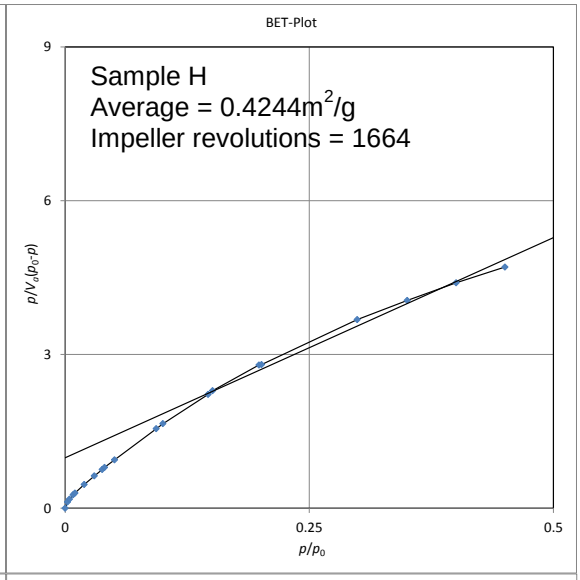
BET-Plot
Sample H
Average = 0.4244m²/g
Impeller revolutions = 1664
p/Va(p0-p)
p/p0
0
3
6
9
0.25
0.5

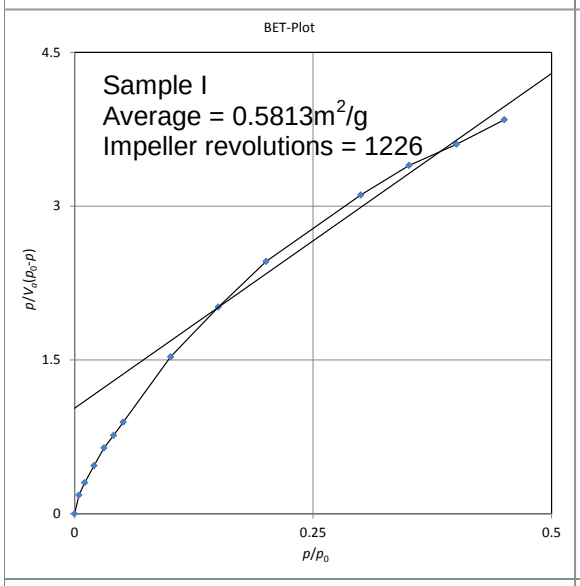
BET-Plot
Sample I
Average = 0.5813m²/g
Impeller revolutions = 1226
p/Va(p0-p)
p/p0
0
1.5
3
4.5
0.25
0.5

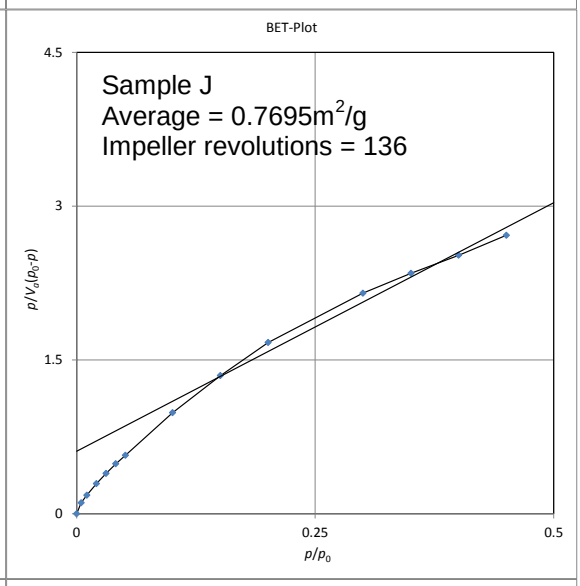
BET-Plot
Sample J
Average = 0.7695m²/g
Impeller revolutions = 136
p/Va(p0-p)
p/p0
0
1.5
3
4.5
0.25
0.5

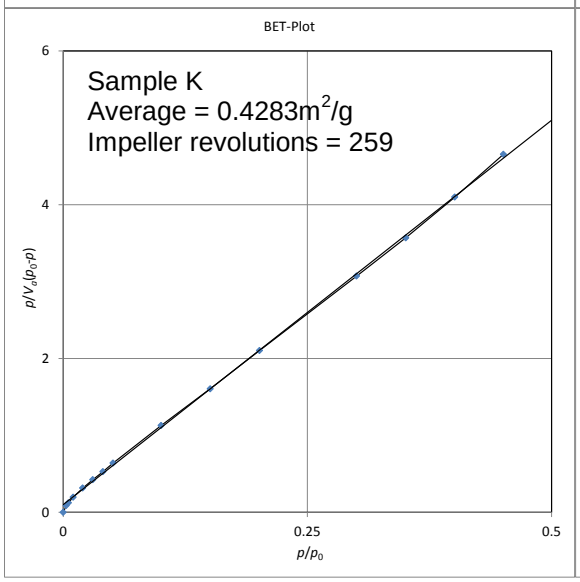
BET-Plot
Sample K
Average = 0.4283m²/g
Impeller revolutions = 259
p/Va(p0-p)
p/p0
0
2
4
6
0.25
0.5

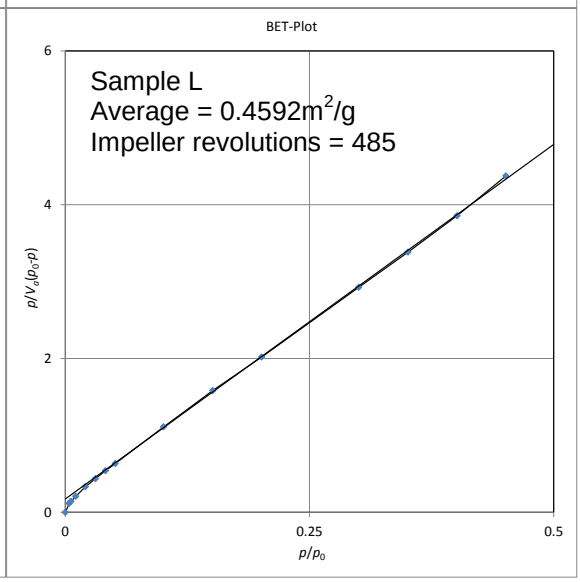
BET-Plot
Sample L
Average = 0.4592m²/g
Impeller revolutions = 485
p/Va(p0-p)
p/p0
0
2
4
6
0.25
0.5

H. MERCURY INTRUSION POROSIMETRY RAW DATA AND GRANULE POROSITY CALCULATIONS

The granule porosity was measured for selected granular samples in *Chapter 5: Effect of the Granulator Compaction Pressure on the Granule Properties*. The granule porosimetry was measured using mercury intrusion porosimetry (Micromeritics). The instrument conducts two sets of tests: low pressure (0-33,000psia) and high pressure test (33,000-65,000psia). During the low pressure test, the mercury fills the penetrometer stem and the bulb with the intention of filling the interstitial pores between the sample powder particles when the low pressure test is completed. The mercury then penetrates the sample internal pores during the high pressure test.

The mercury intrusion porosimetry results can be considered in three main sections (see Figure H.1:

(1) Filling of the interstitial pores between the powder particles and powder compression by the mercury medium,

(2) Filling of the powder internal pores,

(3) Sample brittle failure or permanent particle deformation.

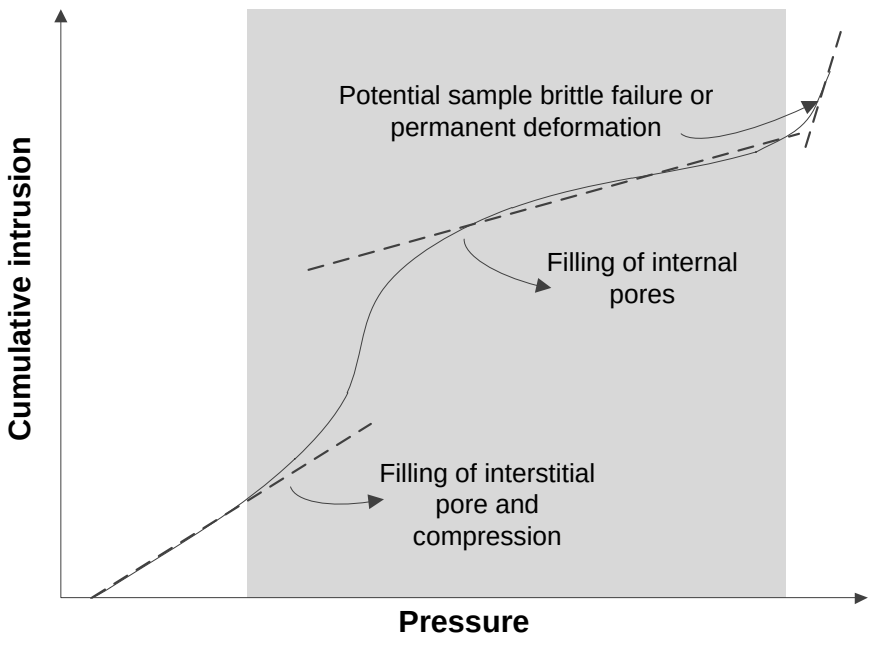

Figure H.1: Schematic diagram of mercury intrusion porosimetry results and the progression of mercury penetrating the sample particles.

When the granule porosity was measured using the mercury intrusion porosimetry, the results from the instrument did not accurately reflect the granule porosity which is expected to be at 50% and below. This is due to the instrument measuring the envelope density of the bulk powder sample during the low pressure test. Therefore during the high pressure test, the instrument measures the porosity from the penetration of mercury through the interstitial and internal granule pores, rather than through the internal pores only. Hence to determine the granule porosity, the results from the mercury intrusion porosimetry instrument needs to be re-calculated to determine the granule porosity from the internal pore measurement only.

Let the following parameters be defined:

Parameter	Definition
$V_{Hg,internal}$	volume of mercury filling the internal pores of the sample particles
$V_{interstitial}$	cumulative interstitial pore volume
$V_{internal}$	cumulative internal pore volume
V_{Hg}	volume of mercury in the penetrometer (upon completion of the low pressure test)
$V_{Hg,interstitial}$	volume of mercury filling the interstitial pores of between the sample particles
V_P	volume of the penetrometer
V_{SA}	absolute volume of the sample particles
V_{SE}	envelope volume of the sample particles
W_S	sample weight
W_P	weight of the penetrometer
W_T	total weight of the sample, penetrometer and mercury within the penetrometer
ε	sample porosity
ρ_{Hg}	density of mercury
ρ_{SA}	absolute density of the sample particles
ρ_{SE}	envelope density of the sample particles

Total volume of mercury filling interstitial pores:

$$V_{Hg,\text{interstitial}} = W_s \times V_{\text{interstitial}}$$
$$= 0.4093g \times 0.4657mL/g = 0.1906mL$$

Total volume of mercury filling internal pores:

$$V_{Hg,\text{internall}} = W_s \times V_{\text{internal}}$$
$$= 0.4093g \times 0.5233mL/g = 0.2142mL$$

Volume of mercury (at low pressure test):

$$V_{Hg} = \frac{W_T - W_P - W_S}{\rho_{Hg}}$$
$$= \frac{106.684g - 61.7715g - 0.4093g}{13.5335g/mL} = 3.2884mL$$

Envelope volume of sample:

$$V_{SE} = V_P - \left(V_{Hg} + V_{Hg,\text{interstitial}}\right)$$
$$= 3.9498mL - \left(3.2884mL + 0.1906mL\right) = 0.4708mL$$

Envelope density of sample:

$$\rho_{SE} = \frac{W_S}{V_{SE}}$$
$$= \frac{0.4093g}{0.4708mL} = 0.8693g/mL$$

Absolute volume of sample:

$$V_{SA} = V_{SE} - V_{Hg,\text{internal}}$$
$$= 0.4708mL - 0.2142mL = 0.2566mL$$

Envelope density of sample:

$$\rho_{SA} = \frac{W_S}{V_{SA}}$$
$$= \frac{0.4093g}{0.2566mL} = 1.5949g/mL$$

Sample porosity:

$$\varepsilon = \left(1 - \frac{\rho_{SE}}{\rho_{SA}}\right) \times 100\%$$
$$= \left(1 - \frac{0.8693g/mL}{1.5949g/mL}\right) \times 100\% = \frac{0.4093g}{0.2566mL} = 45.49\%$$

I. TARGETING THE TABLET STRENGTH USING THE GRANULATOR IMPELLER REVOLUTIONS

The Unified Compaction Curve model can be used to predict the final tablet strength using the wet granulation compaction pressure, P_{WGC}, and the number of granulator impeller revolutions, which can then be used to set up a 'Quality by Design' (QbD) matrix to help design the wet granulation conditions to target the desired tablet strength, as shown in Figure I.1.

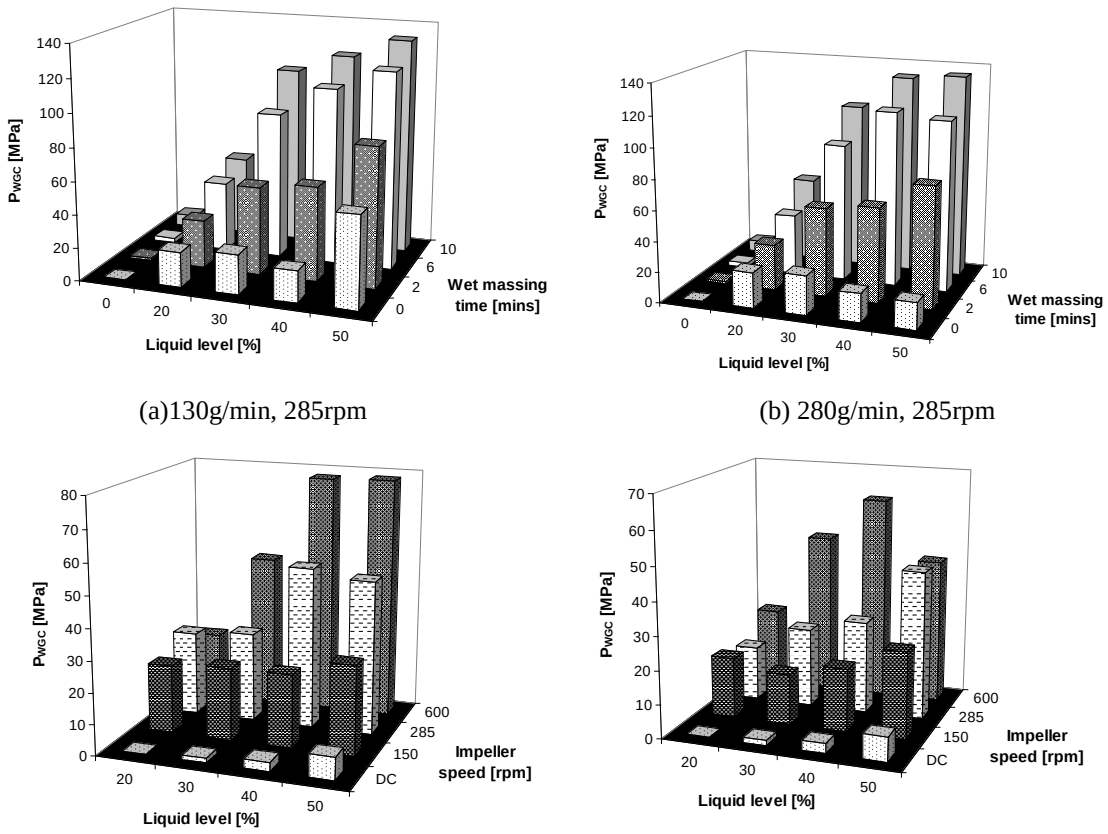

(a)130g/min, 285rpm (b) 280g/min, 285rpm

(c)130g/min (d) 280g/min

Figure I.1: Matrix graphs showing various relationships between the wet granulation compaction pressure P_{WGC}, wet massing time, liquid level, binder flow rate (BF) and impeller speed. (a) BF = 130g/min, 285rpm; (b) BF = 280g/min, 285rpm; (c) BF = 130g/min; and (d) BF = 280g/min.

The wet granulation process can be designed to target a desired tablet strength as presented below for a formulation comprising of 1:1 microcrystalline cellulose and lactose 200mesh, granulated with 5w/v% aqueous PVP liquid binder.

The target tablet strength and known wet granulation and tableting variables are summarised in Table I.1 below:

Table I.1: Summary of the target and known wet granulation, tableting processes and tablet strength.

Target/known variables	Target/known value
Target tablet strength, *T'*	2.2MPa
Tablet diameter	13mm
Theoretical maximum tablet strength, T_{max}	3.54MPa
UCC co-efficient, *b*	0.0062
Tabletting compaction pressure, *P'*	337.5MPa
Maximum wet granulation compaction pressure, $P_{WGC,max}$	134.8MPa

Firstly the ideal wet granulation compaction pressure, P_{WGC}, that would consequently produce a tablet with a tensile strength of 2.2MPa is determined by using the '*goal seek*' facility in *Microsoft Excel* spreadsheet to equate the right and left hand side of Equation H.1 by changing P_{WGC}.

$$T' = T_{\max}\left(e^{-bP_{WGC}} - e^{-b(P'+P_{WGC})}\right) \tag{I.1}$$

$$2.2 = 3.54\left(e^{-0.0062P_{WGC}} - e^{-0.0062(337.5+P_{WGC})}\right) \tag{I.2}$$

The ideal wet granulation compaction pressure was determined to be 55.5MPa. Now that the wet granulation compaction pressure is known, the number of revolutions required to achieve a wet granulation compaction pressure of 55.5MPa is calculated using Equation H.3.

$$P_{WGC} = P_{WGC,\max}\left(1 - e^{-bN}\right) \tag{I.3}$$

$$55.5 = 134.8\left(1 - e^{-0.0062N}\right) \tag{I.4}$$

This gives the number of required granulator impeller revolutions to be 86 revolutions using the '*goal seek*' function in the spreadsheet. With the ideal wet granulation pressure, the wet granulation conditions can be determined using the matrix in Figure I.1. Therefore the ideal wet granulation pressure becomes the primary criterion to establish the wet granulation conditions as demonstrated below:

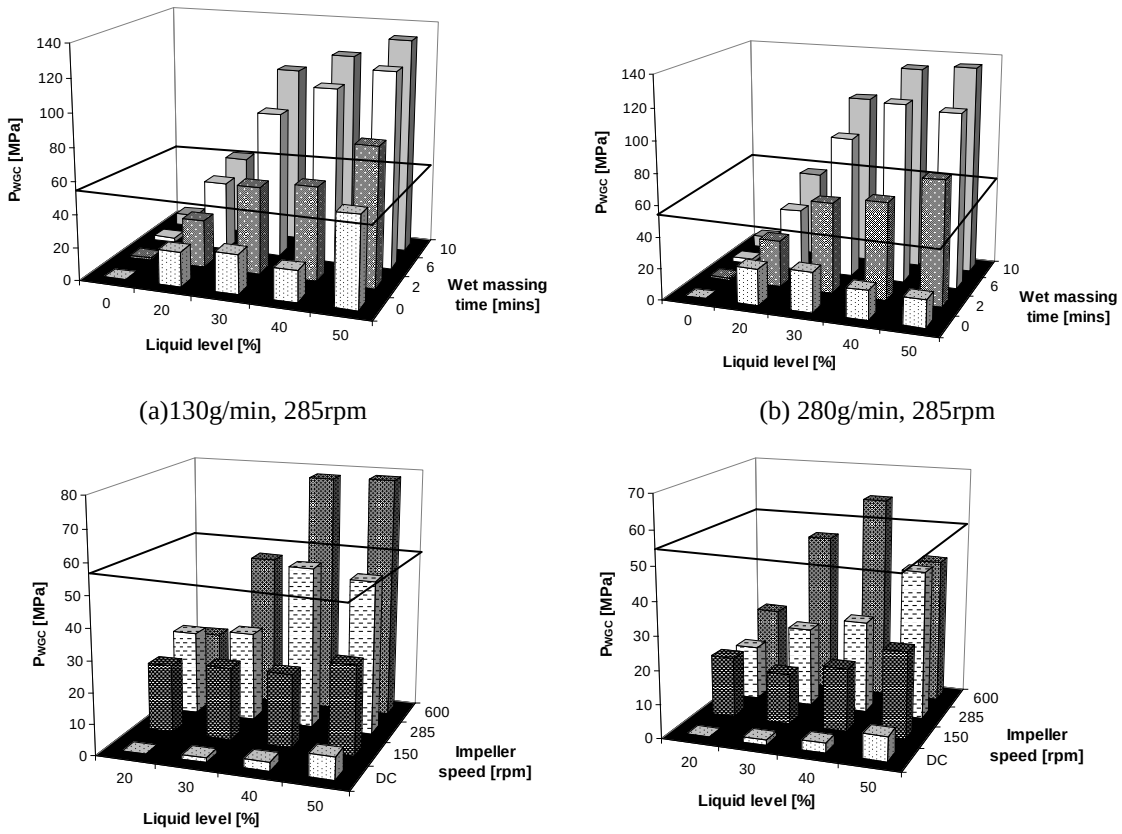

(a)130g/min, 285rpm

(b) 280g/min, 285rpm

(c)130g/min

(d) 280g/min

Figure I.2: Matrix graphs showing various relationships between the wet granulation compaction pressure P_{WGC}, wet massing time, liquid level, binder flow rate (BF) and impeller speed. The area below the high-lighted threshold at P_{WGC} = 55.5MPa determines the potential wet granulation conditions to achieve a tablet tensile strength of 2.2MPa. (a) BF = 130g/min, 285rpm; (b) BF = 280g/min, 285rpm; (c) BF = 130g/min; and (d) BF = 280g/min.

Therefore the wet granulation processing conditions that could be used to achieve a wet granulation compaction pressure of 55.5MPa, which would lead to a resulting tablet tensile strength of 2.2MPa are summarised in Table I.2. The wet granulation conditions that comprise of 20% liquid level are not taken into account because the moisture content of the granules are insufficient for the Unified Compaction Curve model to be valid, as shown in *Chapter 4*. Wet granulation conditions that comprise of zero wet massing time are also not taken into consideration as a suitable wet granulation condition due to the possibility of uneven liquid distribution with the lack of wet massing during the process.

From Table I.2, it can be seen that a wide combinations of liquid level, wet massing time, binder flow rate and impeller speed can be incorporated to achieve a tablet tensile strength of 2.2MPa. The final choice of the wet granulation process conditions will depend on the total number of impeller revolutions of the wet granulation process. This would be dependent on the capacity of the granulator bowl and the dry formulation

powder mass. However the Unified Compaction Curve model and the QbD matrix will be very useful for tablet manufacturing where the wet granulation process can be flexible to accommodate the up-stream or down-stream processes or fine-tune the wet granulation conditions to optimise the process.

Table I.2: Potential wet granulation conditions to achieve the desired tablet strength of 2.2MPa.

Figure	Liquid Level [%]	Wet Massing Time	Binder flow rate [g/min]	Impeller speed [rpm]
a	30	2 minutes	130	285
	40			
b	30		280	
	40			
	50			
c	30	10 seconds	150	130
			285	
			600	
	40		150	
			285	
	50		150	
			285	
d	30		150	280
			285	
			600	
	40		150	
			285	
	50		150	
			285	
			600	